



Gravity Separation and Desliming using Inclined Channels Subject to Different G-Forces

James Lachlan Carpenter

B.Eng. (Chemical) (Hons)

A thesis submitted in fulfilment of the requirements for the degree of
Doctor of Philosophy in Chemical Engineering

January 2021

*This research was supported by an Australian Government Research
Training Program (RTP) Scholarship*

STATEMENT OF ORIGINALITY

I hereby certify that the work embodied in the thesis is my own work, conducted under normal supervision. The thesis contains no material which has been accepted, or is being examined, for the award of any other degree or diploma in any university or other tertiary institution and, to the best of my knowledge and belief, contains no material previously published or written by another person, except where due reference has been made. I give consent to the final version of my thesis being made available worldwide when deposited in the University's Digital Repository, subject to the provisions of the Copyright Act 1968 and any approved embargo.

I hereby certify that the work embodied in this thesis contains published paper/s/scholarly work of which I am a joint author. I have included as part of the thesis a written declaration endorsed in writing by my supervisor, attesting to my contribution to the joint publication/s/scholarly work.

By signing below I confirm that James Carpenter contributed to the research and writing of the publications listed in this thesis.

James L. Carpenter

Kevin P. Galvin

Acknowledgements

Firstly, I would like to express my gratitude to both of my supervisors, Laureate Professor Kevin Galvin and Dr Simon Iveson. Your guidance, mentorship and support throughout my candidature has been invaluable. I must also make a similar thanks to Dr James Zhou for involving me in his experiments, allowing me to expand and add great depth to the thesis.

I would also like to thank the workshop and laboratory staff, colleagues in NIER and the Iron Ore Hub, and my fellow PhD candidates. Your friendship, engaging discussions (rarely about work), assistance in running experiments, and shared pain of wet sieving has made my time here far easier, and above all, enjoyable. Thank you all.

Most importantly, I need to thank my wonderful support network of family and friends. Your love and understanding has kept me motivated throughout these sometimes difficult years. Special thanks go to my parents, Helen and Warwick, my brother Rowan, and my partner Bianca, who have offered endless support and encouragement throughout all of my studies and beyond.

Finally, I am very thankful for the financial support of the University of Newcastle and the Australian Research Council (ARC) Research Hub for Advanced Technologies for Australian Iron Ore, IH130200031. The additional support from the industry partners, which led to a much stronger applied focus, is very much appreciated, as is the research and thesis feedback provided by Kylie Nettleton and Greg Elphick.

Abstract

The separation of ultrafine particles is a difficult and costly process. Low particle inertia and the viscous effects of clay – type slimes reduce the recovery of valuable particles and leads to further issues in downstream processing such as materials handling and dewatering. It is therefore common practise to implement a desliming stage, usually consisting of hydrocyclones, to remove these problematic ultrafines. With this comes an inherent loss of valuable particles. Current desliming processes also demonstrate an incomplete removal of the slimes, thus, downstream processing is still hindered by their presence.

As the minerals industry explores lower grade deposits, it is of increasing interest to develop new technologies to remove slimes at the finest sizes, and in doing so, improve the recovery across all particle sizes. This thesis investigates the issues of ultrafine separations and desliming from two standpoints; a quantitative study of the effects of slimes on separation performance, and the development of a new technology capable of high throughput desliming.

An initial systematic series of experiments was performed in the REFLUX™ Classifier using a high-grade iron ore feed containing a high concentration of slimes. The separation performance was quantified by the solids yield to underflow and Fe recovery across the entire size range. Variations to the solids throughput, through both the solids concentration and volumetric flowrate, revealed the performance to increase for more dilute feeds. At a throughput of 7 t/(m² h), a feed of 36.5 wt.% solids achieved a low recovery and yield of approximately 30 %. By halving the solids concentration, and simultaneously doubling the flowrate to maintain the same throughput, the recovery and yield both doubled to nearly 60 %. Further reductions in the solids concentration showed no further improvement. Thus, a sharp transition in system behaviour occurred at approximately 18.5 wt.%. Additional experiments were conducted with the inclined channel spacing halved, thus inducing a higher shear rate within the channels. A high solids concentration experiment achieved an Fe recovery and yield of approximately

50 %, roughly double that of an identical experiment with the wider channels. Thus, it was shown the performance could be improved without altering feed conditions.

Rheological experiments performed on the overflow solids from the REFLUX™ Classifier experiments showed the slimes to have both a strong shear thinning behaviour and strong dependence on the particle volume fraction. A sharp increase in viscosity with increasing solids fractions corresponded well with the transition in separation performance at 18.5 wt.% solids. A comparison of the slimes viscosity data to an 'ideal' solids model of Krieger & Dougherty (1959) indicated that the slimes effectively occupied a volume 5.5 times larger than their actual solids volume.

The second part of this research involved the novel REFLUX™ Graviton, which subjects inclined channel modules to a centrifugal force, thus combining the hydrodynamic advantage of the inclined channels with the G-Force advantage. An initial series of experiments using a fine silica feed determined the effects of different variables on the continuous system and confirmed the significant throughput advantage discovered in earlier semi-batch studies. This silica work showed the solids rate to underflow to be critical in providing sharp and fine size separations. A range of iron ore feeds, extending up to particle sizes of 1000 μm , were then investigated using the Graviton. This work showed the Graviton to be remarkably effective at desliming, especially when operated as a two – stage process. By removing the ultrafine particles, significant upgrades in the sub 20 μm size fraction were observed. From a feed grade of 55 wt.% Fe, this process achieved product grades of up to 64 wt.% Fe. Thus, desliming in the Graviton proved effective in upgrading an ultrafine waste stream to a saleable product.

Finally, the high-grade, high-slimes feed used in the REFLUX™ Classifier experiments was deslimed in the Graviton at approximately 10 μm , achieving a high yield and Fe recovery of over 90 %. The deslimed product was then processed in the REFLUX™ Classifier. At high solids concentrations, the deslimed runs showed recoveries up to 55 % Fe, roughly double that achieved in the original experiments, however at low solids concentrations the results were much closer. A comparison of

selected experiments for the original, narrow channels, and deslimed experiments showed very similar results. Thus, the viscous effects of the slimes could be practically eliminated through the use of dilution, high shear rates, and by highly efficient desliming at approximately 10 microns. Rheological experiments conducted on the deslimed overflow solids were far closer to the ideal model case of Krieger & Dougherty (1959), with the sharp increase in viscosity not evident until much higher particle volume fractions. Hence, the viscous issues predominantly came from these ultrafine slimes.

In summary, two classifier units were used to investigate the separations of ultrafine particles and slimes. Experiments in the REFLUX™ Classifier, supported by rheology, examined the separation performance in the presence slimes. Dilution and high shear rates proved effective in reducing the viscous effects of slimes, greatly improving the separation performance. Experiments in the REFLUX™ Graviton demonstrated an effective, high-throughput desliming process. With high yields and recoveries, removal of the ultrafines also resulted in high product grades.

Table of Contents

Acknowledgements	i
Abstract	iii
List of Figures	x
List of Tables	xix
Publications	xxi
Nomenclature	xxii
Chapter 1: Introduction	
1.1 Background to Ultrafine Beneficiation	3
1.2 Objectives of Thesis	7
1.3 Structure of Thesis	9
Chapter 2: Literature Review - Particle Sedimentation	
2.1 Single Particle Settling.....	13
2.2 Hindered Settling	17
2.3 Slurry Rheology	20
2.4 Fluidised Beds	23
2.5 Inclined Settling.....	28
2.6 Particle Motion down an Incline.....	30
2.7 Conclusion.....	32
Chapter 3: Literature Review - Gravity Separations and Desliming	
3.1 Introduction to Beneficiation.....	35
3.1.1 <i>Ultrafines and Clays</i>	38
3.1.2 <i>The “Fish Hook” Effect</i>	40
3.2 REFLUX Classifier	41
3.2.1 <i>Design</i>	41
3.2.2 <i>Throughput Advantage</i>	42
3.2.3 <i>Application of Closely Spaced Channels</i>	44
3.2.4 <i>Modelling</i>	50
3.3 Enhanced Gravity Separation.....	51
3.3.1 <i>The effect of Centrifugal Force</i>	51
3.3.2 <i>Existing Technologies</i>	54

3.4	REFLUX™ Graviton	59
3.4.1	<i>Design</i>	59
3.4.2	<i>Throughput Advantage under Centrifugal Force</i>	60
3.4.3	<i>Fine Coal Work</i>	62
3.5	Conclusion.....	63

Chapter 4: Experimental Methods

4.1	REFLUX™ Graviton	67
4.1.1	<i>Equipment</i>	67
4.1.2	<i>Changes to Equipment</i>	75
4.1.3	<i>Procedure</i>	79
4.1.4	<i>Sample Analysis</i>	81
4.2	REFLUX™ Classifier	86
4.2.1	<i>Equipment</i>	86
4.2.2	<i>Procedure</i>	89
4.2.3	<i>Sample Analysis</i>	90
4.3	Supplementary Experiments.....	90
4.3.1	<i>Rheology</i>	90
4.4	Summary	91

Chapter 5: REFLUX™ Classifier Results

5.1	Experimental Conditions.....	95
5.2	Results with 3 mm Channels.....	97
5.3	Results with 1.8 mm Channels.....	103
5.4	Rheology	107
5.5	Concluding Summary	114

Chapter 6: REFLUX™ Graviton Results

6.1	Introduction	119
6.2	Silica Feed.....	119
6.3	Iron Ore Feeds.....	135
6.3.1	<i>Iron Ore Feed 1</i>	136
6.3.2	<i>Iron Ore Feed 2</i>	141
6.3.3	<i>Iron Ore Feed 3</i>	149
6.3.4	<i>Iron Ore Feeds 4 and 5</i>	154
6.4	Comparing the Graviton and REFLUX™ Classifier	158

6.4.1	<i>Feed top size 300 micron.....</i>	158
6.4.2	<i>Feed top size 1000 micron.....</i>	160
6.5	Concluding Summary	163
Chapter 7: Graviton and REFLUX™ Classifier Two-Stage Separation		
7.1	Introduction	167
7.2	First stage: Desliming in the REFLUX™ Graviton.....	167
7.3	Second stage: Processing deslimed feed in the REFLUX™ Classifier.....	169
7.4	Rheology	174
7.5	Concluding Summary	178
Chapter 8: Conclusions and Recommendations		
8.1	Summary of Present Work	181
8.1.1	<i>Initial REFLUX™ Classifier Results with High-Slimes Feed</i>	181
8.1.2	<i>Rheological Experiments</i>	182
8.1.3	<i>REFLUX™ Classifier and Rheological Results with Deslimed Feed.....</i>	183
8.1.4	<i>REFLUX™ Graviton Results</i>	184
8.2	Recommendations for Future work.....	186
References		189
Appendix A: Summary of Run Conditions		199
Appendix B: Laser Sizing Data		203
Appendix C: Experimental Data and Sampling.....		265
Appendix D: Size × Assay Data		343
Appendix E: Rheology Data.....		369
Appendix F: Chapter 5 Calculations.....		378
Appendix G: Chapter 6 Calculations		382
Appendix H: Graviton Splashing Raw Data		385
Appendix I: Copyright Permissions		387

List of Figures

Figure 1.1: Diagram of the REFLUX™ Classifier.	5
Figure 1.2: Diagram of the REFLUX™ Graviton.	7
Figure 2.1: Drag coefficient for solids spheres moving relative to a fluid. Adapted from Bird et al. (1960).	15
Figure 2.2: Drag coefficient versus particle Reynolds number for non-spherical particles, either isometric or disks. Adapted from Rhodes (2008).	17
Figure 2.3: Viscosity, calculated from the Krieger-Dougherty model, versus particle concentration in water for different shaped particles at a shear rate of 300 s^{-1} . Adapted from Barnes et al. (1989).	23
Figure 2.4: Diagram of the bed pressure drop versus fluid velocity for packed and fluidised beds. Adapted from Rhodes (2008).	25
Figure 2.5: Phase inversion in a fluidised bed at increasing fluidisation rates using a binary system of large low-density particles (open circles) and small high-density particles (filled circles). Adapted from Galvin (2003).	28
Figure 2.6: Settling area and sedimentation phases in vertical and inclined channels. Adapted from Davis and Acrivos (1985).	29
Figure 3.1: A general guide to the suitability of various particle separation devices as a function of particle size (Perry & Green, 1999).	36
Figure 3.2: Illustration of the "fish-hook" effect. Adapted from Zhu and Liow (2014).	41
Figure 3.3:(a) Parabolic velocity profile for laminar flow in a closely spaced channel with (b) a detailed view of different sized particles at the inclined surface. The critical elutriation condition is seen when the local fluid velocity is equal and opposite to the particle terminal settling velocity in the tangential direction to the inclined surface (Galvin et al., 2009).	46

Figure 3.4: Equilibrium position of a particle subjected to laminar flow and a high shear rate. Equilibrium occurs when the lift force, L_f , is equal and opposite to the net weight force of the particle, F_n (Galvin & Liu, 2011).	47
Figure 3.5: Comparison of the experimental data and theoretical model of Galvin et al. (2009). Open symbols are for experiments conducted using one species at a time and the closed symbols applicable to the mixed suspension. The triangles denote particles of density 1400 kg/m ³ , the squares denote particles of density 2600 kg/m ³ , the small circles denote particles of density 4300 kg/m ³ and the large circles denote particles of density 4600 kg/m ³ . The model curve for the densest particles was based on the average density of 4450 kg/m ³ .	49
Figure 3.6: Comparison of the experimental data of Galvin et al. (2009) with the theoretical model of (Galvin & Liu, 2011). The squares denote particles of density 1400 kg/m ³ , the circles denote particles of density 2600 kg/m ³ , the plus symbols denote particles of density 4300 kg/m ³ and the cross symbols denote particles of density 4600 kg/m ³ . The model curve for the densest particles was based on the average density of 4450 kg/m ³ .	49
Figure 3.7: Theoretical settling velocities versus the particle diameter for three particle species of specific gravities 1.3, 2.5, and 4.8. The dashed lines show the settling velocities under normal gravity (1 G) and the solid lines show the settling velocities under a centrifugal force of 200 G. Adapted from Luttrell et al. (1995).	53
Figure 3.8: Diagram of the Knelson concentrator (Das & Sarkar, 2018).	56
Figure 3.9: Diagram of the Falcon concentrator (Das & Sarkar, 2018).	57
Figure 3.10: Diagram of the Multi - Gravity Separator (MGS) (Das & Sarkar, 2018).	58
Figure 3.11: Diagram of the Kelsey centrifugal jig (Singh & Das, 2013).	59
Figure 3.12: Throughput advantage given by ratio of superficial fluid velocity to particle terminal velocity, U/u_t , versus $Gz/(3d)$. This result shows that the benefits of the G force and the inclined channels multiply, Key: ○ G = 14, □ G = 28, △ G = 55, × G = 73 (Galvin & Dickinson, 2013).	61
Figure 3.13: Variation in the particle separation density with the particle diameter. Experimental results with $G = 73$ are shown together with the theoretical results for	

inclined channels with $G = 1$ and a conventional fluidised bed at $G = 1$ (Galvin & Dickinson, 2013)	63
Figure 4.1: Swinging arms of the Graviton centrifuge with an open mount (top) and with the inclined channel module in place (bottom). The centrifuge is contained within a stainless steel housing.	68
Figure 4.2: Picture of the original 3-D printed inclined channel module (left) and the face of the module showing the reinforced channels (right).	69
Figure 4.3: Picture of the fluidisation chamber from the inside (left) and a close up of the fluidisation arrangement (right). Fluidisation enters via 100 holes spaced around the centre of the chamber. Underflow exits through an opening at the very centre of the chamber. Feed enters via one or more of the four tangential entry points around the chamber.	70
Figure 4.4: Picture of the fluidisation chamber from the outside (left) and the chamber mounted to the centrifuge arm with all lines attached (right).	70
Figure 4.5: Diagram of the 3-D printed REFLUX™ Classifier module from the side (left) and from the front (right). The side view shows the angle of incline, channel length and the overflow exit for the channels on the side shown. The front view shows the 9 elements in the 3×3 grid each with 22 channels broken into 3 smaller sections by the supports.	71
Figure 4.6: Diagram showing close up details of one of the nine channel elements of the 3-D printed module. Twenty-two channels are shown, each divided into three smaller channels by the supports. The dimensions of each channel and the spacing between them are shown.	71
Figure 4.7: Diagrams of the fluidisation chamber that is mounted to the face of each REFLUX™ Classifier module. On the left is a side view of the chamber with one of the four feed entry points, showing the length of the pyramidal and conical sections connected by the flange. On the right is a top view showing the dimensions of the feed entries, conical section, two fluidisation line inlets and the underflow outlet.	72
Figure 4.8: The different underflow attachment sizes. From top to bottom: 2 mm, 3 mm, 4 mm, 6 mm, 8 mm, 10 mm internal diameter. The 3 and 2 mm parts screw onto the body of the 4 mm piece.	73

Figure 4.9: Mechanical seal of the Graviton. All lines enter the top of the seal and are fed to the rotating system via an annular arrangement. The lines are split evenly and diverted to the modules on opposite arms of the centrifuge.	73
Figure 4.10: Size distributions of the sampled underflow for Run CF222 and the particles washed out of the launder after the run.	74
Figure 4.11: Picture of one of the underflow discharge points and collection in drums (left) and on the opposite side, the other underflow discharge point and below it the overflow discharge and sump (right). The overflow was pumped from this sump into a secondary tank.	75
Figure 4.12: Photo of modification to fluidisation chamber showing flange where cylindrical section was reattached.	76
Figure 4.13: Diagram of the overflow splashing mechanisms believed to occur in the Graviton.	77
Figure 4.14: Temporary solutions to overflow material splashing into underflow launder: launder rail guard (left) and the two overflow exits, the top one is blocked off (right).	78
Figure 4.15: Splashing tests showing the comparison of overflow and underflow rates before and after modifications to the system.	79
Figure 4.16: Process flow diagram of the Graviton experimental setup.	80
Figure 4.17: Overall solids volume yield to underflow calculated by the two product formula (Equation 4.1) applied to each size interval. The solid line shows a yield of 71 vol.%.	82
Figure 4.18: Partition to underflow as calculated by Equations 4.2a and 4.2b. The solid line shows the best fit of Equation 4.4 to the results of Equation 4.2b in the range of 5 to 50 μm .	83
Figure 4.19: Example of a partition curve with the defining characteristic values highlighted. For this curve $d_{75} = 21 \mu\text{m}$, $d_{50} = 14 \mu\text{m}$, $d_{25} = 8 \mu\text{m}$.	84
Figure 4.20: Photo of the RC™100 (left) and the inside of the fluidisation distributor showing four holes on each face of the inverted pyramid (right).	87

Figure 4.21: Photo of the bed density plot during operation of the RC™100. The blue line tracked the measured density as the bed developed, before reaching the set point of 2500 kg/m ³ and levelling out.	88
Figure 4.22: Diagram of the underflow buffer arrangement for the RC™ 100	89
Figure 5.1: Feed size distribution measured as volume percentage by a Malvern Mastersizer 3000.	95
Figure 5.2: Feed size distribution measured as mass percentage by sieving at screen sizes of 0.038, 0.045, 0.063, 0.090, 0.125, 0.180 and 0.250 mm.	95
Figure 5.3: Fe recovery as a function of feed solids concentration for the 3.0 mm channels (mass-balanced data from Table 5.1).	99
Figure 5.4: Fe recovery as a function of feed solids throughput for the 3.0 mm channels (mass balanced data from Table 5.1).	100
Figure 5.5: Solids yield to underflow as a function of mean particle size (mass-balanced data).	101
Figure 5.6: Fe recovery as a function of mean particle size (mass-balanced data).	101
Figure 5.7 Fe recovery as a function of the feed solids concentration for both sets of channels (mass-balanced data from Table 5.1).	104
Figure 5.8: Fe recovery as a function of feed solids throughput for both sets of channels (mass-balanced data from Table 5.1).	105
Figure 5.9: Comparison of the yield curves across the entire size range for the two sets of channels. The empty symbols and dashed lines are for 3.0 mm channels, the filled symbols and solid lines are for 1.8 mm channels. Mass-balanced data.	106
Figure 5.10: Comparison of the recovery curves across the entire size range for both sets of channels. The empty symbols and dashed lines are for 3.0 mm channels, the filled symbols and solid lines are for 1.8 mm channels. Mass-balanced data.	106
Figure 5.11: Shear stress versus shear rate for varying volume fractions of the sub 0.038 mm overflow particles.	108

Figure 5.12: Apparent viscosity as a function of shear rate for suspensions of varying volume fractions of the sub 0.038 mm overflow particles.	108
Figure 5.13: Comparison of the measured apparent viscosities with those predicted from Equation 5.1 for the entire set of rheology data.	109
Figure 5.14: Viscosity of the overflow -0.038 mm solids as a function of particle volume fraction for shear rates of 1, 10, 20, and 40 s ⁻¹ . The solid line shows the model of Krieger and Dougherty (1959) with a maximum packing fraction of $\phi_{\max} = 0.64$. The data at a shear rate of 10 s ⁻¹ was fit to this model using a scaling factor of 5.5.	112
Figure 5.15: Comparison of a standard hindered settling velocity and one calculated to describe the hindered settling of non-slime particles in a slimes suspension.	113
Figure 6.1: Feed particle size distribution for the initial, middle and final runs of the silica suspension experiments. Distributions measured using a Malvern Mastersizer 3000.	120
Figure 6.2: Partition curves for the Runs CF145, CF146, and CF147 demonstrating the effect of fluidisation rate (shown in legend) at a constant feed solids concentration of 2 wt.% and feed flowrate of 100 L/min.	122
Figure 6.3: Partition curves for the Runs of CF148, CF149, and CF150 demonstrating the effect of fluidisation rate (shown in legend) at a constant feed solids concentration of 4 wt.% and feed flowrate of 112 L/min.	122
Figure 6.4: Partition curves the Runs CF153, CF154, and CF157 performed at a constant feed flowrate of 50 L/min and fluidisation rate of 18 L/min. Increasing the feed solids concentration (shown in legend) exceeds the solids capacity of the 4 mm underflow.	125
Figure 6.5: Partition curves for the Runs CF158, CF159, and CF160 performed at a constant feed solids concentration of approximately 30 wt.% and fluidisation of 18 L/min. Increasing the feed flowrate (shown in legend) exceeds the solids capacity of the 6 mm underflow.	126
Figure 6.6: Partition curves for the Runs CF152, CF153, and CF155 performed at a fluidisation rate of 18 L/min with an underflow outlet diameter of 4 mm. The results show the effect	

of balancing an increasing feed solids concentration by lowering the feed flowrate (both shown in legend).	127
Figure 6.7: Partition curves for the Runs CF155 and CF156 performed with a feed flowrate of 36 L/min and solids concentration of 28 wt.% with the 4 mm underflow outlet.	128
Figure 6.8: Partition curves for the Runs CF164, CF160, CF163, and CF162 performed at a feed solids concentration of 30 wt.% with the 6 mm underflow outlet.	129
Figure 6.9: Ep values versus the underflow solids flux, defined by the area of the underflow opening for one module. Open symbols are used for the runs showing a poor separation with $Ep \geq 10 \mu\text{m}$.	131
Figure 6.10: Overflow solids concentration versus the underflow solids concentration. Open symbols are used for the high Ep runs identified in Figure 6.9.	131
Figure 6.11: Solids rate in the underflow versus the solids rate in the feed. Open symbols are used for the high Ep runs identified in Figure 6.9. The linear trend line was fitted using all the data points.	132
Figure 6.12: Throughput advantage as calculated by Equation 3.16. The terminal settling velocity in inclined channel, u'_t , was calculated using Stokes law (under normal gravity) for a particle of the separation size d_{50} . Open symbols are used for the high Ep runs identified in Figure 6.9. The red crosses show the results from the semi-batch study of Galvin and Dickinson (2013) at $G = 55$.	133
Figure 6.13: Theoretical separation size, calculated from Equation 3.16, versus the actual separation size. Open symbols are used for the high Ep runs identified in Figure 6.9.	134
Figure 6.14: Particle size distributions of the feed samples taken for Iron Ore Feed 1 experiments as measured by a Malvern Mastersizer 3000.	136
Figure 6.15: Partition curves for Runs CF184, CF185, and CF186 performed on Iron Ore Feed 1 with the 8 mm underflow opening at a fluidisation rate of 36 L/min and feed flowrate of 140 L/min.	137
Figure 6.16: Partition curves for the Runs CF186 and CF188 that form a two-stage separation, the underflow of CF186 being used as the feed for CF188. The overall partition curve for the combined separation is also shown.	138

Figure 6.17: Particle size distributions of the feed samples taken for Iron Ore Feed 2 experiments as measured by a Malvern Mastersizer 3000.	142
Figure 6.18: Partition curves for the Runs CF195, CF197, CF201, CF202, and CF209 showing the effect of decreasing underflow outlet size.	143
Figure 6.19: Partition curves for the Runs CF197 and CF200 showing the effect of increasing the fluidisation rate by using larger sized holes in the distribution chamber.	145
Figure 6.20: Partition curves for the Runs CF195 and CF196 that form a two-stage separation using the 8 mm underflow outlet. The partition curve for the combined separation is also shown.	146
Figure 6.21: Partition curves for the Runs CF197 and CF198 that form a two-stage separation using the 6 mm underflow outlet. The partition curve for the combined separation is also shown.	147
Figure 6.22: Partition curves for the Runs CF202 and CF203, and repeat runs of CF206 and CF207, that form two-stage separations using the 3 mm underflow outlet. The partition curves for the combined separations are also shown.	147
Figure 6.23: Particle size distributions of the feed samples taken for Iron Ore Feed 3 experiments as measured by a Malvern Mastersizer 3000.	149
Figure 6.24: Partition curves for the Runs CF215, CF217, CF218, CF219, CF220, and CF221 performed with a feed solids concentration of 10 wt.% and the 3 mm underflow outlet.	150
Figure 6.25: Partition curves for the Runs CF222 and CF223 that form a two-stage separation using the 3 mm underflow outlet. The partition curve for the combined separation is also shown.	152
Figure 6.26: Particle size distributions of the 1st stage feed, 1st stage product, and 2nd stage product. The distributions show the near complete removal of sub 10 μm particles in the two-stage separation.	153
Figure 6.27: Particle size distributions of the feed samples taken for Iron Ore Feed 4 and Iron Ore Feed 5 experiments as measured by a Malvern Mastersizer 3000.	155

Figure 6.28: Partition curves for Runs CF232, CF233, CF235, CF236, and CF238 on Iron Ore Feed 4 performed using the 3 mm underflow outlet.	156
Figure 6.29: Partition curves for Runs CF247, CF245, and CF246 performed on Iron Ore Feed 5 with the 3 mm underflow outlet, a feed flowrate of 52 L/min and solids concentration 10 wt.%.	157
Figure 6.30: Particle size distributions for the feed and underflow of Run CF246.	157
Figure 6.31: Particle size distributions for the feed at top sizes of 300 and 1000 μm .	158
Figure 6.32: Partition curves for the Runs CF249, CF250, CF251, CF252, and CF253 performed with an 8 mm underflow outlet. The partition curves remain level as the particle size approaches 300 μm .	160
Figure 6.33: Partition curves for Runs CF256, CF257, and CF258 performed with a 10 mm underflow outlet. The partition curves remain level as the particle size approaches 1000 μm .	162
Figure 7.1: Partition curves for Run CF254 and Run CF251	167
Figure 7.2: Particle size distributions for the feed and underflow of Run CF254, as measured by a Malvern Mastersizer 3000.	169
Figure 7.3: Overall Fe recovery for each run using the deslimed feed as well as the original feed (Chapter 5) in both the 3 mm and 1.8 mm channels.	171
Figure 7.4: Solids yield to underflow as a function of mean particle size for the deslimed feed (mass-balance data).	172
Figure 7.5: Fe recovery as a function of mean particle size for the deslimed feed (mass-balanced data).	172
Figure 7.6: Comparison of Fe recovery curves for runs utilising different methods of combatting the slimes issue. The poor performing run (S24B3) and deslimed run (S24F4) are given as reference points. The lower solids concentration run (S24D) and narrow channel run (S24G2) demonstrate how the slimes issue can be overcome (mass-balanced data).	174

Figure 7.7: Particle size distributions for the -0.038 mm overflow solids from the original rheology experiments and the deslimed experiments, as measured by a Malvern Mastersizer 3000.	175
Figure 7.8: Apparent viscosity as a function of shear rate for suspensions with varying volume fractions of the -0.038 mm overflow particles from the deslimed feed experiment S24F2.	176
Figure 7.9: Apparent viscosity of the overflow solids as a function of particle volume fraction for a shear rate of 10 s^{-1} for the original and deslimed feed. The solid line shows the model of Krieger and Dougherty (1959) with a maximum packing fraction of $\phi_{\text{max}} = 0.64$. The deslimed feed data is also scaled by a factor of 1.44 to fit the Kreiger and Dougherty model (filled circles).	177

List of Tables

Table 5.1: Feed conditions used for each run as well as the mass balanced head grades of the feed, underflow (product) and overflow (reject) streams, overall solids yield to underflow and Fe recovery.	97
Table 6.1: Summary of the experimental conditions of the eighteen runs using the Silica feed along with the d_{50} and Ep values from the partition curves.	121
Table 6.2: Summary of the run conditions for all experiments across the five iron ore feeds. Partition d_{50} and Ep results, head grades of the Feed, Underflow and Overflow streams and the solids yield to underflow and Fe recovery are also listed.	135
Table 6.3: Mass balanced size assay data for Run CF184.	140
Table 6.4: Mass balanced size assay data for Run CF185.	140
Table 6.5: Mass balanced size assay data for Run CF186. This run formed Stage 1 of the two-stage separation.	140
Table 6.6: Mass balanced size assay data for Run CF188. This run formed Stage 2 of the two-stage separation.	141

Table 6.7: Head grades of each stream, yield to underflow and Fe recoveries for the two-stage separation experiments (raw data)	148
Table 6.8: Iron and phosphorus contents of each stream, solids yield to underflow and Fe recovery for the Iron Ore Feed 3 experiments (raw data)	151
Table 6.9: Mass balanced size assay data for the two-stage separation of Iron Ore Feed 3.	154
Table 6.10: Run conditions, partition d_{50} and E_p results, head grades for each stream, solids yield to underflow and Fe recovery (raw data) for the five runs performed with the feed top size of 300 μm . All runs used an 8 mm underflow outlet.	159
Table 6.11: Run conditions, partition d_{50} and E_p results ,head grades for each stream, solids yield to underflow and Fe recovery (raw data) for the runs performed with the feed top size of 1000 μm . All runs used a 10 mm underflow	161
Table 7.1: Mass balanced size \times assay data for Run CF254	168
Table 7.2: Feed conditions, mass balanced head grades of each stream, solids yield to underflow and Fe recovery for the experiments performed using the deslimed feed as a second stage separation.	170

Publications

- Carpenter, J. L., Iveson, S. M., & Galvin, K. P. (2017). *Separation of ultra-fine particles using the REFLUX™ Graviton*. Paper presented at Iron Ore 2017, Perth, Australia.
- Carpenter, J. L., Iveson, S. M., & Galvin, K. P. (2018). Desliming ultra-fine iron ore in the REFLUX graviton. *Chemeca 2018*, 92.
- Carpenter, J. L., Iveson, S. M., & Galvin, K. P. (2019a). Ultrafine desliming using a REFLUX™ classifier subjected to centrifugal G forces. *Minerals Engineering*, 134, 372-380.
- Carpenter, J. L., Iveson, S. M., Zhou, J., Sutherland, J., & Galvin, K. P. (2019b). *Influence of Slimes on Gravity Separation of Iron Ore Fines in a REFLUX Classifier*. Paper presented at Iron Ore 2019, Perth, WA.
- Carpenter, J. L., Zhou, J., Iveson, S. M., & Galvin, K. P. (2019c). Gravity separation in the REFLUX™ Classifier in the presence of slimes. *Minerals Engineering*, 143, 105941.

Nomenclature

Symbol	Meaning	Units
a	Viscosity model exponent	-
A_p	Surface area of particle	m^2
Ar	Archimedes number	-
b	Viscosity model exponent	-
B_i	Mass balanced value	-
C_D	Drag Coefficient	-
d	Particle diameter	μm (mm)
D	Vessel diameter	mm
d_{25}	25 % partition size	μm
d_{50}	50 % partition size, separation size	μm
d_{75}	75 % partition size	μm
E_i	Experimental value	-
Ep	Ecart probable	μm
F	Throughput advantage	-
F	Feed solids rate	kg/min
$f(\phi)$	Hindered settling function	-
F_D	Net drag force on particle	N
F_f	Net force on particle due to the fluid	N
F_n	Net weight force of particle in fluid	N
g	Acceleration due to gravity	m/s^2
G	G -force	-
G	Objective function	-
Ga	Galileo number	-
H	Height of bed	-
K	Consistency constant	$Pa s^{np}$
K_1	Viscosity model constant	s^a
K_2	Viscosity model constant	s
L	Channel length	mm
L_f	Inertial lift force	N
n	Dimensionless exponent	-
n_p	power law index	-

Symbol	Meaning	Units
OF	Overflow solids rate	kg/min
p	Pressure	Pa
P	Partition value	%
R_C	Recovery value	%
Re_{mf}	Reynolds number at minimum fluidisation velocity	-
Re_p	Particle Reynolds numbers	-
Re_s	Shear Reynolds number	-
S	Rate of clarified fluid layer formation	m ³ /s
U	Fluid velocity	m/s
u	Particle velocity	m/s
U'	Fluid velocity through inclined section	m/s
u'_t	Terminal settling velocity tangential to surface	m/s
UF	Underflow solids rate	kg/min
u_h	Hindered settling velocity	m/s
U_L	Local fluid velocity	m/s
U_{mf}	Minimum fluidisation velocity	m/s
u_{slip}	Slip velocity	m/s
u_{slip_i}	Slip velocity of species i	m/s
u_t	Terminal settling velocity	m/s
u_{tG}	Terminal settling velocity under enhanced gravity	m/s
u_{ti}	Terminal settling velocity of species i	m/s
V_p	Surface area of a sphere of equal volume to the particle	m ²
w	Channel depth into the page	m
w_i	Weighting factor	-
x	Distance	m
x_F	Volume fraction of solids in the Feed	-
x_{OF}	Volume fraction of solids in the Overflow	-
x_{UF}	Volume fraction of solids in the Underflow	-
Y	Volume yield	-
y_F	Mass fraction in feed	-
Y_M	Mass yield	-
y_{OF}	Mass fraction in overflow	-
y_{UF}	Mass fraction in underflow	-
z	Channel perpendicular width	mm

Symbol	Meaning	Units
γ	Shear rate	s^{-1}
Δp	Pressure drop	Pa
θ	Angle of incline to the horizontal	-
μ	Fluid viscosity	Pa s
μ_{∞}	Infinite shear viscosity	Pa s
μ_s	Suspension viscosity	Pa s
ρ	Fluid density	kg/m^3
ρ_i	Density of species i	kg/m^3
ρ_p	Density of the particle	kg/m^3
ρ_s	Density of suspension	kg/m^3
σ_i	Standard deviation	-
τ	Shear stress	Pa
τ_0	Yield stress	Pa
ϕ	Volume fraction of solids	-
ϕ_{max}	Maximum packing fraction	-
Ψ	Sphericity	-
α	Exponent factor	-
ε	Voidage	-
$[\eta]$	Intrinsic viscosity	-

Chapter 1

Introduction

1.1 Background to Ultrafine Beneficiation

After extraction, ores undergo a series of processes in order to remove unwanted gangue particles and purify the valuable mineral. This stage of the process chain is known as beneficiation. Iron ore for example is sold at a grade of 62 wt.% Fe, however, as the run of mine ore grade is usually lower, beneficiation is needed to reach this target grade. This can be achieved through processes such as crushing, grinding, screening, gravity separation, and flotation. In general, as particle size decreases, beneficiation becomes more difficult to apply and costly, however, liberation delivers the potential for much higher grade. The term 'ultrafine' has a different definition depending on not only the industry, but also the individual process. In the mining industry, the term is used broadly depending on the individual process, with some extending the term up to 500 μm . In this work the term is used to describe particles finer than 45 μm .

Due to limitations in beneficiation equipment, ultrafine particles are often discarded as part of the tailings, resulting in a significant loss of high-grade well-liberated material. As demand increases, interest grows in maximising the recovery from the entire resource. Developing technologies must therefore be capable of handling particles of all sizes. With industry pushing the recovery of iron to finer sizes, ore is subjected to higher levels of comminution for better liberation. With this comes an inherent increase in the amount of ultrafine gangue particles such as silica, alumina and phosphorous that present problems for the downstream processes of sintering and smelting. The ultrafine gangue is commonly in the form of clay particles, of which there are many types that vary in shape, surface charges and other factors, all of which can alter the behaviour of a slurry. The term used to describe this ultrafine gangue is 'slimes'. With this gangue representing a large portion of ultrafine feeds, effective separation and beneficiation are essential.

Historically ultrafine particles have largely been discarded due to difficulties in processing and handling. Their small mass results in low particle inertia, meaning these particles settle in the Stokes regime where the settling velocity dependence on particle diameter, d , is amplified to d^2 . Separating

ultrafine particles on the basis of density is thus more difficult. The low settling velocity also limits the throughput of separation devices. The presence of slimes carries many negative effects that are detrimental to handling and beneficiation processes. Increased pulp viscosity reduces the efficiency of slurry transport and of separation devices. Slimes can also coat desirable particles and are easily entrained to the product stream. This contamination of the final product also diminishes the filterability due to the moisture retention of the slimes.

These issues have made it more practical for feeds to undergo a desliming stage prior to either gravity separation or flotation. Here, common practice sees large banks of hydrocyclones cut the feed at sizes between 10 and 50 μm . Whilst this approach provides a low cost solution, the reality is that a significant portion of the slimes still report to the underflow, impacting on downstream processes. The ultrafine “waste” stream also contains large numbers of high-grade particles that are discarded as tailings. To minimise their loss, the desliming can be performed at finer sizes. To achieve this, however, smaller diameter cyclones must be used, significantly increasing the total number of units needed. Alternative processing methods for ultrafine feeds that not only reduce the volume of tailings but also increase the Fe recovery are thus of growing interest.

The REFLUX™ Classifier is a hydraulic gravity separation device consisting of a fluidised bed situated below a set of inclined channels. Figure 1.1 shows a diagram of this arrangement. Fluidising water creates a uniform medium for particle segregation with the bulk flow transporting fine and low density particles up to the inclined channels. Within the inclined channels, the water flow conveys the low-density particles upwards toward to the overflow. The inclined channels increase the total sedimentation area, increasing the opportunity for any high-density particles in the channels to settle and slide down to remix in the fluidised bed below. The REFLUX™ Classifier was originally applied to coal but has more recently found success in the wider minerals industry. Like all classification devices, the feed size range affects the performance. The REFLUX™ Classifier has been applied to feed sizes up

to 8 mm (Galvin et al., 2010) and more recently to ultrafine feeds less than 0.015 mm (Hunter et al., 2016), albeit at much lower throughputs.

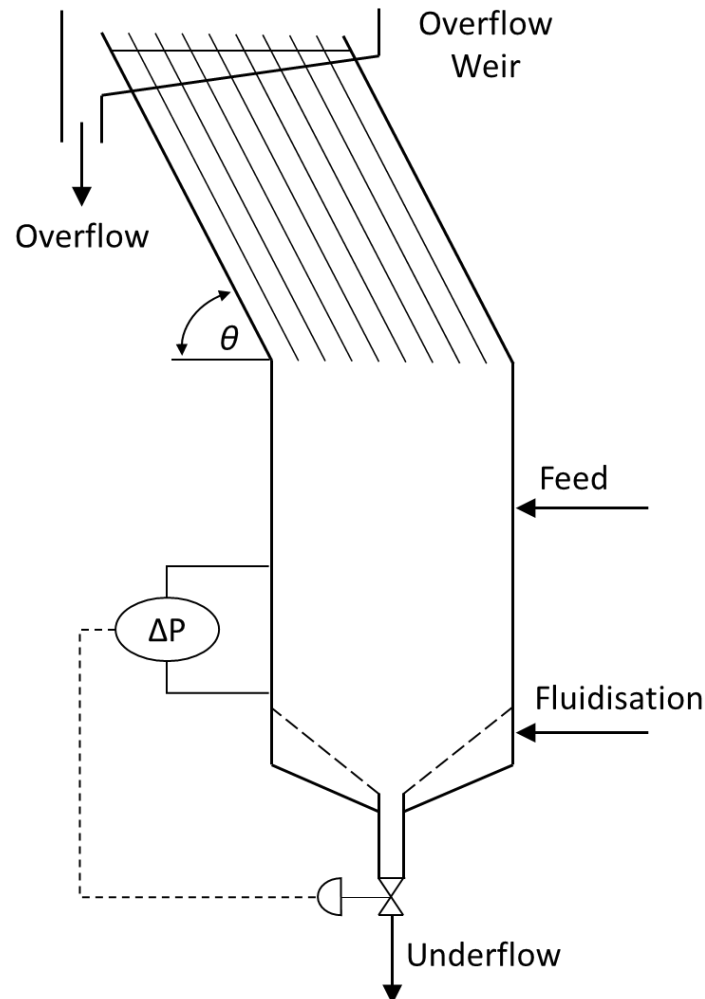


Figure 1.1: Diagram of the REFLUX™ Classifier.

Ideally, mineral separation should be driven only by the difference in density between the particles, not their size difference. However, the slow terminal settling velocity of ultrafine particles places a large dependence on particle size, making a density-based separation less effective. Enhanced gravity devices provide a solution to this problem by increasing the effective inertial forces. This results in faster settling rates and the possibility of a lower dependence of the settling velocity on the particle size by shifting the settling regime from Stokes to intermediate, allowing density to play a greater role

in the separation. Faster settling rates also increase the throughput and allow the normally slow settling ultrafine particles to be recovered efficiently.

Many industries such as oil, dairy and water treatment use centrifugal devices to combat slow settling and increase the throughput (Colic et al., 2007; Batalović, 2011; Das & Sarkar, 2018). Primarily used for immiscible liquid and solid-liquid separations, these devices usually consist of inclined plates within a rotating bowl. In the minerals industry, enhanced gravity devices such as the Knelson concentrator, Falcon concentrator and the multi-gravity separator (MGS) promote density-based separations of particles as fine as 10 μm . Despite shortcomings in capacity, water requirements and bypass issues, these devices have found some industry use for low grade, high value fines, primarily gold (Majumder & Barnwal, 2006; Wills & Finch, 2016). Although not commonly used at large scale, research continues into the application of these devices to other ores such as iron and tin (Roy, 2009; Angadi et al., 2017; Chaurasia & Nikkam, 2017; Marion et al., 2019).

A new application of enhanced gravity is in the device known as the REFLUX™ Graviton, shown in Figure 1.2. This device consists of small REFLUX™ Classifier units inside a high-speed centrifuge. A powerful synergy develops between the effects of the inclined channels and the mechanism of enhanced gravity. With this combination, the Graviton offers the potential for much higher throughput than observed for other enhanced gravity devices. Previously Galvin and Dickinson (2013) studied the Graviton under semi-batch conditions. They obtained sharp size separations using a fine silica feed, and observed other benefits in the separation of lower density coal from higher density particles. Perhaps the most important result of their study was the finding that the overall throughput advantage could be described by simply multiplying the throughput advantage achieved by the inclined channels with the number of G applied.

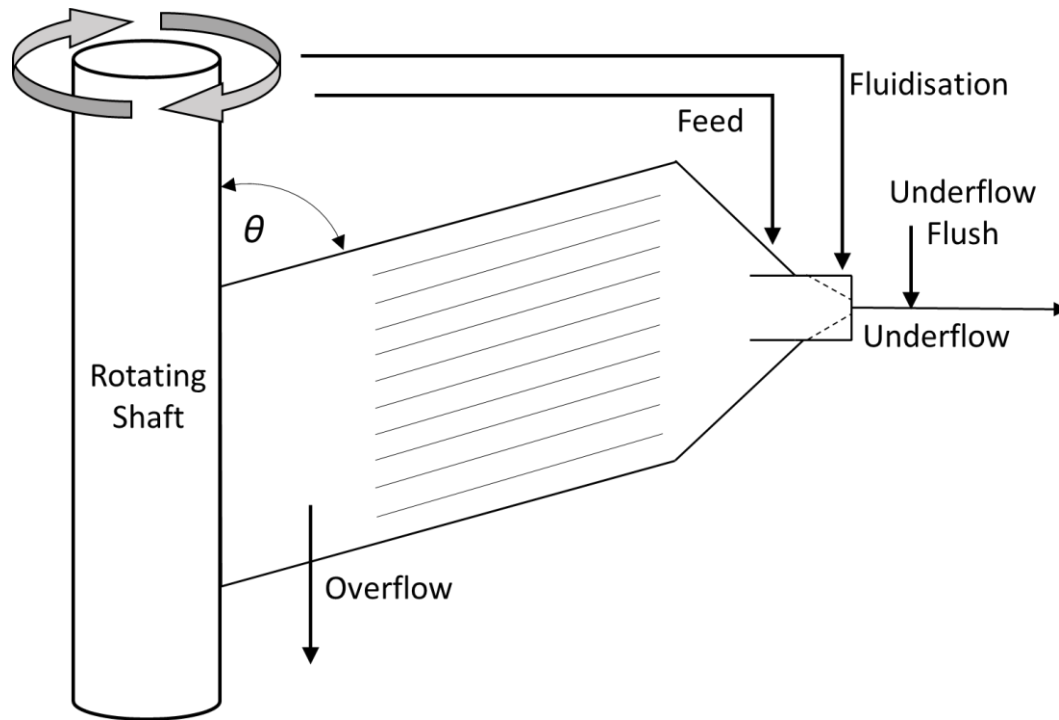


Figure 1.2: Diagram of the REFLUX™ Graviton.

1.2 Objectives of Thesis

Due to inefficiencies in the operation of hydrocyclones installed in most operating plants, significant levels of the so-called “slimes” remain with the “deslimed” feed. It is well known that the presence of such slimes causes deterioration in downstream separation performance, especially at ultrafine particle sizes below 0.1 mm. This thesis addresses the challenges of ultrafine particle separation in the presence of these retained slimes.

Two related technologies, the REFLUX™ Classifier and the REFLUX™ Graviton, in principle offer strong prospects for overcoming the effects of these retained slimes due to the action of the fluidising water, the intense segregation due to the presence of the inclined channels, and the influence of the shear rate within the inclined channels on the slimes rheology. Moreover, the enhanced gravity applied to the Graviton offers the potential to shift the problem of the slimes to much finer sizes, thus improving separation performance.

In principle, the operating conditions applied to both technologies can be adjusted to reduce the effects of the slimes. Thus, the overall objective of this study was to undertake a systematic investigation to quantify the separation performance of the technologies over a broad range of conditions and in turn establish the circumstances required to overcome the negative effects of the slimes. This objective is covered in two main parts, using the REFLUX™ Classifier which operates according to gravitational acceleration only, and then the REFLUX™ Graviton which is subjected to elevated G forces. If the ultrafine particles are subjected to enhanced gravity, the degree of variation in particle settling velocity with particle size should be reduced, thus improving the separation performance. Moreover, the higher particle inertia should be more effective in overcoming the strong viscous effects of the slimes.

The research was conducted primarily on a high-grade iron ore feed containing significant levels of the so-called “slimes”, in order to simplify the assessment of the separation performance. Thus, the feed was binary in nature, either high density hematite over a broad size range, or ultrafine viscous slimes. The separation performance was quantified in terms of the yield to underflow and Fe recovery as a function of the particle size, covering a systematic range of operating conditions.

The aims of the first section of the thesis are to:

- i. investigate the performance of the REFLUX™ Classifier using different inclined channel spacings and feed conditions. The slimes rheology depends upon the solids concentration and the shear rate, which are both influenced by the feed solids concentration, flow velocity, and the inclined channel spacing;
- ii. quantify the rheology of the ultrafine material as a function of the solids concentration and shear rate, and hence use this information to interpret the separation performance in the REFLUX™ Classifier;
- iii. draw conclusions on how best to overcome the effects of the slimes on separation performance.

Thus, the aims of the second part of the research are to:

- i. develop an understanding of the effect of key variables on the performance of the continuous system using the silica feed and identify the optimal conditions;
- ii. quantify the performance of the REFLUX™ Graviton in terms of both gravity separation and desliming using iron ore feeds;
- iii. investigate the effectiveness of the REFLUX™ Graviton on several feed types, covering increasingly broader particle size distributions and levels of slimes.

The REFLUX™ Graviton, which operates at up to $G = 73$, utilises relatively high flow velocities and a relatively narrow channel spacing of only 1 mm, hence, has elevated shear rates. The REFLUX™ Graviton thus provides more extreme process intensification than is possible via the REFLUX™ Classifier. It is of interest therefore to assess whether the simpler REFLUX™ Classifier offers a sufficient solution to the desliming problem, or whether it is necessary to utilise the enhanced gravity of the REFLUX™ Graviton.

1.3 Structure of Thesis

This thesis commences with a review of literature relevant to these investigations of gravity separation and desliming. Chapter 2 outlines the fundamental theories of particle and flow behaviours, commencing with the settling of a single, isolated particle, through to multiple particle suspensions and fluidised beds. Chapter 3 then outlines standard methods, and challenges of fine particle beneficiation. This chapter contains a comprehensive review of the REFLUX™ Classifier and enhanced gravity technologies, including past work concerned with semi-batch operation of the REFLUX™ Graviton.

Descriptions of the REFLUX™ Graviton and the REFLUX™ Classifier used to conduct the experimental work are provided in Chapter 4. This chapter also outlines the methodology used to investigate the rheology of the ultrafine suspensions, data analysis, and the ongoing modifications to the experimental apparatus.

This thesis is built based on the experiments of two different, but related, systems. Chapter 5 outlines the results of experiments performed in the REFLUX™ Classifier along with supporting rheological data, and Chapter 6 contains the results from the REFLUX™ Graviton. Results from a two-stage process utilising both systems are presented in Chapter 7. Details of the feed material and experimental conditions are provided at the beginning of each subchapter.

Finally, conclusions and recommendations for future work are discussed in Chapter 8. The raw sizing, mass flow, assay and rheology data are provided in the appendices along with details of the calculations performed.

Chapter 2

Literature Review - Particle Sedimentation

2.1 Single Particle Settling

If we consider a single spherical particle falling through an incompressible, unbounded, quiescent, Newtonian fluid, the primary forces acting on the particle are gravity, buoyancy and drag forces. The motion of the fluid can be described by the Navier-Stokes equation,

$$\rho \frac{D}{Dt} U = -\nabla p + \mu \nabla^2 U + \rho g \quad (2.1)$$

and the continuity equation,

$$\nabla \cdot U = 0 \quad (2.2)$$

where ρ is the fluid density, μ is the fluid viscosity, g is the acceleration due to gravity, p is the pressure and U the fluid velocity. Stokes (1851) solved the equation using stream functions at zero particle Reynolds number. Here the inertial terms of Equation 2.1 are neglected and the pressure and velocity components of the fluid can be found (Lamb, 1953). The net force acting on a particle due to the fluid, F_f , is found by integrating the forces over the particle surface. Integration of the normal force gives the 'buoyant force' and 'form drag'. Integration of the tangential surface force gives the 'friction drag' (Bird et al., 1960). The sum of these forces is given as,

$$F_f = \underbrace{\frac{1}{6} \pi d^3 \rho g}_{\text{Bouyant force}} + \underbrace{\pi \mu d u}_{\text{Form drag}} + \underbrace{2 \pi \mu d u}_{\text{Friction drag}} \quad (2.3)$$

where d is the particle diameter and u the velocity of the particle relative to the bulk fluid. The sum of the two drag forces is often expressed as the total particle drag force, F_D . At steady state the sum of the forces acting on the particle must be zero, hence the force of the fluid matches the gravitational force on the particle,

$$\frac{1}{6} \pi d^3 \rho_p g = \frac{1}{6} \pi d^3 \rho g + 3 \pi \mu d u \quad (2.4)$$

where ρ_p is the density of the particle. At this steady state the particle velocity relative to the bulk fluid is defined as its terminal settling velocity, u_t , and is found by rearranging Equation 2.4 to give,

$$u_t = \frac{d^2(\rho_p - \rho)g}{18\mu} \quad (2.5)$$

Equations 2.4 and 2.5 are a form of Stokes law with the original derivation using a particle Reynolds number of zero. The particle Reynolds number, Re_p , is given by,

$$Re_p = \frac{\rho u d}{\mu} \quad (2.6)$$

Stokes law becomes invalid at higher Reynolds numbers. Bird et al. (1960) states that with a Reynolds number of 1 Stokes law predicts a drag force that is 10 % too low. This is because the contribution of inertial terms starts to become significant. The drag forces on a particle are often expressed in the form of the dimensionless drag coefficient, C_D , given by,

$$C_D = \frac{2F_D}{\rho u_t^2 \pi \left(\frac{d}{2}\right)^2} \quad (2.7)$$

The relationship between the particles Reynolds number and the drag coefficient is shown in Figure 2.1.

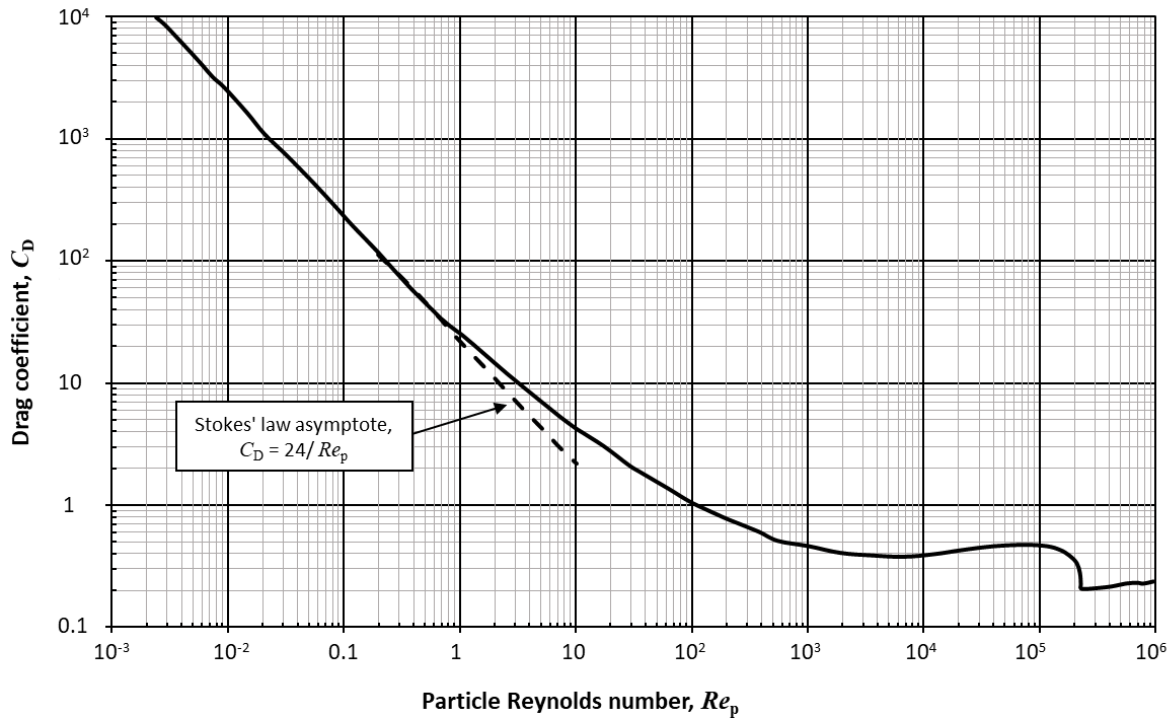


Figure 2.1: Drag coefficient for solids spheres moving relative to a fluid. Adapted from Bird et al. (1960).

Figure 2.1 shows that at a low Reynolds number, the linear relationship of $C_D = 24/Re_p$ holds true. This corresponds to the particle terminal settling velocity of Stokes law (Equation 2.5). As inertial forces become significant, the particle Reynolds number increases and enters what is called the intermediate regime. Here, as evidenced by the curve in Figure 2.1, there are no explicit equations for the drag coefficient or settling velocity, instead, empirical equations are used. In practise, the point at which one stops using Stokes law and moves to the intermediate regime, as well as the empirical equations used, varies. This can depend on factors such as particle shape and size, as well as the actual application.

In this work we will assume the Stokes regime to be valid at $Re_p < 2$ and define the intermediate regime as being the region $2 < Re_p < 500$. Bird et al. (1960) states that although the Stokes regime predicts a drag force that is 10 % too low at $Re_p = 1$, Stokes law is still more accurate than the empirical correlations of the intermediate regime for $Re_p < 2$. There are many empirical equations for the intermediate regime, each vary in accuracy over different ranges of Reynolds numbers. For the range

of $2 < Re_p < 500$ the relationship of $C_D = 18.5/Re_p^{0.6}$ is generally accepted (Lapple, 1950; Vance & Moulton, 1965). The terminal settling velocity in this regime is thus,

$$u_t = \frac{0.153g^{0.71}d^{1.14}(\rho_p - \rho)^{0.71}}{\rho^{0.29}\mu^{0.43}} \quad (2.8)$$

As the Reynolds number moves higher again, the curve in Figure 2.1 flattens out into what is called Newtons regime, that is $500 < Re_p < 10^5$. Here the drag coefficient is approximately constant at $C_D \approx 0.44$. In this regime the particle settling velocity is given by,

$$u_t = 1.74\sqrt{\frac{d(\rho_p - \rho)g}{\rho}} \quad (2.9)$$

For $Re_p > 10^5$ the boundary layer becomes turbulent, which delays boundary layer detachment, resulting in a significant drop in the total drag force. Again, empirical equations are needed to predict the drag behaviour and the exact point of transition is very sensitive to the flow conditions and particle smoothness. This regime, however, is outside the scope of this thesis.

The equations and relationships discussed so far have all related to spherical particles. In practise, particles take on many shapes, some that are hard to define. A simple, although not necessarily accurate, way to describe particle shape is through its sphericity, Ψ , given by,

$$\Psi = \frac{\pi^{1/3}(6V_p)^{2/3}}{A_p} \quad (2.10)$$

where A_p is the surface area of the particle, and V_p is the surface area of a sphere of equal volume to the particle. The sphericity is a measure a how closely the particle resembles a perfect sphere. For non-spherical particles, calculations requiring a diameter, such as the Reynolds number, are based on the spherical particle of equal diameter. This is the case for Figure 2.2, which shows the drag curve (the same as Figure 2.1), but for a range of particle sphericities. Often, real particles have a sphericity of order ~ 0.7 .

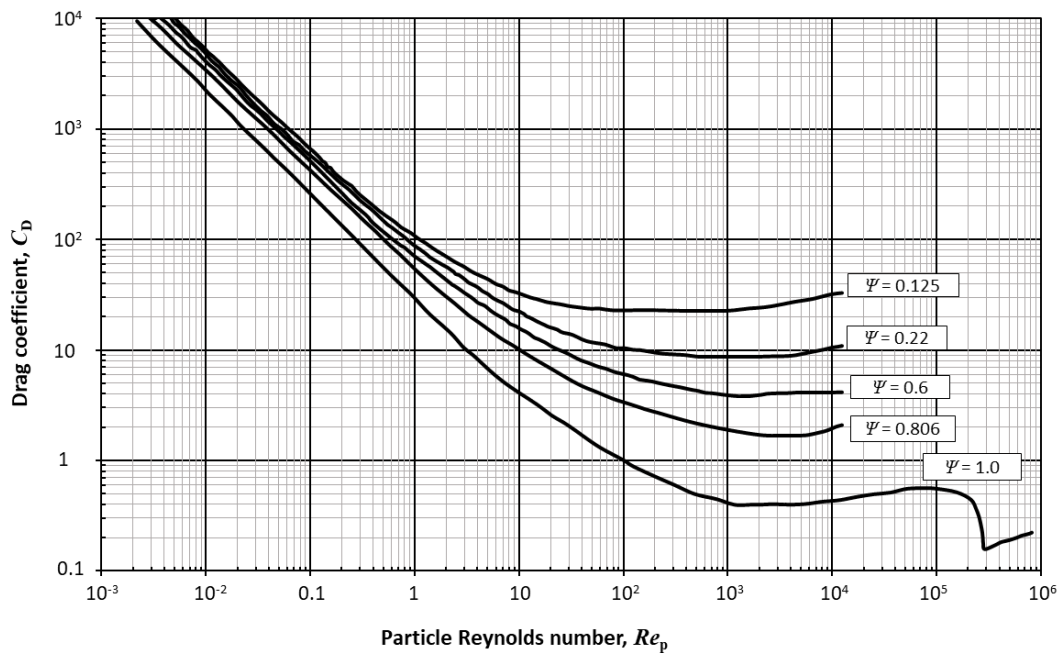


Figure 2.2: Drag coefficient versus particle Reynolds number for non-spherical particles, either isometric or disks. Adapted from Rhodes (2008).

As Figure 2.2 shows, the particle sphericity has a greater effect at higher Reynolds numbers. Drag is also influenced by particle orientation. In the Stokes regime particles fall, presenting their smallest cross-sectional area to the direction of movement. In the Newtons regime, however, particles orientate to present their largest cross-sectional area perpendicular to the direction of movement, creating more drag (Rhodes, 2008).

The effect that particle shape has on the settling velocity is highly dependent on the actual shape, orientation, and Reynolds number. There are many empirical correlations available, which multiply the standard spherical settling velocity by a constant that takes into account the sphericity, or some other shape-related factor (Pettyjohn, 1948; Becker, 1959; Hartman et al., 1994; Perry & Green, 1999; Gabitto & Tsouris, 2008).

2.2 Hindered Settling

In the previous section, the settling behaviour of a single particle was considered. However, in most industrial processes the particles are in suspension and the motion of one particle is influenced by those around it. This change in behaviour is termed hindered settling, as the settling velocity in a multi

particle system is generally lower than for a single particle. The relationship between the single particle settling velocity and the hindered velocity, u_h , is defined by the hindered settling function $f(\phi)$, which is a strong function of the volume fraction of the solids, ϕ . Thus,

$$u_h = u_t f(\phi) \quad (2.11)$$

For suspensions in fluidised beds, discussed further in Section 2.3, it is often more appropriate to refer to the slip velocity, u_{slip} , defined as the difference between the particle velocity, u , and the interstitial fluid velocity, U , both relative to a fixed frame of reference,

$$u_{\text{slip}} = u - U \quad (2.12)$$

Many models have been proposed to describe the relationship between the slip velocity and the solids volume fraction, an extensive review of which is provided by Di Felice (1995). The most commonly used and simplest model is that of Richardson and Zaki (1954) which can also be expressed in terms of the slip velocity,

$$f(\phi) = (1 - \phi)^n \quad (2.13)$$

$$u_{\text{slip}} = u_t (1 - \phi)^{n-1} \quad (2.14)$$

where n is a dimensionless exponent.

Whilst this expression refers to suspensions of a single species, it can also apply to suspensions with species of different size, provided there is little variation in density (Lockett & Al-Habbooby, 1973). Richardson and Zaki (1954) proposed that the value of n was dependent only on the particle Reynolds number, Re_p , and under some conditions the wall effect, defined by the ratio of the particle diameter, d , and the diameter of the vessel, D . However, the influence of the wall effect has been shown to be less than originally predicted and is hence sometimes omitted from equations (Chong et al., 1979; Di

Felice, 1995). The relationship for the exponent n is thus broken into 4 sections, shown here including the wall effect term,

$$\begin{aligned}
 n &= 4.65 + 19.5 \frac{d}{D} & Re_p < 0.2 \\
 n &= \left(4.35 + 17.5 \frac{d}{D} \right) Re_p^{-0.03} & 0.2 < Re_p < 1 \\
 n &= \left(4.45 + 18 \frac{d}{D} \right) Re_p^{-0.1} & 1 < Re_p < 500 \\
 n &= 2.39 & 500 < Re_p
 \end{aligned} \tag{2.15}$$

Many researchers have since proposed their own relationships that cover the entire range of Reynolds numbers, including that of Garside and Al-Dibouni (1977),

$$\frac{5.1 - n}{n - 2.7} = 0.1 Re_p^{0.9} \tag{2.16}$$

and also that of Khan and Richardson (1989), which uses the Galileo number, Ga , rather than the particle Reynolds number,

$$\frac{4.8 - n}{n - 2.35} = 0.043 Ga^{0.57} \tag{2.17}$$

where the Galileo number is defined as,

$$Ga = \frac{d^3 (\rho_p - \rho) \rho g}{\mu^2} \tag{2.18}$$

Other researchers have since further generalised the Richardson and Zaki equation for use in multi-component suspensions, regardless of the variations in particle size or density. Galvin et al. (1999) utilised an approach first proposed by Asif (1997). They proposed that although the pressure gradient across a fluidised bed is formed by the sum of the drag forces of the different species, only the total

pressure gradient is necessary in determining the slip velocity of a single species in the suspension.

The slip velocity for a species i , $u_{\text{slip},i}$, can then be determined by,

$$u_{\text{slip},i} = u_{ti} \left(\frac{\rho_i - \rho_s}{\rho_i - \rho} \right)^{n_i-1} \quad (2.19)$$

where ρ_i and u_{ti} are the density and terminal settling velocity of the species i and ρ_s is the density of the suspension. Reasonable agreement between the results of Moritomi et al. (1986) and this model have been published (Galvin et al., 1999; Beetstra et al., 2007). Sarkar and Das (2010) compared experimental partition results from a Floatex Density Separator with simulations of four different slip velocity models (Masliyah, 1979; Patwardhan & Tien, 1985; Van Der Wielen et al., 1996; Galvin et al., 1999). The comparison found that the approach adopted by Galvin et al (Equation 2.19) offered the best predictions of the experimental data. The authors attributed this to the dissipative pressure gradient being the main basis of separation.

2.3 Slurry Rheology

A Newtonian fluid is defined by a linear relationship between the shear stress, τ , and the shear rate, $\dot{\gamma}$, given by the equation,

$$\tau = \mu \dot{\gamma} \quad (2.20)$$

The slope of the straight line when the shear stress is plotted against the shear rate is equal to the dynamic viscosity. For slurries, Newtonian behaviour can usually be seen at very low solids concentrations, however as the solids concentration increases, stronger non-Newtonian effects are seen. The majority of mineral slurries are shear thinning, meaning that the viscosity decreases with higher shear rates. Many slurries also exhibit a yield stress, τ_0 , which indicates the minimum force needed to initiate flow. To describe the shear stress – shear rate relationship for non-Newtonian, shear thinning suspensions, many empirical models have been proposed, with some common ones

being the power law, Herschel–Bulkley, and Sisko models (Herschel & Bulkley, 1926; Sisko, 1958; Barnes et al., 1989; Turian et al., 1997) given respectively by the equations,

$$\tau = K\dot{\gamma}^{n_p} \quad (2.21)$$

$$\tau = \tau_0 + K\dot{\gamma}^{n_p} \quad (2.22)$$

$$\tau = \mu_\infty \dot{\gamma} + K\dot{\gamma}^{n_p} \quad (2.23)$$

where K is the consistency constant, the units of which (Pa s^n), depend on the power law index, n_p , which describes the deviation from a Newtonian fluid, and μ_∞ is the viscosity at infinite shear rate. Which model is most applicable depends on many factors including particle type, shear rate range and the presence or absence of a yield stress. Both the power law, and the Herschel–Bulkley models are accurate across lower and intermediate shear rate ranges. Several authors have suggested the Sisko model is best when covering higher and larger ranges of shear rate (Barnes et al., 1989; Turian et al., 1997; Rhodes, 2008).

The viscosity of a suspension can depend on many factors including the fluid properties, particle size distribution and shape, pH, temperature, surface forces between particles and, most notably, the volume fraction of solids, ϕ . Early work in this area focussed on spherical particles in very low concentrations. Einstein (1906) proposed a linear relationship for infinitely dilute suspensions such that the presence of one particle has no effect on any other particle,

$$\mu_s = \mu(1 + 2.5\phi) \quad (2.24)$$

As more particles are introduced, their interactions become important. Batchelor (1977) extended the Einstein equation with a higher order term for the volume fraction of solids,

$$\mu_s = \mu(1 + 2.5\phi + 6.2\phi^2) \quad (2.25)$$

To account for particle interactions in slurries of much high concentrations, the maximum packing fraction, ϕ_{\max} , is introduced. This term represents the physical limit when so many particles are present in the suspension that flow becomes impossible and the viscosity tends to infinity. The term depends on particle shape, size distribution and other factors such as flocculation. A commonly used value throughout the literature is that for random close packing of rigid spheres, where $\phi_{\max} = 0.64$. To predict the suspension viscosity at these high concentrations semi-empirical models are used such as that of Krieger and Dougherty (1959),

$$\mu_s = \mu \left(1 - \frac{\phi}{\phi_{\max}} \right)^{-[\eta]\phi_{\max}} \quad (2.26)$$

where $[\eta]$ is the dimensionless intrinsic viscosity. For spherical particles the value of $[\eta]$ is 2.5, and $\phi_{\max} = 0.64$. For this case, a simpler version of equation 2.26 was presented by Quemada (1977),

$$\mu_s = \mu \left(1 - \frac{\phi}{\phi_{\max}} \right)^{-2} \quad (2.27)$$

At low solids concentrations, Equations 2.26 and 2.27 both reduce to the Einstein equation, and approach infinite viscosity as $\phi \rightarrow \phi_{\max}$. In real applications, the particles are rarely rigid spheres. Equation 2.26 accounts for this through the intrinsic viscosity and maximum packing fraction which both can vary considerably depending on particle shape, and are also shear dependant. Figure 2.3 demonstrates this with the viscosity – concentration curves, calculated using Equation 2.26, for spheres, rods, grains and plates. Non-spherical particles produce much higher slurry viscosities, with the rods and plates seeing the largest increase due to their much lower sphericity (Barnes et al., 1989). Particles with higher asymmetry and higher aspect ratios exhibit lower maximum packing fractions, hence the slurry viscosity tends toward infinity at lower solids volume fractions. The influence of shear adds an extra complexity as the particle geometry influences its rotation and alignment at different shear rates, resulting in more variation to the packing fraction and, hence, slurry viscosity.

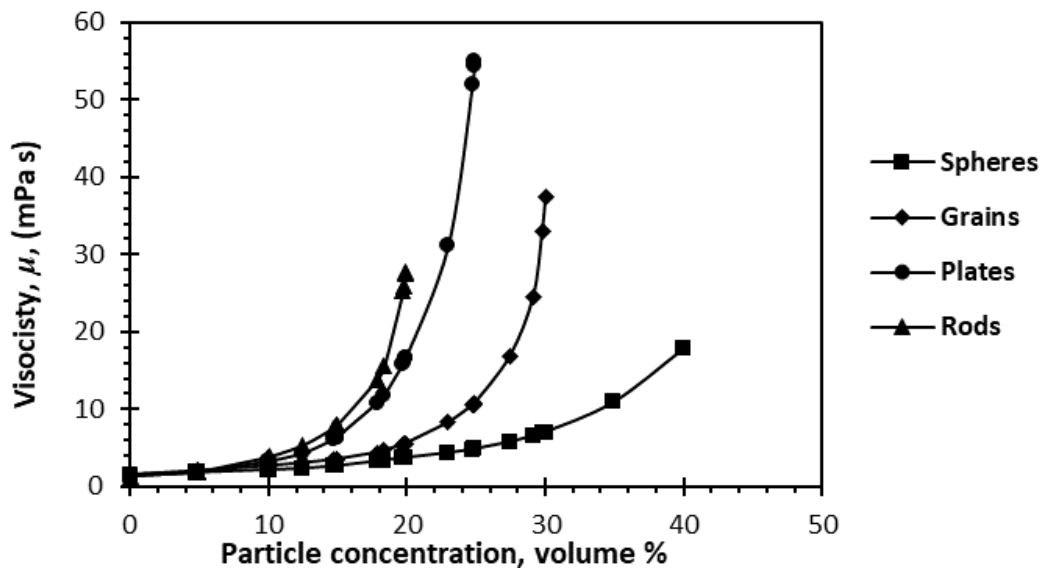


Figure 2.3: Viscosity, calculated from the Krieger-Dougherty model, versus particle concentration in water for different shaped particles at a shear rate of 300 s^{-1} . Adapted from Barnes et al. (1989).

The surface charge of particles also greatly influences the stability, and hence viscosity of suspensions. Colloidal forces cause repulsion, preventing aggregation, thus creating a zone of exclusion around each particle, increasing the effective particle radius and hence, volume fraction. The result is an increase in the zero-shear viscosity of the suspension. At higher shear rates however, the effects of colloidal forces become far less significant and the effective viscosity decreases back towards that predicted for non-interacting rigid spheres in the Krieger-Dougherty model (Barnes et al., 1989; Willenbacher & Georgieva, 2013).

2.4 Fluidised Beds

Fluidised beds are formed by an upward flow of fluid through a suspension of particles. When fluidised, the suspension has several advantageous properties including good solids mixing, uniform and enhanced mass and heat transfer rates and, under the right conditions, particle segregation. The fluidised bed system is very similar to that of a regular suspension. The upwards liquid velocity present in a suspension is a result of the liquid displaced by the settling particles, whereas in a fluidised system the upwards velocity is the superficial fluid velocity imposed on the system. Hence, the relationships between the slip velocity and solids volume fractions presented in Section 2.2 also apply to fluidised beds.

Before fluidisation occurs, the fluid flows through a fixed bed of particles. As the fluid velocity increases, so does the frictional resistance, which increases the pressure loss, Δp , across the particle bed. For laminar flow this is described by the Carman-Kozeny equation (Carman, 1937),

$$\frac{\Delta p}{H} = 180 \frac{\mu U}{d^2} \frac{(1-\varepsilon)^2}{\varepsilon^3} \quad (2.28)$$

where H is the height of the bed and ε is the voidage. Similarly, for turbulent flow the Burke-Plummer is used (Burke & Plummer, 1928),

$$\frac{\Delta p}{H} = 1.75 \frac{\rho U^2}{d} \frac{(1-\varepsilon)}{\varepsilon^3} \quad (2.29)$$

For intermediate flow the two terms are combined to take the form of the well-known Ergun equation (Ergun, 1952),

$$\frac{\Delta p}{H} = 150 \frac{\mu U}{d^2} \frac{(1-\varepsilon)^2}{\varepsilon^3} + 1.75 \frac{\rho U^2}{d} \frac{(1-\varepsilon)}{\varepsilon^3} \quad (2.30)$$

It is noted that a slight change to the constant in the laminar term comes from differences in the experiments used to develop these equations (Rhodes, 2008). Comparison with experimental data has revealed that although very good for compacted beds, the Ergun equation is not valid for high voidage systems or for very high Reynolds number flows (Gibilario et al., 1986; Di Felice, 1995; Niven, 2002). Several modifications have thus been made to the Ergun equation. One such modification by Gibilaro et al. (1986) allows for more accurate descriptions of the pressure drop across a wide range of flows and voidages,

$$\frac{\Delta p}{H} = \left[\left(\frac{17.3}{Re_p} \right)^\alpha + 0.336^\alpha \right]^{1/\alpha} \frac{\rho U^2}{d} (1-\varepsilon) \varepsilon^{-4.8} \quad (2.31)$$

This equation works equally well for fixed beds and also provided accurate descriptions of some fluidisation characteristics. An added advantage Equation 2.31 is the exponent factor α can be

obtained from Equation 2.32 below, or has the flexibility to be chosen to more closely match empirical data (Gibilaro et al., 1986),

$$\alpha = 2.55 - 2.1 \left[\tanh(20\varepsilon - 8)^{0.33} \right]^3 \quad (2.32)$$

The pressure drop through the bed goes through several phases as the fluid velocity increases to the point of fluidisation and beyond. A plot of this is shown in Figure 2.4. The first region, the line AB, describes the fixed bed condition. Here Equations 2.28 – 2.30 are used to describe the pressure drop versus fluid velocity relationship. The peak in the pressure drop at point B in Figure 2.4 is due to the extra forces required to overcome friction and adhesive forces within the packed bed and from the vessel walls. When the fluidised bed is formed, the pressure loss across the bed height equals the weight of the bed. This is shown by the horizontal line CD, expressed as,

$$\frac{\Delta p}{H} = (1 - \varepsilon)(\rho_p - \rho)g \quad (2.33)$$

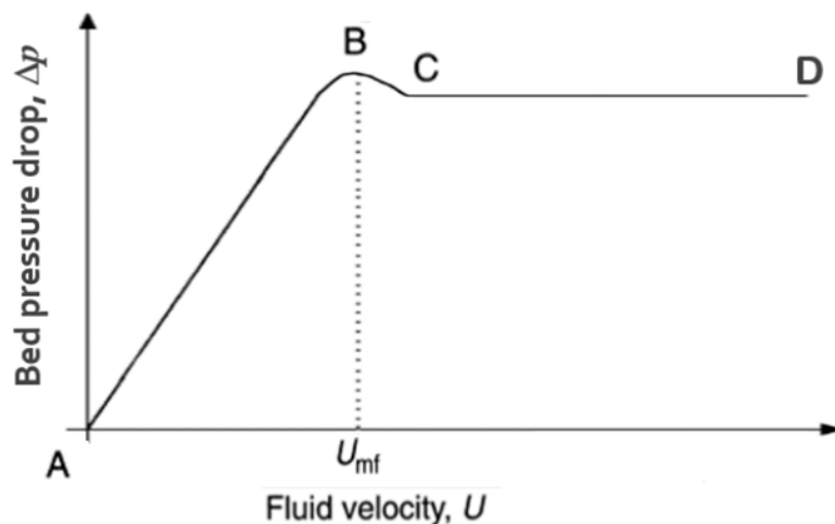


Figure 2.4: Diagram of the bed pressure drop versus fluid velocity for packed and fluidised beds. Adapted from Rhodes (2008).

The fluid velocity at which the bed becomes fluidised is known as the minimum fluidisation velocity, U_{mf} . This value is dependent on factors such as particle size, density, and properties of the fluid and the

bed, however a reasonable estimate can be made by equating the pressure loss equation for a fluidised bed (Equation 2.33) with that for a fixed bed (Equation 2.30),

$$(1-\varepsilon)(\rho_p - \rho)g = 150 \frac{\mu U_{mf}}{d^2} \frac{(1-\varepsilon)^2}{\varepsilon^3} + 1.75 \frac{\rho U_{mf}^2}{d} \frac{(1-\varepsilon)}{\varepsilon^3} \quad (2.34)$$

Rearranging, this expression is commonly put in a dimensionless form,

$$150 \frac{(1-\varepsilon)}{\varepsilon^3} Re_{mf} + 1.75 \frac{1}{\varepsilon^3} Re_{mf}^2 - Ar = 0 \quad (2.35)$$

where Ar is the dimensionless Archimedes number, and Re_{mf} is the Reynolds number at the minimum fluidisation value given by,

$$Ar = \frac{\rho(\rho_p - \rho)gd^3}{\mu^2} \quad (2.36)$$

$$Re_{mf} = \frac{\rho U_{mf} d}{\mu} \quad (2.37)$$

To determine U_{mf} , the bed voidage at fluidisation must be known. This is often estimated as the same voidage as the fixed bed, however in practice can be significantly greater. Hence, it is best to determine this value experimentally or use empirical correlations. The accuracy of these, however, varies greatly with particle, bed and fluid properties (Niven, 2002; Rhodes, 2008).

As with the particle terminal velocity relationships presented in Section 2.1, the relationships presented in this section have been for spherical particles. One can similarly alter the equations for non-spherical particles by substituting the particle diameter term for the particle diameter of a sphere that has the same surface to volume ratio as the particle (Rhodes, 2008).

Particle segregation in fluidised beds is a result of the different settling rates of the individual species. When the particles differ only in size or only in density, the separation behaviour is well understood and can be accurately predicted. Very sharp separations can occur. The denser or larger particles will

settle against the fluidising liquid and congregate in a layer at the base whilst the lower density or smaller particles are lifted upwards and form a layer on top. For a binary system, two mono-component layers will potentially form with a mixed interface between them (Di Felice, 1995).

When a fluidised bed contains particles differing in both size and density, where the larger particles have low densities and the smaller particles have high densities, a phenomenon known as phase inversion may occur (Moritomi et al., 1982). This is illustrated in Figure 2.5, which shows that at a low fluidisation rate, the bed density is high, and the small dense particles reside below the larger less dense particles. This is because the slip velocity of the finer particles is greater than the larger ones. As the fluidisation velocity increases the slip velocity of the two species become equal and complete mixing in the bed is seen. This is called the inversion point. As the fluidisation continues to increase and the bed density lowers further, the two species invert with the slip velocity of the coarser particles now higher than the fine particles. Predictive models of this behaviour have shown close agreement to experimental results (Gibilaro et al., 1986; Moritomi et al., 1986; Di Felice, 1995).

From the phase inversion phenomenon, it is clear density-based separations (where the denser species is removed in the underflow and the less dense species in the overflow) are favoured at lower fluidisation velocities, and hence a higher suspension density. Thus, it is important to understand the conditions that govern the minimum fluidisation velocity and operate close to that value. Conversely, separations driven by particle size are achieved at high fluidisation rates with lower suspension densities. Hence, both variables will always have some effect on the separation regardless of the fluidisation rate used.

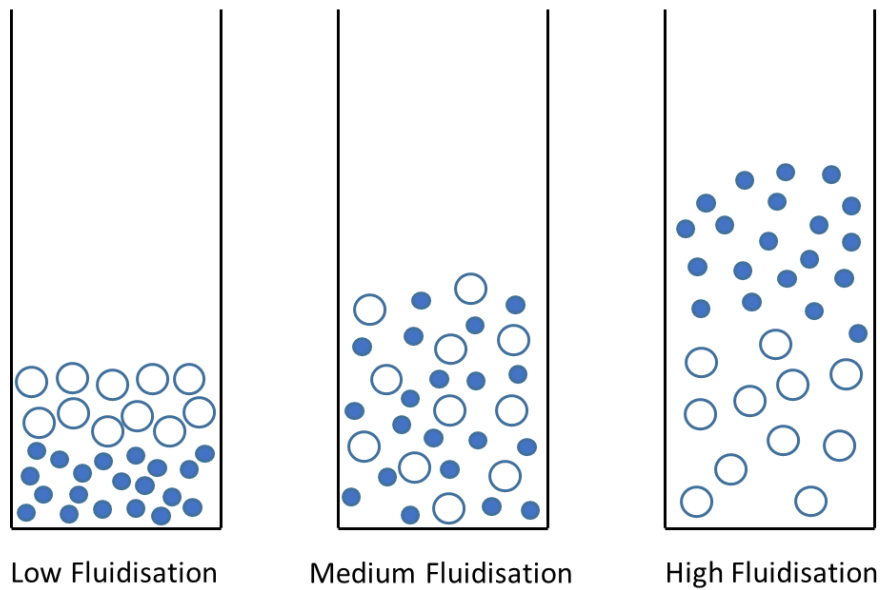


Figure 2.5: Phase inversion in a fluidised bed at increasing fluidisation rates using a binary system of large low-density particles (open circles) and small high-density particles (filled circles). Adapted from Galvin (2003).

2.5 Inclined Settling

Enhanced sedimentation rates in inclined channels is a phenomenon first described by Boycott (1920). In this work it was observed that blood corpuscles in a tube sediment far quicker if the tube is inclined rather than vertical. Enhanced sedimentation in inclined channels has since become known as the Boycott effect. As described by Davis and Acrivos (1985), there are three distinct regions in the sedimentation flow field present in both vertical and inclined channels. These are the clarified particle-free fluid, the suspension and the sediment layer. These regions are shown in Figure 2.6.

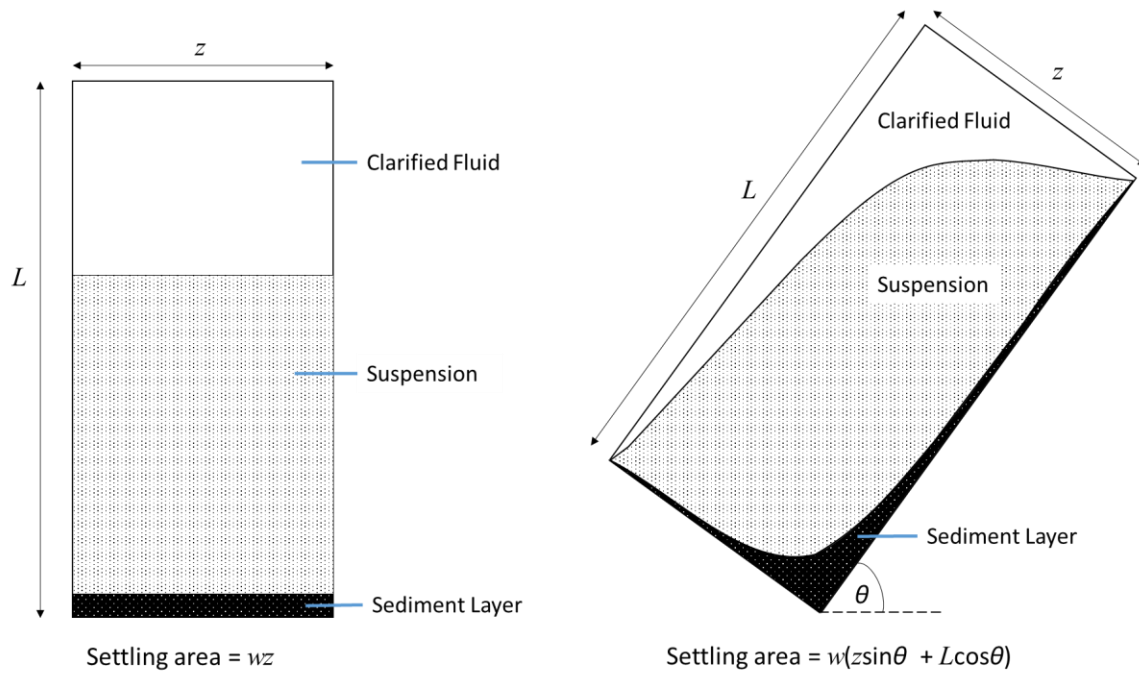


Figure 2.6: Settling area and sedimentation phases in vertical and inclined channels. Adapted from Davis and Acrivos (1985).

The greater sedimentation rate can be viewed as a direct result of the increased sedimentation area as seen in Figure 2.6. Experimental observations of inclined settling show that the particles deposit from the suspension to form a sediment layer that rapidly slides down the upward facing surface. This increased settling rate coincides with the production of the clarified particle-free layer at the top of the vessel and along the downward facing surface. As this clarified fluid layer is more buoyant than the suspension it flows to the top. As a result there is a bulk circulation pattern established which causes the horizontal interface between the particle-free layer and the suspension to fall at a velocity far greater than that of the interface in a vertical channel (Acrivos & Herbolzheimer, 1979; Davis & Acrivos, 1985).

A kinematic description of inclined settling was first developed by Ponder (1925) and Nakamura and Kuroda (1937), a model now termed the PNK theory. Developed in the context water clarification, the model assumes a laminar flow of liquid moving up the channel as well as the formation of a clarified fluid layer. Their theory predicts the enhanced sedimentation rate in terms of the volumetric rate at which the clarified fluid layer is formed, S , based on the assumption that all the particles have the

same settling velocity, u . The consequence of this assumption is that the higher volumetric rate equals u times the projected area of the vessel at the top of the suspension plus the horizontally projected area of the downward facing surface. This result is given by,

$$S = uw(L \sin \theta + z \cos \theta) \quad (2.38)$$

where θ is the angle of incline to the horizontal and w , L and z are respectively the depth (into the page), length and perpendicular width of the channel (Figure 2.6). Many attempts have been made testing the validity and bounds of the PNK theory which are summarised well by Davis and Acrivos (1985). The consensus of these investigations is that the PNK theory does accurately describe the inclined settling behaviour for stagnant and laminar conditions. However, the assumptions behind Equation 2.38 break down when waves form at the interface between the particle-free fluid and suspension layers, remixing the clarified fluid into the suspension and hence limiting the efficiency of the settling process.

2.6 Particle Motion down an Incline

The previous sections have detailed the settling behaviour of smooth spherical particles in suspensions. In practice, particles have asperities of varying sizes that can greatly affect their flow behaviour and solid-solid interactions. In the ideal case of a smooth sphere approaching another particle or surface, the fluid displaced as it approaches produces an increasingly strong lubrication force that resists contact and relative motion. On a smooth inclined surface a smooth particle will neither rotate nor slide down (Smart et al., 1993). A particle with a surface roughness can, however, make contact if the separation distance becomes small enough so that the asperities make contact. In this case, the particle can exhibit both translation and rotation down the inclined plane.

The hydrodynamic roughness is an important factor in the behaviour of a particle near a planar surface or another particle. It is a measure of the normal distance between the nominal surface of the sphere and the plane when in contact with a roughness element. Smart and Leighton (1989) presented a

technique for measuring the hydrodynamic surface roughness by inverting a horizontal surface onto which the sphere had settled and measuring the sphere's fall time. The method compared well to results obtained through scanning electron microscopy. Smart et al. (1993) later used this surface roughness measurement in their analysis of the motion of spheres down an inclined plane under stagnant bulk conditions. Their work described the motion of a sphere uniformly covered by asperities of the same small size. The sphere's motion was broken down into the translational and rotational velocities arising from force and torque balances on the sphere. Whilst this work provided a reasonable description of the sphere's motion, the model could not describe the motion at angles of inclination above 60° and does not account for the behaviour if a larger roughness element makes contact with the plane.

Galvin et al. (2001) continued this line of work using a sphere primarily covered by small roughness elements but with larger elements spaced periodically apart such that the smaller elements can still contact the surface. With such a sphere, the motion of the particle is largely governed by the position and frequency of the large asperities and the angle of incline. Three distinct forms of motion were considered: contact between small roughness elements and the plane, contact between a large roughness element and the plane, and the motion with no contact between the sphere and the plane. When a large roughness element contacts the plane, the sphere appears to stop, gradually lifting further from the surface as it slowly rotates over the peak and eventually loses contact. Slip is then evident in the period after contact as the normal component of gravity causes the sphere to settle towards the plane, with the lubrication force slowing this motion.

The angle of inclination will affect how long the particle takes to re-establish contact with the smaller roughness elements after being lifted by the rotation over a large element. However, on a steep incline the gravitational force normal to the plane is weaker and hence contact may be made with another large element before settling fully towards the smaller ones. The hydrodynamic roughness is hence governed by the height of the smallest roughness elements on a horizontal plane and the largest

elements when a steep incline is used. The experimental results of (Galvin et al., 2001) were consistent with this theoretical model.

2.7 Conclusion

The relationships and physical behaviours presented in this chapter are for the most part well established. Most of the equations and empirical correlations have been developed over many decades of research and verified or modified using many sets of data to cover a broad range of applications.

Through the knowledge of particle behaviour presented in this chapter, it has become easier to design and optimise devices used to separate particles according to their size and/or density. The application of this in beneficiation devices is explored in the following chapter.

Chapter 3

Literature Review- Gravity Separations and Desliming

3.1 Introduction to Beneficiation

The previous chapter outlined the fundamental laws and equations that describe particle behaviour under various conditions. This chapter reviews literature on the industrial practices and technologies relevant to this thesis. Here it is appropriate to present a general view of mineral beneficiation processes and the gaps and inefficiencies that are the targeted areas of this thesis. Beneficiation is the process of removing gangue particles from an ore in order to increase its economic value. To achieve this, a comminution step of crushing and grinding the run of mine ore is usually performed to liberate the mineral grains from the gangue material. A physical separation process is then performed to concentrate the valuable mineral, leaving behind a tailings or reject portion with higher levels of the gangue material. The size and density distribution of the feed material, along with other properties such as magnetism and wettability, are critical parameters for selecting a suitable separation device. Figure 3.1 shows a general guide to the particle size ranges suitable for the most common separation methods. Historically, the abundance of high grade deposits has meant that the separation processes do not need to be overly complex to produce a saleable product. Simple, low cost technologies such as screens, spirals and hydrocyclones have thus dominated the industry.

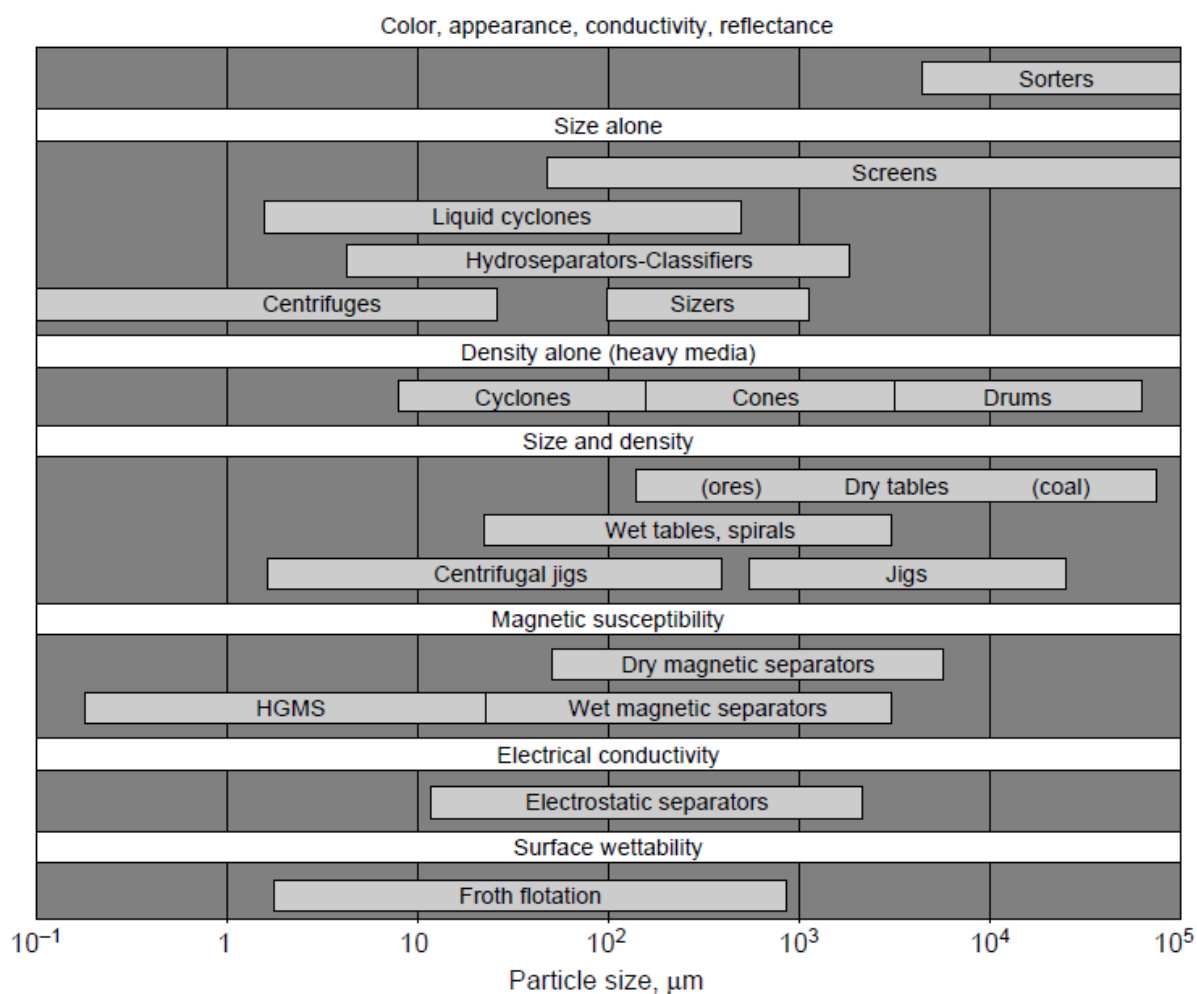


Figure 3.1: A general guide to the suitability of various particle separation devices as a function of particle size (Perry & Green, 1999).

Due to the difficulties in efficiently separating ultrafine particles, discussed in the following section, it has long been common practice to remove the ultrafines in a process called ‘desliming’. This process is usually carried out in hydrocyclones with, depending on requirements, a cut size usually somewhere in the range 10 to 50 μm . The removed ultrafines are then sent to tailings dams. Not only does this incur a significant loss of values, it is adding to the already complex and costly practice of tailings disposal (Wills & Finch, 2016). Additionally, due to the poor partitioning of cyclones at these sizes, large amounts of slimes still pass through the process, causing problems for downstream operations.

As factors such as consumer demands, operating costs and environmental concerns increase, it is becoming increasingly important to maximise use of the entire resource. Additionally, lower grade deposits are being mined that require higher degrees of comminution to liberate the minerals. This in

turn leads to an overall reduction in particle size and generation of larger portions of ultrafine particles. Ultimately, this means separation technologies must evolve to be able to efficiently separate particles at these finer sizes.

Currently, few industrial scale options exist for separating particles below 50 μm and those that potentially can have significant shortcomings. Flotation recoveries decline at both the ultrafine and coarse ends of the size distribution. Efficient flotation processes rely on collision and stable attachment between particles and bubbles (Wills & Finch, 2016). At the ultrafine end, particles lack sufficient inertia to cross water streamlines around the bubbles that would lead to a collision. Fines entrainment is also an issue with flotation. A solution to this is to wash the foam, but this results in a higher demand for fresh water (Trahar, 1981). Although there is some debate, the decline in flotation recovery at coarse sizes is usually attributed to the decrease in the stability of the bubble attachment (Jameson, 2012).

Cyclones operate in the ultrafine range for the purpose of desliming. As discussed above, this process suffers from a significant amount of bypass to the underflow. Data from literature and manufacturers often makes use of a 'corrected' partition curve, which takes into account the liquid fraction reporting to the underflow (Wills & Finch, 2016). Whilst useful for data analysis purposes, the correction doesn't change the fact that, in reality, the cyclones are allowing large volumes of ultrafine particles into the "de-slimes" product, producing what is ultimately a poor separation. As the desired cut point moves to finer sizes, the size of the hydrocyclone must also become smaller. To achieve reasonable separations at 10 μm or below, each unit must be as small as 10 mm in diameter with outlet diameters of only 1 mm diameter. In order to process large throughputs, banks of thousands of cyclone units must be used (Neesse et al., 2015; Wills & Finch, 2016; Vega et al., 2018). The operational complexities of such a large number of units can be substantial.

In the case of gravitational separators, the separation efficiency sharply decreases at the finest sizes due to the greater influence of Brownian motion, increased viscosity and much longer settling times.

Enhanced gravity separators attempt to overcome these effects by exposing the particles to forces many times greater than the acceleration due to gravity. These types of separators are discussed in detail in Section 3.3.2.

3.1.1 Ultrafines and Clays

At first glance, the difficulties in processing ultrafine particles are simply due to their low mass to surface area ratio. This results in the ultrafines having low inertia and settling velocities, a high degree of entrainment, low bubble collision probability, increased chemical adsorption per unit mass, higher slurry viscosity and increased coating of bubbles and minerals (Sivamohan, 1990). Whilst these are indeed all difficulties associated with ultrafine particles, the problem gets considerably more complex when considering the chemical makeup of the ultrafines, namely the frequent presence of clays. Clays are often designated as any particle below a certain size, but more correctly, in the context of mineral processing, this term refers to particles of the silica or phyllosilicate mineral groups. These clay groups contain many different particles types that vary in composition and structure; because of this they exhibit different properties and behaviours in mineral slurries (Arnold & Aplan, 1986; Ndlovu et al., 2013; Wang et al., 2014). Gräfe et al. (2017) outline some of the key areas of clay behaviour being their:

- water absorption/ desorption and capacity
- suspension rheology
- suspension settling
- species adsorption/desorption (including cation and anion exchange)
- dissolution/precipitation
- mineral adhesion (particle – particle interactions)
- polymer adhesion

These behaviours all vary depending on factors such as chemical composition, structure, morphology and surface charges. For example, in the case of a swelling clay type like smectite, the layer structure results in a permanent negative charge that attracts water molecules. The accumulation of water between the layers causes a swelling of the clay. This leads to rheological problems including higher

viscosity and a larger volumetric solids fraction. In contrast, this does not occur in other clay types, such as kaolinite, due to the different layer structure giving a neutral charge and, hence, no attraction of water molecules (Ndlovu et al., 2013; Gräfe et al., 2017). Different slurry behaviours such as this are what make separations and handling more difficult for feeds involving clay minerals.

It is because of these issues that the presence of clays can be detrimental across all processes including comminution, materials handling, flotation, physical separations and iron making (Arnold & Aplan, 1986; Kawatra et al., 1996; He et al., 2004; Ndlovu et al., 2013; Gräfe et al., 2017). The economic benefits of correctly characterising the clay types present in an ore body are becoming increasingly recognised. The differences in particle behaviour are key in selecting the appropriate beneficiation or treatment process. In addition to cyclones and enhanced gravity devices, discussed later, some researchers are developing techniques for selective flocculation, flotation and even leaching of slimes using microorganisms (Pradhan et al., 2006; Rocha et al., 2010; Wang et al., 2014; Gräfe et al., 2017; Panda et al., 2018). The success of these specialised techniques is, however, very dependent on the size and type of clay present.

It is, however, exceedingly difficult to accurately characterise clay types. In any sample, there is often a range of clay types with overlapping properties and compositions. The clays are also intimately mixed and dispersed within other mineral matter. Thus multiple test methods, some quite expensive, are required to accurately determine the relevant parameters such as composition, structure and size distribution (Srivastava et al., 2001; Ndlovu et al., 2013; Jena et al., 2015; Gräfe et al., 2017). Nevertheless, as the demand for beneficiation at finer sizes grows, clay characterisation will likely prove an important step in designing and selecting efficient ultrafine separation methods.

Whilst the combination of correct characterization and the use of suitable technologies can alleviate the issues of ultrafine separations, and the complications of clays, questions are often raised about what practical use ultrafine particles have. For example, it has been argued that ultrafine iron particles reduce the efficiency of blast furnaces due to the lower permeability of the sinter hindering gas and

liquid flow. The higher typical alumina content of iron ore fines also increases the volume and viscosity of the slag, requiring a higher coke rate, and reducing the sinter strength (Roy et al., 2007; Kim et al., 2016). These issues have largely been answered by many studies which show that, with proper beneficiation, the ultrafines can be used in the sinter or be blended into pellets, even with some high alumina fines (Roy et al., 2007; Dey et al., 2012; Jena et al., 2015; Kim et al., 2016). Additionally, researchers are finding value in the slimes with potential uses as raw building materials for bricks, cement, ceramics and even pigments (Zhao et al., 2014; Luo et al., 2016; Mandal & Sinha, 2016; Forbes et al., 2017).

3.1.2 The “Fish Hook” Effect

A common issue in the separation of ultrafine particles is the phenomenon known as the “fish hook” effect, which can be seen in size partition curves. Due to the widespread usage, most of the reporting and research into the fish-hook effect has been in cyclones, although it is an issue for many separation devices. Below a critical particle size, usually less than 10 μm , as the particle size decreases the recovery to underflow levels out and then starts to increase again, rather than continuing to decrease. This creates a large hook at the start of the curve, contrary to the “S” shape normally seen (Roldán-Villasana et al., 1993; Majumder et al., 2003; Zhu & Liow, 2014). An example of this phenomenon is shown in Figure 3.2. Having been reported for decades, opinions have varied greatly as to whether the fish-hook was a real physical phenomenon, and if so then what was causing it, or whether it was simply an artefact of measurement errors in the ultrafine size range. Majumder et al. (2007b) and Bourgeois and Majumder (2013) showed that the fish-hook was not random experimental error but a definite physical phenomenon that exists when processing fines in any kind of centrifugal separator. Variables affecting the size of the fish hook curve include inlet velocity, feed size distribution and particle sphericity, with the major cause of the effect believed to be fine particle entrainment to the underflow in the wakes of larger particles. Liquid bypass to the underflow and ultrafine particle agglomeration via van der Waals forces can also affect the curve, though are less significant (Kraipech et al., 2002; Kraipech et al., 2005; Zhu & Liow, 2014).

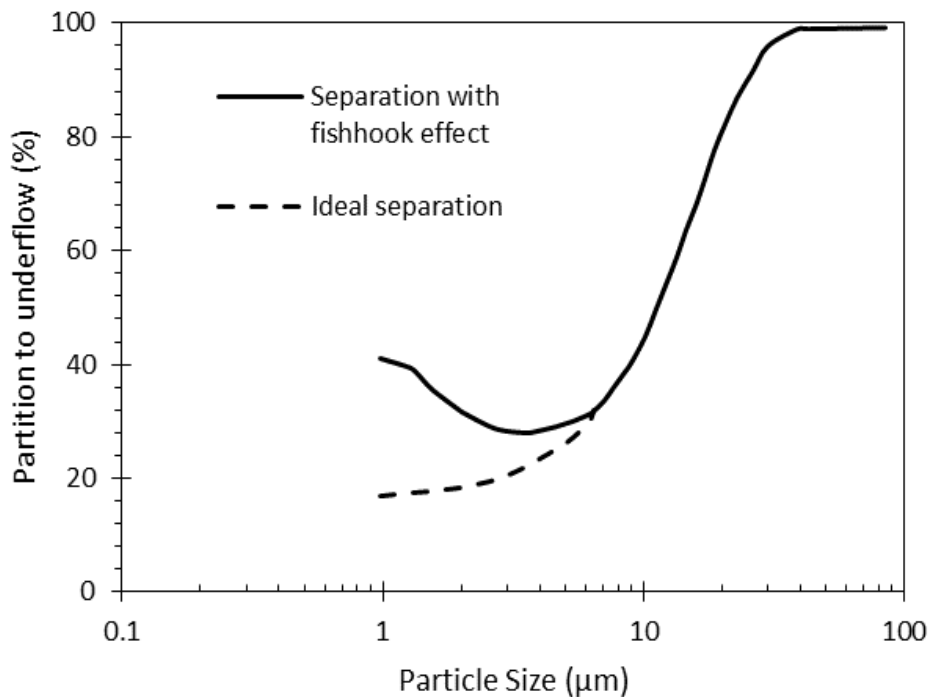


Figure 3.2: Illustration of the "fish-hook" effect. Adapted from Zhu and Liow (2014).

3.2 REFLUX Classifier

3.2.1 Design

The REFLUX™ Classifier is a novel invention consisting of a set of inclined parallel plates positioned above a fluidised bed. The system was developed to provide a higher throughput than conventional fluidised bed devices whilst producing an efficient particle separation on the basis of size or density (Nguyentranlam & Galvin, 2000). The motivation for introducing inclined plates to the system came from the observation by Boycott (1920), discussed in Section 2.5. An early application of this principle was in lamella settlers, devices used for thickening or clarifying. These settlers feature parallel inclined plates that form channels through which the feed can flow. The feed enters from below the channels and is designed such that all particles have time to settle onto the plates and slide down resulting in a clean overflow (Thompson & Galvin, 1997). A similar concept was used for particle classification in the inclined settler, a single plate lamella settler. Whilst this device was capable of achieving sharp classification in particle size (Davis et al., 1989) and density (Nelson et al., 1997) its single plate design is difficult to scale up to an industrial level (Nguyentranlam & Galvin, 2000).

The REFLUX™ Classifier utilises the multiple channel design of a lamella settler but positions the inclined plates above a fluidisation zone. This arrangement is shown in Figure 1.1. The fluidised bed section provides a uniform flow distribution into each of the inclined channels allowing for the same separation to occur in each channel, an important factor for a sharp partition curve (Nguyentranlam & Galvin, 2001). This fluidisation also provides the key difference between the REFLUX™ Classifier and a lamella settler. Lamella thickeners were designed to capture all particles, even the fine and lower density ones, to achieve a clean overflow. In the RC™ however, the upward current of fluidisation water through the channels prevents slower settling particles from settling on the inclined surface and are instead conveyed to the overflow (Galvin et al., 2002). Those particles that can settle against the upward flow slide down the plates and are re-mixed into the bulk of the suspension from where they may be re-fed by the fluidisation water back up into the channels. Thus, the combination of the inclined plates and a fluidised bed creates a ‘reflux’ action, hence the name. This internal recycling effect makes it harder for fast settling particles to be misplaced to the overflow whilst the higher fluidisation rates help prevent fines from being entrained to the underflow (Nguyentranlam & Galvin, 2000; Nguyentranlam & Galvin, 2001).

3.2.2 Throughput Advantage

The benefits of inclined channels in the REFLUX™ Classifier can be quantified by defining the “throughput advantage”, F , as the ratio of the superficial fluid velocity through the vertical section, U , to the terminal settling velocity, u_t , of the critical particle, defined as one with a 50 % probability of being elutriated into the overflow. This value indicates the degree to which the rate of segregation is increased as a result of the inclined surfaces. Based on the PNK theory, Laskovski et al. (2006) determined the theoretical value for this throughput advantage was,

$$F = \frac{U}{u_t} = 1 + \frac{L}{z} \sin \theta \cos \theta \quad (3.1)$$

where L is the channel length, z the perpendicular channel spacing and θ the angle of incline relative to the horizontal. It is noted that this throughput advantage refers to a single inclined section above a vertical section of the same size. In real applications with multiple inclined plates, space is occupied by the width of the plates, lowering the actual throughput. According to Equation 3.1 there is no limit to how much the throughput advantage can be increased by simply increasing the channel “aspect ratio”, defined as L/z . However, in reality, larger aspect ratios coincide with increased segregation areas and the re-suspension of particles due to the sediment layer sliding down the incline surfaces, adjacent to the rising flow. This gradually reduces the overall segregation efficiency in the channels. Laskovski et al. (2006) measured the actual throughput advantage and through dimensional analysis fitted their data to the following empirical equation,

$$F = \frac{U}{u_t} = \frac{1 + \sin\theta \cos\theta (L/z)}{1 + 0.133 \cos\theta Re_p^{1/3} (L/z)} \quad (3.2)$$

Zhou et al. (2006) used this equation to examine the optimum angle of incline on the throughput advantage. Their analysis used the density and size information of a mineral sands feed to obtain a general value for the particle Reynolds number, $Re_p = 0.75$. Applying this value to Equation 3.2, and assuming high aspect ratios of 100 and 200, the optimum angle was found to be between 68° and 72°, hence designs have since adopted an incline of 70°. The predicted throughput advantage using different particle Reynolds numbers, applicable to feeds of coal and mineral matter, showed good agreement with experimental data.

The actual throughput advantage determined by Equation 3.2 reaches an asymptotic level depending on the particle Reynolds number. Taking the limit as the aspect ratio (L/z) goes to infinity and replacing the fluid velocity in the vertical section, U , with the fluid velocity in the inclined section, U' , (i.e. $U' = U/\sin\theta$) gives,

$$\frac{U'}{u_t} = 7.5Re_p^{-1/3}$$

(3.3)

Equation 3.3 describes the superficial velocity required to transport a particle of any size as being independent of the system dimensions. This expression thus provides an upper bound to the throughput achieved in the system.

3.2.3 Application of Closely Spaced Channels

The correlations developed by Laskovski et al. (2006) provided an accurate model of the throughput advantage over a broad range of feed flowrates, densities and size distributions. However, that study used relatively wide channel spacings, with the smallest being 5 mm. These correlations failed to describe results when closely spaced channels were used. To address this Galvin et al. (2009) developed a new model to describe the separation mechanism observed in their work using the relatively narrow channel spacing of $z = 1.77$ mm. A conventional force balance in the direction of the inclined surface was used to describe the transport mechanism of particles of different sizes. A schematic representation of this balance and the parabolic velocity profile that forms in the channel under laminar flow is shown in Figure 3.3. In this balance the friction force and particle rotation are neglected due to the steep angle of incline. When narrow channels are used, higher local velocities are achieved near the surface due to the higher shear rate. With a high enough shear rate there is a near linear relationship between distance from the surface and the local fluid velocity. At the same time, for particle Reynolds numbers in the intermediate range ($2 < Re_p < 500$) a near linear relationship also exists between particle diameter and the terminal settling velocity (Equation 2.8). Hence, at a critical fluid velocity through the inclined channels, U' , the local fluid velocity is equal in magnitude to the opposing component of the particle settling velocity simultaneously for particles across a wide range of sizes (Galvin et al., 2009; Galvin et al., 2010a). This is the condition seen in Figure 3.3. Hence, under these conditions the effect of particle size on the elutriation is suppressed, which promotes separation on the basis of density.

For the more formal development of this model, the local fluid velocity, U_L , experienced by a particle lying on the inclined surface is governed by the velocity at one particle radius from the surface. Taking a linear approximation of the parabolic velocity profile of the laminar flow in the channel (Bird et al., 1960), the local fluid velocity is,

$$U_L = \frac{3}{2} U' \frac{d}{z} \left(2 - \frac{d}{z} \right) \quad (3.4)$$

So, for relatively small particles such that $d \ll z$, the local fluid velocity becomes approximately,

$$U_L = \frac{3U'd}{z} \quad (3.5)$$

The critical elutriation condition occurs when the critical particle terminal settling velocity in the tangent direction to the surface, u'_t , is equal to the local fluid velocity,

$$u'_t = U_L = \frac{3U'd}{z} \quad (3.6)$$

Thus, a simple theoretical relationship for the throughput advantage using only the channel spacing and critical particle diameter is found for inclined channels (i.e. $U = U' \sin \theta$ and $u_t = u'_t \sin \theta$) with a large aspect ratio under laminar conditions,

$$F = \frac{U}{u_t} = \frac{U'}{u'_t} = \frac{z}{3d} \quad (3.7)$$

Again, it must be noted that the throughput advantage determined by Equation 3.7 represents an upper limit. The space occupied by the channel wall directly reduces the total flow. Hence, with a greater number of channels or with thicker channel walls the throughput advantage is reduced.

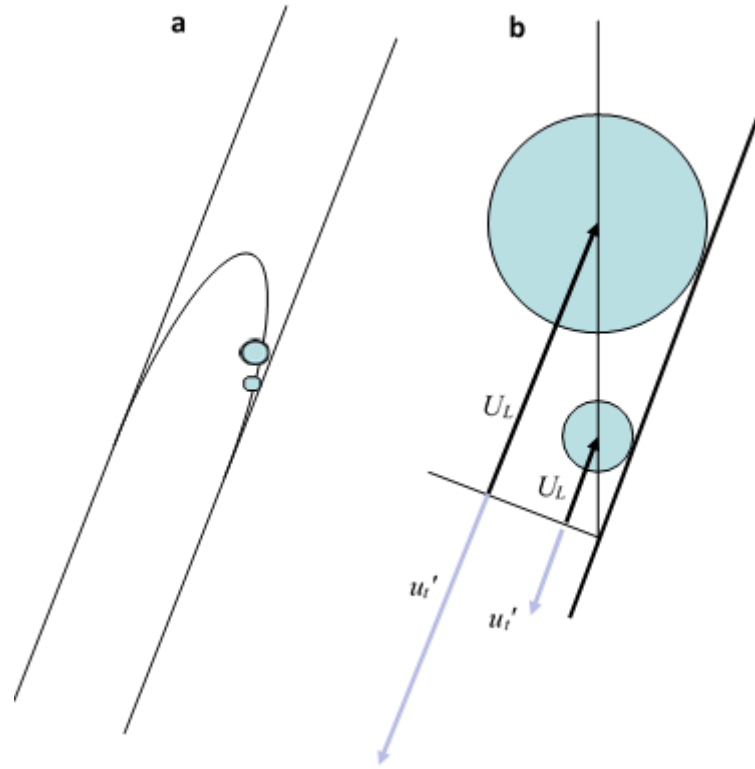


Figure 3.3:(a) Parabolic velocity profile for laminar flow in a closely spaced channel with (b) a detailed view of different sized particles at the inclined surface. The critical elutriation condition is seen when the local fluid velocity is equal and opposite to the particle terminal settling velocity in the tangential direction to the inclined surface (Galvin et al., 2009).

The application of closely spaced channels was further analysed by Galvin and Liu (2011), where the role of the inertial lift force was included. As seen in Figure 3.4, the analysis was performed on a particle located at a perpendicular distance, x , above the inclined surface. At this position the expression for the local fluid velocity is,

$$U_L = \frac{6U'x}{z} \left(1 - \frac{x}{z}\right) \quad (3.8)$$

This expression can then be differentiated with respect to x to give the shear rate, γ ,

$$\gamma = \frac{6U'}{z} \left(1 - \frac{2x}{z}\right) \quad (3.9)$$

Acting in the normal direction to the inclined surface is the net weight force of the particle in the fluid,

F_n , given by,

$$F_n = (\rho_p - \rho)g\cos(\theta)\left(\frac{\pi}{6}\right)d^3 \quad (3.10)$$

Acting in the opposite direction, away from the surface, is the inertial lift force, L_f . Whether or not the particle will indeed lift away from the surface depends on the ratio of the particle Reynolds number, Re_p , and the shear Reynolds number, Re_s , which is given by,

$$Re_s = \frac{\rho\gamma d^2}{\mu} \quad (3.11)$$

Based on the model by King and Leighton (1997), the equilibrium position of the particle illustrated in Figure 3.4 is found when $Re_s^2 = 32Re_p$. By equating the weight force of the particle at the equilibrium position, this model provides an explicit expression for the lift force,

$$L_f = 0.0567 \frac{\rho^{1.8} \gamma^{2.8} d^{5.6}}{\mu^{0.8}} = 0.0567 Re_s^{0.8} \rho \gamma^2 d^4 \quad (3.12)$$

It is noted that Equation 3.12 is valid for particle Reynolds numbers in the intermediate regime.

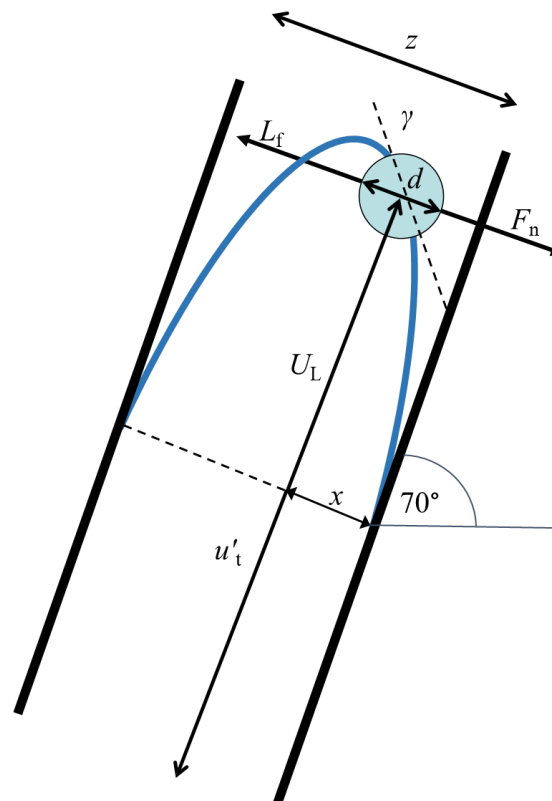


Figure 3.4: Equilibrium position of a particle subjected to laminar flow and a high shear rate. Equilibrium occurs when the lift force, L_f , is equal and opposite to the net weight force of the particle, F_n (Galvin & Liu, 2011).

This analysis provided a very accurate description of the experimental data from Galvin et al. (2009) and further validation of a similar lift force model by King and Leighton (1997). Equation 3.12 also provides a useful tool in discrete element modelling when an expression for the lift force is needed.

Figure 3.5 and 3.6 compare the predicted dependence of elutriation velocity on the separation size from the models of Galvin et al. (2009) and Galvin and Liu (2011) with the same set of experimental data. The predictions in Figure 3.5 show good agreement with the experimental data, however they fail to describe the 'nose' shape seen predominately in the densest particles and somewhat in the mid-range set. This 'nose' in the data indicates the point at which the lift force matches the normal weight force of the particle. As the lift force exceeds the weight force, the particle migrates away from the surface and in doing so experiences a large fluid velocity. The curve turns back in for larger sizes due to the lower superficial velocity needed to achieve the required balance between the local and terminal velocities in the critical elutriation condition. By incorporating the lift force, the model of Galvin and Liu (2011) provides excellent prediction of this trend as shown in Figure 3.6. Overall, the vertical trend of the models and data for each density set indicate the indifference of elutriation velocity to particle size.

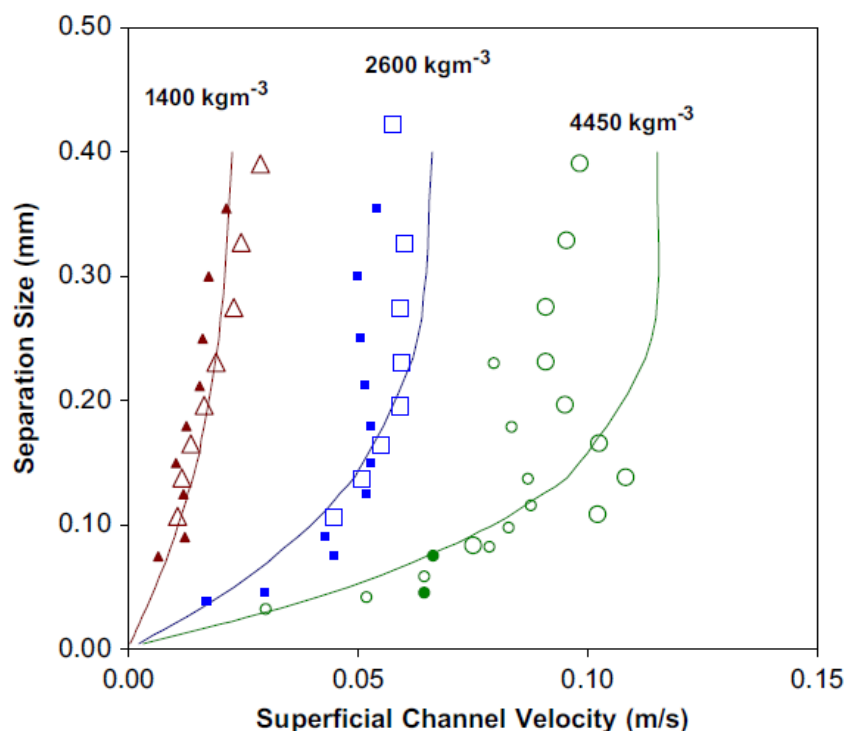


Figure 3.5: Comparison of the experimental data and theoretical model of Galvin et al. (2009). Open symbols are for experiments conducted using one species at a time and the closed symbols applicable to the mixed suspension. The triangles denote particles of density 1400 kg/m^3 , the squares denote particles of density 2600 kg/m^3 , the small circles denote particles of density 4300 kg/m^3 and the large circles denote particles of density 4600 kg/m^3 . The model curve for the densest particles was based on the average density of 4450 kg/m^3 .

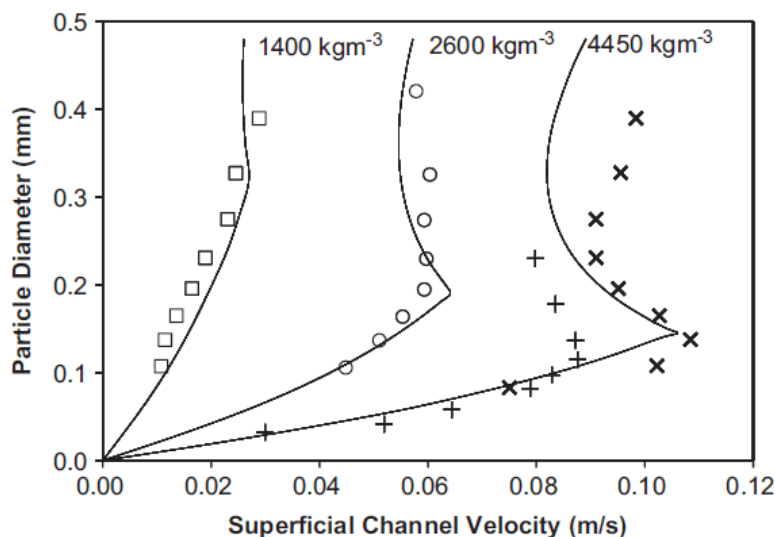


Figure 3.6: Comparison of the experimental data of Galvin et al. (2009) with the theoretical model of Galvin & Liu (2011). The squares denote particles of density 1400 kg/m^3 , the circles denote particles of density 2600 kg/m^3 , the plus symbols denote particles of density 4300 kg/m^3 and the cross symbols denote particles of density 4600 kg/m^3 . The model curve for the densest particles was based on the average density of 4450 kg/m^3 .

3.2.4 Modelling

An important tool in understanding any system is the use of a model. This can, however, present difficulties when dealing with suspensions containing particles of varying size and density as well as the unique combination of fluidised bed and inclined channel systems used in the REFLUX™ Classifier. Initial segregation and dispersion models ignored the complexity of the inclined channels, focusing only on the fluidised bed (Ramirez & Galvin, 2005; Galvin et al., 2006). Although these models provided useful analytical descriptions of the particle dispersion, they were limited in actual use for several reasons. Firstly, the two models describe only binary systems with narrow size distributions and assume that the fluidised bed was at steady state with constant fluidisation velocities. Both are unrealistic in real applications where feeds and fluidisation velocities can vary greatly and dynamically. Finally, both models were sensitive to the boundary conditions at the top of the bed and hence failed to accurately describe the concentration gradient at the top of the bed. This poses a problem if extending the model to describe a REFLUX™ Classifier system where the conditions at the top of the bed become the boundary condition controlling the behaviour in the inclined channels directly above. Patel et al. (2008) therefore later improved on the model, accounting for a multi-component system and successfully describing the dispersion at the top of the bed. For the binary component case, the steady state model also showed excellent agreement with experimental data and could describe the phase inversion phenomena outlined in Section 2.5.

Following this work, a simple 2-D segregation and dispersion model that incorporated both the fluidised bed system and inclined channels was developed, first for a binary system with 0.3 mm particles having densities of 1400 kg/m³ and 2400 kg/m³ (Syed et al., 2015). The model was then further developed for a multiple component system in order to better explain particle segregation on the basis of density difference (Syed et al., 2016). The model considers a distribution of particles with a size range of 1.70 mm to 0.35 mm and densities from 2000 kg/m³ to 1400 kg/m³. This was the first form of a continuous model of the REFLUX™ Classifier system and as such ignored the added complexities of shear-induced lift that occur within narrow spaced channels (Galvin et al., 2009). The

model therefore was validated against experimental data from earlier work featuring wider channels (Galvin et al., 2005).

The REFLUX™ Classifier covers a wide range of feed densities, size distributions, and is adaptable to the type of separation required. As such, the segregation and dispersion models were improved to reflect this. Syed et al. (2018) altered the model to include the shear induced lift force and covered a larger range of particle sizes (1.7 mm – 0.19 mm) and densities (2500 kg/m³ – 1275 kg/m³). The model demonstrated good agreement with the experimental data from the strong density-based separations of coal and mineral matter of (Galvin et al., 2010b). The model did, however, show discrepancies in the finest size fraction studied. By changing the internal state of the REFLUX™ Classifier, sharp size classification can also be achieved. To model this, Syed et al. (2019) input binary and multicomponent mixtures of a single density, 2490 kg/m³, into the system with much wider channel spacings and lower volumetric flowrates, achieving very good agreement with the experimental data from Doroodchi et al. (2006). Additionally, this work also covered the much finer particle sizes (49 - 421 µm) that were problematic for the previous models. For a more fundamental understanding of particle behaviour in the REFLUX™ Classifier, Syed and Khan (2019) ran simulations using mono-sized particles of a single density. This work demonstrated the influence of the fluidisation velocity, underflow rate and water flux in the feed stream on the transport of the particles throughout the fluidised bed and the inclines.

3.3 Enhanced Gravity Separation

3.3.1 The effect of Centrifugal Force

As discussed in Section 3.1.1, the relatively low settling velocities of ultrafine particles presents a major limitation to separation processes. Enhanced gravity devices, or centrifugal separators, are devices that subject the particles to a higher G-force. In doing this, the inertial forces on the particles increase, resulting in higher terminal settling velocities and reducing the effects of Brownian motion. Section 2.1 discussed the terminal settling velocities relationships for single particles across different ranges

of particle Reynolds numbers. The difference in these relationships becomes especially relevant under enhanced gravity conditions. Most ultrafine particles will settle under normal gravity in the Stokes regime ($Re_p < 2$) according to the equation,

$$u_t = \frac{d^2(\rho_p - \rho)g}{18\mu} \quad (2.5)$$

In this regime, the dependence on particle diameter is d^2 . However, under a high enough centrifugal force, the extra particle inertia can shift the Reynolds number into the intermediate regime ($2 < Re_p < 500$) where the settling velocity is given by,

$$u_t = \frac{0.153g^{0.71}d^{1.14}(\rho_p - \rho)^{0.71}}{\rho^{0.29}\mu^{0.43}} \quad (2.8)$$

The significance of this shift is that the dependence on particle diameter is now only $d^{1.14}$. Hence, the ultrafine particles can settle faster, but more importantly, settle at velocities which are much less sensitive to particle size. This allows a separation on the basis of density to be far more efficient. This benefit of enhanced gravity is depicted in Figure 3.7. The plot shows the calculated settling velocities under normal gravity and under 200 G for three particle species of specific gravities of 1.3, 2.5 and 4.8. For the case of normal gravity (dashed lines), the settling velocities of the three species at 0.1 mm are practically indistinguishable. However, at 200 G (solid lines), the settling velocities of the three species vary greatly. This demonstrates how under centrifugal force, differences in particle densities can be used as a basis for separation, even at very fine sizes (Luttrell et al., 1995; Majumder & Barnwal, 2006).

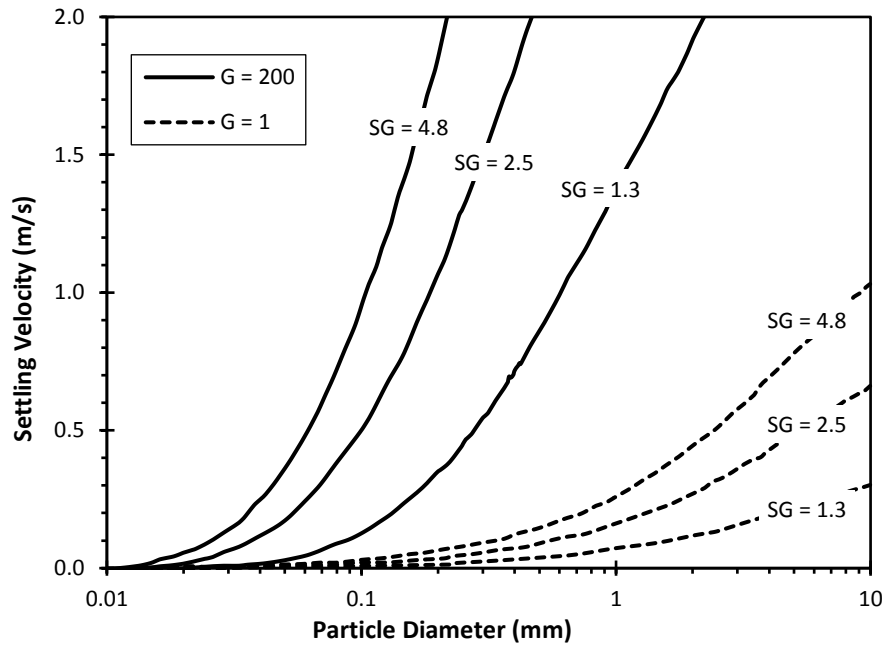


Figure 3.7: Theoretical settling velocities versus the particle diameter for three particle species of specific gravities 1.3, 2.5, and 4.8. The dashed lines show the settling velocities under normal gravity (1 G) and the solid lines show the settling velocities under a centrifugal force of 200 G. Adapted from Luttrell et al. (1995).

To relate the settling velocity under normal gravity with that under enhanced gravity, u_{tG} , Hsu and Perry (1981) proposed a simple correlation for the different ranges of particle Reynolds numbers,

$$u_{tG} = Gu_t \quad 10^{-4} < Re_p < 0.4 \text{ (Stokes)} \quad (3.13)$$

$$u_{tG} = G^{1/2}u_t \quad 0.4 < Re_p < 500 \text{ (Intermediate)} \quad (3.14)$$

$$u_{tG} = G^{1/3}u_t \quad 500 < Re_p < 2 \times 10^5 \text{ (Newtons)} \quad (3.15)$$

where G is the centrifugal G – force exerted on the system.

Majumder et al. (2003) used the above relationships to demonstrate and attempt to explain the fish-hook phenomena in hydrocyclones, suggesting that the turning points on the fish hook occur at the particle sizes where the Reynolds number shifts into the next regime.

Of course, the equations discussed above refer to the settling of single particles. The sedimentation of suspensions under enhanced gravity can be considerably more complex than under normal gravity.

The settling rates and profiles can be affected by the angular momentum, geometry of the vessel and the Coriolis force (Greenspan & Ungarish, 1985a; Greenspan & Ungarish, 1985b; Ungarish, 1995). For the case of inclined settling, the flow patterns describing the enhanced sedimentation rates courtesy of the Boycott effect, outlined in Section 2.5, change when the Coriolis force dominates. Firstly, the pure fluid layer on the outer wall does not remain thin, and secondly, the interface between the pure fluid and the mixture does not move perpendicular to the centrifugal force as it would under normal gravity. The result of this is a partial or even complete negation of the enhanced settling rates obtained from the inclined surfaces (Greenspan & Ungarish, 1985a).

Changes to the vessel geometry can, however, suppress the Coriolis force in order to maintain the benefits of enhanced settling rates. This is achieved through using vessels with close walls or narrow channels such that shear rates are high enough to make the Coriolis force insignificant. Further to this, breaking the rotating vessel up into several sectorial compartments such that the walls restrict the circumferential movement of the suspension and the clear fluid around the centre, will further suppress Coriolis effects (Schaflinger, 1987; Schaflinger, 1990).

3.3.2 Existing Technologies

Enhanced gravity devices are widely used for many types of separations across different industries. The extra force on the particles has proven extremely useful for decreasing sedimentation times for solid – liquid and liquid-liquid separations in the dairy, pharmaceutical, oil and water treatment industries to name a few (Haeberle et al., 2006; Colic et al., 2007; Alpha Laval, 2019). The design of these separators varies depending on the application, with many even utilising inclined plates to also gain the benefit of the Boycott effect (Batalović, 2011).

In the mining industry, centrifugal forces play an important role in spirals and cyclone devices. Here, an important distinction must be made. In spirals and cyclones, the tangential velocity of the feed, and in the case of cyclones the developed air core, generates the centrifugal force. In contrast, in an enhanced gravity device, the centrifugal force is generated through the rotation of the device itself.

In these devices much higher G-forces are generated and the differences between the settling velocities of different particles under that force are what drive the separation. Several technologies utilising this mechanism have been developed for use in mineral separation. Whilst they have been implemented for separations involving low concentration, high-value commodities such as gold and platinum, in general, shortcomings such as throughput, process water requirements and upgrading ratios have limited their use for other minerals on an industrial scale. A brief description of some of the better known of these devices is outlined below.

The Knelson concentrator, illustrated in Figure 3.8, is a bowl shaped unit that applies a centrifugal force to a fluidised bed of particles, capable of separating particles as small as 20 μm in diameter. The rotating bowl can generate centrifugal forces of up to 180 G (Koppalkar, 2009) although most processes operate at 60 G (Majumder & Barnwal, 2006). A series of partitions line the wall of the rotating bowl, trapping particles as feed flows upwards over each partition. Perforations within each partition allow wash water to create a fluidised bed. The fluidisation washes out the lower density particles to continue moving up the walls of the bowl whilst the centrifugal force allows denser particles to concentrate in the partition. The low-density particles eventually exit the top of the bowl whilst higher density particles fill each partition in the walls. Batch units then require several minutes to flush out the concentrate whilst continuous units extract the dense particles periodically through pinch valves (Knelson, 1992; Fullam et al., 2001).

Knelson concentrators work best for feeds where the dense particles make up only a small percentage of the total material. They are now widely implemented for recovering free gold within grinding circuits. Although the Knelson concentrator has had some success in the treatment of fine coal (Honaker et al., 2005; Uslu et al., 2012), limitations in capacity and the large requirement of fluidising water have limited its use in other ultrafine beneficiation processes (Majumder & Barnwal, 2006).

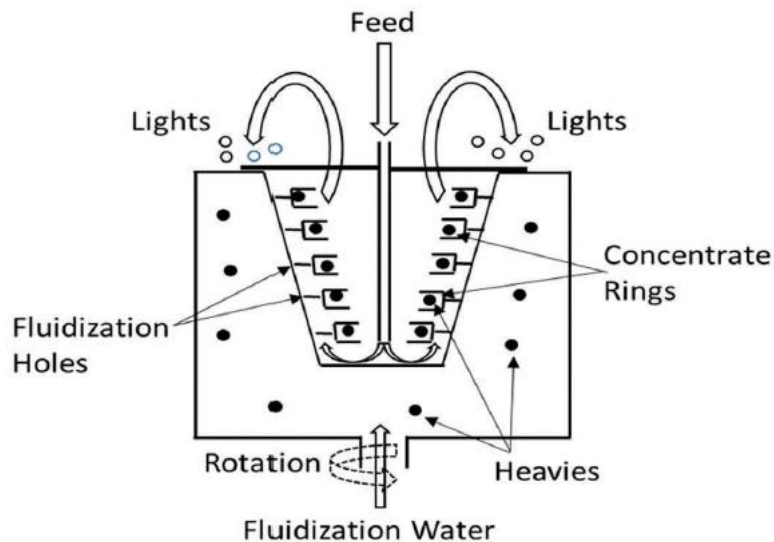


Figure 3.8: Diagram of the Knelson concentrator (Das & Sarkar, 2018).

The Falcon concentrator, shown in Figure 3.9, operates as a kind of centrifugal sluice. Feed enters continuously at the base and is distributed around the smooth angled walls of the bowl. The bowl is divided into two sections: migration/stratification and retention. The migration or stratification zone is where the stratification of particles occurs along the angled walls. The strong centrifugal force, up to 300 G, acting normal to the bowl wall, enhances the difference in the particle densities. Denser and coarser particles are driven towards the surface whilst the less dense and finer particles form a layer resting above. Aided by the angle of the wall, the parallel component of the force pushes the stratified particles up the bowl toward the retention zone at the top. Here, the bowl angles parallel to the axis of rotation, slowing the upward movement of the particles. The dense portion, residing at the surface is withdrawn from a series of ports around the circumference. The lower density portion is then carried over the lip of the bowl (Honaker et al., 1996; Das & Sarkar, 2018).

Most applications and research on the Falcon concentrator have been for coal cleaning (Honaker et al., 1996; Honaker, 1998; Oruç et al., 2010; Zhu et al., 2017) and gold recovery (Alp et al., 2008; Wills & Finch, 2016), although its use for some other minerals has also been explored (Marion et al., 2017; Das & Sarkar, 2018). Compared to the Knelson concentrator, the Falcon concentrator does not separate efficiently at the finest sizes, especially below 45 μm (Honaker et al., 1996; Kroll-Rabotin et

al., 2013). Capacity issues for the industrial scale and low upgrading ratio have also prevented it from becoming widely used across the minerals industry (Falconer, 2003).

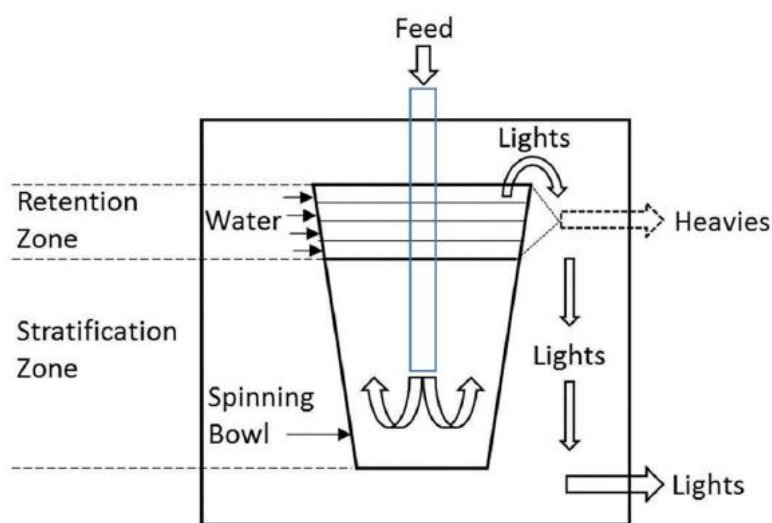


Figure 3.9: Diagram of the Falcon concentrator (Das & Sarkar, 2018).

The Multi-gravity separator (MGS) combines the mechanisms of centrifugal force and a shaking table. Shown in Figure 3.10, the device consists of an angled, rotating drum that is slightly tapered toward the open end. Feed is introduced at the centre of the drum length where a flowing film of the slurry develops. The centrifugal force from the rotation drives higher density particles to settle onto the surface of the drum whilst lower density particles sit at the top of the film layer. The back and forth shaking of the drum adds an extra shearing force to the slurry, improving the particle segregation. Internal scrapers, rotating in the same direction, but at a higher speed reduce entrainment of gangue and move the settled layer of high density particles up the inclined drum, toward the open exit. Flowing in the opposite direction is a stream of wash water to not only wash the exiting concentrate, reducing entrainment, but also to carry the reject towards the opposite end (Chan et al., 1991; Roy, 2009; Das & Sarkar, 2018).

The biggest drawback from the MGS is its lower capacity per unit footprint area compared to other centrifugal devices, largely stemming from the limited rotational speed, capable of achieving only ~ 25 G (Chan et al., 1991; Falconer, 2003; Majumder & Barnwal, 2006). The complexity of the device,

namely the large number of operating variables, also makes optimisation studies more difficult. The MGS does, however, show good upgrading ratios and recoveries for a range of minerals and applications, performing well down to sizes of 5 μm . It has been applied, with varying success, for the cleaning of coal (Majumder et al., 2007a; Özgen et al., 2011), and the recovery of many minerals including tin, chromite, tungsten, lead and iron (Singh et al., 1997; Bhaskar et al., 1999; Özbayoğlu & Atalay, 2000; Cicek & Cöcen, 2002; Göktepe, 2005; Aslan, 2008; Chaurasia & Nikkam, 2017).

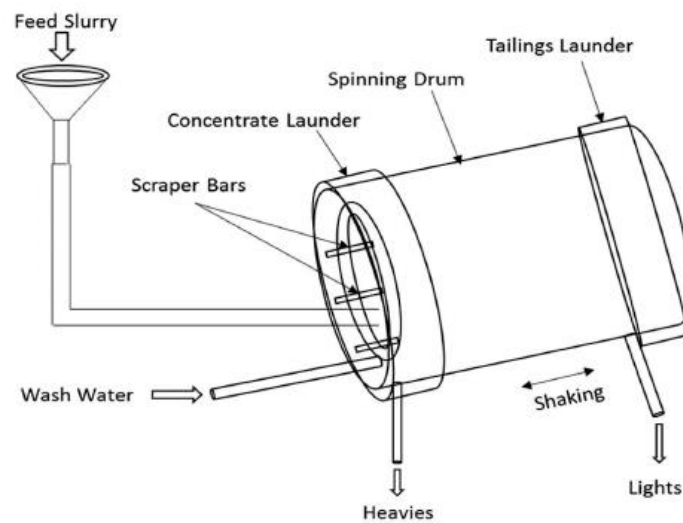


Figure 3.10: Diagram of the Multi - Gravity Separator (MGS) (Das & Sarkar, 2018).

A conventional jig separates particles of different densities by pulsating a bed of coarse particles of intermediate density, known as ragging, over a screen. During the pulsation, denser particles make their way through the ragging and screen to concentrate below while tailings remain above the ragging and are conveyed to the overflow. The Kelsey centrifugal jig, shown in Figure 3.11, takes the same pulsating operation but rotates it in a centrifuge, achieving up to 100 G acceleration. (Luttrell et al., 1995; Richards & Jones, 2004; Nayak & Pal, 2013). Like a conventional jig, the Kelsey jig requires ragging material and is fluidised by additional water. By combining the jigging action with a centrifugal force, the more powerful separation enables processing of much finer particles, down to a few microns (Tucker, 1995; Nayak & Pal, 2013), and for particles of a much narrower density difference.

The Kelsey jig shows excellent results across multiple mineral ultrafines including gold, tin, nickel, coal, mineral sands and iron (Yerriswamy et al., 2003; Richards & Jones, 2004; Majumder & Barnwal, 2006;

Nayak & Pal, 2013; Singh & Das, 2013). It also has the highest capacity of the above described enhanced gravity devices, around 100 t/h (Richards & Jones, 2004; Singh & Das, 2013; Wills & Finch, 2016). There are, however, several major drawbacks for the Kelsey jig. Like the MGS, the Kelsey jig is mechanically complex with many variables. There is also a constant need to monitor and replenish the ragging as it is lost to breakage or conveyed to the overflow. The amount of screening involved is also a drawback. Feed must be screened prior to entering to avoid blinding the internal screen, which itself requires constant cleaning. The tailings must also be screened to recover the ragging particles. The maintenance of these screens and replenishment of ragging drives up the operating costs (Luttrell et al., 1995; Falconer, 2003; Majumder & Barnwal, 2006).

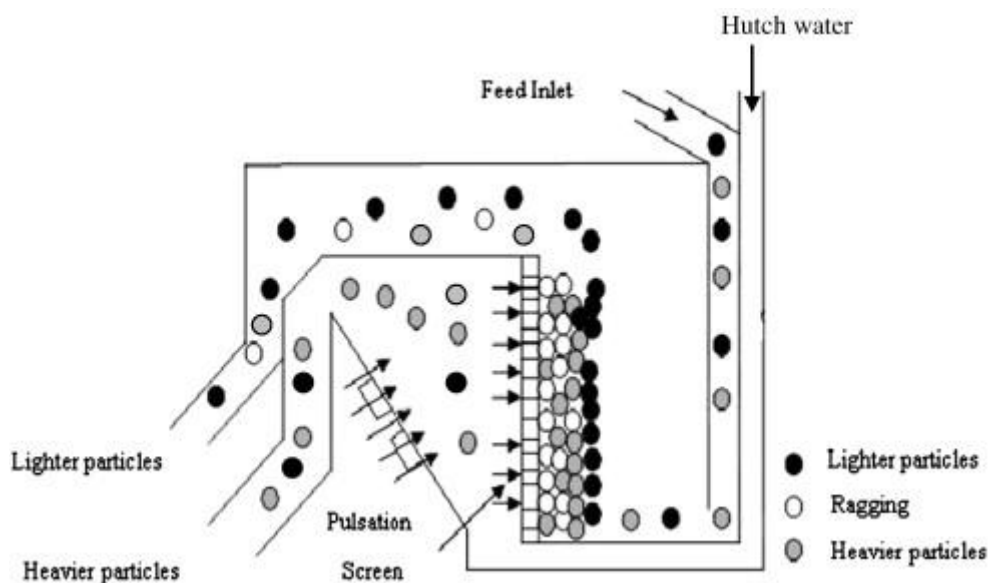


Figure 3.11: Diagram of the Kelsey centrifugal jig (Singh & Das, 2013).

3.4 REFLUX™ Graviton

3.4.1 Design

In addressing the challenge of ultrafine particle separation and the shortcomings of existing technologies, a novel device known as the REFLUX™ Graviton was designed. Like the Kelsey centrifugal jig and MGS, the REFLUX™ Graviton combines a proven separation method, in this case the REFLUX™ Classifier, with centrifugal force. So, this device combines the effects of enhanced gravity separation

with the benefits of the inclined channel system of the REFLUX™ Classifier. With this design the major shortcoming of similar technologies that rely on flowing films, namely their low throughput, is eliminated. The Graviton is also capable of achieving 73 G acceleration, much more than the MGS's 25 G. In fact, minor adjustments to the system speed will yield even higher G values.

The REFLUX™ Graviton consists of multiple REFLUX™ Classifier modules located within a high-speed centrifuge. In the present work, two units were incorporated to simplify operation, while ensuring mechanical stability. Each REFLUX™ Classifier unit consists of a fluidisation and feed entry chamber aligned horizontally, attached to a section of closely-spaced inclined channels aligned at 70° to the vertical, maintaining the optimal angle of inclination found by Zhou et al. (2006). The channels are both closely spaced and compartmentalised, reducing the effects of the Coriolis force. The underflow exits via the outer radius of the units with flush water added to assist the flow and prevent blockage due to material being compacted in the line by the high G forces. Figure 1.2 shows a schematic of the Graviton.

The REFLUX™ Graviton was previously studied at laboratory scale by Galvin and Dickinson (2013) under semi batch conditions. The primary objective of that study was to answer the question: if the system of inclined channels is subjected to a centrifugal force, what happens to the overall throughput advantage? Supplementary to this, the study investigated particle behaviour in the closely spaced channels and evaluated the results with respect to the models developed for the REFLUX™ Classifier (Galvin et al., 2009; Galvin & Liu, 2011) and for sedimentation under centrifugal force.

3.4.2 Throughput Advantage under Centrifugal Force

The primary result of the study by Galvin and Dickinson (2013) was that the hydrodynamic benefits of the centrifugal force and the inclined channels multiply together. This result was found using a single-density suspension of silica, with particle sizes from 0 – 0.060 mm. For the standard REFLUX™ Classifier the throughput advantage was given by,

$$F = \frac{U'}{u'_t} = \frac{z}{3d} \quad (3.7)$$

For the REFLUX™ Graviton system, the centrifugal force increases the gravitational acceleration by a factor of G , which equates to the centrifugal G-force exerted on the system. The throughput advantage is thus modified to give,

$$F = \frac{U'}{u'_t} = \frac{Gz}{3d} \quad (3.16)$$

The accuracy of this model and the scale of its significance are seen in Figure 3.12. Firstly, it is noted that the data follows the line of parity very closely for the lower values of G with a slight divergence at the higher end. Galvin and Dickinson (2013) theorised this divergence to be caused by the laminar flow profile not fully developing at the higher values of flow Reynolds numbers present when operating under higher G-force. It was also possible that the Coriolis force was playing a role here, however the high shear rates through the channels should work to suppress the effect of the Coriolis force as shown by Schaflinger (1987). The significance of the results shown in Figure 3.12 is that with $G = 73$ a throughput advantage of well over 1000 can be achieved.

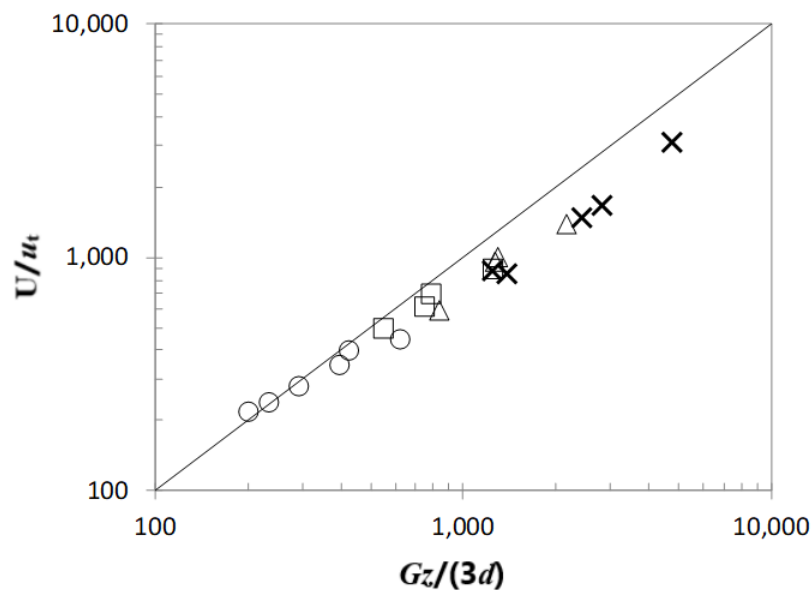


Figure 3.12: Throughput advantage given by ratio of superficial fluid velocity to particle terminal velocity, U/u_t , versus $Gz/(3d)$. This result shows that the benefits of the G force and the inclined channels multiply, Key: \circ $G = 14$, \square $G = 28$, \triangle $G = 55$, \times $G = 73$ (Galvin & Dickinson, 2013).

3.4.3 Fine Coal Work

Galvin and Dickinson (2013) also performed separations on fine coal in the Graviton with excellent consistency. Experiments were conducted using a coal feed with particle sizes in the range 0.038 – 0.260 μm and densities of 1250 – 1600 kg/m^3 . The relationship between the superficial fluid velocity through the channels and the separation diameter d_{50} was examined and compared to that of the single density silica feed. A similar linear relationship was seen in both the silica and coal work, however at higher fluid velocities the separation diameter of coal rapidly increased as the channel velocity increased. This was reminiscent of the similar result reported by Galvin et al. (2009), which was attributed to the inertial lift force (Galvin & Liu, 2011). At this higher end, the velocity scaled with $\sim d^{0.3}$. Hence, the enhanced gravity and channel hydrodynamics had significantly reduced the dependence on the particle diameter compared within the Stokes settling regime.

A series of experiments was then performed, each using a feed with a narrow density range, in order to produce size partition curves based on the particle density and to obtain a relationship between the separation density and the particle size. The density based partitions proved remarkably sharp and consistent given the low solids concentration, low residence time and the fact that they are produced from a series of experiments rather than a single run. The separation density versus the particle size with $G = 73$ is shown in Figure 3.13. The curve shows that there was only a slight increase in the separation density with decreasing particle size down to ~ 0.03 mm, below which there was a sharp increase in separation density. Comparing this result to the theoretical curves for a conventional fluidised bed and inclined channels, both at $G = 1$, it is evident there is more dependence on the separation density than on the particle size.

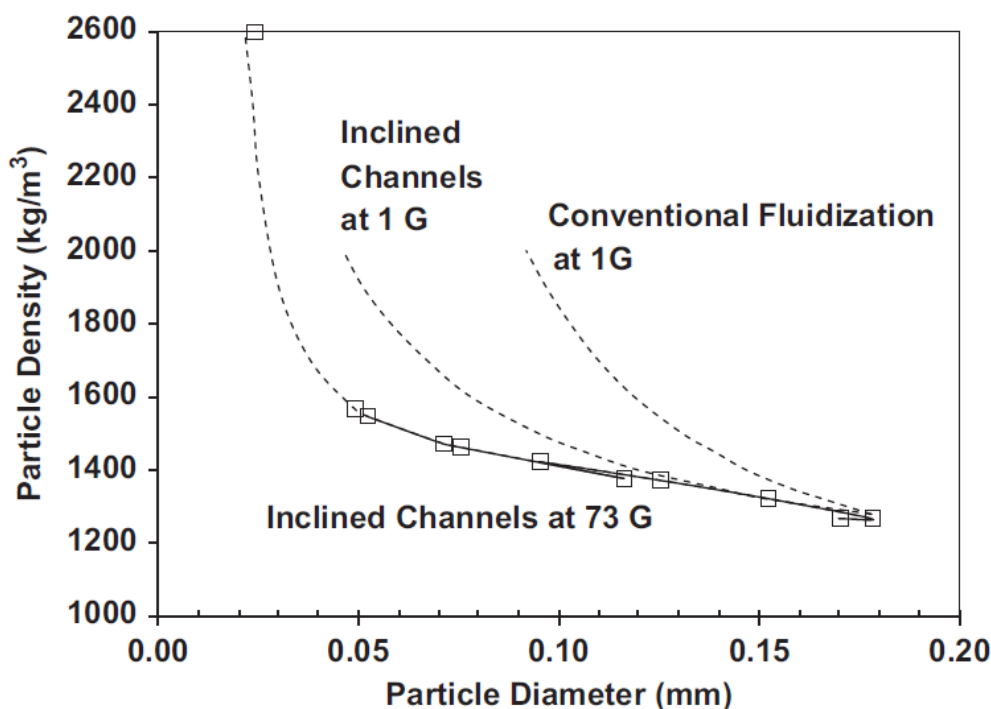


Figure 3.13: Variation in the particle separation density with the particle diameter. Experimental results with $G = 73$ are shown together with the theoretical results for inclined channels with $G = 1$ and a conventional fluidised bed at $G = 1$ (Galvin & Dickinson, 2013)

It was concluded from the relationship seen between separation density and particle size, along with the extremely high throughputs achieved, that a powerful synergy is created by combining the centrifugal forces and inclined channels. The prediction of Galvin and Dickinson (2013) was that with a continuous system a powerful gravity separation should be achievable, with the fully developed Graviton offering an alternative to flotation.

3.5 Conclusion

This chapter has presented a summary of the current state of mineral beneficiation with a particular focus on ultrafine particles. In this, two key points are raised as to what gaps in knowledge and technology exist in the minerals industry. Firstly, there is a unique challenge faced when dealing with ultrafine feeds containing high portions of clay minerals. For the industry to improve recovery at the finest sizes this challenge must be addressed through both better understanding of the issues, and development of new techniques to overcome them. Therein lies the second point identified through this literature review; current technologies developed with ultrafines in mind suffer major drawbacks.

Desliming cyclones result in losses of valuables to tailings whilst also failing to remove large portions of the slimes. Reducing the cut size requires an enormous scale up in the number of units required. Enhanced gravity devices have a range of shortcomings, most importantly, lower capacities and high wash water requirements.

This chapter also presented an in-depth review of two technologies, the REFLUX™ Classifier and REFLUX™ Graviton, the focus of this thesis. The following chapters report on this work which aims to fill the knowledge and technology gaps highlighted above. The experimental apparatus and methods used for these devices are outlined in the following chapter.

Chapter 4

Experimental Methods

4.1 REFLUX™ Graviton

4.1.1 Equipment

The REFLUX™ Graviton consists of a 2.0 m diameter centrifuge that is controlled by a variable speed drive. The swinging arms of the centrifuge, seen in Figure 4.1, are capable of mounting eight REFLUX™ Classifier modules although in the current study only two are used. Each of the modules are mounted via a flange and are opposite to each other to provide mechanical stability. For safety reasons, during operation of the centrifuge the hatch through which the photo in Figure 4.1 was taken was locked closed and the entire area was caged off (see Figure 4.11a).

It is noted that this centrifuge was adapted from a commercial system, stripped back, and modified for use in this study. There are several design elements of this commercial system that compromised the performance of the Graviton system. The impact of this compromise was minimised where possible. However, it should be recognised that ultimately, if the work is taken forward, a new system will be purpose built to further minimise or eliminate these issues. The feed arrangement will ultimately be improved, and the removal and hence sampling of the overflow and underflow will eventually be improved. Issues with the system form part of the discussion in this Chapter.



Figure 4.1: Swinging arms of the Graviton centrifuge with an open mount (top) and with the inclined channel module in place (bottom). The centrifuge is contained within a stainless steel housing.

The modules, shown mounted in Figure 4.1 and close up in Figure 4.2, were 3-D printed from Accura Extreme plastic. Each module contained 9 elements on a 3x3 grid. Each element contained 22 parallel channels inclined at 70° to the vertical, with a channel spacing of 1 mm and separated by a 1 mm wall

thickness. Each channel was nominally 46 mm across, and 227 mm long. The channels were later reinforced with 2 mm wide supports every 14 mm apart. To prevent water absorption the modules were also treated with an acrylic/thinner solution.

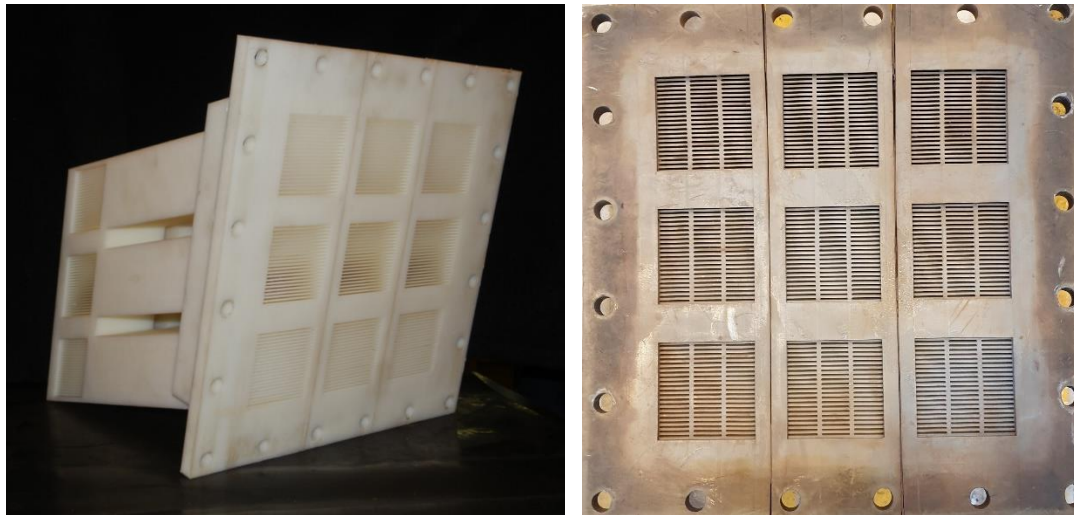


Figure 4.2: Picture of the original 3-D printed inclined channel module (left) and the face of the module showing the reinforced channels (right).

Mounted against the inclined channel modules is the fluidisation chamber. In this chamber the feed and fluidisation water enter the system and the underflow is allowed to exit. The chamber itself, shown from the inside in Figure 4.3, has a cross section of 171 mm × 178 mm that tapers inwards to a cylindrical section with a diameter of 75 mm. Four tangential feed entry points are positioned around the sloping chamber, each with an internal diameter of 12 mm. At the base of the cylindrical chamber are $100 \times \varnothing 0.5$ mm holes through which fluidisation water enters. As discussed in Section 4.1.2 this section was modified part way through the experimental work. Figure 4.4 shows the chamber from the outside as well the chamber mounted to the centrifuge arm with the different inputs labelled. Figures 4.5 - 4.7 show diagrams of the inclined channels and the fluidisation chambers showing all dimensions in detail.

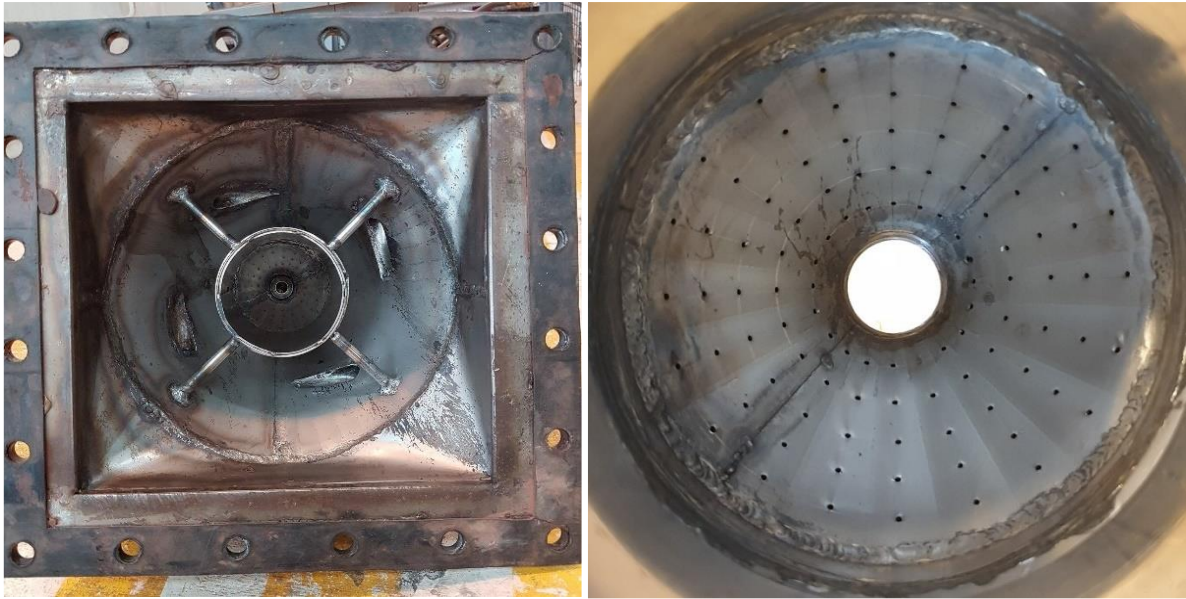


Figure 4.3: Picture of the fluidisation chamber from the inside (left) and a close up of the fluidisation arrangement (right). Fluidisation enters via 100 holes spaced around the centre of the chamber. Underflow exits through an opening at the very centre of the chamber. Feed enters via one or more of the four tangential entry points around the chamber.

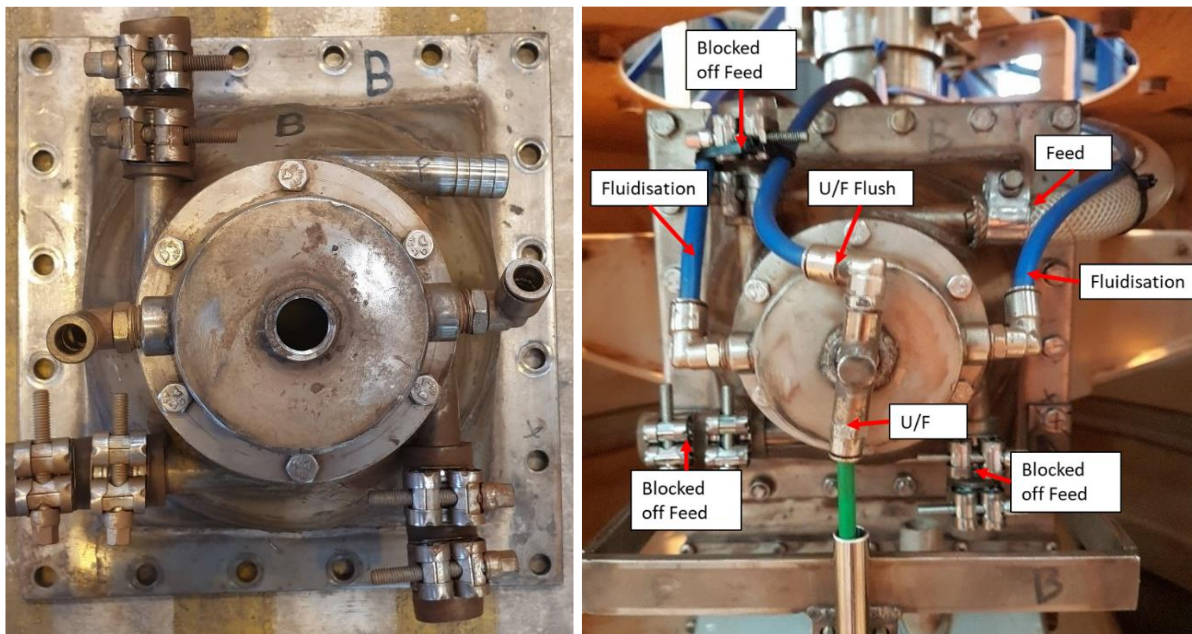


Figure 4.4: Picture of the fluidisation chamber from the outside (left) and the chamber mounted to the centrifuge arm with all lines attached (right).

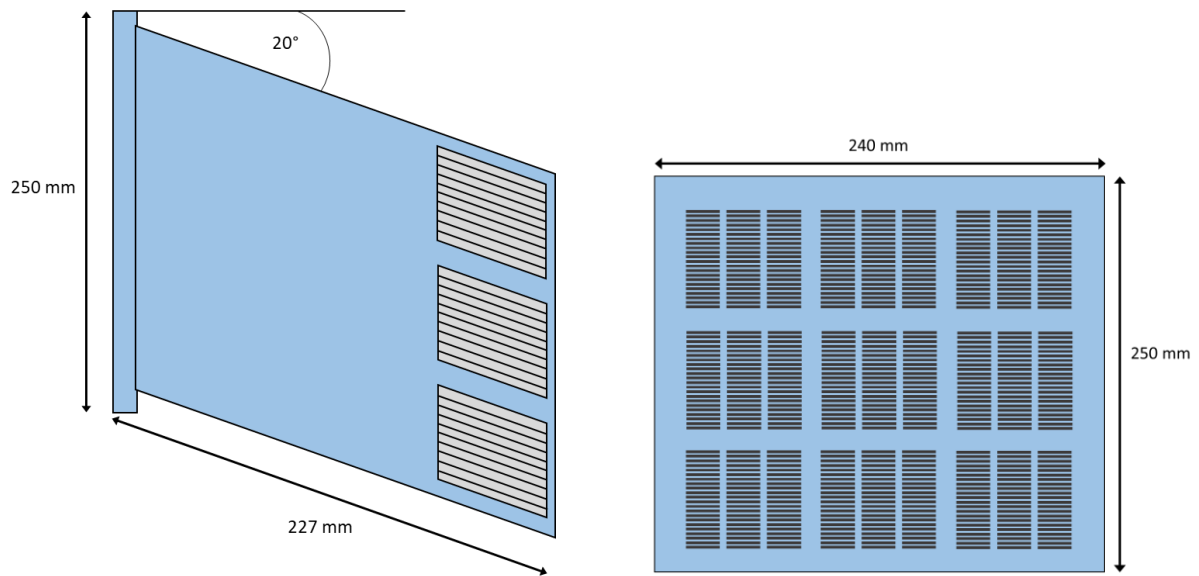


Figure 4.5: Diagram of the 3-D printed REFLUX™ Classifier module from the side (left) and from the front (right). The side view shows the angle of incline, channel length and the overflow exit for the channels on the side shown. The front view shows the 9 elements in the 3 × 3 grid each with 22 channels broken into 3 smaller sections by the supports.

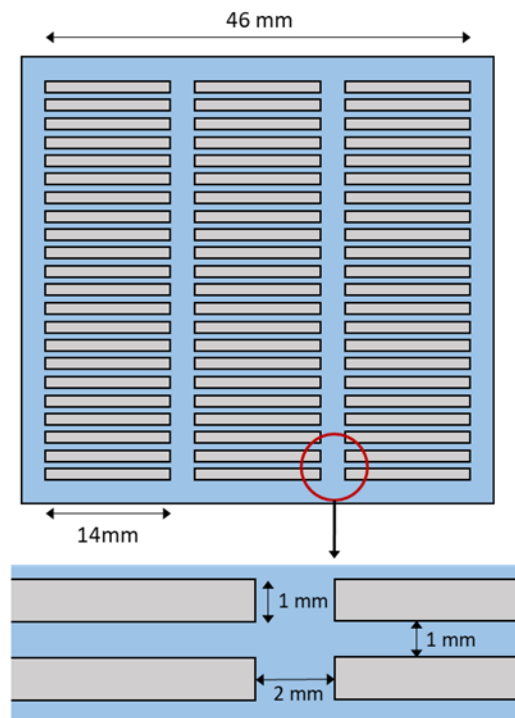


Figure 4.6: Diagram showing close up details of one of the nine channel elements of the 3-D printed module. Twenty-two channels are shown, each divided into three smaller channels by the supports. The dimensions of each channel and the spacing between them are shown.

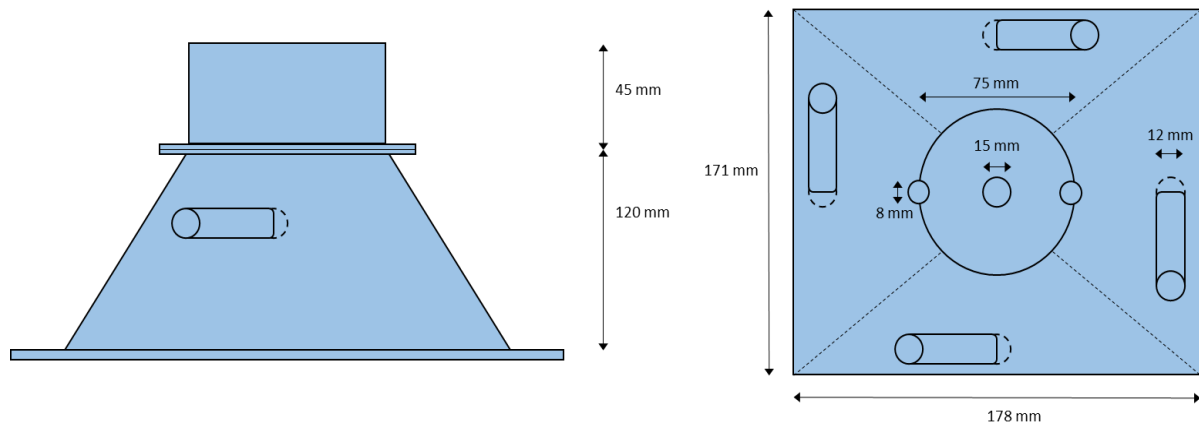


Figure 4.7: Diagrams of the fluidisation chamber that is mounted to the face of each REFLUX™ Classifier module. On the left is a side view of the chamber with one of the four feed entry points, showing the length of the pyramidal and conical sections connected by the flange. On the right is a top view showing the dimensions of the feed entries, conical section, two fluidisation line inlets and the underflow outlet.

At the centre of the fluidisation chamber is the underflow outlet opening with a diameter of 15 mm. The rate of the underflow was limited by the diameter of this outlet. Seen in Figure 4.8, four attachments were made to fit into the opening with internal diameters of 4 mm, 6 mm, 8 mm and 10 mm. Additional sizes of 3 mm and 2 mm were made to be screwed directly onto the 4 mm attachment. To assist in the flow of the solids flush water was added to the underflow via these attachments. This additional flow prevents solids from packing out against the back of the attachment under the high G forces. Feed, fluidisation water and underflow flush water was supplied to the rotating system, along with a defunct air supply line, through a mechanical seal pictured in Figure 4.9.



Figure 4.8: The different underflow attachment sizes. From top to bottom: 2 mm, 3 mm, 4 mm, 6 mm, 8 mm, 10 mm internal diameter. The 3 and 2 mm parts screw onto the body of the 4 mm piece.

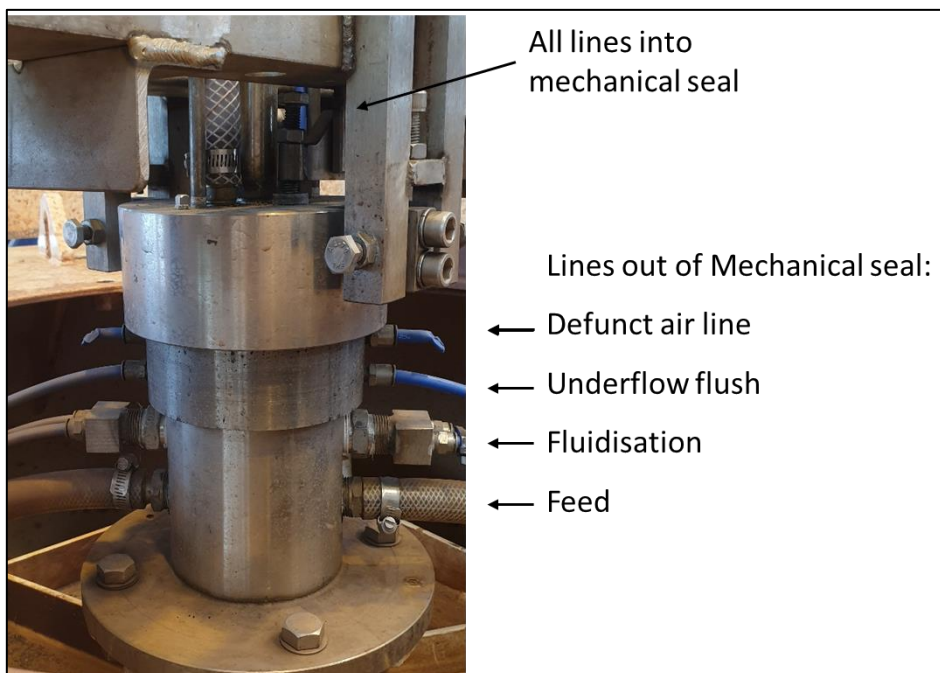


Figure 4.9: Mechanical seal of the Graviton. All lines enter the top of the seal and are fed to the rotating system via an annular arrangement. The lines are split evenly and diverted to the modules on opposite arms of the centrifuge.

The two underflows were discharged into a launder that runs around the inside circumference of the centrifuge housing. An additional flow of water, the “launder wash”, was added to help direct the

solids out of the unit. However, this launder wash was only partially successful, as it was observed after experiments that a significant amount of material had settled in the launder. Size analysis showed that this material was coarser (and also denser) than the underflow sample. Figure 4.10 shows the size analysis of the sampled underflow for Run CF222 along with the particles washed out of the launder after the experiment. These curves clearly show that a high concentration of coarser particles are not represented in the underflow sample. Fe grade analysis indicates that these particles are also of high grade. The sampled underflow from Run CF203 had a reported grade of 53.0 %Fe. After washing out the launder solids and combining with all the collected underflow solids, a second sample was taken. This combined sample showed a grade of 58.5 %Fe, clearly indicating the underflow sample was underrepresenting both coarse and high-grade particles.

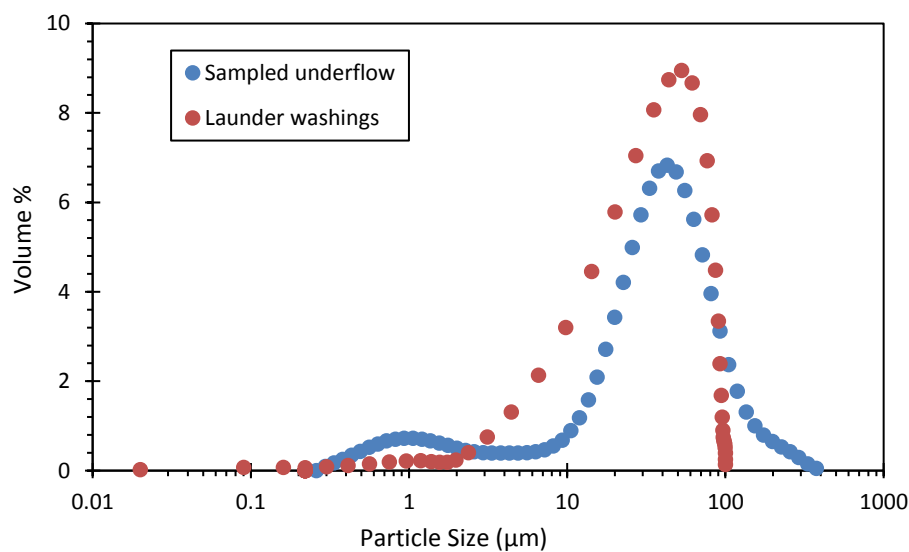


Figure 4.10: Size distributions of the sampled underflow for Run CF222 and the particles washed out of the launder after the run.

Two launder discharge flanges, on opposite sides of the unit, had \varnothing 50 mm pipes attached which directed the underflow into large drums. Samples of the underflow were collected from these pipes as they discharged into the drums (Figure 4.11a). The overflows from the two REFLUX™ Classifier modules were dumped onto the floor of the centrifuge housing where they merged. The combined stream then freely flowed out into a rectangular sump (Figure 4.11b) from where it was pumped by a air-actuated positive displacement pumps (Graco, Huskey 1050) into the overflow holding tank. The

overflow stream was sampled as it discharged into this tank. Figure 4.11 shows the underflow and overflow stream discharge points from the centrifuge.

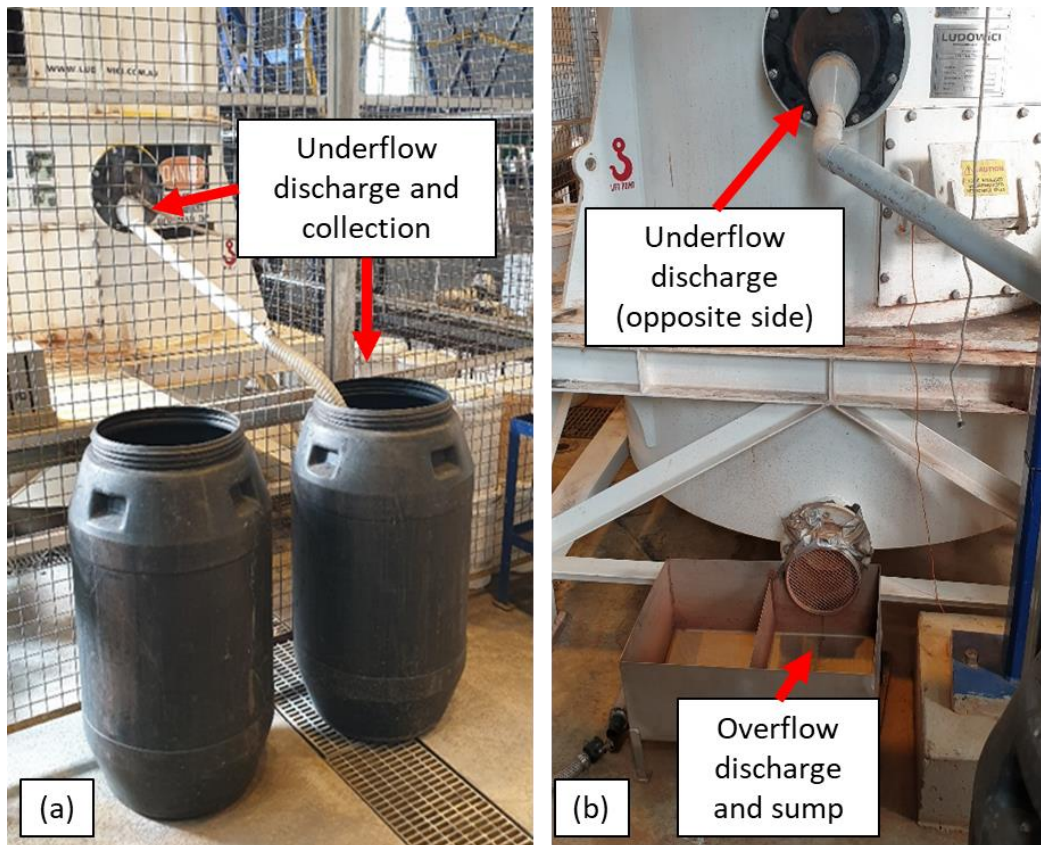


Figure 4.11: Picture of one of the underflow discharge points and collection in drums (left) and on the opposite side, the other underflow discharge point and below it the overflow discharge and sump (right). The overflow was pumped from this sump into a secondary tank.

4.1.2 Changes to Equipment

Under high G forces it was found that the low entry flowrates allowed the feed lines to bow and eventually block with solids. For this reason, the number of entry points for the feed was reduced from four to two, and then later to one. The subsequent higher rate through the remaining entry reduced the risk of early blockage. This modification only affected the initial experiments performed with Silica feed. The first seven experiments, CF145 – CF153, used the original design of four feed inlets. The following six runs, CF154 – CF159, used only two feed entry points. All subsequent runs used only the one feed entry point as is shown in Figure 4.4.

Two fluidisation set ups were used in this study. Initial experiments up to Run CF198 were performed with the fluidisation entering via 100 holes of 0.5 mm diameter. To allow for higher fluidisation rates, a second fluidisation entry was made with 100 holes of 0.8 mm diameter. The cylindrical end of the fluidisation chamber was completely cut off and re-built. The altered section was then reattached to the main body via a flange. This modification is shown in Figure 4.12. The remainder of all experiments were performed with this new fluidisation system.

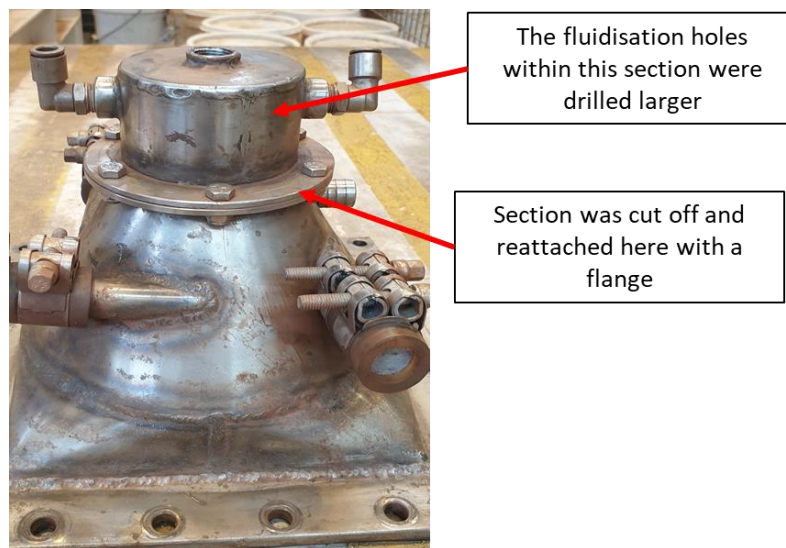


Figure 4.12: Photo of modification to fluidisation chamber showing flange where cylindrical section was reattached.

A noted issue with this design of the Graviton was the tendency for some of the overflow material discharging from the rotating arms to splash outwards into the underflow launder. This caused a significant amount of ultrafine material to be misplaced to the underflow, compromising both the size partition curves and product grades of the underflow samples. To quantify this splashing, the underflow was completely blocked off and mains water fed to the Graviton rotating at the same speed as used for the experiments (351 rpm). Given that the underflow was completely blocked off, all of the water should go to the overflow and hence land on the floor of the unit. Instead, some water reported to underflow via splashing. The overflow and underflow rates were measured by weighing the water collected in a known time. Through these observations and those made after experiments, the 'overflow splashing' was thought to occur via two mechanisms. Firstly, the overflow material exits

the swinging modules at such a velocity, assisted by the G-force and air turbulence in the Graviton, that some sprays out either directly onto the outer shell where it drips down into the launder or splashes off the various support arches into the launder. The second mechanism is not direct splashing, rather, a thin film of overflow that exits below the launder which moves up the launder wall, over the lip and in. This is assisted again by the G-force and air turbulence in the Graviton as well as the design of the launder wall itself, which is angled slightly outwards making it easier for the film to travel upwards. Figure 4.13 shows a diagram of the splashing mechanisms. Of course, due to the enclosed nature of the system it is impossible to observe exactly what is occurring in real time.

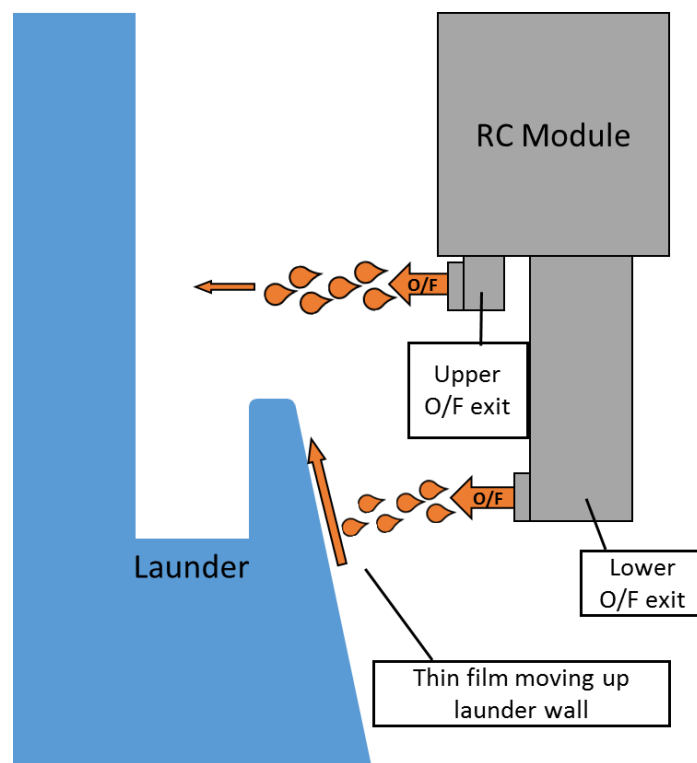


Figure 4.13: Diagram of the overflow splashing mechanisms believed to occur in the Graviton.

This issue was addressed with rudimentary, but seemingly effective solutions. Firstly, the overflow exits via two ports, one above the launder and one below. The upper overflow exit was assumed to be the cause of most of the direct splashing and was thus simply blocked off forcing the material to only exit through the bottom hole. To combat the upwards moving film, several lengths of 1 inch hose were cut along one side and fitted over the lip of the launder rail, covering the entire circumference.

These modifications are shown in Figure 4.14 and were put in place after Run CF202. Figure 4.15 shows the comparison of the overflow and underflow rates of the water splashing test described above. The same test was performed at select feed rates with the upper overflow blocked off, and with the launder rail covered. Appendix H contains the raw data for these tests. Whilst not eliminating the problem, with both modifications in place the splashing was reduced from 8% at the highest rate to less than 3 % of the total flow reporting to the underflow. It must be emphasised that this issue stems from the generic design of the unit, as it was a re-purposed centrifuge. A purpose-built unit would eliminate the problem of overflow splashing through better design.

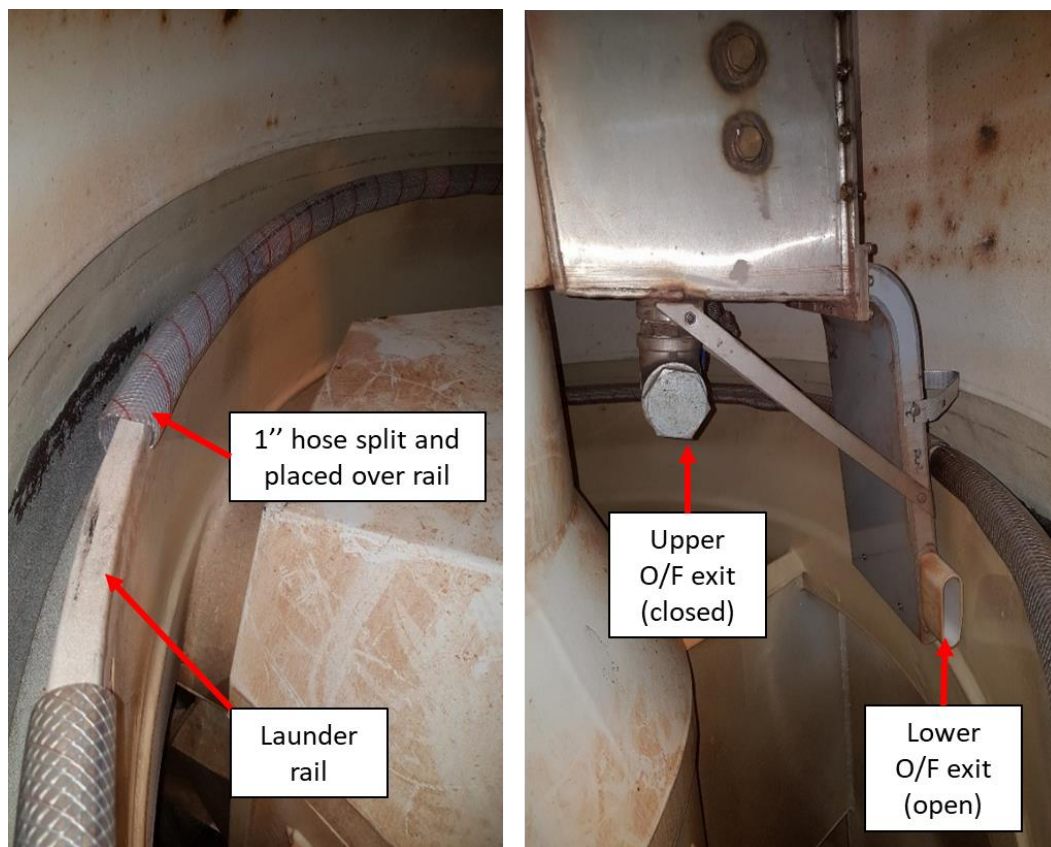


Figure 4.14: Temporary solutions to overflow material splashing into underflow launder: launder rail guard (left) and the two overflow exits, the top one is blocked off (right).

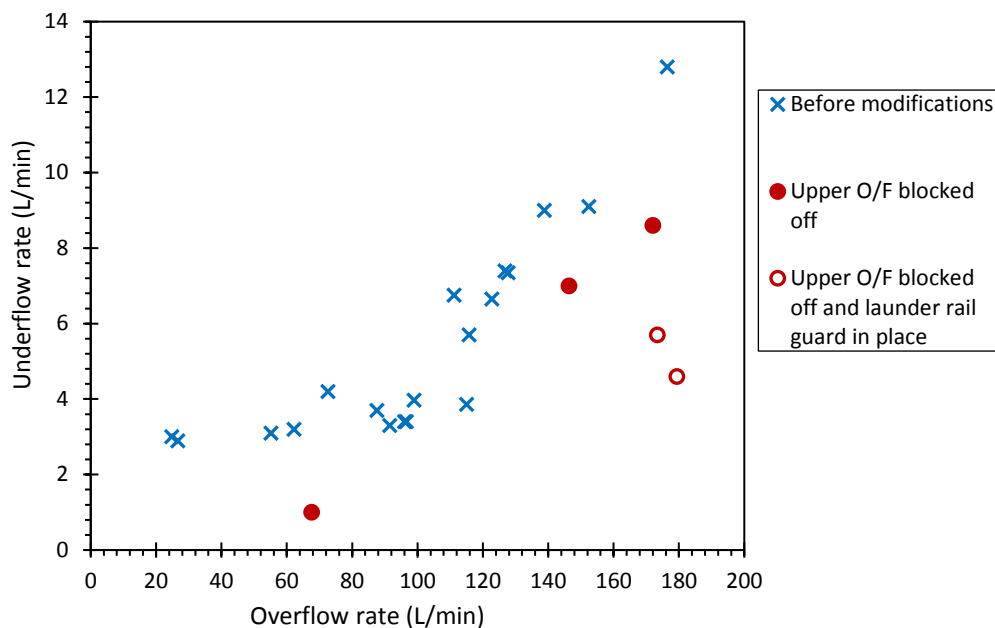


Figure 4.15: Splashing tests showing the comparison of overflow and underflow rates before and after modifications to the system.

4.1.3 Procedure

The feed was made to the desired solids concentration in a well mixed 1.3 m³ tank. For the silica work the feed suspension was pumped into the Graviton using a pneumatic diaphragm pump (Graco, Huskey 1050). The desired flowrate was set by the air pressure powering the pump and although calibrations were performed for this method there was some variability in the actual flowrate. The iron ore studies were performed using an electric centrifugal pump (Warman, Teco, Maxe3 Premium, 4 hP) in order to attain higher flowrates and be more reliable and consistent than the diaphragm pump, and to resist wear. In this case the flowrate was calibrated and controlled by a variable speed drive that adjusted the speed of the pump. For both pumps, the actual flowrate was measured by the volume change in the feed tank over the run time and through a magnetic flowmeter.

The variable speed drive controlling the centrifuge motor was set to rotate at 1298 rpm, which after gearing, according to the manufacturer specifications, gave a centrifuge shaft rotation speed of 351 rpm. The centrifugal force increases radially from the shaft, but the final separation is governed by the force on the particles at the overflow weir of the RC™ assembly. Hence, at this point (0.4 m from the axis) the rotation gives a G-force of 55 G.

The fluidisation water, underflow flush and launder wash water were all supplied directly from the mains through the mechanical seal, with the flowrates measured using calibrated rotameters. Before start up, an initial feed sample was collected from the feed line for analysis. To assist the initial pumping of the feed suspension, mains water was run through the feed line to the Graviton, after the pump. With the centrifuge up to speed and water flows on, the feed pump was started and the assisting feed water shut off. A process flow diagram of the experimental apparatus is shown in Figure 4.16.

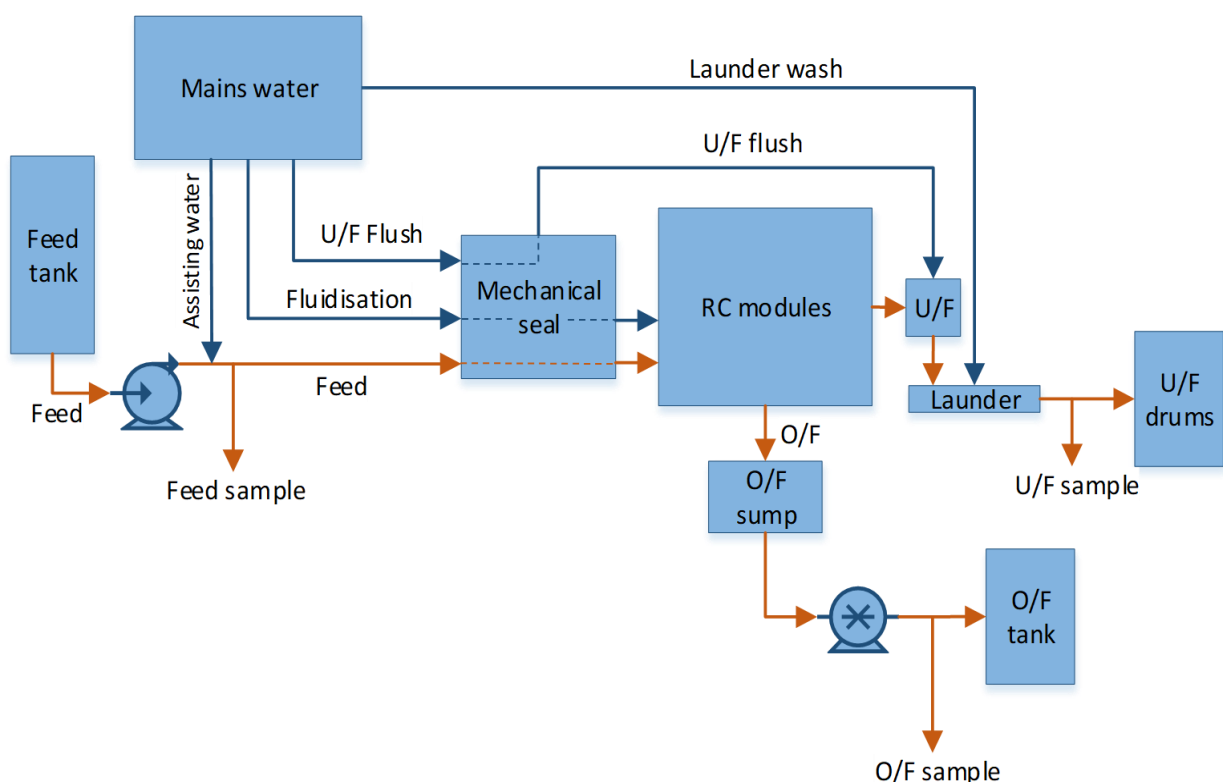


Figure 4.16: Process flow diagram of the Graviton experimental setup.

During the run the feed, launder and wash water flows were monitored and adjusted as necessary to maintain constant rates. During each run several representative full stream samples of the underflow and overflow streams were collected simultaneously into 20 L buckets. These were generally taken at 1 to 3 minute intervals, depending on the total run time. Analysing the samples taken at different times during the run enabled the time taken to reach steady state to be determined. Depending on the flowrate these samples were collected over 7 – 20 seconds to ensure enough solids for later

analysis. At the conclusion of the run, another sample of the feed was taken to ensure the consistency of the feed over the course of the run. All reported values of the underflow flowrate and solids concentrations were adjusted to compensate for the extra water input from the underflow flush and the launder wash.

4.1.4 Sample Analysis

The flowrates of each stream were determined from the mass collected in the sample time. Two sub samples of each stream sample were then taken. To ensure these sub samples were representative, an impellor was lowered into the 20 L sample buckets, along with baffles, and the sub samples taken from the well-mixed sample using a peristaltic pump.

The first was weighed and dried to calculate the solids concentration of the stream, the second was used to measure the solids size distribution using a Malvern Mastersizer 3000 which reports a volume frequency distribution. The sub sample used for laser sizing was again well mixed using a set of baffles and an impellor. A pipette was used to draw several millilitres of the well mixed sub sample for the laser sizing analysis.

At steady state with no breakage or attrition, the rate of material in each size fraction entering the system will equal the combined rate in that size fraction exiting in the overflow and underflow. Assuming steady state, the volume size distributions of each stream from the Malvern can then be used in the two product formula to calculate the volume split (yield) of the feed material that reports to the underflow (Wills & Finch, 2016),

$$Y = \frac{UF}{F} = \frac{x_F(d) - x_{OF}(d)}{x_{UF}(d) - x_{OF}(d)} \quad (4.1)$$

where Y is the volume split of the feed solids, F , to the underflow product, UF , and x_F , x_{OF} and x_{UF} are the volume fractions of solids in the feed, overflow and underflow streams respectively in a size interval with average diameter d . Note that for samples collected at steady state with no measurement errors, the value of Y calculated by Equation 4.1 should not change, regardless of which size fraction is chosen.

A typical example of the application of Equation 4.1 is shown in Figure 4.17. A consistent yield to underflow of 71 % is seen for particle sizes between 2 and 50 μm . The very low amount of material outside of this range explains the drift away from this value. The divergence seen near 18 μm is caused by the increased sensitivity to measurement error when the denominator and numerator of Equation 4.1 both approach values of zero i.e. when $x_F = x_{OF} = x_{UF}$.

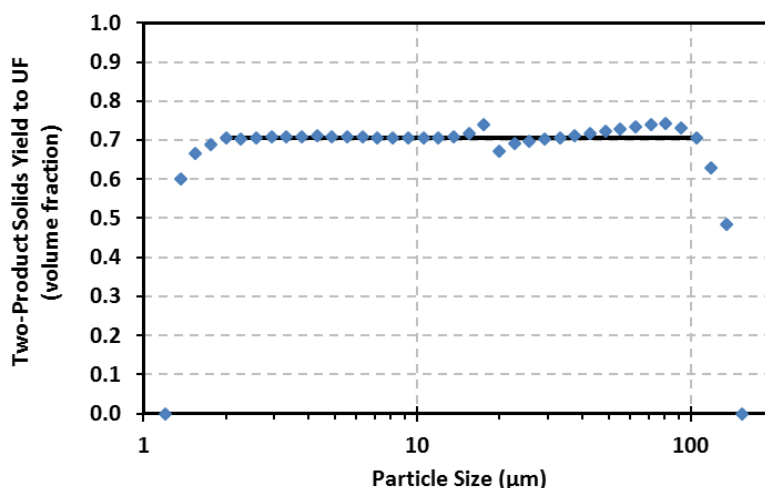


Figure 4.17: Overall solids volume yield to underflow calculated by the two product formula (Equation 4.1) applied to each size interval. The solid line shows a yield of 71 vol.%.

Using this yield, the partition $P(d)$ of the feed material to the underflow as a function of the average size in an interval d can then be calculated in two ways:

$$P(d) = \frac{x_{UF}(d)}{x_F(d)} Y \quad (4.2a)$$

$$P(d) = 1 - \frac{x_{OF}(d)}{x_F(d)} (1 - Y) \quad (4.2b)$$

Equation 4.2a uses the information from the feed and underflow streams whereas Equation 4.2b uses information from the feed and overflow streams. Both equations should give the same result if there were no sampling or measurement errors and the system was at steady state with no breakage or attrition of particles. However, as noted in Section 4.1.1, it was found that the launder wash was not strong enough to prevent large and/or dense particles from settling in the underflow launder. This led to them being underrepresented in the underflow samples. This can be seen in Figure 4.18 where the

partition curve based on the underflow sample (Equation 4.2a) drops away at the larger sizes. This is physically implausible since larger particles should be more likely to exit in the underflow. Hence, Equation 4.2b was preferred as it generally gave stable partition values of 100 % at the largest particle sizes.

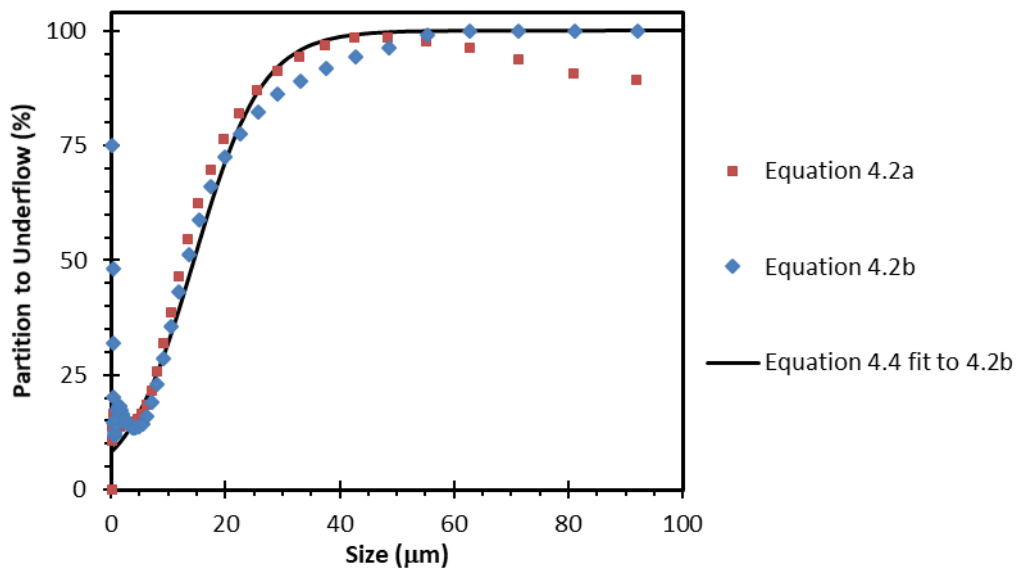


Figure 4.18: Partition to underflow as calculated by Equations 4.2a and 4.2b. The solid line shows the best fit of Equation 4.4 to the results of Equation 4.2b in the range of 5 to 50 µm.

The defining characteristics of a partition curve are the separation size d_{50} , and the Ecart probable Ep value. The d_{50} value is the size of the particle that is equally likely to report to either the underflow or overflow (i.e. a partition value of 50 %), and the Ep value is a measure of the sharpness of the separation, defined as half of the difference between the d_{75} and d_{25} values, that is

$$Ep = \frac{d_{75} - d_{25}}{2} \quad (4.3)$$

An example of these values on a partition curve is shown in Figure 4.19.

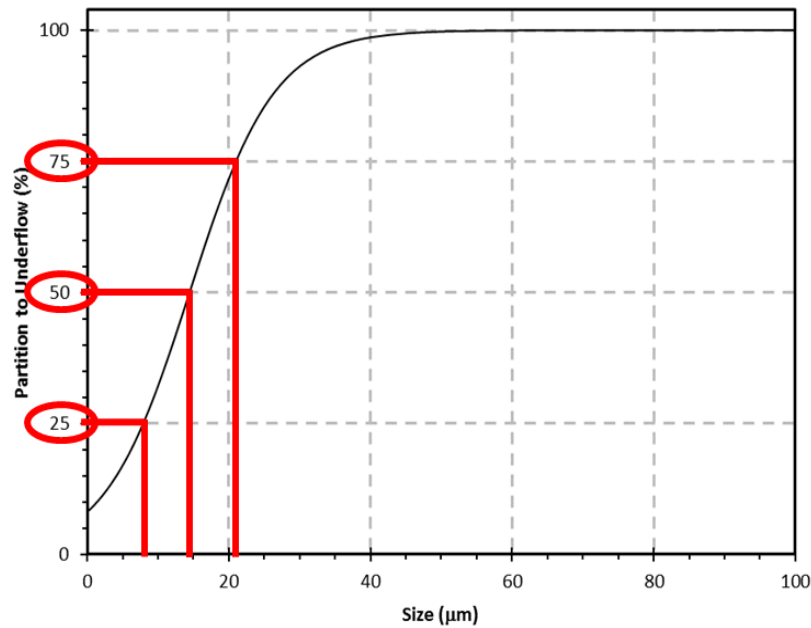


Figure 4.19: Example of a partition curve with the defining characteristic values highlighted. For this curve $d_{75} = 21 \mu\text{m}$, $d_{50} = 14 \mu\text{m}$, $d_{25} = 8 \mu\text{m}$.

To obtain unambiguous values for these parameters, the partition model of Scott and Napier-Munn (1992), Equation 4.4, was fitted to the partition data from Equation 4.2b. The best fit was obtained by varying d_{50} and Ep to minimise the sum of the square of the errors between the experimental and model partition values. The solid line in Figure 4.18 shows the resulting partition curve.

$$P(d) = \frac{1}{1 + \exp\left(\ln(3) \frac{d - d_{50}}{1000Ep}\right)} \quad (4.4)$$

The mass flowrates and solids concentrations calculated from the sub samples allowed the total solids mass rates in the feed F , underflow UF and overflow OF streams to be determined. Using these values, the mass yield of solids to the underflow, Y_M , can be calculated in three different ways:

$$Y_M = \frac{UF}{F} \quad (4.5a)$$

$$Y_M = \frac{UF}{(UF + OF)} \quad (4.5b)$$

$$Y_M = 1 - \frac{OF}{F} \quad (4.5c)$$

Assuming the samples were taken at steady state and with no sampling or measurement errors, these three equations should give the same result. However, the experimental method involved only very short sample times of 7 – 20 seconds for such high flowrates, in addition to other errors in handling, weighing and drying the samples. Therefore, there will be inaccuracies in these values. For single particle density suspensions such as the silica work, the volume yields calculated by Equation 4.1 should equal the mass yields from Equations 4.5a-c. It was observed, however, that the mass yields were systematically higher on average than the volume yields.

For the iron ore work, samples of each stream were dried and sent off for a head grade analysis at an external testing facility. For some runs a wet split of the samples was performed at 20 and 38 μm with the plus 38 μm material also being dry split at various higher sizes, depending the size distribution. Each size fraction was then sent for iron grade analysis. At steady state and with no breakage, attrition, losses or measurements errors, the total mass and iron content of each size fraction entering the unit in the feed stream should equal the total in that size fraction exiting in the unit in the overflow and underflow streams. For real data, however, this is never perfectly achieved, and so mass balance data reconciliation was performed to provide a consistent set of data for analysis. For this process, an objective function, G , based on the mass balance errors, was numerically minimised through the simplex search technique of Nelder and Mead (1965). This results in the mass balance error being dispersed amongst the entire data set. The objective function, G , is defined as,

$$G = \sum_i w_i (E_i - B_i)^2 \quad (4.6)$$

where w_i , E_i and B_i are the i th weighting factor, experimental and balanced values respectively. The weighting factor is given by,

$$w_i = \sigma_i^{-2} \quad (4.7)$$

where the σ_i is the relative standard deviation. Here, data with lower standard deviations should involve less adjustment. The mass balance was performed on the size by assay data along with the

head grades for each stream. The balance did not use the feed or fluidisation rates or the solids concentrations but instead, dummy values for the total solids rate of each stream were used, based on the calculated overall solids yield (Equations 4.5a - c). The standard deviation for this input was relatively large to provide more freedom for adjustment. The standard deviations for the balance varied from 0.3 to 0.01. No bounds or limits existed for this process, and so in some cases the standard deviation had to be set lower to keep the adjustment within physical limits (e.g. to keep adjusted value below maximum hematite grade of 69.99 %Fe). Appendix D contains the raw data, standard deviations, and mass balanced data for all instances of this mass balance reconciliation process.

The two-product formula (Equation 4.1) was previously used to calculate the *volume* yield of solids to underflow by using the *volume* fraction of solids in each size interval. It can also be applied to the *mass* fraction of solids to calculate the *mass* yield. By applying the formula to the mass fractions of iron in each size interval, or to the head grades, the mass-based yield Y_M and recovery R_C of iron can be calculated:

$$Y_M = \left(\frac{y_F(d) - y_{OF}(d)}{y_{UF}(d) - y_{OF}(d)} \right) \quad (4.8)$$

$$R_C = \left(\frac{y_{UF}(d)}{y_F(d)} \right) Y_M \quad (4.9)$$

where y_F , y_{UF} and y_{OF} are the mass fractions of iron in the feed, underflow and overflow streams respectively.

4.2 REFLUX™ Classifier

4.2.1 Equipment

The REFLUX™ Classifier unit used in this research was a pilot scale RC™100, pictured in Figure 4.20, with cross sectional dimensions of 0.1 m width and 0.1 m breadth in the vertical and inclined sections. Both sections had a length of 1.0 m. Inclined plates, 0.5 mm in thickness, were positioned at perpendicular spacings of either 3 mm or 1.77 mm according to the experimental conditions. The 3

mm spacings allowed for 26 channels and the 1.77 mm plates made 38 channels. For all experiments, fluidising water was supplied at 0.55 L/min via a distribution flange at the base of the vertical section. The distributor, pictured in Figure 4.20, was shaped as an inverted pyramid, 90 mm in height, with the water entering via sixteen \varnothing 0.75 mm holes spread evenly across the four faces. At the centre of the distributor was the 9 mm underflow outlet. The feed entry point was a 20 mm inlet located 700 mm above the distributor.



Figure 4.20: Photo of the RC™100 (left) and the inside of the fluidisation distributor showing four holes on each face of the inverted pyramid (right).

Two pressure transducers were located at heights of 60 mm and 440 mm above the distributor. The pressure difference between these transducers determined the average suspension density of the fluidised bed. An automatic PID controller opened and closed the underflow valve to maintain a set bed density of 2500 kg/m³. When the reading fell below the set point, the valve would close allowing dense material to accumulate, increasing the bed height, and hence causing the measured density to

increase. Conversely, when the reading exceeded the set point the valve would open allowing dense/coarse material to discharge from the bed. During each experiment this control system was very successful in maintaining a relatively constant bed density. Figure 4.21 shows the typical behaviour of the bed density during the initial start of an experiment and approach to steady state.

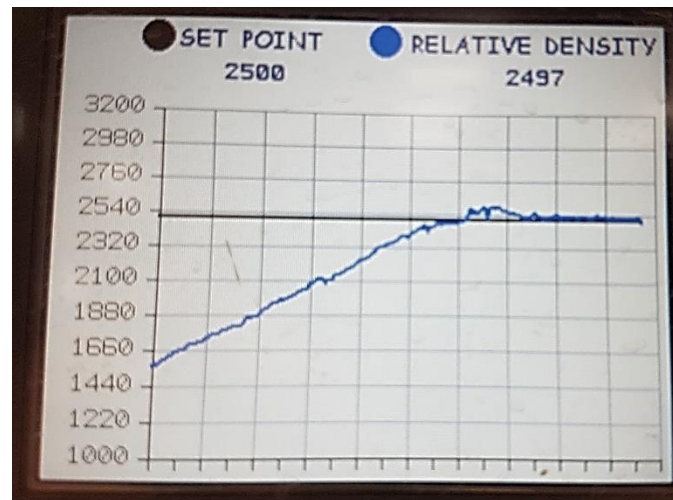


Figure 4.21: Photo of the bed density plot during operation of the RC™100. The blue line tracked the measured density as the bed developed, before reaching the set point of 2500 kg/m³ and levelling out.

The lab scale RC™100 also featured a novel underflow buffer (Galvin et al., 2016) necessary to allow reasonable control of the discharge rate with the valve fully open. The buffer consists of a 22 mm diameter column into which the underflow discharges. The column is fluidised with buffer water at the base and material is withdrawn from a side arm at the top using a positive displacement pump (Figure 4.22). With the valve closed the pump only withdraws water at the buffer rate. When open, the set pump rate controls the discharge rate of the underflow. All reported values for the flow rate and solids concentration of the underflow have been adjusted to remove the additional buffer water being pumped out.

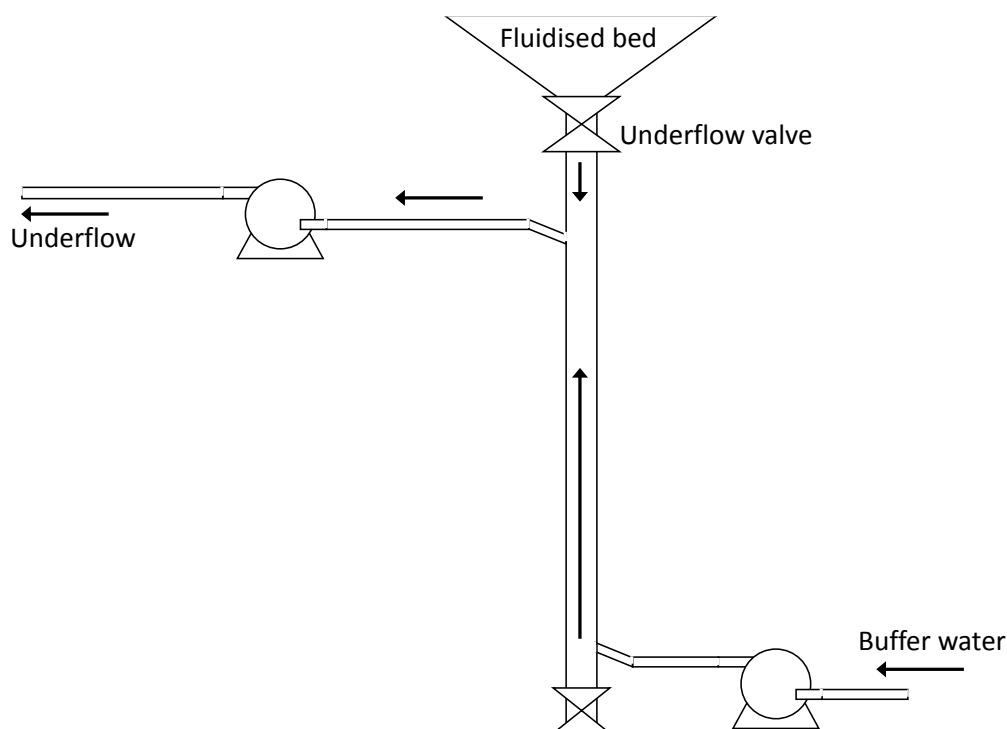


Figure 4.22: Diagram of the underflow buffer arrangement for the RC™ 100

4.2.2 Procedure

Feed was prepared at the required solids concentration in a well-mixed 1300 L tank. For longer running times, additional feed solids were prepared in 200 L drums to be added to the tank, with the appropriate volume of water added periodically as the level decreased. A pump circulated the suspension from the bottom valve of the tank back through the top to prevent faster settling solids building up at the base. A secondary pump supplied the feed to the REFLUX™ Classifier from this circulation line.

To begin each run, the underflow valve remained closed whilst feed entered the system. Larger and denser particles built up in the lower section whilst the fluidising water conveyed the finer/less-dense particles to the overflow. As the bed developed the suspension density approached the set point (Figure 4.21), until eventually the PI controller would begin opening and closing the underflow valve. Throughout this time the enhanced settling in the inclined channels allowed any fine dense particles to reflux back into the lower bed. Steady state was reached after the pressure reading from both probes became steady. This is achieved after the concentration of fine dense particles in the lower

bed had increased to the point where they are fully dispersed across the height of the fluidised bed. Throughout the experiment overflow and underflow flowrates were monitored regularly by collecting small timed samples.

At steady state, simultaneous full stream samples of the underflow and overflow were collected, followed by a feed sample. To allow for at least 800 g of dried solids, these samples were collected over a period of 10 – 30 minutes depending on the mass flow rates. Small additional samples were also collected for supplementary rheology experiments.

4.2.3 Sample Analysis

The solids concentration of each stream was calculated by weighing and drying the full stream samples. A small portion of the dried solids was separated for head grade analysis and the remainder was wet screened at 38 μm . The oversize particles were then dry screened at 45, 63, 90, 125, 180 and 250 μm to obtain a size distribution by mass. The head grade samples and each size fraction were then sent for XRF analysis at an external laboratory.

The raw data was subjected to mass balance reconciliation before using Equation 4.8 and Equation 4.9 to determine the mass yield to underflow and the iron recovery across the size range and in total.

4.3 Supplementary Experiments

4.3.1 Rheology

At steady state, a small sample of the overflow stream was taken and allowed to settle over several days. The supernatant was decanted and set aside and the solids wet screened at 38 μm . The undersize slimes portion was then concentrated and well mixed using an impellor and baffles before dividing into smaller representative samples. This ultrafine portion of the reject stream was used to represent the slimes in the system. Using the original supernatant, the subsamples were diluted to different solids concentrations. An AR-G2 (TA Instruments) rheometer was used to measure the viscosity of each sample. Before testing, two standard fluids of known properties were run through

the rheometer for calibration. Each sample was then mixed well before adding small amounts to the rheometer. The viscosity was then measured across a range of shear rates from 0.002 to more than 100 s⁻¹. The actual range varied for each sample due to the measurable limits. Once complete, the samples were weighed and dried to determine the solids concentration. The pH of each sample was also measured, and found to vary from 7.42 to 7.28, hence the effect of pH on the slimes rheology was negligible.

4.4 Summary

This chapter has presented the apparatus and experimental procedures of the two systems used in this work along with the methods of data analysis. The two systems are closely related, with the main difference being the application of enhanced gravity through the use of a centrifuge for the REFLUX™ Graviton. Chapter 5 discusses the results of the test work done in the REFLUX™ Classifier and Chapter 6 describes the results from the REFLUX™ Graviton. Chapter 7 then follows the results of a two-stage process involving both units.

Chapter 5

REFLUX™ Classifier Results

5.1 Experimental Conditions

This chapter examines the results of experiments performed in the RC™100. The feed used for these experiments was a high grade (65 wt.% Fe) hematite ore with a top size of 0.300 mm, achieved through screening on a Kason vibratory screen. Figures 5.1 and 5.2 show the size distribution of the feed measured as a volume percentage using the Malvern Mastersizer 3000 and mass percentage using laboratory sieves respectively.

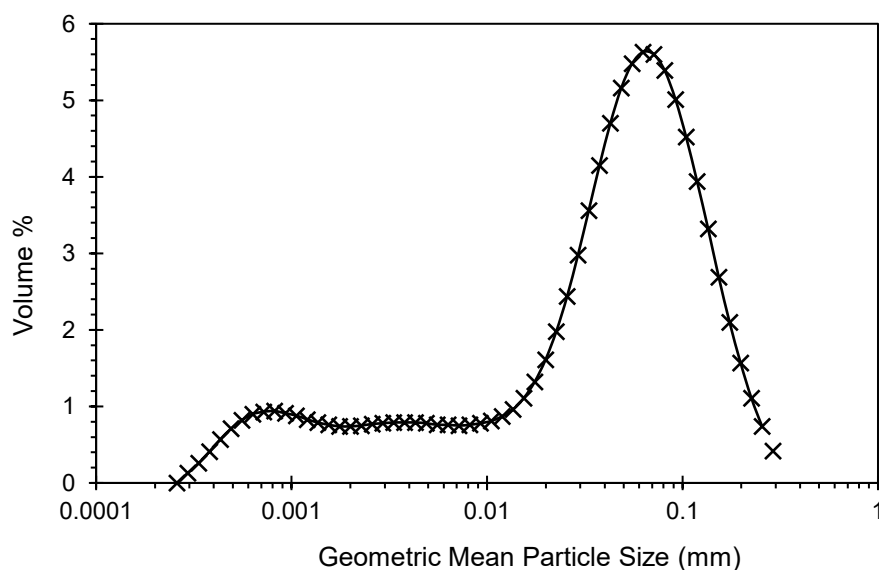


Figure 5.1: Feed size distribution measured as volume percentage by a Malvern Mastersizer 3000.

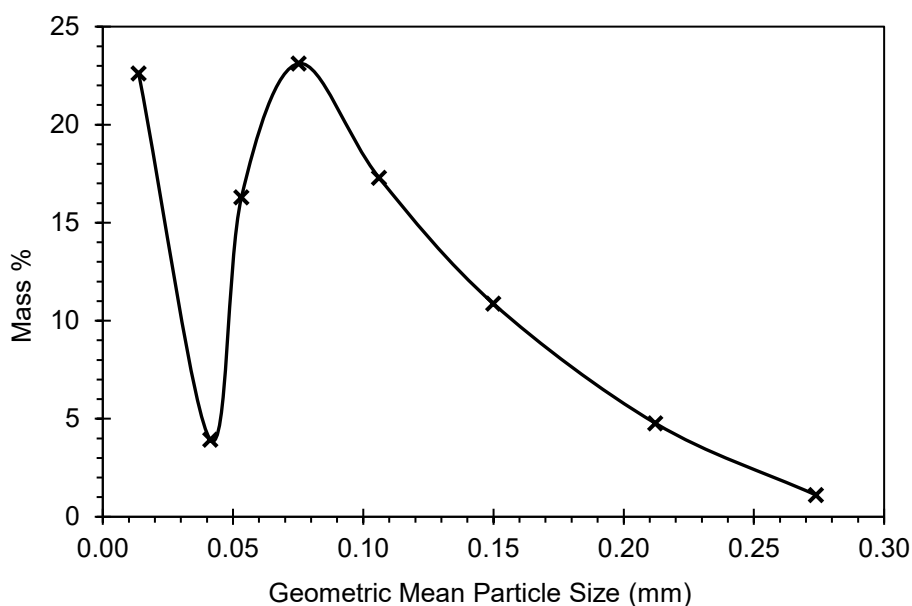


Figure 5.2: Feed size distribution measured as mass percentage by sieving at screen sizes of 0.038, 0.045, 0.063, 0.090, 0.125, 0.180 and 0.250 mm.

The mass distribution (Figure 5.2) shows the effect of a prior desliming stage. A sharp drop is seen at approximately 0.045 mm, the likely cut point of the hydrocyclones, in fact two stages of hydrocyclone desliming. Below that size a significant portion of misplaced slimes, highlighting the inefficiency of that process. That large portion of slimes present in the feed forms the basis of this set of experiments. The aim was to examine the impact of the slimes and how the variables of solids concentration, feed flowrate and channel width alter the separation performance. It must be noted here that the feed is already at a high saleable grade. Pure hematite has a grade of 69.9 % Fe, hence there is limited potential for upgrade. Instead, this series of experiments focusses on the yield and recovery results, rather than simply the product grade. The findings are then supported by rheology experiments on the ultrafine (-0.038 mm) particles taken from the overflow stream.

A total of 11 runs were performed in this series of experiments, seven using a perpendicular channel spacing of 3.0 mm, and four with a spacing of 1.8 mm. Table 5.1 provides a summary of the feed conditions used for each run. Note that solids throughput flux is based on the cross-sectional area of the 0.1 m × 0.1 m vertical section. Additionally, each run used the same fluidisation rate of 0.55 L/min and the same density control set point of 2500 kg/m³. It is noted that the set point had relatively little effect on the separations due to the almost complete liberation of the particles, hence the set point simply resulted in a change in effective bed level as discussed previously. The first tests were conducted at a solids concentration of 36.5 %, a typical concentration seen in beneficiation plants. Halving the solids concentration to 18.5 %, and then again to 9.3 % allowed a large range of concentrations to be tested, covering the typical, the intermediate and dilute conditions. Diluting the feed solids concentration throughout the testing campaign also allowed the tests to be conducted for similarly long run times as the feed solids were exhausted through sampling.

Each set of results obtained in this series of experiments was subject to mass balance reconciliation. The balanced data are presented in this chapter, with the raw data given in Appendix D. Table 5.1 also

contains the mass balanced head grades of each stream and the solids yield to underflow and Fe recovery.

Table 5.1: Feed conditions used for each run as well as the mass balanced head grades of the feed, underflow (product) and overflow (reject) streams, overall solids yield to underflow and Fe recovery.

Run No.	Channel Width (mm)	Feed Conditions			Head grades (wt.% Fe)			Solids Yield (wt.%)	Fe Recovery (%)
		Solids Concentration (wt.%)	Flowrate (L/min)	Throughput (t/(m ² h))	Feed	U/F	O/F		
S24B	3	36.5	9	28	65.2	68.3	64.3	22.5	23.6
S24B2	3	36.5	4.6	14	65.3	68.8	64.1	24.7	26.1
S24B3	3	36.5	2.6	7	65.4	69.1	63.7	32.8	34.7
S24D	3	18.5	5.5	7	66.0	68.9	61.6	61.0	63.6
S24D2	3	18.5	2.8	3.5	65.0	68.6	60.3	56.2	59.3
S24E	3	9.3	11.8	7	65.5	68.8	60.4	60.1	63.2
S24E2	3	9.3	6	3.5	65.2	68.7	60.5	58.2	61.3
S24G	1.8	18.3	5.6	7.0	65.6	69.2	61.0	56.0	59.1
S24G2	1.8	36.5	2.6	7.0	65.9	69.1	62.8	49.0	51.4
S24G3	1.8	36.5	5.2	14.0	65.3	69.0	63.6	31.1	32.9
S24G4	1.8	18.4	11.0	14.0	64.6	68.8	60.8	47.6	50.7

5.2 Results with 3 mm Channels

For each run, head grade samples of the feed, product and reject streams were sent for Fe analysis. These data were then mass-balance reconciled and the overall solids yield and Fe recovery calculated. These results are listed in Table 5.1. The results show that there is little room for improvement in the product grades, with each run approaching ~ 69.0 wt.% Fe with excellent consistency. Examining the reject grades, however, shows a clear trend of decreasing Fe grade as the feed solids concentrations and throughputs decrease. While a dependence on the throughput is expected, the very significant dependence on the feed solids concentration is not expected.

While it is true that a higher solids concentration impacts on the level of hindered settling, at modest concentrations, involving a volume fraction of less than 0.3, the effect is not high, and the impact is mitigated by the option for maintaining the solids throughput by lowering the volumetric feed rate to improve the recovery. It should also be recognised that the solids concentrations within the system,

which represents a form of dynamic hold-up, do not necessarily align with the feed concentration. Nevertheless, for a given volumetric feed rate, a higher feed concentration will likely lead to an increased levels of hindered settling, thus slowing the settling of ultrafine particles within the inclined channels, causing iron ore fines to be misplaced to the overflow. Conversely, lowering the solids concentration reduces those hindered settling effects, increasing the underflow solids yields and Fe recoveries. As noted, lowering the volumetric throughput reduces the velocity in the inclined channels, which similarly reduces the losses of ultrafine iron ore particles to the overflow, thus increasing the underflow solids yield and Fe recovery.

The Fe recovery is plotted against the feed solids concentration and volumetric throughput in Figure 5.3 and Figure 5.4 respectively. These two plots make clear the two general trends mentioned above, namely that higher Fe recoveries are achieved at lower solids concentrations and lower throughputs. However, these trends are non-linear. Figure 5.3 shows that reducing the solids concentration from 36.5 to 18.5 wt.% caused a significant increase in Fe recovery. However, a further reduction in solids concentration down to 9.3 wt.% brought no further improvement in recovery.

Figure 5.4 shows that for the three runs at 36.5 wt.% solids concentration, there was a modest increase in Fe recovery from 23.6 % to 26.1 % and then to 34.7 % as the solids throughput was dropped from 28 down to 14 and then to 7.0 t/(m² h). This improvement reflects the expected effect of reducing the channel velocity on the solids elutriation rates. However, this effect of channel velocity was sometimes dominated by the effect of solids concentration. At a constant solids throughput of 7.0 t/(m² h), the Fe recovery almost doubled from 34.7 to 63.6 % when the feed solids concentrations was halved from 36.5 to 18.5 wt.%, even though the volumetric flowrate had to be doubled to maintain the same throughput. However, only marginal additional improvement in recovery was obtained by further lowering the solids concentration from 18.5 wt.% down to 9.3 wt.%, despite a further doubling of the volumetric throughput. Interestingly, at these higher levels of Fe recovery there was no additional improvement in recovery when the solids throughput was further dropped from 7.0 down to 3.5 t/(m²

h) by halving the feed rate. From these results it is clear that the solids concentration has a large but very non-linear impact on the performance and hence explaining this effect is fundamental to understanding the results.

In the absence of slimes, the system is reasonably insensitive to changes in the feed solids concentration within limits. For example at exceedingly low solids concentrations, it is necessary to increase the volumetric rate significantly to compensate, and hence maintain the same solids throughput. Conversely, at very high solids concentrations, hindered settling can become a major problem. In general, operation between the range 0.05 to 0.20 volume fraction is considered ideal.

Figure 5.4 shows that a halving of the solids concentration, whilst doubling the volumetric flowrate to maintain the same throughput, doubled the recovery. The same dramatic increase is not seen with further reductions to the solids concentration. It is thus concluded that the system is physically very similar at 9.3 and 18.5 wt.% solids concentration, and very different at 36.5 wt.%. This observation is examined in the rheology experiments in Section 5.4 where the suspension viscosity is measured at different solids concentrations.

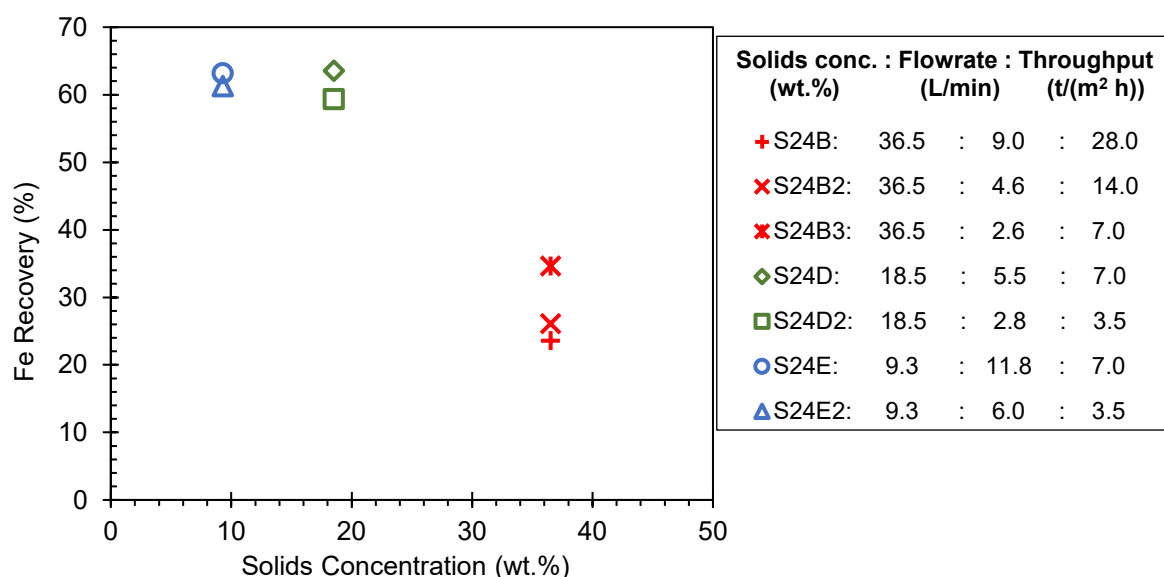


Figure 5.3: Fe recovery as a function of feed solids concentration for the 3.0 mm channels (mass-balanced data from Table 5.1).

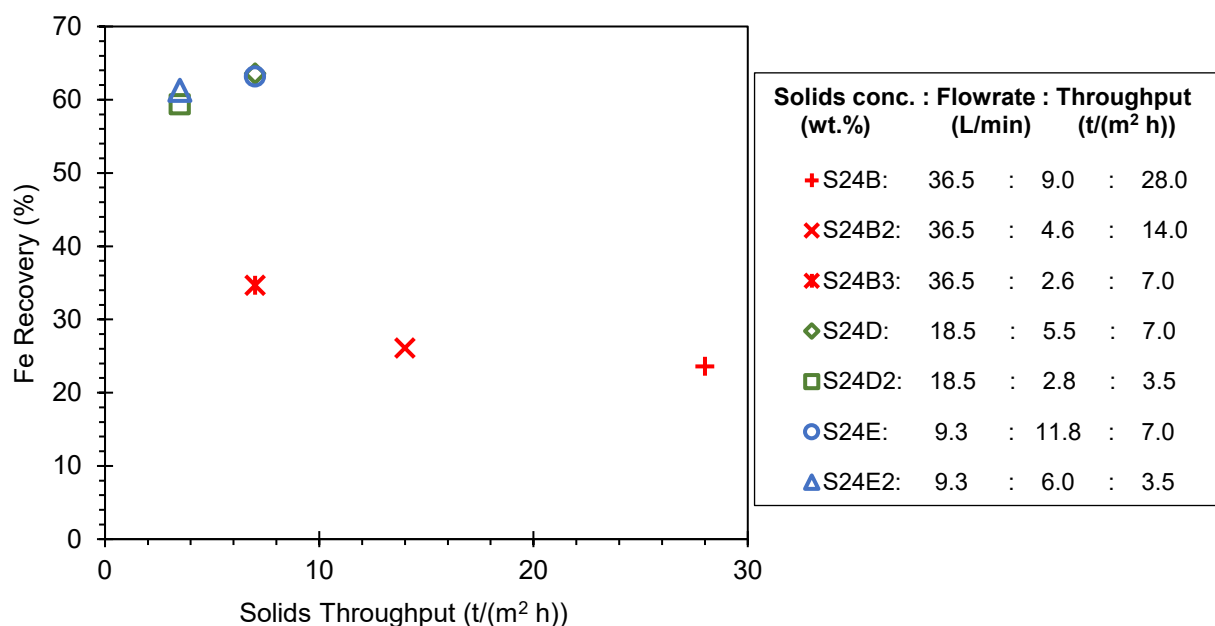


Figure 5.4: Fe recovery as a function of feed solids throughput for the 3.0 mm channels (mass balanced data from Table 5.1).

The samples from each stream were screened to provide more detailed results on the effect of particle size. Figure 5.5 and Figure 5.6 show respectively the solids yield to underflow and Fe recovery, calculated from the mass balanced data, as a function of particle size. Similar trends were observed regardless of feed conditions. With increasing particle size, the yield increases steeply to a maximum and then drops slowly with further increase in particle size. The Fe recovery, however, almost always increased monotonically with increasing particle size with only a very slight decrease at the coarsest size for two of the runs, signifying gangue rejection at all sizes. This is also evident by examining the data tables provided in Appendix D that show the underflow grade being consistently higher than the overflow grade for every size fraction. Again, for any particular size fraction, the separation performance was generally better for the lower throughput, lower solids concentration runs. Figure 5.5 shows that the separation sizes (d_{50} values) were in the range 0.055 – 0.06 mm for the 18.5 and 9.3 wt.% runs compared to coarse sizes of 0.09 – 0.13 mm for the runs at 36.5 wt.%.

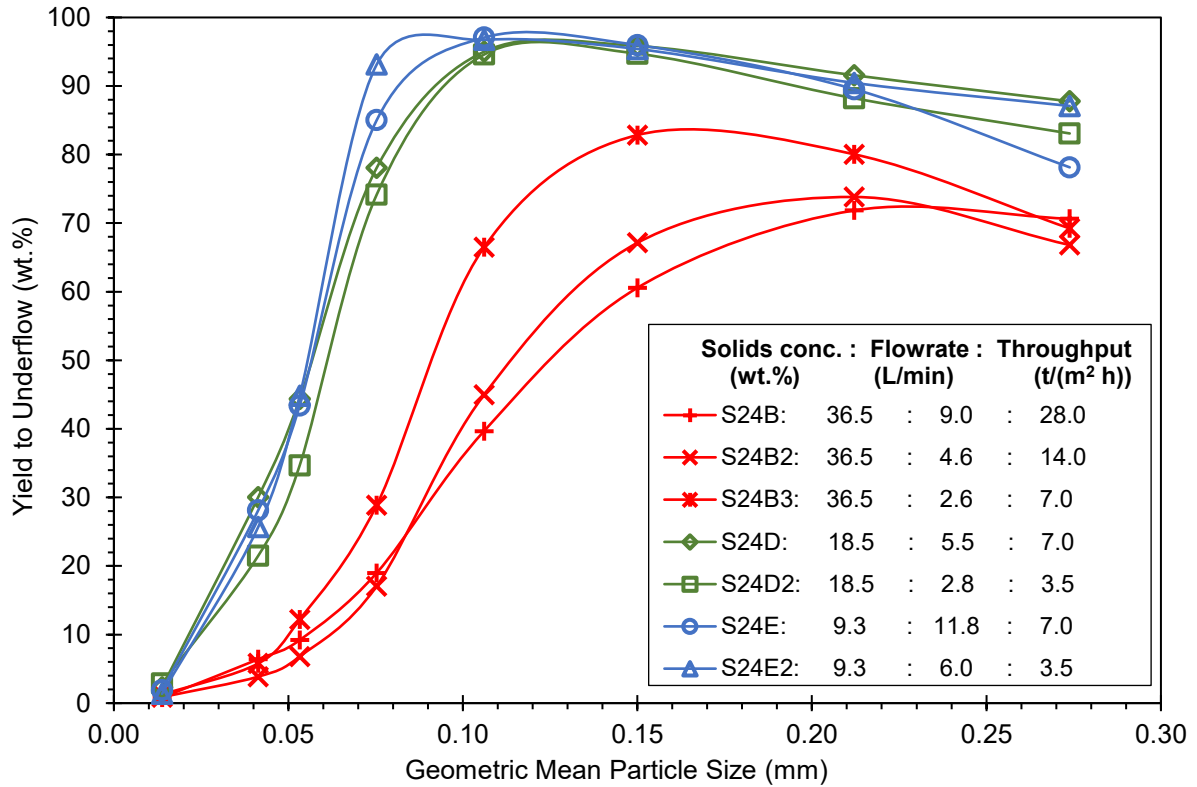


Figure 5.5: Solids yield to underflow as a function of mean particle size (mass-balanced data).

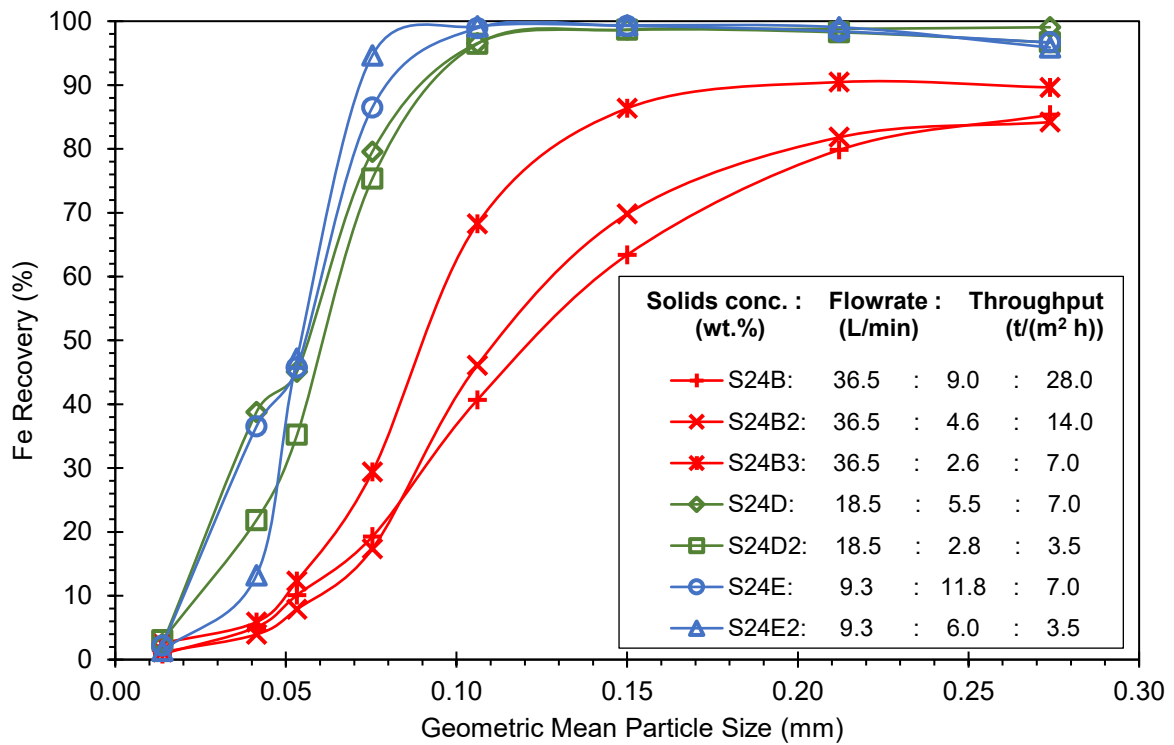


Figure 5.6: Fe recovery as a function of mean particle size (mass-balanced data).

The uncertainty in these values can be inferred through the strong continuity that exists across the various runs. For example, at the highest solids concentration of 36.5 wt.% solids the yield partition numbers, and Fe recovery results show a consistent variation with changes in the feed flow rate. The results at the two highest flow rates are very similar, and arguably equivalent at the finest particle sizes. Each of the partition numbers are within 5 % of each other, with the 4.6 L/min result always higher than the 9.0 L/min result above 0.075 mm, and arguably equivalent below this size. This level of consistency would not be apparent if the error in the partition number exceeded 5 %. For the experiments conducted at 7 t/(m² h) solids throughput, involving different feed solids concentrations, there is similar continuity across the results. For 18.5 wt.% and 9.3 wt.% solids, the results are almost identical, with the partition number consistently higher for the lower solids concentration. The consistency here arises because the powerful effects of viscosity are largely overcome at feed solids concentrations at or below 18.5 wt.% solids. This data suggests the error in the partition number is within 3 % across the full size range. The result obtained at the highest solids concentration is very different but consistent with expectations. For the lowest solids throughput of 3.5 t/(m² h) the consistency continues, however, there is one outlier at about 0.045 mm where the partition number at 9.3 wt.% solids is lower than for the 18.5 wt.% solids case.

It should be noted that in targeting a given solids throughput using different feed solids concentrations, the feed flow rate was adjusted to compensate. Taken to an extreme, for a fixed solids throughput, there must exist a feed solids concentration below which the flow rate would be so high that the separation performance would decline. The data in this work suggests the cross-over point is close to 9.3 wt.% solids. The effect on the partition number is dramatic for a change in the solids concentration from 36.5 to 18.5 wt.% solids, while for the reduction from 18.5 to 9.3 wt.% solids there is minimal change, suggesting that the halving of the solids concentration can be satisfactorily compensated for by a doubling in flow rate. Overall, the strong consistency between the 18.5 wt.% and 9.3 wt.% solids cases confirms the uncertainty in the partition numbers to be less than about 3 %. Finally, it should also be noted that the uncertainty in the partition number in the vicinity of 100 % is

negligible, reflecting the application of mass balance reconciliation, and the precision this brings to the partition numbers.

5.3 Results with 1.8 mm Channels

To investigate the effect of increasing shear rate by narrowing the channel spacing, four runs were completed with a channel spacing of 1.8 mm. Table 5.1 lists the head grades and overall solids yield and recoveries. Like the results for the 3.0 mm channels, the product grades are consistently around 69 wt.% Fe, with the reject grades lower for the more dilute runs (S24G and S24G4). The yield and recovery values also follow the same trends as for the 3.0 mm channels.

The feed conditions of the 1.8 mm channel runs were selected to compare with the results in the 3.0 mm channels around the point where the slimes issue appeared to be overcome, i.e. the very high and very low throughput runs were not repeated. Figure 5.7 and Figure 5.8 compare the recoveries of both sets of results as functions of the feed solids concentration and throughput respectively. In general, the recovery is higher for the narrow channels at high solids concentrations and high throughputs, while the wider channels are superior for the lower concentrations and throughputs. The effect of shear rate is thus more important at the higher solids concentrations. This is potentially a significant finding, related to the rheology of the suspensions.

The interesting Fe recovery increase seen at a throughput of 7 t/(m² h) for the 3.0 mm channels is less pronounced in the 1.8 mm channels. The recovery of 59 % at 18.5 wt.% solids in the 1.8 mm channels is comparable to that obtained in the wider channels. Instead, a similar jump in recovery is observed at the 14 t/(m² h) throughput in Figure 5.8. Here, the one low recovery result (32.9 %) from the 1.8 mm channels was achieved with 36.5 wt.% solids concentration. Diluting this to 18.5 wt.% (shown by the green symbol) produced a much higher recovery of 50 %. A similar result could also be achieved by maintaining the 36.5 wt.% solids concentration and halving the throughput. Both of these higher throughput/solids concentration runs showed higher recoveries than the comparable runs in the 3.0 mm channels.

The results from the 3.0 mm channels revealed that separation performance could be significantly improved through dilution without sacrificing throughput. The 1.8 mm channel result, however, shows that the separation performance could be improved without altering the feed conditions, through an increase in shear rate by using a narrower channel spacing. In this case, the higher fluid velocity through the channels overcomes the detrimental viscous forces of the suspension allowing the denser particles to more easily settle and report correctly to the underflow.

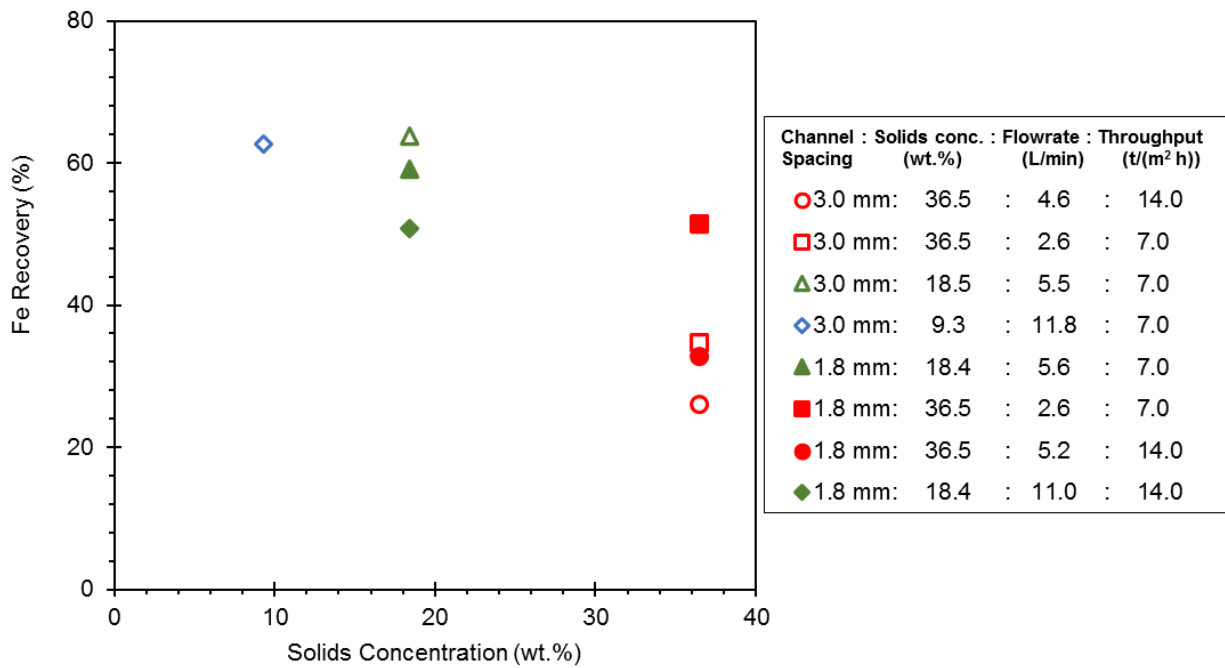


Figure 5.7 Fe recovery as a function of the feed solids concentration for both sets of channels (mass-balanced data from Table 5.1).

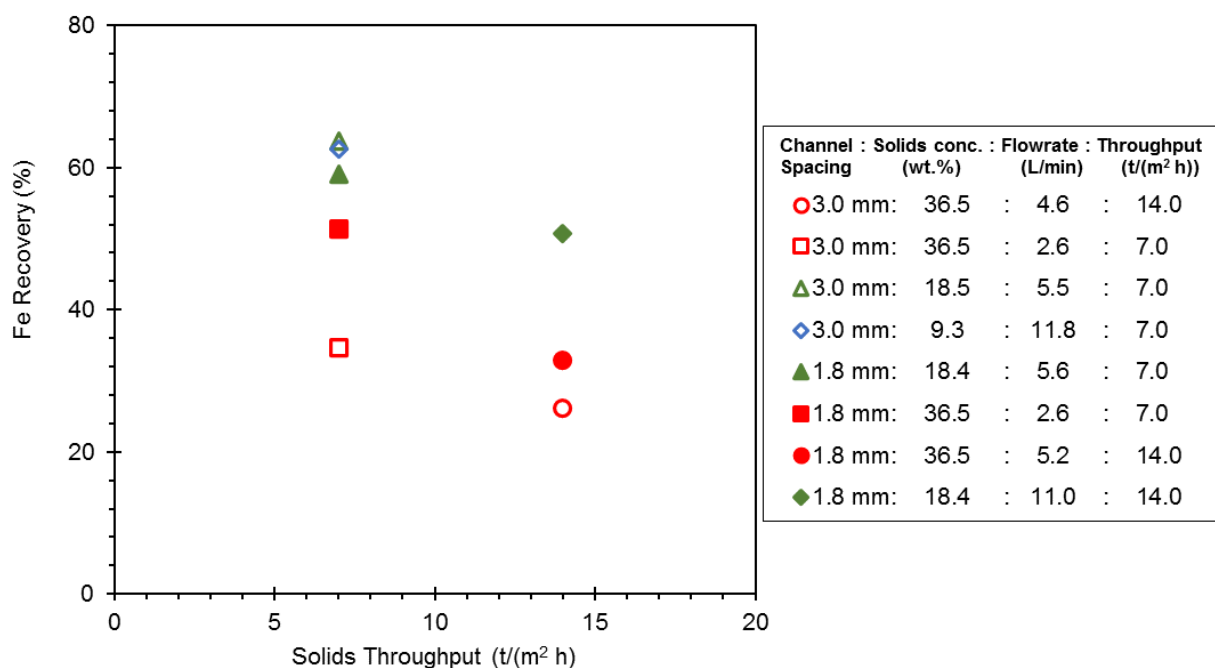


Figure 5.8: Fe recovery as a function of feed solids throughput for both sets of channels (mass-balanced data from Table 5.1).

Across the entire size range, the solids yield to underflow and Fe recovery curves follow the same trends for the 1.8 mm channels as for the 3.0 mm channels. These are shown in Figure 5.9 and Figure 5.10. The yields again decrease at the coarser sizes with the recovery curves levelling out, indicating coarse gangue rejection. For the 36.5 wt.% runs, the 1.8 mm channels have both a finer cut size and higher recovery than the corresponding run in the 3.0 mm channels. For the 18.5 wt.% runs, the 3.0 mm channels appear to have better overall yield and recovery, although the curves are very close. The runs performed at similar conditions of approximately 18.5 wt.% and 5.5 L/min (triangle symbols) show an interesting trend. From 0 – 0.06 mm the yield and recovery from the 1.8 mm channels is higher than that of the 3.0 mm channels. Above 0.06 mm the curves cross over and the 3.0 mm channels appear to be superior. The shear rate of the narrow channels is thus having a greater effect on the ultrafine particles where, importantly, the slimes and majority of gangue particles are present.

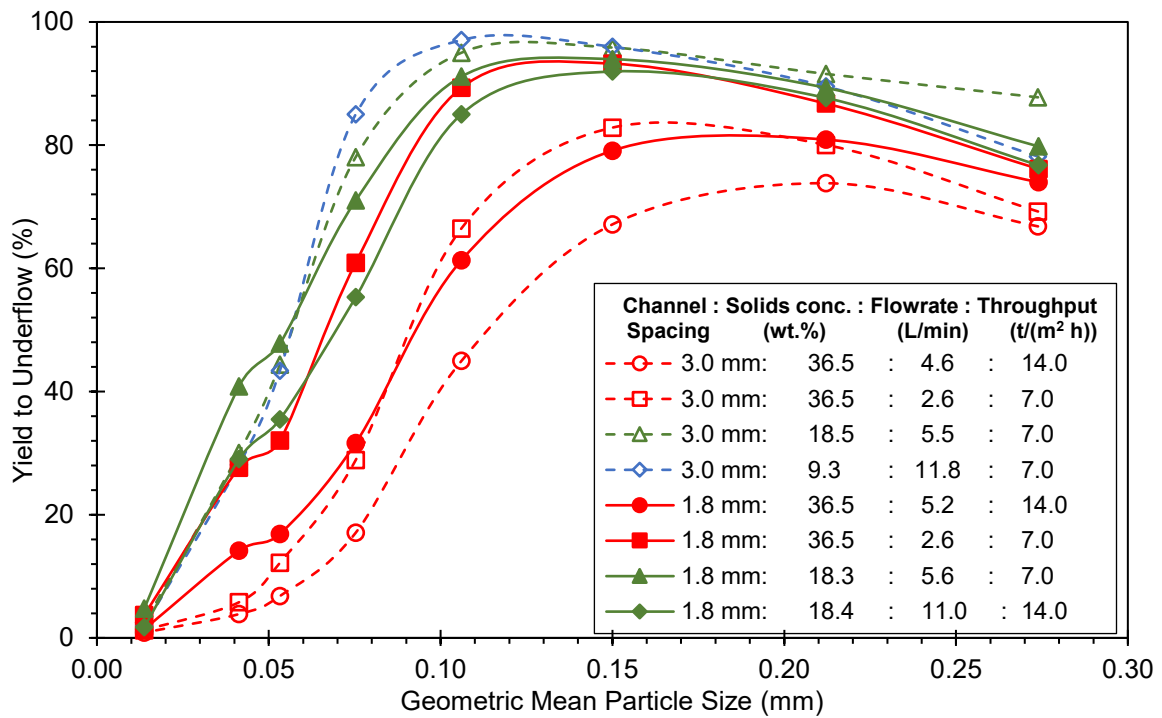


Figure 5.9: Comparison of the yield curves across the entire size range for the two sets of channels. The empty symbols and dashed lines are for 3.0 mm channels, the filled symbols and solid lines are for 1.8 mm channels. Mass-balanced data.

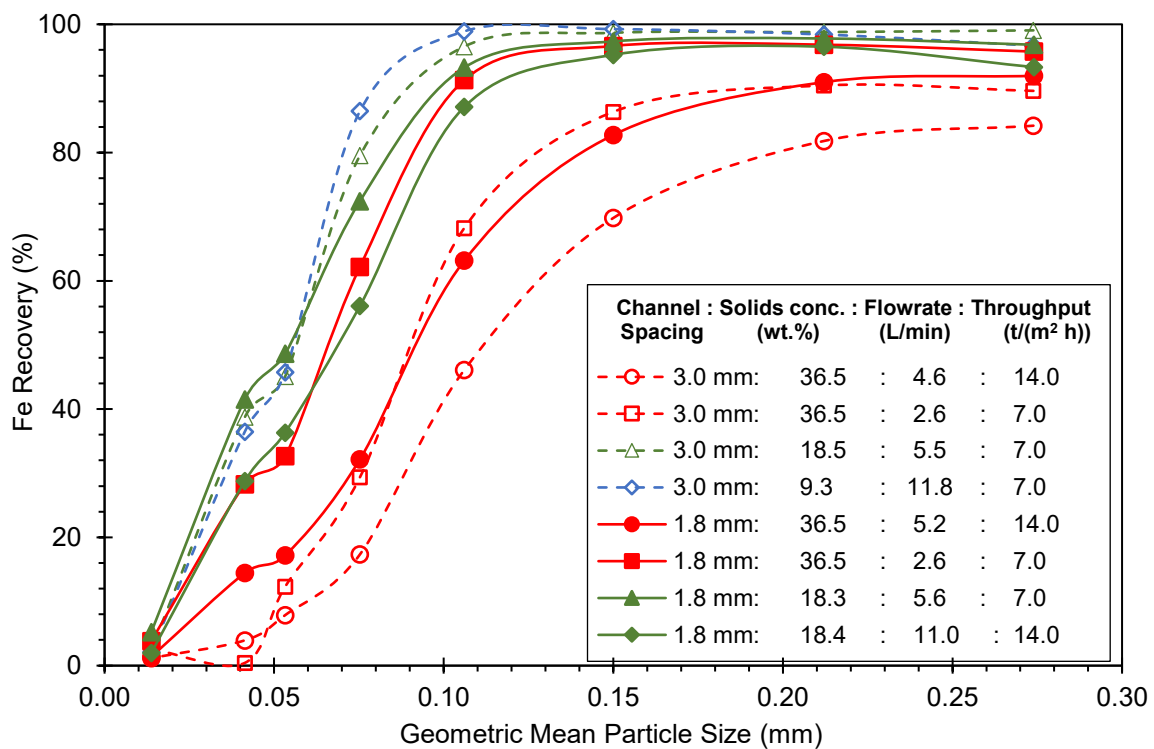


Figure 5.10: Comparison of the recovery curves across the entire size range for both sets of channels. The empty symbols and dashed lines are for 3.0 mm channels, the filled symbols and solid lines are for 1.8 mm channels. Mass-balanced data.

5.4 Rheology

A small sample of the overflow from Run S24E2 was allowed to settle completely before decanting and wet screening to obtain the solids below 0.038 mm. These solids were taken to represent the slimes in the feed. These slimes were diluted to different volume fractions for measurements of the shear stress, and hence apparent viscosity, across a range of shear rates. The actual volume fractions were calculated from the dried mass after the rheology measurements to keep the slimes hydrated. Figure 5.11 shows the shear stress versus the shear rate. Figure 5.12 shows the measured apparent viscosity versus the shear rate. The curvature of the lines in Figures 5.11 and 5.12 clearly demonstrates the shear thinning behaviour of the suspensions. The viscosity initially declined rapidly with increasing shear rate before levelling out at higher shear rates. This finding can help explain some of the results comparing the two channel spacings. The recovery and yield were higher in the narrow channels for runs that achieved higher throughput via a high solids concentration, and low flowrate. In these runs the low volumetric flowrate results in low shear. The narrow channels, halving the channel width, countered this with higher flow velocity, resulting in higher shear. The results from both channel spacings then converged at higher flowrate runs, where the shear rate is higher, and less important than the solids concentration as indicated by flattening of the curves in Figures 5.11 and 5.12.

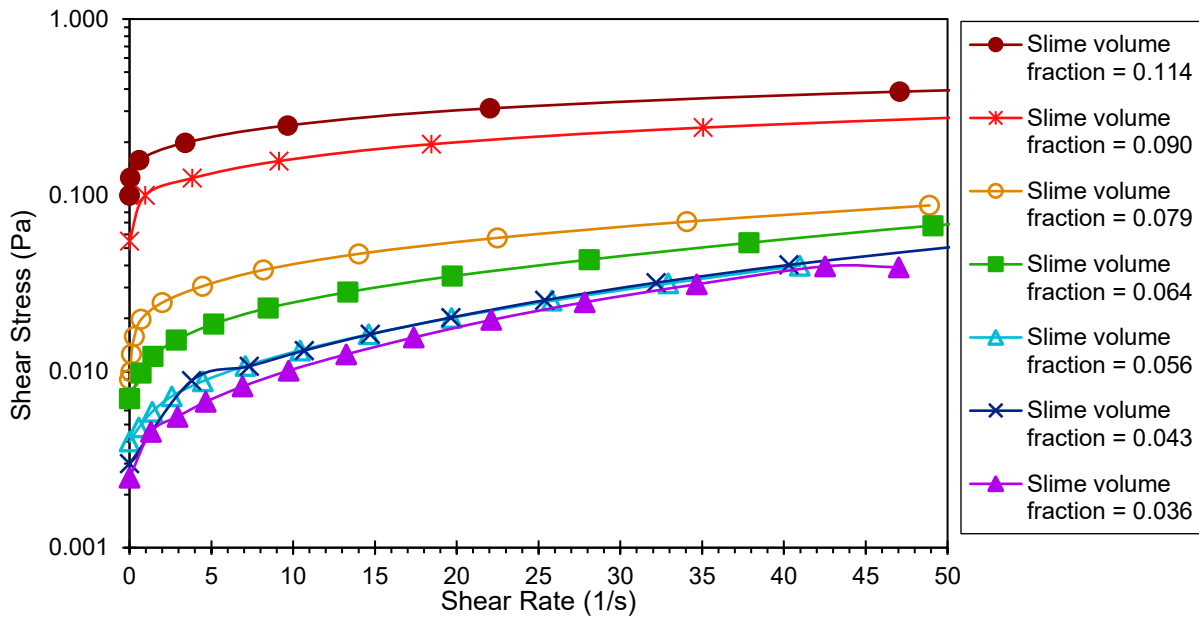


Figure 5.11: Shear stress versus shear rate for varying volume fractions of the sub 0.038 mm overflow particles.

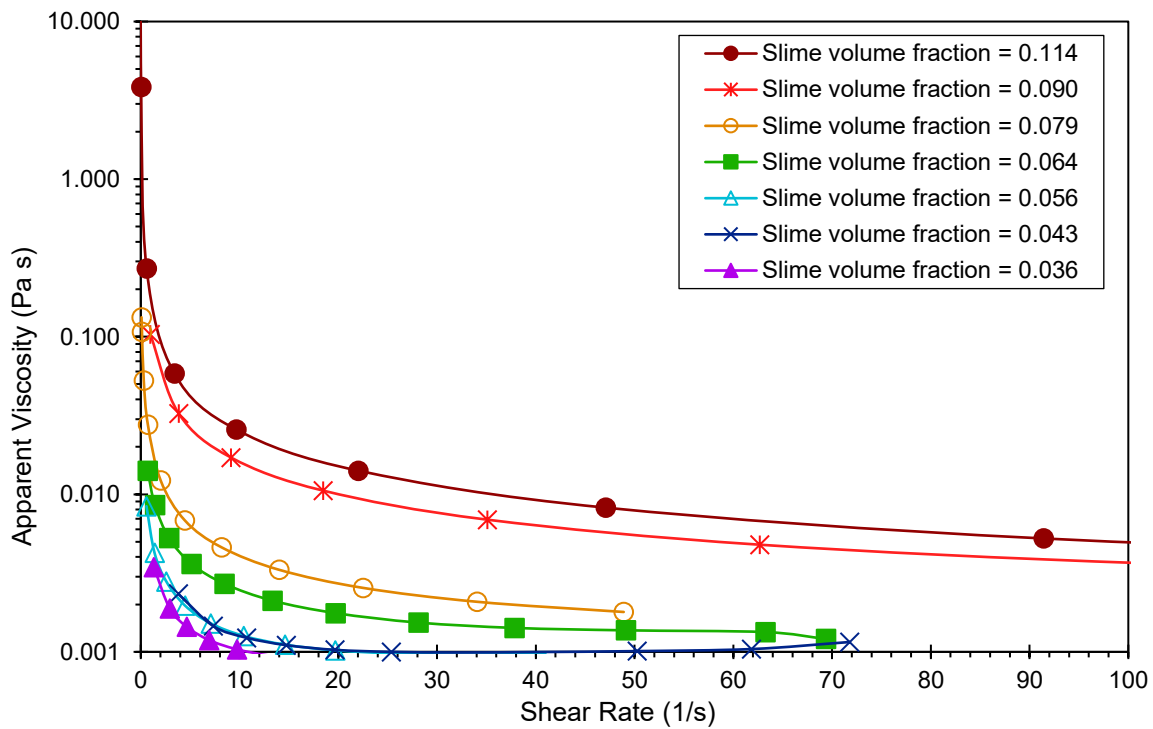


Figure 5.12: Apparent viscosity as a function of shear rate for suspensions of varying volume fractions of the sub 0.038 mm overflow particles.

To collapse all of the data presented in Figure 5.12 into one relationship, an empirical model that included both shear rate and solids volume fraction terms was fitted to the data. The values of the fitted parameters were found by minimising the sum of the squared errors between the model

viscosity and the measured viscosity. Several different forms were trialed, and the following four fitted parameters was selected as the most suitable:

$$\mu_s = \mu \left(1 + K_1 \gamma^a \phi^b + K_2 \gamma \phi \right) \quad (5.1)$$

where K_1 , K_2 , a and b are constants. For dimensional consistency, the units of K_1 and K_2 are (s^a) and (s) respectively. The values of these constants to give the best model fit were: $K_1 = 1.01 \times 10^6 s^a$, $K_2 = 0.40 s$, $a = -0.93$ and $b = 3.98$. Figure 5.13 compares the viscosities calculated using Equation 5.1 with those measured by the rheometer. These are seen to closely follow the line of parity. The raw data and analysis of the rheology are provided in Appendix E.

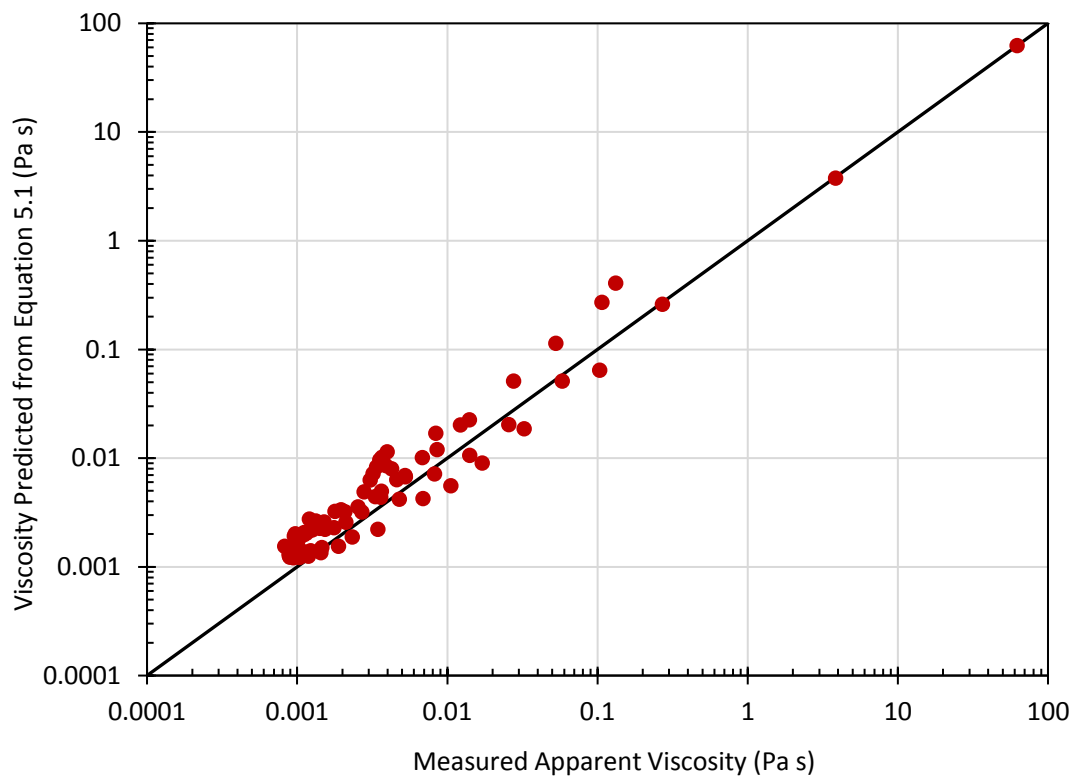


Figure 5.13: Comparison of the measured apparent viscosities with those predicted from Equation 5.1 for the entire set of rheology data.

In addition to the shear rate, the particle volume fraction also has a significant effect on the rheology, as indicated by the large range of shear stresses and viscosities observed for the different samples in Figures 5.11 and 5.12. For a clearer depiction of this, the viscosity values at a fixed shear rate are plotted against the particle volume fraction. In the REFLUX™ Classifier, the shear rate depends on the

fluid velocity through the channels. It also varies depending on the position within the channel, with higher shear rates occurring closer to the walls and zero shear at the centre of the channel. Hence, a range of shear rates must be considered. A simple estimate of the shear rates in these experiments can be made using the flow values of the water component of the overflow stream. From this, the fluid velocity within the inclines can be used to calculate the shear rate according to Equation 3.9.

The shear rate was thus estimated at four locations within the channel; at the surface, at the centre, and at 1/3, and 2/3 of the distance to the centre of the channel. The calculations for this are shown in Appendix F. Using this method, the shear rates across the eleven experiments were estimated to range between 0 and 80 s⁻¹ with an average, across all channel locations, being approximately 16 s⁻¹. It is noted that this value is also roughly where the curves in Figures 5.11 and 5.12 start to become straight. Figure 5.14 shows the viscosity as a function of the particle volume fraction for fixed shear rates of 1, 10, 20, and 40 s⁻¹. It is noted that for the 1 and 10 s⁻¹ shear rate curves, the data points for the sample with particle volume fraction of 0.114 are not shown in order to limit the scale of the graph. Also included in Figure 5.14 is the model of Krieger and Dougherty (1959) (Equation 2.26) with a maximum packing fraction value of 0.64 and intrinsic viscosity of 2.5. This value is for random close packing of rigid spheres. Of course, in these experiments the particles are not rigid spheres and will have some other value for the maximum packing fraction. Here, this model is intended to represent the 'ideal particle' case to which the slimes suspensions can be compared.

Firstly, it is observed that the viscosities measured for the slimes samples correspond to particle volume fractions significantly lower than predicted by the model. With an increasing shear rate the experimental data moves slightly toward the model curve, and with decreasing viscosity, but still remains at volume fractions considerably lower. At a shear rate of 10 s⁻¹, a sharp increase in viscosity is seen after a solids volume fraction of around 0.06. This agrees well with the runs of S24B, S24B2, SD24B3, and in the 1.8 mm channels, S24G3, which showed the lowest separation efficiency. In these runs, the solids volume fractions of the overflow were calculated to be 0.085, 0.083, 0.067, and 0.075

respectively, all exceeding that value of 0.06 where the sharp viscosity increase is seen. In fact, these values exceed the sharp increase point in all the shear rate curves in Figure 5.14. Hence, the lower yields and recoveries seen for these runs could be explained by the significantly higher effective viscosities caused by the slimes. Additionally, the overflow solids volume fractions all other runs were calculated to be less than 0.03, where, in Figure 5.14, the viscosity is low.

In order to quantify the difference between the slimes suspensions and one of 'ideal' solids, as described by the Krieger and Dougherty model, the data at a shear rate of 10 s^{-1} is again used. A scaling factor of 5.5 was applied to the volume fractions using a sum of the squared errors to best match the model. The scaled data is shown to then have excellent agreement with the model results. Thus, the slime particles examined here act as though there is a sphere of influence around them, with a volume 5.5 times larger than the ideal solid particle. This analysis provides a simple comparison between the ideal solids that are well studied throughout literature, and the actual solids studied in this thesis that represent the growing challenge to industry. The scaling factor of 5.5 highlights the vast difference between the two and provides some level of quantification to the viscosity effect that is hindering the separation process. Appendix E contains further details of these calculations.

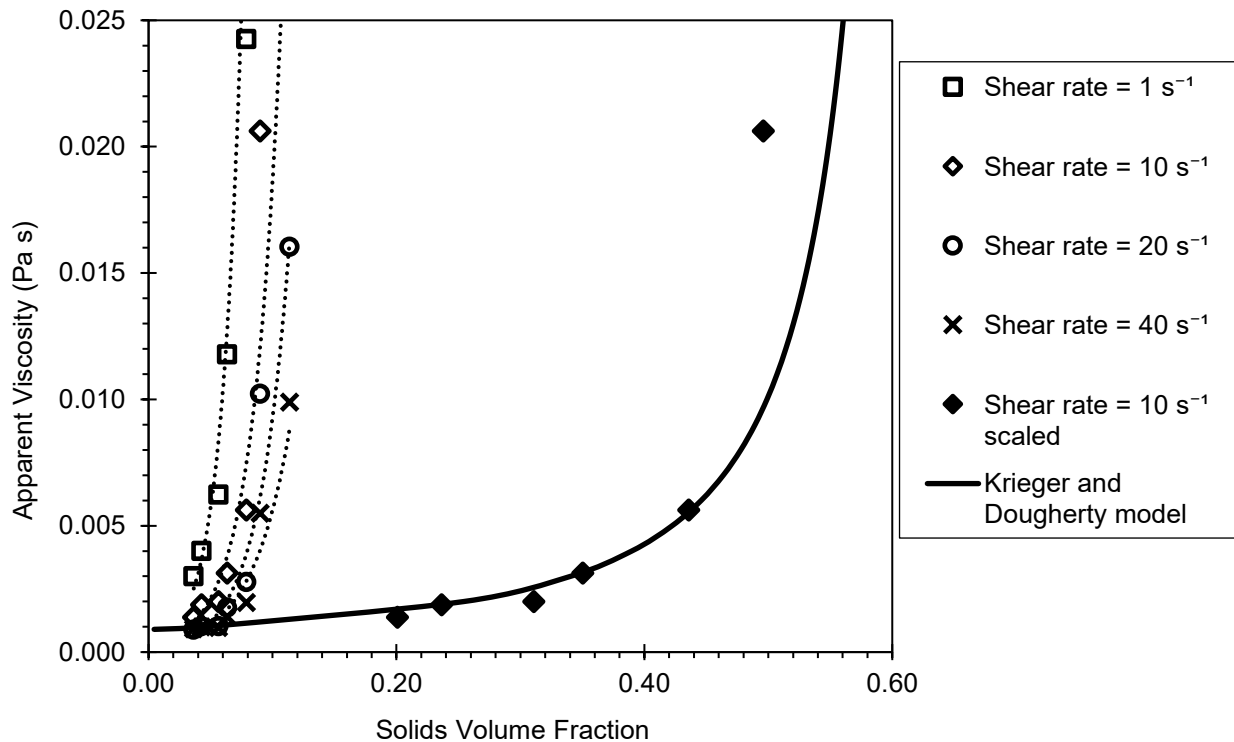


Figure 5.14: Viscosity of the overflow -0.038 mm solids as a function of particle volume fraction for shear rates of 1, 10, 20, and 40 s⁻¹. The solid line shows the model of Krieger and Dougherty (1959) with a maximum packing fraction of $\phi_{max} = 0.64$. The data at a shear rate of 10 s⁻¹ was fit to this model using a scaling factor of 5.5.

The above discussion presented evidence for the significant increase in viscosity that can be caused by the slimes. To demonstrate that the presence of clay particles in the slimes causes adverse effects beyond those that can be described by a standard hindered settling factor, we compared the standard hindered settling approach with a modified one where the slimes were considered part of the liquid phase. This gives it a new apparent viscosity, and only the remaining +0.038 mm material was considered to contribute to the hindered settling effect. Firstly, for the standard approach Stokes law (Equation 2.5) was used to calculate the terminal settling velocities for the d_{50} particles in each run assuming a particle density of 4400 kg/m³. Then using the overflow volume fractions of each run, the Richardson and Zaki equation (Equation 2.13), with the exponent $n = 4.6$, was applied to the Stokes settling velocity to obtain a standard hindered settling velocity for the overflow solids.

In the modified approach, an alternative terminal settling velocity term was calculated to include the effects of the viscous clays. Here, the water viscosity term of Stokes Law was replaced by the effective

viscosity, μ_{eff} , of the -0.038 mm slimes suspension. This term was calculated using the model created to fit our measured viscosity data (Equation 5.1). To be consistent with this model, the solids volume fraction used was for the -0.038 mm overflow solids, calculated for each run using the mass fraction data. The shear rate was assumed to be that experienced by a particle of size d_{50} at the inclined surface as calculated from Equation 3.9 (calculations shown in Appendix F). The Richardson and Zaki equation was again used to find the hindered settling velocity, but this time based only on the solids volume fraction term of the +0.038 mm portion of the overflow solids. Thus, the resulting hindered settling velocity describes the settling of non-slime particles within a slimes suspension. A comparison of this 'slimes hindered settling' velocity to the standard hindered settling velocity is shown in Figure 5.15. It is noted that this figure contains additional data points from runs that will be discussed in Chapter 7.

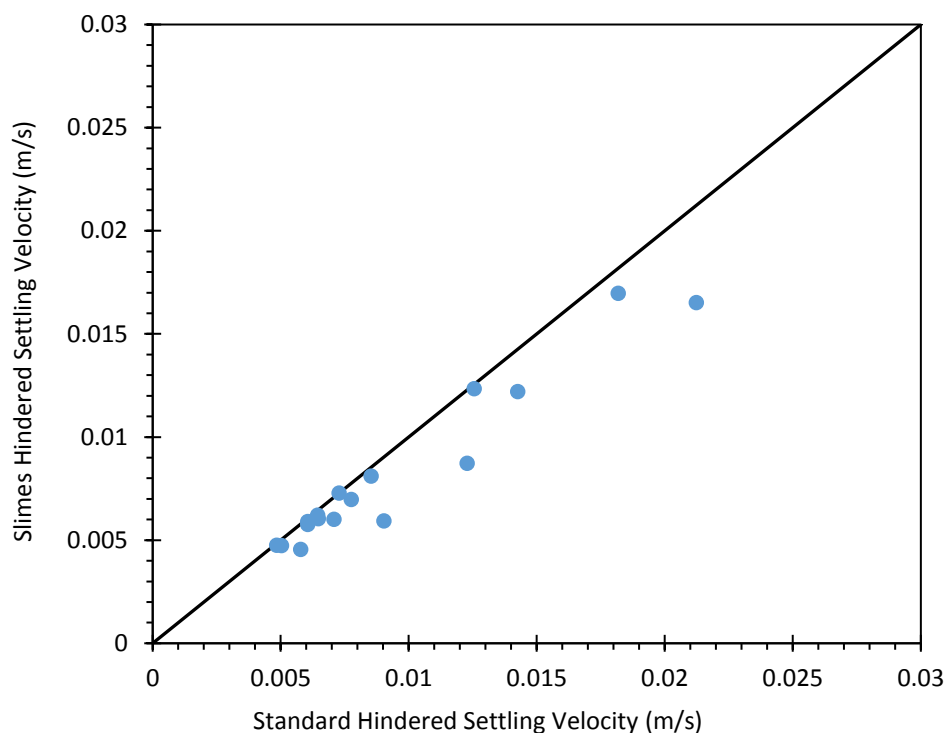


Figure 5.15: Comparison of a standard hindered settling velocity and one calculated to describe the hindered settling of non-slime particles in a slimes suspension.

It is clear that treating the slimes as having an effect on the background liquid viscosity rather than as hindering solids results in a slower settling velocity. Hence, it becomes more difficult to correctly separate denser particles that must settle in this suspension. The points closer to the line of parity

reflect the runs where the viscosity was reduced through dilution and/or higher shear. This analysis was performed for -0.038 mm slimes keeping in line with the rheology work, and because the smallest sieve size used in the mass fraction analysis was 0.038 mm. Hence, the settling of the +0.038 mm particles were considered. If we were to consider the settling of the +20 μm particles, or even all overflow particles in the same slimes suspension, the value of ϕ in the Richardson and Zaki equation increases, hence an even slower settling velocity is attained making the difference between these two settling velocities even greater.

To understand the exact nature of the observations made in this section, in depth characterisation of the slimes would be needed. Correctly identifying the clay type present would inform if this is caused by particle morphology, surface charges, water entrapment, or something else. Knowing this would be valuable in counteracting the effects observed here. The analysis presented here, however, can be used to reasonably explain results of this chapter, showing the significant role of solids concentration and shear rate.

5.5 Concluding Summary

This chapter has presented results from experiments in the REFLUX™ Classifier using a high-grade feed containing a significant portion of slimes. Analysing yield and Fe recovery data showed that the performance varied greatly with changes to the feed solids concentration and flowrates. The effect of shear rate was also examined through experiments using smaller channel spacings. Sudden jumps in Fe recovery, and performance improvements across the entire size range indicated that the solids concentrations and shear rate played a large role in overcoming the difficulties imposed by the slimes.

A clearer explanation of the results was provided through rheological experiments on the overflow slimes. Strong shear thinning effects and sharp increases in viscosity at higher solids volume fractions were observed. Comparison to a semi-empirical model suggested that the slimes particles behave as though they have a volume sphere of influence 5.5 times larger than their actual size. Considering the slimes as part of the liquid phase showed that the hindered settling is greater than predicted by a

standard approach. These observations provided an explanation for the greater separation performance in more dilute and higher shear runs as the viscosity, and hindered settling, was greatly reduced.

The next chapter looks at the separations in REFLUX™ Graviton where high centrifugal force is applied to inclined channel modules, increasing the particle inertia and hence settling velocities. The aim of this is to improve the separation of ultrafines, providing an alternate route for the processing of slimes.

Chapter 6

REFLUX™ Graviton Results

6.1 Introduction

This chapter presents results from experiments performed in the REFLUX™ Graviton. All experiments were performed at a constant centrifuge rotational speed of 351 rpm which, when measured at the overflow weir, is equal to a centrifugal acceleration of 55 G, 539 m s⁻².

Having previously been studied as a semi-batch process (Galvin and Dickinson, 2013), this chapter begins with the first set of experiments trialling the Graviton under continuous steady state conditions. These experiments used a single density feed of ultrafine silica to gain an understanding of the interplay between the operational variables. Results are also compared to the previous study of Galvin and Dickinson (2013). The second section presents results obtained using the iron ore feed material. Here, five different feeds of varying sizes and composition were used to investigate the separation performance of the Graviton in producing a high-grade product, especially in achieving ultrafine desliming. Results are analysed in terms of the size partition curves and in terms of the Fe assays that help quantify the product grade, yield and Fe recovery. Throughout this section, multiple modifications to the system were implemented and hence the effects of these changes are discussed. Finally, experiments were performed on the same high-grade feed used in the REFLUX™ Classifier experiments discussed in the previous chapter. Here, the effectiveness of the Graviton as a desliming unit is discussed and compared to the broader density separation of the RC™. The feed size range was then increased to demonstrate the versatility of the Graviton.

6.2 Silica Feed

This section presents results from the first set of experiments ever performed in the REFLUX™ Graviton under continuous conditions, with the aim of identifying the key variables of operation and comparing the findings to those of the semi-batch study (Galvin & Dickinson, 2013). For simplicity, the feed for these experiments consisted of suspensions of Sibelco Grade 200 G silica powder with a skeletal density of 2650 kg/m³. After each run, the additional process water added during the run (fluidisation, underflow flush and launder wash) was removed by decanting it

from the underflow and overflow tanks. Decantation followed at least 48 hours of settling. After that the solids were recombined for use as feed for the next run. This process resulted in minor losses of some ultrafine particles. Figure 6.1 shows the size distribution of the feed for the initial, middle and final experiments of this campaign of 18 runs, as measured by a Malvern Mastersizer 3000. The distributions shows that there was only a minor reduction in the volume of particles below 10 μm with the measured Sauter mean diameters shifting from 9.5 to 11.9 μm . This variation is not expected to have had any significant effect on the results.

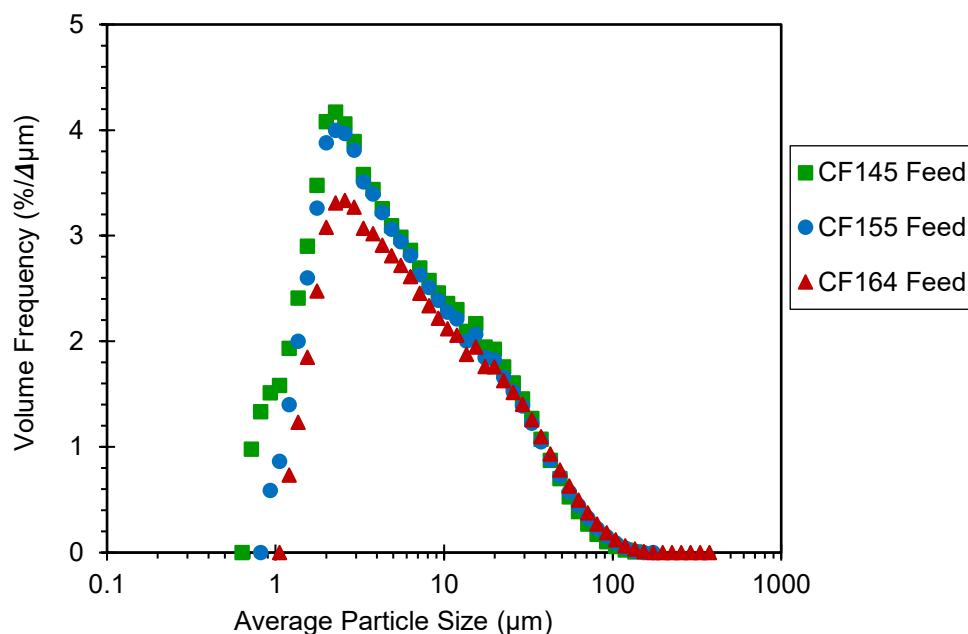


Figure 6.1: Feed particle size distribution for the initial, middle and final runs of the silica suspension experiments. Distributions measured using a Malvern Mastersizer 3000.

Eighteen experiments were performed using the silica feed, altering the variables of feed flowrate, feed solids concentration, fluidisation rate and underflow discharge diameter. Size partition curves were produced for each run from the measured Malvern size distributions of the three streams, as described in Section 4.1.4. In all the partition plots, the solid lines represent the partition curves formed through the best fits of Equation 4.4 using the partition data in the size range 5 – 50 μm , and the reported separation size (d_{50}) and Ep values are the parameters from these fitted curves. Table 6.1 lists the conditions used for each run and the partition d_{50} and Ep results.

Table 6.1: Summary of the experimental conditions of the eighteen runs using the Silica feed along with the d_{50} and Ep values from the partition curves.

Run no.	Feed Flowrate (L/min)	Feed Solids Concentration (wt.%)	Fluidisation Rate (L/min)	Underflow Outlet Diameter (mm)	Separation size, d_{50} (μm)	Ep (μm)
CF145	100	1.9	12	4	9.4	4.6
CF146	98	2.0	18	4	14.4	5.7
CF147	98	2.0	6	4	10.2	5.9
CF148	115	4.0	6	4	11.0	5.3
CF149	111	4.0	12	4	10.7	4.1
CF150	110	3.9	18	4	10.2	4.1
CF152	101	9.9	18	4	12.8	4.5
CF153	49	20.3	18	4	7.8	3.4
CF154	51	29.3	18	4	24.7	14.2
CF155	37	28.0	18	4	5.4	3.0
CF156	35	28.9	30	4	9.0	4.0
CF157	52	30.1	18	4	20.4	12.0
CF158	54	30.2	18	6	6.0	4.9
CF159	115	28.3	18	6	31.5	19.2
CF160	90	28.9	18	6	12.1	5.2
CF162	88	29.6	34	6	19.0	10.0
CF163	82	30.3	24	6	18.6	9.9
CF164	89	30.8	12	6	13.4	7.3

Initial experiments were performed by using a different fluidisation rate, at low feed solids concentrations. Figures 6.2 and 6.3 show the partition curves for sets of runs at 2 wt.% and 4 wt.% solids respectively, each for three different fluidisation rates of 6, 12 and 18 L/min. Similar feed flowrates of 100 and 112 L/min were also used for these two sets of runs. A constant underflow outlet diameter of 4 mm was used throughout, resulting in consistent underflow discharge rates between 18 – 21 L/min.

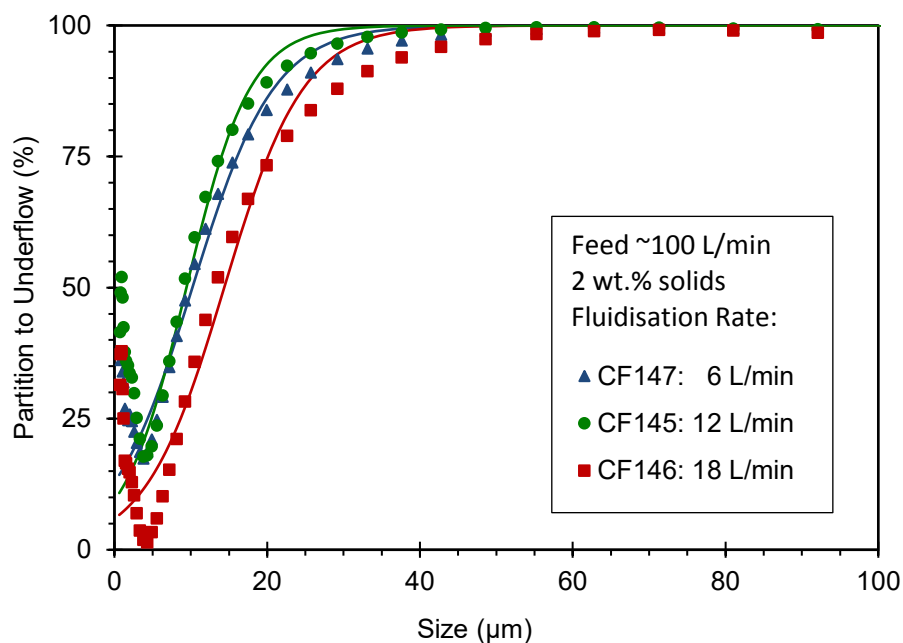


Figure 6.2: Partition curves for the Runs CF145, CF146, and CF147 demonstrating the effect of fluidisation rate (shown in legend) at a constant feed solids concentration of 2 wt.% and feed flowrate of 100 L/min.

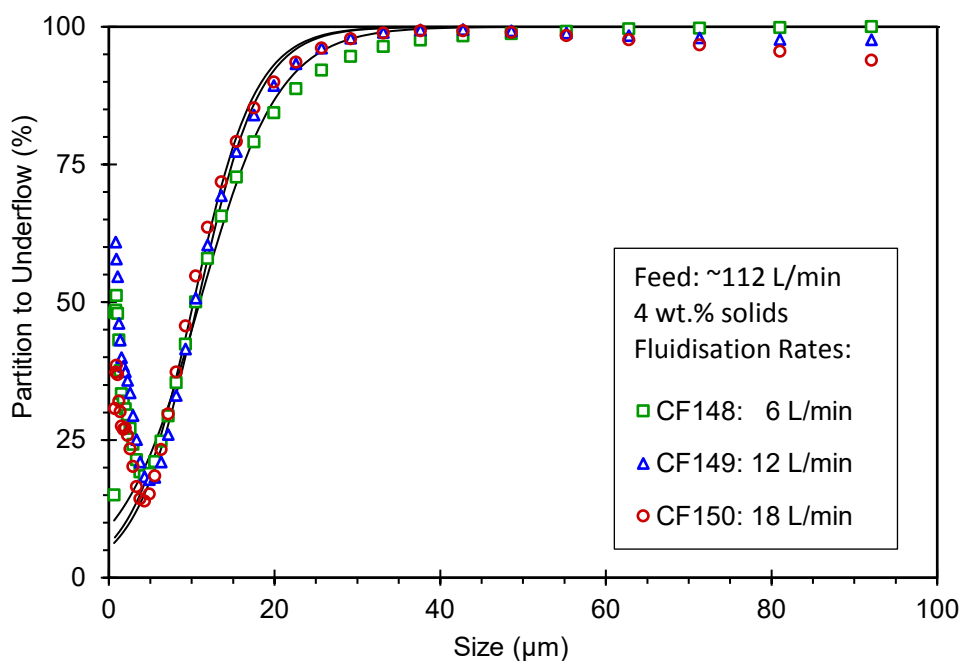


Figure 6.3: Partition curves for the Runs of CF148, CF149, and CF150 demonstrating the effect of fluidisation rate (shown in legend) at a constant feed solids concentration of 4 wt.% and feed flowrate of 112 L/min.

Figures 6.2 and 6.3 display consistent, sharp size partitions. In each case apart from one, the separation size was between 9 and 12 μm with low Ep values of 4 – 6 μm . The one outlier (CF146) was performed at the lowest feed solids concentration, and the

highest fluidisation rate, perhaps indicating an excess of upward fluid entraining more particles to overflow. These initial runs clearly demonstrated that the Graviton is capable of achieving consistently sharp separations at ultrafine sizes.

A feature of all the partition curves here is the so called “fish-hook” effect (Roldán-Villasana et al., 1993; Majumder et al., 2003; Zhu & Liow, 2014) For each run, the partition curve has a minimum at a particle size of approximately 5 µm. The curves then rise sharply at finer sizes. For the 2 wt.% solids runs (Figure 6.2), an increase in fluidisation rate caused a decrease in the minimum partition value. The 4 wt.% solids runs (Figure 6.3) also shows this trend but it is far less pronounced. Hence, as the fluidisation rate increases, the “fish-hook” effect decreases.

The fluidisation of the particles is key for the performance of the system. If the lower bed is not sufficiently fluidised, then more ultrafines are entrained with the coarse particles reporting to the underflow. The discharge is then similar to that observed in a hydrocyclone. With enough fluidisation however, a fluidised bed can form which provides a means for efficiently washing the ultrafines upwards toward the overflow, although some amount of entrainment is always inevitable. The level of entrainment thus depends on the bias flux, the net superficial velocity of water in the lower chamber part of the Graviton. This is given by the fluidisation flux minus the underflow water flux (Galvin et al., 2012). With a positive bias flux, the net flow of water in the fluidisation zone is in the upwards direction towards the overflow, resulting in more efficient desliming. Given that the underflow discharge rate in these initial experiments was very similar, approximately 20 L/min, the increase in fluidisation rate from 6 to 18 L/min increased the bias flux from around negative 14 L/min to close to zero. Hence, the increase in bias flux explains the lowering of the fish-hook minimum at higher fluidisations.

As explained in Section 4.1.2, a design flaw of the Graviton resulted in a portion of the overflow stream being misplaced into the underflow launder. Separate trials, closely monitoring water flows, found that approximately 5 vol.% of the overflow was misplaced into the underflow

launder. The overflow rates throughout this study range between 50 – 100 L/min, hence, up to 5 L/min would be misplaced to the underflow after separation. The underflow rates are considerably lower than the overflow, and thus this misplaced material may contribute to around 25 % of the volumetric flow of the underflow. However, the solids concentration in the overflow is far lower than in the underflow, hence the overflow splashing should only contribute 1 to 2 % of the solids present in the underflow samples. Hence, it is estimated that eliminating this issue would lower the minimum of the fish-hook by around 5 partition percentage units. It is again emphasised that this issue stems from the Graviton being a re-purposed centrifuge, and would be eliminated in a custom designed unit, thus improving the results.

The next set of runs investigated the effect of operating at much higher feed solids concentrations. Figure 6.4 shows the partition results for runs at 20, 29, and 30 wt.% solids, all at a feed rate of 50 L/min and fluidisation rate of 18 L/min. The run performed at 20 wt.% solids achieved a sharp separation similar to the previous low concentration runs with a separation size of 7 μm and E_p value of 5 μm . The two higher concentration runs, however, showed poorer separations. This is attributed to the rate of solids seeking to exit through the underflow, exceeding the solids capacity of the underflow outlet. In the experiments presented thus far, the diameter of the underflow outlet was 4 mm. It is speculated that in these two higher concentration experiments, the solids could not easily exit the underflow, leading to an accumulation of solids in the system. This results in more hindered settling, and more coarse particles reporting to the overflow.

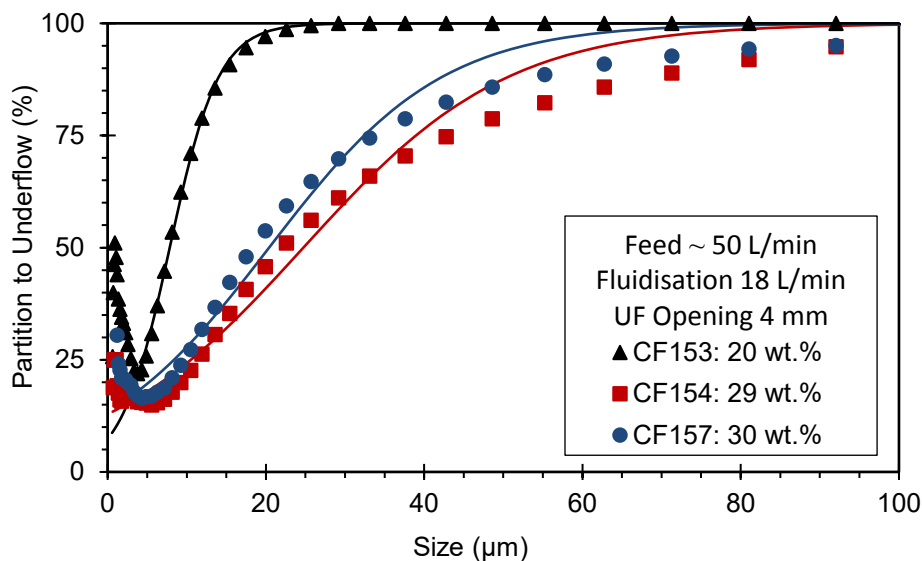


Figure 6.4: Partition curves the Runs CF153, CF154, and CF157 performed at a constant feed flowrate of 50 L/min and fluidisation rate of 18 L/min. Increasing the feed solids concentration (shown in legend) exceeds the solids capacity of the 4 mm underflow.

In order to accommodate higher solids concentrations the underflow outlet diameter was increased from 4 mm to 6 mm. Figure 6.5 shows the partition results for three runs with this 6 mm diameter underflow outlet all performed with a constant fluidisation rate of 18 L/min and feed solids concentration of 30 wt.%, the same concentration that produced poor separations in Figure 6.4. For these runs the feed volumetric rate was increased to the point of significant deterioration. The first increase from 54 to 90 L/min shifted the separation size from 6 to 12 µm whilst maintaining a similar E_p value of ~ 5 µm. Perhaps of greater significance is the dramatic reduction in the ultrafine fish-hook for the 90 L/min run. Here, a higher solids rate in the underflow corresponds to a lower proportion of water reporting to underflow. Thus, with less entrainment of the ultrafines in the liquid bypass, the minimum of the curve was much lower.

Further increasing the feed flowrate to 115 L/min resulted in the separation performance again deteriorating. The “tipping point” for a poor separation is again related to the solids rate in the underflow exceeding the outlet capacity. Thus, neither the feed flowrate nor the solids concentration is individually responsible; rather, it is their combination that affects the solids rate seeking to exit the limited area of the underflow outlet. In Figure 6.4, the poor separation involving a feed flowrate of 50

L/min and solids concentration of 30 wt.% was amended through the use of a larger underflow outlet diameter. With the same conditions, but with the larger underflow diameter, a sharp separation was achieved but with the consequence of a much higher proportion of feed water reporting to the underflow. This resulted in more entrainment of the ultrafine particles to the underflow, hence, a significantly higher fish-hook minimum. This water split was then reduced using the higher feed rate of 90 L/min, achieving a better balance over the underflow size and the amount of solids seeking to discharge.

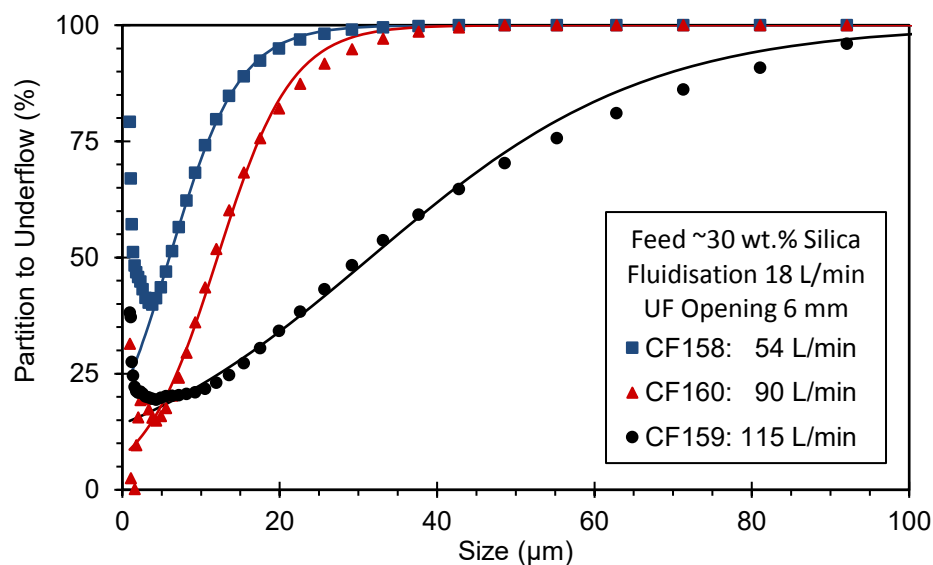


Figure 6.5: Partition curves for the Runs CF158, CF159, and CF160 performed at a constant feed solids concentration of approximately 30 wt.% and fluidisation of 18 L/min. Increasing the feed flowrate (shown in legend) exceeds the solids capacity of the 6 mm underflow.

A series of experiments was then conducted, systematically altering both the feed flowrate and solids concentration, with the aim of demonstrating sharp separations across a range of conditions by maintaining the balance between the solids rate and the underflow capacity. The partition curves for these runs are shown in Figure 6.6. These runs involved the smaller, 4 mm diameter underflow outlet, at a constant fluidisation rate of 18 L/min. To maintain similar solids throughputs, as the feed solids concentration increased, the feed rate was decreased. The results show sharp separations with E_p values between 3 and 5 µm. As the feed flowrate was increased, the separation size shifted from 5.4 to 12.8 µm. With higher feed rates there was also lower minimum in the fish-hook. As with

the results in Figure 6.5, this was due to a lower percentage of the feed water reporting to the underflow, hence, less entrainment of the ultrafine particles.

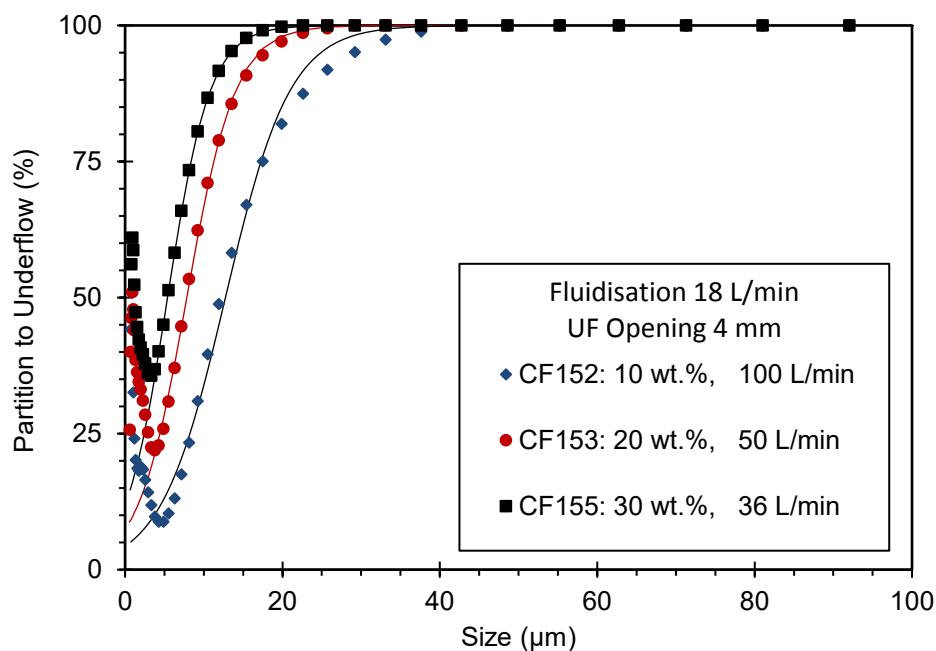


Figure 6.6: Partition curves for the Runs CF152, CF153, and CF155 performed at a fluidisation rate of 18 L/min with an underflow outlet diameter of 4 mm. The results show the effect of balancing an increasing feed solids concentration by lowering the feed flowrate (both shown in legend).

The next sets of experiments examined the effect of fluidisation rates at higher solids concentrations, as opposed to the earlier runs (Figures 6.2 and 6.3) that had very low concentrations. Firstly, runs performed using the 4 mm diameter underflow outlet are shown in Figure 6.7. These two runs used solids concentration of 28 wt.% and a very low feed flowrate of 36 L/min. As seen in Figures 6.2 and 6.3, an increase in the fluidisation rate decreased the minimum of the partition fish-hook effect. In this case, the fluidisation increase was a very large relative to the low feed rate.

The second set of these experiments was performed again at 30 wt.% solids but with the 6 mm diameter underflow outlet, and with much higher feed flowrates, ranging from 82 to 90 L/min (Figure 6.8). Under these conditions a fluidisation rate of 18 L/min was found to give the sharpest separation and also the lowest minimum in the fish-hook. Contrary to previous results, the lower fluidisation rate of 12 L/min actually produced a higher separation size at a slightly higher Ep . Given the much higher solids rates involved (feed rate of ~90L/min compared to 36 L/min in Figure 6.7 for the same solids

concentration), this is possibly due to the low fluidisation allowing excess solids to concentrate near the underflow, edging closer to the capacity of the 6 mm outlet. At the higher fluidisation rates, the separation performance again worsened. For these runs, excess fluidisation limited the rate at which solids can exit the underflow as the greater upward flow reduces the solids concentration in the lower bed. As expected from previous results, the higher fluidisation rates resulted in a slight decrease in the fish-hook minimum. It is noted, however, that with excess fluidisation, turbulent mixing in the lower section can misplace ultrafines to underflow, as is likely the case here. Overall, this work has shown an optimal fluidisation rate of 18 L/min produces a sharp separation whilst minimising the fish-hook effect. This separation is possible even at high solids concentrations, provided the solids rate is within the capacity limit of underflow outlet.

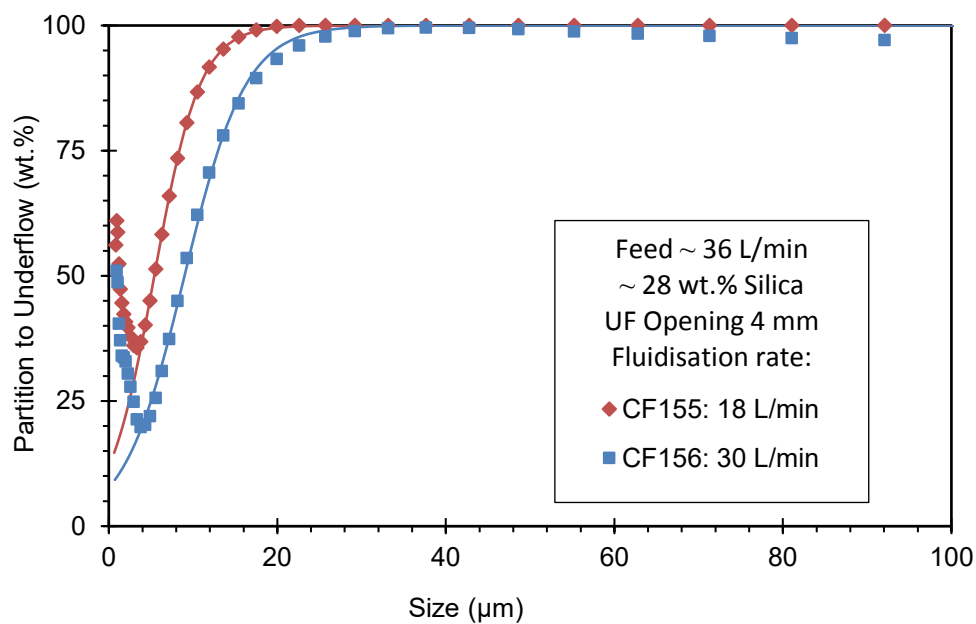


Figure 6.7: Partition curves for the Runs CF155 and CF156 performed with a feed flowrate of 36 L/min and solids concentration of 28 wt.% with the 4 mm underflow outlet.

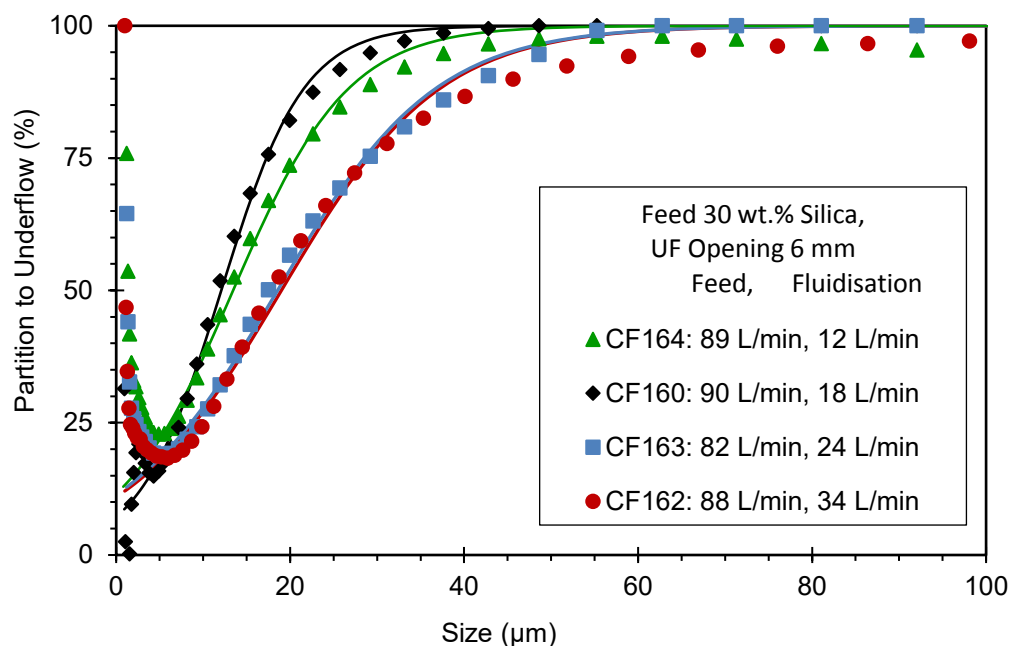


Figure 6.8: Partition curves for the Runs CF164, CF160, CF163, and CF162 performed at a feed solids concentration of 30 wt.% with the 6 mm underflow outlet.

Clearly, the underflow solids capacity is critical in the performance of the Graviton. This is because, unlike in a conventional REFLUX™ Classifier, there are significant technical difficulties in controlling this flowrate in real time using a control valve. Figure 6.9 shows the variation of the E_p value as a function of the underflow solids flux across all the experiments. Here, the underflow solids flux is defined by the area of the underflow opening for just one of the two modules in the Graviton. The data for the 4 mm diameter underflow tube shows a reasonably consistent E_p of around 5 µm for most runs. However, this value increased dramatically above a critical underflow solids flux of approximately $3 \text{ m}^3/(\text{m}^2 \text{ s})$. This finding supports the notion that the underflow outlet diameter governs the volumetric rate and hence, solids capacity, of the underflow discharge. Additionally, the flowrate in the inclined channels governs the particle size classification. This in turn alters the portion of the solids that seek to report to the underflow. At higher feed solids concentrations, or feed volumetric flowrates, the rate in which these solids report to the underflow increases. If this rate exceeds the capacity of the specific underflow outlet, the solids concentration within the system increases, leading to more hindered settling and, as a result, a higher portion of particles reporting to the overflow. This is confirmed by Figure 6.10, which shows the solids concentration in the overflow

versus that in the underflow in terms of volume percentages. This plot shows that the overflow concentration only increased slowly with increasing underflow concentration up to around 20 vol.%. However, beyond that point, which was where the high Ep runs occurred (open symbols), the overflow concentration increased dramatically. It is this point where the underflow capacity has been reached and more solids are forced to report to the overflow, causing the poor Ep values.

In Figure 6.9, the data for the 6 mm diameter underflow is more scattered, with some lower underflow solids flux runs showing high Ep values. Here the critical flux appears to be only $\sim 2.2 \text{ m}^3/(\text{m}^2 \text{ s})$, less than the value of $\sim 3 \text{ m}^3/(\text{m}^2 \text{ s})$ for the 4 mm outlet. This is surprising since it might be expected that the reduced wall effects in a larger outlet would permit a larger underflow solids flux. However, there is evidence to suggest these were flawed measurements. At the conclusion of these high flowrate experiments, as per usual, the RC™ modules were subject to cleaning. During this processes it was observed for Run CF162 that the underflow exit tubes on both sides were partially blocked and for Run CF159 that one of the underflow exit tubes was completely blocked with solids. Hence, the assumption that there was full flow through both these underflow tubes that was used to calculate the underflow flux was incorrect. The actual area available for flow was reduced by the blockage, and so the actual underflow solids flux would have been (as expected) higher than calculated. This hypothesis is supported by Figure 6.11, which shows the underflow solids rate versus the feed solids rate. The high Ep runs identified in Figure 6.9 are again shown by the open symbols. The data from these high Ep runs, and only from these runs, all lie below the trend line of the entire set of runs, suggesting that the underflow capacity was exceeded, creating a partial or complete blockage that lowered the rate measurements.

A similar concept of underflow capacities is also seen in hydrocyclones (Heiskanen, 2000). Here, the diameter of the spigot governs the underflow capacity. Operating above this capacity leads to roping behaviour and a sharp deterioration in performance. To describe this relationship, Jull (1972) and Plitt et al. (1987) proposed that the flow condition for roping scaled with the diameter of the spigot

opening to the power of 2.12 and 2.35 respectively. In the present work, we have presented results in terms of solids flux (volumetric flow per unit of area), hence, scaling the underflow diameter to the power of 2.0. With this limited data set, an exercise in more precise scaling has not been attempted.

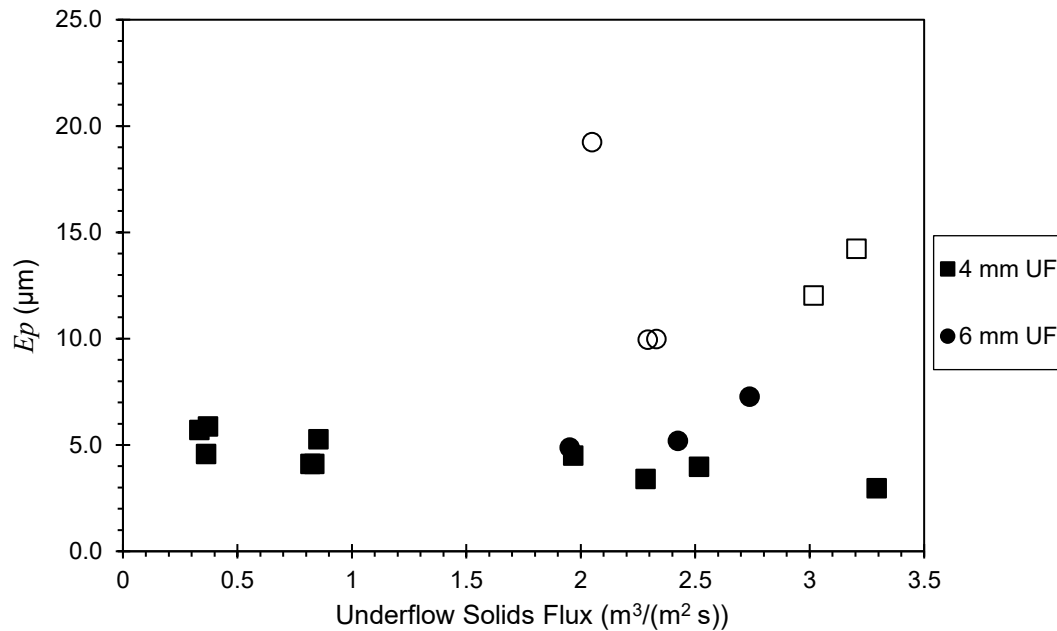


Figure 6.9: E_p values versus the underflow solids flux, defined by the area of the underflow opening for one module. Open symbols are used for the runs showing a poor separation with $E_p \geq 10$ µm.

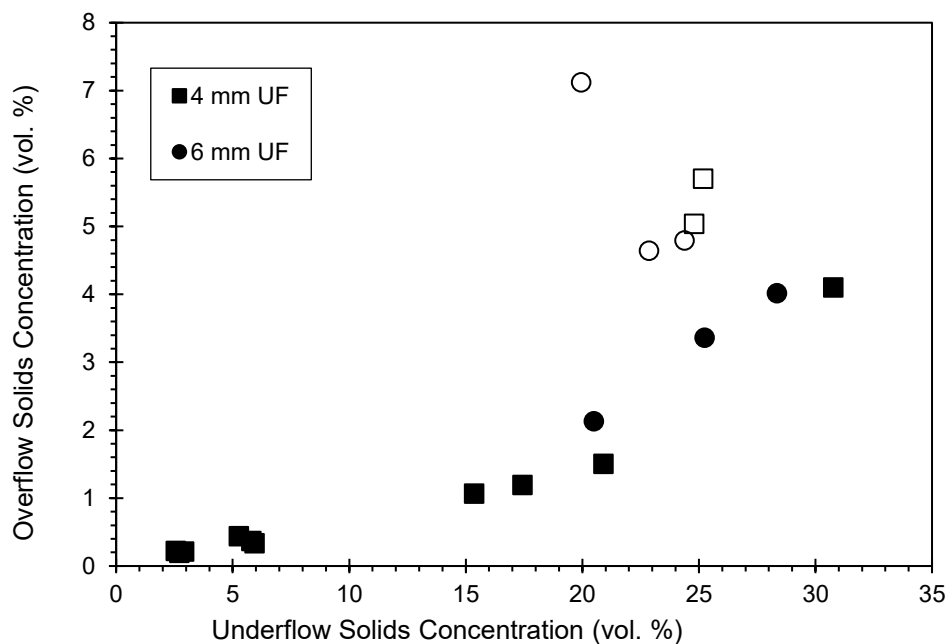


Figure 6.10: Overflow solids concentration versus the underflow solids concentration. Open symbols are used for the high E_p runs identified in Figure 6.9.

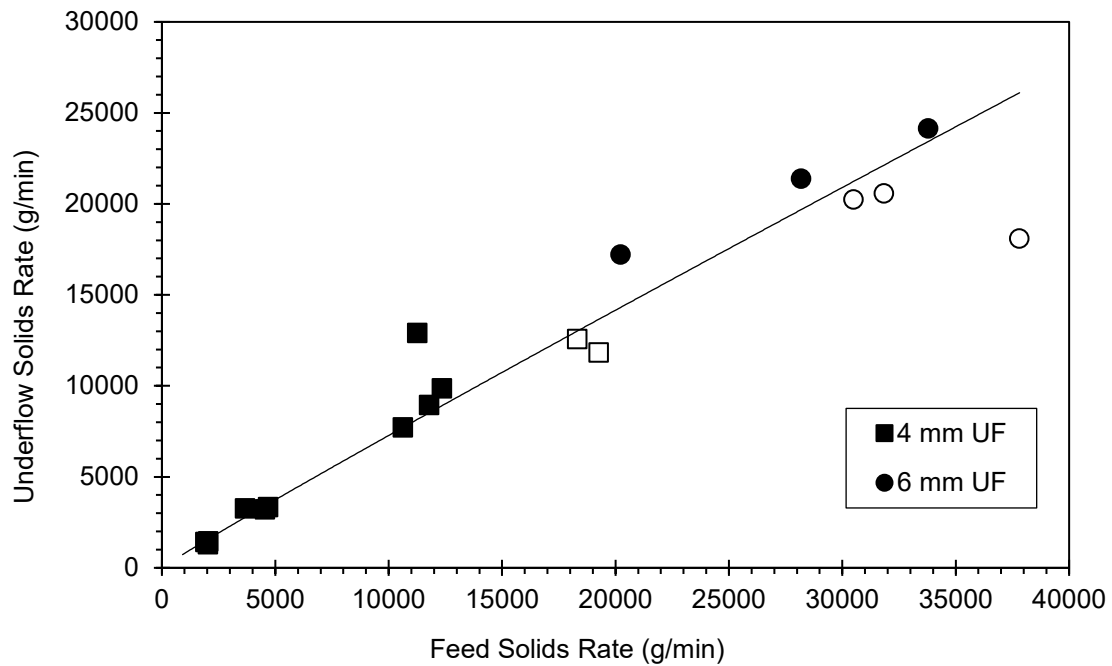


Figure 6.11: Solids rate in the underflow versus the solids rate in the feed. Open symbols are used for the high Ep runs identified in Figure 6.9. The linear trend line was fitted using all the data points.

The throughput advantage for each run was calculated using Equation 3.16, comparing the experimental values, $F = U'/u'_t$ with those predicted from the model, $F = Gz/3d$. This comparison of the actual throughput advantage with the predicted one is presented in Figure 6.12. The clear outliers are again the high Ep runs, shown by the open symbols. Ignoring these points, the rest of the data is in good agreement with the theory. These results show similar accuracy to the results at the same centrifugal force ($G = 55$) in the semi-batch study of Galvin and Dickinson (2013) (Figure 3.12). Throughput advantages of over 1000 were achieved in these experiments.

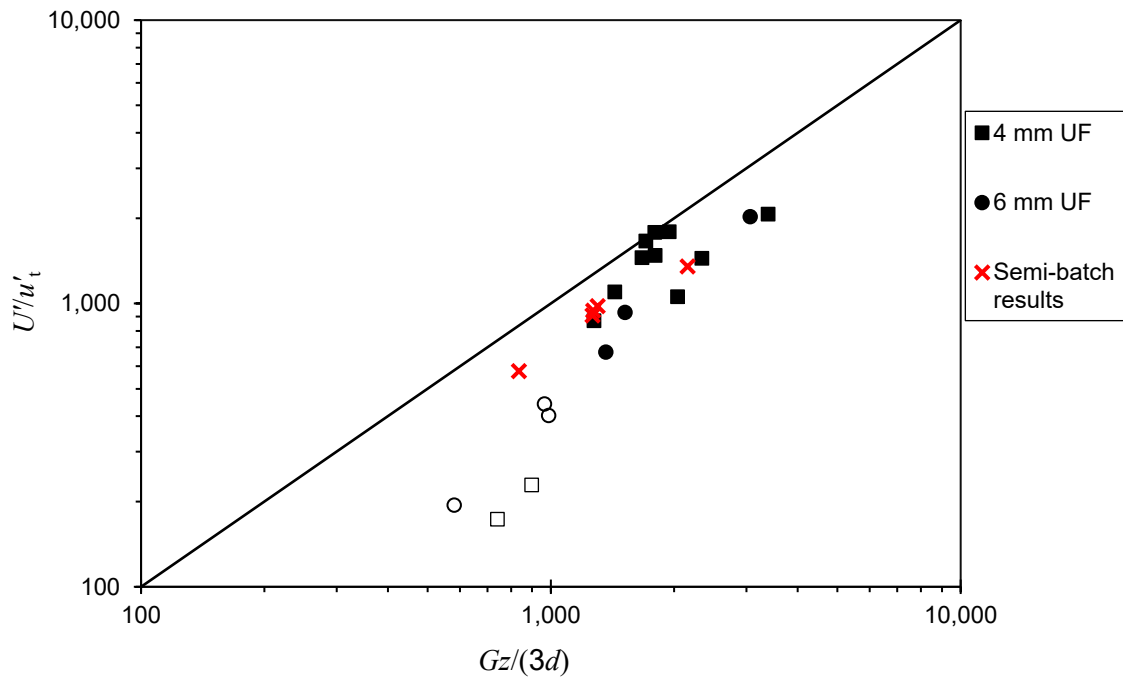


Figure 6.12: Throughput advantage as calculated by Equation 3.16. The terminal settling velocity in inclined channel, u'_t , was calculated using Stokes law (under normal gravity) for a particle of the separation size d_{50} . Open symbols are used for the high Ep runs identified in Figure 6.9. The red crosses show the results from the semi-batch study of Galvin and Dickinson (2013) at $G = 55$.

Equation 3.16 was also used to calculate the theoretical separation size by incorporating the known superficial channel velocity and Stokes law. It is noted that this calculation ignores any effects of hindered settling. Figure 6.13 compares this theoretical separation size with the d_{50} value obtained from the partition curves for each experiment. All of the data points lie below the line of parity, however, given the same divergence is seen for the throughput advantage model in Figure 6.12, this is reasonable. The high Ep runs (open symbols) are again clear outliers.

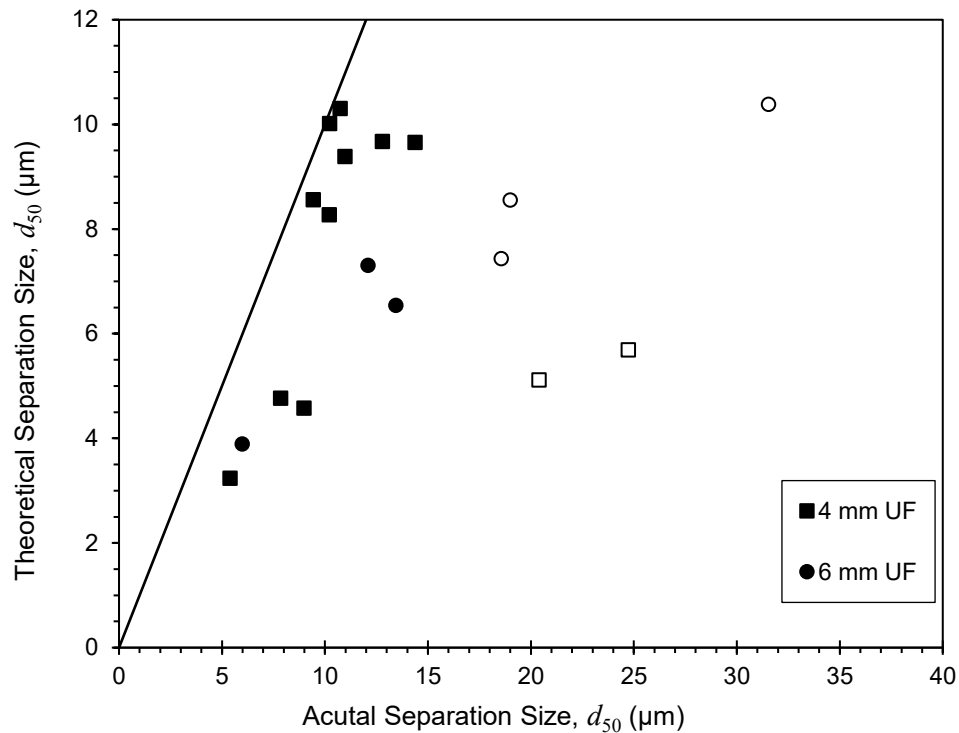


Figure 6.13: Theoretical separation size, calculated from Equation 3.16, versus the actual separation size. Open symbols are used for the high Ep runs identified in Figure 6.9.

These initial studies on the continuous steady state separations using the Graviton unit have made several important findings. Firstly, the capability of the Graviton for producing sharp and consistent separations at ultrafine sizes has been demonstrated. The work has also highlighted the importance of key variables including the fluidisation rate, feed volumetric rate and solids concentration, and the size of the underflow outlet. Ultimately, the solids rate seeking to report to the underflow was found to have the biggest impact on the separation performance. Having identified the role of these variables, better control of the separation, including the minimisation of the fish-hook effect, is possible. Finally, this work has confirmed the findings from the semi batch study (Galvin & Dickinson, 2013), with both sets of results being consistent. The proposed model of Equation 3.16 shows good agreement with the experimental results. The throughput advantage of over 1000-fold confirms the benefits of combining the inclined channels with centrifugal force.

6.3 Iron Ore Feeds

With the knowledge gained from the initial trials based on the silica feed, the Graviton was then used for separations of five different iron ore feeds. These feeds varied in size distribution and grade. In addition to the size partition results, these experiments were also analysed in terms of iron recovery and upgrade. Table 6.2 provides a summary of the run conditions used across each of these feeds along with the d_{50} and Ep values from the partition curve results. The head grades for each stream (raw data) and the associated solids yield to underflow and Fe recovery, calculated using the two-product formula, are also given.

Table 6.2: Summary of the run conditions for all experiments across the five iron ore feeds. Partition d_{50} and Ep results, head grades of the Feed, Underflow and Overflow streams and the solids yield to underflow and Fe recovery are also listed.

Run no.	Feed Flowrate (L/min)	Feed Solids Conc. (wt.%)	Fluidisation Rate (L/min)	Underflow Outlet Diameter (mm)	Sep. Size, d_{50} (μm)	Ep (μm)	Head Grades (wt.% Fe)			Solids Yield (wt.%)	Fe Recovery (%)
							Feed	U/F	O/F		
Iron Ore Feed 1											
CF184	140	4.7	36	8	14.5	6.6	47.5	54.1	35.8	63.9	72.8
CF185	145	18.2	36	8	13.9	6.7	47.1	55.1	36.0	58.1	68.0
CF186	140	24.0	34	8	15.0	7.5	46.9	54.8	36.1	57.8	67.5
CF188*	144	8.5	36	8	9.7	4.4	55.2	58.2	39.4	84.0	88.6
Iron Ore Feed 2											
CF195	149	18.5	34	8	14.2	8.4	31.6	37.8	15.4	72.3	86.5
CF196*	149	14.2	36	8	7.0	7.8	38.8	40.2	16.8	94.0	97.4
CF197	138	19.8	33	6	20.8	9.8	32.7	37.4	14.8	79.2	90.6
CF198*	152	9.2	36	6	14.2	6.5	36.2	42.2	20.4	72.5	84.5
CF200	115	19.0	64	6	20.4	11.3	32.8	39.0	16.8	72.1	85.7
CF201	105	19.5	50	4	32.8	31.8	34.0	46.6	16.5	58.1	79.7
CF202	105	18.6	50	3	51.6	37.6	33.8	51.7	16.9	48.6	74.3
CF203*	93	8.1	50	3	19.2	21.1	47.0	53.0**	36.6	63.4	71.5
CF206	105	19.9	50	3	53.8	42.4	33.6	50.6	18.3	47.4	71.3
CF207*	105	6.1	64	3	22.1	13.1	47.9	53.7	27.0	78.3	87.8
CF209	65	10.1	64	2	53.8	49.7	32.7	48.1	19.5	46.2	67.9
Iron Ore Feed 3											
CF215	63	11.4	18	3	14.7	8.0	55.4	63.5	49.0	44.1	50.6
CF217	62	9.8	36	3	15.4	6.0	56.2	63.0	48.0	54.7	61.3
CF218	60	11.5	54	3	16.9	6.2	56.8	63.8	48.6	54.0	60.6
CF219	100	9.0	18	3	13.6	5.8	55.9	63.8	47.9	50.3	57.4
CF220	92	9.3	36	3	20.6	6.3	54.9	64.0	49.5	37.2	43.4
CF221	99	9.2	54	3	19.7	7.0	52.9	63.5	49.2	25.9	31.1
CF222	96	8.7	54	3	13.3	4.3	56.1	62.4	47.3	58.3	64.8
CF223*	101	3.2	54	3	9.2	2.7	63.6	64.2	49.3	96.0	96.9

Iron Ore Feed 4											
CF232	102	4.1	36	3	16.0	5.8	64.6	67.5	37.9	90.2	94.3
CF233	52	4.1	36	3	15.4	6.0	Not Tested			-	-
CF235	52	8.3	54	3	18.1	6.3				-	-
CF236	101	7.7	54	3	19.4	6.5				-	-
CF238	110	4.0	54	3	17.9	5.8				-	-
Iron Ore Feed 5											
CF245	52	10.1	18	3	15.0	6.1	56.2	63.2	39.9	70.0	78.7
CF246	52	10.2	36	3	16.0	5.8	56.6	63.9	41.7	67.1	75.8
CF247	52	9.9	12	3	13.1	6.3	51.6	62.9	39.1	52.5	64.0

*2nd Stage run

**Head grade re-tested including solids stuck in underflow launder = 58.5 wt.% Fe

6.3.1 Iron Ore Feed 1

The first iron ore experiments were conducted using a hematite feed that was initially diluted, with higher solids concentrations being used for each successive run. Figure 6.14 shows the particle size distributions for each run using this feed. The feed distributions were very consistent across the three runs with the Sauter mean diameter only changing from 2.85 – 2.88 μm . External XRF analysis measured the feed to have a head grade of ~ 47 wt.% Fe.

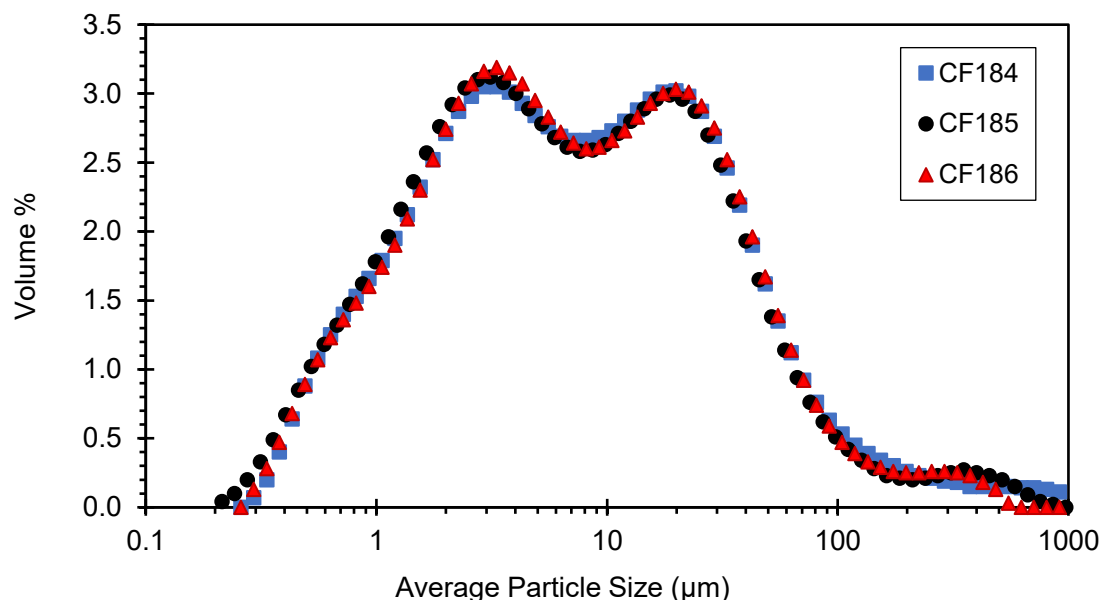


Figure 6.14: Particle size distributions of the feed samples taken for Iron Ore Feed 1 experiments as measured by a Malvern Mastersizer 3000.

Three experiments were performed with this feed at solids concentrations of 5, 18, and 24 wt.%. The feed flowrate and fluidisation rates were kept constant at 140 L/min and 36 L/min respectively. Given that these conditions result in quite high solids throughputs compared to the previous silica work, a larger underflow outlet of 8 mm was used in order to provide adequate underflow capacity. Figure 6.15 shows the partition curves for these runs. Remarkably consistent separations were obtained, with the separation size and E_p values only varying from 14 – 15 μm and 6.6 – 7.5 μm respectively. Run CF186 shows no fish-hook, rather, a flattening of the partition before decreasing again at the finest sizes. This is likely a measurement error in the Malvern laser sizings of the Overflow sample, which when used in Equation 4.2b, resulted in an abnormal partition tail. Using the sizings from the Underflow sample (Equation 4.2a), the fish-hook follows the same trend as Runs CF184 and CF185. This result indicates that the feed solids concentration has little to no effect on the partition in this concentration range. However, it is anticipated that further increasing the solids concentration would reveal the limit to the underflow capacity and the performance would considerably deteriorate as was seen in the silica work.

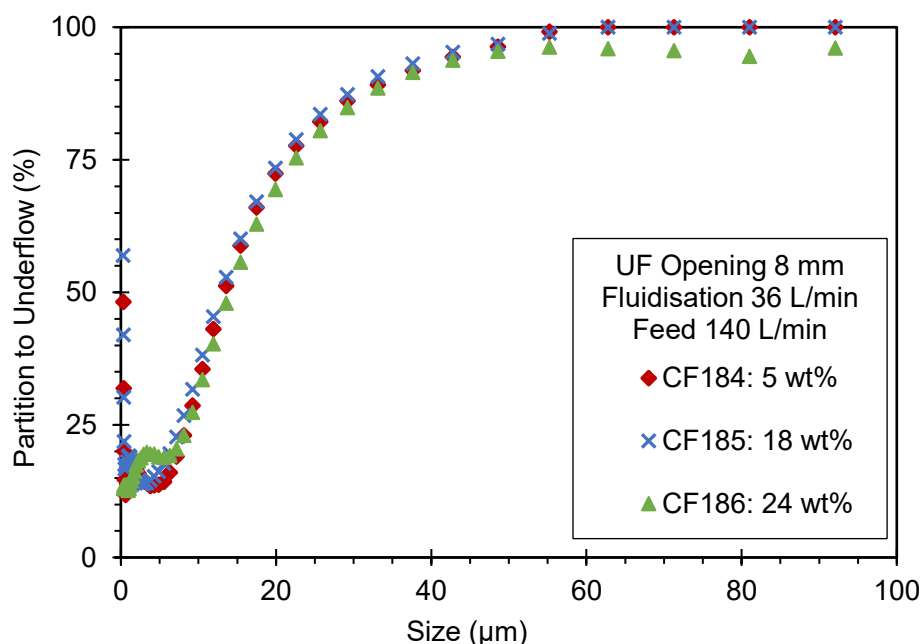


Figure 6.15: Partition curves for Runs CF184, CF185, and CF186 performed on Iron Ore Feed 1 with the 8 mm underflow opening at a fluidisation rate of 36 L/min and feed flowrate of 140 L/min.

The potential of the Graviton as a two-stage separator was assessed by collecting the underflow from Run CF186 and processing it as a feed for Run CF188. Most conditions for the second stage (CF188) were identical to the first (CF186), however in order to allow for a reasonable run time, the first stage underflow had to be diluted to create a sufficient volume of feed. Hence, the second stage was operated at a lower solids concentration, although the results of Figure 6.15 suggest this should have little effect on the separation. Figure 6.16 shows the partition curves for these runs along with the combined curve for the two-stage separation. The second stage partition shows a much finer, sharper separation with an Ep of $4.4\ \mu\text{m}$ and separation size of $9.7\ \mu\text{m}$. This improvement compared with the results in Figure 6.15 is due to the removal of the majority of the slimes in the first stage. The combined partition curve indicates that as a two-stage process the Graviton can effectively remove the tail of ultrafine slimes.

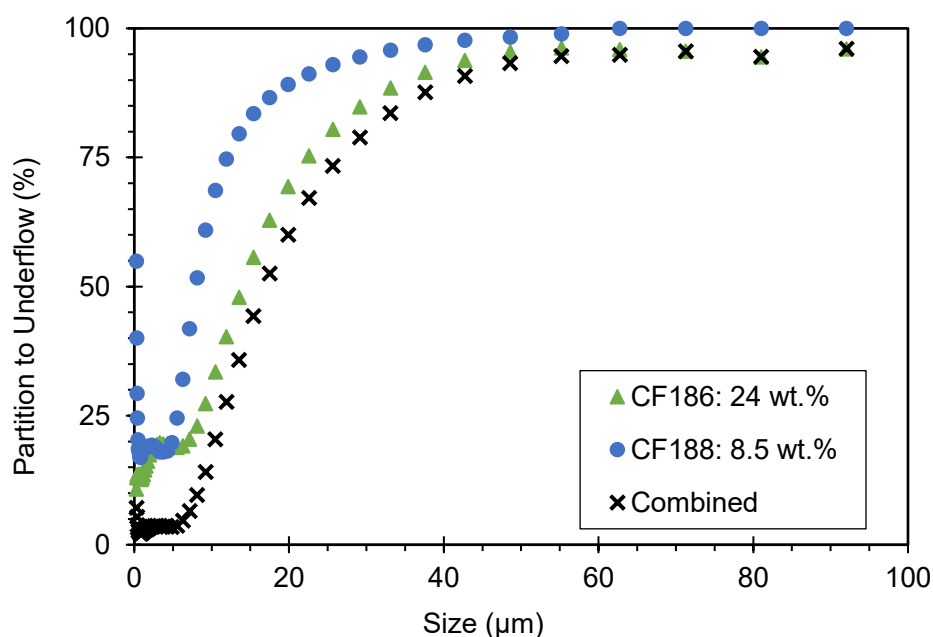


Figure 6.16: Partition curves for the Runs CF186 and CF188 that form a two-stage separation, the underflow of CF186 being used as the feed for CF188. The overall partition curve for the combined separation is also shown.

For each run, samples of the feed, overflow and underflow streams were screened into a number of size fractions (wet screened at 38 and $20\ \mu\text{m}$, dry screened at coarser sizes). These fractions, along with head samples for each stream, were sent for XRF analysis to determine their Fe contents. For a

clearer assessment of the results, this composite size by assay data were subjected to mass balance reconciliation. Tables 6.3 to 6.6 show these mass balanced size assays for Runs CF184 to CF188. The raw assay data are provided in Appendix D.

The size data reveals that the overflow contained negligible material larger than 38 μm . This indicates that the flow conditions were not sufficient to promote enough shear induced lift to convey low density coarse particles to the overflow. The two-product formula (Equation 4.8) was applied to calculate the overall solids yield to underflow and Fe recovery. This calculation was also done for the -20 μm and +20 -38 μm size fractions. As with the partition curves, the single stage runs show very consistent assays. The separation took the feed from a grade of 47 - 48 wt.% Fe and upgraded it to around 55 wt.% Fe in the underflow with the overflow stream being reduced to around 36 % Fe. The overall solids yield and Fe recovery were, however, more varied between the runs.

The two-stage separation (assays shown in Tables 6.5 and 6.6) achieved a final product grade of 57.2 wt.% Fe (the raw head grade was actually 58.2 wt.% Fe). In the first stage the overall solids yield was 64.0 wt.% and the Fe recovery was 73.3 %. The second stage achieved better results with a yield of 88.5 wt.% and recovery of 91.8 %. With the overflow containing no particles larger than 38 μm , it is clear that all of the separation occurs in the ultrafine range below 38 μm . In fact, the assay data show the separation all occurs in the sub 20 μm fraction. In this size fraction the feed increases from a grade of 42.3 to 52.1 % Fe in the first stage, and increases further to 56.1 % Fe in the second stage.

It is interesting to note that for all four runs, the equivalent size fractions of the underflow streams all had similar grades. This suggests that there is potential to achieve a higher upgrade. Operating at higher feed or fluidisation flowrates might provide the shear required to promote lift of coarser low density particles into the overflow. The significant upgrade seen in the finest size fraction provides strong evidence of the Graviton's potential for processing ultrafine feeds.

Table 6.3: Mass balanced size assay data for Run CF184.

CF184: Feed Flowrate 140 L/min, Solids Concentration 5 wt.%, Fluidisation 36 L/min								
Size Range	Feed Mass	Feed Fe	Underflow Mass	Underflow Fe	Overflow Mass	Overflow Fe	Solids Yield	Fe Recovery
(μm)	(wt.%)	(wt.%)	(wt.%)	(wt.%)	(wt.%)	(wt.%)	(wt.%)	(wt.%)
- 1000 + 500	2.0	56.7	3.0	56.7				
- 500 + 250	3.9	60.9	5.7	60.9				
- 250 + 125	4.1	62.2	5.9	62.2				
- 125 + 63	5.6	60.8	8.2	60.8				
- 63 + 38	7.3	55.8	10.6	55.8				
- 38 + 20	16.0	54.4	22.6	55.0	1.4	34.7	97.2	69.4
- 20	61.1	42.3	44.0	49.0	98.6	35.6	49.5	79.6
Head		48.1		53.7		35.6	68.7	76.8

Table 6.4: Mass balanced size assay data for Run CF185.

CF185: Feed Flowrate 145 L/min, Solids Concentration 18 wt.%, Fluidisation 36 L/min								
Size Range	Feed Mass	Feed Fe	Underflow Mass	Underflow Fe	Overflow Mass	Overflow Fe	Solids Yield	Fe Recovery
(μm)	(wt.%)	(wt.%)	(wt.%)	(wt.%)	(wt.%)	(wt.%)	(wt.%)	(wt.%)
- 1000 + 500	0.7	53.4	1.2	53.4				
- 500 + 250	1.8	57.6	3.2	57.6				
- 250 + 125	2.8	60.1	4.8	60.1				
- 125 + 63	4.9	60.2	8.5	60.2				
- 63 + 38	6.9	56.6	11.9	56.6				
- 38 + 20	15.5	55.4	25.6	56.2	1.5	36.3	96.0	58.9
- 20	67.3	42.3	44.8	52.2	98.5	36.0	38.7	71.7
Head		47.0		55.0		36.0	58.1	67.9

Table 6.5: Mass balanced size assay data for Run CF186. This run formed Stage 1 of the two-stage separation.

CF186: Feed Flowrate 140 L/min, Solids Concentration 24 wt.%, Fluidisation 34 L/min (1st Stage)								
Size Range	Feed Mass	Feed Fe	Underflow Mass	Underflow Fe	Overflow Mass	Overflow Fe	Solids Yield	Fe Recovery
(μm)	(wt.%)	(wt.%)	(wt.%)	(wt.%)	(wt.%)	(wt.%)	(wt.%)	(wt.%)
- 1000 + 500	0.7	54.8	1.0	54.8				
- 500 + 250	1.8	58.2	2.8	58.2				
- 250 + 125	3.1	60.9	4.9	60.9				
- 125 + 63	5.3	61.3	8.4	61.3				
- 63 + 38	7.0	57.6	11.0	57.6				
- 38 + 20	17.6	55.3	26.4	56.0	1.8	36.6	96.3	64.9
- 20	64.5	43.2	45.5	52.1	98.2	35.8	45.2	77.3
Head		48.2		55.1		35.8	64.0	73.3

Table 6.6: Mass balanced size assay data for Run CF188. This run formed Stage 2 of the two-stage separation.

CF188: Feed Flowrate 144 L/min, Solids Concentration 8.5 wt.%, Fluidisation 36 L/min (2nd Stage)								
Size Range (μm)	Feed Mass (wt.%)	Feed Fe (wt.%)	Underflow Mass (wt.%)	Underflow Fe (wt.%)	Overflow Mass (wt.%)	Overflow Fe (wt.%)	Solids Yield (wt.%)	Fe Recovery (wt.%)
- 1000 + 500	1.0	54.8	1.2	54.8				
- 500 + 250	2.8	58.2	3.2	58.2				
- 250 + 125	4.9	60.9	5.5	60.9				
- 125 + 63	8.4	61.3	9.4	61.3				
- 63 + 38	11.0	57.6	12.4	57.6				
- 38 + 20	26.4	56.0	29.2	56.3	5.1	41.0	97.9	89.0
- 20	45.5	52.1	39.1	56.1	94.9	39.3	75.9	95.3
Head		55.1		57.2		39.4	88.5	91.8

6.3.2 Iron Ore Feed 2

Following the promising initial trials using Iron Ore Feed 1, a new series of 11 experiments, including 4 two-stage separations, was set up with the purpose of implementing and studying the effects of several key changes to the system. For this series, the iron ore feed was more 'usable', in that it was better liberated, and had a lower percentage of ultrafine slimes. XRF analysis also showed this feed to be of much lower grade, approximately 33 wt.% Fe, which meant that there was more scope for demonstrating the ability of the Graviton to beneficiate fine materials. Figure 6.17 shows the size distributions for the first stage experiments using this feed. Its Sauter mean size varied between 6.33 and 7.35 μm .

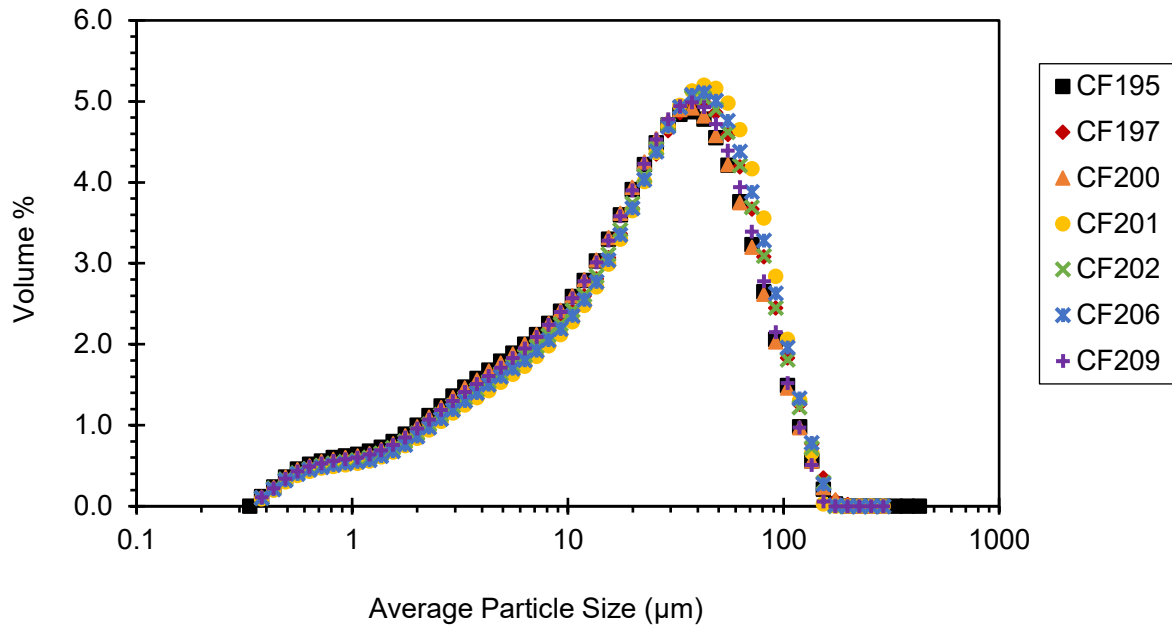


Figure 6.17: Particle size distributions of the feed samples taken for Iron Ore Feed 2 experiments as measured by a Malvern Mastersizer 3000.

The first run with this new feed, CF195, was performed under the same conditions as the highest solids concentration run of the previous feed (CF186). The partition results proved to be very similar with separation size and E_p values of 14.2 μm and 8.4 μm (compared with 15.0 μm and 7.5 μm for CF186). Although the underflow outlet size, feed rate, fluidisation and solids concentration were kept the same as Run CF186, the solids yield to underflow was noticeably higher (67 wt.% versus 42 wt.%). Of course, the coarser size of the feed material can account for some of this difference. Nevertheless, the sharpness of this new partition curve, and the large yield to underflow, led to a series of experiments performed with decreasing underflow outlet sizes in order to limit the amount of material reporting straight to the underflow. The partition curves for these experiments are shown in Figure 6.18.

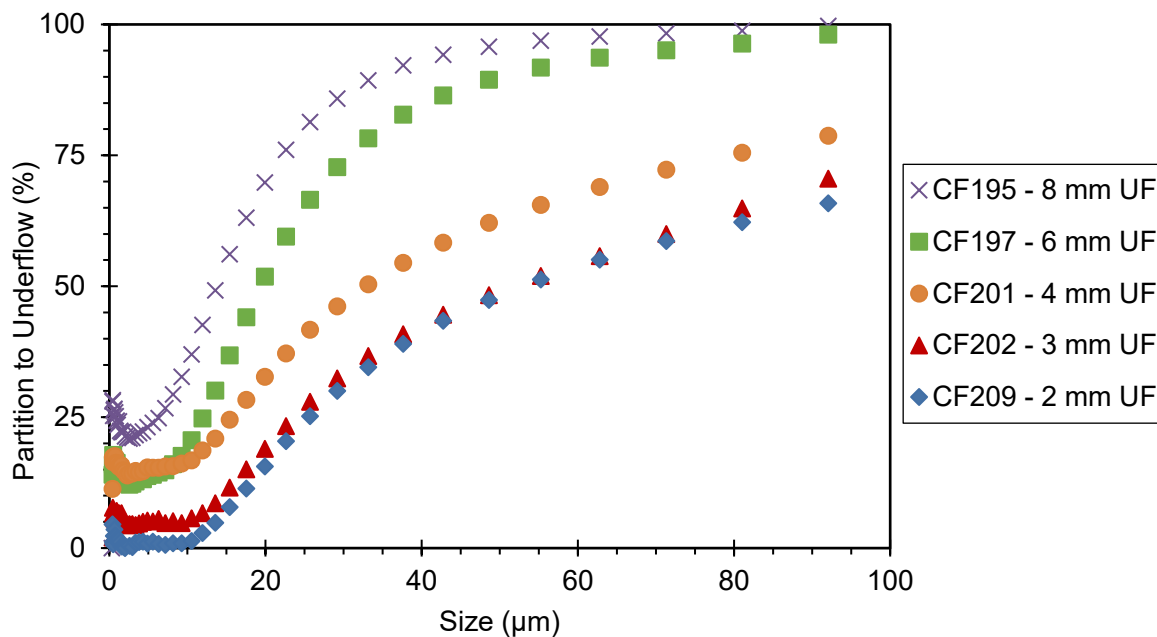


Figure 6.18: Partition curves for the Runs CF195, CF197, CF201, CF202, and CF209 showing the effect of decreasing underflow outlet size.

These experiments all used roughly the same total volumetric flows (feed flowrate + fluidisation) and solids concentrations with the differences discussed in Figures 6.19 – 6.22. However, Run CF209 was operated with both the feed rate and solids concentration halved. This was due to the system blocking mid-run when the original conditions were used. The reported run of CF209 appeared to still block at the new conditions, however this occurred towards the end of the run after two sets of steady state samples had been collected. Comparing these two sets of samples (4 minutes apart) showed no variation that would indicate the system had blocked during those initial 8 min of the run. Hence, the results were deemed valid representations of steady state behaviour. It appears then that these conditions are at the limit of the underflow capacity. In order to allow high solids throughputs, the 2 mm underflow outlet used in Run CF209 was deemed impractical, and given how similar the 3 mm underflow outlet curve is (CF202), no smaller underflow sizes were tested and subsequent experiments were performed using underflow outlets of at least 3 mm diameter.

The partition curves in Figure 6.18 show that as the underflow diameter decreases the separation size and Ep values increase, but the level of fish-hook decreases. In the single density silica experiments, size partition curves behaving like this indicated that the system had reached the limits

of the underflow capacity. Here, where the feed particles vary in both size and density, and with no signs of blockage, the separation occurring over a broader size range could indicate that density is playing a larger role in the separation. Reducing the underflow outlet diameter also reduces the amount of ultrafine material reporting to the underflow.

There is, however, more to the results of Figure 6.18 than just the effects of the decreasing underflow diameter. Throughout the course of these runs, several changes to the Graviton system were implemented. After Run CF201 the issue of overflow material splashing into the launder was addressed through the changes outlined in Section 4.2.1. With these simple alterations in place, the amount of overflow material being misplaced into the underflow launder was greatly reduced. The significant lowering of the ultrafine tail for Runs CF202 and CF209 can be largely attributed to this. However, even for these runs the partition tail still increases towards ~ 10 % below 5 μm indicating that some amount of bypass is occurring. Clearly part of this is unavoidable with the lowest density ultrafine particles still being entrained to the underflow as part of the water split.

Another change made was to the fluidisation chamber. The first two partition curves seen in Figure 6.18, Runs CF195 and CF197, were performed with feed rates of ~150 L/min and fluidisation rates of 33 L/min. For the subsequent runs a higher fluidisation rate was used. To achieve this the fluidisation holes had to be drilled larger to 0.8 mm diameter (previously 0.5 mm). To compensate for the higher fluidisation rate, the subsequent runs used lower feed flowrates between 105 and 115 L/min to maintain roughly the same net flow through the system. Figure 6.19 shows the partition curves from before and after the change. The results show very similar partition curves with almost the same separation size and Ep values. A major benefit from this change was the lowering of the ultrafine hook. The higher rate of fluidisation provides better washing of ultrafine material, minimising its entrainment, and also helping to prevent solids packing out when using the smaller underflow outlets.

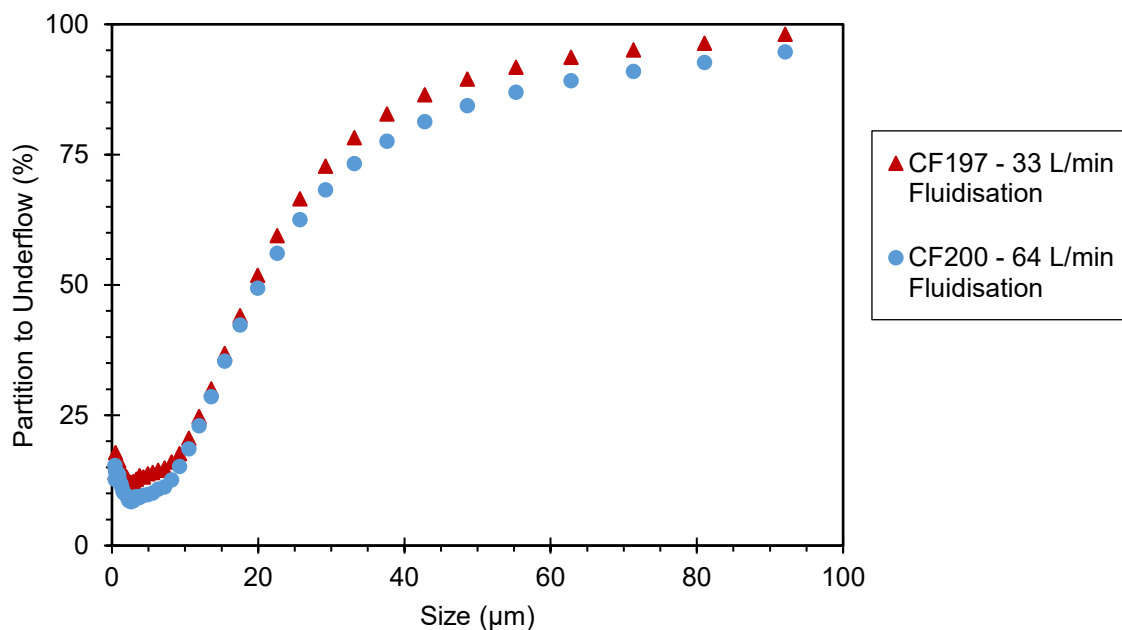


Figure 6.19: Partition curves for the Runs CF197 and CF200 showing the effect of increasing the fluidisation rate by using larger sized holes in the distribution chamber.

The head grades for each stream in these 6 runs, listed in Table 6.2, indicate that as the underflow diameter was reduced the underflow product grade generally increased. Interestingly, the Fe content in the overflow stream also increased and the Fe recovery decreased suggesting that higher product grades should be possible. The slightly lower product grade in CF209 does not follow the trend of increasing grades with decreasing underflow size. This can be attributed to the different flow conditions used that were necessary for a successful run, further justifying the decision not to continue use of the 2 mm outlet.

Several two-stage experiments were also performed using this feed. In the same fashion as the two-stage separation for the previous feed, the underflow product (including that which had settled out in the launder) was collected and re-used as the feed for the second stage. The conditions of the second stage were made identical to the first stage, again with the exception of the feed solids concentration which was diluted to allow for sufficient run time. The two-stage experiments were performed on the 8 mm, 6 mm and 3 mm underflow diameters, the last of which was also repeated to assess the consistency of the results. The size partition curves for these experiments are shown in Figures 6.20 – 6.22.

Similar to the two-stage separation of Iron Ore Feed 1, these experiments show that the very sharp size partition curve in the second stage effectively eliminates the tail of the ultrafine material, particularly for the 6 and 3 mm underflow outlets. The repeat experiments using the 3 mm underflow (Figure 6.22) show excellent consistency. The unavoidable small variations in flowrates and solids concentrations across the experiments may account for the slight variations in the separation size and Ep values.

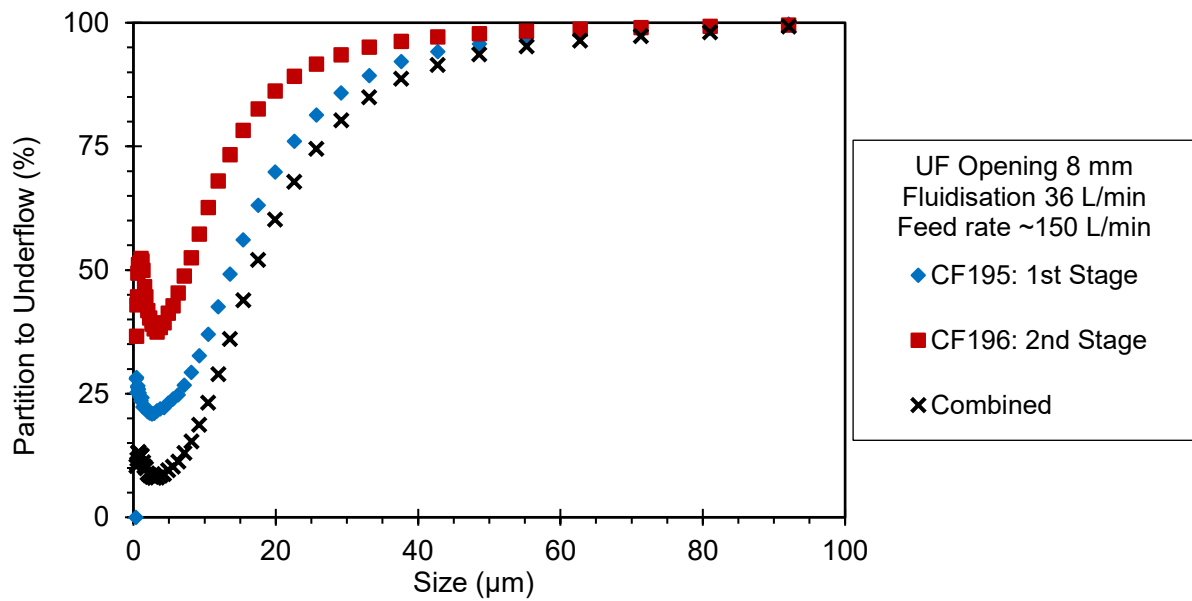


Figure 6.20: Partition curves for the Runs CF195 and CF196 that form a two-stage separation using the 8 mm underflow outlet. The partition curve for the combined separation is also shown.

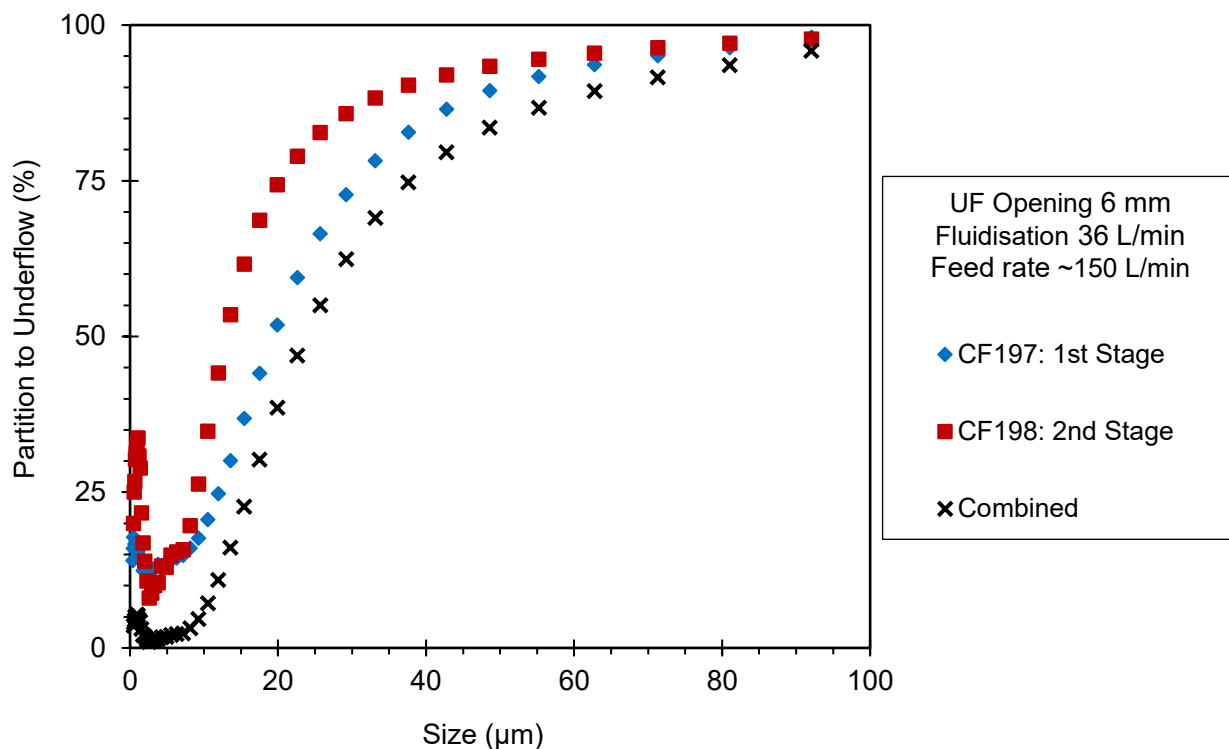


Figure 6.21: Partition curves for the Runs CF197 and CF198 that form a two-stage separation using the 6 mm underflow outlet. The partition curve for the combined separation is also shown.

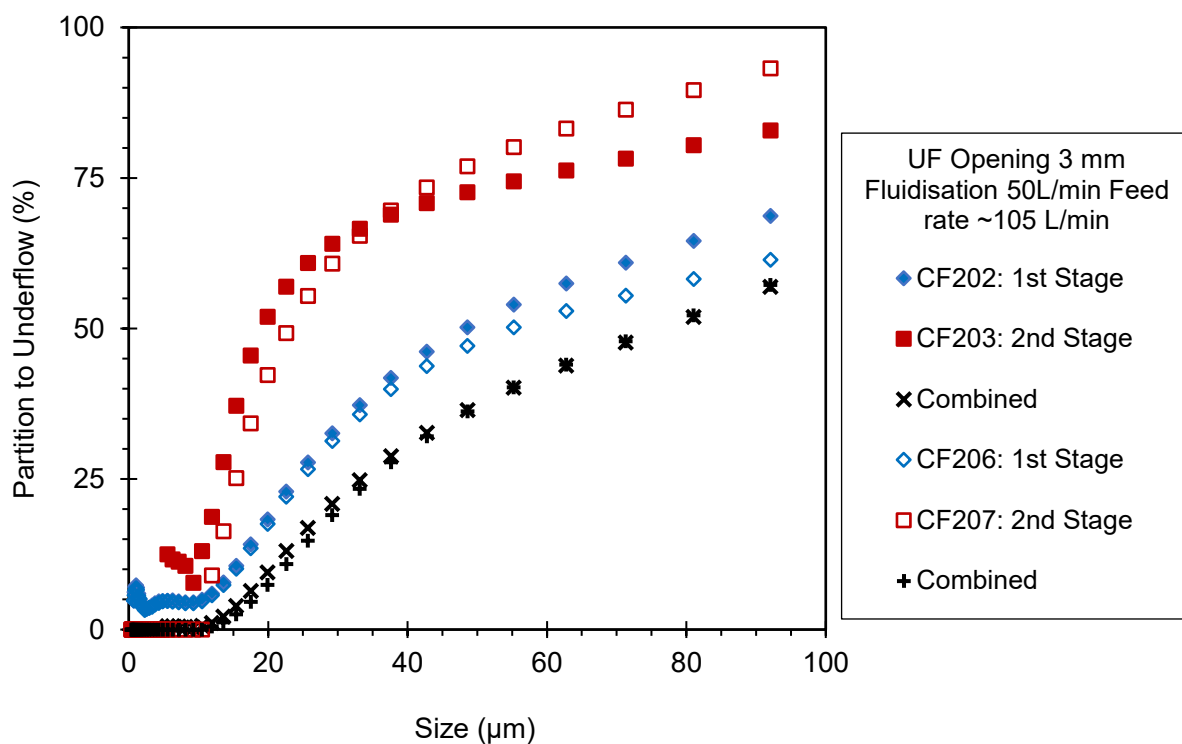


Figure 6.22: Partition curves for the Runs CF202 and CF203, and repeat runs of CF206 and CF207, that form two-stage separations using the 3 mm underflow outlet. The partition curves for the combined separations are also shown.

The head grades for each stream in the two-stage experiments are shown in Table 6.7. As expected, the second stage product grade in the 3 mm underflow experiments far surpassed those of the larger underflow runs. Again, the repeat experiments of CF206 and CF207 show good reproducibility in the results. In Run CF203, a repeat measurement of the underflow product grade was performed on a sample taken from the underflow drum after the solids that had settled in the launder had been added (unlike normal product samples collected as a cut from the stream exiting the unit during the run). The resulting grade of 58.5 % Fe was far higher than the grade of the regular underflow sample collected during the run which was only 53.0 % Fe. This indicates that the design of the launder, and the washing lines was inadequate to transport all of the particles to the collection points. Importantly, it also means that the true product grades of all previous runs were very likely higher than the reported values. This grade check with inclusion of the launder solids was only performed for Run CF203. Unfortunately, there was some time delay for receiving results back from the external laboratory that performed the XRF analysis. This meant that the grades for the rest of the runs in this series were analysed without considering the launder solids and are hence inaccurate. Experiments presented in following sections and chapters all report the underflow grades with the launder solids included.

Table 6.7: Head grades of each stream, yield to underflow and Fe recoveries for the two-stage separation experiments (raw data)

Run No.	Stage	Feed Flowrate (L/min)	Feed Solids Conc. (wt.%)	Fluidisation Rate (L/min)	Underflow Outlet Diameter (mm)	Head Grades (wt.% Fe)			Solids Yield (wt.%)	Fe Recovery (%)
						Feed	U/F	O/F		
CF195	1	149	18.5	34	8	31.6	37.8	15.4	72.3	86.5
CF196	2	149	14.2	36	8	38.8	40.2	16.8	94.0	97.4
CF197	1	138	19.8	33	6	32.7	37.4	14.8	79.2	90.6
CF198	2	152	9.2	36	6	36.2	42.2	20.4	72.5	84.5
CF202	1	105	18.6	50	3	33.8	51.7	16.9	48.6	74.3
CF203	2	93	8.1	50	3	47.0	53.0**	36.6	63.4	71.5
CF206	1	105	19.9	50	3	33.6	50.6	18.3	47.4	71.3
CF207	2	105	6.1	64	3	47.9	53.7	27.0	78.3	87.8

* When this underflow grade was re-measured after inclusion of the solids settled in the launder, it was found to be 58.5 wt.%.

Although the separations and final products in these runs was not great, the knowledge gained and improvements made to the system during this series of experiments formed the basis of later work.

6.3.3 Iron Ore Feed 3

With the improvements made to the Graviton, and the better understanding of the benefit of limiting the underflow size, a third series of experiments was completed. For this series, the feed was similar to that of Iron Ore Feed 1, in that it contained a very large volume of ultrafine slimes. This new feed, however, also contained a reasonable portion of mostly high-grade solids from 20 – 100 μm in diameter. Hence, the aim of this series of experiments was to assess the potential of the Graviton as a desliming unit. Removing the ultrafine slimes should then give a high-grade product. The feed used in these runs had a head grade of ~ 55 wt.% Fe and the particle size distribution is shown in Figure 6.23. Two major peaks are seen at the finest and the largest end of the distribution. The aim of desliming is thus to remove the peak at the fine end.

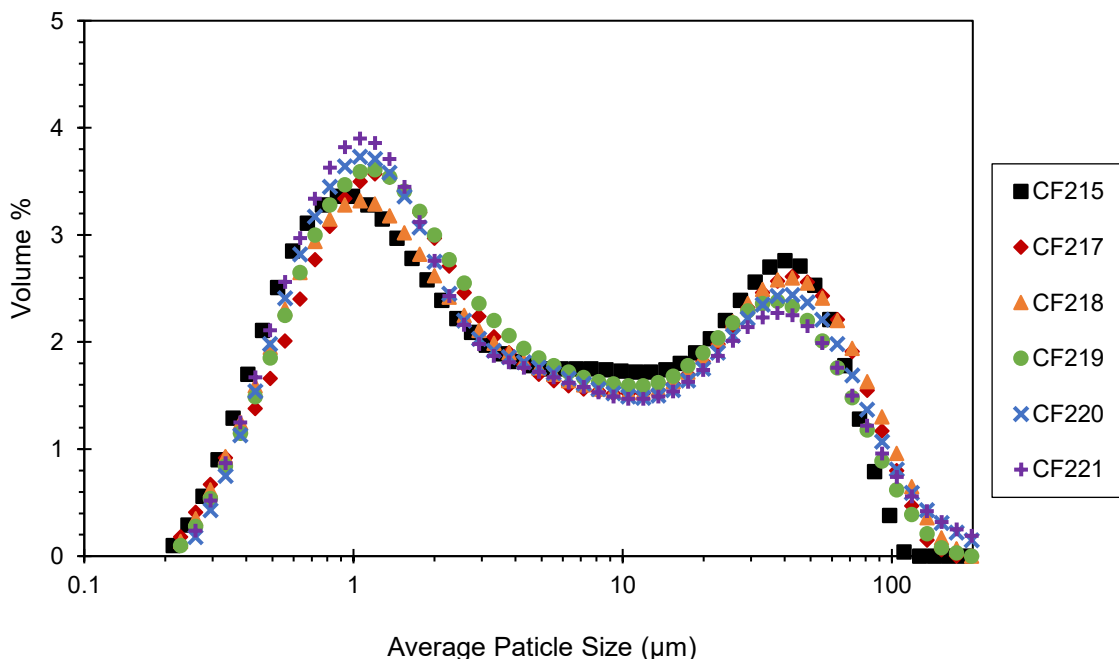


Figure 6.23: Particle size distributions of the feed samples taken for Iron Ore Feed 3 experiments as measured by a Malvern Mastersizer 3000.

Six runs were performed with this feed at a solids concentration of approximately 10 wt.%. From the previous results, it was decided that each run would use the 3 mm underflow outlet in order to

limit the amount of solids going straight to underflow. The first three runs used fluidisation rates of 18, 36 and 54 L/min with a feed flowrate of ~ 60 L/min. The next three runs repeated the varying fluidisation rates but at a higher feed flowrate of ~ 100 L/min. Figure 6.24 shows the partition results for these runs.

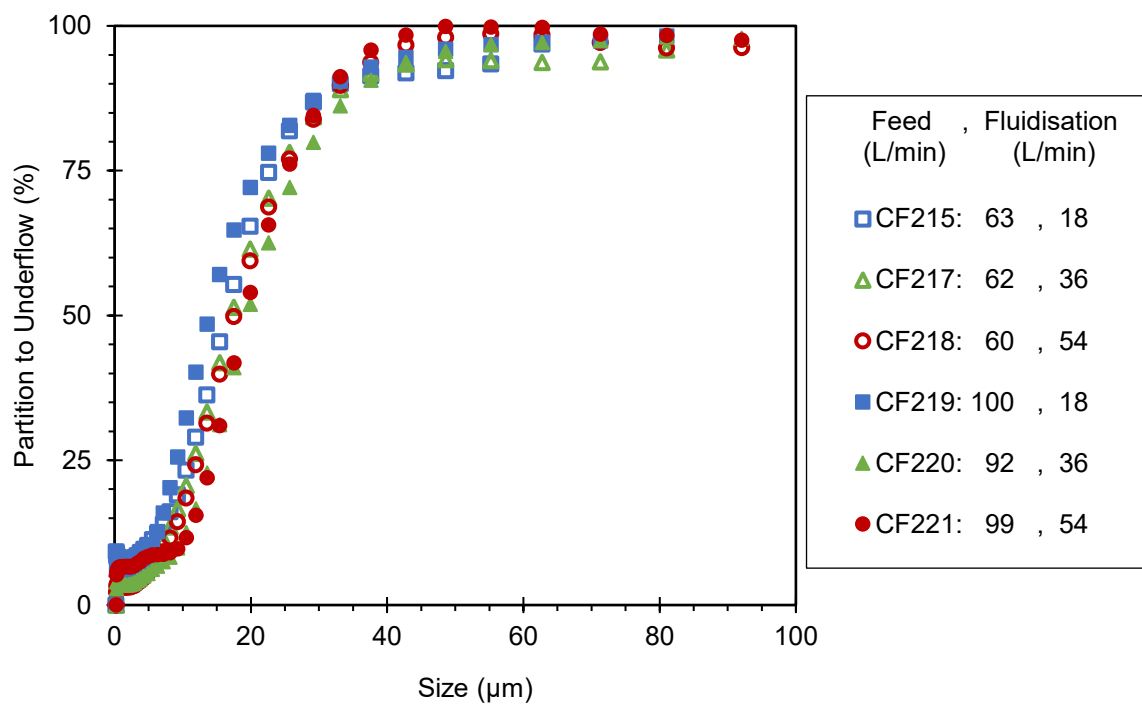


Figure 6.24: Partition curves for the Runs CF215, CF217, CF218, CF219, CF220, and CF221 performed with a feed solids concentration of 10 wt.% and the 3 mm underflow outlet.

The results show that as the fluidisation increases, the separation size increases from 13 to 20 µm. In each run a consistent Ep value between 6 and 8 µm was maintained. The results at the higher feed rate show more spread than the lower feed rate runs, with both the coarsest and finest separation sizes achieved at the 100 L/min feed rate. Excluding the Run CF221, increases in both feed flowrate and fluidisation rate had the effect of lowering the ultrafine tail of the partition curves. This is due to the increase in the net water flow within the lower fluidisation zone creating a better washing process that carries ultrafine particles towards the inclined channels and reduces entrainment to the underflow.

To better analyse these separations, the iron as well as the phosphorus contents of each stream were measured. Table 6.8 shows these grades as well as the yield to underflow and Fe recovery. As expected from the similar partition results, the variations to the feed flowrate and fluidisation had minimal effect on the grade of the underflow product. All of the runs achieved an iron upgrade from approximately 55 wt.% Fe to around 65.5 wt.% Fe, in addition to reducing the overflow grades to around 49 wt.% Fe. As the feed grade of each run varied slightly, and the product grades were also similar, determining any trend from the iron data is difficult. In the phosphorus data, however, there is an indication that the runs performed with the higher feed flowrate achieved better phosphorus removal from the underflow. This supports the idea that better washing was achieved with the higher net water flow through the system. The higher flow also increases the shear rate within the inclined channels which, as discussed in Chapter 5, reduces the viscous effect, allowing for better gangue rejection and Fe recovery.

Table 6.8: Iron and phosphorus contents of each stream, solids yield to underflow and Fe recovery for the Iron Ore Feed 3 experiments (raw data)

Run No.	Feed Rate (L/min)	Fluidisation (L/min)	Head grades					Phosphorus content		
			Feed (%Fe)	U/F (%Fe)	O/F (%Fe)	Yield (%)	Recovery (%)	Feed (%P)	O/F (%P)	U/F (%P)
CF215	63	18	55.4	63.5	49.0	44.14	50.59	0.11	0.16	0.062
CF217	62	36	56.2	63.0	48.0	54.67	61.28	0.11	0.16	0.063
CF218	60	54	56.8	63.8	48.6	53.95	60.6	0.11	0.16	0.061
CF219	100	18	55.9	63.8	47.9	50.31	57.43	0.11	0.16	0.06
CF220	92	36	54.9	64.0	49.5	37.24	43.41	0.12	0.15	0.058
CF221	99	54	52.9	63.5	49.2	25.87	31.06	0.13	0.15	0.059

For the best possible washing, the highest net flow run (CF221) was later repeated as the first stage of a two-stage separation. As with other two-stage separation trials, the second stage was performed with the same flow conditions as the first, in this case at feed and fluidisation rates of 100 and 54 L/min respectively, but with a diluted feed to create enough volume to run the experiment. For this experiment, the 8.7 wt.% solids underflow of the first stage (CF222) was diluted to 3.2 wt.% solids for

the second stage feed (CF223). Figure 6.25 shows the partition curves for this two-stage separation and the combined partition curve.

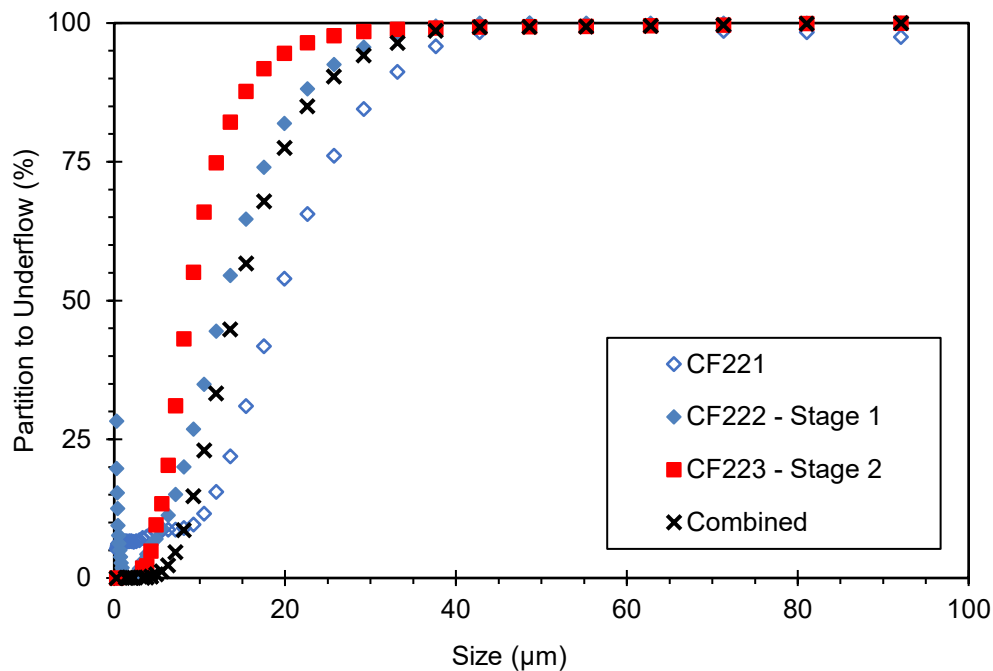


Figure 6.25: Partition curves for the Runs CF222 and CF223 that form a two-stage separation using the 3 mm underflow outlet. The partition curve for the combined separation is also shown.

The partition curve for the first stage actually shows a better partition than the previous run of the same conditions, achieving a separation size and Ep of 13.3 μm and 4.3 μm compared to 19.7 and 7.0 μm in CF221. The separation of the second stage is very sharp with an Ep of just 2.7 μm, and a fine separation size of 9.2 μm. The combined separation is shown to remove almost all of the particles finer than 10 μm. This was indeed the aim of the experiments with this feed. Recalling the feed size distribution in Figure 6.23, the aim of the desliming process was to remove the peak at the ultrafine end. Figure 6.26 shows the particle size distributions of the original feed, the first stage product and the second stage product. From this figure, it is clear that the first stage does a good job at removing the ultrafine particles, with an almost complete removal in stage two.

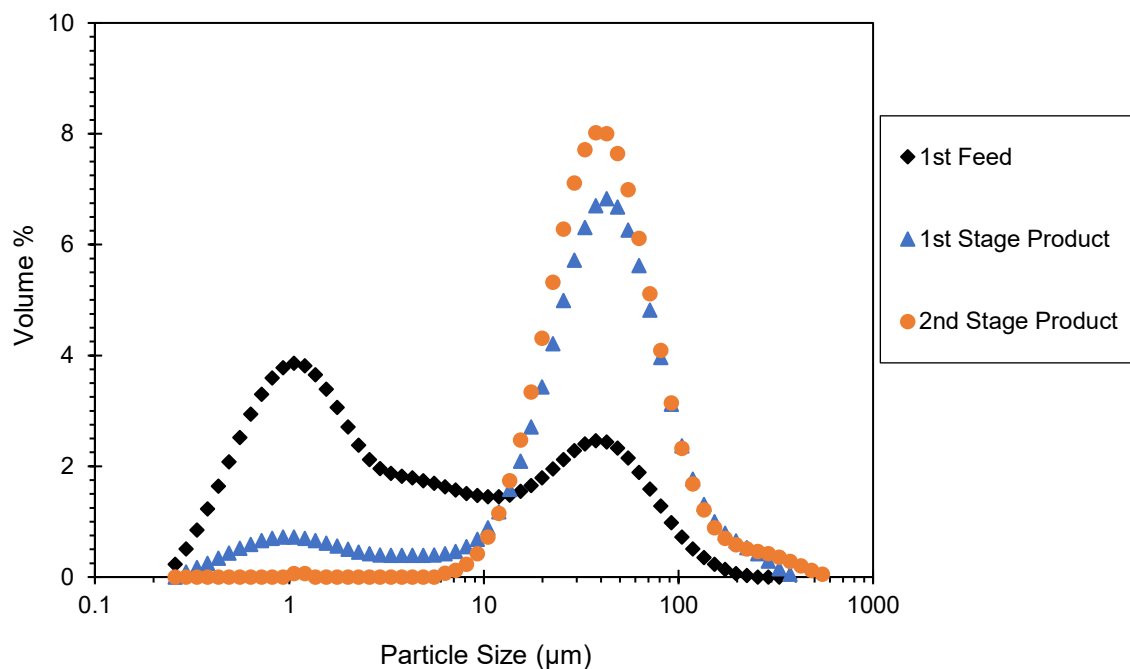


Figure 6.26: Particle size distributions of the 1st stage feed, 1st stage product, and 2nd stage product. The distributions show the near complete removal of sub 10 µm particles in the two-stage separation.

Each stream of the two-stage separation was split into three size fractions and the Fe content measured. Table 6.9 shows the mass balanced size assay data for these runs with the raw data supplied in Appendix D. The overflow streams show no material above 20 µm despite the partition curves indicating that a 20 µm particle had only a 75 % chance to report to the underflow. The raw data shown in Appendix D does actually show some particles in the coarser size fractions, however there was insufficient mass for XRF analysis, hence without data the mass balance assumed there were zero particles in that size range. Regardless, it is clear that essentially all of the iron upgrade occurred in the sub 20 µm fraction as a result of the desliming process. In this size fraction the Fe content increased significantly from 49.9 to 59.9 % Fe in the first stage, although the Fe recovery was only 25 % in that size range. A very high grade of 67.1 % Fe was then reached in the second stage, at a stage two recovery of 67 % (overall two-stage recovery of 17 % in the -20 µm size fraction). The final total product grade from the two-stage separation was 64.9 % Fe with 93 % Fe recovery. Overall, this series of experiments has demonstrated the potential of the Graviton as a desliming unit. Through the removal of the ultrafine slimes a high-grade product was achieved.

Table 6.9: Mass balanced size assay data for the two-stage separation of Iron Ore Feed 3.

1st Stage								
Size Range	Feed Mass	Feed Fe	Underflow Mass	Underflow Fe	Overflow Mass	Overflow Fe	Solids Yield	Fe Recovery
(μm)	(wt.%)	(wt.%)	(wt.%)	(wt.%)	(wt.%)	(wt.%)	(wt.%)	(%)
+ 38	27.4	63.7	50.2	63.7	0.0	0.0	100.0	100.0
- 38 + 20	15.2	66.0	27.8	66.0	0.0	0.0	100.0	100.0
- 20	57.3	49.9	21.9	59.9	100.0	47.2	20.9	25.1
Head		56.1		63.5		47.2	54.6	61.8
2nd Stage								
Size Range	Feed Mass	Feed Fe	Underflow Mass	Underflow Fe	Overflow Mass	Overflow Fe	Solids Yield	Fe Recovery
(μm)	(wt.%)	(wt.%)	(wt.%)	(wt.%)	(wt.%)	(wt.%)	(wt.%)	(%)
+ 38	50.2	63.7	55.1	63.7	0.0	0.0	100.0	100.0
- 38 + 20	27.8	66.0	30.5	66.0	0.0	0.0	100.0	100.0
- 20	21.9	59.9	14.4	67.1	100.0	49.2	60.0	67.2
Head		63.5		64.9		49.2	91.2	93.2

6.3.4 Iron Ore Feeds 4 and 5

To further assess the capabilities of the Graviton, two other feeds were processed. Figure 6.27 shows the particle size distributions for these two feeds, both screened for a top size of 130 μm . The Sauter mean diameter varied from 6.3 – 8.18 μm for Iron Ore Feed 4 and 3.46 – 3.52 μm for Iron Ore Feed 5. XRF analysis showed head grades to be 64.6 and 56 wt.% Fe respectively.

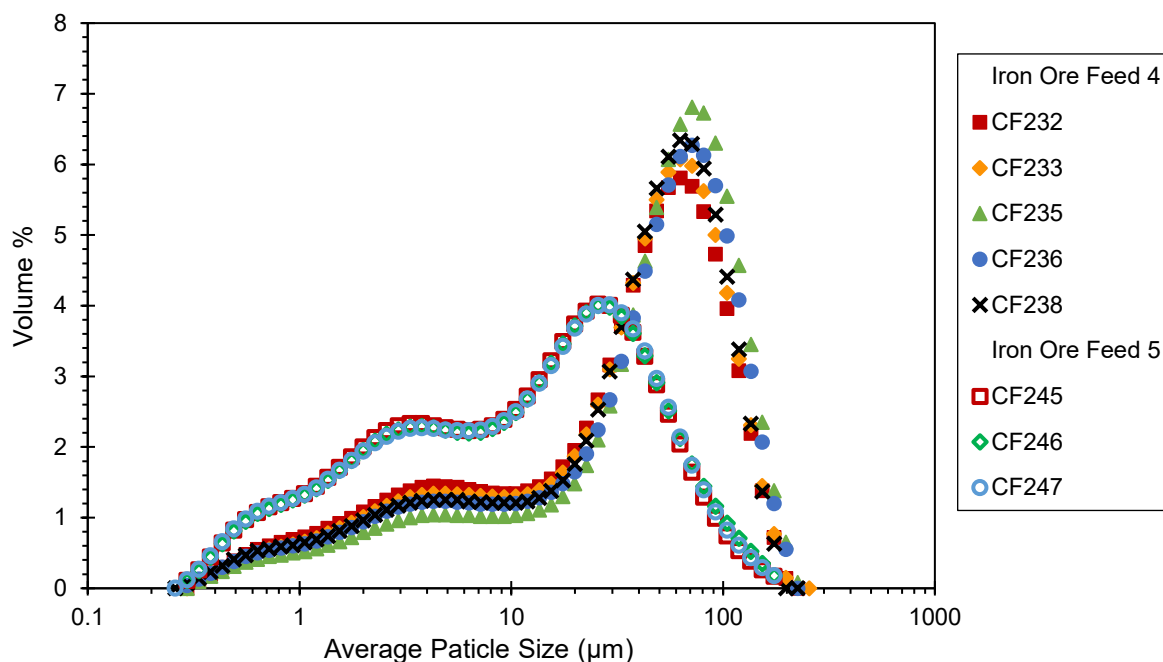


Figure 6.27: Particle size distributions of the feed samples taken for Iron Ore Feed 4 and Iron Ore Feed 5 experiments as measured by a Malvern Mastersizer 3000.

The series of runs performed using Iron Ore Feed 4 used the 3 mm diameter underflow tube, with the fluidisation, feed flowrate and solids concentration varied. Table 6.2 lists the conditions used for each run. The head grades of the first run (CF232) were obtained and are also listed in Table 6.2. Figure 6.28 shows the partition curves for these runs. The curves are all very similar with separation sizes increasing from 15.4 to 19.4 μm as the feed flowrate and fluidisation rate increased. The ultrafine tail also appears to be lower at the higher feed flow and fluidisation rates, although the data appear cluttered. All runs tend towards a partition value close to 0 at the finest sizes with almost no evidence of the fish-hook effect. A sharp E_p between 5.8 and 6.5 μm was maintained throughout.

The grades shown in Table 6.2 indicate that the feed was already at a very high grade of 64.6 wt.% Fe. The separation produced a higher product grade of 67.5 wt.% Fe and a low reject grade of 37.9 wt.% Fe with a very high solids yield and Fe recovery. Although this upgrade, with almost no loss of Fe, shows a successful separation, the runs that followed were not analysed using XRF. It was decided that given the already high grade, and similarity in the partition curves, there was not much value in obtaining these extra results.

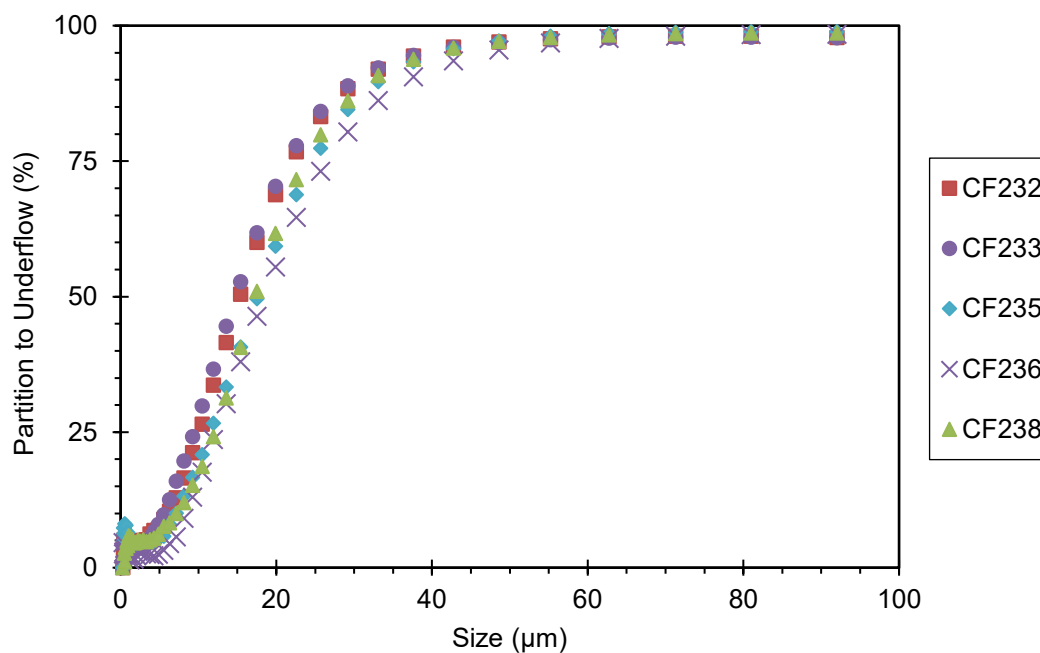


Figure 6.28: Partition curves for Runs CF232, CF233, CF235, CF236, and CF238 on Iron Ore Feed 4 performed using the 3 mm underflow outlet.

Three experiments were conducted using Iron Ore Feed 5, again all with the 3 mm underflow outlet. The feed flowrate and solids concentration were kept constant at 52 L/min and 10 wt.% respectively, and the fluidisation rate was varied from 12 to 36 L/min. Figure 6.29 shows the partition curves for these runs and the head grades, solids yield to underflow and Fe recoveries can be found in Table 6.2. Again, the partition curves are very similar with the separation size increasing from 13.1 to 16 µm as the fluidisation increased, maintaining E_p values between 5.8 and 6.3 µm. The ultrafine tail of the curve also became lower at higher fluidisation rates. The head grade results show good Fe upgrades, with the best results coming from the highest fluidisation run. Here a feed of 56.6 wt.% Fe was upgraded to a product grade of 63.9 wt.% Fe with a solids yield and Fe recovery of 67.1 % and 75.8 wt.% respectively. Given the information from the partition curves, it is safe to say that, as with the other feeds, the separation occurs primarily in the sub 20 µm size range. The particle size distributions for the feed and underflow of the best performing (lowest E_p , highest product grade) run (CF246) are shown in Figure 6.30. These distributions show that the underflow has removed practically all of the particles finer than 10 µm. This shows a significant improvement over the work presented for Iron Ore

Feed 3 (Figure 6.26) where a two-stage process was required to achieve the same level of desliming, although that feed did contain a larger portion of slimes.

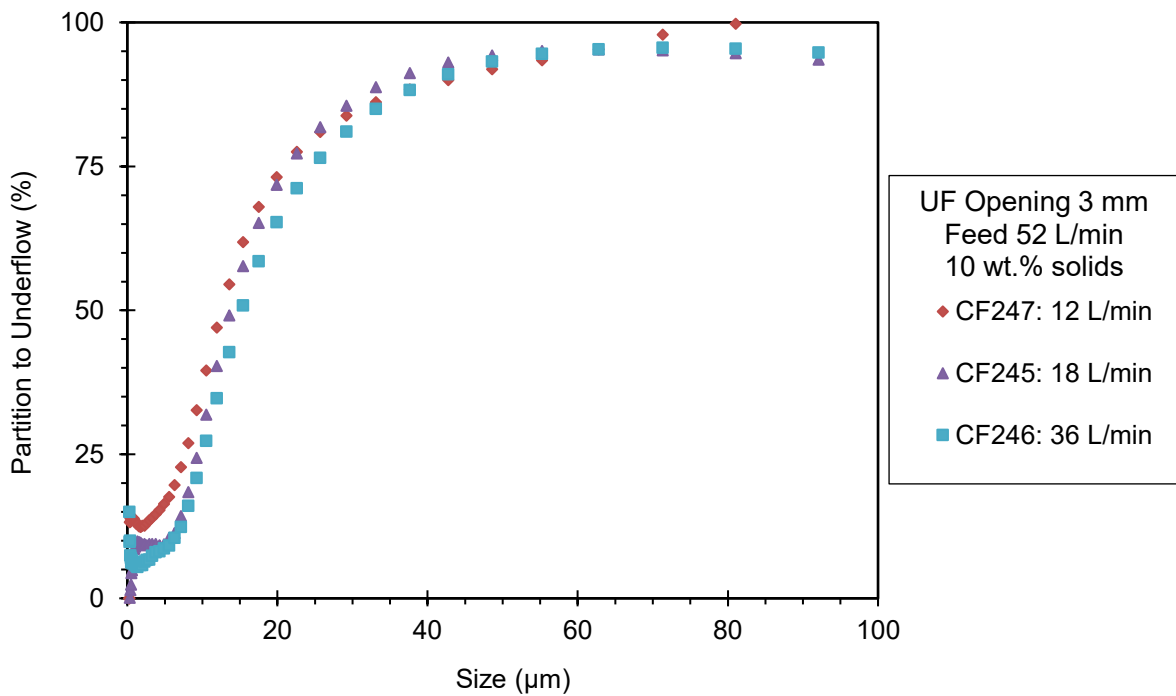


Figure 6.29: Partition curves for Runs CF247, CF245, and CF246 performed on Iron Ore Feed 5 with the 3 mm underflow outlet, a feed flowrate of 52 L/min and solids concentration 10 wt.%.

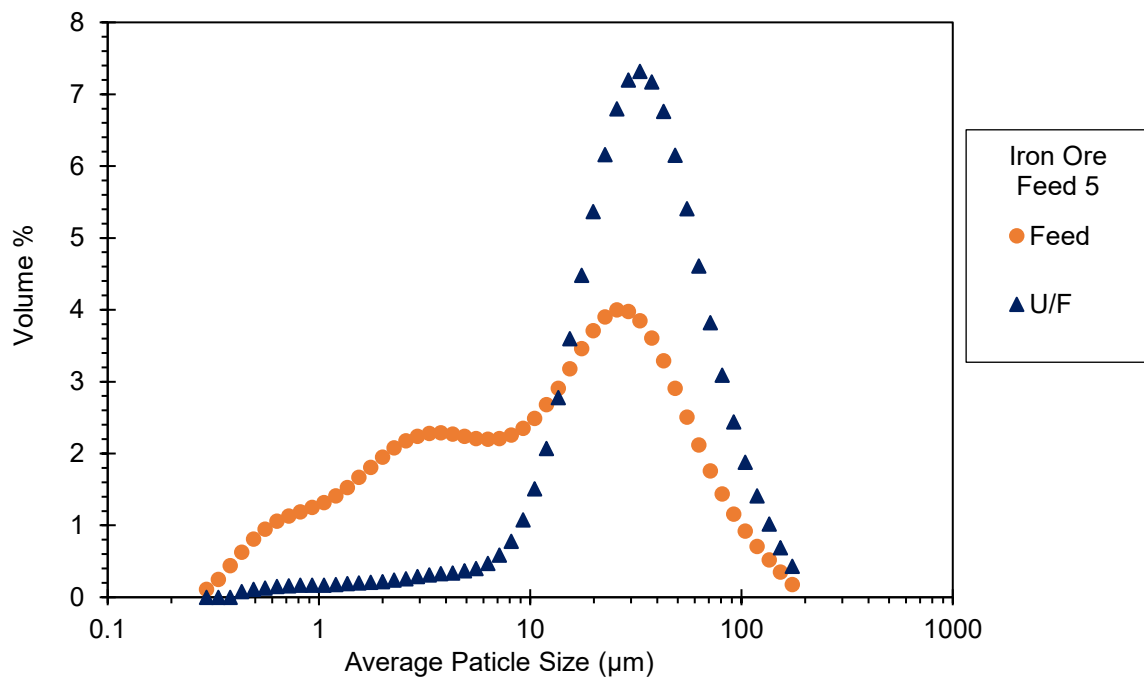


Figure 6.30: Particle size distributions for the feed and underflow of Run CF246.

6.4 Comparing the Graviton and REFLUX™ Classifier

The final series of experiments conducted using the REFLUX™ Graviton used the same feed as the REFLUX™ Classifier experiments presented in Chapter 5. This was a high-grade hematite feed (~65 wt.% Fe) screened for a top size of 300 μm . The high-grade material was present across all sizes, with the majority of the gangue being the ultrafine slimes. Compared to the REFLUX™ Classifier, the Graviton will not show the same kind of coarse gangue rejection. Thus, the aim of these experiments was to provide a more effective desliming process with the endgame of processing the Graviton underflow in the REFLUX™ Classifier. This work will be discussed in Chapter 7. In this chapter, the desliming separation of the Graviton is analysed and compared to the results of the RC™ experiments in Chapter 5. Finally, the versatility of the Graviton to process coarser feed size distributions was explored using the same feed but with the original pre-screened particles added back in. Thus, the size distribution extended up to 1000 μm . Figure 6.31 shows the size distributions for the two feeds.

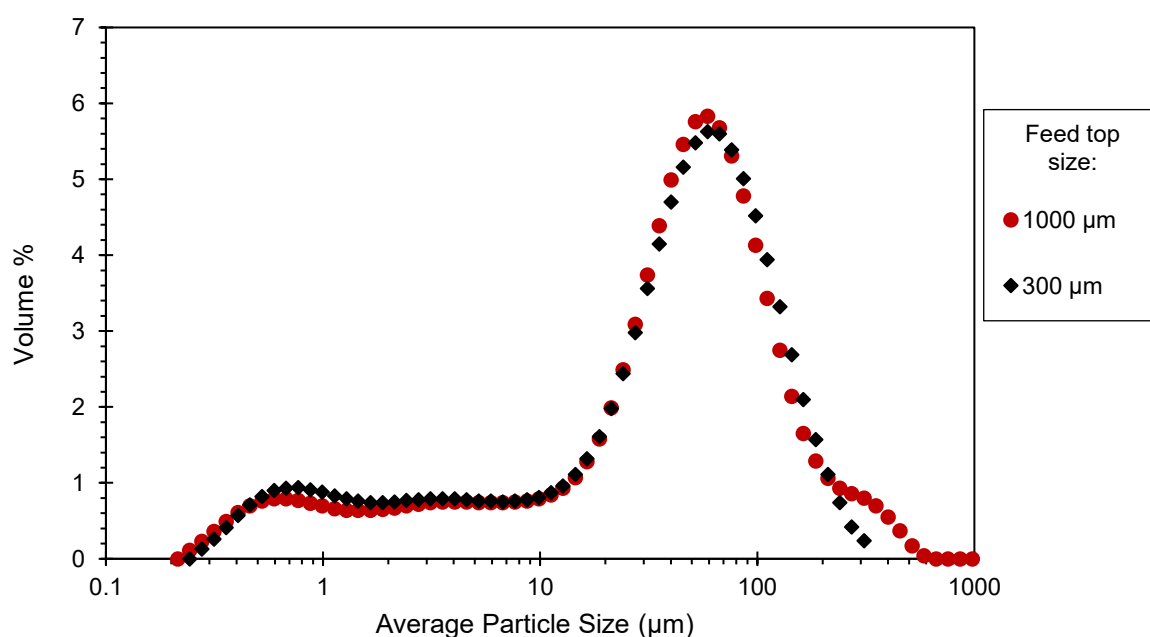


Figure 6.31: Particle size distributions for the feed at top sizes of 300 and 1000 μm .

6.4.1 Feed top size 300 micron

For the screened feed, the same as used in Chapter 5, five runs were performed in the Graviton, all with an 8 mm underflow opening. Table 6.10 lists the various run conditions and head grades of each

stream and Figure 6.32 shows the partition curves. The feed flowrate was kept at around 100 L/min with variations made to the feed solids concentration and fluidisation rate. The product head grades are all fairly similar, with the highest grade obtained from the run using the highest feed solids concentration at 25 wt.% (CF251). The lowest product grade was obtained using the lowest fluidisation rate (CF253), suggesting there was poor washing of the slimes. Given the dispersion of high-grade particles, and concentration of ultrafine slimes being removed, it is unsurprising that the yields and Fe recoveries are all very high, exceeding 86 wt.% and 90 % respectively.

The partition curves confirm the best performing run to be CF251 as it had the sharpest separation ($Ep = 4.4 \mu\text{m}$) and only a very small fish-hook effect. The separation size for this run was also coarser, at $12.4 \mu\text{m}$. Three of the runs, CF249, CF250 and CF252, were almost identical with a separation size between 8 and $9 \mu\text{m}$ and Ep of $5.5 \mu\text{m}$. The tail of these partition curves sits at a higher partition value than CF251. Along with the lowest head grades, Run CF253 demonstrated the highest Ep value. It is clear that the low fluidisation rate did not efficiently wash the slimes to the overflow, resulting in the higher partition curve and lower product grade.

Table 6.10: Run conditions, partition d_{50} and Ep results, head grades for each stream, solids yield to underflow and Fe recovery (raw data) for the five runs performed with the feed top size of $300 \mu\text{m}$. All runs used an 8 mm underflow outlet.

Run no.	Feed Flowrate (L/min)	Feed Solids Conc. (wt.%)	Fluidisation Rate (L/min)	Separation Size, d_{50} (μm)	Ep (μm)	Head Grades (wt.% Fe)			Solids Yield (wt.%)	Fe Recovery (%)
						Feed	U/F	O/F		
CF249	105	6.9	36	8.7	5.5	63.3	66.4	43.1	86.7	90.9
CF250	103	16.6	36	9.0	5.6	64.9	66.0	44.1	95.0	96.6
CF251	98	25.0	36	12.4	4.4	64.7	67.1	43.1	90.0	93.3
CF252	105	14.8	54	8.0	5.5	65.2	66.2	42.9	95.7	97.2
CF253	103	18.0	18	2.6	7.0	64.5	65.6	43.7	95.0	96.6

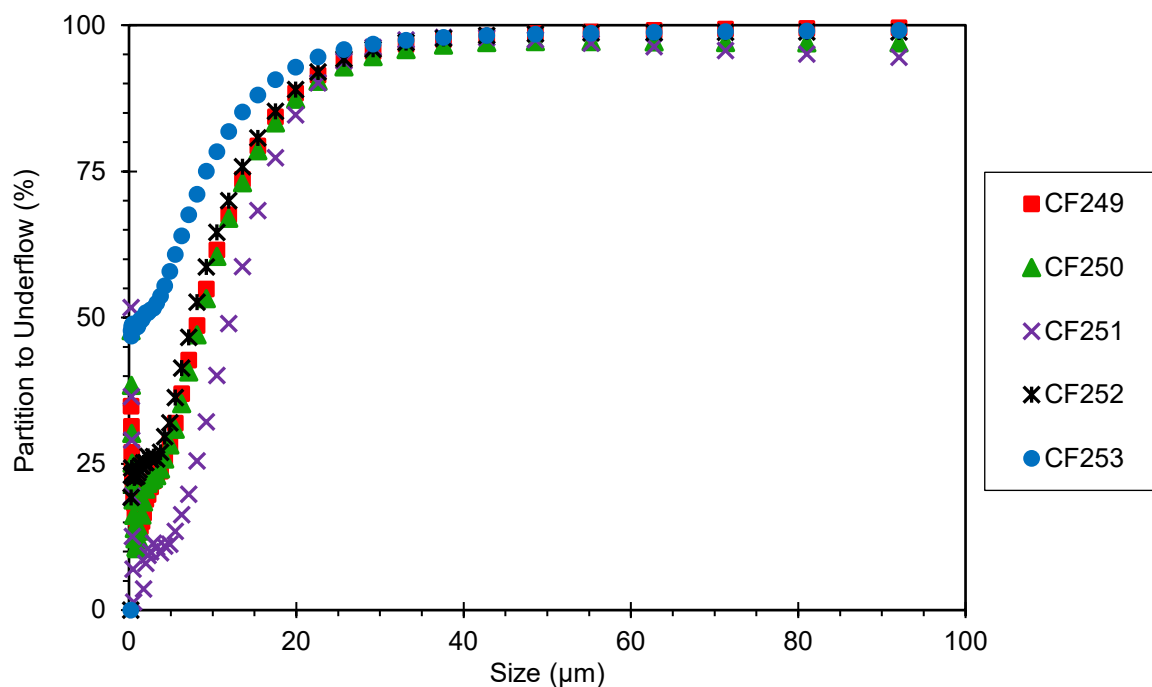


Figure 6.32: Partition curves for the Runs CF249, CF250, CF251, CF252, and CF253 performed with an 8 mm underflow outlet. The partition curves remain level as the particle size approaches 300 μm .

The product grades achieved in the Graviton were slightly lower than those obtained using the RC™, 67.1 wt.% Fe versus 69.1 wt.% Fe, however this is not of the greatest importance, given the already high feed grade. Whilst the RC™ achieved gangue rejection across all sizes, the Graviton showed a very sharp size separation, cutting at 12.4 μm . The Graviton desliming also showed a very high Fe recovery, meaning a second stage process can be used to recover the high-grade particles without the hindrance of slimes. This concept is explored in Chapter 7.

6.4.2 Feed top size 1000 micron

Three runs were performed to assess whether the Graviton could produce a similarly sharp and fine separation when the feed had a wider size distribution. Table 6.11 lists the run conditions and head grades of each stream with the partition curves shown in Figure 6.33. This feed, with particles up to 1 mm in size, posed several issues. Firstly, the inclined channels had a spacing of only 1 mm, hence there was a physical potential for blockages. The hypothesis, however, was that under the high centrifugal forces, the coarse particles will immediately be forced to the underflow, hence even against

the fluidisation water they will never reach the channels to cause a blockage, and importantly, they will not affect the separation performance. The same issue was present for the underflow, where the high concentration of particles can block the outlet. This was accommodated for by increasing the outlet size to 10 mm diameter. Finally, the coarse particles make the mixing and pumping of feed to the unit difficult due to the high settling rates. It is noted that the three runs were performed over successive days with the same feed. The 1300 L mixing tank was filled at the one solids concentration with each run drawing from it across the three days, without any material being returned to the tank. Hence, there was the possibility that the feed composition was changing across the three runs. This suspicion was confirmed by the fact that both the feed solids concentration and the feed head grade decreased over these three runs (Table 6.11). With limited data, the actual impact this had on the performance is difficult to determine.

Table 6.11: Run conditions, partition d_{50} and Ep results ,head grades for each stream, solids yield to underflow and Fe recovery (raw data) for the runs performed with the feed top size of 1000 μm . All runs used a 10 mm underflow

Run no.	Feed Flowrate	Feed Solids Conc.	Fluidisation Rate	Separation Size, d_{50}	Ep	Head Grades (wt.% Fe)			Solids Yield	Fe Recovery
	(L/min)	(wt.%)	(L/min)	(μm)	(μm)	Feed	U/F	O/F	(wt.%)	(%)
CF256	105	16.5	42	7.0	5.9	64.7	66.3	43.8	92.9	95.2
CF257	73	14.3	60	3.1	7.3	64.2	64.8	43.3	97.2	98.1
CF258	52	12.6	60	3.9	9.9	63.4	64.7	46.0	93.0	95.0

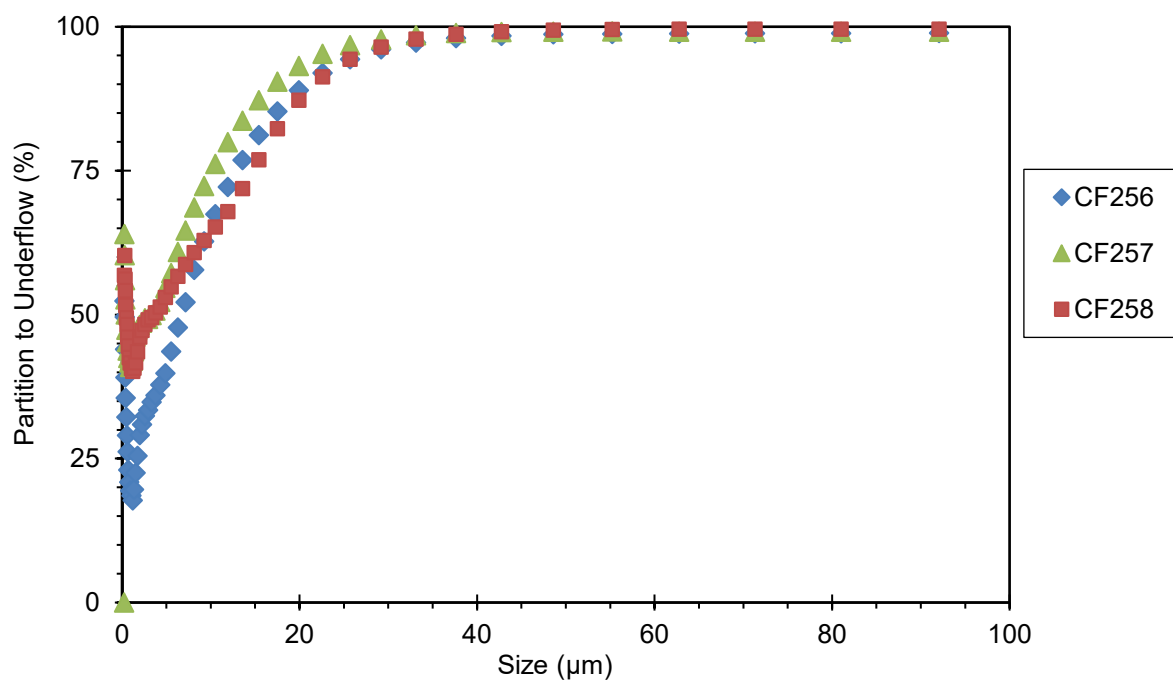


Figure 6.33: Partition curves for Runs CF256, CF257, and CF258 performed with a 10 mm underflow outlet. The partition curves remain level as the particle size approaches 1000 µm.

The product grades and partitions were not as good as the optimal run found for the 300 µm feed (CF251), but with only three runs performed here, the results are promising. The best results were obtained from Run CF256 which had the highest feed flowrate, and more importantly the highest net water flow. This run shows very similar results to the three overlapping results of the 300 µm feed (CF249, CF250 and CF252). The product grade, partition minimum and E_p values were practically identical, and the separation size was actually one micron finer. The other two runs had much poorer separations, similar to the poorest run of the 300 µm feed (CF253). Here the lower net fluid rates did not provide enough washing of the slimes, resulting in more slimes reporting to the underflow and lower product grades. The hypothesis that the coarse particles will report straight to the underflow without affecting the separation appears to be correct. With additional tests using higher fluidisation rates or a reverting back to the 8 mm underflow, it is likely that a separation close to the optimal run of CF251 could be produced.

Overall, these two series of runs demonstrate a very promising application for the Graviton. A very sharp separation, cutting out ultrafine particles and in turn providing an upgrade to the Fe content is

possible. With an efficient deslime and very high Fe recovery, downstream processes can perform strong density separations without the negative effects of the slimes. An additional benefit is seen with the Graviton being able to process feeds of a wide size distribution, eliminating the need for fine pre-screening.

6.5 Concluding Summary

The first series of experiments of the Graviton under continuous conditions were performed with an ultrafine silica feed. The work demonstrated consistently sharp partitions, with Ep values as low as 4 μm and separation sizes ranging from 5 – 20 μm . This work built a foundation of knowledge on the effect of the different operating variables. Understanding these conditions proved important in controlling the separation size and reducing the size of the fish-hook effect. The size of the underflow outlet was the most important factor in ensuring a successful separation. Where a conventional REFLUX™ Classifier controls the underflow discharge in real-time, the Graviton has only the set opening to limit the flow and hence must be selected carefully to avoid blockage. This work also confirmed results obtained in the semi-batch system, again showing a throughput advantage of over 1000.

Following the positive results from the silica work, five iron ore feeds were trialled in the Graviton. With different size distributions and feed grades the results were varied but overall showed that sharp size separations at ultrafine sizes were possible, producing high-grade products. Several feeds highlighted the potential of the Graviton to be used as a desliming unit.

The high-grade feed containing a significant amount of slimes that was used for the REFLUX™ Classifier experiments in Chapter 5 was then processed in the Graviton. Here, the Graviton produced remarkably sharp size separations below 13 μm . Similar results were achieved when separating a feed containing a much larger size distribution of particles, up to 1000 μm . Through the removal of just the finest fraction of particles, the product grade was increased from 65 wt.% Fe to 67.1 wt.% Fe. Importantly, the yield to underflow and Fe recovery were both greater than 90 %, meaning that the

bulk of the Fe is recovered, allowing further processes to be applied without the hindrance of the slimes. This issue will be focus of Chapter 7. An extended run in the Graviton was performed to produce enough deslimed product to use as a feed for the REFLUX™ Classifier. Results using this deslimed feed were then compared to the original results of Chapter 5. The rheology experiments are also repeated for the overflow solids of the deslimed runs.

Chapter 7

Graviton and REFLUX™ Classifier Two-Stage Separation

7.1 Introduction

This chapter describes results from a two-stage separation process comprising of a desliming stage in the Graviton followed by a strong density separation in the REFLUX™ Classifier. In keeping with the previous chapters, sizes are given in μm for the Graviton work, and mm for the RC™100 results. The second stage was run several times at different solids throughputs. This process uses the same high-grade feed as the experiments in Chapter 5 and Section 6.3, with the top size of 0.3 mm. The results then build upon the rheology work of Chapter 5 in describing the viscosity issue caused by the slimes.

7.2 First stage: Desliming in the REFLUX™ Graviton

The optimal run identified in Section 6.4.1 (CF251) was repeated to form stage one of the two-stage process. This first stage, CF254, was thus run at a feed flowrate of 103 L/min, solids concentration of 23.2 wt.% and fluidisation rate of 36 L/min. The underflow outlet diameter was 8 mm. Figure 7.1 shows the partition curve for this run, together with the original CF251 for comparison.

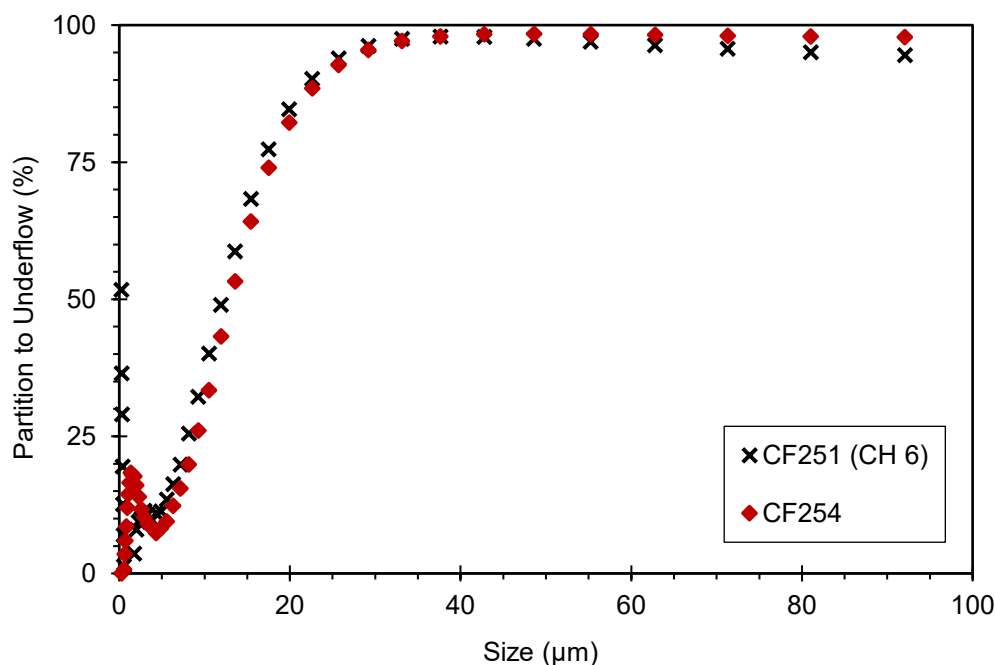


Figure 7.1: Partition curves for Run CF254 and Run CF251

The partition curve shows a very sharp deslime was achieved with a separation size of $13.4 \mu\text{m}$ and E_p of just $4.3 \mu\text{m}$. The partition tail comes down almost to zero at the ultrafine end with only a small

fish-hook. The similarity between this run and the previous run under the same conditions (CF251) also demonstrates the repeatability of the Graviton separations. Each flow stream was sieved into different size fractions to obtain the mass distribution and Fe contents. Table 7.1 lists this data after mass balancing along with the head grades, solids yield and Fe recovery. The raw data are provided in Appendix D.

Table 7.1: Mass balanced size × assay data for Run CF254

Sieve Aperture (μm)	Feed Mass (wt.%)	Feed Fe (wt.%)	Underflow Mass (wt.%)	Underflow Fe (wt.%)	Overflow Mass (wt.%)	Overflow Fe (wt.%)	Solids Yield (wt.%)	Fe Recovery (%)
250	0.8	48.9	0.9	48.9				
180	4.2	60.5	4.6	60.5				
125	10.4	65.7	11.4	65.7				
90	17.3	68.7	18.9	68.7				
63	25.4	67.8	27.9	67.8				
45	15.7	68.5	17.2	68.5				
38	1.1	68.0	1.2	68.0				
20	11.5	67.2	12.6	67.5	0.7	15.2	99.5	99.9
-20	13.5	50.3	5.2	63.9	99.3	42.9	35.2	44.7
Head		65.0		67.1		42.7	91.2	94.2

As intended, the overflow stream shows practically no material above 20 μm , leaving the high grade particles above this size in their original state. The desliming process upgraded the sub 20 μm size fraction from 50.3 up to 63.9 wt.% Fe. This large upgrade of the finest particles results in an overall product grade of 67.1 % Fe with an overall yield and Fe recovery of 91.2 wt.% and 94.2 % respectively, and a reject grade of 42.7 wt.% Fe. It is noted that the coarsest size fractions still have relatively low grades, and thus have the potential for further upgrade. The purpose of this run was not to target this material *per se* but to remove the slimes so that the REFLUX™ Classifier could then more easily beneficiate these coarser particles in the second stage.

In order to illustrate the effects of the desliming step, the particle size distributions of the feed and underflow of Run CF254 are shown in Figure 7.2. The distributions show that the Graviton has removed practically all particles below 10 μm . This, along with the high yield and Fe recovery, shows

that this first stage separation did not alter the majority of this feed, removing only the finest of the size fractions.

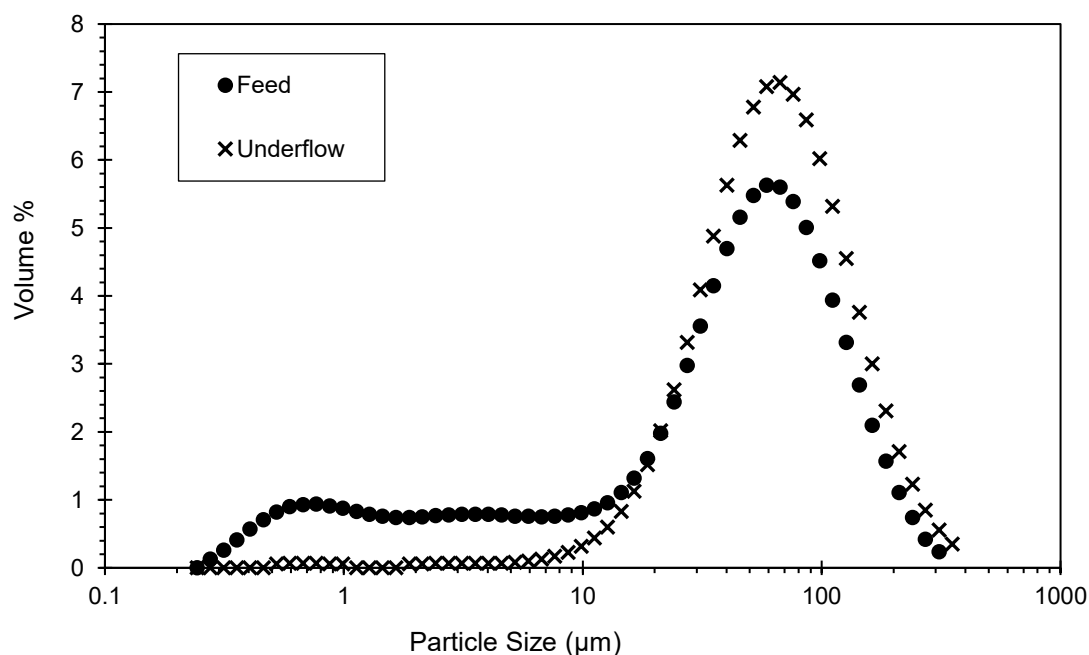


Figure 7.2: Particle size distributions for the feed and underflow of Run CF254, as measured by a Malvern Mastersizer 3000.

7.3 Second stage: Processing deslimed feed in the REFLUX™ Classifier

The deslimed underflow stream from the Graviton was then used as feed for six experiments operated using different feed flowrates and solids concentrations. These were all performed with a 3 mm channel spacing and a fluidisation rate of 0.55 L/min. Table 7.2 lists the conditions used for each run along with the head grades of each stream and the overall solids yield and Fe recovery. As with the original feed, and particularly now for the deslimed feed, there was little room for any further upgrade with the product grades approaching pure hematite (69.9 wt.% Fe). Only the coarser size fractions, identified in Table 7.1 showed relatively lower grades that can be increased. However, these particles sizes account for very little of the mass and hence do not impact the final grade significantly. The product grades show no real trend with each run achieving between 68.1 and 68.9 wt.% Fe. The reject grades, however, decreased with lower solids throughputs. Lower throughput, and more dilute runs, also show high yields and recoveries, as with the original un-deslimed feed.

Table 7.2: Feed conditions, mass balanced head grades of each stream, solids yield to underflow and Fe recovery for the experiments performed using the deslimed feed as a second stage separation.

Run No.	Feed Conditions			Head grades (wt.% Fe)			Solids Yield (wt.%)	Fe Recovery (%)
	Solids Conc. (wt.%)	Flowrate (L/min)	Throughput (t/(m ² h))	Feed	U/F	O/F		
S24F	36.5	9.2	28.0	66.8	68.8	65.9	31.5	32.4
S24F2	36.5	4.6	14.0	66.9	68.9	65.2	45.8	47.1
S24F3	18.3	11.5	14.0	66.6	68.5	64.5	53.5	55.0
S24F4	18.3	5.6	7.0	66.8	68.6	64.3	57.3	58.9
S24F5	9.2	13.2	7.0	67.0	68.1	64.7	69.0	70.1
S24F6	9.2	6.0	3.5	66.4	68.5	62.1	67.6	69.7

Figure 7.3 compares the overall Fe recovery data, as a function of solids throughput, of these deslimed feed runs with those performed on the original feed (Chapter 5) for both the 3 mm and 1.8 mm channels. With the exception of one run, for the same solids throughputs the deslimed feed runs achieved higher recoveries than the original feed in the 3 mm channels. For the deslimed feed, the lowest solids concentration runs achieved Fe recoveries of ~70 %. The best recovery seen in the original was 63 %.

The biggest difference is seen at a throughput of 14 t/m² h where the recoveries for the deslimed feed are roughly double that of the original feed in same 3 mm channels. Additionally, the two data points here from the deslimed feed are not dilute, being 18.3 and 36.5 wt.% respectively. This large difference in recovery shows the benefits of the prior desliming stage. Also at this throughput, one run in the 1.8 mm channels (S24G4, 18.5 wt.%) approached the same recovery as the deslimed Run S24F3 which had the same feed conditions, and exceeded the more concentrated deslimed Run S24F2. This again highlights the effectiveness of dilution and high shear rates. It is clear that the benefits of a first-stage desliming step are more evident when the second stage is operated at a higher solids throughput.

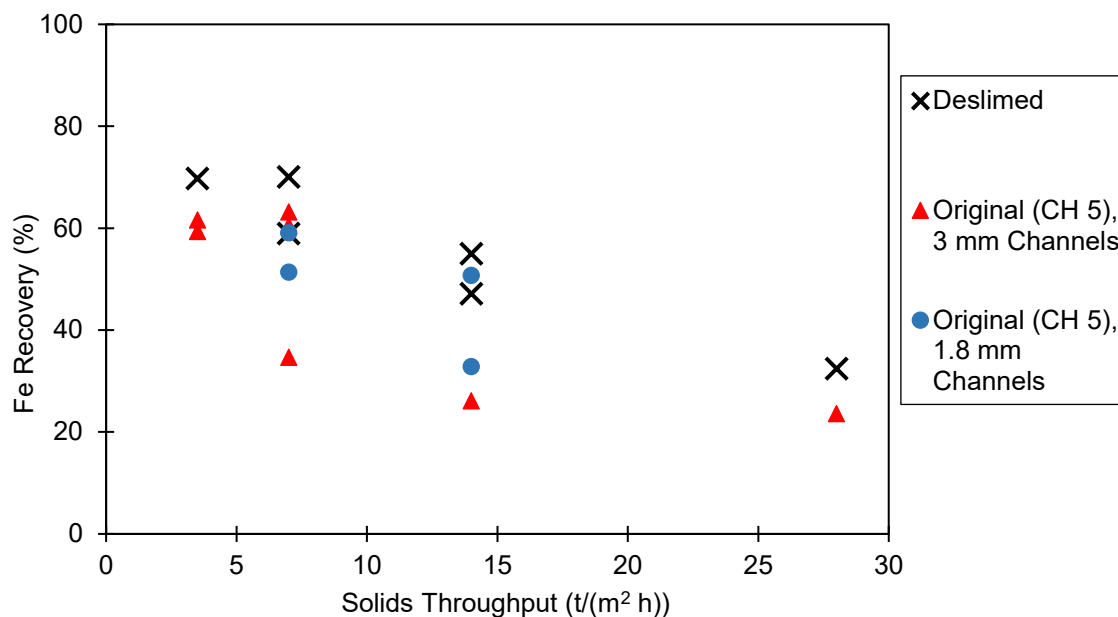


Figure 7.3: Overall Fe recovery for each run using the deslimed feed as well as the original feed (Chapter 5) in both the 3 mm and 1.8 mm channels.

Samples from each stream were screened and assayed. This size \times assay data were used to generate the curves of solids yield to underflow and Fe recovery shown in Figures 7.4 and 7.5 respectively. Again, for such high grades the Fe contents were of secondary importance. Figures 7.4 and 7.5 were prepared using the mass balanced data with the raw data presented in Appendix D.

The yield curves all show a slight drop toward the coarse end, with the recovery curves all remaining constant at the maximum partition value. These results, unlike those in the Graviton, indicate gangue rejection across the entire particle size range. These data can be seen in the size \times assay tables in Appendix D. As with the overall results in Table 7.2, the separation performance improved for lower throughput and lower solids concentration runs. Comparing the runs at the same throughput, i.e. S24F2 and S24F3 at 14 t/(m² h), and S24F4 and S24F5 at 7 t/(m² h) shows the benefit of operating at lower solids concentration and higher flowrates. For each case, the more dilute run showed a finer separation size and higher recovery across the size range.

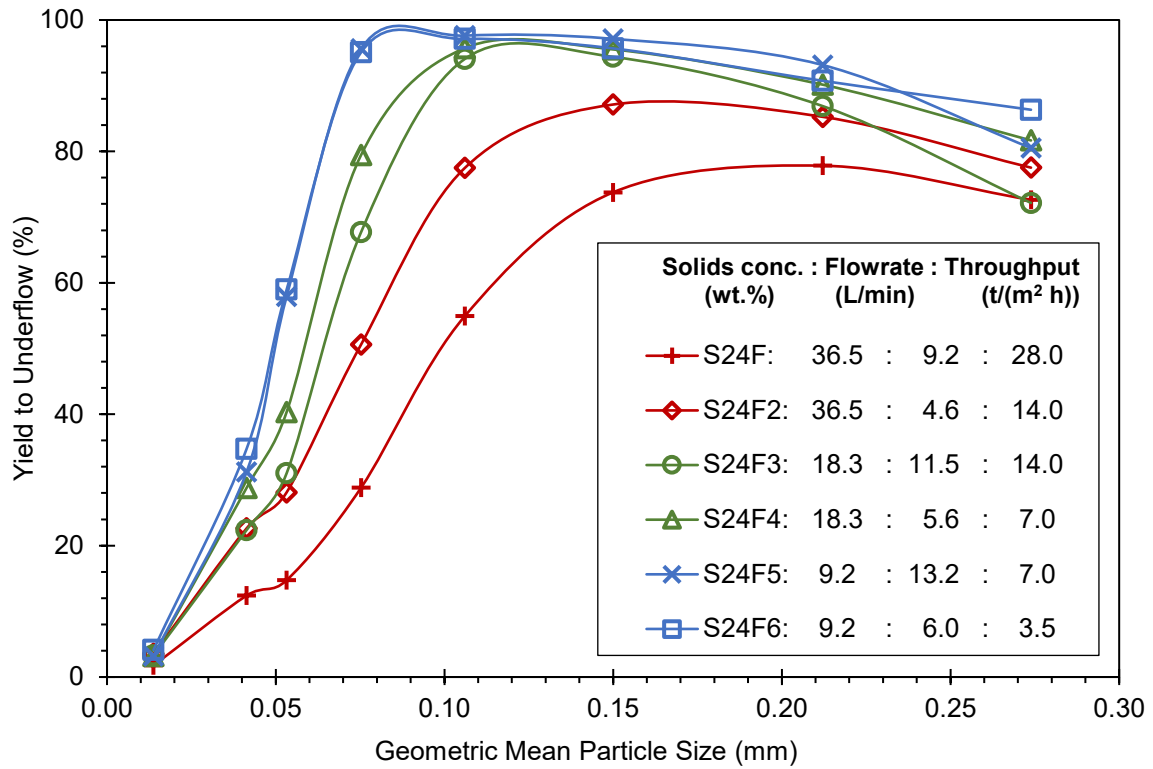


Figure 7.4: Solids yield to underflow as a function of mean particle size for the deslimed feed (mass-balance data).

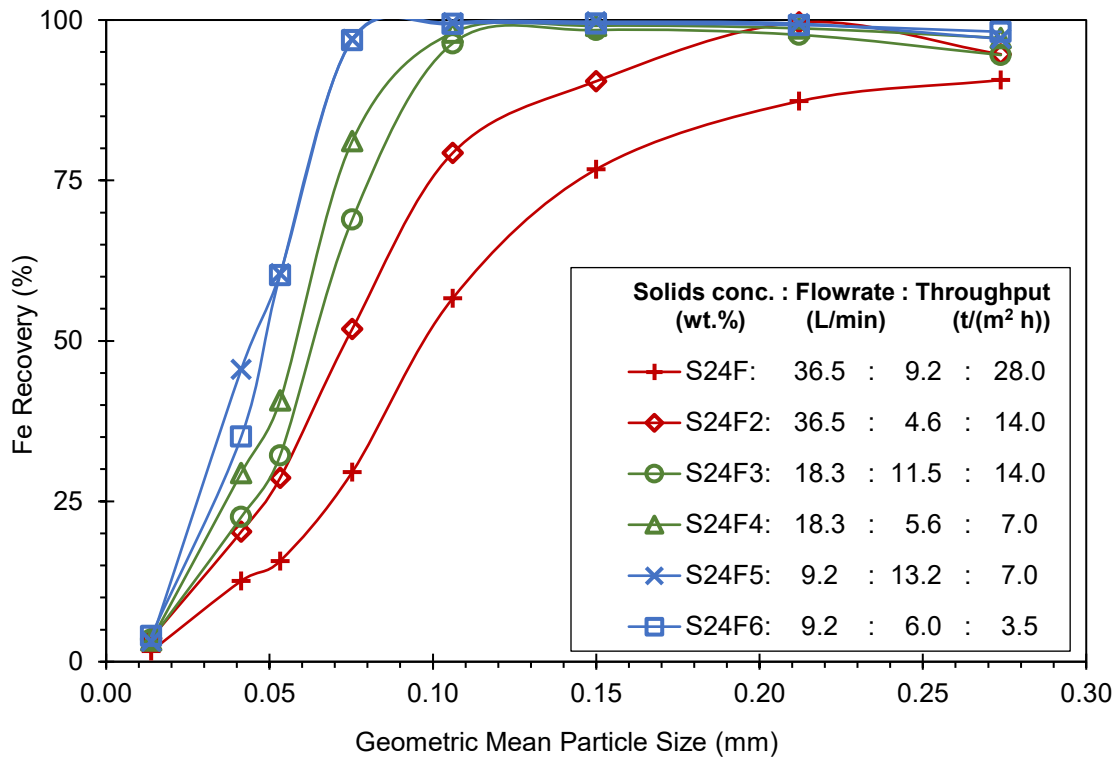


Figure 7.5: Fe recovery as a function of mean particle size for the deslimed feed (mass-balanced data).

Figure 7.6 compares the Fe recovery curves for select runs from this work and Chapter 5, all with the same solids throughputs, to highlight the significance of the results in terms of the impact of slimes. Firstly, the poor performing Run S24B3 (36.5 wt.%, 2.6 L/min) is shown as a benchmark. This run had a high solids concentration and low shear rate, which causes a high level of hindered settling and limits the settling of dense particles. Hence, this run showed a low recovery and yield. To combat this, two methods were investigated. The first method was lowering the solids concentration and increasing the feed flowrate to maintain the same solids throughput. Run S24D (18.5 wt.%, 5.5 L/min) had improved separation through both a higher shear rate and less interference from the slimes in the more dilute suspension. The second method was to simply increase the shear rate through the use of narrow channel spacings. For this Run S24G2 used the same feed conditions (36.5 wt.%, 2.6 L/min) as S24B3. In this run the positive effect of higher shear rate is clearly seen. The deslimed Run S24F4 (18.3 wt.%, 5.6 L/min) shows the 'ideal' case where the separation occurs without any hindrance from the presence of slimes. Comparing this run to the other two shows very similar results. The significance of this is that by simply diluting the feed, and increasing the flowrate for higher shear and maintaining the solids throughput, the separation performance of the REFLUX™ Classifier is similar to those runs performed with the 'ideal' deslimed feed. The 1.8 mm channel run does not quite reach the same recovery as the deslimed or diluted run, but it is still worth noting the improved performance compared to the S24B3 under the same conditions.

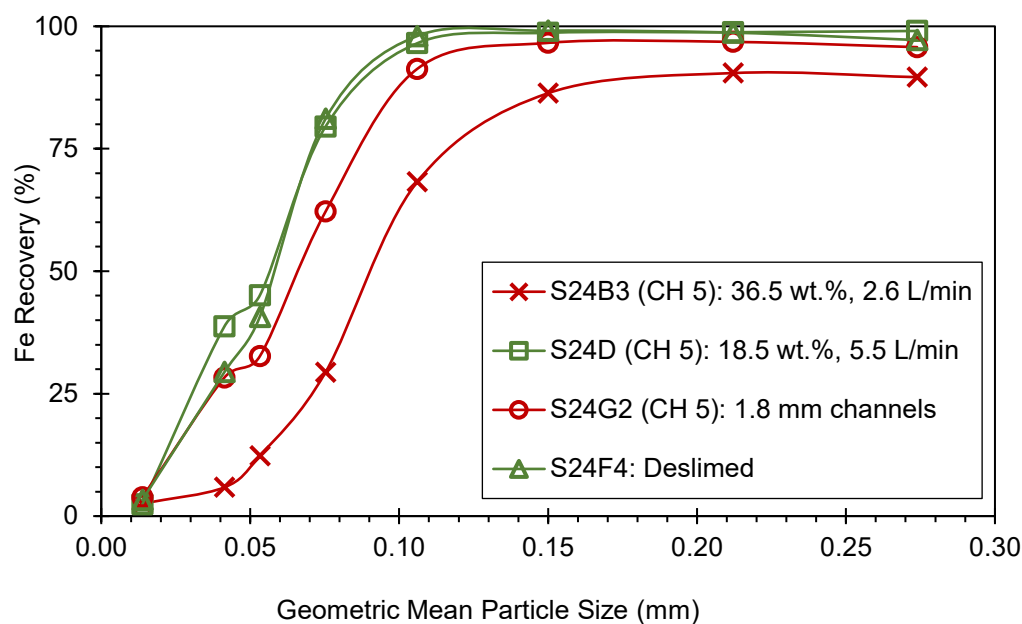


Figure 7.6: Comparison of Fe recovery curves for runs utilising different methods of combatting the slimes issue. The poor performing run (S24B3) and deslimed run (S24F4) are given as reference points. The lower solids concentration run (S24D) and narrow channel run (S24G2) demonstrate how the slimes issue can be overcome (mass-balanced data).

7.4 Rheology

Following the same methodology as the rheology experiments on the original feed (Section 5.4), a small sample of the overflow stream of Run S24F2 was allowed to settle before decanting. The solids were then screened at 0.038 mm. The -0.038 mm solids represent the ultrafines/slimes remaining in the feed after desliming in the Graviton. Figure 7.7 shows a comparison between the particle size distributions for these samples. The distributions show that the deslimed overflow solids contain minimal particles below 0.010 mm, again a testimony to the success of the desliming stage in the Graviton. The Sauter mean diameter increased from 0.0023 mm for the original sample to 0.011 mm in the deslimed sample.

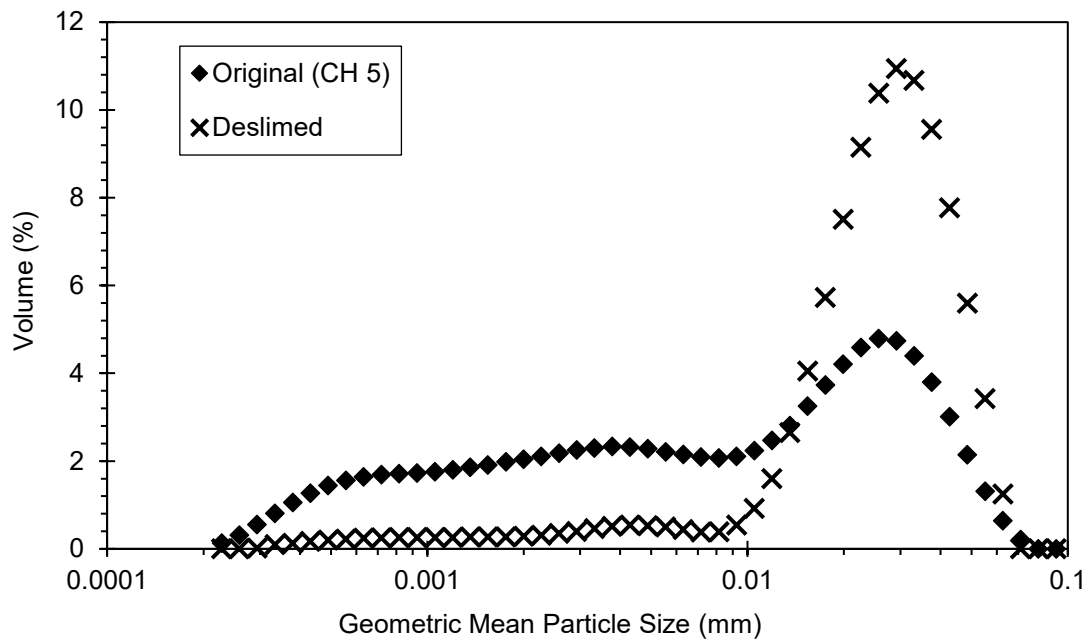


Figure 7.7: Particle size distributions for the -0.038 mm overflow solids from the original rheology experiments and the deslimed experiments, as measured by a Malvern Mastersizer 3000.

The solids were diluted to several different volume fractions and the viscosity was measured for a range of shear rates. This data is shown in Figure 7.8. Like the original feed, there is a strong shear thinning behaviour before levelling out. The key difference between this data set and that for the original feed (Figure 5.12) is that the slimes volume fractions being tested here is considerably higher. The highest volume fraction tested in the original feed was only 0.114, half of the lowest fraction tested in this work. For this deslimed feed, the rheometer was unable to detect any significant shear stress reading below a volume fraction of 0.22. Here it is noted that the highest overflow volume fraction observed in the deslimed feed experiments was only 0.075. Thus, the viscosity effect imposed by the ultrafine particles still present in those runs would have been minimal. Appendix E contains the raw rheology data.

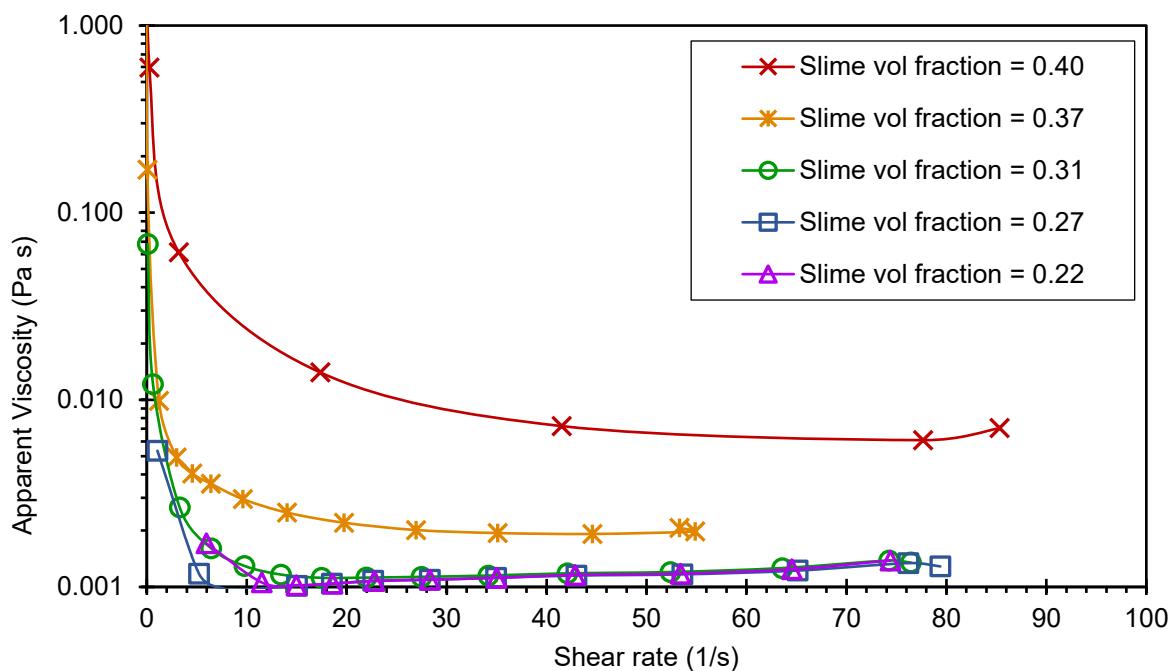


Figure 7.8: Apparent viscosity as a function of shear rate for suspensions with varying volume fractions of the -0.038 mm overflow particles from the deslimed feed experiment S24F2.

Particle volume fraction again has a large effect on the viscosity. Across the entire shear rate range, Figure 7.8 shows the viscosity of the highest volume fraction, 0.40, to be almost an order of magnitude higher than the next highest volume fraction. To clearly show this, the viscosity is plotted as a function of particle volume fraction in Figure 7.9. The viscosity values are selected at a shear rate of 10 s^{-1} and compared to the viscosity values from the original feed experiments and the model of Krieger and Dougherty (1959) with a maximum packing fraction value of 0.64. The data for the deslimed feed is far closer to the 'ideal' case of the model. The sharp viscosity increase occurs at a much higher particle volume fraction, and more suddenly, although there are limited data points. A scaling factor was again applied to this data to fit the Krieger and Dougherty model. For this deslimed feed the best fit was obtained with a scaling factor of only 1.4, compared to 5.5 for the original feed (Chapter 5). As stated before, these volume fractions are far higher than those observed in the overflows of the experiments, and hence the actual effective viscosity experienced in the REFLUX™ Classifier was much lower.

The peak of the sudden inflection occurs at a volume fraction of 0.40. For the model curve, the value for the maximum packing fraction, ϕ_{\max} , used is 0.64, the value for random close packing of rigid spheres of a similar size. This is the value of the peak of the inflection where the viscosity tends toward infinity. As ϕ_{\max} is dependent on the particle shape, shear rate, and size distribution, and the particles of this feed are not necessarily rigid spheres the suspension will have a lower maximum packing fraction. Barnes et al. (1989) lists several empirically determined ϕ_{\max} values for suspensions of asymmetric particles including different clay types, rods and plates. These values are as low as 0.3. Hence an alternative to scaling to fit the model with $\phi_{\max} = 0.64$ would be to assume that the value of ϕ_{\max} for this suspension is not 0.64, rather it is only slightly greater than 0.40.

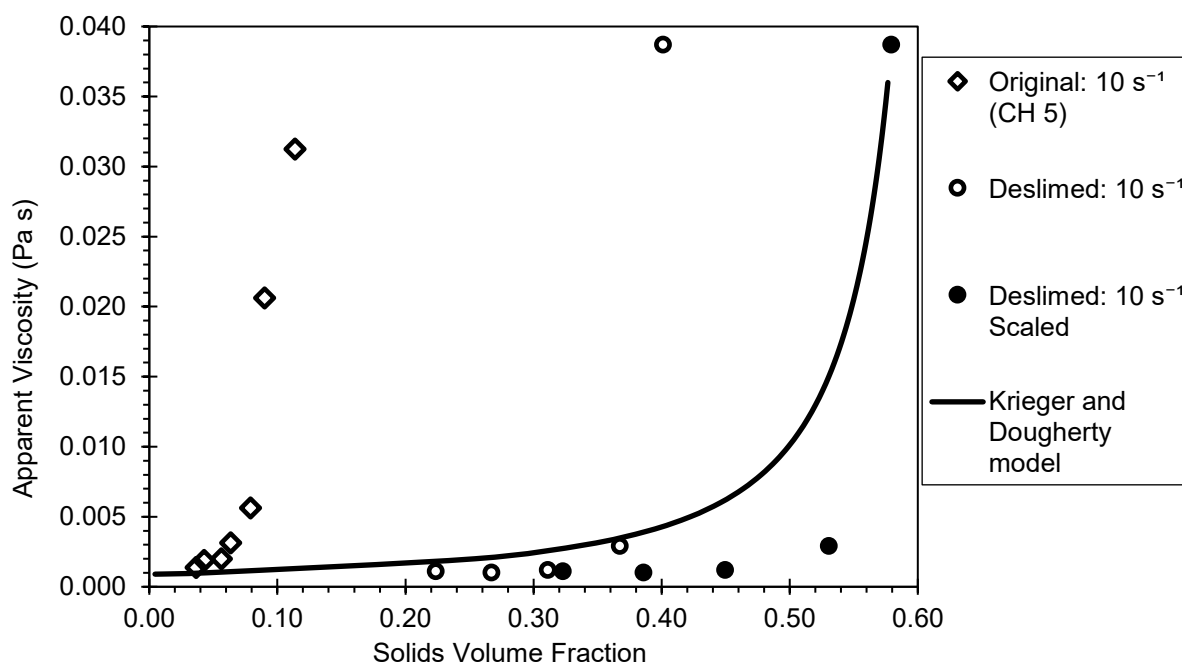


Figure 7.9: Apparent viscosity of the overflow solids as a function of particle volume fraction for a shear rate of 10 s^{-1} for the original and deslimed feed. The solid line shows the model of Krieger and Dougherty (1959) with a maximum packing fraction of $\phi_{\max} = 0.64$. The deslimed feed data is also scaled by a factor of 1.44 to fit the Krieger and Dougherty model (filled circles).

Clearly, the two slimes suspensions show very different behaviour. The size distributions shown in Figure 7.7 indicates the only difference between the two is the amount of -0.010 mm particles. The resulting difference in viscosity seen in Figure 7.9 suggests that the majority of viscous clay particles resided in that size fraction and were successfully removed in the Graviton. The raw size \times assay data

in Appendix D also suggests this distribution, with the grade of the deslimed -0.038 mm overflow fraction being 65.4 wt.% Fe compared to 60.1 wt.% Fe in the original experiments.

7.5 Concluding Summary

This chapter has demonstrated the Graviton to be successful in eliminating the high viscosity problem caused by the slimes. Rheological data showed that through the removal of the -0.010 mm particles, the slimes suspension could reach much higher solids fractions before a sharp increase in viscosity was seen. The deslimed overflow solids exhibited sedimentation characteristics similar to that of 'ideal' solids behaviour.

The benefits of the desliming stage were best seen at higher solids throughputs where the Fe recovery was double that of the original feed under the same conditions. When operated at lower solids concentrations and throughputs, although still higher, the difference in Fe recovery between the deslimed and original feeds was much lower. Clearly, the slimes issue was most potent at higher solids concentrations.

Operating the REFLUX™ Classifier using the deslimed feed also provided further insights into the results presented in Chapter 5. In Figure 7.6, it was evident that with the same solids throughput, a more dilute suspension (from Chapter 5) behaved almost identically to the deslimed case. Without altering the feed conditions, the higher shear rate produced by using a more-narrow channel spacing of 1.8 mm resulted in the Fe recovery increasing towards that of the deslimed run, however the performance was poorer than that observed for the diluted run. Hence, in combatting the negative viscous effects of the clays, dilution and increased shear rates provide ideal conditions to perform the separation as if the clays were completely absent. Importantly, these methods were applied without sacrificing throughput.

Chapter 8

Conclusions and Recommendations

8.1 Summary of Present Work

The minerals industry has long found the separation of ultrafine particles to be a difficult and costly process. The viscous effects of slimes reduce the recovery of valuable ultrafines and pose issues for further downstream processes including dewatering. Hence, in conventional plants a desliming stage, usually involving hydrocyclones, has been widely implemented. However, with this measure comes a significant loss of valuable particles, not to mention the negative impact on downstream performance arising from incomplete removal of the slimes.

Therefore, it is highly desirable that the industry establish new technologies that can efficiently remove slimes, at the finest possible size, and in turn improve recovery at all particle sizes to achieve the highest possible grade. The need for such technology was identified in this study. The focus of the work was on the rheology of the slimes, the direct effects of the slimes viscosity on gravity separation across a broad size range, and how to mitigate the impact of the slimes. This was examined through their efficient removal, and through changes to the hydrodynamic conditions such as solids concentration and shear rate.

8.1.1 Initial REFLUX™ Classifier Results with High-Slimes Feed

The REFLUX™ Classifier is an established separation process that is becoming widely adopted. This separation device combines a fluidised bed with hydrodynamic transport through inclined channels to produce strong density-based separations. In the presence of slimes, however, the separation performance deteriorates due to higher viscous forces. A systematic series of experiments was conducted, utilising a high-grade iron ore feed containing a significant portion of slimes, to quantify the effects of varying slimes concentration on performance.

Initial experiments at high solids throughputs of 14 and 28 t/(m² h) and a high feed slurry solids concentration of 36.5 wt.% produced relatively poor solids yields and Fe recoveries to the underflow of both only around 30 wt.%. Upon reducing the solids throughput to 7 and then 3.5 t/(m² h), these values improved. Interestingly, at a throughput of 7 t/(m² h), by simultaneously halving the solids

concentration to 18.5 wt.% solids and doubling the volumetric feed flowrate to maintain to same overall solids throughput, the separation performance also improved significantly with both the yield to underflow and Fe recoveries doubling to around 60 wt.%. Size assay data revealed that these higher yields and Fe recoveries were achieved across the entire size range. The separation cut point size was also finer at the higher flowrate. However, a further reduction in the solids concentration and increase in the volumetric feed rate resulted in no further improvement in separation performance.

These findings were contrary to usual expectation and practice. Normally the solids throughput is improved by elevating the solids concentration so that the volumetric flow rate can be reduced. Physically, there appears to be a transition at a feed concentration of about 18.5 wt.% solids, with a strong deterioration in performance at higher feed concentrations, but highly effective performance below this concentration. This finding can be attributed to the presence of slimes in this feed.

Experiments using a narrower channel spacing revealed that the separation performance could be improved without altering the feed conditions. The higher shear rate created through the smaller channels was effective at reducing the viscous effects of the slimes, even at the higher solids concentrations. At 36.5 wt.% solids and a feed flowrate of 2.6 L/min the yield to underflow and Fe recovery were both approximately 50 wt.%. A run at identical flow conditions, but with the wider 3 mm channels, only achieved a yield and Fe recovery of around 30 wt.%.

8.1.2 Rheological Experiments

The rheology of the slimes was studied by using the -0.038 mm fraction from a REFLUX™ Classifier overflow sample. Suspensions were prepared at different solids volume fractions and a rheometer used to measure the shear stress and thus apparent viscosity across a range of shear rates. Strong shear thinning behaviour was observed. There was also a strong dependence on particle volume fraction, with an exponential increase beyond a critical point.

The rheological data provided a clear explanation for the deterioration in the separation performance of the REFLUX™ Classifier. The critical change in behaviour at a feed solids concentration of around

18.5 wt.% solids corresponded to a strong increase in the suspension viscosity across all shear rates. It was therefore possible to explain the consistent separation performance at 18.5 wt.% and 9.5 wt.% solids, but significantly poorer performance at 36.5 wt.%. The shear thinning behaviour of the slimes also provided an explanation for the superior performance of both the narrower channel spacings and the higher flowrate runs, both of which induced higher shear rates within the inclined channels. Calculations based on the water component of the overflow rates indicated that the shear rates within the channels varied between 0 and 80 s^{-1} with an average being approximately 16 s^{-1} . This value roughly coincided with the beginning of the sharp increase in viscosity seen at low shears in the rheology data. For runs with high solids concentrations, those with shear rates below this value all showed poorer yields and Fe recoveries.

The viscosity data for the slimes was compared to a well-known model for an 'ideal' suspension of rigid spheres (Krieger & Dougherty, 1959). The experimental data required a volume scaling factor of 5.5 to fit the model curve. This indicated that the slimes particles occupy a volume, or a sphere of influence, 5.5 times larger than their actual solids volume.

8.1.3 REFLUX™ Classifier and Rheological Results with Deslimed Feed

Further REFLUX™ Classifier experiments were performed over a range of feed solids concentrations and flowrates on a feed that had been deslimed at a particle size of about 0.010 mm using the Graviton. At the higher solids concentrations the overall Fe recovery was notably better than in the previous work. For instance a run at a throughput of $14 \text{ t}/(\text{m}^2 \text{ h})$ using the deslimed feed achieved a recovery of 55 %, roughly double that achieved with the original feed. However, at the lower solids concentrations the separation performance was similar to that observed in the previous work with the deslimed Fe recovery being around 70 % versus about 63 % in the original runs.

Four experiments were compared in terms of the Fe recovery across the entire size range: a high concentration run, a low concentration run (both on the original feed), a high concentration run with the narrow channel spacings (original feed), and a deslimed run. Little difference was seen between

the deslimed case and the diluted, higher flowrate run of the original feed. The identical run in the narrower channels for the original feed also approached the same separation performance as the deslimed run. All three showed a significant improvement over the high concentration run of the original feed. This set of results shows that the effect of slimes in the REFLUX™ Classifier can be practically eliminated through use of dilution or higher shear rates.

The rheological experiments were repeated using overflow samples taken from these REFLUX™ Classifier experiments that had been deslimed first in the Graviton. Following the desliming, the new overflow samples had significantly less particles below 0.010 mm. A strong shear thinning behaviour was again observed. The viscosity versus solids volume fraction relationship of the deslimed overflow solids was far closer to that of the 'ideal' solids case, requiring a scaling factor of only 1.4 to match the model compared to a factor of 5.5 for the original overflow samples. The key difference between the measurements of the original and deslimed overflow samples was the volume fraction of solids tested. For the deslimed samples, the rheometer could not detect any shear stress below a volume fraction of 0.22, almost three times higher than the actual maximum overflow solids volume fraction observed in any of the REFLUX™ Classifier experiments on the deslimed feed. Thus, any ultrafines remaining after desliming had minimal effect on the slurry viscosity within the inclined channels.

8.1.4 REFLUX™ Graviton Results

This thesis also explored the use of a new technology, the REFLUX™ Graviton. By subjecting REFLUX™ Classifier modules to centrifugal forces, it is possible to combine the hydrodynamic benefits of the inclined channels with those from centrifugal forces. Previous work on this system had only been conducted under semi-batch conditions. Here continuous steady-state experiments in the Graviton were conducted for the first time.

Initial experiments were undertaken using a feed of fine silica to determine the effect of different variables on the system. This work demonstrated sharp, consistent partitions with separation sizes as low as 5 µm and $\bar{E}p$ values as low as 4 µm. The diameter of the underflow discharge tube governed

the maximum transport rate of the solids to the underflow. Thus, when the outlet diameter was too small, some of the solids that could have exited in the underflow were instead displaced to the overflow, resulting in a poor separation. Similarly, when the outlet diameter was too large, then excess slimes that would normally report to the overflow were instead misplaced to the underflow. However, strong robust performance was achieved through satisfactory selection of the outlet diameter for a given application. The so-called fish-hook effect of the partition curve was then minimised through optimisation of the fluidisation rate. Results from the silica experiments were also compared with the prior semi-batch data. The significant throughput advantage originally reported by Galvin and Dickinson (2013) was shown to hold true for the continuous system.

Building upon the knowledge and understanding gained from the silica experiments, a program of experiments was conducted using the Graviton covering a range of iron ore feeds. This work was unsuccessful in achieving gravity separation, in which the solids separate across a broad size range according to their density. However, the work showed the system produced remarkably effective desliming at particle sizes of about 10 μm , especially as a two-stage process. Through this removal of ultrafine particles, significant Fe upgrades in the sub 20 μm size fraction were seen. The subsequent product grades achieved were up to 64 wt.% Fe (from a feed grade of 55 wt.% Fe). Hence, for some feeds a single stage desliming process in the Graviton is enough to upgrade an ultrafine waste stream to a saleable grade.

The desliming application was investigated further, processing the same feed as trialed in the REFLUX™ Classifier. The entire upgrade was due to the desliming, and hence removal of the ultrafine particles. There was no upgrade achieved at the coarser sizes, as occurs using the REFLUX™ Classifier. The desliming process did, however, produce extremely high yields and Fe recoveries in excess of 90 %, whilst successfully removing the vast majority of particles finer than 10 μm . This Graviton desliming step provided the feed for the set of subsequent experiments in the REFLUX™ Classifier.

Finally, the Graviton was tested to cover more extreme conditions by adding coarse particles up to 1000 μm in size to the feed. Given the high G forces, the probability of these coarse particles reporting to the inclined channels was expected to be negligible. The goal was to effectively strip the finest portion of the particles from the feed i.e. to deslime at about 10 μm . Although only a limited number of runs was performed, the results indicated that results similar to those for the feed with the 300 μm top size should be attainable.

8.2 Recommendations for Future work

This thesis has presented a large body of work investigating the capabilities of the REFLUX™ Graviton and the effects of slimes concentration and throughput on the beneficiation performance of a standard REFLUX™ Classifier. From this work new opportunities for utilising the REFLUX™ Graviton and Classifier systems are evident. Within the limitations of the existing Graviton machine, the following recommendations are made for further potential investigation:

1. In this thesis, the effect of different channel spacings on separations in the REFLUX™ Classifier was investigated. In the Graviton, however, only one channel spacing and one fixed speed was used. Future investigations could cover the use of different modules with different channel spacing and also confirm the performance of the Graviton over a range of speeds.
2. The current set up of the Graviton only uses two modules. Future investigations could also scale up the number of modules, enabling higher throughputs to be processed. The feed system might require some re-design to handle this.
3. The work in this thesis has highlighted the desliming application of the Graviton with efficient, reproducible size separations. To promote density driven separations, improved control of the fluidised bed and underflow discharge is needed. It is therefore recommended to implement an automatic underflow valve controlled in a similar fashion to the REFLUX™ Classifier. This will be a challenge due to the complexities of a rotating system, higher forces and multiple modules.

The experiments conducted on the REFLUX™ Classifier covered new areas concerned specifically with the effects of slimes and the benefits of using closely spaced inclined channels, down to 1.8 mm. The results from this work also invite further investigation. The high-grade feed allowed for easy analysis of Fe recovery, however moving forward it would be beneficial to investigate the separation of a lower grade feed, still with a significant portion of slimes, to assess whether the findings of this work hold true more generally. A wealth of knowledge could also be gained through proper identification and characterisation of the slimes and clay types present. Understanding the full nature of the problem could reveal new ways of overcoming the effects of the slimes.

References

- Acrivós, A., & Herbolzheimer, E. (1979). Enhanced sedimentation in settling tanks with inclined walls. *Journal of fluid mechanics*, 92(03), 435-457.
- Alp, I., Celep, O., Deveci, H., & Vicil, M. (2008). Recovery of gold from a free-milling ore by centrifugal gravity separator. *Iranian Journal of Science & Technology, Transaction B, Engineering*, 32(B1), 67-71.
- Alpha Laval. (2019). Separators. Retrieved from <https://www.alfalaval.com/products/separation/centrifugal-separators/separators/>
- Arnold, B., & Aplan, F. (1986). The effect of clay slimes on coal flotation, part I: The nature of the clay. *International Journal of Mineral Processing*, 17(3-4), 225-242.
- Asif, M. (1997). Modeling of multi-solid liquid fluidized bed. *Chemical Engineering & Technology: Industrial Chemistry-Plant Equipment-Process Engineering-Biotechnology*, 20(7), 485-490.
- Aslan, N. (2008). Multi-objective optimization of some process parameters of a multi-gravity separator for chromite concentration. *Separation and Purification Technology*, 64(2), 237-241.
- Barnes, H. A., Hutton, J. F., & Walters, K. (1989). *An introduction to rheology*: Elsevier.
- Batalović, V. (2011). Centrifugal separator, the new technical solution, application in mineral processing. *International Journal of Mineral Processing*, 100(3-4), 86-95.
- Batchelor, G. (1977). The effect of Brownian motion on the bulk stress in a suspension of spherical particles. *Journal of fluid mechanics*, 83(1), 97-117.
- Becker, H. (1959). The effects of shape and Reynolds number on drag in the motion of a freely oriented body in an infinite fluid. *The Canadian Journal of Chemical Engineering*, 37(2), 85-91.
- Beetstra, R., van der Hoef, M. A., & Kuipers, J. A. M. (2007). Numerical study of segregation using a new drag force correlation for polydisperse systems derived from lattice-Boltzmann simulations. *Chemical Engineering Science*, 62(1), 246-255.
- Bhaskar, K. U., Barnwal, J., Rao, T., & Venugopal, R. (1999). Multigravity separator to enrich heavy minerals from a lead flotation concentrate. *Mining, Metallurgy & Exploration*, 16(2), 61-64.
- Bird, R. B., Stewart, W. E., & Lightfoot, E. N. (1960). *Transport Phenomena*. New York: John Wiley & Sons.
- Bourgeois, F., & Majumder, A. K. (2013). Is the fish-hook effect in hydrocyclones a real phenomenon? *Powder Technology*, 237, 367-375.
- Boycott, A. E. (1920). Sedimentation of blood corpuscles. *Nature*, 104, 532-532.
- Burke, S. P., & Plummer, W. (1928). Gas flow through packed columns¹. *Industrial & Engineering Chemistry*, 20(11), 1196-1200.
- Carman, P. C. (1937). Fluid flow through granular beds. *Trans. Inst. Chem. Eng.*, 15, 150-166.

- Chan, B., Mozley, R. H., & Childs, G. (1991). Extended trials with the high tonnage multi-gravity separator. *Minerals Engineering*, 4(3-4), 489-496.
- Chaurasia, R. C., & Nikkam, S. (2017). Beneficiation of low-grade iron ore fines by multi-gravity separator (MGS) using optimization studies. *Particulate Science and Technology*, 35(1), 45-53.
- Chong, Y. S., Ratkowsky, D. A., & Epstein, N. (1979). Effect of particle shape on hindered settling in creeping flow. *Powder Technology*, 23(1), 55-66.
- Cicek, T., & Cöcen, I. (2002). Applicability of Mozley multigravity separator (MGS) to fine chromite tailings of Turkish chromite concentrating plants. *Minerals Engineering*, 15(1-2), 91-93.
- Colic, M., Morse, W., & Miller, J. D. (2007). The development and application of centrifugal flotation systems in wastewater treatment. *International Journal of Environment and Pollution*, 30(2), 296-312.
- Das, A., & Sarkar, B. (2018). Advanced gravity concentration of fine particles: A review. *Mineral Processing and Extractive Metallurgy Review*, 39(6), 359-394.
- Davis, R. H., & Acrivos, A. (1985). Sedimentation of noncolloidal particles at low Reynolds numbers. *Annual Review of Fluid Mechanics*, 17(1), 91-118.
- Davis, R. H., Zhang, X., & Agarwala, J. (1989). Particle classification for dilute suspensions using an inclined settler. *Industrial & engineering chemistry research*, 28(6), 785-793.
- Dey, S., Pani, S., Mohanta, M., & Singh, R. (2012). Utilization of iron ore slimes: a future prospective. *Separation Science and Technology*, 47(5), 769-776.
- Di Felice, R. (1995). Hydrodynamics of liquid fluidisation. *Chemical engineering science*, 50(8), 1213-1245.
- Doroodchi, E., Zhou, J., Fletcher, D., & Galvin, K. P. (2006). Particle size classification in a fluidized bed containing parallel inclined plates. *Minerals Engineering*, 19(2), 162-171.
- Einstein, A. (1906). Eine neue bestimmung der moleküldimensionen. *Annalen der Physik*, 324(2), 289-306.
- Ergun, S. (1952). Fluid flow through packed columns. *Chem. Eng. Prog.*, 48, 89-94.
- Falconer, A. (2003). Gravity separation: old technique/new methods. *Physical Separation in Science and Engineering*, 12(1), 31-48.
- Forbes, E., Ma, M., & Bruckard, W. (2017). Clay Minerals in Flotation and Comminution Operations. In A. J. McFarlane, C. Klauber, D. J. Robinson, & M. Gräfe (Eds.), *Clays in the Minerals Processing Value Chain* (pp. 302-326). Cambridge: Cambridge University Press.
- Fullam, M., Eng, P., Grewal, I., & Eng, M. S. P. (2001). The Knelson Continuous Variable Discharge (CVD) Concentrator. *The Knelson Group*, 1-6.
- Gabitto, J., & Tsouris, C. (2008). Drag coefficient and settling velocity for particles of cylindrical shape. *Powder Technology*, 183(2), 314-322.

References

- Galvin, K. (2003). On the phenomena of hindered settling in liquid fluidized beds. *Advances in Gravity Concentration, SME*, 19-38.
- Galvin, K., Callen, A., Spear, S., Walton, K., & Zhou, J. (2010a). Gravity Separation of Coal in the Reflux Classifier—New Mechanisms for Suppressing the Effects of Particle Size. *International Journal of Coal Preparation and Utilization*, 30(2-5), 130-144.
- Galvin, K., Doroodchi, E., Callen, A., Lambert, N., & Pratten, S. (2002). Pilot plant trial of the reflux classifier. *Minerals Engineering*, 15(1), 19-25.
- Galvin, K., Pratten, S., & Lam, G. N. T. (1999). A generalized empirical description for particle slip velocities in liquid fluidized beds. *Chemical Engineering Science*, 54(8), 1045-1052.
- Galvin, K., Swann, R., & Ramirez, W. (2006). Segregation and dispersion of a binary system of particles in a fluidized bed. *AIChE journal*, 52(10), 3401-3410.
- Galvin, K., Zhao, Y., & Davis, R. (2001). Time-averaged hydrodynamic roughness of a noncolloidal sphere in low Reynolds number motion down an inclined plane. *Physics of Fluids*, 13(11), 3108-3119.
- Galvin, K., Zhou, J., Dickinson, J., & Ramadhani, H. (2012). Desliming of dense minerals in fluidized beds. *Minerals Engineering*, 39, 9-18.
- Galvin, K., Zhou, J., Price, A., Agrwal, P., & Iveson, S. (2016). Single-stage recovery and concentration of mineral sands using a reflux™ classifier. *Minerals Engineering*, 93, 32-40.
- Galvin, K. P., Callen, A., Zhou, J., & Doroodchi, E. (2005). Performance of the reflux classifier for gravity separation at full scale. *Minerals Engineering*, 18(1), 19-24.
- Galvin, K. P., & Dickinson, J. E. (2013). Particle transport and separation in inclined channels subject to centrifugal forces. *Chemical Engineering Science*, 87, 294-305.
- Galvin, K. P., & Liu, H. (2011). Role of inertial lift in elutriating particles according to their density. *Chemical Engineering Science*, 66(16), 3687-3691.
- Galvin, K. P., Walton, K., & Zhou, J. (2009). How to elutriate particles according to their density. *Chemical Engineering Science*, 64(9), 2003-2010.
- Galvin, K. P., Zhou, J., & Walton, K. (2010b). Application of closely spaced inclined channels in gravity separation of fine particles. *Minerals Engineering*, 23(4), 326-338.
- Garside, J., & Al-Dibouni, M. R. (1977). Velocity-voidage relationships for fluidization and sedimentation in solid-liquid systems. *Industrial & engineering chemistry process design and development*, 16(2), 206-214.
- Gibilaro, L. G., Di Felice, R., Waldram, S. P., & Foscolo, P. U. (1986). A predictive model for the equilibrium composition and inversion of binary-solid liquid fluidized beds. *Chemical Engineering Science*, 41(2), 379-387.
- Göktepe, F. (2005). Treatment of lead mine waste by a Mozley multi-gravity separator (MGS). *Journal of environmental management*, 76(4), 277-281.

- Gräfe, M., Klauber, C., McFarlane, A. J., & Robinson, D. J. (2017). *Clays in the Minerals Processing Value Chain*. Cambridge: Cambridge University Press.
- Greenspan, H., & Ungarish, M. (1985a). On the centrifugal separation of a bulk mixture. *International journal of multiphase flow*, 11(6), 825-835.
- Greenspan, H., & Ungarish, M. (1985b). On the enhancement of centrifugal separation. *Journal of Fluid Mechanics*, 157, 359-373.
- Haeberle, S., Brenner, T., Zengerle, R., & Ducreé, J. (2006). Centrifugal extraction of plasma from whole blood on a rotating disk. *Lab on a Chip*, 6(6), 776-781.
- Hartman, M., Trnka, O., & Svoboda, K. (1994). Free settling of nonspherical particles. *Industrial & engineering chemistry research*, 33(8), 1979-1983.
- He, M., Wang, Y., & Forssberg, E. (2004). Slurry rheology in wet ultrafine grinding of industrial minerals: a review. *Powder technology*, 147(1-3), 94-112.
- Heiskanen, K. (2000). Experimental hydrocyclone roping models. *Chemical Engineering Journal*, 80(1-3), 289-293.
- Herschel, W. H., & Bulkley, R. (1926). Konsistenzmessungen von gummi-benzollösungen. *Colloid & Polymer Science*, 39(4), 291-300.
- Honaker, R. (1998). High capacity fine coal cleaning using an enhanced gravity concentrator. *Minerals engineering*, 11(12), 1191-1199.
- Honaker, R., Das, A., & Nombe, M. (2005). Improving the separation efficiency of the Knelson concentrator using air injection. *Coal Preparation*, 25(2), 99-116.
- Honaker, R., Wang, D., & Ho, K. (1996). Application of the Falcon concentrator for fine coal cleaning. *Minerals Engineering*, 9(11), 1143-1156.
- Hsu, H.-W., & Perry, E. S. (1981). *Separations by centrifugal phenomena*. New York: Wiley.
- Jameson, G. J. (2012). The effect of surface liberation and particle size on flotation rate constants. *Minerals Engineering*, 36, 132-137.
- Jena, S., Sahoo, H., Rath, S., Rao, D., Das, S., & Das, B. (2015). Characterization and processing of iron ore slimes for recovery of iron values. *Mineral Processing and Extractive Metallurgy Review*, 36(3), 174-182.
- Jull, N. (1972). Parameters for hydrocyclone selection. *Proceedings Canadian Mineral Processors*.
- Kawatra, S., Bakshi, A., & Rusesky, M. (1996). Effect of viscosity on the cut (d₅₀) size of hydrocyclone classifiers. *Minerals Engineering*, 9(8), 881-891.
- Khan, A., & Richardson, J. (1989). Fluid-particle interactions and flow characteristics of fluidized beds and settling suspensions of spherical particles. *Chemical Engineering Communications*, 78(1), 111-130.

References

- Kim, S.-W., Jeon, J.-W., Suh, I.-K., & Jung, S.-M. (2016). Improvement of sintering characteristics by selective granulation of high Al₂O₃ iron ores and ultrafine iron ores. *Ironmaking & Steelmaking*, 43(7), 500-507.
- King, M. R., & Leighton, J., David T. (1997). Measurement of the inertial lift on a moving sphere in contact with a plane wall in a shear flow. *Physics of Fluids*, 9(5), 1248-1255.
- Knelson, B. (1992). The Knelson concentrator. Metamorphosis from crude beginning to sophisticated world wide acceptance. *Minerals Engineering*, 5(10-12), 1091-1097.
- Koppalkar, S. (2009). Effect of operating variables in knelson concentrators: A pilot-scale study. *McGill University*.
- Kraipech, W., Chen, W., Parma, F. J., & Dyakowski, T. (2002). Modelling the fish-hook effect of the flow within hydrocyclones. *International Journal of Mineral Processing*, 66(1-4), 49-65.
- Kraipech, W., Nowakowski, A., Dyakowski, T., & Suksangpanomrung, A. (2005). An investigation of the effect of the particle-fluid and particle-particle interactions on the flow within a hydrocyclone. *Chemical Engineering Journal*, 111(2-3), 189-197.
- Krieger, I. M., & Dougherty, T. J. (1959). A mechanism for non-Newtonian flow in suspensions of rigid spheres. *Transactions of the Society of Rheology*, 3(1), 137-152.
- Kroll-Rabotin, J.-S., Bourgeois, F., & Climent, E. (2013). Physical analysis and modeling of the Falcon concentrator for beneficiation of ultrafine particles. *International Journal of Mineral Processing*, 121, 39-50.
- Lamb, H. (1953). *Hydrodynamics* (6th ed.). Cambridge: Cambridge University Press.
- Lapple, C. E. (1950). Dust and Mist Collection. In J. H. Perry (Ed.), *Chemical Engineers' Handbook* (3rd ed.): McGraw-Hill Book Co.
- Laskovski, D., Duncan, P., Stevenson, P., Zhou, J., & Galvin, K. P. (2006). Segregation of hydraulically suspended particles in inclined channels. *Chemical Engineering Science*, 61, 7269 - 7278.
- Lockett, M., & Al-Habbooby, H. (1973). Differential settling by size of two particle species in a liquid. *Trans. Inst. Chem. Eng*, 51(2), 281.
- Luo, L., Zhang, Y., Bao, S., & Chen, T. (2016). Utilization of iron ore tailings as raw material for portland cement clinker production. *Advances in Materials Science and Engineering*, 2016.
- Luttrell, G., Phillips, D., & Honaker, R. (1995). *Enhanced gravity separators: new alternatives for fine coal cleaning*. Paper presented at the 12th International coal preparation conference, Lexington, Kentucky.
- Majumder, A., & Barnwal, J. (2006). Modeling of enhanced gravity concentrators—present status. *Mineral Processing and Extractive Metallurgy Review*, 27(1), 61-86.
- Majumder, A., Bhoi, K., & Barnwal, J. (2007a). Multi-gravity separator: an alternate gravity concentrator to process coal fines. *Mining, Metallurgy & Exploration*, 24(3), 133-138.
- Majumder, A., Shah, H., Shukla, P., & Barnwal, J. (2007b). Effect of operating variables on shape of “fish-hook” curves in cyclones. *Minerals Engineering*, 20(2), 204-206.

- Majumder, A., Yerriswamy, P., & Barnwal, J. (2003). The “fish-hook” phenomenon in centrifugal separation of fine particles. *Minerals Engineering*, 16(10), 1005-1007.
- Mandal, A. K., & Sinha, O. P. (2016). Preparation and characterization of fired bricks made from bottom ash and iron slime. *Journal of Materials in Civil Engineering*, 29(4), 04016245.
- Marion, C., Williams, H., Langlois, R., Kökkılıç, O., Coelho, F., Awais, M., Rowson, N., & Waters, K. (2017). The potential for dense medium separation of mineral fines using a laboratory Falcon Concentrator. *Minerals Engineering*, 105, 7-9.
- Masliyah, J. H. (1979). Hindered settling in a multi-species particle system. *Chemical Engineering Science*, 34(9), 1166-1168.
- Moritomi, H., Iwase, T., & Chiba*, T. (1982). A comprehensive interpretation of solid layer inversion in liquid fluidised beds. *Chemical Engineering Science*, 37(12), 1751-1757.
- Moritomi, H., Yamagishi, T., & Chiba, T. (1986). Prediction of complete mixing of liquid-fluidized binary solid particles. *Chemical Engineering Science*, 41(2), 297-305.
- Nakamura, H., & Kuroda, K. (1937). La cause de l'accélération de la vitesse de sédimentation des suspensions dans les récipients inclinés. *Keijo J. Med*, 8, 256-296.
- Nayak, N. P., & Pal, B. K. (2013). Separation behaviour of iron ore fines in Kelsey centrifugal jig. *Journal of Minerals and Materials Characterization and Engineering*, 1(03), 85.
- Ndlovu, B., Farrokhpay, S., & Bradshaw, D. (2013). The effect of phyllosilicate minerals on mineral processing industry. *International Journal of Mineral Processing*, 125, 149-156.
- Neesse, T., Dueck, J., Schwemmer, H., & Farghaly, M. (2015). Using a high pressure hydrocyclone for solids classification in the submicron range. *Minerals Engineering*, 71, 85-88.
- Nelder, J. A., & Mead, R. (1965). A simplex method for function minimization. *The computer journal*, 7(4), 308-313.
- Nelson, D., Liu, J., & Galvin, K. (1997). Autogenous dense medium separation using an inclined counterflow settler. *Minerals engineering*, 10(8), 871-881.
- Nguyentranlam, G., & Galvin, K. (2000). The development of an innovative classifier. *Chemeca 2000: Opportunities and Challenges for the Resource and Processing Industries*, 375.
- Nguyentranlam, G., & Galvin, K. P. (2001). Particle classification in the reflux classifier. *Minerals Engineering*, 14(9), 1081-1091.
- Niven, R. K. (2002). Physical insight into the Ergun and Wen & Yu equations for fluid flow in packed and fluidised beds. *Chemical Engineering Science*, 57(3), 527-534.
- Oruç, F., Özgen, S., & Sabah, E. (2010). An enhanced-gravity method to recover ultra-fine coal from tailings: Falcon concentrator. *Fuel*, 89(9), 2433-2437.
- Özbayoğlu, G., & Atalay, M. Ü. (2000). Beneficiation of bastnaesite by a multi-gravity separator. *Journal of alloys and compounds*, 303, 520-523.

References

- Özgen, S., Malkoç, Ö., Doğancik, C., Sabah, E., & Şapçı, F. O. (2011). Optimization of a multi gravity separator to produce clean coal from Turkish lignite fine coal tailings. *Fuel*, *90*(4), 1549-1555.
- Panda, L., Biswal, S., Venugopal, R., & Mandre, N. (2018). Recovery of ultra-fine iron ore from iron ore tailings. *Transactions of the Indian Institute of Metals*, *71*(2), 463-468.
- Patel, B. K., Ramirez, W. F., & Galvin, K. P. (2008). A generalized segregation and dispersion model for liquid-fluidized beds. *Chemical Engineering Science*, *63*(6), 1415-1427.
- Patwardhan, V., & Tien, C. (1985). Sedimentation and liquid fluidization of solid particles of different sizes and densities. *Chemical Engineering Science*, *40*(7), 1051-1060.
- Perry, R., & Green, D. (1999). *Perry's Chemical Engineers' Handbook* (7th ed.). Ney York: McGraw-Hill
- Pettyjohn, E. (1948). Effect of particle shape on free settling rates of isometric particles. *Chem. Eng. Prog.*, *44*, 157-172.
- Plitt, L., Flintoff, B., & Stuffco, T. (1987). *Roping in hydrocyclones*. Paper presented at the Proceedings of the 3rd International Conference on Hydrocyclones, Oxford, BHRA. Elsevier, Amsterdam, Paper A-3.
- Ponder, E. (1925). ON SEDIMENTATION AND ROULEAUX FORMATION-I. *Quarterly journal of experimental physiology*, *15*(3), 235-252.
- Pradhan, N., Das, B., Gahan, C. S., Kar, R. N., & Sukla, L. B. (2006). Beneficiation of iron ore slime using *Aspergillus niger* and *Bacillus circulans*. *Bioresource technology*, *97*(15), 1876-1879.
- Quemada, D. (1977). Rheology of concentrated disperse systems and minimum energy dissipation principle. *Rheologica Acta*, *16*(1), 82-94.
- Ramirez, W. F., & Galvin, K. P. (2005). Dynamic model of multi-species segregation and dispersion in liquid fluidized beds. *AIChE journal*, *51*(7), 2103-2108.
- Rhodes, M. (2008). *Introduction to particle technology*. Hoboken, NJ: Wiley.
- Richards, R., & Jones, T. (2004). Kelsey Centrifugal Jig—an update on technology and application. *Mining, Metallurgy & Exploration*, *21*(4), 179-182.
- Richardson, J., & Zaki, W. (1954). Sedimentation and fluidisation, Part 1. *Trans. Ins. Chem. Engrs*, *31*, 35-53.
- Rocha, L., Cançado, R., & Peres, A. (2010). Iron ore slimes flotation. *Minerals Engineering*, *23*(11-13), 842-845.
- Roldán-Villasana, E. J., Williams, R. A., & Dyakowski, T. (1993). The origin of the fish-hook effect in hydrocyclone separators. *Powder Technology*, *77*(3), 243-250.
- Roy, S. (2009). Recovery improvement of fine iron ore particles by multi gravity separation. *The Open Mineral Processing Journal*, *2*(14), 17-30.
- Roy, S., Das, A., & Mohanty, M. (2007). Feasibility of producing pellet grade concentrate by beneficiation of iron ore slime in India. *Separation Science and Technology*, *42*(14), 3271-3287.

- Sarkar, B., & Das, A. (2010). A comparative study of slip velocity models for the prediction of performance of floatex density separator. *International Journal of Mineral Processing*, 94(1), 20-27.
- Schaflinger, U. (1987). Enhanced centrifugal separation with finite Rossby numbers in cylinders with compartment-walls. *Chemical Engineering Science*, 42(5), 1197-1205.
- Schaflinger, U. (1990). Centrifugal separation of a mixture. *Fluid Dynamics Research*, 6(5), 213-249.
- Scott, I., & Napier-Munn, T. (1992). A dense medium cyclone model based on the pivot phenomenon. *Transactions of the Institute of Mining and Metallurgy Section C Mineral Processing and Extractive Metallurgy*, 101, C61-C76.
- Singh, R., Bhattacharyya, K., & Maulik, S. (1997). Gravity concentration of fines and ultrafines.
- Singh, R. K., & Das, A. (2013). Analysis of separation response of Kelsey centrifugal jig in processing fine coal. *Fuel processing technology*, 115, 71-78.
- Sisko, A. (1958). The flow of lubricating greases. *Industrial & Engineering Chemistry*, 50(12), 1789-1792.
- Sivamohan, R. (1990). The problem of recovering very fine particles in mineral processing—a review. *International Journal of Mineral Processing*, 28(3-4), 247-288.
- Smart, J. R., Beimfohr, S., & Leighton Jr, D. T. (1993). Measurement of the translational and rotational velocities of a noncolloidal sphere rolling down a smooth inclined plane at low Reynolds number. *Physics of Fluids A: Fluid Dynamics*, 5(1), 13-24.
- Smart, J. R., & Leighton, D. T. (1989). Measurement of the hydrodynamic surface roughness of noncolloidal spheres. *Physics of Fluids A: Fluid Dynamics*, 1(1), 52-60.
- Srivastava, M., Pan, S., Prasad, N., & Mishra, B. (2001). Characterization and processing of iron ore fines of Kiriburu deposit of India. *International Journal of Mineral Processing*, 61(2), 93-107.
- Stokes, G. G. (1851). *On the effect of the internal friction of fluids on the motion of pendulums* (Vol. 9): Pitt Press.
- Syed, N., Dickinson, J., Galvin, K., & Moreno-Atanasio, R. (2018). Continuous, dynamic and steady state simulation of the reflux classifier using a segregation-dispersion model. *Minerals Engineering*, 115, 53-67.
- Syed, N., Galvin, K., & Moreno-Atanasio, R. (2016). Segregation-dispersion model of a fluidized bed system incorporating inclined channels operated with no shear induced lift. *Chemeca 2016: Chemical Engineering-Regeneration, Recovery and Reinvention*, 570.
- Syed, N., Galvin, K., & Moreno-Atanasio, R. (2019). Application of a 2D segregation-dispersion model to describe binary and multi-component size classification in a Reflux Classifier. *Minerals Engineering*, 133, 80-90.
- Syed, N. H., Dickinson, J., Galvin, K., & Moreno-Atanasio, R. (2015). *A continuum simulation model for the Reflux classifier*. Paper presented at the Asia Pacific Confederation of Chemical Engineering Congress 2015: APCChE 2015, incorporating CHEMECA 2015.

References

- Syed, N. H., & Khan, N. A. (2019). Simulations of mono-sized solid particles in the Reflux Classifier under continuous process conditions. *PHYSICOCHEMICAL PROBLEMS OF MINERAL PROCESSING*, 55(3), 631-642.
- Thompson, P., & Galvin, K. (1997). An empirical description for the classification in an inclined counter-flow settler. *Minerals engineering*, 10(1), 97-109.
- Trahar, W. J. (1981). A rational interpretation of the role of particle size in flotation. *International Journal of Mineral Processing*, 8(4), 289-327.
- Tucker, P. (1995). Modelling the Kelsey centrifugal jig. *Minerals engineering*, 8(3), 333-336.
- Turian, R., Ma, T., Hsu, F., & Sung, D. (1997). Characterization, settling, and rheology of concentrated fine particulate mineral slurries. *Powder Technology*, 93(3), 219-233.
- Ungarish, M. (1995). On the modeling and investigation of polydispersed rotating suspensions. *International Journal of Multiphase Flow*, 21(2), 267-284.
- Uslu, T., Sahinoglu, E., & Yavuz, M. (2012). Desulphurization and deashing of oxidized fine coal by Knelson concentrator. *Fuel Processing Technology*, 101, 94-100.
- Van Der Wielen, L., Van Dam, M., & Luyben, K. C. A. (1996). On the relative motion of a particle in a swarm of different particles. *Chemical engineering science*, 51(6), 995-1008.
- Vance, W. H., & Moulton, R. (1965). A study of slip ratios for the flow of steam-water mixtures at high void fractions. *AIChE Journal*, 11(6), 1114-1124.
- Vega, D., Brito-Parada, P. R., & Cilliers, J. J. (2018). *Small hydrocyclones for classification of particles in the micron size range*. Paper presented at IMPC 2018 Conference, Moscow.
- Wang, C., Harbottle, D., Liu, Q., & Xu, Z. (2014). Current state of fine mineral tailings treatment: A critical review on theory and practice. *Minerals Engineering*, 58, 113-131.
- Willenbacher, N., & Georgieva, K. (2013). *Rheology of disperse systems*. Product Design and Engineering, 7-49.
- Wills, B. A., & Finch, J. A. (2016). *Wills' Mineral Processing Technology: An Introduction to the Practical Aspects of Ore Treatment and Mineral Recovery* (Eighth ed.). Oxford: Butterworth-Heinemann.
- Yerriswamy, P., Majumder, A., Barnwal, J., Govindarajan, B., & Rao, T. (2003). Study on Kelsey jig treating Indian coal fines. *Mineral processing and Extractive metallurgy*, 112(3), 206-210.
- Zhao, S., Fan, J., & Sun, W. (2014). Utilization of iron ore tailings as fine aggregate in ultra-high performance concrete. *Construction and Building Materials*, 50, 540-548.
- Zhou, J., Walton, K., Laskovski, D., Duncan, P., & Galvin, K. P. (2006). Enhanced separation of mineral sands using the Reflux Classifier. *Minerals Engineering*, 19(15), 1573-1579.
- Zhu, G., & Liow, J.-L. (2014). Experimental study of particle separation and the fishhook effect in a mini-hydrocyclone. *Chemical Engineering Science*, 111, 94-105.

Zhu, X.-n., Tao, Y.-j., Sun, Q.-x., & Man, Z.-p. (2017). Enrichment and migration regularity of fine coal particles in enhanced gravity concentrator. *International Journal of Mineral Processing*, 163, 48-54.

Appendix A: Summary of Run Conditions

This appendix contains a summary of the conditions used in all REFLUX™ Graviton and REFLUX™ Classifier experiments. Table A1 contains details of the REFLUX™ Graviton experiments and Table A2 contains details of the REFLUX™ Classifier experiments.

Table A1: Summary of REFLUX™ Graviton experimental conditions.

Run no.	Feed Flowrate (L/min)	Feed Solids Concentration (wt.%)	Fluidisation Rate (L/min)	Underflow Outlet Diameter (mm)	Separation Size, d_{50} (μm)	Ep (μm)	Head Grades (wt.% Fe)			Solids Yield (wt.%)	Fe Recovery (%)
							Feed	U/F	O/F		
Silica Feed											
CF145	100	1.9	12	4	9.4	4.6					
CF146	98	2.0	18	4	14.4	5.7					
CF147	98	2.0	6	4	10.2	5.9					
CF148	115	4.0	6	4	11.0	5.3					
CF149	111	4.0	12	4	10.7	4.1					
CF150	110	3.9	18	4	10.2	4.1					
CF152	101	9.9	18	4	12.8	4.5					
CF153	49	20.3	18	4	7.8	3.4					
CF154	51	29.3	18	4	24.7	14.2					
CF155	37	28.0	18	4	5.4	3.0					
CF156	35	28.9	30	4	9.0	4.0					
CF157	52	30.1	18	4	20.4	12.0					
CF158	54	30.2	18	6	6.0	4.9					
CF159	115	28.3	18	6	31.5	19.2					
CF160	90	28.9	18	6	12.1	5.2					
CF162	88	29.6	34	6	19.0	10.0					
CF163	82	30.3	24	6	18.6	9.9					
CF164	89	30.8	12	6	13.4	7.3					
Iron Ore Feed 1											
CF184	140	4.7	36	8	14.5	6.6	47.5	54.1	35.8	63.9	72.8
CF185	145	18.2	36	8	13.9	6.7	47.1	55.1	36.0	58.1	68.0
CF186	140	24.0	34	8	15.0	7.5	46.9	54.8	36.1	57.8	67.5
CF188*	144	8.5	36	8	9.7	4.4	55.2	58.2	39.4	84.0	88.6
Iron Ore Feed 2											
CF195	149	18.5	34	8	14.2	8.4	31.6	37.8	15.4	72.3	86.5
CF196*	149	14.2	36	8	7.0	7.8	38.8	40.2	16.8	94.0	97.4
CF197	138	19.8	33	6	20.8	9.8	32.7	37.4	14.8	79.2	90.6
CF198*	152	9.2	36	6	14.2	6.5	36.2	42.2	20.4	72.5	84.5

Gravity Separation and Desliming Using Inclined Channels Subject to Different G-Forces

Run no.	Feed Flowrate (L/min)	Feed Solids Concentration (wt.%)	Fluidisation Rate (L/min)	Underflow Outlet Diameter (mm)	Separation Size, d_{50} (μm)	E_p (μm)	Head Grades (wt.% Fe)			Solids Yield (wt.%)	Fe Recovery (%)
							Feed	U/F	O/F		
CF200	115	19.0	64	6	20.4	11.3	32.8	39.0	16.8	72.1	85.7
CF201	105	19.5	50	4	32.8	31.8	34.0	46.6	16.5	58.1	79.7
CF202	105	18.6	50	3	51.6	37.6	33.8	51.7	16.9	48.6	74.3
CF203*	93	8.1	50	3	19.2	21.1	47.0	53.0**	36.6	63.4	71.5
CF206	105	19.9	50	3	53.8	42.4	33.6	50.6	18.3	47.4	71.3
CF207*	105	6.1	64	3	22.1	13.1	47.9	53.7	27.0	78.3	87.8
CF209	65	10.1	64	2	53.8	49.7	32.7	48.1	19.5	46.2	67.9
Iron Ore Feed 3											
CF215	63	11.4	18	3	14.7	8.0	55.4	63.5	49.0	44.1	50.6
CF217	62	9.8	36	3	15.4	6.0	56.2	63.0	48.0	54.7	61.3
CF218	60	11.5	54	3	16.9	6.2	56.8	63.8	48.6	54.0	60.6
CF219	100	9.0	18	3	13.6	5.8	55.9	63.8	47.9	50.3	57.4
CF220	92	9.3	36	3	20.6	6.3	54.9	64.0	49.5	37.2	43.4
CF221	99	9.2	54	3	19.7	7.0	52.9	63.5	49.2	25.9	31.1
CF222	96	8.7	54	3	13.3	4.3	56.1	62.4	47.3	58.3	64.8
CF223*	101	3.2	54	3	9.2	2.7	63.6	64.2	49.3	96.0	96.9
Iron Ore Feed 4											
CF232	102	4.1	36	3	16.0	5.8	64.6	37.9	67.5	90.2	94.3
CF233	52	4.1	36	3	15.4	6.0	Not Tested			-	-
CF235	52	8.3	54	3	18.1	6.3				-	-
CF236	101	7.7	54	3	19.4	6.5				-	-
CF238	110	4.0	54	3	17.9	5.8				-	-
Iron Ore Feed 5											
CF245	52	10.1	18	3	15.0	6.1	56.2	39.9	63.2	70.0	78.7
CF246	52	10.2	36	3	16.0	5.8	56.6	41.7	63.9	67.1	75.8
CF247	52	9.9	12	3	13.1	6.3	51.6	39.1	62.9	52.5	64.0
Iron Ore Feed - Top Size 300 μm											
CF249	105	6.9	36	8	8.7	5.5	63.3	66.4	43.1	86.7	90.9
CF250	103	16.6	36	8	9.0	5.6	64.9	66.0	44.1	95.0	96.6
CF251	98	25.0	36	8	12.4	4.4	64.7	67.1	43.1	90.0	93.3
CF252	105	14.8	54	8	8.0	5.5	65.2	66.2	42.9	95.7	97.2
CF253	103	18.0	18	8	2.6	7.0	64.5	65.6	43.7	95.0	96.6
CF254	103	23.2	36	8	13.4	4.3	65.0	67.1	42.7	91.2	94.2
Iron Ore Feed - Top Size 1000 μm											
CF256	105	16.5	42	10	7.0	5.9	64.7	66.3	43.8	92.9	95.2
CF257	73	14.3	60	10	3.1	7.3	64.2	64.8	43.3	97.2	98.1
CF258	52	12.6	60	10	3.9	9.9	63.4	64.7	46.0	93.0	95.0

Table A2: Summary of REFLUX™ Classifier experimental conditions.

Run no.	Feed Flowrate	Feed Solids Concentration	Fluidisation Rate	Solids Throughput	Channel Width	Head Grades (wt.% Fe)			Solids Yield	Fe Recovery
	(L/min)	(wt.%)	(L/min)	(t/(m ² h))	(mm)	Feed	U/F	O/F	(wt.%)	(%)
S24B	9.0	36.5	0.55	28	3.0	65.2	68.3	64.3	22.5	23.6
S24B2	4.6	36.5	0.55	14	3.0	65.3	68.8	64.1	24.7	26.1
S24B3	2.6	36.5	0.55	7	3.0	65.4	69.1	63.7	32.8	34.7
S24D	5.5	18.5	0.55	7	3.0	66	68.9	61.6	61	63.6
S24D2	2.8	18.5	0.6	3.5	3.0	65.0	68.6	60.3	56.2	59.3
S24E	11.8	9.3	0.55	7	3.0	65.5	68.8	60.4	60.1	63.2
S24E2	6.0	9.3	0.55	3.5	3.0	65.2	68.7	60.5	58.2	61.3
S24G	5.6	18.3	0.55	7	1.8	65.6	69.2	61	56	59.1
S24G2	2.6	36.5	0.55	7	1.8	65.9	69.1	62.8	49	51.4
S24G3	5.2	36.5	0.55	14	1.8	65.3	69	63.6	31.1	32.9
S24G4	11.0	18.4	0.55	14	1.8	64.6	68.8	60.8	47.6	50.7

Appendix B: Laser Sizing Data

This appendix contains the raw data obtained from laser sizing in the Malvern Mastersizer 3000. The size distributions of each stream were used to generate the partition curves presents in the Results chapters according to Equations 4.1 and 4.2b. For each result the cumulative distribution sizes of dx (10), dx (50) and dx (90), which represent the particle sizes at which 10, 50, and 90 % of particles are finer than, as well as the Sauter mean, d [3,2], and volume mean, d [4,3], diameters are given in μm . The sizing data lists the volume % of particles in the interval below the adjacent size value.

It is noted that the sequence of run numbers (i.e. CF145, CF146 ...) skips several numbers throughout the work presented. One or two missing run numbers from a block of work indicates runs that were abandoned mid-run. Such instances occurred due to issues with the experimental equipment, for example feed blockages or failing pumps, and also from external interruptions to the experiment forcing the run to be stopped. Larger blocks of missing run numbers (for example CF164 – CF184) are from experiments in the Graviton or REFLUX™ Classifier that were not performed as part of this thesis.

A sample calculation for the use of Equations 4.1 and 4.2b is shown below for Run CF145. These calculations are for the size interval below (adjacent to in the data tables) $0.872 \mu\text{m}$. This calculation is performed for each size interval, resulting in the full partition curve.

$$\begin{aligned} Y &= (x_F - x_{OF}) / (x_{UF} - x_{OF}) \\ &= (0.15 - 0.4) / (0.1 - 0.4) = 0.83 \text{ i.e. a yield of 83 \% (volume basis)} \\ P &= 1 - (x_{OF} / x_F)(1 - Y) \\ &= 1 - (0.4 / 0.15)(1 - 0.83) = 0.55 \text{ i.e. a partition to underflow of 55 \%} \end{aligned}$$

CF145

Feed				Overflow				Underflow			
<i>dx</i> (10)	4.03	<i>d</i> [3,2]	9.91	<i>dx</i> (10)	2.29	<i>d</i> [3,2]	4.84	<i>dx</i> (10)	10.9	<i>d</i> [3,2]	17.7
<i>dx</i> (50)	22.1	<i>d</i> [4,3]	29.4	<i>dx</i> (50)	7.12	<i>d</i> [4,3]	9.46	<i>dx</i> (50)	29.6	<i>d</i> [4,3]	36.3
<i>dx</i> (90)	65.0			<i>dx</i> (90)	18.8			<i>dx</i> (90)	70.7		
Size (µm)	% Volume In										
0.523	0	9.86	3.04	0.523	0.08	9.86	5.86	0.523	0	9.86	2.16
0.594	0	11.2	3.33	0.594	0.17	11.2	5.46	0.594	0	11.2	2.83
0.675	0.06	12.7	3.66	0.675	0.26	12.7	4.92	0.675	0	12.7	3.57
0.767	0.012	14.5	4.01	0.767	0.34	14.5	4.29	0.767	0.08	14.5	4.36
0.872	0.15	16.4	4.36	0.872	0.4	16.4	3.61	0.872	0.1	16.4	5.15
0.991	0.23	18.7	4.7	0.991	0.49	18.7	2.92	0.991	0.11	18.7	5.87
1.13	0.28	21.2	4.99	1.13	0.64	21.2	2.26	1.13	0.12	21.2	6.47
1.28	0.38	24.1	5.2	1.28	0.9	24.1	1.66	1.28	0.14	24.1	6.9
1.45	0.53	27.4	5.3	1.45	1.28	27.4	1.14	1.45	0.2	27.4	7.12
1.65	0.71	31.1	5.28	1.65	1.73	31.1	0.74	1.65	0.27	31.1	7.11
1.88	0.91	35.3	5.12	1.88	2.21	35.3	0.44	1.88	0.34	35.3	6.88
2.13	1.07	40.1	4.84	2.13	2.65	40.1	0.25	2.13	0.38	40.1	6.44
2.42	1.2	45.6	4.43	2.42	3.04	45.6	0.14	2.42	0.39	45.6	5.84
2.75	1.29	51.8	3.94	2.75	3.41	51.8	0.1	2.75	0.36	51.8	5.13
3.12	1.38	58.9	3.37	3.12	3.81	58.9	0.09	3.12	0.32	58.9	4.35
3.55	1.5	66.9	2.78	3.55	4.25	66.9	0.09	3.55	0.29	66.9	3.55
4.03	1.64	76	2.19	4.03	4.74	76	0.1	4.03	0.29	76	2.78
4.58	1.8	86.4	1.63	4.58	5.22	86.4	0.09	4.58	0.33	86.4	2.06
5.21	1.96	98.1	1.15	5.21	5.64	98.1	0.08	5.21	0.42	98.1	1.43
5.92	2.14	111	0.74	5.92	5.96	111	0.05	5.92	0.58	111	0.91
6.72	2.33	127	0.44	6.72	6.16	127	0	6.72	0.81	127	0.51
7.64	2.54	144	0.22	7.64	6.22	144	0	7.64	1.15	144	0.23
8.68	2.77	163	0.08	8.68	6.12	163	0	8.68	1.6	163	0.05

CF146

Feed				Overflow				Underflow			
<i>dx</i> (10)	5.52	<i>d</i> [3,2]	12.4	<i>dx</i> (10)	2.59	<i>d</i> [3,2]	5.74	<i>dx</i> (10)	13.2	<i>d</i> [3,2]	20.4
<i>dx</i> (50)	26.3	<i>d</i> [4,3]	33.8	<i>dx</i> (50)	8.88	<i>d</i> [4,3]	12.1	<i>dx</i> (50)	34.8	<i>d</i> [4,3]	41.6
<i>dx</i> (90)	72.3			<i>dx</i> (90)	24.4			<i>dx</i> (90)	76.0		
Size (µm)	% Volume In										
0.594	0	11.2	3.08	0.594	0.09	11.2	5.77	0.594	0	11.2	1.79
0.675	0.07	12.7	3.47	0.675	0.16	12.7	5.56	0.675	0	12.7	2.4
0.767	0.11	14.5	3.88	0.767	0.23	14.5	5.22	0.767	0.08	14.5	3.14
0.872	0.14	16.4	4.31	0.872	0.29	16.4	4.76	0.872	0.09	16.4	3.97
0.991	0.16	18.7	4.72	0.991	0.37	18.7	4.2	0.991	0.1	18.7	4.87
1.13	0.2	21.2	5.1	1.13	0.5	21.2	3.58	1.13	0.1	21.2	5.76
1.28	0.26	24.1	5.41	1.28	0.72	24.1	2.92	1.28	0.12	24.1	6.56
1.45	0.37	27.4	5.63	1.45	1.03	27.4	2.27	1.45	0.16	27.4	7.21
1.65	0.5	31.1	5.72	1.65	1.41	31.1	1.67	1.65	0.21	31.1	7.63
1.88	0.63	35.3	5.66	1.88	1.79	35.3	1.15	1.88	0.27	35.3	7.77
2.13	0.74	40.1	5.46	2.13	2.15	40.1	0.75	2.13	0.31	40.1	7.61
2.42	0.82	45.6	5.11	2.42	2.45	45.6	0.45	2.42	0.33	45.6	7.16
2.75	0.88	51.8	4.64	2.75	2.73	51.8	0.26	2.75	0.32	51.8	6.45
3.12	0.94	58.9	4.06	3.12	3.02	58.9	0.15	3.12	0.3	58.9	5.56
3.55	1.03	66.9	3.43	3.55	3.37	66.9	0.1	3.55	0.29	66.9	4.57
4.03	1.15	76	2.77	4.03	3.78	76	0.09	4.03	0.3	76	3.56
4.58	1.31	86.4	2.13	4.58	4.22	86.4	0.1	4.58	0.32	86.4	2.61
5.21	1.48	98.1	1.55	5.21	4.64	98.1	0.11	5.21	0.35	98.1	1.77
5.92	1.68	111	1.05	5.92	5.03	111	0.11	5.92	0.42	111	1.09
6.72	1.9	127	0.65	6.72	5.37	127	0.1	6.72	0.52	127	0.58
7.64	2.14	144	0.35	7.64	5.63	144	0.06	7.64	0.69	144	0.19
8.68	2.42	163	0.15	8.68	5.79	163	0	8.68	0.95	163	0.06
9.86	2.73			9.86	5.84			9.86	1.31		

CF147

Feed				Overflow				Underflow			
<i>dx</i> (10)	5.31	<i>d</i> [3,2]	12.3	<i>dx</i> (10)	2.30	<i>d</i> [3,2]	5.00	<i>dx</i> (10)	10.7	<i>d</i> [3,2]	17.7
<i>dx</i> (50)	26.4	<i>d</i> [4,3]	32.8	<i>dx</i> (50)	7.43	<i>d</i> [4,3]	10.2	<i>dx</i> (50)	31.4	<i>d</i> [4,3]	37.0
<i>dx</i> (90)	69.8			<i>dx</i> (90)	21.1			<i>dx</i> (90)	71.4		
Size (µm)	% Volume In										
0.594	0	9.86	2.67	0.594	0.12	9.86	5.52	0.594	0	9.86	1.83
0.675	0	11.2	3	0.675	0.21	11.2	5.29	0.675	0	11.2	2.37
0.767	0.1	12.7	3.38	0.767	0.29	12.7	4.94	0.767	0.08	12.7	3.02
0.872	0.13	14.5	3.79	0.872	0.37	14.5	4.5	0.872	0.1	14.5	3.75
0.991	0.16	16.4	4.21	0.991	0.48	16.4	3.98	0.991	0.11	16.4	4.54
1.13	0.21	18.7	4.64	1.13	0.65	18.7	3.4	1.13	0.12	18.7	5.33
1.28	0.28	21.2	5.03	1.28	0.93	21.2	2.8	1.28	0.15	21.2	6.06
1.45	0.39	24.1	5.37	1.45	1.31	24.1	2.2	1.45	0.2	24.1	6.67
1.65	0.52	27.4	5.62	1.65	1.78	27.4	1.64	1.65	0.27	27.4	7.11
1.88	0.67	31.1	5.76	1.88	2.26	31.1	1.15	1.88	0.34	31.1	7.31
2.13	0.79	35.3	5.77	2.13	2.71	35.3	0.75	2.13	0.4	35.3	7.27
2.42	0.88	40.1	5.63	2.42	3.1	40.1	0.45	2.42	0.42	40.1	6.96
2.75	0.95	45.6	5.34	2.75	3.44	45.6	0.26	2.75	0.41	45.6	6.43
3.12	1.02	51.8	4.9	3.12	3.77	51.8	0.15	3.12	0.4	51.8	5.71
3.55	1.1	58.9	4.33	3.55	4.13	58.9	0.09	3.55	0.4	58.9	4.86
4.03	1.22	66.9	3.66	4.03	4.51	66.9	0.08	4.03	0.42	66.9	3.95
4.58	1.36	76	2.91	4.58	4.88	76	0.08	4.58	0.46	76	3.04
5.21	1.52	86.4	2.15	5.21	5.2	86.4	0.08	5.21	0.54	86.4	2.2
5.92	1.69	98.1	1.43	5.92	5.44	98.1	0.08	5.92	0.65	98.1	1.47
6.72	1.89	111	0.81	6.72	5.6	111	0.02	6.72	0.83	111	0.88
7.64	2.11	127	0.24	7.64	5.68	127	0	7.64	1.07	127	0.38
8.68	2.37	144	0	8.68	5.65	144	0	8.68	1.4	144	0.09

CF148

Feed				Overflow				Underflow			
<i>dx</i> (10)	4.28	<i>d</i> [3,2]	10.4	<i>dx</i> (10)	2.23	<i>d</i> [3,2]	4.76	<i>dx</i> (10)	10.7	<i>d</i> [3,2]	17.8
<i>dx</i> (50)	23.7	<i>d</i> [4,3]	30.6	<i>dx</i> (50)	7.02	<i>d</i> [4,3]	9.23	<i>dx</i> (50)	31.4	<i>d</i> [4,3]	37.8
<i>dx</i> (90)	66.8			<i>dx</i> (90)	18.8			<i>dx</i> (90)	74.1		
% Size (µm)	% Volume In										
0.523	0	11.2	3.19	0.523	0.08	11.2	5.37	0.523	0	11.2	2.48
0.594	0.05	12.7	3.54	0.594	0.17	12.7	4.87	0.594	0	12.7	3.13
0.675	0.13	14.5	3.91	0.675	0.27	14.5	4.27	0.675	0	14.5	3.85
0.767	0.17	16.4	4.3	0.767	0.35	16.4	3.6	0.767	0.07	16.4	4.61
0.872	0.21	18.7	4.66	0.872	0.41	18.7	2.91	0.872	0.09	18.7	5.34
0.991	0.24	21.2	4.99	0.991	0.5	21.2	2.25	0.991	0.11	21.2	6.01
1.13	0.29	24.1	5.25	1.13	0.66	24.1	1.66	1.13	0.12	24.1	6.54
1.28	0.38	27.4	5.41	1.28	0.95	27.4	1.17	1.28	0.15	27.4	6.9
1.45	0.51	31.1	5.45	1.45	1.36	31.1	0.79	1.45	0.2	31.1	7.05
1.65	0.68	35.3	5.36	1.65	1.85	35.3	0.53	1.65	0.27	35.3	6.97
1.88	0.85	40.1	5.14	1.88	2.36	40.1	0.35	1.88	0.35	40.1	6.68
2.13	1	45.6	4.78	2.13	2.82	45.6	0.24	2.13	0.4	45.6	6.2
2.42	1.1	51.8	4.31	2.42	3.21	51.8	0.15	2.42	0.42	51.8	5.56
2.75	1.17	58.9	3.75	2.75	3.55	58.9	0.06	2.75	0.41	58.9	4.8
3.12	1.24	66.9	3.12	3.12	3.9	66.9	0.04	3.12	0.39	66.9	3.98
3.55	1.33	76	2.47	3.55	4.3	76	0.02	3.55	0.38	76	3.16
4.03	1.45	86.4	1.83	4.03	4.73	86.4	0	4.03	0.4	86.4	2.37
4.58	1.59	98.1	1.25	4.58	5.16	98.1	0	4.58	0.44	98.1	1.66
5.21	1.75	111	0.75	5.21	5.53	111	0	5.21	0.52	111	1.06
5.92	1.93	127	0.38	5.92	5.81	127	0	5.92	0.65	127	0.6
6.72	2.12	144	0.14	6.72	5.99	144	0	6.72	0.84	144	0.28
7.64	2.34	163	0.03	7.64	6.05	163	0	7.64	1.1	163	0.07
8.68	2.59	186	0	8.68	5.97	186	0	8.68	1.46	186	0.07
9.86	2.87			9.86	5.74			9.86	1.92		

CF149

Feed				Overflow				Underflow			
<i>dx</i> (10)	4.92	<i>d</i> [3,2]	11.7	<i>dx</i> (10)	2.5	<i>d</i> [3,2]	5.14	<i>dx</i> (10)	11.2	<i>d</i> [3,2]	18.3
<i>dx</i> (50)	24.8	<i>d</i> [4,3]	32.1	<i>dx</i> (50)	7.04	<i>d</i> [4,3]	9.44	<i>dx</i> (50)	31	<i>d</i> [4,3]	37.5
<i>dx</i> (90)	69.4			<i>dx</i> (90)	16.9			<i>dx</i> (90)	73.9		
% Size (µm)	% Volume In										
0.675	0	11.2	3.18	0.675	0.09	11.2	5.73	0.675	0	11.2	2.69
0.767	0.09	12.7	3.55	0.767	0.16	12.7	4.95	0.767	0.07	12.7	3.38
0.872	0.12	14.5	3.94	0.872	0.23	14.5	4.06	0.872	0.09	14.5	4.11
0.991	0.16	16.4	4.34	0.991	0.33	16.4	3.16	0.991	0.1	16.4	4.84
1.13	0.2	18.7	4.73	1.13	0.49	18.7	2.3	1.13	0.11	18.7	5.53
1.28	0.29	21.2	5.07	1.28	0.75	21.2	1.55	1.28	0.14	21.2	6.13
1.45	0.41	24.1	5.35	1.45	1.12	24.1	0.95	1.45	0.19	24.1	6.6
1.65	0.56	27.4	5.52	1.65	1.57	27.4	0.52	1.65	0.26	27.4	6.89
1.88	0.72	31.1	5.57	1.88	2.05	31.1	0.26	1.88	0.32	31.1	6.98
2.13	0.86	35.3	5.48	2.13	2.51	35.3	0.14	2.13	0.36	35.3	6.87
2.42	0.97	40.1	5.26	2.42	2.93	40.1	0.12	2.42	0.36	40.1	6.57
2.75	1.05	45.6	4.89	2.75	3.37	45.6	0.17	2.75	0.34	45.6	6.09
3.12	1.13	51.8	4.41	3.12	3.85	51.8	0.23	3.12	0.3	51.8	5.47
3.55	1.23	58.9	3.84	3.55	4.42	58.9	0.28	3.55	0.27	58.9	4.74
4.03	1.36	66.9	3.21	4.03	5.05	66.9	0.3	4.03	0.28	66.9	3.95
4.58	1.52	76	2.56	4.58	5.68	76	0.27	4.58	0.32	76	3.15
5.21	1.68	86.4	1.94	5.21	6.25	86.4	0.21	5.21	0.42	86.4	2.38
5.92	1.86	98.1	1.38	5.92	6.68	98.1	0.14	5.92	0.57	98.1	1.68
6.72	2.06	111	0.91	6.72	6.93	111	0.05	6.72	0.81	111	1.08
7.64	2.29	127	0.53	7.64	6.97	127	0.03	7.64	1.13	127	0.61
8.68	2.55	144	0.27	8.68	6.78	144	0	8.68	1.55	144	0.18
9.86	2.84	163	0.1	9.86	6.36	163	0	9.86	2.07	163	0.03

CF150

Feed				Overflow				Underflow			
<i>dx</i> (10)	4.46	<i>d</i> [3,2]	10.8	<i>dx</i> (10)	2.2	<i>d</i> [3,2]	4.58	<i>dx</i> (10)	11.7	<i>d</i> [3,2]	18.9
<i>dx</i> (50)	23.9	<i>d</i> [4,3]	30.8	<i>dx</i> (50)	6.47	<i>d</i> [4,3]	11.2	<i>dx</i> (50)	31.7	<i>d</i> [4,3]	38.2
<i>dx</i> (90)	67.3			<i>dx</i> (90)	17.9			<i>dx</i> (90)	74.2		
% Size (µm)		% Volume In		% Size (µm)		% Volume In		% Size (µm)		% Volume In	
0.523	0	11.2	3.21	0.523	0.07	11.2	4.87	0.523	0	11.2	2.52
0.594	0	12.7	3.55	0.594	0.17	12.7	4.17	0.594	0	12.7	3.22
0.675	0.09	14.5	3.92	0.675	0.26	14.5	3.41	0.675	0	14.5	3.98
0.767	0.13	16.4	4.3	0.767	0.34	16.4	2.65	0.767	0.07	16.4	4.76
0.872	0.16	18.7	4.66	0.872	0.41	18.7	1.95	0.872	0.09	18.7	5.5
0.991	0.19	21.2	4.98	0.991	0.5	21.2	1.34	0.991	0.1	21.2	6.15
1.13	0.24	24.1	5.24	1.13	0.68	24.1	0.85	1.13	0.11	24.1	6.67
1.28	0.34	27.4	5.4	1.28	0.99	27.4	0.5	1.28	0.14	27.4	7.01
1.45	0.47	31.1	5.44	1.45	1.42	31.1	0.27	1.45	0.18	31.1	7.15
1.65	0.64	35.3	5.36	1.65	1.95	35.3	0.17	1.65	0.25	35.3	7.07
1.88	0.82	40.1	5.14	1.88	2.49	40.1	0.16	1.88	0.31	40.1	6.77
2.13	0.97	45.6	4.8	2.13	3	45.6	0.21	2.13	0.35	45.6	6.29
2.42	1.08	51.8	4.34	2.42	3.45	51.8	0.29	2.42	0.35	51.8	5.64
2.75	1.16	58.9	3.78	2.75	3.86	58.9	0.38	2.75	0.32	58.9	4.88
3.12	1.23	66.9	3.17	3.12	4.28	66.9	0.44	3.12	0.28	66.9	4.05
3.55	1.33	76	2.52	3.55	4.75	76	0.47	3.55	0.25	76	3.21
4.03	1.46	86.4	1.89	4.03	5.24	86.4	0.48	4.03	0.24	86.4	2.4
4.58	1.61	98.1	1.3	4.58	5.69	98.1	0.44	4.58	0.27	98.1	1.67
5.21	1.78	111	0.79	5.21	6.05	111	0.39	5.21	0.35	111	1.06
5.92	1.96	127	0.4	5.92	6.27	127	0.31	5.92	0.48	127	0.58
6.72	2.16	144	0.1	6.72	6.33	144	0.22	6.72	0.69	144	0.25
7.64	2.38	163	0	7.64	6.22	163	0.14	7.64	0.99	163	0.05
8.68	2.62	186	0	8.68	5.93	186	0.05	8.68	1.39	186	0
9.86	2.9	211	0	9.86	5.47	211	0.02	9.86	1.91	211	0

CF152

Feed				Overflow				Underflow			
<i>dx</i> (10)	3.89	<i>d</i> [3,2]	9.84	<i>dx</i> (10)	2.21	<i>d</i> [3,2]	4.66	<i>dx</i> (10)	13	<i>d</i> [3,2]	20.9
<i>dx</i> (50)	22.2	<i>d</i> [4,3]	29.3	<i>dx</i> (50)	6.63	<i>d</i> [4,3]	8.3	<i>dx</i> (50)	36.5	<i>d</i> [4,3]	44.7
<i>dx</i> (90)	65.4			<i>dx</i> (90)	16.8			<i>dx</i> (90)	88.8		
% Size (µm)		% Volume In		% Size (µm)		% Volume In		% Size (µm)		% Volume In	
0.594	0	11.2	3.24	0.594	0.09	11.2	5.35	0.594	0	11.2	1.99
0.675	0.1	12.7	3.54	0.675	0.18	12.7	4.77	0.675	0	12.7	2.58
0.767	0.15	14.5	3.85	0.767	0.27	14.5	4.09	0.767	0.07	14.5	3.25
0.872	0.19	16.4	4.18	0.872	0.37	16.4	3.36	0.872	0.09	16.4	3.95
0.991	0.23	18.7	4.5	0.991	0.5	18.7	2.62	0.991	0.1	18.7	4.66
1.13	0.29	21.2	4.78	1.13	0.71	21.2	1.93	1.13	0.11	21.2	5.32
1.28	0.4	24.1	5.01	1.28	1.03	24.1	1.31	1.28	0.13	24.1	5.9
1.45	0.56	27.4	5.15	1.45	1.47	27.4	0.81	1.45	0.17	27.4	6.36
1.65	0.75	31.1	5.19	1.65	1.98	31.1	0.43	1.65	0.22	31.1	6.66
1.88	0.96	35.3	5.1	1.88	2.51	35.3	0.18	1.88	0.28	35.3	6.79
2.13	1.14	40.1	4.9	2.13	3	40.1	0	2.13	0.31	40.1	6.74
2.42	1.27	45.6	4.57	2.42	3.42	45.6	0	2.42	0.32	45.6	6.51
2.75	1.37	51.8	4.13	2.75	3.79	51.8	0	2.75	0.3	51.8	6.12
3.12	1.47	58.9	3.6	3.12	4.18	58.9	0	3.12	0.26	58.9	5.59
3.55	1.58	66.9	3	3.55	4.6	66.9	0	3.55	0.24	66.9	4.95
4.03	1.72	76	2.37	4.03	5.06	76	0	4.03	0.23	76	4.23
4.58	1.87	86.4	1.74	4.58	5.5	86.4	0	4.58	0.25	86.4	3.47
5.21	2.03	98.1	1.16	5.21	5.87	98.1	0	5.21	0.3	98.1	2.71
5.92	2.19	111	0.68	5.92	6.14	111	0	5.92	0.39	111	1.98
6.72	2.36	127	0.31	6.72	6.28	127	0	6.72	0.55	127	1.33
7.64	2.54	144	0.09	7.64	6.28	144	0	7.64	0.77	144	0.78
8.68	2.75	163	0	8.68	6.12	163	0	8.68	1.08	163	0.37
9.86	2.98	186	0	9.86	5.81	186	0	9.86	1.49	186	0.12

CF153

Feed				Overflow				Underflow			
<i>dx</i> (10)	3.71	<i>d</i> [3,2]	9.43	<i>dx</i> (10)	1.96	<i>d</i> [3,2]	3.74	<i>dx</i> (10)	8.43	<i>d</i> [3,2]	15.3
<i>dx</i> (50)	21.5	<i>d</i> [4,3]	28.5	<i>dx</i> (50)	4.91	<i>d</i> [4,3]	5.9	<i>dx</i> (50)	27.3	<i>d</i> [4,3]	33.2
<i>dx</i> (90)	63.3			<i>dx</i> (90)	11.2			<i>dx</i> (90)	66.8		
% Size (µm)	% Volume In										
0.523	0	9.86	3.01	0.523	0.14	9.86	4.36	0.523	0	9.86	2.77
0.594	0.07	11.2	3.27	0.594	0.26	11.2	3.45	0.594	0	11.2	3.32
0.675	0.12	12.7	3.57	0.675	0.36	12.7	2.57	0.675	0	12.7	3.9
0.767	0.16	14.5	3.89	0.767	0.43	14.5	1.79	0.767	0.08	14.5	4.49
0.872	0.2	16.4	4.22	0.872	0.49	16.4	1.15	0.872	0.11	16.4	5.05
0.991	0.23	18.7	4.55	0.991	0.6	18.7	0.67	0.991	0.13	18.7	5.56
1.13	0.3	21.2	4.84	1.13	0.84	21.2	0.33	1.13	0.15	21.2	5.98
1.28	0.41	24.1	5.06	1.28	1.26	24.1	0.13	1.28	0.19	24.1	6.29
1.45	0.59	27.4	5.19	1.45	1.88	27.4	0	1.45	0.26	27.4	6.46
1.65	0.8	31.1	5.2	1.65	2.62	31.1	0	1.65	0.34	31.1	6.48
1.88	1.02	35.3	5.08	1.88	3.41	35.3	0	1.88	0.41	35.3	6.32
2.13	1.21	40.1	4.82	2.13	4.17	40.1	0	2.13	0.46	40.1	6.01
2.42	1.35	45.6	4.44	2.42	4.83	45.6	0	2.42	0.47	45.6	5.54
2.75	1.45	51.8	3.95	2.75	5.42	51.8	0	2.75	0.46	51.8	4.94
3.12	1.54	58.9	3.38	3.12	5.97	58.9	0	3.12	0.45	58.9	4.23
3.55	1.66	66.9	2.77	3.55	6.48	66.9	0	3.55	0.47	66.9	3.46
4.03	1.79	76	2.15	4.03	6.91	76	0	4.03	0.54	76	2.66
4.58	1.94	86.4	1.56	4.58	7.19	86.4	0	4.58	0.67	86.4	1.89
5.21	2.1	98.1	1.04	5.21	7.26	98.1	0	5.21	0.86	98.1	1.21
5.92	2.25	111	0.61	5.92	7.08	111	0	5.92	1.11	111	0.65
6.72	2.41	127	0.3	6.72	6.66	127	0	6.72	1.43	127	0.1
7.64	2.59	144	0.1	7.64	6.03	144	0	7.64	1.82	144	0
8.68	2.79			8.68	5.25			8.68	2.27		

CF154

Feed				Overflow				Underflow			
<i>dx</i> (10)	3.98	<i>d</i> [3,2]	10.1	<i>dx</i> (10)	2.81	<i>d</i> [3,2]	6.79	<i>dx</i> (10)	11.3	<i>d</i> [3,2]	19
<i>dx</i> (50)	22.3	<i>d</i> [4,3]	29.3	<i>dx</i> (50)	12.1	<i>d</i> [4,3]	16.7	<i>dx</i> (50)	37.6	<i>d</i> [4,3]	43.6
<i>dx</i> (90)	65.1			<i>dx</i> (90)	37.2			<i>dx</i> (90)	84.3		
% Size (µm)	% Volume In										
0.594	0	11.2	3.25	0.594	0.07	11.2	4.79	0.594	0	11.2	1.65
0.675	0.08	12.7	3.56	0.675	0.13	12.7	4.94	0.675	0	12.7	2.08
0.767	0.12	14.5	3.89	0.767	0.18	14.5	5.03	0.767	0.08	14.5	2.62
0.872	0.16	16.4	4.24	0.872	0.24	16.4	5.03	0.872	0.11	16.4	3.26
0.991	0.2	18.7	4.56	0.991	0.3	18.7	4.95	0.991	0.12	18.7	3.98
1.13	0.26	21.2	4.86	1.13	0.42	21.2	4.76	1.13	0.13	21.2	4.73
1.28	0.37	24.1	5.08	1.28	0.61	24.1	4.46	1.28	0.16	24.1	5.48
1.45	0.53	27.4	5.22	1.45	0.89	27.4	4.06	1.45	0.21	27.4	6.16
1.65	0.73	31.1	5.24	1.65	1.23	31.1	3.57	1.65	0.27	31.1	6.72
1.88	0.94	35.3	5.14	1.88	1.57	35.3	3.04	1.88	0.35	35.3	7.09
2.13	1.12	40.1	4.92	2.13	1.86	40.1	2.49	2.13	0.4	40.1	7.24
2.42	1.26	45.6	4.58	2.42	2.09	45.6	1.95	2.42	0.43	45.6	7.13
2.75	1.36	51.8	4.13	2.75	2.27	51.8	1.46	2.75	0.44	51.8	6.78
3.12	1.46	58.9	3.59	3.12	2.44	58.9	1.02	3.12	0.44	58.9	6.18
3.55	1.57	66.9	2.99	3.55	2.65	66.9	0.66	3.55	0.46	66.9	5.4
4.03	1.71	76	2.36	4.03	2.89	76	0.38	4.03	0.48	76	4.48
4.58	1.86	86.4	1.73	4.58	3.15	86.4	0.18	4.58	0.53	86.4	3.51
5.21	2.01	98.1	1.16	5.21	3.42	98.1	0.05	5.21	0.58	98.1	2.55
5.92	2.17	111	0.67	5.92	3.67	111	0	5.92	0.65	111	1.68
6.72	2.34	127	0.27	6.72	3.92	127	0	6.72	0.75	127	0.96
7.64	2.53	144	0.05	7.64	4.16	144	0	7.64	0.88	144	0.37
8.68	2.74	163	0	8.68	4.39	163	0	8.68	1.06	163	0.09
9.86	2.98			9.86	4.61			9.86	1.31		

CF155

Feed				Overflow				Underflow			
<i>dx</i> (10)	4.03	<i>d</i> [3,2]	10.3	<i>dx</i> (10)	1.91	<i>d</i> [3,2]	3.49	<i>dx</i> (10)	7.4	<i>d</i> [3,2]	14.5
<i>dx</i> (50)	22.4	<i>d</i> [4,3]	29.6	<i>dx</i> (50)	4.26	<i>d</i> [4,3]	4.98	<i>dx</i> (50)	26.8	<i>d</i> [4,3]	32.9
<i>dx</i> (90)	65.6			<i>dx</i> (90)	9.12			<i>dx</i> (90)	67.9		
% Size (µm)	% Volume In										
0.594	0	11.2	3.26	0.594	0.13	11.2	2.09	0.594	0	11.2	3.41
0.675	0	12.7	3.56	0.675	0.2	12.7	1.29	0.675	0	12.7	3.87
0.767	0.08	14.5	3.9	0.767	0.27	14.5	0.69	0.767	0.06	14.5	4.34
0.872	0.12	16.4	4.24	0.872	0.36	16.4	0.29	0.872	0.09	16.4	4.79
0.991	0.17	18.7	4.57	0.991	0.54	18.7	0.08	0.991	0.12	18.7	5.2
1.13	0.24	21.2	4.87	1.13	0.88	21.2	0	1.13	0.15	21.2	5.56
1.28	0.36	24.1	5.09	1.28	1.46	24.1	0	1.28	0.2	24.1	5.84
1.45	0.53	27.4	5.23	1.45	2.26	27.4	0	1.45	0.27	27.4	6.01
1.65	0.73	31.1	5.25	1.65	3.24	31.1	0	1.65	0.36	31.1	6.07
1.88	0.94	35.3	5.14	1.88	4.28	35.3	0	1.88	0.45	35.3	6
2.13	1.13	40.1	4.9	2.13	5.25	40.1	0	2.13	0.51	40.1	5.79
2.42	1.27	45.6	4.54	2.42	6.07	45.6	0	2.42	0.53	45.6	5.43
2.75	1.37	51.8	4.07	2.75	6.74	51.8	0	2.75	0.54	51.8	4.94
3.12	1.47	58.9	3.52	3.12	7.28	58.9	0	3.12	0.56	58.9	4.32
3.55	1.58	66.9	2.92	3.55	7.68	66.9	0	3.55	0.62	66.9	3.59
4.03	1.72	76	2.31	4.03	7.92	76	0	4.03	0.74	76	2.81
4.58	1.87	86.4	1.72	4.58	7.91	86.4	0	4.58	0.92	86.4	2.01
5.21	2.03	98.1	1.19	5.21	7.6	98.1	0	5.21	1.15	98.1	1.27
5.92	2.18	111	0.74	5.92	7	111	0	5.92	1.43	111	0.66
6.72	2.35	127	0.4	6.72	6.16	127	0	6.72	1.75	127	0.05
7.64	2.53	144	0.17	7.64	5.17	144	0	7.64	2.12	144	0
8.68	2.74	163	0.02	8.68	4.1	163	0	8.68	2.52	163	0
9.86	2.98			9.86	3.05			9.86	2.95		

CF156

Feed				Overflow				Underflow			
<i>dx</i> (10)	4.08	<i>d</i> [3,2]	10.4	<i>dx</i> (10)	2.17	<i>d</i> [3,2]	4.37	<i>dx</i> (10)	9.45	<i>d</i> [3,2]	16.6
<i>dx</i> (50)	22.7	<i>d</i> [4,3]	30.6	<i>dx</i> (50)	5.75	<i>d</i> [4,3]	8.4	<i>dx</i> (50)	29.8	<i>d</i> [4,3]	37.2
<i>dx</i> (90)	68			<i>dx</i> (90)	14.5			<i>dx</i> (90)	75.7		
% Size (µm)		% Volume In		% Size (µm)		% Volume In		% Size (µm)		% Volume In	
0.594	0	11.2	3.25	0.594	0.07	11.2	4.35	0.594	0	11.2	2.92
0.675	0	12.7	3.55	0.675	0.14	12.7	3.55	0.675	0	12.7	3.53
0.767	0.1	14.5	3.89	0.767	0.21	14.5	2.76	0.767	0.07	14.5	4.16
0.872	0.13	16.4	4.23	0.872	0.29	16.4	2.03	0.872	0.09	16.4	4.78
0.991	0.18	18.7	4.56	0.991	0.42	18.7	1.4	0.991	0.11	18.7	5.35
1.13	0.24	21.2	4.85	1.13	0.65	21.2	0.89	1.13	0.13	21.2	5.84
1.28	0.36	24.1	5.07	1.28	1.03	24.1	0.52	1.28	0.17	24.1	6.21
1.45	0.52	27.4	5.2	1.45	1.56	27.4	0.28	1.45	0.23	27.4	6.43
1.65	0.73	31.1	5.2	1.65	2.2	31.1	0.14	1.65	0.31	31.1	6.48
1.88	0.94	35.3	5.08	1.88	2.87	35.3	0.1	1.88	0.39	35.3	6.36
2.13	1.11	40.1	4.82	2.13	3.51	40.1	0.11	2.13	0.44	40.1	6.08
2.42	1.24	45.6	4.45	2.42	4.07	45.6	0.16	2.42	0.45	45.6	5.65
2.75	1.34	51.8	3.99	2.75	4.58	51.8	0.22	2.75	0.43	51.8	5.1
3.12	1.42	58.9	3.45	3.12	5.08	58.9	0.26	3.12	0.41	58.9	4.46
3.55	1.53	66.9	2.89	3.55	5.58	66.9	0.28	3.55	0.41	66.9	3.78
4.03	1.67	76	2.32	4.03	6.06	76	0.27	4.03	0.45	76	3.09
4.58	1.82	86.4	1.79	4.58	6.46	86.4	0.24	4.58	0.53	86.4	2.42
5.21	1.98	98.1	1.32	5.21	6.7	98.1	0.19	5.21	0.67	98.1	1.79
5.92	2.15	111	0.92	5.92	6.75	111	0.13	5.92	0.86	111	1.24
6.72	2.32	127	0.59	6.72	6.61	127	0.05	6.72	1.12	127	0.77
7.64	2.51	144	0.35	7.64	6.28	144	0.04	7.64	1.46	144	0.41
8.68	2.73	163	0.17	8.68	5.77	163	0.02	8.68	1.87	163	0.16
9.86	2.97	186	0.03	9.86	5.11	186	0	9.86	2.36	186	0

Appendix B: Laser Sizing Data

CF157

Feed				Overflow				Underflow			
<i>dx</i> (10)	4.05	<i>d</i> [3,2]	10.3	<i>dx</i> (10)	2.83	<i>d</i> [3,2]	6.74	<i>dx</i> (10)	10.5	<i>d</i> [3,2]	18.2
<i>dx</i> (50)	21.7	<i>d</i> [4,3]	28.7	<i>dx</i> (50)	10.9	<i>d</i> [4,3]	15.2	<i>dx</i> (50)	34.9	<i>d</i> [4,3]	40.7
<i>dx</i> (90)	63.5			<i>dx</i> (90)	33			<i>dx</i> (90)	78.9		
% Size (µm)	% Volume In										
0.767	0	12.7	3.68	0.767	0	12.7	5.18	0.767	0.04	12.7	2.37
0.872	0.08	14.5	4.02	0.872	0.09	14.5	5.16	0.872	0.09	14.5	2.97
0.991	0.14	16.4	4.37	0.991	0.19	16.4	5.05	0.991	0.1	16.4	3.67
1.13	0.22	18.7	4.7	1.13	0.34	18.7	4.83	1.13	0.12	18.7	4.43
1.28	0.35	21.2	4.98	1.28	0.59	21.2	4.5	1.28	0.15	21.2	5.2
1.45	0.53	24.1	5.19	1.45	0.91	24.1	4.07	1.45	0.21	24.1	5.93
1.65	0.74	27.4	5.29	1.65	1.3	27.4	3.55	1.65	0.29	27.4	6.55
1.88	0.96	31.1	5.26	1.88	1.69	31.1	2.99	1.88	0.37	31.1	7
2.13	1.15	35.3	5.11	2.13	2.03	35.3	2.42	2.13	0.44	35.3	7.22
2.42	1.29	40.1	4.82	2.42	2.3	40.1	1.88	2.42	0.47	40.1	7.2
2.75	1.4	45.6	4.41	2.75	2.51	45.6	1.39	2.75	0.49	45.6	6.91
3.12	1.49	51.8	3.91	3.12	2.72	51.8	0.99	3.12	0.49	51.8	6.39
3.55	1.61	58.9	3.33	3.55	2.97	58.9	0.67	3.55	0.51	58.9	5.66
4.03	1.75	66.9	2.72	4.03	3.25	66.9	0.44	4.03	0.54	66.9	4.8
4.58	1.92	76	2.12	4.58	3.55	76	0.27	4.58	0.58	76	3.86
5.21	2.08	86.4	1.56	5.21	3.84	86.4	0.17	5.21	0.64	86.4	2.92
5.92	2.25	98.1	1.06	5.92	4.11	98.1	0.08	5.92	0.72	98.1	2.05
6.72	2.42	111	0.66	6.72	4.37	111	0.06	6.72	0.82	111	1.3
7.64	2.62	127	0.36	7.64	4.6	127	0.03	7.64	0.97	127	0.71
8.68	2.84	144	0.15	8.68	4.81	144	0	8.68	1.18	144	0.24
9.86	3.08	163	0	9.86	4.98	163	0	9.86	1.48	163	0.03
11.2	3.37	163	0.17	11.2	5.11	163	0.02	11.2	1.87	163	0.16

CF158

Feed				Overflow				Underflow			
<i>dx</i> (10)	4.01	<i>d</i> [3,2]	10.3	<i>dx</i> (10)	2.13	<i>d</i> [3,2]	4.27	<i>dx</i> (10)	6.75	<i>d</i> [3,2]	13.8
<i>dx</i> (50)	22.2	<i>d</i> [4,3]	29.5	<i>dx</i> (50)	5.42	<i>d</i> [4,3]	6.85	<i>dx</i> (50)	26.3	<i>d</i> [4,3]	33
<i>dx</i> (90)	65.5			<i>dx</i> (90)	13.5			<i>dx</i> (90)	68.7		
% Size (µm)		% Volume In		% Size (µm)		% Volume In		% Size (µm)		% Volume In	
0.872	0.1	12.7	3.6	0.872	0.13	12.7	3.43	0.872	0.09	12.7	3.78
0.991	0.16	14.5	3.93	0.991	0.33	14.5	2.7	0.991	0.12	14.5	4.3
1.13	0.25	16.4	4.26	1.13	0.67	16.4	2.03	1.13	0.16	16.4	4.81
1.28	0.38	18.7	4.58	1.28	1.16	18.7	1.44	1.28	0.23	18.7	5.27
1.45	0.56	21.2	4.87	1.45	1.81	21.2	0.95	1.45	0.33	21.2	5.66
1.65	0.77	24.1	5.09	1.65	2.56	24.1	0.58	1.65	0.45	24.1	5.93
1.88	0.98	27.4	5.21	1.88	3.32	27.4	0.32	1.88	0.56	27.4	6.08
2.13	1.16	31.1	5.22	2.13	4	31.1	0.15	2.13	0.64	31.1	6.07
2.42	1.29	35.3	5.1	2.42	4.58	35.3	0.07	2.42	0.69	35.3	5.91
2.75	1.38	40.1	4.85	2.75	5.06	40.1	0	2.75	0.71	40.1	5.61
3.12	1.47	45.6	4.48	3.12	5.49	45.6	0	3.12	0.73	45.6	5.17
3.55	1.57	51.8	4	3.55	5.9	51.8	0	3.55	0.78	51.8	4.63
4.03	1.71	58.9	3.45	4.03	6.28	58.9	0	4.03	0.87	58.9	4.01
4.58	1.86	66.9	2.86	4.58	6.56	66.9	0	4.58	1	66.9	3.34
5.21	2.02	76	2.26	5.21	6.7	76	0	5.21	1.18	76	2.65
5.92	2.19	86.4	1.69	5.92	6.66	86.4	0	5.92	1.4	86.4	1.98
6.72	2.37	98.1	1.18	6.72	6.44	98.1	0	6.72	1.67	98.1	1.36
7.64	2.57	111	0.76	7.64	6.06	111	0	7.64	2	111	0.84
8.68	2.79	127	0.43	8.68	5.54	127	0	8.68	2.37	127	0.43
9.86	3.03	144	0.21	9.86	4.89	144	0	9.86	2.8	144	0.12
11.2	3.3	163	0.06	11.2	4.18	163	0	11.2	3.28	163	0

CF159

Feed				Overflow				Underflow			
<i>dx</i> (10)	4.05	<i>d</i> [3,2]	10.4	<i>dx</i> (10)	3.17	<i>d</i> [3,2]	7.88	<i>dx</i> (10)	8.53	<i>d</i> [3,2]	17.6
<i>dx</i> (50)	22.4	<i>d</i> [4,3]	29.5	<i>dx</i> (50)	14.2	<i>d</i> [4,3]	18.5	<i>dx</i> (50)	39	<i>d</i> [4,3]	44.2
<i>dx</i> (90)	65.9			<i>dx</i> (90)	40.1			<i>dx</i> (90)	86.3		
Size (µm)	% Volume In										
0.872	0.08	12.7	3.55	0.872	0.09	12.7	4.86	0.872	0.08	12.7	1.96
0.991	0.14	14.5	3.87	0.991	0.16	14.5	5.12	0.991	0.11	14.5	2.36
1.13	0.22	16.4	4.2	1.13	0.29	16.4	5.31	1.13	0.14	16.4	2.86
1.28	0.35	18.7	4.52	1.28	0.48	18.7	5.41	1.28	0.19	18.7	3.46
1.45	0.53	21.2	4.8	1.45	0.75	21.2	5.38	1.45	0.27	21.2	4.16
1.65	0.74	24.1	5.02	1.65	1.06	24.1	5.19	1.65	0.36	24.1	4.9
1.88	0.96	27.4	5.16	1.88	1.38	27.4	4.85	1.88	0.46	27.4	5.63
2.13	1.15	31.1	5.19	2.13	1.65	31.1	4.37	2.13	0.54	31.1	6.29
2.42	1.29	35.3	5.1	2.42	1.86	35.3	3.78	2.42	0.6	35.3	6.79
2.75	1.39	40.1	4.88	2.75	2.02	40.1	3.13	2.75	0.64	40.1	7.09
3.12	1.49	45.6	4.56	3.12	2.17	45.6	2.46	3.12	0.67	45.6	7.11
3.55	1.6	51.8	4.12	3.55	2.34	51.8	1.82	3.55	0.71	51.8	6.86
4.03	1.74	58.9	3.6	4.03	2.55	58.9	1.24	4.03	0.78	58.9	6.32
4.58	1.9	66.9	3.02	4.58	2.77	66.9	0.76	4.58	0.85	66.9	5.54
5.21	2.06	76	2.4	5.21	2.99	76	0.4	5.21	0.93	76	4.59
5.92	2.22	86.4	1.79	5.92	3.22	86.4	0.13	5.92	1.01	86.4	3.57
6.72	2.39	98.1	1.23	6.72	3.46	98.1	0.02	6.72	1.09	98.1	2.55
7.64	2.57	111	0.74	7.64	3.71	111	0	7.64	1.19	111	1.64
8.68	2.77	127	0.36	8.68	3.98	127	0	8.68	1.3	127	0.9
9.86	3	144	0.04	9.86	4.27	144	0	9.86	1.46	144	0.38
11.2	3.26			11.2	4.56			11.2	1.67		

CF160

Feed				Overflow				Underflow			
<i>dx</i> (10)	4.03	<i>d</i> [3,2]	10.4	<i>dx</i> (10)	2.5	<i>d</i> [3,2]	5.43	<i>dx</i> (10)	10.3	<i>d</i> [3,2]	17.7
<i>dx</i> (50)	22	<i>d</i> [4,3]	29.1	<i>dx</i> (50)	7.56	<i>d</i> [4,3]	9.58	<i>dx</i> (50)	32.7	<i>d</i> [4,3]	39.2
<i>dx</i> (90)	65.2			<i>dx</i> (90)	19.6			<i>dx</i> (90)	76.8		
% Size (µm)		% Volume In		% Size (µm)		% Volume In		% Size (µm)		% Volume In	
0.872	0.07	14.5	3.93	0.872	0	14.5	4.79	0.872	0.08	14.5	3.44
0.991	0.12	16.4	4.25	0.991	0.16	16.4	4.15	0.991	0.1	16.4	4.18
1.13	0.21	18.7	4.56	1.13	0.39	18.7	3.44	1.13	0.12	18.7	4.94
1.28	0.34	21.2	4.82	1.28	0.74	21.2	2.72	1.28	0.16	21.2	5.66
1.45	0.52	24.1	5.03	1.45	1.2	24.1	2.02	1.45	0.22	24.1	6.28
1.65	0.75	27.4	5.14	1.65	1.73	27.4	1.39	1.65	0.31	27.4	6.75
1.88	0.97	31.1	5.15	1.88	2.26	31.1	0.88	1.88	0.4	31.1	7.01
2.13	1.16	35.3	5.04	2.13	2.73	35.3	0.49	2.13	0.47	35.3	7.05
2.42	1.31	40.1	4.82	2.42	3.12	40.1	0.23	2.42	0.5	40.1	6.85
2.75	1.41	45.6	4.49	2.75	3.45	45.6	0.08	2.75	0.51	45.6	6.42
3.12	1.51	51.8	4.07	3.12	3.78	51.8	0	3.12	0.5	51.8	5.81
3.55	1.63	58.9	3.56	3.55	4.16	58.9	0	3.55	0.5	58.9	5.05
4.03	1.77	66.9	2.98	4.03	4.59	66.9	0	4.03	0.52	66.9	4.22
4.58	1.93	76	2.38	4.58	5.02	76	0	4.58	0.56	76	3.37
5.21	2.09	86.4	1.77	5.21	5.41	86.4	0	5.21	0.61	86.4	2.55
5.92	2.25	98.1	1.2	5.92	5.74	98.1	0	5.92	0.7	98.1	1.83
6.72	2.42	111	0.7	6.72	5.98	111	0	6.72	0.83	111	1.21
7.64	2.61	127	0.24	7.64	6.12	127	0	7.64	1.03	127	0.73
8.68	2.82	144	0	8.68	6.13	144	0	8.68	1.31	144	0.39
9.86	3.05	163	0	9.86	6.01	163	0	9.86	1.69	163	0.17
11.2	3.32	186	0	11.2	5.74	186	0	11.2	2.17	186	0.03
12.7	3.61			12.7	5.33			12.7	2.76		

CF162

Feed				Overflow				Underflow			
<i>dx</i> (10)	4.44	<i>d</i> [3,2]	11.2	<i>dx</i> (10)	3.06	<i>d</i> [3,2]	7.14	<i>dx</i> (10)	11.2	<i>d</i> [3,2]	19.1
<i>dx</i> (50)	23.3	<i>d</i> [4,3]	30.5	<i>dx</i> (50)	11.1	<i>d</i> [4,3]	14.8	<i>dx</i> (50)	36.1	<i>d</i> [4,3]	41
<i>dx</i> (90)	67.2			<i>dx</i> (90)	30.9			<i>dx</i> (90)	78		
% Size (µm)	Volume In										
0.872	0	12.7	3.53	0.872	0	12.7	5.61	0.872	0.08	12.7	2.06
0.991	0.08	14.5	3.86	0.991	0	14.5	5.58	0.991	0.09	14.5	2.66
1.13	0.15	16.4	4.2	1.13	0.19	16.4	5.43	1.13	0.11	16.4	3.38
1.28	0.27	18.7	4.54	1.28	0.42	18.7	5.13	1.28	0.14	18.7	4.2
1.45	0.43	21.2	4.85	1.45	0.74	21.2	4.69	1.45	0.19	21.2	5.06
1.65	0.63	24.1	5.11	1.65	1.13	24.1	4.13	1.65	0.26	24.1	5.9
1.88	0.84	27.4	5.27	1.88	1.52	27.4	3.49	1.88	0.34	27.4	6.64
2.13	1.02	31.1	5.32	2.13	1.87	31.1	2.82	2.13	0.41	31.1	7.21
2.42	1.16	35.3	5.24	2.42	2.15	35.3	2.18	2.42	0.45	35.3	7.54
2.75	1.28	40.1	5.04	2.75	2.38	40.1	1.6	2.75	0.48	40.1	7.59
3.12	1.38	45.6	4.7	3.12	2.61	45.6	1.13	3.12	0.5	45.6	7.35
3.55	1.51	51.8	4.26	3.55	2.88	51.8	0.77	3.55	0.52	51.8	6.82
4.03	1.66	58.9	3.72	4.03	3.19	58.9	0.51	4.03	0.55	58.9	6.06
4.58	1.83	66.9	3.13	4.58	3.54	66.9	0.34	4.58	0.6	66.9	5.12
5.21	2	76	2.5	5.21	3.88	76	0.23	5.21	0.64	76	4.09
5.92	2.17	86.4	1.88	5.92	4.22	86.4	0.15	5.92	0.69	86.4	3.04
6.72	2.35	98.1	1.3	6.72	4.54	98.1	0.09	6.72	0.76	98.1	2.05
7.64	2.54	111	0.8	7.64	4.85	111	0.03	7.64	0.87	111	1.21
8.68	2.74	127	0.37	8.68	5.12	127	0	8.68	1.02	127	0.43
9.86	2.97	144	0.09	9.86	5.36	144	0	9.86	1.26	144	0
11.2	3.23	163	0.02	11.2	5.53	163	0	11.2	1.6	163	0

CF163

Feed				Overflow				Underflow			
<i>dx</i> (10)	4.47	<i>d</i> [3,2]	11.3	<i>dx</i> (10)	3.02	<i>d</i> [3,2]	6.87	<i>dx</i> (10)	11.5	<i>d</i> [3,2]	19.8
<i>dx</i> (50)	23.1	<i>d</i> [4,3]	29.8	<i>dx</i> (50)	10.2	<i>d</i> [4,3]	13	<i>dx</i> (50)	36.5	<i>d</i> [4,3]	42
<i>dx</i> (90)	65.5			<i>dx</i> (90)	27.3			<i>dx</i> (90)	80.3		
% Size (µm)		% Volume In		% Size (µm)		% Volume In		% Size (µm)		% Volume In	
0.991	0	14.5	3.88	0.991	0	14.5	5.61	0.991	0.07	14.5	2.68
1.13	0.11	16.4	4.23	1.13	0.1	16.4	5.41	1.13	0.09	16.4	3.39
1.28	0.23	18.7	4.57	1.28	0.33	18.7	5.08	1.28	0.13	18.7	4.18
1.45	0.4	21.2	4.89	1.45	0.69	21.2	4.62	1.45	0.18	21.2	5.02
1.65	0.61	24.1	5.14	1.65	1.13	24.1	4.04	1.65	0.25	24.1	5.83
1.88	0.83	27.4	5.31	1.88	1.58	27.4	3.36	1.88	0.33	27.4	6.54
2.13	1.02	31.1	5.37	2.13	1.97	31.1	2.63	2.13	0.4	31.1	7.09
2.42	1.17	35.3	5.3	2.42	2.3	35.3	1.9	2.42	0.44	35.3	7.41
2.75	1.29	40.1	5.1	2.75	2.57	40.1	1.23	2.75	0.46	40.1	7.47
3.12	1.41	45.6	4.76	3.12	2.84	45.6	0.66	3.12	0.48	45.6	7.25
3.55	1.54	51.8	4.3	3.55	3.15	51.8	0.1	3.55	0.5	51.8	6.76
4.03	1.7	58.9	3.74	4.03	3.52	58.9	0	4.03	0.53	58.9	6.05
4.58	1.88	66.9	3.11	4.58	3.9	66.9	0	4.58	0.58	66.9	5.16
5.21	2.05	76	2.44	5.21	4.27	76	0	5.21	0.62	76	4.17
5.92	2.22	86.4	1.78	5.92	4.6	86.4	0	5.92	0.68	86.4	3.16
6.72	2.39	98.1	1.17	6.72	4.9	98.1	0	6.72	0.75	98.1	2.2
7.64	2.58	111	0.65	7.64	5.17	111	0	7.64	0.86	111	1.36
8.68	2.78	127	0.19	8.68	5.4	127	0	8.68	1.03	127	0.71
9.86	3	144	0.03	9.86	5.57	144	0	9.86	1.27	144	0.2
11.2	3.26	163	0	11.2	5.67	163	0	11.2	1.62	163	0.02
12.7	3.56			12.7	5.69			12.7	2.09		

CF164

Feed				Overflow				Underflow			
<i>dx</i> (10)	4.69	<i>d</i> [3,2]	11.9	<i>dx</i> (10)	2.88	<i>d</i> [3,2]	6.32	<i>dx</i> (10)	10.5	<i>d</i> [3,2]	18.6
<i>dx</i> (50)	24.7	<i>d</i> [4,3]	32.3	<i>dx</i> (50)	8.74	<i>d</i> [4,3]	13.3	<i>dx</i> (50)	34.1	<i>d</i> [4,3]	40.9
<i>dx</i> (90)	71.5			<i>dx</i> (90)	24.8			<i>dx</i> (90)	80.6		
% Size (µm)	Volume In										
0.872	0	14.5	3.7	0.872	0	14.5	5.04	0.872	0.06	14.5	3.17
0.991	0	16.4	4.05	0.991	0	16.4	4.53	0.991	0.08	16.4	3.88
1.13	0.11	18.7	4.4	1.13	0.09	18.7	3.93	1.13	0.09	18.7	4.63
1.28	0.21	21.2	4.72	1.28	0.33	21.2	3.27	1.28	0.13	21.2	5.37
1.45	0.37	24.1	5	1.45	0.73	24.1	2.6	1.45	0.19	24.1	6.04
1.65	0.57	27.4	5.2	1.65	1.23	27.4	1.96	1.65	0.27	27.4	6.57
1.88	0.77	31.1	5.29	1.88	1.75	31.1	1.39	1.88	0.36	31.1	6.91
2.13	0.96	35.3	5.27	2.13	2.22	35.3	0.94	2.13	0.43	35.3	7.03
2.42	1.1	40.1	5.13	2.42	2.62	40.1	0.6	2.42	0.47	40.1	6.92
2.75	1.21	45.6	4.86	2.75	2.96	45.6	0.4	2.75	0.49	45.6	6.58
3.12	1.32	51.8	4.48	3.12	3.31	51.8	0.3	3.12	0.5	51.8	6.03
3.55	1.45	58.9	3.99	3.55	3.72	58.9	0.27	3.55	0.51	58.9	5.33
4.03	1.6	66.9	3.43	4.03	4.17	66.9	0.29	4.03	0.55	66.9	4.53
4.58	1.77	76	2.82	4.58	4.63	76	0.32	4.58	0.59	76	3.69
5.21	1.93	86.4	2.19	5.21	5.04	86.4	0.34	5.21	0.65	86.4	2.87
5.92	2.09	98.1	1.58	5.92	5.39	98.1	0.34	5.92	0.73	98.1	2.1
6.72	2.26	111	1.02	6.72	5.65	111	0.31	6.72	0.85	111	1.44
7.64	2.43	127	0.56	7.64	5.83	127	0.25	7.64	1.01	127	0.89
8.68	2.62	144	0.18	8.68	5.91	144	0.18	8.68	1.25	144	0.48
9.86	2.84	163	0.03	9.86	5.88	163	0.09	9.86	1.57	163	0.2
11.2	3.09	186	0	11.2	5.72	186	0.02	11.2	2	186	0.03
12.7	3.38			12.7	5.44			12.7	2.53		

CF184

Feed				Overflow				Underflow			
<i>dx</i> (10)	1.05	<i>d</i> [3,2]	2.85	<i>dx</i> (10)	0.835	<i>d</i> [3,2]	2.08	<i>dx</i> (10)	2.76	<i>d</i> [3,2]	6.80
<i>dx</i> (50)	6.72	<i>d</i> [4,3]	24.4	<i>dx</i> (50)	3.43	<i>d</i> [4,3]	5.72	<i>dx</i> (50)	23.1	<i>d</i> [4,3]	40.0
<i>dx</i> (90)	46.6			<i>dx</i> (90)	13.6			<i>dx</i> (90)	81.2		
% Size (µm)	% Volume In										
0.243	0	14.5	2.9	0.243	0	14.5	2.06	0.243	0	14.5	4.3
0.276	0.14	16.4	2.95	0.276	0.06	16.4	1.73	0.276	0	16.4	4.89
0.314	0.28	18.7	2.96	0.314	0.25	18.7	1.41	0.314	0.07	18.7	5.37
0.357	0.46	21.2	2.91	0.357	0.54	21.2	1.12	0.357	0.15	21.2	5.68
0.405	0.66	24.1	2.8	0.405	0.91	24.1	0.86	0.405	0.24	24.1	5.8
0.46	0.87	27.4	2.63	0.46	1.28	27.4	0.63	0.46	0.33	27.4	5.7
0.523	1.05	31.1	2.4	0.523	1.59	31.1	0.45	0.523	0.41	31.1	5.39
0.594	1.21	35.3	2.13	0.594	1.84	35.3	0.3	0.594	0.47	35.3	4.91
0.675	1.36	40.1	1.85	0.675	2.05	40.1	0.18	0.675	0.51	40.1	4.33
0.767	1.51	45.6	1.57	0.767	2.24	45.6	0.1	0.767	0.55	45.6	3.68
0.872	1.66	51.8	1.31	0.872	2.42	51.8	0.02	0.872	0.59	51.8	3.04
0.991	1.83	58.9	1.07	0.991	2.62	58.9	0	0.991	0.62	58.9	2.45
1.13	2.01	66.9	0.87	1.13	2.85	66.9	0	1.13	0.67	66.9	1.94
1.28	2.22	76	0.71	1.28	3.13	76	0	1.28	0.73	76	1.53
1.45	2.43	86.4	0.58	1.45	3.43	86.4	0	1.45	0.79	86.4	1.23
1.65	2.64	98.1	0.48	1.65	3.76	98.1	0	1.65	0.86	98.1	1.02
1.88	2.83	111	0.4	1.88	4.07	111	0	1.88	0.93	111	0.9
2.13	2.99	127	0.34	2.13	4.34	127	0	2.13	1	127	0.84
2.42	3.1	144	0.29	2.42	4.54	144	0	2.42	1.05	144	0.81
2.75	3.15	163	0.25	2.75	4.65	163	0	2.75	1.07	163	0.78
3.12	3.15	186	0.22	3.12	4.67	186	0	3.12	1.08	186	0.74
3.55	3.09	211	0.21	3.55	4.61	211	0	3.55	1.08	211	0.68
4.03	3	240	0.22	4.03	4.47	240	0	4.03	1.06	240	0.6
4.58	2.89	272	0.24	4.58	4.3	272	0	4.58	1.06	272	0.5
5.21	2.78	310	0.26	5.21	4.11	310	0	5.21	1.09	310	0.39
5.92	2.7	352	0.28	5.92	3.91	352	0	5.92	1.18	352	0.28
6.72	2.65	400	0.28	6.72	3.7	400	0	6.72	1.35	400	0.2
7.64	2.63	454	0.25	7.64	3.49	454	0	7.64	1.61	454	0.13
8.68	2.64	516	0.2	8.68	3.25	516	0	8.68	1.99	516	0.1
9.86	2.69	586	0.13	9.86	2.99	586	0	9.86	2.47	586	0.06
11.2	2.75	666	0.08	11.2	2.7	666	0	11.2	3.04	666	0.02
12.7	2.83	756	0.02	12.7	2.38	756	0	12.7	3.66	756	0

CF185

Feed				Overflow				Underflow			
<i>dx</i> (10)	1.02	<i>d</i> [3,2]	2.8	<i>dx</i> (10)	0.818	<i>d</i> [3,2]	2.02	<i>dx</i> (10)	2.42	<i>d</i> [3,2]	6.15
<i>dx</i> (50)	7.3	<i>d</i> [4,3]	23.6	<i>dx</i> (50)	3.38	<i>d</i> [4,3]	5.69	<i>dx</i> (50)	22.4	<i>d</i> [4,3]	36.1
<i>dx</i> (90)	52.1			<i>dx</i> (90)	13.6			<i>dx</i> (90)	72.9		
% Size (µm)	% Volume In										
0.214	0.07	11.2	2.73	0.214	0	11.2	2.71	0.214	0	11.2	3
0.243	0.13	12.7	2.81	0.243	0	12.7	2.41	0.243	0	12.7	3.64
0.276	0.23	14.5	2.88	0.276	0.18	14.5	2.09	0.276	0.09	14.5	4.29
0.314	0.36	16.4	2.94	0.314	0.38	16.4	1.76	0.314	0.15	16.4	4.89
0.357	0.52	18.7	2.96	0.357	0.66	18.7	1.43	0.357	0.22	18.7	5.38
0.405	0.69	21.2	2.93	0.405	0.98	21.2	1.13	0.405	0.29	21.2	5.7
0.46	0.86	24.1	2.84	0.46	1.29	24.1	0.85	0.46	0.37	24.1	5.82
0.523	1.03	27.4	2.69	0.523	1.56	27.4	0.62	0.523	0.43	27.4	5.72
0.594	1.19	31.1	2.48	0.594	1.8	31.1	0.42	0.594	0.49	31.1	5.41
0.675	1.34	35.3	2.23	0.675	2.02	35.3	0.28	0.675	0.54	35.3	4.94
0.767	1.49	40.1	1.97	0.767	2.22	40.1	0.17	0.767	0.59	40.1	4.35
0.872	1.65	45.6	1.7	0.872	2.43	45.6	0.1	0.872	0.64	45.6	3.7
0.991	1.81	51.8	1.45	0.991	2.66	51.8	0.03	0.991	0.69	51.8	3.06
1.13	1.98	58.9	1.22	1.13	2.92	58.9	0	1.13	0.75	58.9	2.46
1.28	2.16	66.9	1.02	1.28	3.21	66.9	0	1.28	0.82	66.9	1.95
1.45	2.34	76	0.86	1.45	3.52	76	0	1.45	0.89	76	1.54
1.65	2.51	86.4	0.72	1.65	3.83	86.4	0	1.65	0.96	86.4	1.23
1.88	2.67	98.1	0.61	1.88	4.11	98.1	0	1.88	1.03	98.1	1
2.13	2.79	111	0.53	2.13	4.35	111	0	2.13	1.09	111	0.85
2.42	2.88	127	0.48	2.42	4.51	127	0	2.42	1.13	127	0.75
2.75	2.93	144	0.44	2.75	4.59	144	0	2.75	1.15	144	0.68
3.12	2.93	163	0.42	3.12	4.58	163	0	3.12	1.15	163	0.63
3.55	2.89	186	0.41	3.55	4.49	186	0	3.55	1.13	186	0.58
4.03	2.83	211	0.39	4.03	4.36	211	0	4.03	1.1	211	0.52
4.58	2.75	240	0.38	4.58	4.19	240	0	4.58	1.09	240	0.45
5.21	2.68	272	0.35	5.21	4.01	272	0	5.21	1.1	272	0.37
5.92	2.62	310	0.31	5.92	3.83	310	0	5.92	1.17	310	0.29
6.72	2.59	352	0.24	6.72	3.64	352	0	6.72	1.33	352	0.21
7.64	2.59	400	0.16	7.64	3.45	400	0	7.64	1.58	400	0.14
8.68	2.61	454	0.07	8.68	3.24	454	0	8.68	1.95	454	0.08
9.86	2.66	516	0	9.86	2.99	516	0	9.86	2.43	516	0.05

CF186

Feed				Overflow				Underflow			
<i>dx</i> (10)	1.05	<i>d</i> [3,2]	2.88	<i>dx</i> (10)	0.803	<i>d</i> [3,2]	2.03	<i>dx</i> (10)	6.40	<i>d</i> [3,2]	23.4
<i>dx</i> (50)	6.87	<i>d</i> [4,3]	21.4	<i>dx</i> (50)	3.50	<i>d</i> [4,3]	6.19	<i>dx</i> (50)	37.7	<i>d</i> [4,3]	77.2
<i>dx</i> (90)	45.7			<i>dx</i> (90)	14.7			<i>dx</i> (90)	2.58		
% Size (µm) Volume In	Size (µm)	% Volume In	Size (µm)								
0.243	0	12.7	0.243	0	12.7	0.243	0	12.7	0.243	0	12.7
0.276	0.13	14.5	0.276	0.13	14.5	0.276	0.13	14.5	0.276	0.13	14.5
0.314	0.28	16.4	0.314	0.28	16.4	0.314	0.28	16.4	0.314	0.28	16.4
0.357	0.47	18.7	0.357	0.47	18.7	0.357	0.47	18.7	0.357	0.47	18.7
0.405	0.68	21.2	0.405	0.68	21.2	0.405	0.68	21.2	0.405	0.68	21.2
0.46	0.89	24.1	0.46	0.89	24.1	0.46	0.89	24.1	0.46	0.89	24.1
0.523	1.07	27.4	0.523	1.07	27.4	0.523	1.07	27.4	0.523	1.07	27.4
0.594	1.23	31.1	0.594	1.23	31.1	0.594	1.23	31.1	0.594	1.23	31.1
0.675	1.36	35.3	0.675	1.36	35.3	0.675	1.36	35.3	0.675	1.36	35.3
0.767	1.48	40.1	0.767	1.48	40.1	0.767	1.48	40.1	0.767	1.48	40.1
0.872	1.6	45.6	0.872	1.6	45.6	0.872	1.6	45.6	0.872	1.6	45.6
0.991	1.74	51.8	0.991	1.74	51.8	0.991	1.74	51.8	0.991	1.74	51.8
1.13	1.9	58.9	1.13	1.9	58.9	1.13	1.9	58.9	1.13	1.9	58.9
1.28	2.09	66.9	1.28	2.09	66.9	1.28	2.09	66.9	1.28	2.09	66.9
1.45	2.3	76	1.45	2.3	76	1.45	2.3	76	1.45	2.3	76
1.65	2.52	86.4	1.65	2.52	86.4	1.65	2.52	86.4	1.65	2.52	86.4
1.88	2.74	98.1	1.88	2.74	98.1	1.88	2.74	98.1	1.88	2.74	98.1
2.13	2.93	111	2.13	2.93	111	2.13	2.93	111	2.13	2.93	111
2.42	3.07	127	2.42	3.07	127	2.42	3.07	127	2.42	3.07	127
2.75	3.16	144	2.75	3.16	144	2.75	3.16	144	2.75	3.16	144
3.12	3.19	163	3.12	3.19	163	3.12	3.19	163	3.12	3.19	163
3.55	3.15	186	3.55	3.15	186	3.55	3.15	186	3.55	3.15	186
4.03	3.07	211	4.03	3.07	211	4.03	3.07	211	4.03	3.07	211
4.58	2.95	240	4.58	2.95	240	4.58	2.95	240	4.58	2.95	240
5.21	2.83	272	5.21	2.83	272	5.21	2.83	272	5.21	2.83	272
5.92	2.72	310	5.92	2.72	310	5.92	2.72	310	5.92	2.72	310
6.72	2.64	352	6.72	2.64	352	6.72	2.64	352	6.72	2.64	352
7.64	2.6	400	7.64	2.6	400	7.64	2.6	400	7.64	2.6	400
8.68	2.61	454	8.68	2.61	454	8.68	2.61	454	8.68	2.61	454
9.86	2.66	516	9.86	2.66	516	9.86	2.66	516	9.86	2.66	516
11.2	2.73		11.2	2.73		11.2	2.73		11.2	2.73	

CF188

Feed				Overflow				Underflow			
<i>dx</i> (10)	2.31	<i>d</i> [3,2]	5.91	<i>dx</i> (10)	0.874	<i>d</i> [3,2]	2.34	<i>dx</i> (10)	11.3	<i>d</i> [3,2]	14.9
<i>dx</i> (50)	22.3	<i>d</i> [4,3]	35.8	<i>dx</i> (50)	4.59	<i>d</i> [4,3]	8.03	<i>dx</i> (50)	22.9	<i>d</i> [4,3]	50.1
<i>dx</i> (90)	75.1			<i>dx</i> (90)	20			<i>dx</i> (90)	113		
% Size (µm) In	% Volume In										
0.276	0.08	12.7	3.57	0.276	0.08	12.7	3.47	0.276	0	12.7	3.59
0.314	0.15	14.5	4.2	0.314	0.26	14.5	3.29	0.314	0	14.5	4.47
0.357	0.23	16.4	4.79	0.357	0.53	16.4	3.03	0.357	0.07	16.4	5.32
0.405	0.32	18.7	5.26	0.405	0.87	18.7	2.71	0.405	0.09	18.7	6.03
0.46	0.41	21.2	5.58	0.46	1.19	21.2	2.33	0.46	0.11	21.2	6.55
0.523	0.48	24.1	5.69	0.523	1.47	24.1	1.92	0.523	0.12	24.1	6.81
0.594	0.54	27.4	5.59	0.594	1.69	27.4	1.5	0.594	0.13	27.4	6.8
0.675	0.59	31.1	5.29	0.675	1.86	31.1	1.12	0.675	0.14	31.1	6.52
0.767	0.63	35.3	4.83	0.767	2.01	35.3	0.78	0.767	0.15	35.3	6.02
0.872	0.67	40.1	4.26	0.872	2.14	40.1	0.52	0.872	0.16	40.1	5.37
0.991	0.72	45.6	3.63	0.991	2.27	45.6	0.32	0.991	0.17	45.6	4.63
1.13	0.77	51.8	3.01	1.13	2.41	51.8	0.19	1.13	0.18	51.8	3.9
1.28	0.83	58.9	2.45	1.28	2.59	58.9	0.1	1.28	0.19	58.9	3.21
1.45	0.89	66.9	1.96	1.45	2.78	66.9	0	1.45	0.21	66.9	2.62
1.65	0.96	76	1.57	1.65	3	76	0	1.65	0.23	76	2.15
1.88	1.03	86.4	1.27	1.88	3.21	86.4	0	1.88	0.26	86.4	1.79
2.13	1.09	98.1	1.06	2.13	3.39	98.1	0	2.13	0.28	98.1	1.55
2.42	1.14	111	0.92	2.42	3.54	111	0	2.42	0.3	111	1.39
2.75	1.17	127	0.83	2.75	3.64	127	0	2.75	0.31	127	1.29
3.12	1.18	144	0.77	3.12	3.69	144	0	3.12	0.3	144	1.24
3.55	1.17	163	0.72	3.55	3.69	163	0	3.55	0.29	163	1.2
4.03	1.16	186	0.67	4.03	3.66	186	0	4.03	0.27	186	1.15
4.58	1.15	211	0.6	4.58	3.62	211	0	4.58	0.27	211	1.06
5.21	1.16	240	0.51	5.21	3.58	240	0	5.21	0.3	240	0.94
5.92	1.23	272	0.4	5.92	3.57	272	0	5.92	0.4	272	0.77
6.72	1.37	310	0.28	6.72	3.58	310	0	6.72	0.59	310	0.57
7.64	1.61	352	0.16	7.64	3.6	352	0	7.64	0.91	352	0.35
8.68	1.95	400	0.07	8.68	3.62	400	0	8.68	1.37	400	0.15
9.86	2.41	454	0	9.86	3.62	454	0	9.86	1.99	454	0.03
11.2	2.96			11.2	3.57			11.2	2.74		

CF195

Feed				Overflow				Underflow			
<i>dx</i> (10)	2.77	<i>d</i> [3,2]	6.71	<i>dx</i> (10)	1.25	<i>d</i> [3,2]	3.24	<i>dx</i> (10)	10.4	<i>d</i> [3,2]	14.9
<i>dx</i> (50)	24.5	<i>d</i> [4,3]	32.6	<i>dx</i> (50)	6.94	<i>d</i> [4,3]	10.4	<i>dx</i> (50)	39	<i>d</i> [4,3]	45.8
<i>dx</i> (90)	75			<i>dx</i> (90)	23.8			<i>dx</i> (90)	90.8		
% Size (µm)	% Volume In										
0.314	0	7.64	2.12	0.314	0.06	7.64	4.54	0.314	0	7.64	0.88
0.357	0.11	8.68	2.26	0.357	0.24	8.68	4.61	0.357	0	8.68	1.05
0.405	0.23	9.86	2.42	0.405	0.5	9.86	4.62	0.405	0.07	9.86	1.28
0.46	0.34	11.2	2.61	0.46	0.77	11.2	4.54	0.46	0.11	11.2	1.58
0.523	0.43	12.7	2.84	0.523	0.96	12.7	4.37	0.523	0.14	12.7	1.96
0.594	0.49	14.5	3.1	0.594	1.09	14.5	4.12	0.594	0.17	14.5	2.44
0.675	0.53	16.4	3.39	0.675	1.19	16.4	3.79	0.675	0.19	16.4	3.01
0.767	0.56	18.7	3.71	0.767	1.27	18.7	3.39	0.767	0.2	18.7	3.66
0.872	0.58	21.2	4.05	0.872	1.33	21.2	2.94	0.872	0.21	21.2	4.36
0.991	0.6	24.1	4.37	0.991	1.39	24.1	2.47	0.991	0.22	24.1	5.06
1.13	0.64	27.4	4.65	1.13	1.47	27.4	2	1.13	0.23	27.4	5.72
1.28	0.68	31.1	4.86	1.28	1.6	31.1	1.57	1.28	0.24	31.1	6.28
1.45	0.75	35.3	4.97	1.45	1.77	35.3	1.18	1.45	0.25	35.3	6.69
1.65	0.84	40.1	4.96	1.65	1.98	40.1	0.87	1.65	0.27	40.1	6.9
1.88	0.94	45.6	4.82	1.88	2.24	45.6	0.62	1.88	0.29	45.6	6.89
2.13	1.05	51.8	4.55	2.13	2.51	51.8	0.43	2.13	0.32	51.8	6.65
2.42	1.16	58.9	4.15	2.42	2.78	58.9	0.29	2.42	0.35	58.9	6.19
2.75	1.27	66.9	3.64	2.75	3.04	66.9	0.19	2.75	0.38	66.9	5.54
3.12	1.38	76	3.05	3.12	3.28	76	0.11	3.12	0.41	76	4.75
3.55	1.48	86.4	2.43	3.55	3.5	86.4	0.02	3.55	0.45	86.4	3.88
4.03	1.57	98.1	1.81	4.03	3.7	98.1	0	4.03	0.49	98.1	3
4.58	1.67	111	1.23	4.58	3.89	111	0	4.58	0.54	111	2.16
5.21	1.77	127	0.74	5.21	4.08	127	0	5.21	0.6	127	1.42
5.92	1.87	144	0.32	5.92	4.26	144	0	5.92	0.67	144	0.81
6.72	1.99	163	0.05	6.72	4.42	163	0	6.72	0.76	163	0.25

CF196

Feed				Overflow				Underflow			
<i>dx</i> (10)	10.8	<i>d</i> [3,2]	15.6	<i>dx</i> (10)	1.66	<i>d</i> [3,2]	4.15	<i>dx</i> (10)	16.4	<i>d</i> [3,2]	23.7
<i>dx</i> (50)	42.6	<i>d</i> [4,3]	49.4	<i>dx</i> (50)	10	<i>d</i> [4,3]	14.7	<i>dx</i> (50)	44.6	<i>d</i> [4,3]	51.6
<i>dx</i> (90)	97.6			<i>dx</i> (90)	33.8			<i>dx</i> (90)	97.6		
Size (µm)	% Volume In										
0.357	0	8.68	1	0.357	0.18	8.68	4.27	0.357	0	8.68	0.64
0.405	0.06	9.86	1.2	0.405	0.38	9.86	4.48	0.405	0	9.86	0.86
0.46	0.1	11.2	1.45	0.46	0.57	11.2	4.64	0.46	0	11.2	1.16
0.523	0.13	12.7	1.77	0.523	0.72	12.7	4.72	0.523	0	12.7	1.56
0.594	0.16	14.5	2.17	0.594	0.81	14.5	4.72	0.594	0.07	14.5	2.05
0.675	0.18	16.4	2.65	0.675	0.88	16.4	4.62	0.675	0.09	16.4	2.65
0.767	0.19	18.7	3.2	0.767	0.93	18.7	4.42	0.767	0.11	18.7	3.34
0.872	0.2	21.2	3.81	0.872	0.97	21.2	4.11	0.872	0.13	21.2	4.1
0.991	0.21	24.1	4.46	0.991	1	24.1	3.73	0.991	0.14	24.1	4.89
1.13	0.22	27.4	5.11	1.13	1.06	27.4	3.29	1.13	0.14	27.4	5.67
1.28	0.23	31.1	5.72	1.28	1.15	31.1	2.82	1.28	0.13	31.1	6.38
1.45	0.24	35.3	6.25	1.45	1.28	35.3	2.35	1.45	0.13	35.3	6.95
1.65	0.26	40.1	6.64	1.65	1.44	40.1	1.9	1.65	0.12	40.1	7.35
1.88	0.28	45.6	6.85	1.88	1.63	45.6	1.5	1.88	0.12	45.6	7.51
2.13	0.31	51.8	6.85	2.13	1.85	51.8	1.15	2.13	0.12	51.8	7.42
2.42	0.34	58.9	6.61	2.42	2.07	58.9	0.85	2.42	0.12	58.9	7.06
2.75	0.37	66.9	6.15	2.75	2.29	66.9	0.6	2.75	0.14	66.9	6.47
3.12	0.4	76	5.48	3.12	2.5	76	0.38	3.12	0.15	76	5.67
3.55	0.44	86.4	4.65	3.55	2.71	86.4	0.21	3.55	0.17	86.4	4.74
4.03	0.48	98.1	3.72	4.03	2.91	98.1	0.07	4.03	0.19	98.1	3.73
4.58	0.53	111	2.76	4.58	3.11	111	0	4.58	0.22	111	2.74
5.21	0.58	127	1.85	5.21	3.32	127	0	5.21	0.26	127	1.83
5.92	0.65	144	1.07	5.92	3.55	144	0	5.92	0.31	144	1.07
6.72	0.74	163	0.41	6.72	3.79	163	0	6.72	0.38	163	0.43
7.64	0.85	186	0	7.64	4.04	186	0	7.64	0.49	186	0.01

CF197

Feed				Overflow				Underflow			
<i>dx</i> (10)	2.82	<i>d</i> [3,2]	6.79	<i>dx</i> (10)	1.46	<i>d</i> [3,2]	3.75	<i>dx</i> (10)	14.9	<i>d</i> [3,2]	19.1
<i>dx</i> (50)	24.8	<i>d</i> [4,3]	33	<i>dx</i> (50)	8.81	<i>d</i> [4,3]	13.1	<i>dx</i> (50)	42.2	<i>d</i> [4,3]	48.8
<i>dx</i> (90)	75.6			<i>dx</i> (90)	30.4			<i>dx</i> (90)	92.5		
% Size (µm)	Volume In										
0.357	0.1	8.68	2.25	0.357	0.2	8.68	4.31	0.357	0	8.68	0.65
0.405	0.22	9.86	2.41	0.405	0.43	9.86	4.45	0.405	0	9.86	0.83
0.46	0.34	11.2	2.6	0.46	0.65	11.2	4.55	0.46	0.07	11.2	1.1
0.523	0.42	12.7	2.81	0.523	0.82	12.7	4.57	0.523	0.1	12.7	1.48
0.594	0.48	14.5	3.07	0.594	0.93	14.5	4.51	0.594	0.12	14.5	1.99
0.675	0.52	16.4	3.36	0.675	1.01	16.4	4.37	0.675	0.14	16.4	2.63
0.767	0.55	18.7	3.68	0.767	1.07	18.7	4.12	0.767	0.15	18.7	3.4
0.872	0.57	21.2	4.02	0.872	1.11	21.2	3.79	0.872	0.16	21.2	4.25
0.991	0.59	24.1	4.35	0.991	1.16	24.1	3.39	0.991	0.17	24.1	5.14
1.13	0.62	27.4	4.64	1.13	1.23	27.4	2.94	1.13	0.17	27.4	6
1.28	0.67	31.1	4.86	1.28	1.33	31.1	2.46	1.28	0.17	31.1	6.75
1.45	0.74	35.3	4.99	1.45	1.48	35.3	2	1.45	0.17	35.3	7.32
1.65	0.82	40.1	4.99	1.65	1.67	40.1	1.57	1.65	0.18	40.1	7.64
1.88	0.93	45.6	4.86	1.88	1.88	45.6	1.19	1.88	0.19	45.6	7.67
2.13	1.04	51.8	4.59	2.13	2.12	51.8	0.88	2.13	0.2	51.8	7.4
2.42	1.15	58.9	4.19	2.42	2.35	58.9	0.62	2.42	0.22	58.9	6.86
2.75	1.26	66.9	3.67	2.75	2.57	66.9	0.42	2.75	0.24	66.9	6.08
3.12	1.37	76	3.08	3.12	2.78	76	0.26	3.12	0.26	76	5.15
3.55	1.47	86.4	2.45	3.55	2.96	86.4	0.11	3.55	0.29	86.4	4.14
4.03	1.56	98.1	1.83	4.03	3.15	98.1	0	4.03	0.32	98.1	3.14
4.58	1.66	111	1.26	4.58	3.33	111	0	4.58	0.35	111	2.22
5.21	1.76	127	0.77	5.21	3.52	127	0	5.21	0.38	127	1.44
5.92	1.87	144	0.35	5.92	3.72	144	0	5.92	0.42	144	0.82
6.72	1.98	163	0.07	6.72	3.92	163	0	6.72	0.46	163	0.39
7.64	2.11	186	0.02	7.64	4.12	186	0	7.64	0.54	186	0.06

CF198

Feed				Overflow				Underflow			
<i>dx</i> (10)	12.8	<i>d</i> [3,2]	16.9	<i>dx</i> (10)	2.37	<i>d</i> [3,2]	5.58	<i>dx</i> (10)	20.4	<i>d</i> [3,2]	34
<i>dx</i> (50)	38.8	<i>d</i> [4,3]	44.2	<i>dx</i> (50)	15.5	<i>d</i> [4,3]	20.1	<i>dx</i> (50)	47	<i>d</i> [4,3]	54.2
<i>dx</i> (90)	83.7			<i>dx</i> (90)	44.2			<i>dx</i> (90)	98.6		
% Size (µm)	Volume In										
0.357	0	8.68	0.84	0.357	0.13	8.68	3.44	0.357	0	8.68	0.34
0.405	0	9.86	1.06	0.405	0.27	9.86	3.84	0.405	0	9.86	0.49
0.46	0.09	11.2	1.37	0.46	0.4	11.2	4.25	0.46	0	11.2	0.74
0.523	0.12	12.7	1.8	0.523	0.5	12.7	4.65	0.523	0	12.7	1.1
0.594	0.14	14.5	2.35	0.594	0.57	14.5	5.01	0.594	0	14.5	1.6
0.675	0.16	16.4	3.03	0.675	0.62	16.4	5.28	0.675	0	16.4	2.25
0.767	0.17	18.7	3.82	0.767	0.65	18.7	5.44	0.767	0.02	18.7	3.04
0.872	0.18	21.2	4.67	0.872	0.67	21.2	5.46	0.872	0.03	21.2	3.94
0.991	0.19	24.1	5.53	0.991	0.7	24.1	5.31	0.991	0.04	24.1	4.92
1.13	0.19	27.4	6.34	1.13	0.73	27.4	5.01	1.13	0.04	27.4	5.89
1.28	0.2	31.1	7	1.28	0.79	31.1	4.56	1.28	0.04	31.1	6.79
1.45	0.2	35.3	7.46	1.45	0.87	35.3	4.01	1.45	0.04	35.3	7.52
1.65	0.21	40.1	7.65	1.65	0.97	40.1	3.4	1.65	0.03	40.1	8.01
1.88	0.23	45.6	7.56	1.88	1.1	45.6	2.78	1.88	0.02	45.6	8.21
2.13	0.25	51.8	7.17	2.13	1.24	51.8	2.18	2.13	0.02	51.8	8.09
2.42	0.27	58.9	6.51	2.42	1.38	58.9	1.63	2.42	0	58.9	7.65
2.75	0.3	66.9	5.65	2.75	1.52	66.9	1.15	2.75	0	66.9	6.93
3.12	0.33	76	4.64	3.12	1.65	76	0.75	3.12	0.07	76	6
3.55	0.36	86.4	3.59	3.55	1.79	86.4	0.45	3.55	0.09	86.4	4.93
4.03	0.4	98.1	2.56	4.03	1.93	98.1	0.19	4.03	0.1	98.1	3.83
4.58	0.43	111	1.64	4.58	2.08	111	0.04	4.58	0.12	111	2.77
5.21	0.48	127	0.9	5.21	2.27	127	0	5.21	0.14	127	1.84
5.92	0.53	144	0.16	5.92	2.49	144	0	5.92	0.16	144	1.07
6.72	0.59	163	0	6.72	2.76	163	0	6.72	0.19	163	0.51
7.64	0.69	186	0	7.64	3.08	186	0	7.64	0.25	186	0.11

CF200

Feed				Overflow				Underflow			
<i>dx</i> (10)	2.67	<i>d</i> [3,2]	6.44	<i>dx</i> (10)	1.51	<i>d</i> [3,2]	3.87	<i>dx</i> (10)	14.3	<i>d</i> [3,2]	18.9
<i>dx</i> (50)	22.4	<i>d</i> [4,3]	30.4	<i>dx</i> (50)	9.2	<i>d</i> [4,3]	14.1	<i>dx</i> (50)	41.3	<i>d</i> [4,3]	47.3
<i>dx</i> (90)	70			<i>dx</i> (90)	33.4			<i>dx</i> (90)	89.9		
% Size (µm)	% Volume In										
0.357	0.11	8.68	2.42	0.357	0.19	8.68	4.19	0.357	0	8.68	0.74
0.405	0.23	9.86	2.6	0.405	0.41	9.86	4.32	0.405	0	9.86	0.95
0.46	0.36	11.2	2.8	0.46	0.63	11.2	4.4	0.46	0.06	11.2	1.25
0.523	0.45	12.7	3.04	0.523	0.79	12.7	4.43	0.523	0.09	12.7	1.65
0.594	0.5	14.5	3.32	0.594	0.89	14.5	4.38	0.594	0.12	14.5	2.17
0.675	0.55	16.4	3.62	0.675	0.97	16.4	4.26	0.675	0.14	16.4	2.82
0.767	0.58	18.7	3.94	0.767	1.02	18.7	4.07	0.767	0.15	18.7	3.56
0.872	0.6	21.2	4.25	0.872	1.06	21.2	3.81	0.872	0.16	21.2	4.38
0.991	0.62	24.1	4.54	0.991	1.11	24.1	3.47	0.991	0.17	24.1	5.23
1.13	0.65	27.4	4.77	1.13	1.17	27.4	3.09	1.13	0.17	27.4	6.03
1.28	0.7	31.1	4.9	1.28	1.27	31.1	2.67	1.28	0.17	31.1	6.73
1.45	0.77	35.3	4.92	1.45	1.41	35.3	2.25	1.45	0.17	35.3	7.25
1.65	0.87	40.1	4.82	1.65	1.6	40.1	1.84	1.65	0.18	40.1	7.54
1.88	0.98	45.6	4.58	1.88	1.81	45.6	1.46	1.88	0.19	45.6	7.56
2.13	1.1	51.8	4.22	2.13	2.05	51.8	1.12	2.13	0.2	51.8	7.31
2.42	1.22	58.9	3.75	2.42	2.28	58.9	0.83	2.42	0.22	58.9	6.79
2.75	1.34	66.9	3.2	2.75	2.5	66.9	0.59	2.75	0.24	66.9	6.05
3.12	1.46	76	2.62	3.12	2.7	76	0.39	3.12	0.26	76	5.14
3.55	1.56	86.4	2.03	3.55	2.89	86.4	0.22	3.55	0.29	86.4	4.13
4.03	1.67	98.1	1.46	4.03	3.08	98.1	0.08	4.03	0.32	98.1	3.1
4.58	1.77	111	0.97	4.58	3.26	111	0.03	4.58	0.35	111	2.13
5.21	1.88	127	0.56	5.21	3.45	127	0	5.21	0.39	127	1.29
5.92	2	144	0.23	5.92	3.64	144	0	5.92	0.43	144	0.57
6.72	2.12	163	0.08	6.72	3.84	163	0	6.72	0.5	163	0.06
7.64	2.26			7.64	4.03			7.64	0.6		

CF201

Feed				Overflow				Underflow			
<i>dx</i> (10)	3.13	<i>d</i> [3,2]	7.35	<i>dx</i> (10)	2.11	<i>d</i> [3,2]	5.25	<i>dx</i> (10)	11.6	<i>d</i> [3,2]	15.9
<i>dx</i> (50)	26.9	<i>d</i> [4,3]	34.2	<i>dx</i> (50)	15.7	<i>d</i> [4,3]	22.7	<i>dx</i> (50)	44.3	<i>d</i> [4,3]	49.5
<i>dx</i> (90)	77.3			<i>dx</i> (90)	54.3			<i>dx</i> (90)	94.1		
Size (µm)	% Volume In										
0.357	0.09	7.64	1.98	0.357	0.14	7.64	2.93	0.357	0	7.64	0.71
0.405	0.2	8.68	2.12	0.405	0.29	8.68	3.12	0.405	0.07	8.68	0.77
0.46	0.3	9.86	2.28	0.46	0.44	9.86	3.33	0.46	0.11	9.86	0.87
0.523	0.38	11.2	2.48	0.523	0.55	11.2	3.54	0.523	0.14	11.2	1.03
0.594	0.43	12.7	2.71	0.594	0.63	12.7	3.76	0.594	0.16	12.7	1.28
0.675	0.47	14.5	2.99	0.675	0.68	14.5	3.96	0.675	0.18	14.5	1.64
0.767	0.49	16.4	3.3	0.767	0.72	16.4	4.15	0.767	0.19	16.4	2.12
0.872	0.51	18.7	3.65	0.872	0.75	18.7	4.31	0.872	0.2	18.7	2.75
0.991	0.53	21.2	4.01	0.991	0.78	21.2	4.42	0.991	0.21	21.2	3.49
1.13	0.56	24.1	4.37	1.13	0.83	24.1	4.47	1.13	0.21	24.1	4.33
1.28	0.61	27.4	4.69	1.28	0.9	27.4	4.43	1.28	0.22	27.4	5.2
1.45	0.67	31.1	4.95	1.45	0.99	31.1	4.31	1.45	0.24	31.1	6.03
1.65	0.75	35.3	5.13	1.65	1.12	35.3	4.1	1.65	0.26	35.3	6.76
1.88	0.84	40.1	5.2	1.88	1.26	40.1	3.8	1.88	0.29	40.1	7.31
2.13	0.94	45.6	5.16	2.13	1.42	45.6	3.43	2.13	0.32	45.6	7.61
2.42	1.05	51.8	4.98	2.42	1.58	51.8	3.01	2.42	0.35	51.8	7.61
2.75	1.15	58.9	4.65	2.75	1.73	58.9	2.53	2.75	0.39	58.9	7.31
3.12	1.25	66.9	4.17	3.12	1.87	66.9	2.03	3.12	0.43	66.9	6.71
3.55	1.34	76	3.56	3.55	2.01	76	1.53	3.55	0.47	76	5.85
4.03	1.43	86.4	2.84	4.03	2.14	86.4	1.06	4.03	0.51	86.4	4.82
4.58	1.53	98.1	2.06	4.58	2.27	98.1	0.64	4.58	0.55	98.1	3.68
5.21	1.63	111	1.31	5.21	2.42	111	0.25	5.21	0.59	111	2.55
5.92	1.73	127	0.66	5.92	2.57	127	0.04	5.92	0.62	127	1.54
6.72	1.85	144	0.03	6.72	2.74	144	0	6.72	0.66	144	0.66

CF202

Feed				Overflow				Underflow			
<i>dx</i> (10)	2.9	<i>d</i> [3,2]	6.91	<i>dx</i> (10)	2.16	<i>d</i> [3,2]	5.35	<i>dx</i> (10)	20.5	<i>d</i> [3,2]	26.7
<i>dx</i> (50)	24.9	<i>d</i> [4,3]	32.8	<i>dx</i> (50)	16.2	<i>d</i> [4,3]	23	<i>dx</i> (50)	50.2	<i>d</i> [4,3]	56.6
<i>dx</i> (90)	74.9			<i>dx</i> (90)	54.4			<i>dx</i> (90)	103		
% Size (µm)	Volume In										
0.357	0.1	8.68	2.25	0.357	0.14	8.68	3.06	0.357	0	8.68	0.34
0.405	0.22	9.86	2.42	0.405	0.29	9.86	3.26	0.405	0	9.86	0.4
0.46	0.33	11.2	2.61	0.46	0.44	11.2	3.48	0.46	0	11.2	0.52
0.523	0.41	12.7	2.84	0.523	0.55	12.7	3.71	0.523	0	12.7	0.74
0.594	0.46	14.5	3.11	0.594	0.62	14.5	3.93	0.594	0	14.5	1.1
0.675	0.5	16.4	3.41	0.675	0.67	16.4	4.14	0.675	0.08	16.4	1.61
0.767	0.53	18.7	3.74	0.767	0.71	18.7	4.33	0.767	0.11	18.7	2.28
0.872	0.55	21.2	4.08	0.872	0.73	21.2	4.47	0.872	0.13	21.2	3.12
0.991	0.57	24.1	4.42	0.991	0.76	24.1	4.55	0.991	0.14	24.1	4.09
1.13	0.6	27.4	4.71	1.13	0.8	27.4	4.55	1.13	0.14	27.4	5.12
1.28	0.65	31.1	4.93	1.28	0.87	31.1	4.46	1.28	0.13	31.1	6.13
1.45	0.72	35.3	5.05	1.45	0.96	35.3	4.27	1.45	0.12	35.3	7.04
1.65	0.8	40.1	5.04	1.65	1.08	40.1	3.99	1.65	0.12	40.1	7.76
1.88	0.9	45.6	4.9	1.88	1.22	45.6	3.62	1.88	0.12	45.6	8.2
2.13	1.01	51.8	4.62	2.13	1.38	51.8	3.17	2.13	0.12	51.8	8.31
2.42	1.13	58.9	4.21	2.42	1.54	58.9	2.66	2.42	0.13	58.9	8.07
2.75	1.24	66.9	3.69	2.75	1.69	66.9	2.11	2.75	0.15	66.9	7.5
3.12	1.34	76	3.09	3.12	1.83	76	1.55	3.12	0.18	76	6.65
3.55	1.44	86.4	2.45	3.55	1.96	86.4	1.03	3.55	0.21	86.4	5.61
4.03	1.54	98.1	1.81	4.03	2.09	98.1	0.57	4.03	0.24	98.1	4.45
4.58	1.64	111	1.22	4.58	2.22	111	0.12	4.58	0.26	111	3.29
5.21	1.74	127	0.72	5.21	2.36	127	0	5.21	0.28	127	2.22
5.92	1.86	144	0.29	5.92	2.51	144	0	5.92	0.3	144	1.31
6.72	1.97	163	0	6.72	2.68	163	0	6.72	0.31	163	0.55
7.64	2.11			7.64	2.86			7.64	0.32		

CF203

Feed				Overflow				Underflow			
<i>dx</i> (10)	20.4	<i>d</i> [3,2]	26.6	<i>dx</i> (10)	10.1	<i>d</i> [3,2]	14.1	<i>dx</i> (10)	27.2	<i>d</i> [3,2]	47.6
<i>dx</i> (50)	50.1	<i>d</i> [4,3]	56.6	<i>dx</i> (50)	37.9	<i>d</i> [4,3]	43.2	<i>dx</i> (50)	56.5	<i>d</i> [4,3]	64.2
<i>dx</i> (90)	103			<i>dx</i> (90)	83.2			<i>dx</i> (90)	113		
Size (µm)	% Volume In										
0.405	0	9.86	0.43	0.405	0.09	9.86	1.05	0.405	0	9.86	0.08
0.46	0	11.2	0.56	0.46	0.13	11.2	1.32	0.46	0	11.2	0.15
0.523	0	12.7	0.78	0.523	0.17	12.7	1.72	0.523	0	12.7	0.31
0.594	0	14.5	1.13	0.594	0.19	14.5	2.26	0.594	0	14.5	0.6
0.675	0.08	16.4	1.63	0.675	0.21	16.4	2.93	0.675	0	16.4	1.06
0.767	0.11	18.7	2.29	0.767	0.22	18.7	3.72	0.767	0	18.7	1.7
0.872	0.13	21.2	3.12	0.872	0.23	21.2	4.58	0.872	0	21.2	2.54
0.991	0.14	24.1	4.08	0.991	0.23	24.1	5.46	0.991	0	24.1	3.55
1.13	0.14	27.4	5.1	1.13	0.23	27.4	6.26	1.13	0	27.4	4.67
1.28	0.13	31.1	6.12	1.28	0.24	31.1	6.91	1.28	0	31.1	5.82
1.45	0.12	35.3	7.03	1.45	0.26	35.3	7.34	1.45	0	35.3	6.92
1.65	0.12	40.1	7.75	1.65	0.28	40.1	7.51	1.65	0	40.1	7.84
1.88	0.12	45.6	8.19	1.88	0.31	45.6	7.38	1.88	0	45.6	8.5
2.13	0.12	51.8	8.3	2.13	0.35	51.8	6.96	2.13	0	51.8	8.83
2.42	0.13	58.9	8.06	2.42	0.39	58.9	6.28	2.42	0	58.9	8.78
2.75	0.15	66.9	7.48	2.75	0.44	66.9	5.41	2.75	0	66.9	8.36
3.12	0.17	76	6.63	3.12	0.48	76	4.43	3.12	0	76	7.62
3.55	0.2	86.4	5.58	3.55	0.53	86.4	3.41	3.55	0	86.4	6.61
4.03	0.23	98.1	4.42	4.03	0.57	98.1	2.44	4.03	0	98.1	5.43
4.58	0.26	111	3.27	4.58	0.6	111	1.59	4.58	0	111	4.19
5.21	0.28	127	2.21	5.21	0.63	127	0.9	5.21	0.05	127	2.98
5.92	0.3	144	1.31	5.92	0.66	144	0.34	5.92	0.05	144	1.91
6.72	0.31	163	0.56	6.72	0.7	163	0	6.72	0.05	163	0.96
7.64	0.33	186	0.04	7.64	0.77	186	0	7.64	0.05	186	0.36
8.68	0.36			8.68	0.87			8.68	0.04		

CF206

Feed				Overflow				Underflow			
<i>dx</i> (10)	3.03	<i>d</i> [3,2]	7.13	<i>dx</i> (10)	2.25	<i>d</i> [3,2]	5.53	<i>dx</i> (10)	20.9	<i>d</i> [3,2]	27.3
<i>dx</i> (50)	25.9	<i>d</i> [4,3]	33.8	<i>dx</i> (50)	17.2	<i>d</i> [4,3]	24.4	<i>dx</i> (50)	50.8	<i>d</i> [4,3]	58
<i>dx</i> (90)	76.8			<i>dx</i> (90)	57.4			<i>dx</i> (90)	107		
% Size (µm)		% Volume In		% Size (µm)		% Volume In		% Size (µm)		% Volume In	
0.357	0.1	8.68	2.19	0.357	0.13	8.68	2.93	0.357	0	8.68	0.33
0.405	0.21	9.86	2.35	0.405	0.28	9.86	3.13	0.405	0	9.86	0.38
0.46	0.32	11.2	2.55	0.46	0.42	11.2	3.36	0.46	0	11.2	0.5
0.523	0.4	12.7	2.77	0.523	0.53	12.7	3.6	0.523	0	12.7	0.71
0.594	0.45	14.5	3.04	0.594	0.6	14.5	3.84	0.594	0	14.5	1.06
0.675	0.48	16.4	3.35	0.675	0.65	16.4	4.08	0.675	0.08	16.4	1.56
0.767	0.51	18.7	3.68	0.767	0.68	18.7	4.3	0.767	0.1	18.7	2.23
0.872	0.53	21.2	4.03	0.872	0.71	21.2	4.48	0.872	0.12	21.2	3.07
0.991	0.55	24.1	4.38	0.991	0.73	24.1	4.59	0.991	0.13	24.1	4.03
1.13	0.57	27.4	4.69	1.13	0.77	27.4	4.61	1.13	0.13	27.4	5.07
1.28	0.62	31.1	4.93	1.28	0.83	31.1	4.54	1.28	0.12	31.1	6.08
1.45	0.68	35.3	5.08	1.45	0.91	35.3	4.37	1.45	0.12	35.3	7
1.65	0.76	40.1	5.11	1.65	1.03	40.1	4.1	1.65	0.11	40.1	7.71
1.88	0.86	45.6	5.01	1.88	1.17	45.6	3.74	1.88	0.11	45.6	8.14
2.13	0.97	51.8	4.76	2.13	1.32	51.8	3.3	2.13	0.11	51.8	8.24
2.42	1.08	58.9	4.38	2.42	1.47	58.9	2.8	2.42	0.13	58.9	7.99
2.75	1.19	66.9	3.88	2.75	1.62	66.9	2.27	2.75	0.15	66.9	7.42
3.12	1.3	76	3.28	3.12	1.76	76	1.74	3.12	0.17	76	6.59
3.55	1.4	86.4	2.63	3.55	1.9	86.4	1.23	3.55	0.2	86.4	5.57
4.03	1.5	98.1	1.96	4.03	2.02	98.1	0.79	4.03	0.23	98.1	4.46
4.58	1.6	111	1.33	4.58	2.15	111	0.39	4.58	0.26	111	3.37
5.21	1.7	127	0.78	5.21	2.28	127	0.11	5.21	0.28	127	2.36
5.92	1.8	144	0.27	5.92	2.42	144	0.03	5.92	0.29	144	1.51
6.72	1.92	163	0.01	6.72	2.57	163	0	6.72	0.3	163	0.85
7.64	2.05	186	0	7.64	2.74	186	0	7.64	0.31	186	0.32

Appendix B: Laser Sizing Data

CF207

Feed				Overflow				Underflow			
<i>dx</i> (10)	18.2	<i>d</i> [3,2]	23.3	<i>dx</i> (10)	4.91	<i>d</i> [3,2]	9.31	<i>dx</i> (10)	27.8	<i>d</i> [3,2]	48.5
<i>dx</i> (50)	46.7	<i>d</i> [4,3]	52.6	<i>dx</i> (50)	27.1	<i>d</i> [4,3]	30.5	<i>dx</i> (50)	56.1	<i>d</i> [4,3]	63.3
<i>dx</i> (90)	96.7			<i>dx</i> (90)	59.9			<i>dx</i> (90)	110		
% Size (µm)	Volume In										
0.357	0	8.68	0.44	0.357	0.07	8.68	1.65	0.357	0	8.68	0
0.405	0	9.86	0.54	0.405	0.15	9.86	2	0.405	0	9.86	0
0.46	0	11.2	0.71	0.46	0.22	11.2	2.46	0.46	0	11.2	0.09
0.523	0	12.7	1	0.523	0.28	12.7	3.04	0.523	0	12.7	0.23
0.594	0.08	14.5	1.41	0.594	0.31	14.5	3.73	0.594	0	14.5	0.5
0.675	0.11	16.4	1.99	0.675	0.34	16.4	4.49	0.675	0	16.4	0.96
0.767	0.13	18.7	2.72	0.767	0.36	18.7	5.27	0.767	0	18.7	1.62
0.872	0.14	21.2	3.59	0.872	0.36	21.2	6	0.872	0	21.2	2.49
0.991	0.15	24.1	4.56	0.991	0.37	24.1	6.61	0.991	0	24.1	3.56
1.13	0.15	27.4	5.55	1.13	0.38	27.4	7.03	1.13	0	27.4	4.75
1.28	0.15	31.1	6.49	1.28	0.4	31.1	7.18	1.28	0	31.1	5.98
1.45	0.14	35.3	7.29	1.45	0.44	35.3	7.05	1.45	0	35.3	7.15
1.65	0.14	40.1	7.86	1.65	0.49	40.1	6.63	1.65	0	40.1	8.13
1.88	0.15	45.6	8.14	1.88	0.55	45.6	5.95	1.88	0	45.6	8.82
2.13	0.16	51.8	8.09	2.13	0.62	51.8	5.05	2.13	0	51.8	9.13
2.42	0.17	58.9	7.71	2.42	0.69	58.9	4.03	2.42	0	58.9	9.04
2.75	0.19	66.9	7.03	2.75	0.76	66.9	2.98	2.75	0	66.9	8.55
3.12	0.22	76	6.1	3.12	0.83	76	1.98	3.12	0	76	7.7
3.55	0.25	86.4	5.02	3.55	0.89	86.4	1.13	3.55	0	86.4	6.59
4.03	0.28	98.1	3.87	4.03	0.94	98.1	0.43	4.03	0	98.1	5.32
4.58	0.3	111	2.75	4.58	0.99	111	0	4.58	0	111	4.01
5.21	0.33	127	1.75	5.21	1.05	127	0	5.21	0	127	2.77
5.92	0.34	144	0.94	5.92	1.13	144	0	5.92	0	144	1.7
6.72	0.36	163	0.14	6.72	1.24	163	0	6.72	0	163	0.86
7.64	0.39	186	0	7.64	1.41	186	0	7.64	0	186	0.04

CF209

Feed				Overflow				Underflow			
<i>dx</i> (10)	2.75	<i>d</i> [3,2]	6.61	<i>dx</i> (10)	2.08	<i>d</i> [3,2]	5.21	<i>dx</i> (10)	22.8	<i>d</i> [3,2]	39.2
<i>dx</i> (50)	23.1	<i>d</i> [4,3]	30.6	<i>dx</i> (50)	15.5	<i>d</i> [4,3]	22.5	<i>dx</i> (50)	50	<i>d</i> [4,3]	56.2
<i>dx</i> (90)	70.5			<i>dx</i> (90)	53.3			<i>dx</i> (90)	99.4		
% Size (µm)	% Volume In										
0.357	0.11	8.68	2.4	0.357	0.14	8.68	3.17	0.357	0	8.68	0.22
0.405	0.22	9.86	2.57	0.405	0.29	9.86	3.38	0.405	0	9.86	0.3
0.46	0.34	11.2	2.78	0.46	0.45	11.2	3.6	0.46	0	11.2	0.46
0.523	0.43	12.7	3.01	0.523	0.56	12.7	3.82	0.523	0	12.7	0.73
0.594	0.49	14.5	3.28	0.594	0.63	14.5	4.03	0.594	0	14.5	1.14
0.675	0.53	16.4	3.58	0.675	0.69	16.4	4.23	0.675	0	16.4	1.72
0.767	0.56	18.7	3.9	0.767	0.73	18.7	4.39	0.767	0	18.7	2.48
0.872	0.58	21.2	4.23	0.872	0.76	21.2	4.49	0.872	0	21.2	3.4
0.991	0.6	24.1	4.53	0.991	0.79	24.1	4.52	0.991	0	24.1	4.44
1.13	0.64	27.4	4.78	1.13	0.84	27.4	4.46	1.13	0	27.4	5.53
1.28	0.69	31.1	4.94	1.28	0.91	31.1	4.31	1.28	0	31.1	6.59
1.45	0.76	35.3	4.99	1.45	1.01	35.3	4.06	1.45	0	35.3	7.52
1.65	0.85	40.1	4.93	1.65	1.13	40.1	3.72	1.65	0	40.1	8.23
1.88	0.96	45.6	4.72	1.88	1.28	45.6	3.31	1.88	0	45.6	8.63
2.13	1.07	51.8	4.39	2.13	1.43	51.8	2.85	2.13	0	51.8	8.68
2.42	1.19	58.9	3.94	2.42	1.58	58.9	2.36	2.42	0	58.9	8.37
2.75	1.3	66.9	3.39	2.75	1.73	66.9	1.87	2.75	0	66.9	7.7
3.12	1.41	76	2.78	3.12	1.86	76	1.4	3.12	0.07	76	6.75
3.55	1.51	86.4	2.15	3.55	1.99	86.4	0.98	3.55	0.09	86.4	5.59
4.03	1.61	98.1	1.52	4.03	2.12	98.1	0.63	4.03	0.11	98.1	4.33
4.58	1.71	111	0.97	4.58	2.26	111	0.36	4.58	0.13	111	3.07
5.21	1.83	127	0.51	5.21	2.41	127	0.12	5.21	0.15	127	1.94
5.92	1.95	144	0.06	5.92	2.58	144	0.05	5.92	0.16	144	1.01
6.72	2.09	163	0	6.72	2.77	163	0	6.72	0.17	163	0.1
7.64	2.24			7.64	2.96			7.64	0.18		

CF215

Feed				Overflow				Underflow			
<i>dx</i> (10)	0.609	<i>d</i> [3,2]	1.7	<i>dx</i> (10)	0.54	<i>d</i> [3,2]	1.22	<i>dx</i> (10)	3.26	<i>d</i> [3,2]	6.75
<i>dx</i> (50)	3.84	<i>d</i> [4,3]	15.4	<i>dx</i> (50)	1.63	<i>d</i> [4,3]	3.98	<i>dx</i> (50)	37.3	<i>d</i> [4,3]	46.1
<i>dx</i> (90)	49.4			<i>dx</i> (90)	10.7			<i>dx</i> (90)	94.1		
% Size (µm)	Volume In										
0.214	0.1	9.86	1.73	0.214	0.14	9.86	1.81	0.214	0	9.86	1.06
0.243	0.29	11.2	1.72	0.243	0.39	11.2	1.66	0.243	0.07	11.2	1.31
0.276	0.56	12.7	1.72	0.276	0.77	12.7	1.48	0.276	0.13	12.7	1.64
0.314	0.9	14.5	1.74	0.314	1.21	14.5	1.3	0.314	0.2	14.5	2.08
0.357	1.29	16.4	1.8	0.357	1.69	16.4	1.13	0.357	0.28	16.4	2.62
0.405	1.7	18.7	1.9	0.405	2.21	18.7	0.97	0.405	0.37	18.7	3.27
0.46	2.11	21.2	2.03	0.46	2.77	21.2	0.81	0.46	0.45	21.2	3.99
0.523	2.51	24.1	2.2	0.523	3.35	24.1	0.66	0.523	0.53	24.1	4.74
0.594	2.85	27.4	2.39	0.594	3.91	27.4	0.51	0.594	0.6	27.4	5.46
0.675	3.11	31.1	2.56	0.675	4.39	31.1	0.37	0.675	0.65	31.1	6.06
0.767	3.28	35.3	2.7	0.767	4.75	35.3	0.24	0.767	0.69	35.3	6.49
0.872	3.36	40.1	2.76	0.872	4.99	40.1	0.13	0.872	0.7	40.1	6.67
0.991	3.36	45.6	2.71	0.991	5.1	45.6	0.03	0.991	0.7	45.6	6.58
1.13	3.28	51.8	2.53	1.13	5.08	51.8	0	1.13	0.68	51.8	6.22
1.28	3.15	58.9	2.21	1.28	4.94	58.9	0	1.28	0.65	58.9	5.63
1.45	2.97	66.9	1.78	1.45	4.69	66.9	0	1.45	0.61	66.9	4.89
1.65	2.78	76	1.28	1.65	4.37	76	0	1.65	0.57	76	4.08
1.88	2.58	86.4	0.79	1.88	4.01	86.4	0	1.88	0.53	86.4	3.27
2.13	2.39	98.1	0.38	2.13	3.64	98.1	0	2.13	0.5	98.1	2.53
2.42	2.22	111	0.04	2.42	3.29	111	0	2.42	0.47	111	1.91
2.75	2.09	127	0	2.75	2.98	127	0	2.75	0.45	127	1.42
3.12	1.97	144	0	3.12	2.71	144	0	3.12	0.44	144	1.04
3.55	1.89	163	0	3.55	2.51	163	0	3.55	0.45	163	0.75
4.03	1.82	186	0	4.03	2.35	186	0	4.03	0.46	186	0.52
4.58	1.78	211	0	4.58	2.25	211	0	4.58	0.48	211	0.34
5.21	1.75	240	0	5.21	2.18	240	0	5.21	0.52	240	0.2
5.92	1.75	272	0	5.92	2.14	272	0	5.92	0.57	272	0.12
6.72	1.75	310	0	6.72	2.1	310	0	6.72	0.64	310	0.07
7.64	1.75	352	0	7.64	2.04	352	0	7.64	0.74	352	0.02
8.68	1.74			8.68	1.94			8.68	0.87		

CF217

Feed				Overflow				Underflow			
<i>dx</i> (10)	0.647	<i>d</i> [3,2]	1.75	<i>dx</i> (10)	0.602	<i>d</i> [3,2]	1.33	<i>dx</i> (10)	9.02	<i>d</i> [3,2]	9.87
<i>dx</i> (50)	3.63	<i>d</i> [4,3]	16.9	<i>dx</i> (50)	1.75	<i>d</i> [4,3]	4.31	<i>dx</i> (50)	40.1	<i>d</i> [4,3]	49.5
<i>dx</i> (90)	53.9			<i>dx</i> (90)	10.3			<i>dx</i> (90)	97.1		
% Size (µm)	Volume In										
0.214	0.18	8.68	1.52	0.214	0.07	8.68	1.72	0.214	0	8.68	0.74
0.243	0.41	9.86	1.52	0.243	0.27	9.86	1.58	0.243	0	9.86	0.92
0.276	0.67	11.2	1.52	0.276	0.57	11.2	1.43	0.276	0.07	11.2	1.17
0.314	0.92	12.7	1.55	0.314	0.91	12.7	1.28	0.314	0.11	12.7	1.52
0.357	1.15	14.5	1.61	0.357	1.27	14.5	1.13	0.357	0.15	14.5	1.98
0.405	1.38	16.4	1.7	0.405	1.67	16.4	0.98	0.405	0.19	16.4	2.57
0.46	1.66	18.7	1.82	0.46	2.16	18.7	0.84	0.46	0.24	18.7	3.29
0.523	2.01	21.2	1.98	0.523	2.75	21.2	0.7	0.523	0.3	21.2	4.09
0.594	2.4	24.1	2.15	0.594	3.38	24.1	0.57	0.594	0.36	24.1	4.94
0.675	2.77	27.4	2.32	0.675	3.98	27.4	0.45	0.675	0.41	27.4	5.75
0.767	3.08	31.1	2.46	0.767	4.5	31.1	0.35	0.767	0.46	31.1	6.44
0.872	3.34	35.3	2.57	0.872	4.92	35.3	0.28	0.872	0.49	35.3	6.94
0.991	3.5	40.1	2.61	0.991	5.22	40.1	0.24	0.991	0.5	40.1	7.17
1.13	3.57	45.6	2.56	1.13	5.37	45.6	0.22	1.13	0.5	45.6	7.09
1.28	3.54	51.8	2.43	1.28	5.36	51.8	0.19	1.28	0.49	51.8	6.72
1.45	3.41	58.9	2.21	1.45	5.22	58.9	0.16	1.45	0.46	58.9	6.09
1.65	3.21	66.9	1.91	1.65	4.95	66.9	0.12	1.65	0.43	66.9	5.27
1.88	2.97	76	1.55	1.88	4.6	76	0.07	1.88	0.39	76	4.37
2.13	2.71	86.4	1.17	2.13	4.21	86.4	0	2.13	0.35	86.4	3.48
2.42	2.46	98.1	0.8	2.42	3.81	98.1	0	2.42	0.33	98.1	2.67
2.75	2.24	111	0.47	2.75	3.44	111	0	2.75	0.31	111	1.99
3.12	2.05	127	0.15	3.12	3.11	127	0	3.12	0.3	127	1.48
3.55	1.9	144	0.06	3.55	2.83	144	0	3.55	0.31	144	1.1
4.03	1.79	163	0	4.03	2.59	163	0	4.03	0.33	163	0.83
4.58	1.7	186	0	4.58	2.4	186	0	4.58	0.35	186	0.62
5.21	1.64	211	0	5.21	2.23	211	0	5.21	0.39	211	0.46
5.92	1.59	240	0	5.92	2.1	240	0	5.92	0.45	240	0.31
6.72	1.56	272	0	6.72	1.97	272	0	6.72	0.52	272	0.17
7.64	1.54	310	0	7.64	1.85	310	0	7.64	0.61	310	0.09

CF218

Feed				Overflow				Underflow			
<i>dx</i> (10)	0.619	<i>d</i> [3,2]	1.73	<i>dx</i> (10)	0.552	<i>d</i> [3,2]	1.26	<i>dx</i> (10)	13.2	<i>d</i> [3,2]	12.3
<i>dx</i> (50)	4.01	<i>d</i> [4,3]	18	<i>dx</i> (50)	1.7	<i>d</i> [4,3]	4.11	<i>dx</i> (50)	42.1	<i>d</i> [4,3]	53.2
<i>dx</i> (90)	56.7			<i>dx</i> (90)	10.8			<i>dx</i> (90)	102		
% Size (µm)	Volume In										
0.214	0.14	9.86	1.53	0.214	0.11	9.86	1.77	0.214	0	9.86	0.83
0.243	0.35	11.2	1.53	0.243	0.34	11.2	1.64	0.243	0	11.2	1.09
0.276	0.62	12.7	1.56	0.276	0.7	12.7	1.49	0.276	0.04	12.7	1.44
0.314	0.93	14.5	1.63	0.314	1.13	14.5	1.33	0.314	0.09	14.5	1.91
0.357	1.25	16.4	1.72	0.357	1.6	16.4	1.16	0.357	0.13	16.4	2.52
0.405	1.59	18.7	1.86	0.405	2.11	18.7	0.98	0.405	0.17	18.7	3.25
0.46	1.95	21.2	2.02	0.46	2.66	21.2	0.81	0.46	0.21	21.2	4.08
0.523	2.31	24.1	2.19	0.523	3.24	24.1	0.64	0.523	0.25	24.1	4.96
0.594	2.65	27.4	2.36	0.594	3.8	27.4	0.49	0.594	0.28	27.4	5.82
0.675	2.94	31.1	2.49	0.675	4.27	31.1	0.36	0.675	0.3	31.1	6.57
0.767	3.15	35.3	2.58	0.767	4.64	35.3	0.26	0.767	0.32	35.3	7.11
0.872	3.28	40.1	2.6	0.872	4.89	40.1	0.18	0.872	0.32	40.1	7.39
0.991	3.32	45.6	2.55	0.991	5.01	45.6	0.1	0.991	0.32	45.6	7.35
1.13	3.29	51.8	2.41	1.13	5	51.8	0.07	1.13	0.31	51.8	6.99
1.28	3.18	58.9	2.2	1.28	4.88	58.9	0.02	1.28	0.29	58.9	6.37
1.45	3.02	66.9	1.94	1.45	4.67	66.9	0	1.45	0.27	66.9	5.54
1.65	2.82	76	1.63	1.65	4.38	76	0	1.65	0.25	76	4.61
1.88	2.62	86.4	1.3	1.88	4.06	86.4	0	1.88	0.24	86.4	3.68
2.13	2.42	98.1	0.96	2.13	3.73	98.1	0	2.13	0.22	98.1	2.83
2.42	2.25	111	0.65	2.42	3.42	111	0	2.42	0.21	111	2.11
2.75	2.11	127	0.36	2.75	3.14	127	0	2.75	0.21	127	1.55
3.12	1.99	144	0.17	3.12	2.91	144	0	3.12	0.22	144	1.14
3.55	1.9	163	0.07	3.55	2.71	163	0	3.55	0.23	163	0.86
4.03	1.82	186	0	4.03	2.54	186	0	4.03	0.25	186	0.67
4.58	1.76	211	0	4.58	2.4	211	0	4.58	0.28	211	0.52
5.21	1.7	240	0	5.21	2.28	240	0	5.21	0.32	240	0.39
5.92	1.64	272	0	5.92	2.17	272	0	5.92	0.37	272	0.29
6.72	1.6	310	0	6.72	2.08	310	0	6.72	0.43	310	0.22
7.64	1.56	352	0	7.64	1.98	352	0	7.64	0.53	352	0.15
8.68	1.54	400	0	8.68	1.88	400	0	8.68	0.65	400	0.08

CF219

Feed				Overflow				Underflow			
<i>dx</i> (10)	0.639	<i>d</i> [3,2]	1.71	<i>dx</i> (10)	0.554	<i>d</i> [3,2]	1.22	<i>dx</i> (10)	5.01	<i>d</i> [3,2]	7.62
<i>dx</i> (50)	3.32	<i>d</i> [4,3]	15.1	<i>dx</i> (50)	1.62	<i>d</i> [4,3]	3.5	<i>dx</i> (50)	33.7	<i>d</i> [4,3]	43.4
<i>dx</i> (90)	47.9			<i>dx</i> (90)	8.71			<i>dx</i> (90)	86.6		
% Size (µm)	% Volume In										
0.214	0.1	9.86	1.59	0.214	0.14	9.86	1.55	0.214	0	9.86	1.51
0.243	0.28	11.2	1.59	0.243	0.39	11.2	1.37	0.243	0	11.2	1.88
0.276	0.54	12.7	1.62	0.276	0.75	12.7	1.18	0.276	0.1	12.7	2.31
0.314	0.84	14.5	1.68	0.314	1.15	14.5	1	0.314	0.16	14.5	2.82
0.357	1.15	16.4	1.78	0.357	1.58	16.4	0.82	0.357	0.23	16.4	3.39
0.405	1.49	18.7	1.9	0.405	2.04	18.7	0.66	0.405	0.29	18.7	4.03
0.46	1.85	21.2	2.04	0.46	2.56	21.2	0.52	0.46	0.36	21.2	4.68
0.523	2.25	24.1	2.18	0.523	3.14	24.1	0.39	0.523	0.43	24.1	5.31
0.594	2.65	27.4	2.29	0.594	3.74	27.4	0.28	0.594	0.5	27.4	5.87
0.675	3	31.1	2.36	0.675	4.29	31.1	0.2	0.675	0.56	31.1	6.28
0.767	3.28	35.3	2.38	0.767	4.74	35.3	0.14	0.767	0.59	35.3	6.5
0.872	3.47	40.1	2.33	0.872	5.08	40.1	0.08	0.872	0.61	40.1	6.48
0.991	3.59	45.6	2.2	0.991	5.31	45.6	0.07	0.991	0.62	45.6	6.21
1.13	3.61	51.8	2.01	1.13	5.38	51.8	0.05	1.13	0.61	51.8	5.72
1.28	3.54	58.9	1.76	1.28	5.32	58.9	0.02	1.28	0.59	58.9	5.03
1.45	3.41	66.9	1.48	1.45	5.14	66.9	0	1.45	0.55	66.9	4.24
1.65	3.22	76	1.18	1.65	4.84	76	0	1.65	0.52	76	3.41
1.88	3	86.4	0.89	1.88	4.48	86.4	0	1.88	0.48	86.4	2.63
2.13	2.77	98.1	0.62	2.13	4.09	98.1	0	2.13	0.44	98.1	1.95
2.42	2.55	111	0.39	2.42	3.7	111	0	2.42	0.42	111	1.41
2.75	2.36	127	0.21	2.75	3.34	127	0	2.75	0.4	127	1.02
3.12	2.2	144	0.08	3.12	3.02	144	0	3.12	0.39	144	0.77
3.55	2.06	163	0.03	3.55	2.75	163	0	3.55	0.4	163	0.61
4.03	1.94	186	0	4.03	2.53	186	0	4.03	0.42	186	0.51
4.58	1.85	211	0	4.58	2.35	211	0	4.58	0.46	211	0.43
5.21	1.78	240	0	5.21	2.21	240	0	5.21	0.54	240	0.34
5.92	1.72	272	0	5.92	2.09	272	0	5.92	0.64	272	0.22
6.72	1.67	310	0	6.72	1.97	310	0	6.72	0.78	310	0.13
7.64	1.63	352	0	7.64	1.85	352	0	7.64	0.97	352	0.03
8.68	1.61			8.68	1.71			8.68	1.21		

CF220

Feed				Overflow				Underflow			
<i>dx</i> (10)	0.638	<i>d</i> [3,2]	1.73	<i>dx</i> (10)	0.569	<i>d</i> [3,2]	1.32	<i>dx</i> (10)	11.8	<i>d</i> [3,2]	10.6
<i>dx</i> (50)	3.47	<i>d</i> [4,3]	17.8	<i>dx</i> (50)	1.8	<i>d</i> [4,3]	4.81	<i>dx</i> (50)	41.9	<i>d</i> [4,3]	53.6
<i>dx</i> (90)	54.8			<i>dx</i> (90)	12.9			<i>dx</i> (90)	100		
% Size (µm)	Volume In										
0.243	0.18	11.2	1.48	0.243	0.24	11.2	1.77	0.243	0	11.2	0.82
0.276	0.43	12.7	1.5	0.276	0.58	12.7	1.65	0.276	0.04	12.7	1.14
0.314	0.75	14.5	1.55	0.314	1.01	14.5	1.53	0.314	0.1	14.5	1.61
0.357	1.13	16.4	1.64	0.357	1.49	16.4	1.38	0.357	0.15	16.4	2.24
0.405	1.54	18.7	1.75	0.405	2.03	18.7	1.22	0.405	0.21	18.7	3.03
0.46	1.98	21.2	1.9	0.46	2.58	21.2	1.05	0.46	0.26	21.2	3.96
0.523	2.41	24.1	2.06	0.523	3.13	24.1	0.87	0.523	0.31	24.1	4.95
0.594	2.82	27.4	2.22	0.594	3.65	27.4	0.69	0.594	0.36	27.4	5.91
0.675	3.17	31.1	2.35	0.675	4.1	31.1	0.52	0.675	0.39	31.1	6.75
0.767	3.45	35.3	2.43	0.767	4.46	35.3	0.38	0.767	0.42	35.3	7.34
0.872	3.64	40.1	2.44	0.872	4.72	40.1	0.27	0.872	0.44	40.1	7.62
0.991	3.73	45.6	2.37	0.991	4.87	45.6	0.2	0.991	0.44	45.6	7.55
1.13	3.71	51.8	2.21	1.13	4.88	51.8	0.15	1.13	0.43	51.8	7.13
1.28	3.58	58.9	1.98	1.28	4.77	58.9	0.11	1.28	0.41	58.9	6.41
1.45	3.36	66.9	1.69	1.45	4.55	66.9	0.08	1.45	0.39	66.9	5.49
1.65	3.07	76	1.37	1.65	4.23	76	0.02	1.65	0.35	76	4.48
1.88	2.75	86.4	1.07	1.88	3.87	86.4	0	1.88	0.32	86.4	3.49
2.13	2.45	98.1	0.81	2.13	3.51	98.1	0	2.13	0.29	98.1	2.6
2.42	2.2	111	0.59	2.42	3.21	111	0	2.42	0.27	111	1.88
2.75	2.03	127	0.43	2.75	2.98	127	0	2.75	0.26	127	1.34
3.12	1.92	144	0.31	3.12	2.81	144	0	3.12	0.27	144	0.98
3.55	1.86	163	0.22	3.55	2.69	163	0	3.55	0.28	163	0.76
4.03	1.81	186	0.15	4.03	2.57	186	0	4.03	0.3	186	0.63
4.58	1.76	211	0.09	4.58	2.46	211	0	4.58	0.32	211	0.56
5.21	1.71	240	0.04	5.21	2.35	240	0	5.21	0.35	240	0.5
5.92	1.66	272	0	5.92	2.25	272	0	5.92	0.37	272	0.44
6.72	1.61	310	0	6.72	2.16	310	0	6.72	0.4	310	0.34
7.64	1.56	352	0	7.64	2.06	352	0	7.64	0.43	352	0.23
8.68	1.52	400	0	8.68	1.97	400	0	8.68	0.5	400	0.1
9.86	1.49	454	0	9.86	1.87	454	0	9.86	0.62	454	0.03

CF221

Feed				Overflow				Underflow			
<i>dx</i> (10)	0.614	<i>d</i> [3,2]	1.64	<i>dx</i> (10)	0.57	<i>d</i> [3,2]	1.27	<i>dx</i> (10)	14.9	<i>d</i> [3,2]	11.8
<i>dx</i> (50)	3.06	<i>d</i> [4,3]	17.7	<i>dx</i> (50)	1.63	<i>d</i> [4,3]	4.37	<i>dx</i> (50)	46.4	<i>d</i> [4,3]	60.3
<i>dx</i> (90)	53			<i>dx</i> (90)	11.9			<i>dx</i> (90)	117		
% Size (µm) In	% Volume In										
0.243	0.24	11.2	1.47	0.243	0.21	11.2	1.67	0.243	0	11.2	0.59
0.276	0.52	12.7	1.49	0.276	0.54	12.7	1.56	0.276	0.04	12.7	0.83
0.314	0.87	14.5	1.54	0.314	0.96	14.5	1.44	0.314	0.1	14.5	1.19
0.357	1.25	16.4	1.63	0.357	1.46	16.4	1.3	0.357	0.15	16.4	1.73
0.405	1.67	18.7	1.74	0.405	2.02	18.7	1.15	0.405	0.2	18.7	2.45
0.46	2.11	21.2	1.87	0.46	2.64	21.2	0.98	0.46	0.24	21.2	3.33
0.523	2.56	24.1	2.01	0.523	3.27	24.1	0.79	0.523	0.28	24.1	4.32
0.594	2.97	27.4	2.14	0.594	3.88	27.4	0.61	0.594	0.32	27.4	5.34
0.675	3.34	31.1	2.23	0.675	4.44	31.1	0.45	0.675	0.34	31.1	6.29
0.767	3.63	35.3	2.27	0.767	4.9	35.3	0.32	0.767	0.36	35.3	7.05
0.872	3.82	40.1	2.25	0.872	5.24	40.1	0.22	0.872	0.36	40.1	7.53
0.991	3.9	45.6	2.15	0.991	5.41	45.6	0.15	0.991	0.36	45.6	7.65
1.13	3.86	51.8	1.99	1.13	5.42	51.8	0.1	1.13	0.35	51.8	7.42
1.28	3.71	58.9	1.76	1.28	5.25	58.9	0.06	1.28	0.33	58.9	6.84
1.45	3.45	66.9	1.5	1.45	4.92	66.9	0	1.45	0.31	66.9	6.02
1.65	3.12	76	1.22	1.65	4.46	76	0	1.65	0.29	76	5.05
1.88	2.76	86.4	0.96	1.88	3.94	86.4	0	1.88	0.26	86.4	4.06
2.13	2.43	98.1	0.74	2.13	3.43	98.1	0	2.13	0.24	98.1	3.14
2.42	2.16	111	0.56	2.42	3.01	111	0	2.42	0.23	111	2.38
2.75	1.98	127	0.42	2.75	2.7	127	0	2.75	0.23	127	1.81
3.12	1.87	144	0.32	3.12	2.5	144	0	3.12	0.23	144	1.42
3.55	1.81	163	0.25	3.55	2.37	163	0	3.55	0.25	163	1.18
4.03	1.76	186	0.19	4.03	2.28	186	0	4.03	0.27	186	1.03
4.58	1.72	211	0.15	4.58	2.2	211	0	4.58	0.3	211	0.92
5.21	1.67	240	0.12	5.21	2.14	240	0	5.21	0.32	240	0.79
5.92	1.62	272	0.08	5.92	2.07	272	0	5.92	0.34	272	0.63
6.72	1.58	310	0.06	6.72	2	310	0	6.72	0.35	310	0.43
7.64	1.53	352	0.05	7.64	1.93	352	0	7.64	0.37	352	0.22
8.68	1.49	400	0	8.68	1.85	400	0	8.68	0.4	400	0.05
9.86	1.47			9.86	1.76			9.86	0.47		

CF222

Feed				Overflow				Underflow			
<i>dx</i> (10)	0.619	<i>d</i> [3,2]	1.66	<i>dx</i> (10)	0.547	<i>d</i> [3,2]	1.18	<i>dx</i> (10)	3.7	<i>d</i> [3,2]	7.18
<i>dx</i> (50)	3.21	<i>d</i> [4,3]	16.5	<i>dx</i> (50)	1.48	<i>d</i> [4,3]	3.04	<i>dx</i> (50)	37.6	<i>d</i> [4,3]	47.8
<i>dx</i> (90)	51.6			<i>dx</i> (90)	7.61			<i>dx</i> (90)	95.5		
Size (µm)	% Volume In										
0.243	0.23	9.86	1.45	0.243	0.25	9.86	1.43	0.243	0	9.86	0.89
0.276	0.51	11.2	1.45	0.276	0.62	11.2	1.22	0.276	0.09	11.2	1.18
0.314	0.85	12.7	1.48	0.314	1.09	12.7	1.02	0.314	0.17	12.7	1.58
0.357	1.23	14.5	1.55	0.357	1.63	14.5	0.83	0.357	0.25	14.5	2.09
0.405	1.64	16.4	1.65	0.405	2.25	16.4	0.65	0.405	0.34	16.4	2.71
0.46	2.08	18.7	1.79	0.46	2.91	18.7	0.49	0.46	0.43	18.7	3.43
0.523	2.52	21.2	1.95	0.523	3.58	21.2	0.35	0.523	0.52	21.2	4.21
0.594	2.94	24.1	2.12	0.594	4.23	24.1	0.24	0.594	0.59	24.1	4.99
0.675	3.3	27.4	2.28	0.675	4.81	27.4	0.15	0.675	0.66	27.4	5.72
0.767	3.59	31.1	2.4	0.767	5.29	31.1	0.09	0.767	0.7	31.1	6.31
0.872	3.78	35.3	2.46	0.872	5.62	35.3	0.02	0.872	0.72	35.3	6.7
0.991	3.86	40.1	2.44	0.991	5.79	40.1	0	0.991	0.72	40.1	6.83
1.13	3.81	45.6	2.33	1.13	5.76	45.6	0	1.13	0.7	45.6	6.68
1.28	3.65	51.8	2.15	1.28	5.55	51.8	0	1.28	0.66	51.8	6.26
1.45	3.39	58.9	1.89	1.45	5.17	58.9	0	1.45	0.61	58.9	5.62
1.65	3.06	66.9	1.59	1.65	4.68	66.9	0	1.65	0.56	66.9	4.82
1.88	2.71	76	1.28	1.88	4.13	76	0	1.88	0.5	76	3.96
2.13	2.38	86.4	0.98	2.13	3.62	86.4	0	2.13	0.45	86.4	3.12
2.42	2.12	98.1	0.72	2.42	3.2	98.1	0	2.42	0.42	98.1	2.37
2.75	1.96	111	0.51	2.75	2.92	111	0	2.75	0.4	111	1.77
3.12	1.87	127	0.35	3.12	2.75	127	0	3.12	0.39	127	1.31
3.55	1.82	144	0.23	3.55	2.64	144	0	3.55	0.39	144	1
4.03	1.79	163	0.14	4.03	2.55	163	0	4.03	0.39	163	0.79
4.58	1.74	186	0.06	4.58	2.45	186	0	4.58	0.39	186	0.65
5.21	1.69	211	0.03	5.21	2.33	211	0	5.21	0.4	211	0.53
5.92	1.63	240	0	5.92	2.19	240	0	5.92	0.42	240	0.42
6.72	1.57	272	0	6.72	2.02	272	0	6.72	0.46	272	0.29
7.64	1.51	310	0	7.64	1.83	310	0	7.64	0.55	310	0.15
8.68	1.47	352	0	8.68	1.63	352	0	8.68	0.68	352	0.05

CF223

Feed				Overflow				Underflow			
<i>dx</i> (10)	9.62	<i>d</i> [3,2]	9.42	<i>dx</i> (10)	0.57	<i>d</i> [3,2]	1.37	<i>dx</i> (10)	20.5	<i>d</i> [3,2]	38.6
<i>dx</i> (50)	39	<i>d</i> [4,3]	47.2	<i>dx</i> (50)	1.94	<i>d</i> [4,3]	5.91	<i>dx</i> (50)	47.1	<i>d</i> [4,3]	67.5
<i>dx</i> (90)	93.4			<i>dx</i> (90)	15.7			<i>dx</i> (90)	124		
Size (µm)	% Volume In										
0.243	0	14.5	2.16	0.243	0.2	14.5	2.21	0.243	0	14.5	1.76
0.276	0.04	16.4	2.8	0.276	0.53	16.4	1.92	0.276	0	16.4	2.43
0.314	0.11	18.7	3.54	0.314	0.96	18.7	1.6	0.314	0	18.7	3.24
0.357	0.17	21.2	4.35	0.357	1.48	21.2	1.28	0.357	0	21.2	4.14
0.405	0.24	24.1	5.19	0.405	2.04	24.1	0.99	0.405	0	24.1	5.1
0.46	0.3	27.4	5.97	0.46	2.64	27.4	0.76	0.46	0	27.4	6.02
0.523	0.37	31.1	6.61	0.523	3.22	31.1	0.6	0.523	0	31.1	6.83
0.594	0.42	35.3	7.05	0.594	3.75	35.3	0.5	0.594	0	35.3	7.43
0.675	0.47	40.1	7.21	0.675	4.18	40.1	0.44	0.675	0	40.1	7.75
0.767	0.5	45.6	7.08	0.767	4.49	45.6	0.39	0.767	0	45.6	7.74
0.872	0.52	51.8	6.65	0.872	4.66	51.8	0.33	0.872	0	51.8	7.41
0.991	0.51	58.9	5.98	0.991	4.68	58.9	0.25	0.991	0	58.9	6.78
1.13	0.5	66.9	5.15	1.13	4.56	66.9	0.15	1.13	0	66.9	5.94
1.28	0.47	76	4.25	1.28	4.3	76	0.03	1.28	0	76	4.98
1.45	0.43	86.4	3.38	1.45	3.94	86.4	0	1.45	0	86.4	4.01
1.65	0.39	98.1	2.6	1.65	3.52	98.1	0	1.65	0	98.1	3.12
1.88	0.35	111	1.95	1.88	3.09	111	0	1.88	0	111	2.36
2.13	0.31	127	1.44	2.13	2.71	127	0	2.13	0	127	1.77
2.42	0.28	144	1.05	2.42	2.44	144	0	2.42	0	144	1.34
2.75	0.27	163	0.74	2.75	2.27	163	0	2.75	0	163	1.07
3.12	0.27	186	0.49	3.12	2.21	186	0	3.12	0	186	0.89
3.55	0.27	211	0.27	3.55	2.2	211	0	3.55	0	211	0.79
4.03	0.28	240	0.12	4.03	2.22	240	0	4.03	0	240	0.73
4.58	0.3	272	0.03	4.58	2.26	272	0	4.58	0	272	0.68
5.21	0.32	310	0	5.21	2.31	310	0	5.21	0.07	310	0.62
5.92	0.36	352	0	5.92	2.39	352	0	5.92	0.09	352	0.53
6.72	0.43	400	0	6.72	2.47	400	0	6.72	0.14	400	0.43
7.64	0.54	454	0	7.64	2.56	454	0	7.64	0.21	454	0.32
8.68	0.7	516	0	8.68	2.62	516	0	8.68	0.34	516	0.21
9.86	0.93	586	0	9.86	2.64	586	0	9.86	0.53	586	0.1
11.2	1.23	666	0	11.2	2.58	666	0	11.2	0.82	666	0.04
12.7	1.64			12.7	2.44			12.7	1.22		

Appendix B: Laser Sizing Data

CF232

Feed				Overflow				Underflow			
<i>dx</i> (10)	2.3	<i>d</i> [3,2]	6.3	<i>dx</i> (10)	0.874	<i>d</i> [3,2]	2.31	<i>dx</i> (10)	25.6	<i>d</i> [3,2]	40.4
<i>dx</i> (50)	38.9	<i>d</i> [4,3]	45.9	<i>dx</i> (50)	4.36	<i>d</i> [4,3]	11.1	<i>dx</i> (50)	62	<i>d</i> [4,3]	68.9
<i>dx</i> (90)	103			<i>dx</i> (90)	22.2			<i>dx</i> (90)	123		
% Size (µm)		% Volume In		% Size (µm)		% Volume In		% Size (µm)		% Volume In	
0.276	0	9.86	1.34	0.276	0.15	9.86	3.08	0.276	0	9.86	0.38
0.314	0.11	11.2	1.38	0.314	0.35	11.2	2.86	0.314	0	11.2	0.49
0.357	0.2	12.7	1.44	0.357	0.61	12.7	2.63	0.357	0	12.7	0.64
0.405	0.3	14.5	1.55	0.405	0.89	14.5	2.4	0.405	0	14.5	0.84
0.46	0.39	16.4	1.72	0.46	1.18	16.4	2.15	0.46	0	16.4	1.13
0.523	0.48	18.7	1.95	0.523	1.43	18.7	1.9	0.523	0	18.7	1.51
0.594	0.55	21.2	2.27	0.594	1.64	21.2	1.65	0.594	0	21.2	2.01
0.675	0.6	24.1	2.67	0.675	1.8	24.1	1.4	0.675	0	24.1	2.66
0.767	0.65	27.4	3.16	0.767	1.94	27.4	1.15	0.767	0	27.4	3.46
0.872	0.69	31.1	3.71	0.872	2.06	31.1	0.93	0.872	0.06	31.1	4.38
0.991	0.73	35.3	4.29	0.991	2.2	35.3	0.75	0.991	0.07	35.3	5.39
1.13	0.78	40.1	4.85	1.13	2.35	40.1	0.6	1.13	0.07	40.1	6.41
1.28	0.85	45.6	5.34	1.28	2.54	45.6	0.5	1.28	0.06	45.6	7.35
1.45	0.92	51.8	5.67	1.45	2.75	51.8	0.43	1.45	0	51.8	8.1
1.65	0.99	58.9	5.81	1.65	2.98	58.9	0.38	1.65	0	58.9	8.56
1.88	1.08	66.9	5.69	1.88	3.22	66.9	0.35	1.88	0	66.9	8.64
2.13	1.16	76	5.33	2.13	3.47	76	0.33	2.13	0	76	8.31
2.42	1.25	86.4	4.73	2.42	3.71	86.4	0.32	2.42	0.06	86.4	7.58
2.75	1.32	98.1	3.96	2.75	3.92	98.1	0.3	2.75	0.07	98.1	6.51
3.12	1.38	111	3.08	3.12	4.09	111	0.29	3.12	0.08	111	5.22
3.55	1.43	127	2.19	3.55	4.19	127	0.27	3.55	0.09	127	3.84
4.03	1.45	144	1.38	4.03	4.22	144	0.24	4.03	0.1	144	2.54
4.58	1.44	163	0.72	4.58	4.18	163	0.21	4.58	0.11	163	1.45
5.21	1.43	186	0.14	5.21	4.07	186	0.17	5.21	0.12	186	0.65
5.92	1.4	211	0	5.92	3.92	211	0.13	5.92	0.15	211	0.18
6.72	1.37	240	0	6.72	3.73	240	0.1	6.72	0.18	240	0
7.64	1.35	272	0	7.64	3.52	272	0.09	7.64	0.23	272	0
8.68	1.34			8.68	3.3			8.68	0.29		

CF233

Feed				Overflow				Underflow			
<i>dx</i> (10)	2.5	<i>d</i> [3,2]	6.71	<i>dx</i> (10)	0.841	<i>d</i> [3,2]	2.25	<i>dx</i> (10)	23.4	<i>d</i> [3,2]	38.7
<i>dx</i> (50)	41.4	<i>d</i> [4,3]	47.7	<i>dx</i> (50)	4.32	<i>d</i> [4,3]	11.2	<i>dx</i> (50)	58.9	<i>d</i> [4,3]	65.7
<i>dx</i> (90)	105			<i>dx</i> (90)	23			<i>dx</i> (90)	118		
Size (µm)	% Volume In										
0.276	0	9.86	1.3	0.276	0.2	9.86	3.04	0.276	0	9.86	0.48
0.314	0.11	11.2	1.33	0.314	0.43	11.2	2.81	0.314	0	11.2	0.62
0.357	0.2	12.7	1.39	0.357	0.71	12.7	2.57	0.357	0	12.7	0.8
0.405	0.29	14.5	1.48	0.405	1	14.5	2.33	0.405	0	14.5	1.04
0.46	0.37	16.4	1.64	0.46	1.28	16.4	2.09	0.46	0	16.4	1.36
0.523	0.44	18.7	1.87	0.523	1.51	18.7	1.85	0.523	0	18.7	1.79
0.594	0.5	21.2	2.18	0.594	1.68	21.2	1.61	0.594	0	21.2	2.33
0.675	0.55	24.1	2.6	0.675	1.81	24.1	1.37	0.675	0	24.1	3.01
0.767	0.59	27.4	3.1	0.767	1.92	27.4	1.15	0.767	0.04	27.4	3.82
0.872	0.62	31.1	3.69	0.872	2.02	31.1	0.96	0.872	0.04	31.1	4.73
0.991	0.66	35.3	4.32	0.991	2.13	35.3	0.79	0.991	0.02	35.3	5.7
1.13	0.71	40.1	4.95	1.13	2.29	40.1	0.66	1.13	0.02	40.1	6.64
1.28	0.78	45.6	5.5	1.28	2.48	45.6	0.57	1.28	0	45.6	7.47
1.45	0.85	51.8	5.89	1.45	2.71	51.8	0.51	1.45	0	51.8	8.09
1.65	0.93	58.9	6.07	1.65	2.96	58.9	0.47	1.65	0	58.9	8.4
1.88	1.01	66.9	5.98	1.88	3.23	66.9	0.43	1.88	0.04	66.9	8.35
2.13	1.09	76	5.62	2.13	3.49	76	0.4	2.13	0.07	76	7.91
2.42	1.17	86.4	5	2.42	3.73	86.4	0.37	2.42	0.07	86.4	7.11
2.75	1.23	98.1	4.18	2.75	3.93	98.1	0.33	2.75	0.08	98.1	6.01
3.12	1.29	111	3.25	3.12	4.08	111	0.3	3.12	0.09	111	4.74
3.55	1.32	127	2.31	3.55	4.16	127	0.26	3.55	0.1	127	3.42
4.03	1.34	144	1.45	4.03	4.17	144	0.22	4.03	0.11	144	2.21
4.58	1.34	163	0.77	4.58	4.11	163	0.18	4.58	0.13	163	1.22
5.21	1.33	186	0.15	5.21	4	186	0.15	5.21	0.15	186	0.52
5.92	1.32	211	0.03	5.92	3.85	211	0.12	5.92	0.19	211	0.13
6.72	1.31	240	0	6.72	3.67	240	0.1	6.72	0.24	240	0
7.64	1.3	272	0	7.64	3.48	272	0.07	7.64	0.3	272	0
8.68	1.29			8.68	3.26			8.68	0.38		

CF235

Feed				Overflow				Underflow			
<i>dx</i> (10)	3.28	<i>d</i> [3,2]	8.18	<i>dx</i> (10)	0.898	<i>d</i> [3,2]	2.41	<i>dx</i> (10)	29	<i>d</i> [3,2]	50.4
<i>dx</i> (50)	52.4	<i>d</i> [4,3]	57.5	<i>dx</i> (50)	4.8	<i>d</i> [4,3]	10.3	<i>dx</i> (50)	68.2	<i>d</i> [4,3]	75.6
<i>dx</i> (90)	119			<i>dx</i> (90)	23.9			<i>dx</i> (90)	133		
% Size (µm)	% Volume In										
0.276	0	8.68	1.02	0.276	0.17	8.68	3.4	0.276	0	8.68	0.23
0.314	0.1	9.86	1.03	0.314	0.38	9.86	3.26	0.314	0	9.86	0.3
0.357	0.17	11.2	1.06	0.357	0.63	11.2	3.11	0.357	0	11.2	0.39
0.405	0.24	12.7	1.11	0.405	0.9	12.7	2.96	0.405	0	12.7	0.51
0.46	0.31	14.5	1.18	0.46	1.15	14.5	2.8	0.46	0	14.5	0.67
0.523	0.37	16.4	1.3	0.523	1.36	16.4	2.62	0.523	0	16.4	0.9
0.594	0.41	18.7	1.48	0.594	1.53	18.7	2.41	0.594	0	18.7	1.22
0.675	0.45	21.2	1.74	0.675	1.66	21.2	2.17	0.675	0	21.2	1.64
0.767	0.47	24.1	2.1	0.767	1.77	24.1	1.9	0.767	0	24.1	2.2
0.872	0.5	27.4	2.58	0.872	1.87	27.4	1.6	0.872	0	27.4	2.9
0.991	0.52	31.1	3.17	0.991	2	31.1	1.31	0.991	0	31.1	3.75
1.13	0.56	35.3	3.87	1.13	2.15	35.3	1.03	1.13	0	35.3	4.72
1.28	0.61	40.1	4.63	1.28	2.34	40.1	0.79	1.28	0	40.1	5.75
1.45	0.66	45.6	5.39	1.45	2.56	45.6	0.61	1.45	0.04	45.6	6.78
1.65	0.72	51.8	6.07	1.65	2.8	51.8	0.48	1.65	0.04	51.8	7.69
1.88	0.79	58.9	6.57	1.88	3.04	58.9	0.39	1.88	0.04	58.9	8.39
2.13	0.85	66.9	6.81	2.13	3.28	66.9	0.34	2.13	0	66.9	8.77
2.42	0.91	76	6.73	2.42	3.51	76	0.31	2.42	0	76	8.74
2.75	0.96	86.4	6.3	2.75	3.7	86.4	0.29	2.75	0	86.4	8.28
3.12	1	98.1	5.55	3.12	3.84	98.1	0.26	3.12	0	98.1	7.41
3.55	1.03	111	4.57	3.55	3.93	111	0.22	3.55	0	111	6.22
4.03	1.04	127	3.45	4.03	3.97	127	0.18	4.03	0	127	4.83
4.58	1.04	144	2.35	4.58	3.94	144	0.12	4.58	0	144	3.41
5.21	1.03	163	1.38	5.21	3.88	163	0.04	5.21	0.07	163	2.13
5.92	1.03	186	0.65	5.92	3.79	186	0.02	5.92	0.1	186	1.12
6.72	1.02	211	0.08	6.72	3.67	211	0	6.72	0.13	211	0.44
7.64	1.02			7.64	3.54			7.64	0.17		

CF236

Feed				Overflow				Underflow			
<i>dx</i> (10)	2.61	<i>d</i> [3,2]	6.9	<i>dx</i> (10)	0.881	<i>d</i> [3,2]	2.4	<i>dx</i> (10)	27.8	<i>d</i> [3,2]	49.3
<i>dx</i> (50)	46.8	<i>d</i> [4,3]	53	<i>dx</i> (50)	4.9	<i>d</i> [4,3]	11.3	<i>dx</i> (50)	63.4	<i>d</i> [4,3]	70.8
<i>dx</i> (90)	115			<i>dx</i> (90)	26.1			<i>dx</i> (90)	125		
% Size (µm)	% Volume In										
0.276	0.04	8.68	1.19	0.276	0.19	8.68	3.34	0.276	0	8.68	0.21
0.314	0.13	9.86	1.2	0.314	0.4	9.86	3.19	0.314	0	9.86	0.28
0.357	0.21	11.2	1.23	0.357	0.66	11.2	3.03	0.357	0	11.2	0.37
0.405	0.3	12.7	1.28	0.405	0.94	12.7	2.88	0.405	0	12.7	0.5
0.46	0.38	14.5	1.36	0.46	1.19	14.5	2.72	0.46	0	14.5	0.7
0.523	0.45	16.4	1.48	0.523	1.4	16.4	2.56	0.523	0	16.4	0.99
0.594	0.5	18.7	1.65	0.594	1.57	18.7	2.37	0.594	0	18.7	1.39
0.675	0.54	21.2	1.9	0.675	1.69	21.2	2.17	0.675	0	21.2	1.94
0.767	0.57	24.1	2.24	0.767	1.79	24.1	1.94	0.767	0	24.1	2.63
0.872	0.6	27.4	2.67	0.872	1.88	27.4	1.69	0.872	0	27.4	3.47
0.991	0.63	31.1	3.21	0.991	1.99	31.1	1.43	0.991	0	31.1	4.43
1.13	0.67	35.3	3.83	1.13	2.13	35.3	1.17	1.13	0	35.3	5.47
1.28	0.73	40.1	4.49	1.28	2.3	40.1	0.94	1.28	0	40.1	6.5
1.45	0.79	45.6	5.15	1.45	2.5	45.6	0.75	1.45	0	45.6	7.44
1.65	0.86	51.8	5.71	1.65	2.73	51.8	0.59	1.65	0	51.8	8.18
1.88	0.94	58.9	6.11	1.88	2.96	58.9	0.47	1.88	0	58.9	8.63
2.13	1.02	66.9	6.27	2.13	3.19	66.9	0.39	2.13	0	66.9	8.72
2.42	1.09	76	6.13	2.42	3.41	76	0.33	2.42	0	76	8.41
2.75	1.15	86.4	5.7	2.75	3.6	86.4	0.29	2.75	0	86.4	7.7
3.12	1.19	98.1	4.99	3.12	3.74	98.1	0.26	3.12	0	98.1	6.67
3.55	1.22	111	4.08	3.55	3.84	111	0.24	3.55	0	111	5.4
4.03	1.23	127	3.07	4.03	3.88	127	0.21	4.03	0	127	4.04
4.58	1.23	144	2.07	4.58	3.87	144	0.18	4.58	0.06	144	2.74
5.21	1.22	163	1.2	5.21	3.81	163	0.15	5.21	0.08	163	1.61
5.92	1.21	186	0.55	5.92	3.73	186	0.12	5.92	0.1	186	0.77
6.72	1.19	211	0	6.72	3.62	211	0.07	6.72	0.13	211	0.25
7.64	1.19			7.64	3.49			7.64	0.17		

CF238

Feed				Overflow				Underflow			
<i>dx</i> (10)	2.51	<i>d</i> [3,2]	6.6	<i>dx</i> (10)	0.82	<i>d</i> [3,2]	2.25	<i>dx</i> (10)	25.8	<i>d</i> [3,2]	36.3
<i>dx</i> (50)	43.1	<i>d</i> [4,3]	48.4	<i>dx</i> (50)	4.58	<i>d</i> [4,3]	10.1	<i>dx</i> (50)	59.8	<i>d</i> [4,3]	66.1
<i>dx</i> (90)	104			<i>dx</i> (90)	22.7			<i>dx</i> (90)	116		
% Size (µm)	Volume In										
0.243	0	7.64	1.21	0.243	0.07	7.64	3.55	0.243	0	7.64	0.19
0.276	0.07	8.68	1.21	0.276	0.24	8.68	3.42	0.276	0	8.68	0.23
0.314	0.14	9.86	1.21	0.314	0.48	9.86	3.28	0.314	0	9.86	0.28
0.357	0.23	11.2	1.23	0.357	0.78	11.2	3.11	0.357	0	11.2	0.37
0.405	0.32	12.7	1.28	0.405	1.07	12.7	2.93	0.405	0	12.7	0.51
0.46	0.41	14.5	1.38	0.46	1.33	14.5	2.73	0.46	0	14.5	0.72
0.523	0.47	16.4	1.53	0.523	1.55	16.4	2.5	0.523	0	16.4	1.03
0.594	0.53	18.7	1.76	0.594	1.7	18.7	2.25	0.594	0	18.7	1.47
0.675	0.56	21.2	2.09	0.675	1.8	21.2	1.98	0.675	0.07	21.2	2.06
0.767	0.59	24.1	2.53	0.767	1.87	24.1	1.7	0.767	0.08	24.1	2.81
0.872	0.61	27.4	3.07	0.872	1.95	27.4	1.42	0.872	0.07	27.4	3.72
0.991	0.65	31.1	3.7	0.991	2.04	31.1	1.14	0.991	0.07	31.1	4.76
1.13	0.69	35.3	4.37	1.13	2.17	35.3	0.9	1.13	0.06	35.3	5.85
1.28	0.74	40.1	5.05	1.28	2.35	40.1	0.7	1.28	0	40.1	6.92
1.45	0.81	45.6	5.66	1.45	2.56	45.6	0.55	1.45	0	45.6	7.86
1.65	0.88	51.8	6.11	1.65	2.8	51.8	0.44	1.65	0.06	51.8	8.54
1.88	0.96	58.9	6.34	1.88	3.05	58.9	0.36	1.88	0.07	58.9	8.88
2.13	1.04	66.9	6.29	2.13	3.29	66.9	0.31	2.13	0.08	66.9	8.8
2.42	1.11	76	5.94	2.42	3.52	76	0.27	2.42	0.09	76	8.28
2.75	1.17	86.4	5.29	2.75	3.7	86.4	0.24	2.75	0.1	86.4	7.36
3.12	1.21	98.1	4.41	3.12	3.84	98.1	0.22	3.12	0.1	98.1	6.13
3.55	1.24	111	3.38	3.55	3.92	111	0.2	3.55	0.11	111	4.73
4.03	1.25	127	2.33	4.03	3.94	127	0.18	4.03	0.11	127	3.32
4.58	1.25	144	1.37	4.58	3.91	144	0.15	4.58	0.12	144	2.05
5.21	1.25	163	0.63	5.21	3.85	163	0.12	5.21	0.13	163	1.05
5.92	1.23	186	0	5.92	3.76	186	0.09	5.92	0.14	186	0.39
6.72	1.22	211	0	6.72	3.66	211	0.03	6.72	0.16	211	0.07

CF245

Feed				Overflow				Underflow			
<i>dx</i> (10)	1.2	<i>d</i> [3,2]	3.46	<i>dx</i> (10)	0.77	<i>d</i> [3,2]	2.08	<i>dx</i> (10)	9.04	<i>d</i> [3,2]	12.1
<i>dx</i> (50)	12.5	<i>d</i> [4,3]	21.5	<i>dx</i> (50)	3.96	<i>d</i> [4,3]	7.88	<i>dx</i> (50)	31.5	<i>d</i> [4,3]	40.5
<i>dx</i> (90)	53.4			<i>dx</i> (90)	18.2			<i>dx</i> (90)	84.3		
% Size (µm)	% Volume In										
0.276	0.11	7.64	2.3	0.276	0.22	7.64	3.54	0.276	0	7.64	0.99
0.314	0.26	8.68	2.39	0.314	0.49	8.68	3.41	0.314	0	8.68	1.29
0.357	0.44	9.86	2.53	0.357	0.84	9.86	3.25	0.357	0.09	9.86	1.7
0.405	0.64	11.2	2.72	0.405	1.19	11.2	3.06	0.405	0.13	11.2	2.22
0.46	0.82	12.7	2.95	0.46	1.51	12.7	2.83	0.46	0.17	12.7	2.86
0.523	0.97	14.5	3.22	0.523	1.75	14.5	2.57	0.523	0.2	14.5	3.58
0.594	1.07	16.4	3.49	0.594	1.92	16.4	2.29	0.594	0.22	16.4	4.35
0.675	1.15	18.7	3.74	0.675	2.03	18.7	1.99	0.675	0.24	18.7	5.09
0.767	1.21	21.2	3.92	0.767	2.11	21.2	1.68	0.767	0.25	21.2	5.76
0.872	1.27	24.1	4.02	0.872	2.19	24.1	1.38	0.872	0.25	24.1	6.27
0.991	1.34	27.4	4	0.991	2.3	27.4	1.09	0.991	0.26	27.4	6.58
1.13	1.44	31.1	3.86	1.13	2.46	31.1	0.82	1.13	0.27	31.1	6.66
1.28	1.57	35.3	3.62	1.28	2.67	35.3	0.6	1.28	0.29	35.3	6.51
1.45	1.71	40.1	3.28	1.45	2.91	40.1	0.43	1.45	0.31	40.1	6.16
1.65	1.86	45.6	2.88	1.65	3.17	45.6	0.31	1.65	0.33	45.6	5.65
1.88	2	51.8	2.46	1.88	3.42	51.8	0.23	1.88	0.35	51.8	5.04
2.13	2.13	58.9	2.04	2.13	3.64	58.9	0.18	2.13	0.38	58.9	4.39
2.42	2.23	66.9	1.64	2.42	3.82	66.9	0.15	2.42	0.41	66.9	3.76
2.75	2.3	76	1.29	2.75	3.93	76	0.13	2.75	0.43	76	3.16
3.12	2.33	86.4	0.99	3.12	3.98	86.4	0.12	3.12	0.46	86.4	2.61
3.55	2.33	98.1	0.74	3.55	3.98	98.1	0.11	3.55	0.48	98.1	2.11
4.03	2.3	111	0.53	4.03	3.94	111	0.1	4.03	0.5	111	1.66
4.58	2.27	127	0.38	4.58	3.88	127	0.09	4.58	0.53	127	1.25
5.21	2.25	144	0.26	5.21	3.8	144	0.08	5.21	0.58	144	0.89
5.92	2.23	163	0.17	5.92	3.73	163	0.04	5.92	0.66	163	0.57
6.72	2.25	186	0.1	6.72	3.64	186	0	6.72	0.79	186	0.31

CF246

Feed				Overflow				Underflow			
<i>dx</i> (10)	1.22	<i>d</i> [3,2]	3.52	<i>dx</i> (10)	0.813	<i>d</i> [3,2]	2.19	<i>dx</i> (10)	11.8	<i>d</i> [3,2]	15.4
<i>dx</i> (50)	13	<i>d</i> [4,3]	22.5	<i>dx</i> (50)	4.23	<i>d</i> [4,3]	8.45	<i>dx</i> (50)	32.4	<i>d</i> [4,3]	40.4
<i>dx</i> (90)	56.5			<i>dx</i> (90)	20.1			<i>dx</i> (90)	79.8		
% Size (µm)	Volume In										
0.276	0.11	7.64	2.26	0.276	0.17	7.64	3.45	0.276	0	7.64	0.78
0.314	0.25	8.68	2.35	0.314	0.41	8.68	3.38	0.314	0	8.68	1.08
0.357	0.44	9.86	2.49	0.357	0.72	9.86	3.29	0.357	0	9.86	1.51
0.405	0.63	11.2	2.68	0.405	1.06	11.2	3.18	0.405	0.08	11.2	2.07
0.46	0.81	12.7	2.91	0.46	1.37	12.7	3.03	0.46	0.11	12.7	2.78
0.523	0.95	14.5	3.18	0.523	1.62	14.5	2.84	0.523	0.13	14.5	3.6
0.594	1.06	16.4	3.46	0.594	1.8	16.4	2.61	0.594	0.15	16.4	4.48
0.675	1.13	18.7	3.71	0.675	1.93	18.7	2.34	0.675	0.16	18.7	5.37
0.767	1.19	21.2	3.9	0.767	2.03	21.2	2.04	0.767	0.17	21.2	6.16
0.872	1.25	24.1	4	0.872	2.13	24.1	1.71	0.872	0.17	24.1	6.8
0.991	1.32	27.4	3.98	0.991	2.26	27.4	1.37	0.991	0.17	27.4	7.2
1.13	1.41	31.1	3.85	1.13	2.42	31.1	1.05	1.13	0.18	31.1	7.32
1.28	1.53	35.3	3.61	1.28	2.63	35.3	0.77	1.28	0.19	35.3	7.17
1.45	1.67	40.1	3.29	1.45	2.86	40.1	0.54	1.45	0.2	40.1	6.76
1.65	1.81	45.6	2.91	1.65	3.1	45.6	0.36	1.65	0.21	45.6	6.15
1.88	1.95	51.8	2.51	1.88	3.34	51.8	0.25	1.88	0.22	51.8	5.41
2.13	2.08	58.9	2.12	2.13	3.54	58.9	0.18	2.13	0.24	58.9	4.61
2.42	2.18	66.9	1.76	2.42	3.7	66.9	0.14	2.42	0.26	66.9	3.82
2.75	2.24	76	1.44	2.75	3.8	76	0.12	2.75	0.29	76	3.09
3.12	2.28	86.4	1.16	3.12	3.84	86.4	0.11	3.12	0.31	86.4	2.44
3.55	2.29	98.1	0.92	3.55	3.83	98.1	0.11	3.55	0.33	98.1	1.88
4.03	2.27	111	0.71	4.03	3.79	111	0.11	4.03	0.34	111	1.41
4.58	2.24	127	0.52	4.58	3.72	127	0.1	4.58	0.37	127	1.02
5.21	2.21	144	0.35	5.21	3.65	144	0.08	5.21	0.4	144	0.69
5.92	2.2	163	0.18	5.92	3.58	163	0.03	5.92	0.47	163	0.43
6.72	2.21	186	0.05	6.72	3.52	186	0	6.72	0.59	186	0.23

CF247

Feed				Overflow				Underflow			
<i>dx</i> (10)	1.19	<i>d</i> [3,2]	3.47	<i>dx</i> (10)	0.766	<i>d</i> [3,2]	2.04	<i>dx</i> (10)	6.23	<i>d</i> [3,2]	9.73
<i>dx</i> (50)	12.9	<i>d</i> [4,3]	22.2	<i>dx</i> (50)	3.8	<i>d</i> [4,3]	8.31	<i>dx</i> (50)	28.6	<i>d</i> [4,3]	36
<i>dx</i> (90)	55.3			<i>dx</i> (90)	18.9			<i>dx</i> (90)	74.5		
% Size (µm)	% Volume In										
0.243	0	7.64	2.29	0.243	0.02	7.64	3.38	0.243	0	7.64	1.21
0.276	0.12	8.68	2.37	0.276	0.23	8.68	3.21	0.276	0	8.68	1.52
0.314	0.27	9.86	2.5	0.314	0.51	9.86	3	0.314	0.07	9.86	1.94
0.357	0.46	11.2	2.68	0.357	0.84	11.2	2.77	0.357	0.12	11.2	2.47
0.405	0.66	12.7	2.9	0.405	1.19	12.7	2.53	0.405	0.18	12.7	3.1
0.46	0.84	14.5	3.15	0.46	1.5	14.5	2.27	0.46	0.23	14.5	3.82
0.523	0.98	16.4	3.42	0.523	1.75	16.4	2.02	0.523	0.27	16.4	4.56
0.594	1.09	18.7	3.68	0.594	1.93	18.7	1.76	0.594	0.3	18.7	5.28
0.675	1.16	21.2	3.88	0.675	2.05	21.2	1.52	0.675	0.31	21.2	5.9
0.767	1.21	24.1	4	0.767	2.15	24.1	1.29	0.767	0.33	24.1	6.35
0.872	1.27	27.4	4.01	0.872	2.25	27.4	1.07	0.872	0.34	27.4	6.59
0.991	1.33	31.1	3.9	0.991	2.38	31.1	0.87	0.991	0.35	31.1	6.59
1.13	1.42	35.3	3.67	1.13	2.56	35.3	0.7	1.13	0.36	35.3	6.36
1.28	1.54	40.1	3.36	1.28	2.79	40.1	0.55	1.28	0.39	40.1	5.93
1.45	1.67	45.6	2.97	1.45	3.04	45.6	0.44	1.45	0.41	45.6	5.35
1.65	1.81	51.8	2.56	1.65	3.31	51.8	0.36	1.65	0.44	51.8	4.69
1.88	1.94	58.9	2.14	1.88	3.55	58.9	0.3	1.88	0.48	58.9	4
2.13	2.06	66.9	1.74	2.13	3.76	66.9	0.26	2.13	0.51	66.9	3.34
2.42	2.15	76	1.39	2.42	3.92	76	0.23	2.42	0.55	76	2.72
2.75	2.22	86.4	1.08	2.75	4.02	86.4	0.2	2.75	0.59	86.4	2.17
3.12	2.26	98.1	0.82	3.12	4.06	98.1	0.18	3.12	0.62	98.1	1.68
3.55	2.27	111	0.61	3.55	4.04	111	0.15	3.55	0.65	111	1.25
4.03	2.26	127	0.43	4.03	3.97	127	0.12	4.03	0.68	127	0.87
4.58	2.24	144	0.29	4.58	3.88	144	0.09	4.58	0.72	144	0.54
5.21	2.23	163	0.18	5.21	3.78	163	0.05	5.21	0.77	163	0.26
5.92	2.23	186	0.08	5.92	3.66	186	0.08	5.92	0.86	186	0.02
6.72	2.24			6.72	3.53			6.72	1		

CF249

Feed				Overflow				Underflow			
<i>dx</i> (10)	1.57	<i>d</i> [3,2]	4.98	<i>dx</i> (10)	0.526	<i>d</i> [3,2]	1.29	<i>dx</i> (10)	15.3	<i>d</i> [3,2]	13.1
<i>dx</i> (50)	46.1	<i>d</i> [4,3]	56.3	<i>dx</i> (50)	2.04	<i>d</i> [4,3]	6.27	<i>dx</i> (50)	62.9	<i>d</i> [4,3]	76.1
<i>dx</i> (90)	124			<i>dx</i> (90)	14.1			<i>dx</i> (90)	153		
% Size (µm)	Volume In										
0.243	0.07	9.86	0.87	0.243	0.24	9.86	1.76	0.243	0	9.86	0.56
0.276	0.18	11.2	0.92	0.276	0.65	11.2	1.57	0.276	0.04	11.2	0.65
0.314	0.32	12.7	1.01	0.314	1.23	12.7	1.4	0.314	0.11	12.7	0.76
0.357	0.48	14.5	1.15	0.357	1.91	14.5	1.25	0.357	0.16	14.5	0.92
0.405	0.64	16.4	1.37	0.405	2.6	16.4	1.13	0.405	0.21	16.4	1.15
0.46	0.78	18.7	1.67	0.46	3.22	18.7	1.02	0.46	0.25	18.7	1.45
0.523	0.88	21.2	2.07	0.523	3.71	21.2	0.93	0.523	0.28	21.2	1.87
0.594	0.94	24.1	2.58	0.594	4.04	24.1	0.84	0.594	0.29	24.1	2.4
0.675	0.96	27.4	3.17	0.675	4.2	27.4	0.75	0.675	0.3	27.4	3.03
0.767	0.95	31.1	3.82	0.767	4.21	31.1	0.66	0.767	0.29	31.1	3.76
0.872	0.91	35.3	4.47	0.872	4.11	35.3	0.58	0.872	0.28	35.3	4.53
0.991	0.86	40.1	5.06	0.991	3.93	40.1	0.5	0.991	0.27	40.1	5.28
1.13	0.82	45.6	5.53	1.13	3.72	45.6	0.42	1.13	0.25	45.6	5.96
1.28	0.78	51.8	5.82	1.28	3.52	51.8	0.35	1.28	0.25	51.8	6.48
1.45	0.75	58.9	5.9	1.45	3.35	58.9	0.28	1.45	0.24	58.9	6.81
1.65	0.74	66.9	5.75	1.65	3.25	66.9	0.21	1.65	0.24	66.9	6.9
1.88	0.75	76	5.39	1.88	3.2	76	0.16	1.88	0.25	76	6.75
2.13	0.76	86.4	4.86	2.13	3.21	86.4	0.12	2.13	0.26	86.4	6.36
2.42	0.78	98.1	4.23	2.42	3.24	98.1	0.11	2.42	0.26	98.1	5.79
2.75	0.8	111	3.54	2.75	3.28	111	0.1	2.75	0.27	111	5.07
3.12	0.81	127	2.85	3.12	3.29	127	0.1	3.12	0.27	127	4.28
3.55	0.81	144	2.21	3.55	3.25	144	0.1	3.55	0.28	144	3.47
4.03	0.81	163	1.64	4.03	3.16	163	0.08	4.03	0.29	163	2.69
4.58	0.8	186	1.16	4.58	3.01	186	0.04	4.58	0.3	186	2
5.21	0.79	211	0.77	5.21	2.83	211	0	5.21	0.32	211	1.41
5.92	0.79	240	0.46	5.92	2.62	240	0	5.92	0.35	240	0.95
6.72	0.8	272	0.24	6.72	2.41	272	0	6.72	0.39	272	0.59
7.64	0.81	310	0.09	7.64	2.19	310	0	7.64	0.44	310	0.33
8.68	0.83	352	0	8.68	1.97	352	0	8.68	0.5	352	0.15

CF250

Feed				Overflow				Underflow			
<i>dx</i> (10)	1.35	<i>d</i> [3,2]	4.58	<i>dx</i> (10)	0.538	<i>d</i> [3,2]	1.35	<i>dx</i> (10)	15	<i>d</i> [3,2]	12.9
<i>dx</i> (50)	43.8	<i>d</i> [4,3]	53	<i>dx</i> (50)	2.19	<i>d</i> [4,3]	9.39	<i>dx</i> (50)	61	<i>d</i> [4,3]	71.7
<i>dx</i> (90)	119			<i>dx</i> (90)	22.4			<i>dx</i> (90)	141		
% Size (µm)	% Volume In										
0.243	0.08	9.86	0.93	0.243	0.19	9.86	1.67	0.243	0	9.86	0.59
0.276	0.2	11.2	1	0.276	0.56	11.2	1.5	0.276	0.07	11.2	0.68
0.314	0.35	12.7	1.11	0.314	1.11	12.7	1.36	0.314	0.12	12.7	0.8
0.357	0.52	14.5	1.26	0.357	1.77	14.5	1.23	0.357	0.17	14.5	0.96
0.405	0.69	16.4	1.49	0.405	2.46	16.4	1.13	0.405	0.22	16.4	1.19
0.46	0.84	18.7	1.79	0.46	3.1	18.7	1.03	0.46	0.25	18.7	1.51
0.523	0.95	21.2	2.16	0.523	3.62	21.2	0.94	0.523	0.27	21.2	1.94
0.594	1.02	24.1	2.62	0.594	3.99	24.1	0.85	0.594	0.28	24.1	2.49
0.675	1.05	27.4	3.14	0.675	4.19	27.4	0.77	0.675	0.28	27.4	3.16
0.767	1.04	31.1	3.7	0.767	4.22	31.1	0.7	0.767	0.27	31.1	3.91
0.872	1.01	35.3	4.26	0.872	4.11	35.3	0.66	0.872	0.26	35.3	4.71
0.991	0.96	40.1	4.79	0.991	3.9	40.1	0.65	0.991	0.24	40.1	5.5
1.13	0.91	45.6	5.22	1.13	3.64	45.6	0.67	1.13	0.24	45.6	6.2
1.28	0.86	51.8	5.53	1.28	3.38	51.8	0.7	1.28	0.23	51.8	6.74
1.45	0.83	58.9	5.66	1.45	3.16	58.9	0.74	1.45	0.23	58.9	7.07
1.65	0.81	66.9	5.6	1.65	3	66.9	0.76	1.65	0.24	66.9	7.14
1.88	0.81	76	5.35	1.88	2.92	76	0.74	1.88	0.25	76	6.94
2.13	0.82	86.4	4.91	2.13	2.92	86.4	0.67	2.13	0.25	86.4	6.48
2.42	0.84	98.1	4.33	2.42	2.97	98.1	0.57	2.42	0.26	98.1	5.82
2.75	0.86	111	3.64	2.75	3.03	111	0.44	2.75	0.27	111	5.01
3.12	0.88	127	2.91	3.12	3.08	127	0.3	3.12	0.28	127	4.12
3.55	0.89	144	2.19	3.55	3.07	144	0.17	3.55	0.29	144	3.22
4.03	0.89	163	1.52	4.03	3	163	0.06	4.03	0.3	163	2.38
4.58	0.88	186	0.95	4.58	2.87	186	0	4.58	0.31	186	1.65
5.21	0.86	211	0.5	5.21	2.7	211	0	5.21	0.33	211	1.06
5.92	0.85	240	0.12	5.92	2.5	240	0	5.92	0.36	240	0.62
6.72	0.85	272	0.02	6.72	2.29	272	0	6.72	0.41	272	0.32
7.64	0.86	310	0	7.64	2.07	310	0	7.64	0.46	310	0.13
8.68	0.88			8.68	1.87			8.68	0.52		

CF251

Feed				Overflow				Underflow			
<i>dx</i> (10)	2.09	<i>d</i> [3,2]	5.48	<i>dx</i> (10)	0.552	<i>d</i> [3,2]	1.48	<i>dx</i> (10)	24.5	<i>d</i> [3,2]	32.1
<i>dx</i> (50)	49.5	<i>d</i> [4,3]	59.8	<i>dx</i> (50)	2.86	<i>d</i> [4,3]	14.3	<i>dx</i> (50)	62.4	<i>d</i> [4,3]	76.1
<i>dx</i> (90)	129			<i>dx</i> (90)	49.6			<i>dx</i> (90)	143		
% Size (µm)	Volume In										
0.243	0.1	12.7	0.97	0.243	0.21	12.7	1.74	0.243	0	12.7	0.7
0.276	0.21	14.5	1.11	0.276	0.58	14.5	1.53	0.276	0	14.5	0.93
0.314	0.35	16.4	1.33	0.314	1.08	16.4	1.31	0.314	0	16.4	1.25
0.357	0.48	18.7	1.62	0.357	1.68	18.7	1.08	0.357	0	18.7	1.66
0.405	0.6	21.2	2.01	0.405	2.28	21.2	0.86	0.405	0	21.2	2.2
0.46	0.7	24.1	2.5	0.46	2.83	24.1	0.66	0.46	0.06	24.1	2.85
0.523	0.76	27.4	3.08	0.523	3.26	27.4	0.51	0.523	0.07	27.4	3.61
0.594	0.78	31.1	3.72	0.594	3.54	31.1	0.41	0.594	0.07	31.1	4.46
0.675	0.78	35.3	4.38	0.675	3.68	35.3	0.4	0.675	0.07	35.3	5.33
0.767	0.76	40.1	5	0.767	3.67	40.1	0.47	0.767	0.07	40.1	6.15
0.872	0.72	45.6	5.52	0.872	3.54	45.6	0.6	0.872	0.07	45.6	6.85
0.991	0.68	51.8	5.88	0.991	3.35	51.8	0.78	0.991	0.06	51.8	7.35
1.13	0.65	58.9	6.05	1.13	3.13	58.9	0.97	1.13	0.06	58.9	7.6
1.28	0.63	66.9	6	1.28	2.92	66.9	1.13	1.28	0.06	66.9	7.55
1.45	0.63	76	5.72	1.45	2.74	76	1.23	1.45	0.06	76	7.22
1.65	0.63	86.4	5.26	1.65	2.64	86.4	1.25	1.65	0.07	86.4	6.64
1.88	0.65	98.1	4.65	1.88	2.6	98.1	1.19	1.88	0.07	98.1	5.85
2.13	0.67	111	3.95	2.13	2.64	111	1.05	2.13	0.07	111	4.95
2.42	0.7	127	3.21	2.42	2.74	127	0.85	2.42	0.07	127	4
2.75	0.74	144	2.49	2.75	2.85	144	0.61	2.75	0.07	144	3.08
3.12	0.76	163	1.84	3.12	2.95	163	0.37	3.12	0.07	163	2.25
3.55	0.77	186	1.28	3.55	3.02	186	0.14	3.55	0.08	186	1.56
4.03	0.78	211	0.83	4.03	3.02	211	0.02	4.03	0.08	211	1.02
4.58	0.77	240	0.49	4.58	2.97	240	0	4.58	0.09	240	0.65
5.21	0.76	272	0.25	5.21	2.86	272	0	5.21	0.1	272	0.41
5.92	0.75	310	0.09	5.92	2.73	310	0	5.92	0.13	310	0.26
6.72	0.74	352	0.02	6.72	2.58	352	0	6.72	0.17	352	0.18
7.64	0.75	400	0	7.64	2.43	400	0	7.64	0.22	400	0.13
8.68	0.77	454	0	8.68	2.27	454	0	8.68	0.3	454	0.1
9.86	0.81	516	0	9.86	2.11	516	0	9.86	0.39	516	0.07
11.2	0.87			11.2	1.93			11.2	0.52		

CF252

Feed				Overflow				Underflow			
<i>dx</i> (10)	1.85	<i>d</i> [3,2]	5.28	<i>dx</i> (10)	0.504	<i>d</i> [3,2]	1.29	<i>dx</i> (10)	16.4	<i>d</i> [3,2]	14.3
<i>dx</i> (50)	46.9	<i>d</i> [4,3]	52.9	<i>dx</i> (50)	2.27	<i>d</i> [4,3]	7.92	<i>dx</i> (50)	59	<i>d</i> [4,3]	69
<i>dx</i> (90)	112			<i>dx</i> (90)	17.6			<i>dx</i> (90)	134		
% Size (µm)	% Volume In										
0.214	0	8.68	0.81	0.214	0.09	8.68	1.97	0.214	0	8.68	0.53
0.243	0.08	9.86	0.84	0.243	0.38	9.86	1.75	0.243	0	9.86	0.6
0.276	0.19	11.2	0.89	0.276	0.86	11.2	1.57	0.276	0.04	11.2	0.69
0.314	0.33	12.7	0.99	0.314	1.47	12.7	1.41	0.314	0.1	12.7	0.81
0.357	0.47	14.5	1.13	0.357	2.13	14.5	1.28	0.357	0.15	14.5	0.98
0.405	0.61	16.4	1.36	0.405	2.76	16.4	1.18	0.405	0.19	16.4	1.22
0.46	0.73	18.7	1.67	0.46	3.29	18.7	1.08	0.46	0.22	18.7	1.57
0.523	0.81	21.2	2.1	0.523	3.66	21.2	0.99	0.523	0.24	21.2	2.04
0.594	0.85	24.1	2.63	0.594	3.87	24.1	0.89	0.594	0.25	24.1	2.64
0.675	0.86	27.4	3.26	0.675	3.9	27.4	0.79	0.675	0.25	27.4	3.38
0.767	0.84	31.1	3.95	0.767	3.81	31.1	0.69	0.767	0.24	31.1	4.22
0.872	0.8	35.3	4.65	0.872	3.63	35.3	0.61	0.872	0.23	35.3	5.09
0.991	0.76	40.1	5.31	0.991	3.42	40.1	0.55	0.991	0.22	40.1	5.93
1.13	0.72	45.6	5.85	1.13	3.22	45.6	0.51	1.13	0.21	45.6	6.65
1.28	0.69	51.8	6.23	1.28	3.06	51.8	0.49	1.28	0.2	51.8	7.16
1.45	0.67	58.9	6.39	1.45	2.97	58.9	0.48	1.45	0.2	58.9	7.41
1.65	0.67	66.9	6.32	1.65	2.95	66.9	0.45	1.65	0.21	66.9	7.35
1.88	0.68	76	6.01	1.88	2.99	76	0.42	1.88	0.21	76	6.99
2.13	0.71	86.4	5.47	2.13	3.08	86.4	0.38	2.13	0.22	86.4	6.39
2.42	0.73	98.1	4.75	2.42	3.19	98.1	0.33	2.42	0.23	98.1	5.59
2.75	0.76	111	3.88	2.75	3.3	111	0.28	2.75	0.24	111	4.68
3.12	0.77	127	2.94	3.12	3.36	127	0.21	3.12	0.24	127	3.74
3.55	0.78	144	1.99	3.55	3.35	144	0.15	3.55	0.25	144	2.85
4.03	0.79	163	1.13	4.03	3.27	163	0.1	4.03	0.26	163	2.05
4.58	0.78	186	0.28	4.58	3.12	186	0.02	4.58	0.28	186	1.39
5.21	0.78	211	0	5.21	2.92	211	0	5.21	0.31	211	0.86
5.92	0.78	240	0	5.92	2.69	240	0	5.92	0.35	240	0.48
6.72	0.78	272	0	6.72	2.45	272	0	6.72	0.4	272	0.23
7.64	0.79	310	0	7.64	2.2	310	0	7.64	0.46	310	0.06

CF253

Feed				Overflow				Underflow			
<i>dx</i> (10)	1.92	<i>d</i> [3,2]	5.37	<i>dx</i> (10)	0.499	<i>d</i> [3,2]	1.28	<i>dx</i> (10)	6.97	<i>d</i> [3,2]	8.88
<i>dx</i> (50)	49.7	<i>d</i> [4,3]	58.3	<i>dx</i> (50)	2.23	<i>d</i> [4,3]	8.54	<i>dx</i> (50)	52.6	<i>d</i> [4,3]	61.1
<i>dx</i> (90)	127			<i>dx</i> (90)	21			<i>dx</i> (90)	123		
% Size (µm)	% Volume In										
0.214	0	8.68	0.81	0.214	0.09	8.68	1.84	0.214	0	8.68	0.69
0.243	0.08	9.86	0.84	0.243	0.38	9.86	1.65	0.243	0	9.86	0.76
0.276	0.18	11.2	0.9	0.276	0.87	11.2	1.49	0.276	0.11	11.2	0.85
0.314	0.32	12.7	1	0.314	1.5	12.7	1.35	0.314	0.18	12.7	0.98
0.357	0.47	14.5	1.14	0.357	2.19	14.5	1.24	0.357	0.27	14.5	1.15
0.405	0.61	16.4	1.36	0.405	2.85	16.4	1.15	0.405	0.34	16.4	1.41
0.46	0.73	18.7	1.66	0.46	3.39	18.7	1.08	0.46	0.4	18.7	1.77
0.523	0.81	21.2	2.04	0.523	3.77	21.2	1.01	0.523	0.44	21.2	2.25
0.594	0.85	24.1	2.5	0.594	3.97	24.1	0.95	0.594	0.46	24.1	2.85
0.675	0.85	27.4	3.03	0.675	3.99	27.4	0.9	0.675	0.46	27.4	3.56
0.767	0.83	31.1	3.6	0.767	3.87	31.1	0.84	0.767	0.45	31.1	4.35
0.872	0.78	35.3	4.17	0.872	3.66	35.3	0.79	0.872	0.42	35.3	5.15
0.991	0.73	40.1	4.71	0.991	3.42	40.1	0.75	0.991	0.4	40.1	5.88
1.13	0.69	45.6	5.18	1.13	3.19	45.6	0.72	1.13	0.38	45.6	6.48
1.28	0.66	51.8	5.54	1.28	3.02	51.8	0.69	1.28	0.37	51.8	6.86
1.45	0.64	58.9	5.76	1.45	2.93	58.9	0.64	1.45	0.36	58.9	6.98
1.65	0.64	66.9	5.85	1.65	2.9	66.9	0.59	1.65	0.36	66.9	6.82
1.88	0.66	76	5.77	1.88	2.95	76	0.52	1.88	0.37	76	6.39
2.13	0.68	86.4	5.54	2.13	3.04	86.4	0.44	2.13	0.39	86.4	5.74
2.42	0.71	98.1	5.13	2.42	3.14	98.1	0.36	2.42	0.4	98.1	4.94
2.75	0.73	111	4.55	2.75	3.21	111	0.28	2.75	0.42	111	4.06
3.12	0.75	127	3.8	3.12	3.24	127	0.21	3.12	0.43	127	3.17
3.55	0.76	144	2.93	3.55	3.2	144	0.14	3.55	0.44	144	2.34
4.03	0.76	163	2	4.03	3.08	163	0.07	4.03	0.46	163	1.62
4.58	0.76	186	1.13	4.58	2.91	186	0.02	4.58	0.48	186	1.02
5.21	0.76	211	0.27	5.21	2.71	211	0	5.21	0.5	211	0.56
5.92	0.76	240	0	5.92	2.49	240	0	5.92	0.54	240	0.25
6.72	0.77	272	0	6.72	2.27	272	0	6.72	0.58	272	0.07
7.64	0.78			7.64	2.05			7.64	0.63		

CF254

Feed				Overflow				Underflow			
<i>dx</i> (10)	1.7	<i>d</i> [3,2]	5.68	<i>dx</i> (10)	0.57	<i>d</i> [3,2]	1.44	<i>dx</i> (10)	25.9	<i>d</i> [3,2]	38.2
<i>dx</i> (50)	51.5	<i>d</i> [4,3]	63.9	<i>dx</i> (50)	2.4	<i>d</i> [4,3]	8.82	<i>dx</i> (50)	67.9	<i>d</i> [4,3]	85.8
<i>dx</i> (90)	142			<i>dx</i> (90)	17.3			<i>dx</i> (90)	167		
% Size (µm) Volume In											
0.243	0	14.5	1.02	0.243	0.12	14.5	1.66	0.243	0	14.5	0.83
0.276	0.08	16.4	1.21	0.276	0.42	16.4	1.43	0.276	0	16.4	1.13
0.314	0.18	18.7	1.47	0.314	0.9	18.7	1.19	0.314	0	18.7	1.52
0.357	0.31	21.2	1.83	0.357	1.49	21.2	0.96	0.357	0	21.2	2.02
0.405	0.44	24.1	2.27	0.405	2.13	24.1	0.75	0.405	0	24.1	2.62
0.46	0.58	27.4	2.8	0.46	2.74	27.4	0.58	0.46	0	27.4	3.32
0.523	0.72	31.1	3.39	0.523	3.25	31.1	0.45	0.523	0.06	31.1	4.09
0.594	0.83	35.3	4	0.594	3.64	35.3	0.38	0.594	0.07	35.3	4.88
0.675	0.91	40.1	4.59	0.675	3.89	40.1	0.35	0.675	0.07	40.1	5.63
0.767	0.96	45.6	5.11	0.767	3.99	45.6	0.37	0.767	0.07	45.6	6.29
0.872	0.99	51.8	5.49	0.872	3.96	51.8	0.42	0.872	0.06	51.8	6.78
0.991	0.99	58.9	5.71	0.991	3.85	58.9	0.47	0.991	0.06	58.9	7.08
1.13	0.97	66.9	5.73	1.13	3.68	66.9	0.51	1.13	0	66.9	7.14
1.28	0.94	76	5.56	1.28	3.49	76	0.52	1.28	0	76	6.97
1.45	0.89	86.4	5.21	1.45	3.32	86.4	0.52	1.45	0	86.4	6.59
1.65	0.85	98.1	4.73	1.65	3.18	98.1	0.48	1.65	0	98.1	6.02
1.88	0.81	111	4.14	1.88	3.09	111	0.41	1.88	0.06	111	5.32
2.13	0.78	127	3.51	2.13	3.05	127	0.33	2.13	0.06	127	4.55
2.42	0.76	144	2.87	2.42	3.05	144	0.24	2.42	0.07	144	3.76
2.75	0.75	163	2.26	2.75	3.06	163	0.14	2.75	0.07	163	3
3.12	0.74	186	1.71	3.12	3.06	186	0.05	3.12	0.07	186	2.31
3.55	0.73	211	1.23	3.55	3.04	211	0.02	3.55	0.07	211	1.71
4.03	0.71	240	0.83	4.03	2.99	240	0	4.03	0.07	240	1.23
4.58	0.7	272	0.5	4.58	2.92	272	0	4.58	0.07	272	0.85
5.21	0.69	310	0.25	5.21	2.84	310	0	5.21	0.08	310	0.56
5.92	0.69	352	0	5.92	2.75	352	0	5.92	0.1	352	0.35
6.72	0.69	400	0	6.72	2.65	400	0	6.72	0.13	400	0.21
7.64	0.7	454	0	7.64	2.55	454	0	7.64	0.17	454	0.12
8.68	0.72	516	0	8.68	2.42	516	0	8.68	0.23	516	0.08
9.86	0.75	586	0	9.86	2.27	586	0	9.86	0.32	586	0.03
11.2	0.81	666	0	11.2	2.09	666	0	11.2	0.44	666	0.02
12.7	0.89			12.7	1.89			12.7	0.6		

CF256

Feed				Overflow				Underflow			
<i>dx</i> (10)	2.33	<i>d</i> [3,2]	5.99	<i>dx</i> (10)	0.54	<i>d</i> [3,2]	1.33	<i>dx</i> (10)	21.8	<i>d</i> [3,2]	16.8
<i>dx</i> (50)	53.9	<i>d</i> [4,3]	69	<i>dx</i> (50)	2.08	<i>d</i> [4,3]	7.5	<i>dx</i> (50)	75.8	<i>d</i> [4,3]	111
<i>dx</i> (90)	147			<i>dx</i> (90)	17.5			<i>dx</i> (90)	229		
% Size (µm)	% Volume In										
0.243	0.05	16.4	1.17	0.243	0.17	16.4	1.23	0.243	0	16.4	0.8
0.276	0.15	18.7	1.43	0.276	0.54	18.7	1.13	0.276	0	18.7	1.02
0.314	0.27	21.2	1.79	0.314	1.08	21.2	1.03	0.314	0.09	21.2	1.34
0.357	0.4	24.1	2.26	0.357	1.74	24.1	0.91	0.357	0.13	24.1	1.77
0.405	0.53	27.4	2.82	0.405	2.44	27.4	0.79	0.405	0.17	27.4	2.32
0.46	0.64	31.1	3.46	0.46	3.1	31.1	0.68	0.46	0.2	31.1	2.97
0.523	0.72	35.3	4.14	0.523	3.65	35.3	0.59	0.523	0.22	35.3	3.71
0.594	0.77	40.1	4.79	0.594	4.06	40.1	0.54	0.594	0.23	40.1	4.47
0.675	0.78	45.6	5.37	0.675	4.29	45.6	0.51	0.675	0.23	45.6	5.2
0.767	0.77	51.8	5.8	0.767	4.35	51.8	0.51	0.767	0.22	51.8	5.83
0.872	0.74	58.9	6.03	0.872	4.26	58.9	0.51	0.872	0.21	58.9	6.3
0.991	0.7	66.9	6.03	0.991	4.07	66.9	0.5	0.991	0.19	66.9	6.56
1.13	0.65	76	5.81	1.13	3.82	76	0.47	1.13	0.18	76	6.59
1.28	0.62	86.4	5.38	1.28	3.56	86.4	0.41	1.28	0.18	86.4	6.38
1.45	0.6	98.1	4.8	1.45	3.32	98.1	0.33	1.45	0.18	98.1	5.95
1.65	0.59	111	4.11	1.65	3.14	111	0.24	1.65	0.18	111	5.36
1.88	0.6	127	3.39	1.88	3.04	127	0.14	1.88	0.19	127	4.65
2.13	0.61	144	2.69	2.13	3.01	144	0.05	2.13	0.19	144	3.9
2.42	0.63	163	2.07	2.42	3.04	163	0	2.42	0.2	163	3.18
2.75	0.65	186	1.56	2.75	3.09	186	0	2.75	0.21	186	2.53
3.12	0.67	211	1.17	3.12	3.12	211	0	3.12	0.21	211	2
3.55	0.68	240	0.9	3.55	3.11	240	0	3.55	0.22	240	1.62
4.03	0.68	272	0.7	4.03	3.02	272	0	4.03	0.22	272	1.35
4.58	0.67	310	0.54	4.58	2.88	310	0	4.58	0.23	310	1.18
5.21	0.67	352	0.4	5.21	2.7	352	0	5.21	0.25	352	1.07
5.92	0.67	400	0.26	5.92	2.5	400	0	5.92	0.27	400	0.98
6.72	0.67	454	0.12	6.72	2.29	454	0	6.72	0.3	454	0.88
7.64	0.69	516	0.03	7.64	2.08	516	0	7.64	0.33	516	0.76
8.68	0.71	586	0	8.68	1.89	586	0	8.68	0.37	586	0.61
9.86	0.74	666	0	9.86	1.72	666	0	9.86	0.42	666	0.44
11.2	0.79	756	0	11.2	1.57	756	0	11.2	0.47	756	0.26
12.7	0.87	859	0	12.7	1.44	859	0	12.7	0.54	859	0.11
14.5	0.99	976	0	14.5	1.33	976	0	14.5	0.65	976	0.03

CF257

Feed				Overflow				Underflow			
<i>dx</i> (10)	2.01	<i>d</i> [3,2]	5.42	<i>dx</i> (10)	0.505	<i>d</i> [3,2]	1.26	<i>dx</i> (10)	8.07	<i>d</i> [3,2]	9.44
<i>dx</i> (50)	49.7	<i>d</i> [4,3]	69.5	<i>dx</i> (50)	2.08	<i>d</i> [4,3]	6.81	<i>dx</i> (50)	58.8	<i>d</i> [4,3]	89.5
<i>dx</i> (90)	149			<i>dx</i> (90)	14.6			<i>dx</i> (90)	187		
% Size (µm)	% Volume In										
0.214	0	14.5	1.07	0.214	0.05	14.5	1.24	0.214	0	14.5	1.04
0.243	0.11	16.4	1.28	0.243	0.36	16.4	1.11	0.243	0.05	16.4	1.28
0.276	0.23	18.7	1.58	0.276	0.83	18.7	0.98	0.276	0.12	18.7	1.6
0.314	0.36	21.2	1.99	0.314	1.44	21.2	0.85	0.314	0.19	21.2	2.02
0.357	0.49	24.1	2.49	0.357	2.11	24.1	0.73	0.357	0.26	24.1	2.55
0.405	0.61	27.4	3.09	0.405	2.77	27.4	0.61	0.405	0.32	27.4	3.16
0.46	0.7	31.1	3.74	0.46	3.35	31.1	0.51	0.46	0.37	31.1	3.83
0.523	0.76	35.3	4.39	0.523	3.78	35.3	0.44	0.523	0.39	35.3	4.51
0.594	0.79	40.1	4.99	0.594	4.04	40.1	0.42	0.594	0.41	40.1	5.14
0.675	0.79	45.6	5.46	0.675	4.13	45.6	0.42	0.675	0.4	45.6	5.65
0.767	0.77	51.8	5.76	0.767	4.08	51.8	0.43	0.767	0.39	51.8	6
0.872	0.73	58.9	5.83	0.872	3.92	58.9	0.45	0.872	0.37	58.9	6.13
0.991	0.7	66.9	5.68	0.991	3.71	66.9	0.46	0.991	0.35	66.9	6.04
1.13	0.66	76	5.31	1.13	3.48	76	0.43	1.13	0.34	76	5.74
1.28	0.64	86.4	4.78	1.28	3.28	86.4	0.38	1.28	0.34	86.4	5.27
1.45	0.64	98.1	4.13	1.45	3.13	98.1	0.31	1.45	0.34	98.1	4.66
1.65	0.64	111	3.43	1.65	3.06	111	0.21	1.65	0.35	111	3.98
1.88	0.65	127	2.75	1.88	3.06	127	0.12	1.88	0.36	127	3.29
2.13	0.67	144	2.14	2.13	3.13	144	0	2.13	0.37	144	2.65
2.42	0.7	163	1.65	2.42	3.22	163	0	2.42	0.39	163	2.08
2.75	0.72	186	1.29	2.75	3.32	186	0	2.75	0.4	186	1.63
3.12	0.74	211	1.06	3.12	3.37	211	0	3.12	0.42	211	1.31
3.55	0.75	240	0.93	3.55	3.36	240	0	3.55	0.43	240	1.11
4.03	0.75	272	0.86	4.03	3.26	272	0	4.03	0.44	272	1
4.58	0.75	310	0.8	4.58	3.09	310	0	4.58	0.46	310	0.96
5.21	0.74	352	0.7	5.21	2.88	352	0	5.21	0.47	352	0.92
5.92	0.74	400	0.55	5.92	2.63	400	0	5.92	0.5	400	0.87
6.72	0.74	454	0.37	6.72	2.38	454	0	6.72	0.53	454	0.78
7.64	0.75	516	0.17	7.64	2.14	516	0	7.64	0.57	516	0.65
8.68	0.76	586	0.04	8.68	1.91	586	0	8.68	0.62	586	0.47
9.86	0.79	666	0	9.86	1.71	666	0	9.86	0.68	666	0.28
11.2	0.84	756	0	11.2	1.53	756	0	11.2	0.76	756	0.1
12.7	0.93	859	0	12.7	1.38	859	0	12.7	0.88	859	0.02

CF258

Feed				Overflow				Underflow			
<i>dx</i> (10)	1.92	<i>d</i> [3,2]	5.51	<i>dx</i> (10)	0.548	<i>d</i> [3,2]	1.39	<i>dx</i> (10)	8.49	<i>d</i> [3,2]	9.74
<i>dx</i> (50)	49.1	<i>d</i> [4,3]	67.6	<i>dx</i> (50)	2.33	<i>d</i> [4,3]	6.69	<i>dx</i> (50)	66.2	<i>d</i> [4,3]	111
<i>dx</i> (90)	144			<i>dx</i> (90)	16.8			<i>dx</i> (90)	262		
% Size (µm)	% Volume In										
0.243	0.05	18.7	1.57	0.243	0.18	18.7	1.67	0.243	0	18.7	1.29
0.276	0.16	21.2	1.99	0.276	0.53	21.2	1.44	0.276	0.11	21.2	1.67
0.314	0.29	24.1	2.53	0.314	1.06	24.1	1.19	0.314	0.18	24.1	2.14
0.357	0.44	27.4	3.16	0.357	1.68	27.4	0.93	0.357	0.26	27.4	2.71
0.405	0.58	31.1	3.85	0.405	2.34	31.1	0.69	0.405	0.33	31.1	3.34
0.46	0.7	35.3	4.54	0.46	2.95	35.3	0.5	0.46	0.38	35.3	3.99
0.523	0.8	40.1	5.16	0.523	3.45	40.1	0.36	0.523	0.41	40.1	4.62
0.594	0.85	45.6	5.64	0.594	3.82	45.6	0.27	0.594	0.43	45.6	5.16
0.675	0.87	51.8	5.9	0.675	4.02	51.8	0.22	0.675	0.42	51.8	5.55
0.767	0.85	58.9	5.93	0.767	4.07	58.9	0.2	0.767	0.4	58.9	5.77
0.872	0.82	66.9	5.72	0.872	3.99	66.9	0.19	0.872	0.38	66.9	5.79
0.991	0.77	76	5.29	0.991	3.81	76	0.19	0.991	0.36	76	5.6
1.13	0.72	86.4	4.7	1.13	3.59	86.4	0.17	1.13	0.34	86.4	5.23
1.28	0.68	98.1	4.02	1.28	3.36	98.1	0.15	1.28	0.34	98.1	4.73
1.45	0.65	111	3.32	1.45	3.16	111	0.13	1.45	0.34	111	4.14
1.65	0.64	127	2.66	1.65	3.01	127	0.1	1.65	0.34	127	3.53
1.88	0.65	144	2.08	1.88	2.92	144	0.06	1.88	0.36	144	2.95
2.13	0.66	163	1.62	2.13	2.9	163	0	2.13	0.37	163	2.46
2.42	0.68	186	1.29	2.42	2.93	186	0	2.42	0.39	186	2.08
2.75	0.7	211	1.06	2.75	2.97	211	0	2.75	0.41	211	1.82
3.12	0.71	240	0.92	3.12	2.99	240	0	3.12	0.42	240	1.67
3.55	0.72	272	0.83	3.55	2.98	272	0	3.55	0.43	272	1.58
4.03	0.72	310	0.73	4.03	2.92	310	0	4.03	0.43	310	1.51
4.58	0.72	352	0.61	4.58	2.82	352	0	4.58	0.43	352	1.42
5.21	0.72	400	0.45	5.21	2.71	400	0	5.21	0.44	400	1.28
5.92	0.72	454	0.28	5.92	2.6	454	0	5.92	0.45	454	1.1
6.72	0.73	516	0.14	6.72	2.51	516	0	6.72	0.46	516	0.89
7.64	0.74	586	0.05	7.64	2.42	586	0	7.64	0.48	586	0.67
8.68	0.76	666	0	8.68	2.35	666	0	8.68	0.51	666	0.46
9.86	0.79	756	0	9.86	2.29	756	0	9.86	0.54	756	0.28
11.2	0.83	859	0	11.2	2.22	859	0	11.2	0.6	859	0.12
12.7	0.91	976	0	12.7	2.13	976	0	12.7	0.69	976	0.03
14.5	1.05	1110	0	14.5	2.02	1110	0	14.5	0.82	1110	0.02
16.4	1.26			16.4	1.86			16.4	1.02		

S24E2 and S24F2 -0.038 mm Overflow Fraction

S24E2 (Original)				S24F2 (Deslimed)			
<i>dx</i> (10)	0.741	<i>d</i> [3,2]	2.33	<i>dx</i> (10)	11.4	<i>d</i> [3,2]	11
<i>dx</i> (50)	8.92	<i>d</i> [4,3]	14.6	<i>dx</i> (50)	27.1	<i>d</i> [4,3]	27.9
<i>dx</i> (90)	36.7			<i>dx</i> (90)	45.9		
% Size (µm)	% Volume In	% Size (µm)	% Volume In	% Size (µm)	% Volume In	% Size (µm)	% Volume In
0.214	0.13	4.03	2.32	0.214	0	4.03	0.54
0.243	0.31	4.58	2.28	0.243	0	4.58	0.53
0.276	0.55	5.21	2.21	0.276	0.02	5.21	0.5
0.314	0.81	5.92	2.15	0.314	0.1	5.92	0.44
0.357	1.06	6.72	2.09	0.357	0.13	6.72	0.38
0.405	1.27	7.64	2.07	0.405	0.17	7.64	0.39
0.46	1.44	8.68	2.11	0.46	0.2	8.68	0.54
0.523	1.56	9.86	2.24	0.523	0.22	9.86	0.92
0.594	1.64	11.2	2.47	0.594	0.24	11.2	1.6
0.675	1.69	12.7	2.81	0.675	0.25	12.7	2.65
0.767	1.71	14.5	3.25	0.767	0.26	14.5	4.05
0.872	1.73	16.4	3.73	0.872	0.26	16.4	5.73
0.991	1.76	18.7	4.21	0.991	0.26	18.7	7.51
1.13	1.8	21.2	4.59	1.13	0.26	21.2	9.15
1.28	1.86	24.1	4.79	1.28	0.27	24.1	10.38
1.45	1.91	27.4	4.74	1.45	0.27	27.4	10.94
1.65	1.98	31.1	4.4	1.65	0.27	31.1	10.67
1.88	2.04	35.3	3.8	1.88	0.29	35.3	9.56
2.13	2.11	40.1	3.01	2.13	0.31	40.1	7.77
2.42	2.18	45.6	2.14	2.42	0.35	45.6	5.6
2.75	2.25	51.8	1.31	2.75	0.4	51.8	3.42
3.12	2.3	58.9	0.64	3.12	0.46	58.9	1.25
3.55	2.33	66.9	0.21	3.55	0.51	66.9	0

CF222 Underflow Launder Solids

CF222 Launder Washings			
<i>dx</i> (10)	0.741	<i>d</i> [3,2]	2.33
<i>dx</i> (50)	8.92	<i>d</i> [4,3]	14.6
<i>dx</i> (90)	36.7		
Size (μm)	% Volume In	Size (μm)	% Volume In
0.243	0	12.7	0.23
0.276	0	14.5	0.4
0.314	0	16.4	0.75
0.357	0	18.7	1.31
0.405	0	21.2	2.13
0.46	0	24.1	3.2
0.523	0	27.4	4.45
0.594	0	31.1	5.78
0.675	0.02	35.3	7.04
0.767	0.07	40.1	8.07
0.872	0.07	45.6	8.74
0.991	0.06	51.8	8.95
1.13	0	58.9	8.67
1.28	0	66.9	7.96
1.45	0	76	6.93
1.65	0	86.4	5.72
1.88	0	98.1	4.48
2.13	0	111	3.34
2.42	0	127	2.39
2.75	0	144	1.68
3.12	0	163	1.19
3.55	0	186	0.9
4.03	0.08	211	0.74

Appendix C: Experimental Data and Sampling

This appendix contains the records of the experimental conditions, sample weights and calculated data for each run. Summaries of the conditions used for each run are provided in the thesis body in Tables 5.1, 6.1, 6.2, 6.10 and 6.11. Sample calculations for this appendix refer to Run CF145, and are for the sample “OF 1 min”.

Each table in this appendix contains the weight and time of the samples taken for each stream and the wet and dry masses for the further sub samples taken from which the solids concentration and flowrates were calculated (in some cases the entire sample was dried rather than taking a second sub sample). The solids concentration was calculated by dividing the solids weight (dry) by the slurry weight,

$$\begin{aligned} \text{Solids Conc.} &= 100 \times \text{Solids weight} / \text{Slurry weight} \\ &= 100 \times 75.6 / 14700 = 0.51 \text{ wt.}\% \end{aligned}$$

The solids Rate was calculated by dividing the solids weight by the sample time,

$$\begin{aligned} \text{Solids rate} &= \text{Solids weight} / \text{Sample time} \times 60 \\ &= 75.6 / 10 \times 60 = 454 \text{ g/s} \end{aligned}$$

The same calculation is made for the Mass Flow using the slurry weight in place of the solids weight.

The slurry density (g/mL) was calculated using the concentrations and densities of the solids and water in the equation,

$$\begin{aligned} \text{SlurryDensity} &= \frac{100}{\frac{\text{SolidsConc.}}{\text{SolidsDensity}} + \frac{100 - \text{SolidsConc}}{\text{WaterDensity}}} \\ &= 100 / ((0.51/2.65) + (100 - 0.51)/ 1) = 1.0032 \text{ (g/mL)} \end{aligned}$$

The volumetric flow was calculated by dividing the mass flow by the slurry density,

$$\text{Vol. Flow} = \text{Mass Flow} / \text{Slurry Density} / 1000$$

$$= 88200 / 1.0032 / 1000 = 87.9 \text{ L/min}$$

The measured volume rates and mass rate in/out provide an indication of the internal consistency of the data. These were calculated by dividing all of the volumetric flows into the system by the volumetric flows out using the average values for each stream. Average U/F values are doubled to give the total U/F values as the sample collection is from only one side. This is the row listed as 'Two Sides'. The same In/Out balance was performed for the solids flows.

$$\begin{aligned} \text{Volume Balance Ratio} &= (\text{Feed} + \text{U/F Flush} + \text{Launder Wash} + \text{Fluidisation}) / (\text{U/F} + \text{O/F}) \\ &= (99.7 + 2 + 21.8 + 11.4) / (87.9 + 43.6) = 1.03 \end{aligned}$$

$$\begin{aligned} \text{Solids Balance Ratio} &= \text{Feed} / (\text{U/F} + \text{O/F}) \\ &= 1910 / (454 + 1419) = 1.02 \end{aligned}$$

The solids yields to underflow are calculated using Equations 4.5a -4.5c along with an average of the three. The average solids flow values for each stream were used,

$$\text{Yield} = \text{U/F} / (\text{O/F} + \text{U/F}) = 1419 / (454 + 1419) = 0.758 \text{ i.e. a solids yield of 75.8 wt.}\%$$

$$\text{Yield} = 1 - (\text{O/F} / \text{Feed}) = 1 - (454 / 1910) = 0.763 \text{ i.e. a solids yield of 76.3 wt.}\%$$

$$\text{Yield} = \text{U/F} / \text{F} = 1419 / 1910 = 0.743 \text{ i.e. a solids yield of 74.3 wt.}\%$$

As is discussed in Chapter 4, the underflow samples are often not representative of the true underflow due to particles settling in the Launder. Hence, the yield determined by Equation 4.5a often contains error. Table values highlighted in yellow indicate outliers, inconsistencies and/or measurement errors. These values were not included to calculate average values. Entries highlighted in green are inputs/flows controlled during the experiment.

It is noted that the data presented for the underflow refers to the 'collected' underflow sample and hence includes extra water from the launder wash and underflow flush. In each case the 'true' underflow solids concentration and volumetric flowrate were also calculated,

$$\text{True U/F Flowrate} = \text{U/F Vol.Flow} - \text{Launder wash} - \text{U/F Flush}$$

$$= 43.6 - 21.8 - 2 = 19.8 \text{ L/min}$$

$$\text{True U/F Solids Conc.} = \text{Solids rate} / (\text{Mass Flow} - (\text{Launder} \times 1000) - (\text{U/F Flush} \times 1000)) \times 100$$

$$= 1419 / (44475 - (21.8 \times 1000) - (2 \times 1000)) \times 100 = 6.9 \text{ wt.}\%$$

Any reference to such data in the results chapters refers to these 'true' values. The same adjustment was made in the REFLUX™ Classifier work with the underflow rate and solids concentration adjusted for the underflow buffer water rate.

Underflow samples listed as (N) or (S) refer to samples collected from the two discharge points on the north and south side of the Graviton. Until Run CF238, when not specified, the sample was collected from the south side. From this run onwards, the launder wash system was altered to provide better removal of solids. This involved adjusting the alignment of the launder wash hose, increasing the launder wash flowrate and installing deflectors at either discharge point to help guide solids out of the launder. Following this change, the north side showed better removal of solids than the south side and so unless specified, the underflow sample was taken from the north side.

Gravity Separation and Desliming Using Inclined Channels Subject to Different G-Forces

CF145

			Solids Density						
	Slurry Weight (g)	Solids Weight (g)	Solids Conc. (wt. %)	Sample time (s)	Solids Rate (g/min)	Slurry Density (g/ml)	Mass Flow (g/min)	Volumetric Flow (L/min)	
Feed 1	13052	251.5	1.93		1945	1.0121	100910.4	99.7	
Feed 2	12965	241.1	1.86		1876	1.0117	100867.6	99.7	
OF 8 min	14700	75.6	0.51	10	454	1.0032	88200.0	87.9	
UF 1 min	3362	133.5	3.97	10	801	1.0254	20172.0	19.7	
UF 2 min	3755	122.0	3.25	10	732	1.0206	22530.0	22.1	
UF 4 min	3935	138.1	3.51	10	829	1.0223	23610.0	23.1	
UF 6 min	3783	120.6	3.19	10	724	1.0203	22698.0	22.2	
UF 8 min	3673	79.8	2.17	10	479	1.0137	22038.0	21.7	
UF 10 min	7459	230.8	3.09	20	692	1.0196	22377.0	21.9	
UF average		137.5	3.20		709	1.0203	22237.5	21.8	
				Two sides:	1419		44475.0	43.6	
					UF/(OF+UF)		1 - OF/F	UF/F	
				Solids Yield to UF:	0.758		0.763	0.743	
				Underflow flush (L/min)	2				
				Launder Wash (L/min)	21.8				
				Fluidisation (L/min)	11.4				
				Volume Balance:	In =	134.90			
					Out =	131.51			
					Ratio:	1.03			
				Solids In/Out =		1.02			
				Average Yield =		0.754			

Takes into account water from Launder and U/F Flush

TRUE U/F	
Flowrate	Solids Conc.
L/min	wt. %
19.8	6.9

Appendix C: Experimental Data and Sampling

CF146

			Solids Density									
	Slurry Weight (g)	Solids Weight (g)	Solids Conc. (wt. %)	Sample time (s)	Solids Rate (g/min)	Slurry Density (g/ml)	Mass Flow (g/min)	Volumetric Flow (L/min)				
Feed 1	12705.8	256.6	2.02		2028	1.0127	100441	99.2				
OF 8 min	16582	97.4	0.59	10	584	1.0037	99492	99.1				
UF 1 min	3587	82.4	2.30	10	494	1.0145	21522	21.2				
UF 2 min	3626	124.7	3.44	10	748	1.0219	21756	21.3				
UF 4 min	3787	140.6	3.71	10	844	1.0237	22722	22.2				
UF 6 min	3773	93.5	2.48	10	561	1.0157	22638	22.3				
UF 8 min	3663	120.4	3.29	10	722	1.0209	21978	21.5				
UF 10 min	6990	186.3	2.67	20	559	1.0169	20969	20.6				
<i>UF average</i>		124.7	2.98		655	1.0189	21931	21.5				
				Two sides:	1310		43862	43.0				
					UF/(OF+UF)		1 - OF/F		UF/F			
				Solids Yield to UF:	0.691		0.712		0.646			
				Underflow flush (L/min)	2							
				Launder Wash (L/min)	21.8							
				Fluidisation (L/min)	18							
				Volume Balance:	In =	141.0						
					Out =	142.2						
					Ratio:	0.992						
				Solids In/Out =		1.071						
					Average Yield =	0.683						

Takes into account water from Launder and U/F Flush

TRUE U/F
Flowrate Solids Conc.
L/min wt.%

19.2 6.5

Gravity Separation and Desliming Using Inclined Channels Subject to Different G-Forces

CF147

	Slurry Weight (g)	Solids Weight (g)	Solids Conc. (wt. %)	Sample time (s)	Solids Rate (g/min)	Slurry Density (g/ml)	Mass Flow (g/min)	Volumetric Flow (L/min)
Feed 1	11651	236.9	2.03		2037	1.0128	100162	98.9
OF 1 min	14909	89.0	0.60	10	534	1.0037	89454	89.1
OF 2 min	14446	87.1	0.60	10	523	1.0038	86674	86.3
OF 4 min	13839	62.1	0.45	10	373	1.0028	83034	82.8
OF 6 min	14195	88.0	0.62	10	528	1.0039	85170	84.8
OF 8 min	13601	62.2	0.46	10	373	1.0029	81606	81.4
OF 10 min	14262	86.0	0.60	10	516	1.0038	85572	85.3
OF average	14209	79	0.55		474	1.0035	85252	85
UF 1 min	3652	131.9	3.61	10	791	1.0230	21912	21.4
UF 2 min	3552	89.0	2.51	10	534	1.0158	21312	21.0
UF 4 min	3711	134.1	3.61	10	805	1.0230	22266	21.8
UF 6 min	3616	118.8	3.29	10	713	1.0209	21696	21.3
UF 8 min	3732	133.1	3.57	10	799	1.0227	22392	21.9
UF 10 min	6991	245.7	3.51	20	737	1.0224	20973	20.5
UF average		142.1	3.35		730	1.0213	21759	21.3
				Two sides:	1460		43517	42.6
					UF/(OF+UF)		1 - OF/F	UF/F
				Solids Yield to UF:	0.755		0.755	0.717
				Underflow flush (L/min)	2			
				Launder Wash (L/min)	21.8			
				Fluidisation (L/min)	6			
				Volume Balance:	In =	128.7		
					Out =	127.6		
					Ratio:	1.009		
				Solids In/Out =		1.053		
				Average Yield =		0.742		

Takes into account water from Launder and U/F Flush

TRUE U/F	
Flowrate L/min	Solids Conc. wt. %
18.8	7.4

Appendix C: Experimental Data and Sampling

CF148

		Solids Density		2.65					
	Slurry weight (g)	Sub sample		Solids Conc. (wt. %)	Sample time (s)	Solids Rate (g/min)	Slurry Density (g/ml)	Mass Flow (g/min)	Volumetric Flow (L/min)
		Slurry Weight (g)	Solids Weight (g)						
Feed 1	11354	All	463	4.1	-	4812	1.026	117996	115
Feed 2	13995	All	541	3.9	-	4555	1.025	117836	115
<i>Feed Average</i>	12675			4.0		4683	1.025	117916	115
O/F 6 min	16612	All	179.5	1.1	10	1077	1.007	99672	99
O/F 8 min	15753	486	5.9	1.2	10	1147	1.008	94518	94
<i>O/F Average</i>	16183			1.1	10	1112	1.007	97095	96
U/F 1 min	4098	All	266.8	6.5	10	1601	1.042	24588	24
U/F 2 min	4277	All	289	6.8	10	1734	1.044	25662	25
U/F 4 min	4108	All	281.2	6.8	10	1687	1.045	24648	24
U/F 6 min	4181	All	279.8	6.7	10	1679	1.043	25086	24
U/F 8 min	4115	All	277.6	6.7	10	1666	1.044	24690	24
<i>U/F Average</i>	4156			6.7	10	1673	1.044	24935	24
Two Sides:						3347		49870	48
						UF/(OF+UF)		1 - OF/F	UF/F
						Solids Yield to UF:	0.751	0.763	0.715
						Underflow flush (L/min):	2		
						Launder Wash (L/min):	21.8		
						Fluidisation (L/min):	6		
						Volume Balance: In =	144.8		
						Out =	144.2		
						Ratio:	1.00		
						Solids In/Out =	1.05		
						Average Yield =	0.743		

Takes into account water from Launder and U/F Flush

TRUE U/F	
Flowrate	Solids Conc.
L/min	wt.%
24.0	12.8

Gravity Separation and Desliming Using Inclined Channels Subject to Different G-Forces

CF149

			Solids Density	2.65						
	Slurry weight (g)	Sub sample		Solids Conc. (wt. %)	Sample time (s)	Solids Rate (g/min)	Slurry Density (g/ml)	Mass Flow (g/min)	Volumetric Flow (L/min)	
	Slurry weight (g)	Slurry Weight (g)	Solids Weight (g)							
Feed 1	11415	All	466.5	4.1	-	4655	1.026	113898	111	
Feed 2	9098	All	352.2	3.9	-	4403	1.025	113742	111	
<i>Feed Average</i>	10257			4.0		4529	1.025	113820	111	
O/F 1 min	19736	All	173.3	0.9	10	1040	1.005	118416	118	
O/F 2 min	17418	All	153.1	0.9	10	919	1.006	104508	104	
O/F 4 min	17754	All	160	0.9	10	960	1.006	106524	106	
<i>O/F 6 min</i>	16812	All	146.4	0.9	10	878	1.005	100872	100	
O/F 8 min	16930	All	148	0.9	10	888	1.005	101580	101	
<i>O/F Average</i>	17730			0.9	10	937	1.006	106380	106	
U/F 1 min	3865	All	267.2	6.9	10	1603.2	1.045	23190	22	
U/F 2 min	3842	All	267.4	7.0	10	1604	1.045	23052	22	
U/F 6 min	3855	All	262.2	6.8	10	1573	1.044	23130	22	
U/F 8 min	3839	All	273.8	7.1	10	1643	1.046	23034	22	
<i>U/F Average</i>	3850			7.0	10	1606	1.045	23102	22	
					Two Sides:	3212		46203	44	
						UF/(OF+UF)		1 - OF/F	UF/F	
					Solids Yield to UF:	0.774		0.793	0.709	
					Underflow flush (L/min):	2				
					Laundry Wash (L/min):	21.8				
					Fluidisation (L/min):	16.8				
					Volume Balance: In =		151.6			
					Out =		150.0			
					Ratio:		1.01			
					Solids In/Out =		1.09			
					Average Yield =		0.759			

Takes into account water from Launder and U/F Flush

TRUE U/F	
Flowrate	Solids Conc.
L/min	wt.%
20.4	14.3

Appendix C: Experimental Data and Sampling

CF150

										Solids Density	2.65								
										Sub sample									
	Slurry weight (g)	Slurry Weight (g)	Solids Weight (g)	Solids Conc. (wt. %)	Sample time (s)	Solids Rate (g/min)	Slurry Density (g/ml)	Mass Flow (g/min)	Volumetric Flow (L/min)										
Feed 1	10603	All	439	2.6	-	2889	1.016	111799	110										
Feed 2	10219	All	402	3.9	-	4436	1.025	112762	110										
<i>Feed Average</i>	10411			3.3		3662	1.021	112278	110										
O/F 8 min	17244	508	4.9	1.0	10	998	1.006	103464	103										
<i>O/F Average</i>	17244			1.0	10	998	1.006	103464	103										
U/F 1 min	3913	All	274	7.0	10	1644	1.046	23478	22										
U/F 2 min	3956	All	269	6.8	10	1614	1.044	23736	23										
U/F 4 min	3937	All	279	7.1	10	1674	1.046	23622	23										
U/F 6 min	3892	All	269	6.9	10	1614	1.045	23352	22										
U/F 8 min	3935	All	273	6.9	10	1638	1.045	23610	23										
<i>U/F Average</i>	3927			7.0	10	1637	1.045	23560	23										
						Two Sides:	3273	47119	45										
							UF/(OF+UF)	1 - OF/F	UF/F										
						Solids Yield to UF:	0.766	0.728	0.894										
						Underflow flush (L/min):	2												
						Launder Wash (L/min):	21.8												
						Fluidisation (L/min):	18												
						Volume Balance: In =	151.8												
						Out =	147.9												
						Ratio:	1.03												
						Solids In/Out =	0.86												
						Average Yield =	0.796												

Takes into account water from Launder and U/F Flush

TRUE U/F	
Flowrate	Solids Conc.
L/min	wt. %
21.3	14.0

Gravity Separation and Desliming Using Inclined Channels Subject to Different G-Forces

CF152

	Slurry Weight (g)	Solids Weight (g)	Solids Conc. (wt. %)	Sample time (s)	Solids Rate (g/min)	Slurry Density (g/ml)	Mass Flow (g/min)	Volumetric Flow (L/min)	
			Solids Density	2.65					
Feed 1	12358	1249.5	10.1	-	10898	1.067	107786	101	
Feed 2	13684	1316.7	9.6	-	10338	1.064	107437	101	
<i>Feed Average</i>	13021	1284.7	9.9		10618	1.065	107611	101	
O/F 4 mins	17953	592.0	3.3	10	3552	1.021	107718	106	
O/F 6 mins	15844	391.8	2.5	10	2351	1.016	95064	94	
O/F 8 mins	16747	401.9	2.4	10	2412	1.015	100482	99	
O/F average	16848	458.9	2.7		2753	1.017	101088	99	
U/F 4 mins	4070	670.0	16.5	10	4020	1.114	24420	22	
U/F 8 mins	3970	635.1	16.0	10	3811	1.111	23820	21	
U/F average	3962	652.6	16.2	10	3915	1.112	24120	22	
				Two Sides:	7831		48240	43	
					UF/(OF+UF)		1 - OF/F	UF/F	
				Solids Yield to UF:	0.733		0.736	0.726	
				Underflow flush (L/min):	2				
				Launder Wash (L/min):	21.8				
				Fluidisation (L/min):	18				
				Volume Balance: In =		119.0			
				Out =		118.3			
				Ratio:		1.01			
				Solids In/Out =		1.01			
				Average Yield =		0.732			

Takes into account water from Launder and U/F Flush

TRUE U/F	
Flowrate	Solids Conc.
L/min	wt. %
19.6	32.0

Appendix C: Experimental Data and Sampling

CF153

			Solids Density	2.65						
	Slurry weight (g)	Sub sample		Solids Conc. (wt. %)	Sample time (s)	Solids Rate (g/min)	Slurry Density (g/ml)	Mass Flow (g/min)	Volumetric Flow (L/min)	
	Slurry weight (g)	Slurry Weight (g)	Solids Weight (g)							
Feed 1	12217	274	54.2	19.8	-	11054	1.1405	55883	49	
Feed 2	14203	399	87.9	22.0	-	12511	1.1590	56790	49	
<i>Feed Average</i>	<i>13210</i>	<i>336.5</i>	<i>71.1</i>	<i>20.9</i>		<i>11783</i>	<i>1.1497</i>	<i>56336</i>	<i>49</i>	
O/F 8 min	8619	422	13.2	3.1	10	1618	1.0199	51714	51	
O/F 12 min	7768	347	10.5	3.0	10	1410	1.0192	46608	46	
O/F 16 min	8578	410	12.8	3.1	10	1607	1.0198	51468	50	
<i>O/F Average</i>	<i>8322</i>	<i>393</i>	<i>12</i>	<i>3</i>	<i>10</i>	<i>1545</i>	<i>1.0196</i>	<i>49930</i>	<i>49</i>	
U/F 8 min	4207	340	60.5	19.5	10	4928	1.1246	25242	22	
U/F 12 min	4158	482	74.7	18.2	10	4533	1.1068	24948	23	
U/F 16 min	3819	368	57.8	17.4	10	3984	1.1084	22914	21	
<i>UF Average</i>	<i>4061</i>	<i>397</i>	<i>64</i>	<i>18</i>	<i>10</i>	<i>4482</i>	<i>1.1133</i>	<i>24368</i>	<i>22</i>	
					Two Sides:	8964		48736	44	
						UF/(OF+UF)		1 - OF/F	UF/F	
					Solids Yield to UF:	0.853		0.869	0.761	
					Underflow flush (L/min):	2				
					Launder Wash (L/min):	21.8				
					Fluidisation (L/min):	18				
					Volume Balance: In =		90.8			
					Out =		92.7			
					Ratio:		0.98			
					Solids In/Out =		1.12			
					Average Yield	0.828				

Takes into account water from Launder and U/F Flush

TRUE U/F
Flowrate Solids Conc.
L/min wt.%
20.0 35.9

Gravity Separation and Desliming Using Inclined Channels Subject to Different G-Forces

CF154

				Solids Densit	2.65							
	Slurry weight (g)	Sub sample		Solids Conc. (wt. %)	Sample time (s)	Solids Rate (g/min)	Slurry Density (g/ml)	Mass Flow (g/min)	Volumetric Flow (L/min)			
		Slurry Weight (g)	Solids Weight (g)									
Feed 1	11707	208	63.3	30.4	-	19149	1.2338	62923	51			
Feed 2	8090	212	59.9	28.3	-	17486	1.2135	61888	51			
<i>Feed Average</i>	<i>9898.5</i>	<i>210</i>	<i>61.6</i>	<i>29.3</i>		<i>18318</i>	<i>1.2236</i>	<i>62405</i>	<i>51</i>			
O/F 8 min	10182	179	24.6	13.7	10	8396	1.0936	61092	56			
O/F 10 min	10723	231	32.3	14.0	10	8996	1.0954	64338	59			
O/F 12 min	11059	224	30.7	13.7	10	9094	1.0933	66354	61			
<i>O/F Average</i>	<i>10655</i>	<i>211</i>	<i>29</i>	<i>14</i>	<i>10</i>	<i>8829</i>	<i>1.0941</i>	<i>63928</i>	<i>58</i>			
U/F 8 min	4159	264	50.9	25.3	10	6315	1.1364	24954	22			
U/F 10 min	4222	218	43.5	24.7	10	6246	1.1419	25332	22			
U/F 12 min	4232	175	35.9	24.7	10	6284	1.1464	25392	22			
<i>UF Average</i>	<i>4204</i>	<i>219</i>	<i>43</i>	<i>25</i>	<i>10</i>	<i>6282</i>	<i>1.1416</i>	<i>25226</i>	<i>22</i>			
					Two Sides:	12563		50452	44			
						UF/(OF+UF)		1 - OF/F		UF/F		
					Solids Yield to UF:	0.587		0.518		0.686		
					Underflow flush (L/min):	2						
					Launder Wash (L/min):	21.8						
					Fluidisation (L/min):	18						
					Volume Balance: In =		92.8					
					Out =		102.6					
					Ratio:		0.90					
					Solids In/Out =		0.86					
					Average Yield =		0.597					

Takes into account water from Launder and U/F Flush

TRUE U/F	
Flowrate	Solids Conc.
L/min	wt. %
20.4	47.1

Appendix C: Experimental Data and Sampling

CF155

		Solids Density		2.65					
	Slurry weight (g)	Sub sample		Solids Conc. (wt. %)	Sample time (s)	Solids Rate (g/min)	Slurry Density (g/ml)	Mass Flow (g/min)	Volumetric Flow (L/min)
		Slurry Weight (g)	Solids Weight (g)						
Feed 1	15492	249	64.6	25.9	-	11449	1.1927	44128.3	37.0
Feed 2	14119	239	60.2	25.2	-	11053	1.1860	43882.2	37.0
<i>Feed Average</i>	<i>14805.5</i>	<i>244</i>	<i>62.4</i>	<i>25.6</i>		<i>11251</i>	<i>1.1893</i>	<i>44005.3</i>	<i>37.0</i>
O/F 8 min	6236	164	16.8	10.2	10	3833	1.0681	37416.0	35.0
O/F 12 min	5753	174	16.9	9.7	10	3353	1.0644	34518.0	32.4
O/F 16 min	5767	155	16.4	10.6	10	3661	1.0705	34602.0	32.3
<i>O/F Average</i>	<i>5919</i>	<i>164</i>	<i>17</i>	<i>10</i>	<i>10</i>	<i>3616</i>	<i>1.0677</i>	<i>35512.0</i>	<i>33.3</i>
U/F 8 min	3883	221	49.9	25.5	10	5951	1.1636	23298.0	20.0
U/F 12 min	3971	178	38.9	25.4	10	6058	1.1575	23826.0	20.6
U/F 16 min	4064	170	31.1	30.3	10	7381	1.1285	24384.0	21.6
<i>UF Average</i>	<i>3973</i>	<i>190</i>	<i>40</i>	<i>27</i>	<i>10</i>	<i>6463</i>	<i>1.1499</i>	<i>23836.0</i>	<i>20.7</i>
Two Sides:						12927		47672.0	41.5
						UF/(OF+UF)		1 - OF/F	UF/F
Solids Yield to UF:						0.781		0.679	1.149
Underflow flush (L/min):						2			
Launder Wash (L/min):						21.8			
Fluidisation (L/min):						18			
Volume Balance: In =							78.8		
Out =							74.7		
Ratio:							1.05		
Solids In/Out =							0.68		
Average Yield:							0.730		

Takes into account water from Launder and U/F Flush

TRUE U/F	
Flowrate	Solids Conc.
L/min	wt. %
17.7	54.1

Gravity Separation and Desliming Using Inclined Channels Subject to Different G-Forces

CF156

				Solids Density							
				2.65							
	Slurry weight (g)	Sub sample		Solids Conc. (wt. %)	Sample time (s)	Solids Rate (g/min)	Slurry Density (g/ml)	Mass Flow (g/min)	Volumetric Flow (L/min)		
		Slurry Weight (g)	Solids Weight (g)							Flowrate	Solids Conc.
Feed 1	14228	187	53.9	28.8	-	12295	1.2187	42655.2	35.0		
Feed 2	11848	255	73.9	29.0	-	12376	1.2202	42706.0	35.0		
<i>Feed Average</i>	<i>13038</i>	<i>221</i>	<i>63.9</i>	<i>28.9</i>		<i>12336</i>	<i>1.2194</i>	<i>42680.6</i>	<i>35.0</i>		
O/F 8 min	8148	287	10.5	3.7	10	1789	1.0233	48888.0	47.8		
O/F 14 min	8075	251	10.5	4.2	10	2027	1.0267	48450.0	47.2		
O/F 16 min	7863	267	10.2	3.8	10	1802	1.0244	47178.0	46.1		
<i>O/F Average</i>	<i>8029</i>	<i>268</i>	<i>10</i>	<i>4</i>	<i>10</i>	<i>1873</i>	<i>1.0248</i>	<i>48172.0</i>	<i>47.0</i>		
U/F 8 min	3869	225	41.0	21.0	10	4882	1.1280	23214.0	20.6		
U/F 14 min	4103	222	35.6	19.8	10	4865	1.1109	24618.0	22.2		
U/F 16 min	3963	230	41.7	21.2	10	5040	1.1273	23778.0	21.1		
<i>UF Average</i>	<i>3978</i>	<i>226</i>	<i>39</i>	<i>21</i>	<i>10</i>	<i>4929</i>	<i>1.1221</i>	<i>23870.0</i>	<i>21.3</i>		
Two Sides:						9858		47740.0	42.6		
						UF/(OF+UF)		1 - OF/F		UF/F	
						Solids Yield to UF:	0.840		0.848		0.799
						Underflow flush (L/min):	2				
						Launder Wash (L/min):	21.8				
						Fluidisation (L/min):	30				
						Volume Balance: In =		88.8			
						Out =		89.6			
						Ratio:		0.99			
						Solids In/Out =		1.05			
						Average Yield:		0.829			

Takes into account water from Launder and U/F Flush

TRUE U/F	
Flowrate	Solids Conc.
L/min	wt. %
18.8	41.2

Appendix C: Experimental Data and Sampling

CF157

			Solids Density	2.65									
		Sub sample											
	Slurry weight (g)	Slurry Weight (g)	Solids Weight (g)	Solids Conc. (wt. %)	Sample time (s)	Solids Rate (g/min)	Slurry Density (g/ml)	Mass Flow (g/min)	Volumetric Flow (L/min)				
Feed 1	14132	293	89.9	30.7	-	19723	1.2362	64280.3	52.0				
Feed 2	13337	274	80.9	29.5	-	18812	1.2252	63712.9	52.0				
Feed Average	13734.5	283.5	85.4	30.1		19267	1.2307	63996.6	52.0				
O/F 10 min	9050	299	38.1	12.7	10	6919	1.0862	54300.0	50.0				
O/F 12 min	9912	216	27.2	12.6	10	7489	1.0851	59472.0	54.8				
O/F 14 min	9473	307	35.7	11.6	10	6610	1.0781	56838.0	52.7				
O/F Average	9478	274	34	12	10	7006	1.0831	56870.0	52.5				
U/F 10 min	4138	212	42.9	24.0	10	5961	1.1758	24828.0	21.1				
U/F 12 min	4121	252	54.7	24.0	10	5940	1.1759	24726.0	21.0				
U/F 14 min	4033	170	37.1	24.2	10	5848	1.1771	24198.0	20.6				
UF Average	4097	211	45	24	10	5916	1.1763	24584.0	20.9				
					Two Sides:	11833		49168.0	41.8			18.0	46.6
						UF/(OF+UF)		1 - OF/F		UF/F			
					Solids Yield to UF:	0.631		0.641		0.614			
					Underflow flush (L/min):	2							
					Launder Wash (L/min):	21.8							
					Fluidisation (L/min):	18							
					Volume Balance: In =		93.8						
					Out =		94.3						
					Ratio:		0.99						
					Solids In/Out =		1.03						
					Average Yield =		0.629						

Takes into account water from Launder and U/F Flush

TRUE U/F Flowrate Solids Conc. L/min wt.%

Gravity Separation and Desliming Using Inclined Channels Subject to Different G-Forces

CF158

		Solids Density		2.65					
	Slurry weight (g)	Sub sample		Solids Conc. (wt. %)	Sample time (s)	Solids Rate (g/min)	Slurry Density (g/ml)	Mass Flow (g/min)	Volumetric Flow (L/min)
		Slurry Weight (g)	Solids Weight (g)						
Feed 1	13845	273	82.0	30.0	-	20099	1.2300	66914.4	54.4
Feed 2	13133	277	84.0	30.3	-	20337	1.2328	67062.4	54.4
<i>Feed Average</i>	<i>13489</i>	<i>275</i>	<i>83.0</i>	<i>30.2</i>		<i>20218</i>	<i>1.2314</i>	<i>66988.4</i>	<i>54.4</i>
O/F 10 min	6903	217	12.0	5.5	10	2290	1.0357	41418.0	40.0
O/F 12 min	6998	252	14.0	5.6	10	2333	1.0358	41988.0	40.5
O/F 14 min	6772	227	12.0	5.3	10	2148	1.0340	40632.0	39.3
<i>O/F Average</i>	<i>6891</i>	<i>232</i>	<i>13</i>	<i>5</i>	<i>10</i>	<i>2257</i>	<i>1.0352</i>	<i>41346.0</i>	<i>39.9</i>
U/F 10 min	5504	328	86.0	26.2	10	8659	1.1951	33024.0	27.6
U/F 12 min	5443	328	85.0	25.9	10	8463	1.1924	32658.0	27.4
U/F 14 min	5609	286	74.0	25.9	10	8708	1.1920	33654.0	28.2
<i>UF Average</i>	<i>5519</i>	<i>314</i>	<i>82</i>	<i>26</i>	<i>10</i>	<i>8610</i>	<i>1.1932</i>	<i>33112.0</i>	<i>27.8</i>
Two Sides:						17220		66224.0	55.5
						UF/(OF+UF)		1 - OF/F	UF/F
Solids Yield to UF:						0.883		0.887	0.852
Underflow flush (L/min):						2			
Launder Wash (L/min):						21.8			
Fluidisation (L/min):						18			
Volume Balance: In =							96.2		
Out =							95.4		
Ratio:							1.01		
Solids In/Out =							1.04		
Average Yield =							0.874		

Takes into account water from Launder and U/F Flush

TRUE U/F	
Flowrate	Solids Conc.
L/min	wt. %
31.7	40.6

Appendix C: Experimental Data and Sampling

CF159

		Solids Density		2.65						
		Sub sample								
	Slurry weight (g)	Slurry Weight (g)	Solids Weight (g)	Solids Conc. (wt. %)	Sample time (s)	Solids Rate (g/min)	Slurry Density (g/ml)	Mass Flow (g/min)	Volumetric Flow (L/min)	
Feed 1	12437	398	111.2	27.9		38897	1.2106	139219.1	115.0	
Feed 2	12164	280	74.6	26.6		36733	1.1989	137871.4	115.0	
<i>Feed Average</i>	<i>12300.5</i>	<i>339</i>	<i>92.9</i>	<i>27.3</i>		<i>37815</i>	<i>1.2047</i>	<i>138545.3</i>	<i>115.0</i>	
O/F 4 min	13581	205	36.4	17.8	7	20670	1.1243	116408.6	103.5	
O/F 6 min	12670	158	26.3	16.6	7	18077	1.1156	108600.0	97.3	
O/F 8 min	15422	308	50.0	16.2	7	21459	1.1124	132188.6	118.8	
<i>O/F Average</i>	<i>13891</i>	<i>224</i>	<i>38</i>	<i>17</i>	<i>7</i>	<i>20069</i>	<i>1.1175</i>	<i>119065.7</i>	<i>106.6</i>	
U/F 4 min	5827	228	65.9	28.9	10	10105	1.2195	34962.0	28.7	
U/F 6 min	5657	193	55.7	28.9	10	9796	1.2191	33942.0	27.8	
U/F 8 min	5832	389	80.4	20.7	10	7232	1.1477	34992.0	30.5	
<i>UF Average</i>	<i>5772</i>	<i>270</i>	<i>67</i>	<i>26</i>	<i>10</i>	<i>9044</i>	<i>1.1954</i>	<i>34632.0</i>	<i>29.0</i>	
Two Sides:						18089		69264.0	58.0	
						UF/(OF+UF)		1 - OF/F	UF/F	
Solids Yield to UF:						0.457		0.433	0.478	
Underflow flush (L/min):						2				
Launder Wash (L/min):						21.8				
Fluidisation (L/min):						18				
Volume Balance: In =							156.8			
Out =							164.6			
Ratio:							0.95			
Solids In/Out =							0.99			
Average Yield =							0.456			

Takes into account water from Launder and U/F Flush

TRUE U/F	
Flowrate	Solids Conc.
L/min	wt. %
34.2	39.8

Gravity Separation and Desliming Using Inclined Channels Subject to Different G-Forces

CF160

		Solids Density		2.65					
	Slurry weight (g)	Sub sample Slurry Weight (g)	Solids Weight (g)	Solids Conc. (wt. %)	Sample time (s)	Solids Rate (g/min)	Slurry Density (g/ml)	Mass Flow (g/min)	Volumetric Flow (L/min)
Feed 1	13076	173	45.1	26.1		28009	1.1938	107439.4	90.0
Feed 2	12800	321	84.5	26.3		28336	1.1960	107643.2	90.0
<i>Feed Average</i>	<i>12938</i>	<i>247</i>	<i>64.8</i>	<i>26.2</i>		<i>28172</i>	<i>1.1949</i>	<i>107541.3</i>	<i>90.0</i>
OF 6 min	13258	168	14.6	8.7	10	6913	1.0572	79548.0	75.2
OF 8 min	13237	179	15.1	8.4	10	6700	1.0554	79422.0	75.3
O/F 10 min	13077	287	23.5	8.2	10	6425	1.0537	78462.0	74.5
<i>O/F Average</i>	<i>13191</i>	<i>211</i>	<i>18</i>	<i>8</i>	<i>10</i>	<i>6679</i>	<i>1.0555</i>	<i>79144.0</i>	<i>75.0</i>
UF 6 min	5731	187	57.1	30.5	10	10500	1.2348	34386.0	27.8
UF 8 min	5701	157	48.1	30.6	10	10480	1.2357	34206.0	27.7
U/F 10 min	5838	352	111.5	31.7	10	11096	1.2457	35028.0	28.1
<i>UF Average</i>	<i>5757</i>	<i>232</i>	<i>72</i>	<i>31</i>	<i>10</i>	<i>10692</i>	<i>1.2387</i>	<i>34540.0</i>	<i>27.9</i>
Two Sides:						21383		69080.0	55.8
						UF/(OF+UF)		1 - OF/F	UF/F
Solids Yield to UF:						0.769		0.773	0.755
Underflow flush (L/min):						2			
Launder Wash (L/min):						21.8			
Fluidisation (L/min):						18			
Volume Balance: In =							131.8		
Out =							130.8		
Ratio:							1.01		
Solids In/Out =							1.00		
Average Yield =							0.766		

Takes into account water from Launder and U/F Flush

TRUE U/F	
Flowrate	Solids Conc.
L/min	wt.%
32.0	47.2

Appendix C: Experimental Data and Sampling

CF162

				Solids Density	2.65						
	Slurry weight (g)	Sub sample		Solids Conc. (wt. %)	Sample time (s)	Solids Rate (g/min)	Slurry Density (g/ml)	Mass Flow (g/min)	Volumetric Flow (L/min)		
	Slurry weight (g)	Slurry Weight (g)	Solids Weight (g)								
Feed 1	14167	380	111.5	29.3		31557	1.2235	107548.7	87.9		
Feed 2	14703	342	101.8	29.8		32117	1.2275	107897.2	87.9		
<i>Feed Average</i>	<i>14435</i>	<i>361</i>	<i>106.7</i>	<i>29.6</i>		<i>31837</i>	<i>1.2255</i>	<i>107723.0</i>	<i>87.9</i>		
OF 6 min	15948	383	45.6	11.9	10	11393	1.0801	95688.0	88.6		
OF 8 min	15451	198	22.5	11.4	10	10535	1.0761	92706.0	86.1		
O/F 10 min	15876	209	23.0	11.0	10	10483	1.0736	95256.0	88.7		
<i>O/F Average</i>	<i>15758</i>	<i>263</i>	<i>30</i>	<i>11</i>	<i>10</i>	<i>10803</i>	<i>1.0766</i>	<i>94550.0</i>	<i>87.8</i>		
UF 6 min	5722	191	55.0	28.8	10	9886	1.2185	34332	28.2		
UF 8 min	5776	193	55.9	29.0	10	10038	1.2200	34656	28.4		
U/F 10 min	6133	181	53.7	29.7	10	10917	1.2266	36798	30.0		
<i>UF Average</i>	<i>5877</i>	<i>188</i>	<i>55</i>	<i>29</i>	<i>10</i>	<i>10280</i>	<i>1.2217</i>	<i>35262.0</i>	<i>28.9</i>		
					Two Sides:	20561		70524.0	57.7		
						UF/(OF+UF)		1 - OF/F	UF/F		
						Solids Yield to UF:	0.662	0.674	0.640		
						Underflow flush (L/min):	2				
						Launder Wash (L/min):	21.8				
						Fluidisation (L/min):	34				
						Volume Balance: In =	147.7				
						Out =	145.5				
						Ratio:	1.01				
						Solids In/Out =	1.02				
						Average Yield =	0.659				

Takes into account water from Launder and U/F Flush

TRUE U/F	
Flowrate	Solids Conc.
L/min	wt.%
33.9	44.0

Gravity Separation and Desliming Using Inclined Channels Subject to Different G-Forces

CF163

				Solids Density	2.65								
		Sub sample											
	Slurry weight (g)	Slurry Weight (g)	Solids Weight (g)	Solids Conc. (wt. %)	Sample time (s)	Solids Rate (g/min)	Slurry Density (g/ml)	Mass Flow (g/min)	Volumetric Flow (L/min)				
Feed 1	12396	222	67.8	30.5		30810	1.2348	100883.9	81.7				
Feed 2	12315	233	70.0	30.0		30193	1.2301	100499.4	81.7				
<i>Feed Average</i>	<i>12355.5</i>	<i>227.5</i>	<i>68.9</i>	<i>30.3</i>		<i>30502</i>	<i>1.2325</i>	<i>100691.6</i>	<i>81.7</i>				
OF 1 min	13629	250	31.6	12.6	10	10336	1.0854	81774.0	75.3				
OF 2 min	13281	249	32.4	13.0	10	10369	1.0882	79686.0	73.2				
OF 4 min	13313	226	24.3	10.8	10	8589	1.0718	79878.0	74.5				
OF 6 min	14125	214	24.1	11.3	10	9544	1.0754	84750.0	78.8				
O/F 8 min	14258	295	33.0	11.2	10	9570	1.0749	85548.0	79.6				
<i>O/F Average</i>	<i>13721</i>	<i>247</i>	<i>29</i>	<i>12</i>	<i>10</i>	<i>9682</i>	<i>1.0791</i>	<i>82327.2</i>	<i>76.3</i>				
UF 1 min	5346	216	55.6	25.7	10	8257	1.1909	32076.0	26.9				
UF 2 min	5506	181	49.0	27.1	10	8943	1.2027	33036.0	27.5				
UF 4 min	5730	181	57.6	31.8	10	10941	1.2471	34380	27.6				
UF 6 min	5852	192	61.8	32.2	10	11302	1.2506	35112	28.1				
U/F 8 min	5770	286	91.9	32.1	10	11124	1.2501	34620	27.7				
<i>UF Average</i>	<i>5641</i>	<i>211</i>	<i>63</i>	<i>30</i>	<i>10</i>	<i>10113</i>	<i>1.2283</i>	<i>33844.8</i>	<i>27.5</i>				
					Two Sides:	20227		67689.6	55.1				
						UF/(OF+UF)		1 - OF/F		UF/F			
					Solids Yield to UF:	0.679		0.683		0.670			
					Underflow flush (L/min):	2							
					Launder Wash (L/min):	21.8							
					Fluidisation (L/min):	24							
					Volume Balance: In =		129.5						
					Out =		131.4						
					Ratio:		0.99						
					Solids In/Out =		1.02						
					Average Yield =		0.677						

Takes into account water from Launder and U/F Flush

TRUE U/F	
Flowrate	Solids Conc.
L/min	wt. %
31.3	46.1

Appendix C: Experimental Data and Sampling

CF164

		Solids Density		2.65					
	Slurry weight (g)	Sub sample		Solids Conc. (wt. %)	Sample time (s)	Solids Rate (g/min)	Slurry Density (g/ml)	Mass Flow (g/min)	Volumetric Flow (L/min)
		Slurry Weight (g)	Solids Weight (g)						
Feed 1	16072	314	97.2	31.0		33975	1.2388	109754.2	88.6
Feed 2	14116	242	74.2	30.7		33576	1.2360	109505.6	88.6
<i>Feed Average</i>	<i>15094</i>	<i>278</i>	<i>85.7</i>	<i>30.8</i>		<i>33775</i>	<i>1.2374</i>	<i>109629.9</i>	<i>88.6</i>
OF 4 min	11343	202	19.6	9.7	10	6604	1.0643	68058.0	63.9
OF 6 min	12986	169	17.6	10.4	10	8114	1.0693	77916.0	72.9
OF 8 min	11486	159	15.6	9.8	10	6762	1.0651	68916.0	64.7
<i>O/F Average</i>	<i>11938</i>	<i>177</i>	<i>18</i>	<i>10</i>	<i>10</i>	<i>7160</i>	<i>1.0662</i>	<i>71630.0</i>	<i>67.2</i>
UF 4 min	5926	222	72.7	32.7	10	11644	1.2561	35556	28.3
UF 6 min	5987	207	71.8	34.7	10	12460	1.2755	35922	28.2
UF 8 min	5830	212	73.4	34.6	10	12111	1.2748	34980	27.4
<i>UF Average</i>	<i>5914</i>	<i>214</i>	<i>73</i>	<i>34</i>	<i>10</i>	<i>12072</i>	<i>1.2688</i>	<i>35486.0</i>	<i>28.0</i>
Two Sides:						24143		70972.0	55.9
						UF/(OF+UF)		1 - OF/F	UF/F
Solids Yield to UF:						0.781		0.799	0.719
Underflow flush (L/min):						2			
Launder Wash (L/min):						21.8			
Fluidisation (L/min):						12			
Volume Balance: In =							124.4		
Out =							120.6		
Ratio:							1.03		
Solids In/Out =							1.08		
Average Yield =							0.766		

Takes into account water from Launder and U/F Flush

TRUE U/F	
Flowrate	Solids Conc.
L/min	wt. %
32.1	51.2

Gravity Separation and Desliming Using Inclined Channels Subject to Different G-Forces

CF184

		Solids Density		3.8					
	Slurry weight (g)	Sub sample		Solids Conc. (wt.%)	Sample time (s)	Solids Rate (g/min)	Slurry Density (g/ml)	Mass Flow (g/min)	Volumetric Flow (L/min)
	Slurry weight (g)	Slurry Weight (g)	Solids Weight (g)	(wt.%)	(s)	(g/min)	(g/ml)	(g/min)	(L/min)
Feed 1	13308	575	27.9	4.9	-	7045	1.0371	145191	140
Feed 2	13234	633	28.8	4.5	-	6591	1.0347	144856	140
<i>Feed Average</i>	<i>13271</i>	<i>604</i>	<i>28.4</i>	<i>4.7</i>		<i>6818</i>	<i>1.0359</i>	<i>145024</i>	<i>140</i>
OF 3 min	13431	269	4.8	1.8	6	2397	1.0133	134310	133
OF 4 min	15230	263	5.5	2.1	7	2730	1.0157	130543	129
OF 5 min	15606	430	7.6	1.8	7	2364	1.0132	133766	132
<i>OF Average</i>	<i>14756</i>	<i>321</i>	<i>6.0</i>	<i>1.9</i>		<i>2497</i>	<i>1.0141</i>	<i>132873</i>	<i>131</i>
UF 3 min	5653	276	14.1	5.1	10	1733	1.0391	33918	33
UF 4 min	5624	407	25.2	6.2	10	2089	1.0478	33744	32
UF 5 min	11264	397	22.4	5.6	20	1907	1.0434	33792	32
<i>UF Average</i>	<i>7514</i>	<i>360</i>	<i>20.6</i>	<i>5.4</i>		<i>1820</i>	<i>1.0434</i>	<i>33818</i>	<i>32</i>
Two Sides:						3639		67636	65
						UF/(OF+UF)		1 - OF/F	UF/F
						Solids Yield to UF:	0.593	0.634	0.534
						Underflow flush (L/min):	2		
						Launder Wash (L/min):	21.8		
						Fluidisation (L/min):	36		
						Volume Balance: In =		199.8	
						Out =		195.9	
						Ratio:		1.02	
						Solids In/Out =		1.11	
						Average Yield =		0.587	

Takes into account water from Launder and U/F Flush

TRUE U/F	
Flowrate	Solids Conc.
L/min	wt.%
41.0	8.3

CF185

		Solids Density		3.8					
	Slurry weight (g)	Sub sample		Solids Conc. (wt. %)	Sample time (s)	Solids Rate (g/min)	Slurry Density (g/ml)	Mass Flow (g/min)	Volumetric Flow (L/min)
		Slurry Weight (g)	Solids Weight (g)						
Feed 1	14668	153	28.0	18.3	-	30672	1.1559	167600	145
Feed 2	11015	334	60.7	18.2	-	30426	1.1546	167419	145
<i>Feed Average</i>	<i>12841</i>	<i>244</i>	<i>44.4</i>	<i>18.2</i>		<i>30549</i>	<i>1.1552</i>	<i>167510</i>	<i>145</i>
OF 3 min	16965	295	24.2	8.2	7	11929	1.0643	145413	137
OF 4 min	16543	148	11.9	8.0	7	11401	1.0630	141797	133
OF 5 min	17050	349	28.0	8.0	7	11725	1.0628	146143	138
<i>OF Average</i>	<i>16853</i>	<i>264</i>	<i>21.4</i>	<i>8.1</i>		<i>11685</i>	<i>1.0634</i>	<i>144451</i>	<i>136</i>
UF 3 min	5652	223	52.9	23.7	10	8045	1.2118	33912	28
UF 4 min	6462	246	55.8	22.7	10	8795	1.2007	38772	32
UF 5 min	6671	330	76.4	23.2	10	9267	1.2057	40026	33
<i>UF Average</i>	<i>6262</i>	<i>266</i>	<i>61.7</i>	<i>23.2</i>		<i>8702</i>	<i>1.2061</i>	<i>37570</i>	<i>31</i>
Two Sides:						17404		75140	62
						UF/(OF+UF)	1 - OF/F	UF/F	
Solids Yield to UF:						0.598		0.616	0.572
Underflow flush (L/min):						2			
Launder Wash (L/min):						21.8			
Fluidisation (L/min):						36			
Volume Balance: In =							204.8		
Out =							198.2		
Ratio:							1.03		
Solids In/Out =							1.05		
Average Yield =							0.595		

Takes into account water from Launder and U/F Flush

TRUE U/F	
Flowrate	Solids Conc.
L/min	wt. %
38.5	33.9

Gravity Separation and Desliming Using Inclined Channels Subject to Different G-Forces

CF186

		Solids Density		3.8					
	Slurry weight (g)	Sub sample		Solids Conc. (wt. %)	Sample time (s)	Solids Rate (g/min)	Slurry Density (g/ml)	Mass Flow (g/min)	Volumetric Flow (L/min)
		Slurry Weight (g)	Solids Weight (g)						
Feed 1	9677	243	60.1	24.7	-	42523	1.2229	171933	141
Feed 2	12307	275	63.8	23.2	-	39345	1.2062	169591	141
<i>Feed Average</i>	<i>10992</i>	<i>259</i>	<i>62.0</i>	<i>24.0</i>		<i>40934</i>	<i>1.2145</i>	<i>170762</i>	<i>141</i>
OF 2 min	16376	169	20.4	12.1	7	16944	1.0976	140366	128
OF 2.75 min	16324	150	17.9	11.9	7	16697	1.0964	139920	128
OF 3.5 min	16464	327	37.9	11.6	7	16356	1.0934	141120	129
<i>OF Average</i>	<i>16388</i>	<i>215</i>	<i>25.4</i>	<i>11.9</i>		<i>16666</i>	<i>1.0958</i>	<i>140469</i>	<i>128</i>
UF 2 min	6630	258	64.8	25.1	10	9991	1.2271	39780	32
UF 2.75 min	6540	252	68.2	27.1	10	10620	1.2491	39240	31
UF 3.5 min	6712	257	73.4	28.6	10	11502	1.2665	40272	32
<i>UF Average</i>	<i>6627</i>	<i>256</i>	<i>68.8</i>	<i>26.9</i>		<i>10704</i>	<i>1.2476</i>	<i>39764</i>	<i>32</i>
Two Sides:						21409		79528	64
						UF/(OF+UF)	1 - OF/F	UF/F	
Solids Yield to UF:						0.562	0.593	0.544	
Underflow flush (L/min):						2			
Launder Wash (L/min):						21.8			
Fluidisation (L/min):						34			
Volume Balance: In =						198.4			
Out =						191.9			
Ratio:						1.03			
Solids In/Out =						1.08			
Average Yield =						0.566			

Takes into account water from Launder and U/F Flush

TRUE U/F	
Flowrate	Solids Conc.
L/min	wt. %
40.0	38.4

CF188

		Solids Density		3.8					
	Slurry weight (g)	Sub sample Slurry Weight (g)	Solids Weight (g)	Solids Conc. (wt. %)	Sample time (s)	Solids Rate (g/min)	Slurry Density (g/ml)	Mass Flow (g/min)	Volumetric Flow (L/min)
Feed 1	12093	343	31.8	9.3	-	14329	1.0733	154558	144
Feed 2	11952	343	26.8	7.8	-	11939	1.0611	152797	144
<i>Feed Average</i>	<i>12023</i>	<i>343</i>	<i>29.3</i>	<i>8.5</i>		<i>13134</i>	<i>1.0672</i>	<i>153678</i>	<i>144</i>
OF 3 min	15520	279	3.4	1.2	7	1621	1.0091	133029	132
OF 4 min	15216	348	4.2	1.2	7	1574	1.0090	130423	129
OF 5 min	15311	366	4.4	1.2	7	1578	1.0089	131237	130
<i>OF Average</i>	<i>15349</i>	<i>331</i>	<i>4.0</i>	<i>1.2</i>		<i>1591</i>	<i>1.0090</i>	<i>131563</i>	<i>130</i>
UF 3 min	5955	316	40.5	12.8	10	4579	1.1043	35730	32
UF 4 min	6176	351	42.8	12.2	10	4519	1.0987	37056	34
UF 5 min	6315	343	45.6	13.3	10	5037	1.1086	37890	34
<i>UF Average</i>	<i>6149</i>	<i>337</i>	<i>43.0</i>	<i>12.8</i>		<i>4712</i>	<i>1.1039</i>	<i>36892</i>	<i>33</i>
Two Sides:						9423		73784	67
						UF/(OF+UF)	1 - OF/F	UF/F	
Solids Yield to UF:						0.856	0.879	0.789	
Underflow flush (L/min):						2			
Launder Wash (L/min):						21.8			
Fluidisation (L/min):						36			
Volume Balance: In =						203.8			
Out =						197.2			
Ratio:						1.03		43.0	
Solids In/Out =						1.19			
Average Yield =						0.841			

Takes into account water from Launder and U/F Flush

TRUE U/F	
Flowrate	Solids Conc.
L/min	wt. %
43.0	18.9

Gravity Separation and Desliming Using Inclined Channels Subject to Different G-Forces

CF195

		Solids Density 3.8										
	Slurry weight (g)	Sub sample Slurry Weight (g)	Solids Weight (g)	Solids Conc. (wt. %)	Sample time (s)	Solids Rate (g/min)	Slurry Density (g/ml)	Mass Flow (g/min)	Volumetric Flow (L/min)			
Feed 1	16382	314	59.0	18.8	-	32496	1.1607	172944	149			
Feed 2	10097	353	64.0	18.1	-	31179	1.1542	171974	149			
<i>Feed Average</i>	<i>13240</i>	<i>334</i>	<i>61.5</i>	<i>18.5</i>		<i>31838</i>	<i>1.1574</i>	<i>172459</i>	<i>149</i>			
OF 4 min	15485	378	18.0	4.8	7	6320	1.0364	132729	128			
OF 5 min	14953	390	17.0	4.4	7	5587	1.0332	128169	124			
<i>OF Average</i>	<i>15219</i>	<i>384</i>	<i>17.5</i>	<i>4.6</i>		<i>5954</i>	<i>1.0348</i>	<i>130449</i>	<i>126</i>			
UF 4 min	8259	210	58.0	27.6	10	13686	1.2555	49554	39			
UF 5 min south	8425	414	124.0	30.0	10	15141	1.2832	50550	39			
UF 5 min north	8365	367	97.0	26.4	10	13265	1.2419	50190	40			
<i>UF Average</i>	<i>8342</i>	<i>330</i>	<i>93.0</i>	<i>28.0</i>		<i>14031</i>	<i>1.2602</i>	<i>50098</i>	<i>40</i>			
Two Sides:						28062		100196	80			
						UF/(OF+UF)		1 - OF/F		UF/F		
						Solids Yield to UF:	0.825	0.813		0.900002		
						Underflow flush (L/min):	2					
						Launder Wash (L/min):	21.8					
						Fluidisation (L/min):	34					
						Volume Balance: In =	206.8					
						Out =	205.6					
						Ratio:	1.01					
						Solids In/Out =	0.94					
						Average Yield =	0.846					

Takes into account water from Launder and U/F Flush

TRUE U/F	
Flowrate L/min	Solids Conc. wt.%
55.7	36.7

CF196

		Solids Density		3.8					
	Slurry weight (g)	Sub sample Slurry Weight (g)	Solids Weight (g)	Solids Conc. (wt. %)	Sample time (s)	Solids Rate (g/min)	Slurry Density (g/ml)	Mass Flow (g/min)	Volumetric Flow (L/min)
Feed 1	12642	232	33.0	14.2	-	23675	1.1171	166445	149
Feed 2	8471	563	55.0	9.8	-	15685	1.0776	160557	149
Feed Average	10557	398	44.0	14.2		23675	1.0973	163501	149
OF 4 min	15521	296	3.0	1.0	7	1348	1.0075	133037	132
OF 5.5 min	15268	451	6.0	1.3	7	1741	1.0099	130869	130
OF Average	15395	374	4.5	1.2		1545	1.0087	131953	131
UF 4 min	8129	203	49.5	24.4	10	11893	1.2190	48774	40
UF 5.5 min	12132	209	55.0	26.3	15	12771	1.2405	48528	39
UF Average	10131	206	52.3	25.4		12332	1.2298	48651	40
Two Sides:						24664		97302	79
						UF/(OF+UF)	1 - OF/F	UF/F	
Solids Yield to UF:						0.941	0.902	1.041745	
Underflow flush (L/min):						2			
Launder Wash (L/min):						21.8			
Fluidisation (L/min):						34			
Volume Balance: In =						206.8			
Out =						209.9			
Ratio:						0.99			
Solids In/Out =						0.90			
Average Yield =						0.921			

Takes into account water from Launder and U/F Flush

TRUE U/F	
Flowrate	Solids Conc.
L/min	wt. %
55.3	33.6

CF197

		Solids Density		3.8					
	Slurry weight (g)	Sub sample		Solids Conc. (wt. %)	Sample time (s)	Solids Rate (g/min)	Slurry Density (g/ml)	Mass Flow (g/min)	Volumetric Flow (L/min)
		Slurry Weight (g)	Solids Weight (g)						
Feed 1	11323				-				
Feed 2	8474	248	49.0	19.8	-	31912	1.1704	161514	138
<i>Feed Average</i>	<i>9899</i>	<i>248</i>	<i>49.0</i>	<i>19.8</i>		<i>31912</i>	<i>1.1704</i>	<i>161514</i>	<i>138</i>
OF 4 min	17417	257	14.0	5.4	7	8132	1.0418	149289	143
OF 4.5 min	16964	176	10.0	5.7	7	8262	1.0437	145406	139
<i>OF Average</i>	<i>17191</i>	<i>217</i>	<i>12.0</i>	<i>5.6</i>		<i>8197</i>	<i>1.0428</i>	<i>147347</i>	<i>141</i>
UF 4 min	5898	124	41.0	33.1	10	11701	1.3221	35388	27
UF 4.5 min	6060	163	53.0	32.5	10	11823	1.3151	36360	28
<i>UF Average</i>	<i>5979</i>	<i>144</i>	<i>47.0</i>	<i>32.8</i>		<i>11762</i>	<i>1.3186</i>	<i>35874</i>	<i>27</i>
Two Sides:						23523		71748	54
						UF/(OF+UF)		1 - OF/F	UF/F
						Solids Yield to UF:	0.742	0.743	0.737
						Underflow flush (L/min):	2		
						Launder Wash (L/min):	21.8		
						Fluidisation (L/min):	34		
						Volume Balance: In =	195.8		
						Out =	195.7		
						Ratio:	1.00		
						Solids In/Out =	1.01		
						Average Yield =	0.741		

Takes into account water from Launder and U/F Flush

TRUE U/F	
Flowrate	Solids Conc.
L/min	wt. %
30.6	49.1

CF198

		Solids Density		3.8					
	Slurry weight (g)	Sub sample Slurry Weight (g)	Solids Weight (g)	Solids Conc. (wt. %)	Sample time (s)	Solids Rate (g/min)	Slurry Density (g/ml)	Mass Flow (g/min)	Volumetric Flow (L/min)
Feed 1	7548				-				
Feed 2	7802	153	14.0	9.2	-	14914	1.0723	162989	152
<i>Feed Average</i>	7675	153	14.0	9.2		14914	1.0723	162989	152
OF 4 min	12896	196	2.0	1.0	5	1579	1.0076	154752	154
OF 5.5 min	13142	380	3.0	0.8	5	1245	1.0059	157704	157
<i>OF Average</i>	13019	288	2.5	0.9		1412	1.0067	156228	155
UF 4 min	5842	171	39.0	22.8	10	7994	1.2020	35052	29
UF 5.5 min	8812	223	56.0	25.1	15	8852	1.2270	35248	29
<i>UF Average</i>	7327	197	47.5	24.0		8423	1.2145	35150	29
Two Sides:						16846		70300	58
						UF/(OF+UF)	1 - OF/F	UF/F	
						Solids Yield to UF:	0.923	0.905	1.130
						Underflow flush (L/min):	2		
						Launder Wash (L/min):	21.8		
						Fluidisation (L/min):	33		
						Volume Balance: In =	208.8		
						Out =	213.1		
						Ratio:	0.98		
						Solids In/Out =	0.82		
						Average Yield =	0.914		

Takes into account water from Launder and U/F Flush

TRUE U/F	
Flowrate L/min	Solids Conc. wt. %
34.1	36.2

CF200

Solids Density 3.8									
	Slurry weight (g)	Sub sample Slurry Weight (g)	Solids Weight (g)	Solids Conc. (wt. %)	Sample time (s)	Solids Rate (g/min)	Slurry Density (g/ml)	Mass Flow (g/min)	Volumetric Flow (L/min)
Feed 1	6431				-				
Feed 2	10899	326	62.0	19.0	-	25436	1.1630	133742	115
Feed Average	8665	326	62.0	19.0		25436	1.1630	133742	115
OF 3 min	17315								
OF 5 min	15111	291	15.0	5.2	6	7789	1.0395	151110	145
OF Average	16213	291	15.0	5.2		7789	1.0395	151110	145
UF 4 min	5613								
UF 5 min	5722	251	75.0	29.9	10	10259	1.2823	34332	27
UF Average	5668	251	75.0	29.9		10259	1.2823	34332	27
Two Sides:						20517		68664	54
						UF/(OF+UF)		1 - OF/F	UF/F
Solids Yield to UF:						0.725		0.694	0.807
Underflow flush (L/min):						2			
Launder Wash (L/min):						21.8			
Fluidisation (L/min):						64			
Volume Balance: In =							202.8		
Out =							198.9		
Ratio:							1.02		
Solids In/Out =							0.90		
Average Yield =							0.742		

Takes into account water from Launder and U/F Flush

TRUE U/F	
Flowrate	Solids Conc.
L/min	wt. %
29.7	45.7

CF201

		Solids Density		3.8					
	Slurry weight (g)	Sub sample		Solids Conc. (wt. %)	Sample time (s)	Solids Rate (g/min)	Slurry Density (g/ml)	Mass Flow (g/min)	Volumetric Flow (L/min)
	Slurry weight (g)	Slurry Weight (g)	Solids Weight (g)						
Feed 1	9966				-				
Feed 2	11107	303	59	19.5	-	23870	1.1675	122589	105.0
<i>Feed Average</i>	<i>10536.5</i>	<i>303</i>	<i>59</i>	<i>19.5</i>		<i>23870.41</i>	<i>1.168</i>	<i>122588.7</i>	<i>105</i>
OF 4 min	13565				6				
OF 5 min	12658				6				
OF 6 min	13993	375	26	6.9	6	9702	1.0538	139930.0	132.8
<i>OF Average</i>	<i>13405</i>	<i>375</i>	<i>26</i>	<i>6.9</i>	<i>6</i>	<i>9702</i>	<i>1</i>	<i>139930</i>	<i>132.8</i>
UF 4 min	6476				15				
UF 5 min	6686				15				
UF 6 min	6847	275	55	20.0	15	5478	1.1728	27388	23.4
<i>UF Average</i>	<i>6670</i>	<i>275</i>	<i>55</i>	<i>20</i>	<i>15</i>	<i>5478</i>	<i>1</i>	<i>27388</i>	<i>23</i>
Two Sides:						10955		54776.0	46.7
						UF/(OF+UF)		1 - OF/F	UF/F
						Solids Yield to UF:	0.530	0.594	0.459
						Underflow flush (L/min):	2		
						Launder Wash (L/min):	21.8		
						Fluidisation (L/min):	50		
						Volume Balance: In =	178.8		
						Out =	179.5		
						Ratio:	1.00		
						Solids In/Out =	1.16		
						Average Yield =	0.562		

Takes into account water from Launder and U/F Flush

TRUE U/F	
Flowrate	Solids Conc.
L/min	wt.%
22.9	35.4

CF202

		Solids Density		3.8					
	Slurry weight (g)	Sub sample Slurry Weight (g)	Solids Weight (g)	Solids Conc. (wt. %)	Sample time (s)	Solids Rate (g/min)	Slurry Density (g/ml)	Mass Flow (g/min)	Volumetric Flow (L/min)
Feed 1	10448				-				
Feed 2	11826	210	39	18.6	-	22591	1.1585	121646	105.0
<i>Feed Average</i>	<i>11137</i>	<i>210</i>	<i>39</i>	<i>18.6</i>		<i>22591.46</i>	<i>1.159</i>	<i>121646.3</i>	<i>105</i>
OF 5 min	15250				6				
OF 6 min	14601	318	23.1	7.3	6	10606	1.0566	146010.0	138.2
<i>OF Average</i>	<i>14926</i>	<i>318</i>	<i>23</i>	<i>7.3</i>	<i>6</i>	<i>10606</i>	<i>1</i>	<i>146010</i>	<i>138.2</i>
UF 5 min	7599				20				
UF 6 min	7141	325	73.6	22.6	20	4851	1.2003	21423	17.8
<i>UF Average</i>	<i>7370</i>	<i>325</i>	<i>74</i>	<i>23</i>	<i>15</i>	<i>4851</i>	<i>1</i>	<i>21423</i>	<i>18</i>
Two Sides:						9703		42846.0	35.7
						UF/(OF+UF)		1 - OF/F	UF/F
						Solids Yield to UF:	0.478	0.531	0.429
						Underflow flush (L/min):	2		
						Launder Wash (L/min):	21.8		
						Fluidisation (L/min):	50		
						Volume Balance: In =	178.8		
						Out =	173.9		
						Ratio:	1.03		
						Solids In/Out =	1.11		
						Average Yield =	0.504		

Takes into account water from Launder and U/F Flush

TRUE U/F	
Flowrate	Solids Conc.
L/min	wt.%
11.9	50.9

CF203

		Solids Density		3.8					
	Slurry weight (g)	Sub sample Slurry Weight (g)	Solids Weight (g)	Solids Conc. (wt. %)	Sample time (s)	Solids Rate (g/min)	Slurry Density (g/ml)	Mass Flow (g/min)	Volumetric Flow (L/min)
Feed 1	8036				-				
Feed 2	9479	296	23.9	8.1	-	7984.138	1.0633	98883	93.0
<i>Feed Average</i>	<i>8757.5</i>	<i>296</i>	<i>23.9</i>	<i>8.1</i>		<i>7984.138</i>	<i>1.0633</i>	<i>98883.0</i>	<i>93</i>
OF 3 min	13227				6				
OF 4 min	13585	463	8.2	1.8	6	2406	1.0132	135850.0	134.1
<i>OF Average</i>	<i>13406</i>	<i>463</i>	<i>8</i>	<i>1.8</i>	<i>6</i>	<i>2406</i>	<i>1.0132</i>	<i>135850</i>	<i>134.1</i>
UF 3 min	5301				20				
UF 4 min	5319	221	22.1	10.0	20	1596	1.0795	15957	14.8
<i>UF Average</i>	<i>5310</i>	<i>221</i>	<i>22</i>	<i>10</i>	<i>15</i>	<i>1596</i>	<i>1.0795</i>	<i>15957</i>	<i>15</i>
Two Sides:						3191		31914.0	29.6
						UF/(OF+UF)		1 - OF/F	UF/F
						Solids Yield to UF:	0.570	0.699	0.400
						Underflow flush (L/min):	2		
						Launder Wash (L/min):	21.8		
						Fluidisation (L/min):	50		
						Volume Balance: In =	166.8		
						Out =	163.6		
						Ratio:	1.02		
						Solids In/Out =	1.43		
						Average Yield =	0.634		

Takes into account water from Launder and U/F Flush

TRUE U/F	
Flowrate L/min	Solids Conc. wt. %
5.8	39.3

CF206

		Solids Density		3.8					
	Slurry weight (g)	Sub sample Slurry Weight (g)	Solids Weight (g)	Solids Conc. (wt. %)	Sample time (s)	Solids Rate (g/min)	Slurry Density (g/ml)	Mass Flow (g/min)	Volumetric Flow (L/min)
Feed 1	9537				-				
Feed 2	12025	267	53	19.9	-	24413.53	1.1713	122989	105.0
<i>Feed Average</i>	<i>10781</i>	<i>267</i>	<i>53</i>	<i>19.9</i>		<i>24413.53</i>	<i>1.1713</i>	<i>122988.9</i>	<i>105</i>
OF 3 min	14239				6				
OF 4 min	15331	482	39	8.1	6	12405	1.0634	153310.0	144.2
<i>OF Average</i>	<i>14785</i>	<i>482</i>	<i>39</i>	<i>8.1</i>	<i>6</i>	<i>12405</i>	<i>1.0634</i>	<i>153310</i>	<i>144.2</i>
UF 3 min	6520				20				
UF 4 min	7130	316	73	23.1	20	4941	1.2051	21390	17.7
<i>UF Average</i>	<i>6825</i>	<i>316</i>	<i>73</i>	<i>23</i>	<i>15</i>	<i>4941</i>	<i>1.2051</i>	<i>21390</i>	<i>18</i>
Two Sides:						9883		42780.0	35.5
						UF/(OF+UF)		1 - OF/F	UF/F
						Solids Yield to UF:	0.443	0.492	0.405
						Underflow flush (L/min):	2		
						Launder Wash (L/min):	21.8		
						Fluidisation (L/min):	50		
						Volume Balance: In =	178.8		
						Out =	179.7		
						Ratio:	1.00		
						Solids In/Out =	1.10		
						Average Yield =	0.447		

Takes into account water from Launder and U/F Flush

TRUE U/F	
Flowrate	Solids Conc.
L/min	wt. %
11.7	52.1

CF207

		Solids Density		3.8					
	Slurry weight (g)	Sub sample		Solids Conc. (wt. %)	Sample time (s)	Solids Rate (g/min)	Slurry Density (g/ml)	Mass Flow (g/min)	Volumetric Flow (L/min)
		Slurry Weight (g)	Solids Weight (g)						
Feed 1	6196				-				
Feed 2	9030	347	21	6.1	-	6651.056	1.0467	109901	105.0
<i>Feed Average</i>	<i>7613</i>	<i>347</i>	<i>21</i>	<i>6.1</i>		<i>6651.056</i>	<i>1.0467</i>	<i>109900.8</i>	<i>105</i>
OF 3 min	16910				6				
OF 4 min	16148	630	4	0.6	6	1025	1.0047	161480.0	160.7
<i>OF Average</i>	<i>16529</i>	<i>630</i>	<i>4</i>	<i>0.6</i>	<i>6</i>	<i>1025</i>	<i>1.0047</i>	<i>161480</i>	<i>160.7</i>
UF 3 min	6731				20				
UF 4 min	6984	331	56	16.9	20	3545	1.1424	20952	18.3
<i>UF Average</i>	<i>6858</i>	<i>331</i>	<i>56</i>	<i>17</i>	<i>15</i>	<i>3545</i>	<i>1.1424</i>	<i>20952</i>	<i>18</i>
Two Sides:						7089		41904.0	36.7
						UF/(OF+UF)		1 - OF/F	UF/F
						Solids Yield to UF:	0.874	0.846	1.066
						Underflow flush (L/min):	2		
						Launder Wash (L/min):	21.8		
						Fluidisation (L/min):	64		
						Volume Balance: In =	192.8		
						Out =	197.4		
						Ratio:	0.98		
						Solids In/Out =	0.82		
						Average Yield =	0.860		

Takes into account water from Launder and U/F Flush

TRUE U/F	
Flowrate L/min	Solids Conc. wt. %
12.9	39.2

CF209

		Solids Density		3.8					
	Slurry weight (g)	Sub sample		Solids Conc. (wt. %)	Sample time (s)	Solids Rate (g/min)	Slurry Density (g/ml)	Mass Flow (g/min)	Volumetric Flow (L/min)
		Slurry Weight (g)	Solids Weight (g)						
Feed 1	8623				-				
Feed 2	8623	297	30	10.1	-	7093.624	1.0804	70227	65.0
<i>Feed Average</i>	<i>8623</i>	<i>297</i>	<i>30</i>	<i>10.1</i>		<i>7093.624</i>	<i>1.0804</i>	<i>70226.9</i>	<i>65</i>
OF 4 min	13212				6				
OF 8 min	14164	392	10	2.6	7	3097	1.0192	121405.7	119.1
<i>OF Average</i>	<i>13688</i>	<i>392</i>	<i>10</i>	<i>2.6</i>	<i>6</i>	<i>3097</i>	<i>1.0192</i>	<i>121406</i>	<i>119.1</i>
UF 4 min	5732				20				
UF 8 min	5737	283	26	9.2	20	1581	1.0726	17211	16.0
<i>UF Average</i>	<i>5735</i>	<i>283</i>	<i>26</i>	<i>9</i>	<i>15</i>	<i>1581</i>	<i>1.0726</i>	<i>17211</i>	<i>16</i>
Two Sides:						3162		34422.0	32.1
						UF/(OF+UF)		1 - OF/F	UF/F
						Solids Yield to UF:	0.505	0.563	0.446
						Underflow flush (L/min):	3		
						Launder Wash (L/min):	21.8		
						Fluidisation (L/min):	64		
						Volume Balance: In =	153.8		
						Out =	151.2		
						Ratio:	1.02		
						Solids In/Out =	1.13		
						Average Yield =	0.534		

Takes into account water from Launder and U/F Flush

TRUE U/F	
Flowrate	Solids Conc.
L/min	wt. %
7.3	32.9

CF215

Solids Density 3.8									
	Slurry weight (g)	Sub sample Slurry Weight (g)	Solids Weight (g)	Solids Conc. (wt. %)	Sample time (s)	Solids Rate (g/min)	Slurry Density (g/ml)	Mass Flow (g/min)	Volumetric Flow (L/min)
Feed 1	9231	440	50	11.4	-				
Feed 2	11610	467	54	11.6	-	7963	1.0931	68868	63.0
<i>Feed Average</i>	<i>10420.5</i>	<i>453.5</i>	<i>52</i>	<i>11.5</i>		<i>7963</i>	<i>1.0931</i>	<i>68867.7</i>	<i>63</i>
OF 4 min	12180	451	20.3	4.5	10	3289	1.0343	73080.0	70.7
OF 5 min	12091	601	27.6	4.6	10	3332	1.0350	72546.0	70.1
<i>OF Average</i>	<i>12136</i>	<i>526</i>	<i>24</i>	<i>4.5</i>	<i>10</i>	<i>3289</i>	<i>1.0347</i>	<i>72813</i>	<i>70.4</i>
<i>UF 4 min (N)</i>	<i>4126</i>	<i>241</i>	<i>25</i>	<i>10.3</i>	<i>15</i>	<i>1698</i>	<i>1.0820</i>	<i>16504</i>	<i>15.3</i>
<i>UF 4 min (S)</i>	<i>5330</i>	<i>140</i>	<i>12</i>	<i>8.2</i>	<i>15</i>	<i>1751</i>	<i>1.0644</i>	<i>21320</i>	<i>20</i>
UF 5 min (N)	4097	231	24.3	10.5	15	1724	1.0840	16388	15.1
UF 5 min (S)	5084	217	19.6	9.0	15	1837	1.0713	20336	19.0
<i>UF Average</i>	<i>9319</i>	<i>275</i>	<i>24</i>	<i>9</i>	<i>15</i>	<i>1753</i>	<i>1.0754</i>	<i>18637</i>	<i>17</i>
Two Sides:						3505		37274.0	34.7
						UF/(OF+UF)		1 - OF/F	UF/F
						Solids Yield to UF:	0.516	0.587	0.440
						Underflow flush (L/min):	3		
						Launder Wash (L/min):	21.8		
						Fluidisation (L/min):	18		
						Volume Balance: In =	105.8		
						Out =	105.1		
						Ratio:	1.01		
						Solids In/Out =	1.17		
						Average Yield =	0.551		

Takes into account water from Launder and U/F Flush

TRUE U/F	
Flowrate L/min	Solids Conc. wt. %
9.9	28.1

CF217

		Solids Density		3.8					
	Slurry weight (g)	Sub sample		Solids Conc. (wt. %)	Sample time (s)	Solids Rate (g/min)	Slurry Density (g/ml)	Mass Flow (g/min)	Volumetric Flow (L/min)
		Slurry Weight (g)	Solids Weight (g)						
Feed 1	7157				-				
Feed 2	9072	297	29	9.8	-	6523	1.0775	66807	62.0
<i>Feed Average</i>	<i>8114.5</i>	<i>297</i>	<i>29</i>	<i>9.8</i>		<i>6523</i>	<i>1.0775</i>	<i>66806.6</i>	<i>62</i>
OF 4 min	16055								
OF 5 min	15414	489	16	3.3	8	3783	1.0247	115605.0	112.8
<i>OF Average</i>	<i>15735</i>	<i>489</i>	<i>16</i>	<i>3.3</i>		<i>3783</i>	<i>1.0247</i>	<i>115605</i>	<i>112.8</i>
UF 4 min	9001								
UF 5 min	8859	346	22	6.4	30	1127	1.0492	17718	16.9
<i>UF Average</i>	<i>8930</i>	<i>346</i>	<i>22</i>	<i>6</i>	<i>30</i>	<i>1127</i>	<i>1.0492</i>	<i>17718</i>	<i>17</i>
Two Sides:						2253		35436.0	33.8
						UF/(OF+UF)		1 - OF/F	UF/F
						Solids Yield to UF:	0.373	0.420	0.345
						Underflow flush (L/min):	3		
						Launder Wash (L/min):	21.8		
						Fluidisation (L/min):	36		
						Volume Balance: In =	122.8		
						Out =	146.6		
						Ratio:	0.84		
						Solids In/Out =	1.08		
						Average Yield =	0.397		

Takes into account water from Launder and U/F Flush

TRUE U/F	
Flowrate	Solids Conc.
L/min	wt. %
9.0	21.2

CF218

Solids Density 3.8									
	Slurry weight (g)	Sub sample Slurry Weight (g)	Solids Weight (g)	Solids Conc. (wt. %)	Sample time (s)	Solids Rate (g/min)	Slurry Density (g/ml)	Mass Flow (g/min)	Volumetric Flow (L/min)
Feed 1					-				
Feed 2	9605	358	41	11.5	-	7505	1.0922	65530	60.0
<i>Feed Average</i>	<i>9605</i>	<i>358</i>	<i>41</i>	<i>11.5</i>		<i>7505</i>	<i>1.0922</i>	<i>65529.9</i>	<i>60</i>
OF 4 min									
OF 5 min	14491	325	10	3.1	8	3344	1.0232	108682.5	106.2
<i>OF Average</i>	<i>14491</i>	<i>325</i>	<i>10</i>	<i>3.1</i>		<i>3344</i>	<i>1.0232</i>	<i>108683</i>	<i>106.2</i>
UF 4 min									
UF 5 min	9228	338	26	7.7	30	1420	1.0601	18456	17.4
<i>UF Average</i>	<i>9228</i>	<i>338</i>	<i>26</i>	<i>8</i>	<i>30</i>	<i>1420</i>	<i>1.0601</i>	<i>18456</i>	<i>17</i>
Two Sides:						2839		36912.0	34.8
						UF/(OF+UF)		1 - OF/F	UF/F
						Solids Yield to UF:	0.459	0.554	0.378
						Underflow flush (L/min):	3		
						Launder Wash (L/min):	21.8		
						Fluidisation (L/min):	54		
						Volume Balance: In =	138.8		
						Out =	141.0		
						Ratio:	0.98		
						Solids In/Out =	1.21		
						Average Yield =	0.507		

Takes into account water from Launder and U/F Flush

TRUE U/F	
Flowrate	Solids Conc.
L/min	wt. %
10.0	23.4

CF219

Solids Density 3.8									
	Slurry weight (g)	Sub sample Slurry Weight (g)	Solids Weight (g)	Solids Conc. (wt. %)	Sample time (s)	Solids Rate (g/min)	Slurry Density (g/ml)	Mass Flow (g/min)	Volumetric Flow (L/min)
Feed 1	11698				-				
Feed 2	10267	445	40	9.0	-	9626	1.0709	107093	100.0
<i>Feed Average</i>	<i>10982.5</i>	<i>445</i>	<i>40</i>	<i>9.0</i>		<i>9626</i>	<i>1.0709</i>	<i>107093.1</i>	<i>100</i>
OF 3 min	11545								
OF 4 min	10955	581	22	3.8	6	4148	1.0287	109550.0	106.5
<i>OF Average</i>	<i>11250</i>	<i>581</i>	<i>22</i>	<i>3.8</i>		<i>4148</i>	<i>1.0287</i>	<i>109550</i>	<i>106.5</i>
UF 3 min	10701				30				
UF 4 min	7243	405	48	11.9	20	2575	1.0957	21729	19.8
<i>UF Average</i>	<i>8972</i>	<i>405</i>	<i>48</i>	<i>12</i>	<i>25</i>	<i>2575</i>	<i>1.0957</i>	<i>21729</i>	<i>20</i>
Two Sides:						5151		43458.0	39.7
						UF/(OF+UF)		1 - OF/F	UF/F
Solids Yield to UF:						0.554		0.569	0.535
Underflow flush (L/min):						3			
Launder Wash (L/min):						21.8			
Fluidisation (L/min):						18			
Volume Balance: In =							142.8		
Out =							146.2		
Ratio:							0.98		
Solids In/Out =							1.04		
Average Yield =							0.553		

Takes into account water from Launder and U/F Flush

TRUE U/F	
Flowrate	Solids Conc.
L/min	wt. %
14.9	27.6

CF220

Solids Density 3.8									
	Slurry weight (g)	Sub sample Slurry Weight (g)	Solids Weight (g)	Solids Conc. (wt. %)	Sample time (s)	Solids Rate (g/min)	Slurry Density (g/ml)	Mass Flow (g/min)	Volumetric Flow (L/min)
Feed 1	9850				-				
Feed 2	9650	514	48	9.3	-	9226	1.0739	98798	92.0
<i>Feed Average</i>	<i>9750</i>	<i>514</i>	<i>48</i>	<i>9.3</i>		<i>9226</i>	<i>1.0739</i>	<i>98798.3</i>	<i>92</i>
OF 3 min	12315				7				
OF 4 min	12890	696	26	3.7	7	4127	1.0283	110485.7	107.4
<i>OF Average</i>	<i>12603</i>	<i>696</i>	<i>26</i>	<i>3.7</i>		<i>4127</i>	<i>1.0283</i>	<i>110486</i>	<i>107.4</i>
UF 3 min	9303				30				
UF 4 min	6104	430	36	8.4	20	1533	1.0657	18312	17.2
<i>UF Average</i>	<i>7704</i>	<i>430</i>	<i>36</i>	<i>8</i>	<i>20</i>	<i>1533</i>	<i>1.0657</i>	<i>18312</i>	<i>17</i>
Two Sides:						3066		36624.0	34.4
						UF/(OF+UF)		1 - OF/F	UF/F
						Solids Yield to UF:	0.426	0.553	0.332
						Underflow flush (L/min):	3		
						Launder Wash (L/min):	21.8		
						Fluidisation (L/min):	36		
						Volume Balance: In =	152.8		
						Out =	141.8		
						Ratio:	1.08		
						Solids In/Out =	1.28		
						Average Yield =	0.489		

Takes into account water from Launder and U/F Flush

TRUE U/F	
Flowrate	Solids Conc.
L/min	wt.%
9.6	25.9

CF221

		Solids Density		3.8					
	Slurry weight (g)	Sub sample Slurry Weight (g)	Solids Weight (g)	Solids Conc. (wt. %)	Sample time (s)	Solids Rate (g/min)	Slurry Density (g/ml)	Mass Flow (g/min)	Volumetric Flow (L/min)
Feed 1	11013				-				
Feed 2	11949	631	58	9.2	-	9860	1.0726	107265	100.0
<i>Feed Average</i>	<i>11481</i>	<i>631</i>	<i>58</i>	<i>9.2</i>		<i>9860</i>	<i>1.0726</i>	<i>107264.9</i>	<i>100</i>
OF 3 min	15252								
OF 4 min	14250	617	21	3.4	6	4850	1.0257	142500.0	138.9
<i>OF Average</i>	<i>14751</i>	<i>617</i>	<i>21</i>	<i>3.4</i>		<i>4850</i>	<i>1.0257</i>	<i>142500</i>	<i>138.9</i>
UF 3 min	6158								
UF 4 min	6718	511	30	5.9	20	1183	1.0452	20154	19.3
<i>UF Average</i>	<i>6438</i>	<i>511</i>	<i>30</i>	<i>6</i>	<i>20</i>	<i>1183</i>	<i>1.0452</i>	<i>20154</i>	<i>19</i>
Two Sides:						2366		40308.0	38.6
						UF/(OF+UF)		1 - OF/F	UF/F
Solids Yield to UF:						0.328		0.508	0.240
Underflow flush (L/min):						3			
Launder Wash (L/min):						21.8			
Fluidisation (L/min):						54			
Volume Balance: In =							178.8		
Out =							177.5		
Ratio:							1.01		
Solids In/Out =							1.37		
Average Yield =							0.418		

Takes into account water from Launder and U/F Flush

TRUE U/F	
Flowrate	Solids Conc.
L/min	wt. %
13.8	15.3

CF222

		Solids Density		3.8					
	Slurry weight (g)	Sub sample Slurry Weight (g)	Solids Weight (g)	Solids Conc. (wt. %)	Sample time (s)	Solids Rate (g/min)	Slurry Density (g/ml)	Mass Flow (g/min)	Volumetric Flow (L/min)
Feed 1	13100				-				
Feed 2	12785	481	42	8.7	-	8959	1.0688	102601	96.0
<i>Feed Average</i>	<i>12942.5</i>	<i>481</i>	<i>42</i>	<i>8.7</i>		<i>8959</i>	<i>1.0688</i>	<i>102601.3</i>	<i>96</i>
OF 3 min	14518								
OF 4 min	13919	562	16	2.8	6	3963	1.0214	139190.0	136.3
<i>OF Average</i>	<i>14219</i>	<i>562</i>	<i>16</i>	<i>2.8</i>		<i>3963</i>	<i>1.0214</i>	<i>139190</i>	<i>136.3</i>
UF 3 min	6588								
UF 4 min	7266	464	39	8.4	20	1832	1.0660	21798	20.4
<i>UF Average</i>	<i>6927</i>	<i>464</i>	<i>39</i>	<i>8</i>	<i>20</i>	<i>1832</i>	<i>1.0660</i>	<i>21798</i>	<i>20</i>
Two Sides:						3664		43596.0	40.9
						UF/(OF+UF)		1 - OF/F	UF/F
						Solids Yield to UF:	0.480	0.558	0.409
						Underflow flush (L/min):	3		
						Launder Wash (L/min):	21.8		
						Fluidisation (L/min):	54		
						Volume Balance: In =	174.8		
						Out =	177.2		
						Ratio:	0.99		
						Solids In/Out =	1.17		
						Average Yield =	0.519		

Takes into account water from Launder and U/F Flush

TRUE U/F	
Flowrate L/min	Solids Conc. wt.%
16.1	19.5

CF223

		Solids Density		3.8					
	Slurry weight (g)	Sub sample Slurry Weight (g)	Solids Weight (g)	Solids Conc. (wt. %)	Sample time (s)	Solids Rate (g/min)	Slurry Density (g/ml)	Mass Flow (g/min)	Volumetric Flow (L/min)
Feed 1	11815				-				
Feed 2	11124	437	14	3.2	-	3314	1.0242	103442	101.0
<i>Feed Average</i>	<i>11469.5</i>	<i>437</i>	<i>14</i>	<i>3.2</i>		<i>3314</i>	<i>1.0242</i>	<i>103441.8</i>	<i>101</i>
OF 2.5 min	14930								
OF 3.5 min	14355	863	1	0.1	6	166	1.0009	143550.0	143.4
<i>OF Average</i>	<i>14643</i>	<i>863</i>	<i>1</i>	<i>0.1</i>		<i>166</i>	<i>1.0009</i>	<i>143550</i>	<i>143.4</i>
UF 2.5 min	9175								
UF 3.5 min	9249	546	25	4.6	30	847	1.0349	18498	17.9
<i>UF Average</i>	<i>9212</i>	<i>546</i>	<i>25</i>	<i>5</i>	<i>30</i>	<i>847</i>	<i>1.0349</i>	<i>18498</i>	<i>18</i>
Two Sides:						1694		36996.0	35.7
						UF/(OF+UF)		1 - OF/F	UF/F
						Solids Yield to UF:	0.911	0.950	0.511
						Underflow flush (L/min):	3		
						Launder Wash (L/min):	21.8		
						Fluidisation (L/min):	54		
						Volume Balance: In =	179.8		
						Out =	179.2		
						Ratio:	1.00		
						Solids In/Out =	1.78		
						Average Yield =	0.930		

Takes into account water from Launder and U/F Flush

TRUE U/F	
Flowrate	Solids Conc.
L/min	wt.%
10.9	13.9

CF232

		Solids Density		3.9					
	Slurry weight (g)	Sub sample Slurry Weight (g)	Solids Weight (g)	Solids Conc. (wt. %)	Sample time (s)	Solids Rate (g/min)	Slurry Density (g/ml)	Mass Flow (g/min)	Volumetric Flow (L/min)
Feed 1	12596	597	25.4	4.3	-	4481	1.0327	105332	102.0
Feed 2	10886	630	24.4	3.9	-	4068	1.0297	105025	102.0
<i>Feed Average</i>	<i>11741</i>	<i>613.5</i>	<i>24.9</i>	<i>4.1</i>		<i>4275</i>	<i>1.0312</i>	<i>105178.5</i>	<i>102</i>
OF 3 min	15425	1735	6.1	0.4	7	465	1.0026	132214.3	131.9
OF 4 min	15117	1782	6.9	0.4	7	502	1.0029	129574.3	129.2
<i>OF Average</i>	<i>15271</i>	<i>1759</i>	<i>7</i>	<i>0.4</i>		<i>502</i>	<i>1.0028</i>	<i>130894</i>	<i>130.5</i>
UF 3 min	6854	491	32	6.6	20	1353	1.0514	20562	19.6
UF 4 min	6828	619	39.1	6.3	20	1294	1.0493	20484	19.5
<i>UF Average</i>	<i>6841</i>	<i>555</i>	<i>36</i>	<i>6</i>	<i>20</i>	<i>1294</i>	<i>1.0493</i>	<i>20484</i>	<i>20</i>
Two Sides:						2588		40968.0	39.0
						UF/(OF+UF)	1 - OF/F	UF/F	
						Solids Yield to UF:	0.838	0.877	0.605
						Underflow flush (L/min):	3		
						Launder Wash (L/min):	21.8		
						Fluidisation (L/min):	36		
						Volume Balance: In =	162.8		
						Out =	169.6		
						Ratio:	0.96		
						Solids In/Out =	1.38		
						Average Yield =	0.857		

Takes into account water from Launder and U/F Flush

TRUE U/F	
Flowrate L/min	Solids Conc. wt.%
14.2	16.0

CF233

		Solids Density		3.9					
	Slurry weight (g)	Sub sample		Solids Conc. (wt. %)	Sample time (s)	Solids Rate (g/min)	Slurry Density (g/ml)	Mass Flow (g/min)	Volumetric Flow (L/min)
		Slurry Weight (g)	Solids Weight (g)						
Feed 1	13201				-				
Feed 2	12027	585	24	4.1	-	2200	1.0315	53636	52.0
<i>Feed Average</i>	<i>12614</i>	<i>585</i>	<i>24</i>	<i>4.1</i>		<i>2200</i>	<i>1.0315</i>	<i>53636.2</i>	<i>52</i>
OF 4 min	13175								
OF 5 min	12846	1879	5.79	0.3	10	238	1.0023	77076.0	76.9
<i>OF Average</i>	<i>13011</i>	<i>1879</i>	<i>6</i>	<i>0.3</i>		<i>238</i>	<i>1.0023</i>	<i>77076</i>	<i>76.9</i>
UF 4 min	10377								
UF 5 min	10365	783	28	3.6	30	741	1.0273	20730	20.2
<i>UF Average</i>	<i>10371</i>	<i>783</i>	<i>28</i>	<i>4</i>	<i>30</i>	<i>741</i>	<i>1.0273</i>	<i>20730</i>	<i>20</i>
Two Sides:						1483		41460.0	40.4
						UF/(OF+UF)		1 - OF/F	UF/F
						Solids Yield to UF:	0.862	0.892	0.674
						Underflow flush (L/min):	3		
						Launder Wash (L/min):	21.8		
						Fluidisation (L/min):	36		
						Volume Balance: In =	112.8		
						Out =	117.3		
						Ratio:	0.96		
						Solids In/Out =	1.28		
						Average Yield =	0.877		

Takes into account water from Launder and U/F Flush

TRUE U/F	
Flowrate L/min	Solids Conc. wt.%
15.6	8.9

CF235

Solids Density 3.9									
	Slurry weight (g)	Sub sample Slurry Weight (g)	Solids Weight (g)	Solids Conc. (wt. %)	Sample time (s)	Solids Rate (g/min)	Slurry Density (g/ml)	Mass Flow (g/min)	Volumetric Flow (L/min)
Feed 1	13655				-				
Feed 2	11410	640	53.3	8.3	-	4617	1.0660	55433	52.0
<i>Feed Average</i>	<i>12532.5</i>	<i>640</i>	<i>53.3</i>	<i>8.3</i>		<i>4617</i>	<i>1.0660</i>	<i>55432.8</i>	<i>52</i>
OF 4 min	17500								
OF 5 min	16729	1472	6.7	0.5	10	457	1.0034	100374.0	100.0
<i>OF Average</i>	<i>17115</i>	<i>1472</i>	<i>7</i>	<i>0.5</i>		<i>457</i>	<i>1.0034</i>	<i>100374</i>	<i>100.0</i>
UF 4 min	9725								
UF 5 min	10469	658	53.8	8.2	30	1712	1.0647	20938	19.7
<i>UF Average</i>	<i>10097</i>	<i>658</i>	<i>54</i>	<i>8</i>	<i>30</i>	<i>1712</i>	<i>1.0647</i>	<i>20938</i>	<i>20</i>
Two Sides:						3424		41876.0	39.3
						UF/(OF+UF)		1 - OF/F	UF/F
						Solids Yield to UF:	0.882	0.901	0.742
						Underflow flush (L/min):	3		
						Launder Wash (L/min):	21.8		
						Fluidisation (L/min):	54		
						Volume Balance: In =	130.8		
						Out =	139.4		
						Ratio:	0.94		
						Solids In/Out =	1.19		
						Average Yield =	0.892		

Takes into account water from Launder and U/F Flush

TRUE U/F	
Flowrate	Solids Conc.
L/min	wt. %
14.5	20.1

CF236

		Solids Density		3.9					
	Slurry weight (g)	Sub sample Slurry Weight (g)	Solids Weight (g)	Solids Conc. (wt. %)	Sample time (s)	Solids Rate (g/min)	Slurry Density (g/ml)	Mass Flow (g/min)	Volumetric Flow (L/min)
Feed 1					-				
Feed 2	13165	690	52.9	7.7	-	8211	1.0605	107106	101.0
<i>Feed Average</i>	13165	690	52.9	7.7		8211	1.0605	107106.0	101
OF 4 min	17090								
OF 5 min	17346	1545	9.2	0.6	7	885	1.0044	148680.0	148.0
<i>OF Average</i>	17218	1545	9	0.6		885	1.0044	148680	148.0
UF 4 min	10047								
UF 5 min	10583	528	65.4	12.4	30	2622	1.1014	21166	19.2
<i>UF Average</i>	10315	528	65	12	30	2622	1.1014	21166	19
Two Sides:						5243		42332.0	38.4
						UF/(OF+UF)		1 - OF/F	UF/F
						Solids Yield to UF:	0.856	0.892	0.639
						Underflow flush (L/min):	3		
						Launder Wash (L/min):	21.8		
						Fluidisation (L/min):	54		
						Volume Balance: In =	179.8		
						Out =	186.5		
						Ratio:	0.96		
						Solids In/Out =	1.34		
						Average Yield =	0.874		

Takes into account water from Launder and U/F Flush

TRUE U/F	
Flowrate	Solids Conc.
L/min	wt.%
13.6	29.9

CF238

		Solids Density		3.9							
	Slurry weight (g)	Sub sample Slurry Weight (g)	Sub sample Solids Weight (g)	Solids Conc. (wt. %)	Sample time (s)	Solids Rate (g/min)	Slurry Density (g/ml)	Mass Flow (g/min)	Volumetric Flow (L/min)		
Feed 1	13601	811.8	39.4	4.9	-	5539	1.0374	114118	110.0	Solids washed out of launder after run	
Feed 2	10907	749.3	23.3	3.1	-	3501	1.0237	112604	110.0		
<i>Feed Average</i>	<i>12254</i>	<i>780.55</i>	<i>31.35</i>	<i>4.0</i>		<i>4520</i>	<i>1.0306</i>	<i>113361.1</i>	<i>110</i>		
OF 4 min	15050				5					Launder solids (g) North Side 115.3 934.0	
OF 5 min	14208	947.8	2.6	0.3	5	468	1.0020	170496.0	170.1		
<i>OF Average</i>	<i>14629</i>	<i>948</i>	<i>3</i>	<i>0.3</i>	<i>5</i>	<i>468</i>	<i>1.0020</i>	<i>170496</i>	<i>170.1</i>		
UF 4 min (S)	7905	893	83	9.3	20	2201	1.0741	23715	22	TRUE U/F Flowrate Solids Conc. L/min wt.% 14.6 19.2	
UF 5 min (S)	7912	746	59	8.0	20	1888	1.0629	23736	22		
UF 4 min (N)	8450	745.4	59	8.0	20	2017	1.0629	25350	23.9		
UF 5 min (N)	8379	758	49.5	6.5	20	1642	1.0510	25137	23.9		
<i>UF Average</i>	<i>8415</i>	<i>752</i>	<i>54</i>	<i>7</i>	<i>20</i>	<i>1642</i>	<i>1.0510</i>	<i>25137</i>	<i>24</i>		
Two Sides:						3283		50274.0	47.8		
						UF/(OF+UF)		1 - OF/F		UF/F	Takes into account water from Launder and U/F Flush
						Solids Yield to UF:	0.875	0.866	0.726		
						Underflow flush (L/min):	3				
						Launder Wash (L/min):	30.19				
						Fluidisation (L/min):	54				
						Volume Balance: In =		197.2			
						Out =		218.0			
						Ratio:		0.90			
						Solids In/Out =		1.21			
						Average Yield =		0.871			

CF245

		Solids Density		3.9					
	Slurry weight (g)	Sub sample Slurry Weight (g)	Solids Weight (g)	Solids Conc. (wt. %)	Sample time (s)	Solids Rate (g/min)	Slurry Density (g/ml)	Mass Flow (g/min)	Volumetric Flow (L/min)
Feed 1	11559								
Feed 2	10900	847	85.7	10.1	-	5689	1.0814	56231	52.0
<i>Feed Average</i>	<i>11229.5</i>	<i>847</i>	<i>85.7</i>	<i>10.1</i>		<i>5689</i>	<i>1.0814</i>	<i>56230.6</i>	<i>52</i>
OF 3 min	12113								
OF 4 min	11990	797	23	2.9	11	1887	1.0219	65400.0	64.0
<i>OF Average</i>	<i>12052</i>	<i>797</i>	<i>23</i>	<i>2.9</i>		<i>1887</i>	<i>1.0219</i>	<i>65400</i>	<i>64.0</i>
UF 3 min	7614								
UF 4 min	7498	764	65.5	8.6	20	1928	1.0681	22494	21.1
<i>UF Average</i>	<i>7556</i>	<i>764</i>	<i>66</i>	<i>9</i>	<i>20</i>	<i>1928</i>	<i>1.0681</i>	<i>22494</i>	<i>21</i>
Two Sides:						3857		44988.0	42.1
						UF/(OF+UF)		1 - OF/F	UF/F
						Solids Yield to UF:	0.671	0.668	0.678
						Underflow flush (L/min):	3.5		
						Launder Wash (L/min):	30.2		
						Fluidisation (L/min):	18		
						Volume Balance: In =	103.7		
						Out =	106.1		
						Ratio:	0.98		
						Solids In/Out =	0.99		
						Average Yield =	0.673		

Takes into account water from Launder and U/F Flush

TRUE U/F	
Flowrate	Solids Conc.
L/min	wt.%
8.4	34.2

CF246

		Solids Density		3.9					
	Slurry weight (g)	Sub sample		Solids Conc. (wt. %)	Sample time (s)	Solids Rate (g/min)	Slurry Density (g/ml)	Mass Flow (g/min)	Volumetric Flow (L/min)
		Slurry Weight (g)	Solids Weight (g)						
Feed 1	11448								
Feed 2	11243	758	77.4	10.2	-	5746	1.0822	56273	52.0
<i>Feed Average</i>	<i>11345.5</i>	<i>758</i>	<i>77.4</i>	<i>10.2</i>		<i>5746</i>	<i>1.0822</i>	<i>56272.7</i>	<i>52</i>
OF 3 min	11103				8				
OF 4 min	10801	802	20	2.5	8	2020	1.0189	81007.5	79.5
<i>OF Average</i>	<i>10952</i>	<i>802</i>	<i>20</i>	<i>2.5</i>		<i>2020</i>	<i>1.0189</i>	<i>81008</i>	<i>79.5</i>
UF 3 min	7525								
UF 4 min	7408	725	58.7	8.1	20	1799	1.0641	22224	20.9
<i>UF Average</i>	<i>7467</i>	<i>725</i>	<i>59</i>	<i>8</i>	<i>20</i>	<i>1799</i>	<i>1.0641</i>	<i>22224</i>	<i>21</i>
Two Sides:						3599		44448.0	41.8
						UF/(OF+UF)		1 - OF/F	UF/F
						Solids Yield to UF:	0.640	0.648	0.626
						Underflow flush (L/min):	3		
						Launder Wash (L/min):	30.2		
						Fluidisation (L/min):	36		
						Volume Balance: In =	121.2		
						Out =	121.3		
						Ratio:	1.00		
						Solids In/Out =	1.02		
						Average Yield =	0.638		

Takes into account water from Launder and U/F Flush

TRUE U/F	
Flowrate	Solids Conc.
L/min	wt. %
8.6	32.0

CF247

		Solids Density		3.9					
	Slurry weight (g)	Sub sample Slurry Weight (g)	Solids Weight (g)	Solids Conc. (wt. %)	Sample time (s)	Solids Rate (g/min)	Slurry Density (g/ml)	Mass Flow (g/min)	Volumetric Flow (L/min)
Feed 1	12423								
Feed 2	10715	791	78	9.9	-	5533	1.0791	56115	52.0
<i>Feed Average</i>	<i>11569</i>	<i>791</i>	<i>78</i>	<i>9.9</i>		<i>5533</i>	<i>1.0791</i>	<i>56114.6</i>	<i>52</i>
OF 3 min	9489								
OF 4 min	9564	898	26	2.9	10	1661	1.0220	57384.0	56.1
<i>OF Average</i>	<i>9527</i>	<i>898</i>	<i>26</i>	<i>2.9</i>		<i>1661</i>	<i>1.0220</i>	<i>57384</i>	<i>56.1</i>
UF 3 min	7395								
UF 4 min	7543	638	56	8.8	20	1986	1.0698	22629	21.2
<i>UF Average</i>	<i>7469</i>	<i>638</i>	<i>56</i>	<i>9</i>	<i>20</i>	<i>1986</i>	<i>1.0698</i>	<i>22629</i>	<i>21</i>
Two Sides:						3972		45258.0	42.3
						UF/(OF+UF)		1 - OF/F	UF/F
						Solids Yield to UF:	0.705	0.700	0.718
						Underflow flush (L/min):	3		
						Launder Wash (L/min):	30.2		
						Fluidisation (L/min):	12		
						Volume Balance: In =	97.2		
						Out =	98.5		
						Ratio:	0.99		
						Solids In/Out =	0.98		
						Average Yield =	0.708		

Takes into account water from Launder and U/F Flush

TRUE U/F	
Flowrate	Solids Conc.
L/min	wt. %
9.1	32.9

CF249

		Solids Density		3.9					
	Slurry weight (g)	Sub sample		Solids Conc. (wt. %)	Sample time (s)	Solids Rate (g/min)	Slurry Density (g/ml)	Mass Flow (g/min)	Volumetric Flow (L/min)
		Slurry Weight (g)	Solids Weight (g)						
Feed 1	11326	721	50.2	7.0		7636	1.0546	109678	104.0
Feed 2	10938	897	59.1	6.6	-	7274	1.0515	110409	105.0
<i>Feed Average</i>	<i>11132</i>	<i>809</i>	<i>54.65</i>	<i>6.8</i>		<i>7455</i>	<i>1.0531</i>	<i>110043.8</i>	<i>105</i>
OF 3 min	13505				10				
OF 4 min	13768	835	5.2	0.6	10	514	1.0047	82608.0	82.2
<i>OF Average</i>	<i>13637</i>	<i>835</i>	<i>5</i>	<i>0.6</i>		<i>514</i>	<i>1.0047</i>	<i>82608</i>	<i>82.2</i>
UF 3 min	8502				10				
UF 4 min	8565	906	98.2	10.8	10	5570	1.0877	51390	47.2
<i>UF Average</i>	<i>8534</i>	<i>906</i>	<i>98</i>	<i>11</i>	<i>10</i>	<i>5570</i>	<i>1.0877</i>	<i>51390</i>	<i>47</i>
Two Sides:						11140		102780.0	94.5
						UF/(OF+UF)		1 - OF/F	UF/F
						Solids Yield to UF:	0.956	0.931	1.494
						Underflow flush (L/min):	3		
						Launder Wash (L/min):	30.2		
						Fluidisation (L/min):	36		
						Volume Balance: In =	174.2		
						Out =	176.7		
						Ratio:	0.99		
						Solids In/Out =	0.66		
						Average Yield =	0.943		

Takes into account water from Launder and U/F Flush

TRUE U/F	
Flowrate L/min	Solids Conc. wt.%
61.3	16.0

CF250

		Solids Density		3.9					
	Slurry weight (g)	Sub sample Slurry Weight (g)	Solids Weight (g)	Solids Conc. (wt. %)	Sample time (s)	Solids Rate (g/min)	Slurry Density (g/ml)	Mass Flow (g/min)	Volumetric Flow (L/min)
Feed 1	12072	678	124.4	18.3		22097	1.1580	120431	104.0
Feed 2	10997	770	116.6	15.1	-	17918	1.1269	118323	105.0
<i>Feed Average</i>	<i>11534.5</i>	<i>724</i>	<i>120.5</i>	<i>16.6</i>		<i>20007</i>	<i>1.1424</i>	<i>119377.1</i>	<i>105</i>
OF 3 min	13770				10				
OF 4 min	15213	662	9.5	1.4	10	1310	1.0108	91278.0	90.3
<i>OF Average</i>	<i>14492</i>	<i>662</i>	<i>10</i>	<i>1.4</i>		<i>1310</i>	<i>1.0108</i>	<i>91278</i>	<i>90.3</i>
UF 3 min	12742				15				
UF 4 min	12620	872	164.8	18.9	15	9540	1.1635	50480	43.4
<i>UF Average</i>	<i>12681</i>	<i>872</i>	<i>165</i>	<i>19</i>	<i>15</i>	<i>9540</i>	<i>1.1635</i>	<i>50480</i>	<i>43</i>
Two Sides:						19081		100960.0	86.8
						UF/(OF+UF)		1 - OF/F	UF/F
						Solids Yield to UF:	0.936	0.935	0.954
						Underflow flush (L/min):	3		
						Launder Wash (L/min):	30.2		
						Fluidisation (L/min):	36		
						Volume Balance: In =	174.2		
						Out =	177.1		
						Ratio:	0.98		
						Solids In/Out =	0.98		
						Average Yield =	0.941		

Takes into account water from Launder and U/F Flush

TRUE U/F	
Flowrate L/min	Solids Conc. wt.%
53.6	28.2

CF251

		Solids Density		3.9					
	Slurry weight (g)	Sub sample		Solids Conc. (wt. %)	Sample time (s)	Solids Rate (g/min)	Slurry Density (g/ml)	Mass Flow (g/min)	Volumetric Flow (L/min)
		Slurry Weight (g)	Solids Weight (g)						
Feed 1	9708	771	224.6	29.1		36442	1.2765	125098	98.0
Feed 2	13454	665	139	20.9	-	24254	1.1840	116035	98.0
<i>Feed Average</i>	<i>11581</i>	<i>718</i>	<i>181.8</i>	<i>25.3</i>		<i>30348</i>	<i>1.2303</i>	<i>120566.6</i>	<i>98</i>
OF 3 min	15788				8				
OF 4 min	15195	834	17.7	2.1	8	2419	1.0160	113962.5	112.2
<i>OF Average</i>	<i>15492</i>	<i>834</i>	<i>18</i>	<i>2.1</i>		<i>2419</i>	<i>1.0160</i>	<i>113963</i>	<i>112.2</i>
UF 3 min	12587				15				
UF 4 min	9075	658	246.1	37.4	15	13577	1.3853	36300	26.2
<i>UF Average</i>	<i>10831</i>	<i>658</i>	<i>246</i>	<i>37</i>	<i>15</i>	<i>13577</i>	<i>1.3853</i>	<i>36300</i>	<i>26</i>
Two Sides:						27153		72600.0	52.4
						UF/(OF+UF)		1 - OF/F	UF/F
						Solids Yield to UF:	0.918	0.920	0.895
						Underflow flush (L/min):	3		
						Launder Wash (L/min):	30.2		
						Fluidisation (L/min):	36		
						Volume Balance: In =	167.2		
						Out =	164.6		
						Ratio:	1.02		
						Solids In/Out =	1.03		
						Average Yield =	0.911		

Takes into account water from Launder and U/F Flush

TRUE U/F	
Flowrate L/min	Solids Conc. wt.%
19.2	68.9

CF252

		Solids Density 3.9							
	Slurry weight (g)	Sub sample Slurry Weight (g)	Solids Weight (g)	Solids Conc. (wt. %)	Sample time (s)	Solids Rate (g/min)	Slurry Density (g/ml)	Mass Flow (g/min)	Volumetric Flow (L/min)
Feed 1	10516	717.6	115.9	16.2		19273	1.1365	119331	105.0
Feed 2	9711	795.8	108.4	13.6	-	15915	1.1127	116834	105.0
<i>Feed Average</i>	<i>10113.5</i>	<i>756.7</i>	<i>112.15</i>	<i>14.8</i>		<i>17594</i>	<i>1.1246</i>	<i>118082.7</i>	<i>105</i>
OF 3 min	13518								
OF 4 min	13509	788.6	9.5	1.2	8	1221	1.0090	101317.5	100.4
<i>OF Average</i>	<i>13514</i>	<i>789</i>	<i>10</i>	<i>1.2</i>		<i>1221</i>	<i>1.0090</i>	<i>101318</i>	<i>100.4</i>
UF 3 min	13244								
UF 4 min	13473	726.5	124	17.1	15	9198	1.1454	53892	47.1
<i>UF Average</i>	<i>13359</i>	<i>727</i>	<i>124</i>	<i>17</i>	<i>15</i>	<i>9198</i>	<i>1.1454</i>	<i>53892</i>	<i>47</i>
Two Sides:						18397		107784.0	94.1
						UF/(OF+UF)		1 - OF/F	UF/F
						Solids Yield to UF:	0.938	0.931	1.046
						Underflow flush (L/min):	3		
						Launder Wash (L/min):	30.2		
						Fluidisation (L/min):	54		
						Volume Balance: In =	192.2		
						Out =	194.5		
						Ratio:	0.99		
						Solids In/Out =	0.90		
						Average Yield =	0.934		

Takes into account water from Launder and U/F Flush

TRUE U/F	
Flowrate L/min	Solids Conc. wt.%
60.9	24.7

CF253

		Solids Density		3.9					
	Slurry weight (g)	Sub sample Slurry Weight (g)	Solids Weight (g)	Solids Conc. (wt. %)	Sample time (s)	Solids Rate (g/min)	Slurry Density (g/ml)	Mass Flow (g/min)	Volumetric Flow (L/min)
Feed 1	13480	480	92	19.2		23023	1.1662	120120	103.0
Feed 2	10936	877	152	17.3	-	20493	1.1479	118238	103.0
<i>Feed Average</i>	<i>12208</i>	<i>678.5</i>	<i>122</i>	<i>18.0</i>		<i>21758</i>	<i>1.1571</i>	<i>119178.9</i>	<i>103</i>
OF 3 min	11629				10				
OF 4 min	11131	661	23	3.5	10	2324	1.0266	66786.0	65.1
<i>OF Average</i>	<i>11380</i>	<i>661</i>	<i>23</i>	<i>3.5</i>		<i>2324</i>	<i>1.0266</i>	<i>66786</i>	<i>65.1</i>
UF 3 min	13245				15				
UF 4 min	13325	671	135	20.1	15	10724	1.1759	53300	45.3
<i>UF Average</i>	<i>13285</i>	<i>671</i>	<i>135</i>	<i>20</i>	<i>15</i>	<i>10724</i>	<i>1.1759</i>	<i>53300</i>	<i>45</i>
Two Sides:						21447		106600.0	90.7
						UF/(OF+UF)		1 - OF/F	UF/F
						Solids Yield to UF:	0.902	0.893	0.986
						Underflow flush (L/min):	3		
						Launder Wash (L/min):	30.2		
						Fluidisation (L/min):	18		
						Volume Balance: In =	154.2		
						Out =	155.7		
						Ratio:	0.99		
						Solids In/Out =	0.92		
						Average Yield =	0.898		

Takes into account water from Launder and U/F Flush

TRUE U/F	
Flowrate L/min	Solids Conc. wt.%
57.5	29.2

CF254

		Solids Density		3.9						
		Slurry weight (g)	Sub sample Slurry Weight (g)	Solids Weight (g)	Solids Conc. (wt. %)	Sample time (s)	Solids Rate (g/min)	Slurry Density (g/ml)	Mass Flow (g/min)	Volumetric Flow (L/min)
	Feed 1	3002.5	3002.5	713.8964	23.8		29785	1.2150	125148	103.0
	Feed 2	2581	2581	667.7938	25.9	-	33040	1.2385	127568	103.0
	Feed 3	3939.6	3939.6	896.3649	22.8		28278	1.2041	124027	103.0
	Feed 4	3863.6	3863.6	783.401	20.3		24626	1.1778	121312	103.0
	<i>Feed Average</i>				23.2		28932	1.2089	124513.9	103
	OF 4 min	16478.3	16153.9	302.3	1.9	8	2313	1.0141	123587.3	121.9
	OF 8 min	16127.5	15817.1	267	1.7	8	2042	1.0127	120956.3	119.4
Large sample taken in Drum	OF DRUM	140556.9	140556.9	2376.8	1.7	70	2037	1.0127	120477.3	119.0
	OF 14 min	15749.7	15461.6	244.9	1.6	8	1871	1.0119	118122.8	116.7
	<i>OF Average</i>	47228	46997	798	1.7		2066	1.0129	120786	119.2
	UF 4 min	23566	23092.6	8474.9	36.7	40	12973	1.3753	35348.9	25.7
	UF 8 min	23769	23392.9	8651.8	37.0	40	13186	1.3793	35652.9	25.8
	UF 14 min	20378	20020.1	6965.9	34.8	30	14181	1.3490	40755.2	30.2
Second sample for assays	UF 14 min b	18715	18393.4	5822.4	31.7	30	11849	1.3078	37430.6	28.6
	<i>UF Average</i>	21607	21225	7479	35	35	13047	1.3529	37297	28
Two Sides:							26094		74593.8	55.2
							UF/(OF+UF)	1 - OF/F	UF/F	
							Solids Yield to UF:	0.927	0.929	0.902
							Underflow flush (L/min):	3		
							Laundry Wash (L/min):	30.2		
							Fluidisation (L/min):	36		
							Volume Balance: In =	172.2		
							Out =	174.4		
							Ratio:	0.99		
							Solids In/Out =	1.03		
							Average Yield =	0.919		

Takes into account water from Launder and U/F Flush

TRUE U/F	
Flowrate L/min	Solids Conc. wt. %
22.0	63.0

CF256

		Solids Density		3.9					
	Slurry weight (g)	Sub sample Slurry Weight (g)	Solids Weight (g)	Solids Conc. (wt. %)	Sample time (s)	Solids Rate (g/min)	Slurry Density (g/ml)	Mass Flow (g/min)	Volumetric Flow (L/min)
Feed 1	12777	906	146.3	16.1		19269	1.1365	119328	105.0
Feed 2	12870	811	134.1	16.5	-	19796	1.1402	119720	105.0
<i>Feed Average</i>	<i>12823.5</i>	<i>858.5</i>	<i>140.2</i>	<i>16.3</i>		<i>19532</i>	<i>1.1383</i>	<i>119524.1</i>	<i>105</i>
OF 1.5 min	13438	772	7.8	1.0	10	815	1.0076	80628.0	80.0
OF 2 min	14443	666	6.7	1.0	10	872	1.0075	86658.0	86.0
<i>OF Average</i>	<i>13941</i>	<i>719</i>	<i>7</i>	<i>1.0</i>	<i>10</i>	<i>843</i>	<i>1.0076</i>	<i>83643</i>	<i>83.0</i>
UF 1.5 min	13694	792	145	18.3	15	10042	1.1578	54776	47.3
UF 2 min	14324	885	205.7	23.2	15	13317	1.2089	57296	47.4
<i>UF Average</i>	<i>14009</i>	<i>839</i>	<i>175</i>	<i>21</i>	<i>15</i>	<i>11680</i>	<i>1.1834</i>	<i>56036</i>	<i>47</i>
Two Sides:						23360		112072.0	94.7
						UF/(OF+UF)		1 - OF/F	UF/F
						Solids Yield to UF:	0.965	0.957	1.196
						Underflow flush (L/min):	3		
						Launder Wash (L/min):	30.2		
						Fluidisation (L/min):	42		
						Volume Balance: In =	180.2		
						Out =	177.7		
						Ratio:	1.01		
						Solids In/Out =	0.81		
						Average Yield =	0.961		

Takes into account water from Launder and U/F Flush

TRUE U/F	
Flowrate L/min	Solids Conc. wt.%
61.5	29.6

Gravity Separation and Desliming Using Inclined Channels Subject to Different G-Forces

CF257

		Solids Density		3.9					
	Slurry weight (g)	Sub sample		Solids Conc. (wt. %)	Sample time (s)	Solids Rate (g/min)	Slurry Density (g/ml)	Mass Flow (g/min)	Volumetric Flow (L/min)
		Slurry Weight (g)	Solids Weight (g)						
Feed 1	13237	824	86.4	10.5		8302	1.0846	79173	73.0
Feed 2	14017	889	127.4	14.3	-	11709	1.1193	81707	73.0
<i>Feed Average</i>	<i>13627</i>	<i>856.5</i>	<i>106.9</i>	<i>12.4</i>		<i>10005</i>	<i>1.1019</i>	<i>80439.9</i>	<i>73</i>
OF 2 min	15777				15				
OF 3 min	15773				15				
<i>OF 4 min</i>	<i>15170</i>	<i>904</i>	<i>7</i>	<i>0.8</i>	<i>15</i>	<i>490</i>	<i>1.0060</i>	<i>60680</i>	<i>60.3</i>
<i>OF Average</i>	<i>15573</i>	<i>904</i>	<i>7</i>	<i>0.8</i>	<i>15</i>	<i>490</i>	<i>1.0060</i>	<i>60680</i>	<i>60</i>
UF 2 min	10940				10				
UF 3 min	10161				10				
UF 4 min	10195	702	55.1	7.8	10	4801	1.0620	61170	57.6
<i>UF Average</i>	<i>10568</i>	<i>702</i>	<i>55</i>	<i>7.8</i>	<i>10</i>	<i>4801</i>	<i>1.0620</i>	<i>61170</i>	<i>58</i>
Two Sides:						9602		122340.0	115.2
						UF/(OF+UF)		1 - OF/F	UF/F
Solids Yield to UF:						0.951		0.951	0.960
Underflow flush (L/min):						3			
Launder Wash (L/min):						30.2			
Fluidisation (L/min):						60			
Volume Balance: In =							166.2		
Out =							175.5		
Ratio:							0.95		
Solids In/Out =							0.99		
Average Yield =							0.954		

Takes into account water from Launder and U/F Flush

TRUE U/F	
Flowrate	Solids Conc.
L/min	wt. %
82.0	10.8

CF258

		Solids Density		3.9					
	Slurry weight (g)	Sub sample		Solids Conc. (wt. %)	Sample time (s)	Solids Rate (g/min)	Slurry Density (g/ml)	Mass Flow (g/min)	Volumetric Flow (L/min)
		Slurry Weight (g)	Solids Weight (g)						
Feed 1	14490								
Feed 2	14566	900	113.7	12.6	-	7250	1.1037	57391	52.0
<i>Feed Average</i>	<i>14528</i>	<i>900</i>	<i>113.7</i>	<i>12.6</i>		<i>7250</i>	<i>1.1037</i>	<i>57391.4</i>	<i>52</i>
OF 2 min	31471				55				
OF 4 min	36820				55				
<i>OF 6 min</i>	<i>31053</i>	<i>1019</i>	<i>9</i>	<i>0.9</i>	<i>55</i>	<i>309</i>	<i>1.0068</i>	<i>33876</i>	<i>33.6</i>
<i>OF Average</i>	<i>33115</i>	<i>1019</i>	<i>9</i>	<i>0.9</i>	<i>55</i>	<i>309</i>	<i>1.0068</i>	<i>33876</i>	<i>34</i>
UF 2 min	18229				20				
UF 4 min	19192				20				
UF 6 min	19005	833	43.5	5.2	20	2977	1.0404	57015	54.8
<i>UF Average</i>	<i>18617</i>	<i>833</i>	<i>44</i>	<i>5.2</i>	<i>20</i>	<i>2977</i>	<i>1.0404</i>	<i>57015</i>	<i>55</i>
Two Sides:						5955		114030.0	109.6
						UF/(OF+UF)		1 - OF/F	UF/F
						Solids Yield to UF:	0.951	0.957	0.821
						Underflow flush (L/min):	3		
						Launder Wash (L/min):	30.2		
						Fluidisation (L/min):	60		
						Volume Balance: In =	145.2		
						Out =	143.2		
						Ratio:	1.01		
						Solids In/Out =	1.16		
						Average Yield =	0.954		

Takes into account water from Launder and U/F Flush

TRUE U/F	
Flowrate	Solids Conc.
L/min	wt. %
76.4	7.4

Gravity Separation and Desliming Using Inclined Channels Subject to Different G-Forces

S24B

					Solids Density	4.4						
	Sample time (s)	Slurry Weight (g)	Solids Weight (g)	Solids Conc. (wt. %)	Solids Rate (g/min)	Slurry Density (g/ml)	Mass Flow (g/min)	Volumetric Flow (L/min)				
Feed												
1	120	25380.5	8782.9	34.6	4391.5	1.4	12690.3	9.3				
Average				34.6	4391.5	1.4	12690.3	9.3				
Overflow												
1	90	17408.2	5149.0	29.6	3432.7	1.3	11605.5	9.0				
2	90	18001	5352.1	29.7	3568.1	1.3	12000.7	9.2				
3	90	17484.6	4930.1	28.2	3286.7	1.3	11656.4	9.1				
4	90	17953.5	5343.7	29.8	3562.5	1.3	11969.0	9.2				
5	90	18280.4	5429.5	29.7	3619.7	1.3	12186.9	9.4				
6	90	17536.3	4969.0	28.3	3312.7	1.3	11690.9	9.1				
7	90	17675.4	5070.8	28.7	3380.5	1.3	11783.6	9.2				
8	90	17688.1	5136.7	29.0	3424.5	1.3	11792.1	9.1				
Average				29.1	3448.4	1.3	11835.6	9.2				
Underflow												
1	180	6741.5	4068.6	60.4	1356.2	1.9	2247.2	1.2				
2	180	7031.7	3901.6	55.5	1300.5	1.8	2343.9	1.3				
3	180	6597.9	3554.4	53.9	1184.8	1.7	2199.3	1.3	TRUE U/F	TRUE U/F		
4	180	6680.4	3608.6	54.0	1202.9	1.7	2226.8	1.3	L/min	wt. %		
Average				55.9	1261.1	1.8	2254.3	1.3	0.6	81.1		
					U/F buffer (L/min)	0.7						
					Fluidisation (L/min)	0.7						
					Volume Balance: In =	10.7			Solids Yield to	UF/(OF+UF)	1 - OF/F	UF/F
					Out =	10.5			0.268	0.215	0.287	
					Ratio:	1.02			UF:	Average Yield =	0.257	
					Solids In/Out =	0.93						

Appendix C: Experimental Data and Sampling

S24B2

					Solids Densi	4.4							
	Sample time (s)	Slurry Weight (g)	Solids Weight (g)	Solids Conc. (wt. %)	Solids Rate (g/min)	Slurry Density (g/ml)	Mass Flow (g/min)	Volumetric Flow (L/min)					
Feed													
1	120	12692.9	4717.6	37.2	2358.8	1.4	6346.5	4.5					
2	120	12653.9	4687.4	37.0	2343.7	1.4	6327.0	4.5					
Average				37.1	2351.3	1.4	6336.7	4.5					
Overflow													
1	150	15799.7	4472.8	28.3	1789.1	1.3	6319.9	4.9					
2	150	15655.9	4548.9	29.1	1819.6	1.3	6262.4	4.9					
3	150	16049.4	4700.0	29.3	1880.0	1.3	6419.8	5.0					
4	150	15990.3	4664.0	29.2	1865.6	1.3	6396.1	5.0					
5	150	14960.8	3843.2	25.7	1537.3	1.2	5984.3	4.8					
6	150	16387.1	5002.3	30.5	2000.9	1.3	6554.8	5.0					
7	150	15539.4	4235.3	27.3	1694.1	1.3	6215.8	4.9					
8	150	15743.6	4532.8	28.8	1813.1	1.3	6297.4	4.9					
9	150	16120.5	4787.6	29.7	1915.0	1.3	6448.2	5.0					
10	150	14968.6	3859.1	25.8	1543.6	1.2	5987.4	4.8					
Average				28.4	1785.8	1.3	6288.6	4.9					
Underflow													
1	300	7345.6	3850.2	52.4	770.0	1.7	1469.1	0.9					
2	300	6039.8	2636.4	43.7	527.3	1.5	1208.0	0.8					
3	300	7321.2	3827.7	52.3	765.5	1.7	1464.2	0.9	TRUE U/F	TRUE U/F			
4	300	6971	3463.0	49.7	692.6	1.6	1394.2	0.9	L/min	wt.%			
5	300	6963.2	3510.5	50.4	702.1	1.6	1392.6	0.9	0.5	70.2			
Average				49.7	691.5	1.6	1385.6	0.9					
					U/F buffer (L/min)		0.4						
					Fluidisation (L/min)		0.7						
					Volume Balance: In =		5.6						
					Out =		5.8		Solids	UF/(OF+UF)	1 - OF/F	UF/F	
					Ratio:		0.98		Yield to	0.279	0.240	0.294	
					Solids In/Out =		0.95		UF:	Average Yield =		0.271	

S24B3

					Solids Dens	4.4				
	Sample time (s)	Slurry Weight (g)	Solids Weight (g)	Solids Conc. (wt. %)	Solids Rate (g/min)	Slurry Density (g/ml)	Mass Flow (g/min)	Volumetric Flow (L/min)		
Feed										
1	240	13984.2	5209.1	37.2	1302.3	1.4	3496.1	2.5		
2	240	13921.7	5169.6	37.1	1292.4	1.4	3480.4	2.5		
<i>Average</i>				37.2	1297.3	1.4	3488.2	2.5		
Overflow										
1	240	14268	3509.6	24.6	877.4	1.2	3567.0	2.9		
2	240	14105.1	3447.9	24.4	862.0	1.2	3526.3	2.9		
3	240	13890.5	3363.2	24.2	840.8	1.2	3472.6	2.8		
4	240	13795.7	3204.7	23.2	801.2	1.2	3448.9	2.8		
5	240	13928.6	3312.7	23.8	828.2	1.2	3482.2	2.8		
6	240	13742.4	3075.6	22.4	768.9	1.2	3435.6	2.8		
7	240	13765.9	3248.1	23.6	812.0	1.2	3441.5	2.8		
8	240	14438.1	3643.8	25.2	911.0	1.2	3609.5	2.9		
<i>Average</i>				23.9	837.7	1.2	3497.9	2.9		
Underflow										
1	480	8175.9	3208.6	39.2	401.1	1.4	1022.0	0.7		
2	480	9299.5	4311.7	46.4	539.0	1.6	1162.4	0.7		
3	480	8724.1	3722.7	42.7	465.3	1.5	1090.5	0.7		
4	480	8162	3215.0	39.4	401.9	1.4	1020.3	0.7		
<i>Average</i>				41.9	451.8	1.5	1073.8	0.7		
					U/F buffer (L/min)		0.4		TRUE U/F	TRUE U/F
					Fluidisation (L/min)		0.7		L/min	wt. %
								0.3		67.1
					Volume Balance: In =		3.6			
					Out =		3.6		Solids	
					Ratio:		1.00		UF/(OF+UF)	1 - OF/F
					Solids In/Out =		1.01		0.350	0.354
									UF/F	UF/F
									Average Yield =	0.351

S24D

					Solids Der	4.4					
	Sample time (s)	Slurry Weight (g)	Solids Weight (g)	Solids Conc. (wt. %)	Solids Rate (g/min)	Slurry Density (g/ml)	Mass Flow (g/min)	Volumetric Flow (L/min)			
Feed											
1	180	18847.9	4030.4	21.4	1343.5	1.2	6282.6	5.2			
2	180	18782.9	4004.9	21.3	1335.0	1.2	6261.0	5.2			
Average				21.4	1339.2	1.2	6271.8	5.2			
Overflow											
1	180	17373.4	1525.5	8.8	508.5	1.1	5791.1	5.4			
2	180	17154.5	1506.1	8.8	502.0	1.1	5718.2	5.3			
3	180	17389.4	1556.0	8.9	518.7	1.1	5796.5	5.4			
4	180	17606.9	1665.3	9.5	555.1	1.1	5869.0	5.4			
5	180	17278.8	1510.3	8.7	503.4	1.1	5759.6	5.4			
6	180	17797.6	1874.7	10.5	624.9	1.1	5932.5	5.4			
Average				9.2	535.4	1.1	5811.1	5.4			
Underflow											
1	360	8590	4378.7	51.0	729.8	1.6	1431.7	0.9			
2	360	7463.1	3367.6	45.1	561.3	1.5	1243.9	0.8	TRUE U/F	TRUE U/F	
3	360	7814	3694.6	47.3	615.8	1.6	1302.3	0.8	L/min	wt. %	
Average				47.8	635.6	1.6	1326.0	0.8	0.4	68.6	
					U/F buffer (L/min)	0.4					
					Fluidisation (L/min)	0.55					
					Volume Balance: In =	6.2	Solids Yield to	UF/(OF+UF)	1 - OF/F	UF/F	
					Out =	6.2	UF:	0.543	0.600	0.475	
					Ratio:	0.99	Average Yield =				
					Solids In/Out =	1.14					

S24D2

					Solids Densi	4.4					
	Sample time (s)	Slurry Weight (g)	Solids Weight (g)	Solids Conc. (wt. %)	Solids Rate (g/min)	Slurry Density (g/ml)	Mass Flow (g/min)	Volumetric Flow (L/min)			
Feed											
1	300	13563.1	2632.3	19.4	526.5	1.2	2712.6	2.3			
2	300	13346.8	2552.3	19.1	510.5	1.2	2669.4	2.3			
Average				19.3	518.5	1.2	2691.0	2.3			
Overflow											
1	300	14092.2	1160.0	8.2	232.0	1.1	2818.4	2.6			
2	300	13881.3	1113.2	8.0	222.6	1.1	2776.3	2.6			
3	300	14290.3	1388.5	9.7	277.7	1.1	2858.1	2.6			
4	300	13731.7	840.3	6.1	168.1	1.0	2746.3	2.6			
5	300	14370.3	1302.0	9.1	260.4	1.1	2874.1	2.7			
6	300	13623	1021.3	7.5	204.3	1.1	2724.6	2.6			
7	300	14312.7	1240.5	8.7	248.1	1.1	2862.5	2.7			
8	300	14178.5	1370.4	9.7	274.1	1.1	2835.7	2.6			
Average				8.4	235.9	1.1	2812.0	2.6			
Underflow											
1	600	9327.2	2997.0	32.1	299.7	1.3	932.7	0.7			
2	600	9763.1	3342.5	34.2	334.3	1.4	976.3	0.7			
3	600	9351.1	3032.3	32.4	303.2	1.3	935.1	0.7			
4	600	8478.9	2254.5	26.6	225.5	1.3	847.9	0.7			
Average				31.3	290.7	1.3	923.0	0.7			
						U/F buffer (L/min)	0.4		TRUE U/F	TRUE U/F	
						Fluidisation (L/min)	0.7		L/min	wt. %	
								0.3		55.6	
						Volume Balance: In =	3.4				
						Out =	3.3		Solids	UF/(OF+UF)	
						Ratio:	1.02		Yield to	1 - OF/F	
						Solids In/Out =	0.98		UF:	UF/F	
									0.552	0.545	
									Average Yield =	0.553	

Appendix C: Experimental Data and Sampling

S24E

						Solids Densi	4.4						
		Sample time (s)	Slurry Weight (g)	Solids Weight (g)	Solids Conc. (wt. %)	Solids Rate (g/min)	Slurry Density (g/ml)	Mass Flow (g/min)	Volumetric Flow (L/min)				
	Feed												
	1	90	17557.6	1628.2	9.3	1085.5	1.1	11705.1	10.9				
	2	90	17708.1	1632.9	9.2	1088.6	1.1	11805.4	11.0				
	3	90	17602.6	1616	9.2	1077.3	1.1	11735.1	10.9				
	4	90	17626.9	1643.2	9.3	1095.5	1.1	11751.3	10.9				
	5	90	17616.2	1661.6	9.4	1107.7	1.1	11744.1	10.9				
	Average				9.3	1090.9	1.1	11748.2	10.9				
	Overflow												
	1	240	49338.3	1850.6	3.8	462.7	1.0	12334.6	12.0				
	2	240	48458.2	1768.3	3.6	442.1	1.0	12114.6	11.8				
	3	240	49257.8	1733.6	3.5	433.4	1.0	12314.5	12.0				
	4	240	48667.8	1710.4	3.5	427.6	1.0	12167.0	11.8				
	5	240	49755.5	2529.9	5.1	632.5	1.0	12438.9	12.0				
	Average				3.9	479.6	1.0	12273.9	11.9				
	Underflow												
	1	300	6619	3154.2	47.7	630.8	1.6	1323.8	0.8				
	2	300	7607.5	4121.9	54.2	824.4	1.7	1521.5	0.9				
	3	300	7176.8	3731.4	52.0	746.3	1.7	1435.4	0.9				
	4	300	5810.7	2542.2	43.8	508.4	1.5	1162.1	0.8				
	Average				49.4	677.5	1.6	1360.7	0.8				
						U/F buffer (L/min)	0.4				TRUE U/F	TRUE U/F	
						Fluidisation (L/min)	0.55				L/min	wt. %	
											0.4	70.5	
						Volume Balance: In =	11.9						
						Out =	12.7			Solids	UF/(OF+UF)	1 - OF/F	UF/F
						Ratio:	0.93			Yield to	0.585	0.560	0.621
						Solids In/Out =	0.94			UF:	Average Yield =		0.589

S24E2

					Solids Density (g/ml)	4.4						
	Sample time (s)	Slurry Weight (g)	Solids Weight (g)	Solids Conc. (wt. %)	Solids Rate (g/min)	Slurry Density (g/ml)	Mass Flow (g/min)	Volumetric Flow (L/min)				
Feed												
1	150	15519.3	1475.6	9.5	590.2	1.1	6207.7	5.8				
2	150	15489.7	1356.8	8.8	542.7	1.1	6195.9	5.8				
3	150	15497.7	1356.1	8.8	542.4	1.1	6199.1	5.8				
4	150	15472.2	1346.1	8.7	538.4	1.1	6188.9	5.8				
5	150	15478	1327.4	8.6	531.0	1.1	6191.2	5.8				
6	150	15019.9	1373.9	9.1	549.6	1.1	6008.0	5.6				
Average				8.9	549.1	1.1	6165.1	5.7				
Overflow												
1	1500	155516.7	5752.2	3.7	230.1	1.0	6220.7	6.0				
2	1500	155610.4	5594.0	3.6	223.8	1.0	6224.4	6.1				
Average				3.6	226.9	1.0	6222.5	6.0				
Underflow												
1	600	9923.1	3627.2	36.6	362.7	1.4	992.3	0.7				
2	600	10385.3	4015.6	38.7	401.6	1.4	1038.5	0.7				
3	600	9786.4	3475.9	35.5	347.6	1.4	978.6	0.7				
4	600	10773.8	4349.1	40.4	434.9	1.5	1077.4	0.7		TRUE U/F	TRUE U/F	
5	600	9715.5	3381.2	34.8	338.1	1.4	971.6	0.7		L/min	wt. %	
Average				37.2	377.0	1.4	1011.7	0.7		0.3	61.6	
					U/F buffer (L/min)		0.4					
					Fluidisation (L/min)		0.55					
					Volume Balance: In =		6.7		Solids	UF/(OF+UF) 1 - OF/F	UF/F	
					Out =		6.8		Yield to	0.624	0.587	0.687
					Ratio:		0.99		UF:	Average Yield =	0.633	
					Solids In/Out =		0.91					

Appendix C: Experimental Data and Sampling

S24F

					Solids Density	4.4							
	Sample time (s)	Slurry Weight (g)	Solids Weight (g)	Solids Conc. (wt. %)	Solids Rate (g/min)	Slurry Density (g/ml)	Mass Flow (g/min)	Volumetric Flow (L/min)					
Feed													
1	75	13856.6	4816.2	34.8	3853.0	1.4	11085.3	8.1					
2	75	13855.8	4805.9	34.7	3844.7	1.4	11084.6	8.1					
Average				34.7	3848.8	1.4	11085.0	8.1					
Overflow													
1	90	15939	4120.9	25.9	2747.3	1.2	10626.0	8.5					
2	90	16021.3	4230.0	26.4	2820.0	1.3	10680.9	8.5					
3	90	16080.1	4288.0	26.7	2858.7	1.3	10720.1	8.5					
4	90	16218.9	4428.3	27.3	2952.2	1.3	10812.6	8.5					
5	90	16238.7	4423.5	27.2	2949.0	1.3	10825.8	8.5					
6	90	15844	4049.0	25.6	2699.3	1.2	10562.7	8.5					
7	90	15996.7	4147.2	25.9	2764.8	1.3	10664.5	8.5					
8	90	15859.1	3990.1	25.2	2660.1	1.2	10572.7	8.5					
Average	90			26.3	2806.4	1.3	10683.2	8.5					
Underflow													
1	180	6609.1	4120.1	62.3	1373.4	1.9	2203.0	1.1					
2	180	6420.3	3958.4	61.7	1319.5	1.9	2140.1	1.1					
3	180	6782.3	4319.1	63.7	1439.7	2.0	2260.8	1.1			TRUE U/F	TRUE U/F	
4	180	6877.5	4398.9	64.0	1466.3	2.0	2292.5	1.2			L/min	wt.%	
Average	180			62.9	1399.7	1.9	2224.1	1.1			0.7	76.7	
					U/F buffer (L/min)		0.4						
					Fluidisation (L/min)		0.6						
					Volume Balance: In =		9.1		Solids Yield to UF:	UF/(OF+UF)	1 - OF/F	UF/F	
					Out =		9.7			0.333	0.271	0.364	
					Ratio:		0.94			Average Yield =		0.322	
					Solids In/Out =		0.92						

S24F2

					Solids Densi	4.4						
	Sample time (s)	Slurry Weight (g)	Solids Weight (g)	Solids Conc. (wt. %)	Solids Rate (g/min)	Slurry Density (g/ml)	Mass Flow (g/min)	Volumetric Flow (L/min)				
Feed												
1	90	9447	3408.1	36.1	2272.1	1.4	6298.0	4.5				
2	90	9323.2	3327	35.7	2218.0	1.4	6215.5	4.5				
Average				35.9	2245.0	1.4	6256.7	4.5				
Overflow												
1	180	15992.3	3408.7	21.3	1136.2	1.2	5330.8	4.5				
2	180	16150	3483.7	21.6	1161.2	1.2	5383.3	4.5				
3	180	16439.1	3813.7	23.2	1271.2	1.2	5479.7	4.5				
4	180	16163	3590.2	22.2	1196.7	1.2	5387.7	4.5				
5	180	15964.1	3365.8	21.1	1121.9	1.2	5321.4	4.5				
6	180	16505.3	3898.6	23.6	1299.5	1.2	5501.8	4.5				
Average				22.2	1197.8	1.2	5400.8	4.5				
Underflow												
1	360	10269.6	5900.4	57.5	983.4	1.8	1711.6	1.0				
2	360	10104.2	5760.1	57.0	960.0	1.8	1684.0	0.9	TRUE U/F	TRUE U/F		
3	360	10338.3	5972.9	57.8	995.5	1.8	1723.1	1.0	L/min	wt.%		
Average				57.4	979.6	1.8	1706.2	0.9	0.5	75.0		
					U/F buffer (L/min)		0.4					
					Fluidisation (L/min)		0.55					
					Volume Balance: In =		5.5		Solids	UF/(OF+UF)	1 - OF/F	UF/F
					Out =		5.4		Yield to	0.450	0.466	0.436
					Ratio:		1.01		UF:	Average Yield =		0.451
					Solids In/Out =		1.03					

S24F3

					Solids Density	4.4						
	Sample time (s)	Slurry Weight (g)	Solids Weight (g)	Solids Conc. (wt. %)	Solids Rate (g/min)	Slurry Density (g/ml)	Mass Flow (g/min)	Volumetric Flow (L/min)				
Feed												
1	90	18741.9	3200.5	17.1	2133.7	1.2	12494.6	10.8				
2	90	18334.1	3060.1	16.7	2040.1	1.1	12222.7	10.6				
Average				16.9	2086.9	1.2	12358.7	10.7				
Overflow												
1	90	17692.5	1521.0	8.6	1014.0	1.1	11795.0	11.0				
2	90	17248	1422.4	8.2	948.3	1.1	11498.7	10.8				
3	90	17369	1455.9	8.4	970.6	1.1	11579.3	10.8				
4	90	17615	1500.3	8.5	1000.2	1.1	11743.3	11.0				
5	90	17633.7	1557.1	8.8	1038.1	1.1	11755.8	11.0				
6	90	17409.1	1383.4	7.9	922.3	1.1	11606.1	10.9				
7	90	17354.3	1424.8	8.2	949.9	1.1	11569.5	10.8				
8	90	17693.2	1540.6	8.7	1027.1	1.1	11795.5	11.0				
Average	90			8.4	983.8	1.1	11667.9	10.9				
Underflow									TRUE U/F	TRUE U/F		
1	180	6188.1	3865.5	62.5	1288.5	1.9	2062.7	1.1	L/min	wt. %		
2	180	5758.8	3455.8	60.0	1151.9	1.9	1919.6	1.0	0.6	76.5		
3	180	5864.4	3571.2	60.9	1190.4	1.9	1954.8	1.0				
4	180	5727.8	3448.3	60.2	1149.4	1.9	1909.3	1.0				
Average	180			60.9	1195.1	1.9	1961.6	1.0				
					U/F buffer (L/min)		0.4					
					Fluidisation (L/min)		0.55					
					Volume Balance: In =		11.7					
					Out =		11.9		Solids	UF/(OF+UF)	1 - OF/F	UF/F
					Ratio:		0.98		Yield to	0.548	0.529	0.573
					Solids In/Out =		0.96		UF:	Average Yield =		0.550

S24F4

					Solids Density					
					4.4					
	Sample time (s)	Slurry Weight (g)	Solids Weight (g)	Solids Conc. (wt. %)	Solids Rate (g/min)	Slurry Density (g/ml)	Mass Flow (g/min)	Volumetric Flow (L/min)		
Feed										
1	150	15920.5	2909.2	18.3	1163.7	1.2	6368.2	5.5		
2	150	15796.4	2827.6	17.9	1131.0	1.2	6318.6	5.4		
3	150	15716.4	2805.1	17.8	1122.0	1.2	6286.6	5.4		
Average				18.0	1138.9	1.2	6324.4	5.4		
Overflow										
1	180	17788.6	1292.7	7.3	430.9	1.1	5929.5	5.6		
2	180	17791.8	1291.4	7.3	430.5	1.1	5930.6	5.6		
3	180	17833.9	1322.0	7.4	440.7	1.1	5944.6	5.6		
4	180	17842.4	1284.6	7.2	428.2	1.1	5947.5	5.6		
5	180	18087.9	1325.1	7.3	441.7	1.1	6029.3	5.7		
6	180	17778.8	1340.3	7.5	446.8	1.1	5926.3	5.6		
7	180	17716.8	1197.3	6.8	399.1	1.1	5905.6	5.6		
8	180	18312.5	1485.9	8.1	495.3	1.1	6104.2	5.7		
Average				7.4	439.1	1.1	5964.7	5.6		
Underflow										
1	360	8386.5	4391.0	52.4	731.8	1.7	1397.8	0.8	TRUE U/F	TRUE U/F
2	360	7900.1	3895.3	49.3	649.2	1.6	1316.7	0.8	L/min	wt.%
3	360	7988.8	4008.7	50.2	668.1	1.6	1331.5	0.8	0.4	71.5
4	360	7587.2	3615.8	47.7	602.6	1.6	1264.5	0.8		
Average				49.9	663.0	1.6	1327.6	0.8		
					U/F buffer (L/min)		0.4			
					Fluidisation (L/min)		0.55			
					Volume Balance: In =		6.4		Solids Yield to	UF/(OF+UF)
					Out =		6.4		1 - OF/F	UF/F
					Ratio:		0.99		Average Yield =	0.582
					Solids In/Out =		1.03			0.599

S24F5

					Solids Density	4.4						
	Sample time (s)	Slurry Weight (g)	Solids Weight (g)	Solids Conc. (wt. %)	Solids Rate (g/min)	Slurry Density (g/ml)	Mass Flow (g/min)	Volumetric Flow (L/min)				
Feed												
1	90	19323.5	1474	7.6	982.7	1.1	12882.3	12.1				
2	90	19277.2	1426.1	7.4	950.7	1.1	12851.5	12.1				
3	90	19066.4	1392.4	7.3	928.3	1.1	12710.9	12.0				
4	90	18940.3	1449.8	7.7	966.5	1.1	12626.9	11.9				
Average				7.5	957.1	1.1	12767.9	12.0				
Overflow												
1	180	38085.5	1106.2	2.9	368.7	1.0	12695.2	12.4				
2	180	38617.6	1322.0	3.4	440.7	1.0	12872.5	12.5				
3	180	38090.2	1122.2	2.9	374.1	1.0	12696.7	12.4				
4	180	38652.5	1360.4	3.5	453.5	1.0	12884.2	12.5				
5	180	38242.6	1325.1	3.5	441.7	1.0	12747.5	12.4				
6	180	37879.1	1197.3	3.2	399.1	1.0	12626.4	12.3				
Average				3.2	413.0	1.0	12753.8	12.4				
Underflow												
1	180	5428.7	3116.5	57.4	1038.8	1.8	1809.6	1.0				
2	180	3994.4	1818.4	45.5	606.1	1.5	1331.5	0.9				
3	180	5114.4	2810.0	54.9	936.7	1.7	1704.8	1.0		TRUE U/F	TRUE U/F	
4	180	4490.9	2254.6	50.2	751.5	1.6	1497.0	0.9		L/min	wt. %	
5	180	5267.8	2958.7	56.2	986.2	1.8	1755.9	1.0		0.6	70.7	
6	180	4737.7	2481.6	52.4	827.2	1.7	1579.2	0.9				
Average				52.8	857.8	1.7	1613.0	1.0				
					U/F buffer (L/min)		0.4					
					Fluidisation (L/min)		0.55					
					Volume Balance: In =		13.0		Solids Yield to	UF/(OF+UF)	1 - OF/F	UF/F
					Out =		13.4			0.675	0.569	0.896
					Ratio:		0.97		UF:	Average Yield =		0.713
					Solids In/Out =		0.75					

S24F6

					Solids Der	4.4					
	Sample time (s)	Slurry Weight (g)	Solids Weight (g)	Solids Conc. (wt. %)	Solids Rate (g/min)	Slurry Density (g/ml)	Mass Flow (g/min)	Volumetric Flow (L/min)			
Feed											
1	150	15888	1366.2	8.6	546.5	1.1	6355.2	5.9			
2	150	15902.7	1375.6	8.7	550.2	1.1	6361.1	5.9			
3	150	15854.2	1344.2	8.5	537.7	1.1	6341.7	5.9			
4	150	15827.5	1343.2	8.5	537.3	1.1	6331.0	5.9			
5	150	15800.6	1296.5	8.2	518.6	1.1	6320.2	5.9			
<i>Average</i>				8.5	538.1	1.1	6341.8	5.9			
Overflow											
1	1200	128285	3814.5	3.0	190.7	1.0	6414.3	6.3			
2	1200	127577	3254.0	2.6	162.7	1.0	6378.9	6.3			
<i>Average</i>				2.8	176.7	1.0	6396.6	6.3			
Underflow											
1	600	11194.9	4397.9	39.3	439.8	1.4	1119.5	0.8			
2	600	11786.4	4982.7	42.3	498.3	1.5	1178.6	0.8			
3	600	11176.8	4417.9	39.5	441.8	1.4	1117.7	0.8	TRUE U/F	TRUE U/F	
4	600	10550.1	3801.1	36.0	380.1	1.4	1055.0	0.8	L/min	wt.%	
<i>Average</i>				39.3	440.0	1.4	1117.7	0.8	0.4	61.3	
					U/F buffer (L/min)	0.4					
					Fluidisation (L/min)	0.55					
					Volume Balance: In =	6.9	Solids	UF/(OF+UF)	1 - OF/F	UF/F	
					Out =	7.0	Yield to	0.713	0.672	0.818	
					Ratio:	0.98	UF:	Average Yield =		0.734	
					Solids In/Out =	0.87					

S24G

					Solids Densit	4.4						
	Sample time (s)	Slurry Weight (g)	Solids Weight (g)	Solids Conc. (wt. %)	Solids Rate (g/min)	Slurry Density (g/ml)	Mass Flow (g/min)	Volumetric Flow (L/min)				
Feed												
1	180	18813.9	3452.6	18.4	1150.9	1.2	6271.3	5.4				
2	180	18849.3	3431.5	18.2	1143.8	1.2	6283.1	5.4				
Average				18.3	1147.4	1.2	6277.2	5.4				
Overflow												
1	150	15278.1	1612.7	10.6	645.1	1.1	6111.2	5.6				
2	150	14562.7	1217.7	8.4	487.1	1.1	5825.1	5.4				
3	150	14740	1226.1	8.3	490.4	1.1	5896.0	5.5				
4	150	14633.8	1171.3	8.0	468.5	1.1	5853.5	5.5				
5	150	14660.1	1119.8	7.6	447.9	1.1	5864.0	5.5				
6	150	14790.9	1263.9	8.5	505.6	1.1	5916.4	5.5				
7	150	14619.7	1157.8	7.9	463.1	1.1	5847.9	5.5				
8	150	14340.7	1050.7	7.3	420.3	1.1	5736.3	5.4				
Average				8.3	491.0	1.1	5881.3	5.5				
Underflow									TRUE U/F	TRUE U/F		
1	300	7790	4106.4	52.7	821.3	1.7	1558.0	0.9	L/min	wt. %		
2	300	7794.1	4069.7	52.2	813.9	1.7	1558.8	0.9	0.5	70.5		
3	300	7274.6	3633.4	49.9	726.7	1.6	1454.9	0.9				
4	300	8110.6	4380.5	54.0	876.1	1.7	1622.1	0.9				
Average				52.2	809.5	1.7	1548.5	0.9				
					U/F buffer (L/min)		0.4					
					Fluidisation (L/min)		0.55					
					Volume Balance:	In =	6.3		Solids Yield to	UF/(OF+UF)	1 - OF/F	UF/F
						Out =	6.4		0.622	0.572	0.706	
						Ratio:	0.99		UF:	Average Yield =	0.633	
					Solids In/Out =		0.88					

S24G2

					Solids Density	4.4				
	Sample time (s)	Slurry Weight (g)	Solids Weight (g)	Solids Conc. (wt. %)	Solids Rate (g/min)	Slurry Density (g/ml)	Mass Flow (g/min)	Volumetric Flow (L/min)		
Feed										
1	360	22718.2	8157.4	35.9	1359.6	1.4	3786.4	2.7		
Average				35.9	1359.6	1.4	3786.4	2.7		
Overflow										
1	300	15455.8	2995.6	19.4	599.1	1.2	3091.2	2.6		
2	300	15412.7	2961.0	19.2	592.2	1.2	3082.5	2.6		
3	300	15718.3	3145.6	20.0	629.1	1.2	3143.7	2.7		
4	300	15577.3	3093.2	19.9	618.6	1.2	3115.5	2.6		
Average				19.6	609.8	1.2	3108.2	2.6		
Underflow									TRUE U/F	TRUE U/F
1	600	11029.6	5017.6	45.5	501.8	1.5	1103.0	0.7	L/min	wt. %
2	600	10410.4	4333.3	41.6	433.3	1.5	1041.0	0.7	0.3	69.6
Average				43.6	467.5	1.5	1072.0	0.7		
					U/F buffer (L/min)		0.4			
					Fluidisation (L/min)		0.55			
					Volume Balance: In =		3.7			
					Out =		3.3		Solids	
					Ratio:		1.10		Yield to	
					Solids In/Out =		1.26		UF/(OF+UF)	1 - OF/F
									0.434	0.551
									Average Yield =	0.344
									UF:	0.443

S24G3

						Solids Der	4.4						
		Sample time (s)	Slurry Weight (g)	Solids Weight (g)	Solids Conc. (wt. %)	Solids Rate (g/min)	Slurry Density (g/ml)	Mass Flow (g/min)	Volumetric Flow (L/min)				
	Feed												
	1	180	19301.3	6968.8	36.1	2322.9	1.4	6433.8	4.6				
	<i>Average</i>				36.1	2322.9	1.4	6433.8	4.6				
	Overflow												
	1	150	15720.2	4256.6	27.1	1702.6	1.3	6288.1	5.0				
	2	150	15417.6	4046.7	26.2	1618.7	1.3	6167.0	4.9				
	3	150	15085.7	3856.8	25.6	1542.7	1.2	6034.3	4.8				
	4	150	14929	3708.7	24.8	1483.5	1.2	5971.6	4.8				
	<i>Average</i>				25.9	1586.9	1.3	6115.3	4.9				
	Underflow												
	1	300	6867	3525.3	51.3	705.1	1.7	1373.4	0.8				
	2	300	7553.7	4126.9	54.6	825.4	1.7	1510.7	0.9		TRUE U/F	TRUE U/F	
	<i>Average</i>				53.0	765.2	1.7	1442.1	0.9		L/min	wt. %	
						U/F buffer (L/min)		0.4			0.5	73.4	
						Fluidisation (L/min)		0.55					
						Volume Balance: In =		5.6					
						Out =		5.7		Solids	UF/(OF+UF)	1 - OF/F	UF/F
						Ratio:		0.97		Yield to	0.325	0.317	0.329
						Solids In/Out =		0.99		UF:	Average Yield =		0.324

S24G4

					Solids Density	4.4					
	Sample time (s)	Slurry Weight (g)	Solids Weight (g)	Solids Conc. (wt. %)	Solids Rate (g/min)	Slurry Density (g/ml)	Mass Flow (g/min)	Volumetric Flow (L/min)			
Feed											
1	90	17615.1	3078.8	17.5	2052.5	1.2	11743.4	10.2			
2	90	17521.6	3077.9	17.6	2051.9	1.2	11681.1	10.1			
Average				17.5	2052.2	1.2	11712.2	10.1			
Overflow											
1	90	16857.1	1580.7	9.4	1053.8	1.1	11238.1	10.4			
2	90	16900.1	1719.7	10.2	1146.5	1.1	11266.7	10.4			
3	90	16851.2	1837.0	10.9	1224.7	1.1	11234.1	10.3			
4	90	16994	1762.6	10.4	1175.1	1.1	11329.3	10.4			
5	90	17278.2	1953.7	11.3	1302.5	1.1	11518.8	10.5			
6	90	16863.9	1524.1	9.0	1016.1	1.1	11242.6	10.5			
7	90	16679.3	1636.9	9.8	1091.3	1.1	11119.5	10.3			
8	90	16389.4	1313.3	8.0	875.5	1.1	10926.3	10.2			
Average				9.9	1110.7	1.1	11234.4	10.4			
Underflow											
1	180	4512.5	2506.3	55.5	835.4	1.8	1504.2	0.9			
2	180	4791.5	2785.2	58.1	928.4	1.8	1597.2	0.9			
3	180	4444.9	2462.7	55.4	820.9	1.7	1481.6	0.8	TRUE U/F	TRUE U/F	
4	180	5974.8	3840.2	64.3	1280.1	2.0	1991.6	1.0	L/min	wt.%	
Average				58.3	966.2	1.8	1643.6	0.9	0.5	77.7	
					U/F buffer (L/min)	0.4					
					Fluidisation (L/min)	0.55					
					Volume Balance: In =	11.1	Solids Yield to UF:	UF/(OF+UF)	1 - OF/F	UF/F	
					Out =	11.3	0.465	0.459	0.471		
					Ratio:	0.98	Average Yield =		0.465		
					Solids In/Out =	0.99					

Appendix D: Size × Assay Data

This appendix contains the raw size × assay data along with the mass balanced data and the standard deviation inputs used for each mass balance. The mass balance did not include the feed rate, solids concentration or fluidisation rate but instead, dummy values for the total solids rate of each stream. These values were based on the overall solids yield calculated from the mass flow data (Appendix B). For example, if a run had a solids yield to underflow of 60 wt.%, the solids rate inputs for the feed, underflow, and overflow would be 100, 60, and 40 respectively. The standard deviation inputs varied depending on the feed and in order to constrain the balance to the maximum grade of 69.9 wt.% Fe. In general the mass rate and mass distribution data was given larger standard deviations than the assays to allow more adjustment.

The balanced data tables include the *Solids Yield* to underflow and *Fe Recovery*. These two columns were calculated by applying Equations 4.8 and 4.9 to the *Fe assay* of each size fraction and also to the head grades to calculate the overall values. For the REFLUX™ Classifier assays, an additional column of *Mass Partition* is shown. This column applied Equation 4.8 to the mass distribution data. This column and the *Solids Yield* column should be identical and for the most part are, with only minor differences seen for some size fractions. Below is a sample calculation for Run S24B and the size fraction above 0.250 mm (top row of table).

$$\begin{aligned} \text{Solids Yield} &= (\text{Feed} - \text{O/F}) / (\text{U/F} - \text{O/F}) \times 100 \\ &= (50.5 - 25.0) / (61.2 - 25.0) \times 100 = 70.4 \text{ wt.}\% \end{aligned}$$

$$\begin{aligned} \text{Fe Recovery} &= \text{Yield} \times \text{U/F} / \text{Feed} \\ &= 70.4 \times (61.2 / 50.5) = 85.4 \% \end{aligned}$$

$$\begin{aligned} \text{Mass Partition} &= (\text{Feed} - \text{O/F}) / (\text{U/F} - \text{O/F}) \times (\text{U/F} / \text{Feed}) \times 100 \\ &= (1.0 - 0.4) / (3.2 - 0.4) \times (3.2 / 1.0) \times 100 = 70.6 \% \end{aligned}$$

Entries marked in red indicate size fractions where mass was found, however there was not enough collected to perform XRF analysis on. For these fractions, the mass balanced assumed that there was zero mass in that fraction.

S24B**Raw Data**

Run S24B	Feed		Product		Reject	
Sieve aperture (mm)	Mass (wt.%)	Assay (wt.% Fe)	Mass (wt.%)	Assay (wt.% Fe)	Mass (wt.%)	Assay (wt.% Fe)
0.250	0.9	50.0	3.3	61.9	0.4	24.8
0.180	3.9	60.1	13.6	67.1	1.6	43.5
0.125	9.7	65.7	26.5	68.6	5.1	61.2
0.090	16.8	67.5	29.0	69.0	12.6	66.2
0.063	22.9	68.2	18.0	69.0	21.3	67.7
0.045	17.5	68.6	7.4	69.2	21.7	68.1
0.038	3.9	68.4	1.3	69.6	6.5	68.4
-0.038	24.4	58.9	0.9	62.3	30.9	60.5
Head		65.2		68.4		64.3

Standard Deviations

Run S24B	Feed		Product		Reject	
Sieve aperture (mm)	Mass (wt.%)	Assay (wt.% Fe)	Mass (wt.%)	Assay (wt.% Fe)	Mass (wt.%)	Assay (wt.% Fe)
0.250	0.1	0.05	0.1	0.05	0.1	0.05
0.180	0.1	0.05	0.1	0.05	0.1	0.05
0.125	0.1	0.05	0.1	0.05	0.1	0.05
0.090	0.1	0.05	0.1	0.05	0.1	0.05
0.063	0.1	0.05	0.1	0.05	0.1	0.05
0.045	0.1	0.05	0.1	0.05	0.1	0.05
0.038	0.1	0.05	0.1	0.05	0.1	0.05
-0.038	0.1	0.05	0.1	0.05	0.1	0.05
Head		0.05		0.05		0.05
Solids rate		0.1		0.1		0.1

Balanced Data

Run S24B	Feed		Product		Reject		Mass Partition (%)	Solids Yield (wt.%)	Fe Recovery (%)
Sieve aperture (mm)	Mass (wt.%)	Assay (wt.% Fe)	Mass (wt.%)	Assay (wt.% Fe)	Mass (wt.%)	Assay (wt.% Fe)			
0.250	1.0	50.5	3.2	61.2	0.4	25.0	70.6	70.4	85.4
0.180	4.3	60.3	13.7	66.9	1.6	43.4	71.9	71.9	79.8
0.125	9.9	65.7	26.6	68.6	5.0	61.2	60.6	60.7	63.4
0.090	16.5	67.4	29.1	69.1	12.9	66.3	39.7	39.7	40.7
0.063	21.4	68.0	18.0	69.0	22.4	67.8	19.0	19.0	19.3
0.045	18.0	68.4	7.4	69.3	21.1	68.4	9.2	10.0	10.1
0.038	4.4	68.4	1.3	69.7	5.4	68.3	6.4	5.0	5.1
-0.038	24.4	59.7	0.9	62.6	31.3	59.7	0.8	0.8	0.9
Head		65.2		68.3		64.3		22.5	23.6

S24B2**Raw Data**

Run S24B2	Feed		Product		Reject	
Sieve aperture (mm)	Mass (wt.%)	Assay (wt.% Fe)	Mass (wt.%)	Assay (wt.% Fe)	Mass (wt.%)	Assay (wt.% Fe)
0.250	1.0	51.7	3.2	65.3	0.5	24.2
0.180	4.5	61.1	14.3	67.8	1.7	42.7
0.125	10.7	66.3	29.3	68.7	4.7	60.6
0.090	17.7	67.9	31.4	68.8	12.8	66.3
0.063	22.5	68.1	15.8	69.4	25.4	67.8
0.045	16.7	67.9	4.5	69.6	20.3	68.5
0.038	4.0	67.9	0.6	69.8	4.8	67.8
-0.038	22.9	59.3	0.8	64.4	29.8	58.8
Head		65.5		69.0		64.2

Standard Deviations

Run S24B2	Feed		Product		Reject	
Sieve aperture (mm)	Mass (wt.%)	Assay (wt.% Fe)	Mass (wt.%)	Assay (wt.% Fe)	Mass (wt.%)	Assay (wt.% Fe)
0.250	0.1	0.01	0.1	0.01	0.1	0.01
0.180	0.1	0.01	0.1	0.01	0.1	0.01
0.125	0.1	0.01	0.1	0.01	0.1	0.01
0.090	0.1	0.01	0.1	0.01	0.1	0.01
0.063	0.1	0.01	0.1	0.01	0.1	0.01
0.045	0.1	0.01	0.1	0.01	0.1	0.01
0.038	0.1	0.01	0.1	0.01	0.1	0.01
-0.038	0.1	0.01	0.1	0.01	0.1	0.01
Head		0.01		0.01		0.01
Solids rate		0.1		0.1		0.1

Balanced Data

Run S24B2	Feed		Product		Reject		Mass Partition (%)	Solids Yield (wt.%)	Fe Recovery (%)
Sieve aperture (mm)	Mass (wt.%)	Assay (wt.% Fe)	Mass (wt.%)	Assay (wt.% Fe)	Mass (wt.%)	Assay (wt.% Fe)			
0.250	1.1	51.8	3.0	65.2	0.5	24.7	66.8	66.8	84.2
0.180	4.8	61.2	14.2	67.9	1.7	42.5	73.8	73.8	81.8
0.125	10.9	66.2	29.5	68.8	4.7	60.8	67.1	67.1	69.8
0.090	17.3	67.7	31.4	69.4	12.6	66.3	45.0	45.0	46.1
0.063	23.1	68.2	16.0	69.3	25.5	68.0	17.1	17.1	17.3
0.045	16.3	68.2	4.5	69.7	20.2	68.0	6.8	7.7	7.9
0.038	3.9	68.0	0.6	69.4	5.0	68.0	3.9	3.9	3.9
-0.038	22.6	59.0	0.8	64.2	29.8	58.9	0.9	1.1	1.2
Head		65.3		68.8		64.1		24.7	26.1

S24B3**Raw Data**

Run S24B3	Feed		Product		Reject	
Sieve aperture (mm)	Mass (wt.%)	Assay (wt.% Fe)	Mass (wt.%)	Assay (wt.% Fe)	Mass (wt.%)	Assay (wt.% Fe)
0.250	0.9	51.0	2.1	66.2	0.4	17.9
0.180	4.2	60.7	10.7	68.5	1.3	29.1
0.125	10.3	66.2	25.6	69.0	2.6	51.6
0.090	17.8	67.6	33.9	69.3	8.1	64.1
0.063	22.5	68.4	19.8	69.5	24.1	67.8
0.045	15.7	68.7	6.2	69.2	22.5	68.6
0.038	5.4	68.6	0.8	69.5	5.7	68.1
-0.038	23.1	59.1	0.9	62.8	35.3	60.6
Head		65.4		68.9		63.2

Standard Deviations

Run S24B3	Feed		Product		Reject	
Sieve aperture (mm)	Mass (wt.%)	Assay (wt.% Fe)	Mass (wt.%)	Assay (wt.% Fe)	Mass (wt.%)	Assay (wt.% Fe)
0.250	0.1	0.01	0.1	0.01	0.1	0.01
0.180	0.1	0.01	0.1	0.01	0.1	0.01
0.125	0.1	0.01	0.1	0.01	0.1	0.01
0.090	0.1	0.01	0.1	0.01	0.1	0.01
0.063	0.1	0.01	0.1	0.01	0.1	0.01
0.045	0.1	0.01	0.1	0.01	0.1	0.01
0.038	0.1	0.01	0.1	0.01	0.1	0.01
-0.038	0.1	0.01	0.1	0.01	0.1	0.01
Head		0.01		0.01		0.01
Solids rate		0.1		0.1		0.1

Balanced Data

Run S24B3	Feed		Product		Reject		Mass Partition (%)	Solids Yield (wt.%)	Fe Recovery (%)
Sieve aperture (mm)	Mass (wt.%)	Assay (wt.% Fe)	Mass (wt.%)	Assay (wt.% Fe)	Mass (wt.%)	Assay (wt.% Fe)			
0.250	0.9	51.0	2.0	66.0	0.4	17.2	69.2	69.2	89.6
0.180	4.3	60.7	10.6	68.6	1.3	29.0	80.0	80.0	90.5
0.125	10.2	66.1	25.8	69.1	2.6	51.8	82.8	82.6	86.4
0.090	16.8	67.5	34.0	69.3	8.4	64.0	66.5	66.5	68.2
0.063	22.7	68.2	20.0	69.5	24.1	67.8	28.9	28.9	29.4
0.045	16.3	68.6	6.1	69.3	21.4	68.5	12.2	12.2	12.3
0.038	4.6	68.4	0.8	69.5	6.4	68.4	5.8	5.8	5.9
-0.038	24.1	59.7	0.9	62.1	35.4	59.7	1.2	2.5	2.6
Head		65.4		69.1		63.7		32.8	34.7

S24D**Raw Data**

Run S24D	Feed		Product		Reject	
Sieve aperture (mm)	Mass (wt.%)	Assay (wt.% Fe)	Mass (wt.%)	Assay (wt.% Fe)	Mass (wt.%)	Assay (wt.% Fe)
0.250	1.2	51.8	1.2	57.7	0.3	6.3
0.180	5.4	62.2	6.8	66.4	1.0	9.7
0.125	11.7	66.9	17.7	68.8	1.2	21.7
0.090	18.3	68.3	30.2	69.1	2.5	47.0
0.063	21.3	68.5	29.3	69.3	13.4	64.8
0.045	16.5	68.9	12.1	69.7	25.1	67.7
0.038	3.4	68.2	1.8	69.7	6.7	67.9
-0.038	22.2	60.3	0.8	61.2	49.7	60.3
Head		65.7		68.8		61.7

Standard Deviations

Run S24D	Feed		Product		Reject	
Sieve aperture (mm)	Mass (wt.%)	Assay (wt.% Fe)	Mass (wt.%)	Assay (wt.% Fe)	Mass (wt.%)	Assay (wt.% Fe)
0.250	0.1	0.01	0.1	0.01	0.1	0.01
0.180	0.1	0.01	0.1	0.01	0.1	0.01
0.125	0.1	0.01	0.1	0.01	0.1	0.01
0.090	0.1	0.01	0.1	0.01	0.1	0.01
0.063	0.1	0.01	0.1	0.01	0.1	0.01
0.045	0.1	0.01	0.1	0.01	0.1	0.01
0.038	0.1	0.01	0.1	0.01	0.1	0.01
-0.038	0.1	0.01	0.1	0.01	0.1	0.01
Head		0.01		0.01		0.01
Solids rate		0.1		0.1		0.1

Balanced Data

Run S24D	Feed		Product		Reject		Mass Partition (%)	Solids Yield (wt.%)	Fe Recovery (%)
Sieve aperture (mm)	Mass (wt.%)	Assay (wt.% Fe)	Mass (wt.%)	Assay (wt.% Fe)	Mass (wt.%)	Assay (wt.% Fe)			
0.250	0.9	51.6	1.4	57.6	0.3	4.3	87.8	88.8	99.1
0.180	4.6	61.9	6.9	66.6	1.0	9.1	91.6	91.8	98.8
0.125	11.3	66.9	17.8	68.9	1.2	21.3	95.8	95.8	98.7
0.090	19.3	68.1	30.1	69.2	2.5	47.2	95.0	95.0	96.5
0.063	22.9	68.4	29.3	69.3	12.9	64.8	78.1	78.4	79.5
0.045	16.5	68.7	12.0	69.8	23.6	67.8	44.3	44.4	45.1
0.038	3.5	68.4	1.7	69.5	6.4	67.7	30.0	38.1	38.7
-0.038	20.9	60.3	0.8	61.9	52.3	60.2	2.3	2.3	2.4
Head		66.0		68.9		61.6		61.0	63.6

S24D2**Raw Data**

Run S24D2	Feed		Product		Reject	
Sieve aperture (mm)	Mass (wt.%)	Assay (wt.% Fe)	Mass (wt.%)	Assay (wt.% Fe)	Mass (wt.%)	Assay (wt.% Fe)
0.250	0.6	47.2	1.1	54.2	0.4	8.4
0.180	3.7	59.7	6.6	65.8	1.2	9.6
0.125	9.6	66.1	17.5	68.6	1.3	18.3
0.090	17.4	67.7	30.5	68.7	2.3	42.5
0.063	22.4	68.1	30.8	68.9	14.2	64.7
0.045	18.2	68.8	10.9	69.7	25.5	68.1
0.038	3.8	68.2	1.4	69.7	6.0	67.8
-0.038	24.3	55.2	1.1	60.9	49.2	59.2
Head		65.7		68.6		60.9

Standard Deviations

Run S24D2	Feed		Product		Reject	
Sieve aperture (mm)	Mass (wt.%)	Assay (wt.% Fe)	Mass (wt.%)	Assay (wt.% Fe)	Mass (wt.%)	Assay (wt.% Fe)
0.250	0.1	0.01	0.1	0.01	0.1	0.01
0.180	0.1	0.01	0.1	0.01	0.1	0.01
0.125	0.1	0.01	0.1	0.01	0.1	0.01
0.090	0.1	0.01	0.1	0.01	0.1	0.01
0.063	0.1	0.01	0.1	0.01	0.1	0.01
0.045	0.1	0.01	0.1	0.01	0.1	0.01
0.038	0.1	0.01	0.1	0.01	0.1	0.01
-0.038	0.1	0.01	0.1	0.01	0.1	0.01
Head		0.01		0.01		0.01
Solids rate		0.1		0.1		0.1

Balanced Data

Run S24D2	Feed		Product		Reject		Mass Partition (%)	Solids Yield (wt.%)	Fe Recovery (%)
Sieve aperture (mm)	Mass (wt.%)	Assay (wt.% Fe)	Mass (wt.%)	Assay (wt.% Fe)	Mass (wt.%)	Assay (wt.% Fe)			
0.250	0.7	46.2	1.1	53.7	0.3	9.1	83.1	83.1	96.7
0.180	4.2	59.5	6.5	66.0	1.1	9.1	88.2	88.6	98.3
0.125	10.5	66.0	17.6	68.6	1.3	18.0	94.7	94.9	98.6
0.090	18.2	67.5	30.6	69.0	2.3	42.7	94.6	94.4	96.4
0.063	23.5	68.0	31.0	69.1	13.9	64.9	74.2	74.1	75.3
0.045	17.4	68.8	10.7	69.8	26.0	68.3	34.7	34.7	35.2
0.038	3.7	68.4	1.4	69.4	6.7	68.1	21.5	21.5	21.8
-0.038	21.8	57.3	1.1	60.7	48.4	57.2	2.8	2.8	3.0
Head		65.0		68.6		60.3		56.2	59.3

S24E**Raw Data**

Run S24E	Feed		Product		Reject	
Sieve aperture (mm)	Mass (wt.%)	Assay (wt.% Fe)	Mass (wt.%)	Assay (wt.% Fe)	Mass (wt.%)	Assay (wt.% Fe)
0.250	0.8	49.4	1.2	60.3	0.6	7.7
0.180	4.0	60.7	7.1	66.6	1.3	8.8
0.125	10.1	66.3	17.3	68.6	1.1	12.9
0.090	17.7	67.7	28.2	69.4	1.3	25.1
0.063	21.8	68.0	30.2	69.2	8.0	61.3
0.045	17.8	68.7	13.5	69.7	26.9	68.1
0.038	3.9	68.2	1.8	69.8	7.1	68.2
-0.038	23.8	58.1	0.7	66.8	53.7	59.9
Head		65.8		68.6		60.8

Standard Deviations

Run S24E	Feed		Product		Reject	
Sieve aperture (mm)	Mass (wt.%)	Assay (wt.% Fe)	Mass (wt.%)	Assay (wt.% Fe)	Mass (wt.%)	Assay (wt.% Fe)
0.250	0.1	0.01	0.1	0.01	0.1	0.01
0.180	0.1	0.01	0.1	0.01	0.1	0.01
0.125	0.1	0.01	0.1	0.01	0.1	0.01
0.090	0.1	0.01	0.1	0.01	0.1	0.01
0.063	0.1	0.01	0.1	0.01	0.1	0.01
0.045	0.1	0.01	0.1	0.01	0.1	0.01
0.038	0.1	0.01	0.1	0.01	0.1	0.01
-0.038	0.1	0.01	0.1	0.01	0.1	0.01
Head		0.01		0.01		0.01
Solids rate		0.1		0.1		0.1

Balanced Data

Run S24E	Feed		Product		Reject		Mass Partition (%)	Solids Yield (wt.%)	Fe Recovery (%)
Sieve aperture (mm)	Mass (wt.%)	Assay (wt.% Fe)	Mass (wt.%)	Assay (wt.% Fe)	Mass (wt.%)	Assay (wt.% Fe)			
0.250	0.9	49.2	1.2	60.8	0.5	7.5	78.1	78.1	96.7
0.180	4.7	60.6	7.0	66.7	1.2	9.1	89.5	89.4	98.4
0.125	10.9	66.3	17.4	68.5	1.1	12.5	96.0	96.0	99.3
0.090	17.4	67.8	28.2	69.1	1.3	25.2	97.1	97.1	98.9
0.063	21.4	68.0	30.3	69.2	8.0	61.4	85.0	85.0	86.5
0.045	18.6	68.8	13.4	69.6	26.4	68.2	43.4	45.2	45.7
0.038	4.0	68.5	1.8	69.5	7.1	67.9	28.1	35.9	36.5
-0.038	22.1	59.1	0.7	66.7	54.3	59.0	1.9	1.9	2.1
Head		65.5		68.8		60.4		60.1	63.2

S24E2**Raw Data**

Run S24E2	Feed		Product		Reject	
Sieve aperture (mm)	Mass (wt.%)	Assay (wt.% Fe)	Mass (wt.%)	Assay (wt.% Fe)	Mass (wt.%)	Assay (wt.% Fe)
0.250	0.6	50.2	1.1	57.5	0.2	8.5
0.180	3.3	59.8	6.3	65.7	0.9	6.1
0.125	8.8	65.8	16.0	68.4	1.1	9.4
0.090	16.8	67.5	28.0	69.0	1.3	16.6
0.063	22.9	67.9	31.8	68.7	3.3	50.4
0.045	18.4	68.6	14.4	69.3	24.7	67.6
0.038	3.9	68.7	1.8	69.8	7.8	68.2
-0.038	25.4	60.5	0.6	60.6	60.9	60.1
Head		65.4		68.4		59.9

Standard Deviations

Run S24E2	Feed		Product		Reject	
Sieve aperture (mm)	Mass (wt.%)	Assay (wt.% Fe)	Mass (wt.%)	Assay (wt.% Fe)	Mass (wt.%)	Assay (wt.% Fe)
0.250	0.1	0.01	0.1	0.01	0.1	0.01
0.180	0.1	0.01	0.1	0.01	0.1	0.01
0.125	0.1	0.01	0.1	0.01	0.1	0.01
0.090	0.1	0.01	0.1	0.01	0.1	0.01
0.063	0.1	0.01	0.1	0.01	0.1	0.01
0.045	0.1	0.01	0.1	0.01	0.1	0.01
0.038	0.1	0.01	0.1	0.01	0.1	0.01
-0.038	0.1	0.01	0.1	0.01	0.1	0.01
Head		0.01		0.01		0.01
Solids rate		0.1		0.1		0.1

Balanced Data

Run S24E2	Feed		Product		Reject		Mass Partition (%)	Solids Yield (wt.%)	Fe Recovery (%)
Sieve aperture (mm)	Mass (wt.%)	Assay (wt.% Fe)	Mass (wt.%)	Assay (wt.% Fe)	Mass (wt.%)	Assay (wt.% Fe)			
0.250	0.7	50.0	1.0	57.4	0.2	12.5	87.1	83.5	95.9
0.180	3.8	59.7	5.9	65.7	0.9	5.7	90.5	90.1	99.1
0.125	9.9	65.8	16.1	68.5	1.1	9.3	95.4	95.4	99.4
0.090	17.1	67.3	28.3	69.0	1.3	17.0	96.7	96.7	99.2
0.063	19.9	67.6	31.8	68.9	3.3	50.8	93.1	92.8	94.6
0.045	18.8	68.4	14.4	69.7	25.0	67.2	44.8	46.2	47.1
0.038	4.2	68.4	1.8	69.6	7.4	68.3	25.7	13.0	13.2
-0.038	25.6	60.2	0.6	60.6	60.8	60.2	1.4	1.4	1.4
Head		65.2		68.7		60.5		58.2	61.3

S24G**Raw Data**

Run S24G	Feed		Product		Reject	
Sieve aperture (mm)	Mass (wt.%)	Assay (wt.% Fe)	Mass (wt.%)	Assay (wt.% Fe)	Mass (wt.%)	Assay (wt.% Fe)
0.250	0.6	47.4	1.0	59.1	0.3	7.5
0.180	3.3	59.9	6.9	66.6	1.0	12.5
0.125	10.7	66.4	21.2	68.8	1.7	28.9
0.090	15.3	68.3	24.6	69.5	3.1	51.5
0.063	23.2	68.5	27.1	70.0	14.3	64.7
0.045	17.1	68.8	13.9	69.8	19.3	67.5
0.038	4.9	68.8	3.3	69.5	6.1	67.4
-0.038	24.8	58.4	2.1	66.0	54.2	64.4
Head		65.4		69.6		60.3

Standard Deviations

Run S24G	Feed		Product		Reject	
Sieve aperture (mm)	Mass (wt.%)	Assay (wt.% Fe)	Mass (wt.%)	Assay (wt.% Fe)	Mass (wt.%)	Assay (wt.% Fe)
0.250	0.1	0.05	0.1	0.05	0.1	0.05
0.180	0.1	0.05	0.1	0.05	0.1	0.05
0.125	0.1	0.05	0.1	0.02	0.1	0.05
0.090	0.1	0.05	0.1	0.01	0.1	0.05
0.063	0.1	0.05	0.1	0.01	0.1	0.05
0.045	0.1	0.05	0.1	0.02	0.1	0.05
0.038	0.1	0.05	0.1	0.02	0.1	0.05
-0.038	0.1	0.05	0.1	0.05	0.1	0.05
Head		0.05		0.05		0.05
Solids rate		0.1		0.1		0.1

Balanced Data

Run S24G	Feed		Product		Reject		Mass Partition (%)	Solids Yield (wt.%)	Fe Recovery (%)
Sieve aperture (mm)	Mass (wt.%)	Assay (wt.% Fe)	Mass (wt.%)	Assay (wt.% Fe)	Mass (wt.%)	Assay (wt.% Fe)			
0.250	0.6	48.1	0.9	58.3	0.3	7.6	79.8	79.8	96.8
0.180	4.0	60.7	6.4	66.4	1.0	12.6	89.3	89.3	97.8
0.125	12.3	66.6	20.7	69.0	1.7	29.3	94.0	94.0	97.3
0.090	15.3	67.8	24.8	69.4	3.1	51.5	91.1	91.1	93.3
0.063	21.7	68.5	27.6	69.9	14.3	65.2	71.0	71.0	72.4
0.045	16.5	68.5	14.1	69.9	19.6	67.2	47.8	47.7	48.6
0.038	4.7	68.4	3.4	69.5	6.3	67.6	40.8	40.8	41.5
-0.038	24.8	59.8	2.1	65.6	53.8	59.5	4.8	4.8	5.2
Head		65.6		69.2		61.0		56.0	59.1

S24G2**Raw Data**

Run S24G2	Feed		Product		Reject	
Sieve aperture (mm)	Mass (wt.%)	Assay (wt.% Fe)	Mass (wt.%)	Assay (wt.% Fe)	Mass (wt.%)	Assay (wt.% Fe)
0.250	0.6	47.4	0.6	57.4	0.2	8.4
0.180	3.4	59.7	5.4	67.2	0.8	14.4
0.125	10.6	66.6	20.1	68.6	1.4	33.2
0.090	15.3	67.8	28.0	69.2	3.2	55.0
0.063	23.4	68.1	30.6	69.9	19.3	66.8
0.045	17.4	68.3	11.3	69.8	22.5	67.8
0.038	4.4	68.4	2.1	69.8	5.1	67.6
-0.038	25.0	58.4	1.9	63.3	47.4	65.2
Head		65.6		69.2		61.7

Standard Deviations

Run S24G2	Feed		Product		Reject	
Sieve aperture (mm)	Mass (wt.%)	Assay (wt.% Fe)	Mass (wt.%)	Assay (wt.% Fe)	Mass (wt.%)	Assay (wt.% Fe)
0.250	0.1	0.05	0.1	0.05	0.1	0.05
0.180	0.1	0.05	0.1	0.05	0.1	0.05
0.125	0.1	0.05	0.1	0.05	0.1	0.05
0.090	0.1	0.05	0.1	0.05	0.1	0.05
0.063	0.1	0.05	0.1	0.02	0.1	0.05
0.045	0.1	0.05	0.1	0.02	0.1	0.05
0.038	0.1	0.05	0.1	0.02	0.1	0.05
-0.038	0.1	0.05	0.1	0.05	0.1	0.05
Head		0.05		0.05		0.05
Solids rate		0.1		0.1		0.1

Balanced Data

Run S24G2	Feed		Product		Reject		Mass Partition (%)	Solids Yield (wt.%)	Fe Recovery (%)
Sieve aperture (mm)	Mass (wt.%)	Assay (wt.% Fe)	Mass (wt.%)	Assay (wt.% Fe)	Mass (wt.%)	Assay (wt.% Fe)			
0.250	0.4	46.5	0.7	58.4	0.2	8.3	76.1	76.2	95.7
0.180	3.1	59.9	5.5	66.9	0.8	14.4	86.8	86.8	96.8
0.125	10.5	66.4	20.0	68.8	1.4	33.2	93.2	93.2	96.6
0.090	15.3	67.7	27.9	69.2	3.2	55.1	89.3	89.3	91.3
0.063	24.6	68.5	30.6	69.9	18.9	66.3	60.9	60.9	62.2
0.045	17.1	68.2	11.2	69.8	22.8	67.4	32.0	31.9	32.6
0.038	3.9	68.2	2.2	69.8	5.5	67.6	27.6	27.6	28.3
-0.038	25.0	61.2	1.9	63.2	47.2	61.1	3.7	3.7	3.8
Head		65.9		69.1		62.8		49.0	51.4

S24G3**Raw Data**

Run S24G3	Feed		Product		Reject	
Sieve aperture (mm)	Mass (wt.%)	Assay (wt.% Fe)	Mass (wt.%)	Assay (wt.% Fe)	Mass (wt.%)	Assay (wt.% Fe)
0.250	0.5	47.4	1.3	59.0	0.2	14.7
0.180	3.2	59.5	8.5	67.0	0.9	28.1
0.125	10.0	66.4	25.2	69.0	3.0	54.4
0.090	14.9	68.0	28.1	69.6	7.8	64.3
0.063	23.6	68.6	24.4	69.6	23.9	67.5
0.045	17.5	68.6	9.6	69.6	21.3	68.2
0.038	4.2	68.4	1.8	69.8	4.8	68.2
-0.038	26.0	59.8	1.2	60.5	38.1	59.0
Head		65.5		69.1		63.4

Standard Deviations

Run S24G3	Feed		Product		Reject	
Sieve aperture (mm)	Mass (wt.%)	Assay (wt.% Fe)	Mass (wt.%)	Assay (wt.% Fe)	Mass (wt.%)	Assay (wt.% Fe)
0.250	0.1	0.05	0.1	0.05	0.1	0.05
0.180	0.1	0.05	0.1	0.05	0.1	0.05
0.125	0.1	0.05	0.1	0.02	0.1	0.05
0.090	0.1	0.05	0.1	0.02	0.1	0.05
0.063	0.1	0.05	0.1	0.02	0.1	0.05
0.045	0.1	0.05	0.1	0.02	0.1	0.05
0.038	0.1	0.05	0.1	0.02	0.1	0.05
-0.038	0.1	0.05	0.1	0.05	0.1	0.05
Head		0.05		0.05		0.05
Solids rate		0.1		0.1		0.1

Balanced Data

Run S24G3	Feed		Product		Reject		Mass Partition (%)	Solids Yield (wt.%)	Fe Recovery (%)
Sieve aperture (mm)	Mass (wt.%)	Assay (wt.% Fe)	Mass (wt.%)	Assay (wt.% Fe)	Mass (wt.%)	Assay (wt.% Fe)			
0.250	0.5	47.4	1.2	58.9	0.2	14.6	74.0	74.0	92.0
0.180	3.2	59.5	8.4	66.9	0.9	28.1	80.9	80.9	91.0
0.125	9.9	66.0	25.3	69.1	3.0	54.6	79.1	79.1	82.7
0.090	14.2	67.6	28.0	69.7	8.0	64.4	61.3	61.3	63.2
0.063	24.0	68.3	24.4	69.6	23.8	67.7	31.6	31.6	32.2
0.045	17.5	68.5	9.5	69.6	21.1	68.2	16.9	16.9	17.2
0.038	4.0	68.4	1.8	69.8	5.0	68.1	14.1	14.1	14.4
-0.038	26.6	59.4	1.2	60.6	38.0	59.4	1.4	1.4	1.4
Head		65.3		69.0		63.6		31.1	32.9

S24G4**Raw Data**

Run S24G4	Feed		Product		Reject	
Sieve aperture (mm)	Mass (wt.%)	Assay (wt.% Fe)	Mass (wt.%)	Assay (wt.% Fe)	Mass (wt.%)	Assay (wt.% Fe)
0.250	0.7	49.3	1.1	61.8	0.3	14.2
0.180	3.7	60.4	7.1	67.2	0.9	17.3
0.125	11.1	66.0	21.5	68.8	1.7	39.1
0.090	15.5	67.7	27.0	69.4	4.3	58.5
0.063	23.6	67.9	27.1	69.3	19.8	66.6
0.045	16.5	67.9	12.9	69.8	21.9	67.5
0.038	4.0	68.1	2.4	69.3	5.8	67.9
-0.038	24.8	64.7	0.9	64.2	45.4	51.1
Head		65.3		68.8		62.3

Standard Deviations

Run S24G4	Feed		Product		Reject	
Sieve aperture (mm)	Mass (wt.%)	Assay (wt.% Fe)	Mass (wt.%)	Assay (wt.% Fe)	Mass (wt.%)	Assay (wt.% Fe)
0.250	0.1	0.05	0.1	0.05	0.1	0.05
0.180	0.1	0.05	0.1	0.05	0.1	0.05
0.125	0.1	0.05	0.1	0.05	0.1	0.05
0.090	0.1	0.05	0.1	0.02	0.1	0.05
0.063	0.1	0.05	0.1	0.05	0.1	0.05
0.045	0.1	0.05	0.1	0.01	0.1	0.05
0.038	0.1	0.05	0.1	0.02	0.1	0.05
-0.038	0.1	0.05	0.1	0.05	0.1	0.05
Head		0.05		0.05		0.05
Solids rate		0.1		0.1		0.1

Balanced Data

Run S24G4	Feed		Product		Reject		Mass Partition (%)	Solids Yield (wt.%)	Fe Recovery (%)
Sieve aperture (mm)	Mass (wt.%)	Assay (wt.% Fe)	Mass (wt.%)	Assay (wt.% Fe)	Mass (wt.%)	Assay (wt.% Fe)			
0.250	0.7	49.8	1.1	60.5	0.3	14.3	76.7	76.7	93.3
0.180	3.8	60.8	7.0	67.0	0.9	17.2	87.7	87.6	96.5
0.125	11.1	66.0	21.5	68.3	1.7	39.1	92.0	92.0	95.2
0.090	15.1	67.9	26.9	69.5	4.3	58.3	85.0	85.0	87.1
0.063	23.6	68.2	27.4	69.1	20.1	67.0	55.3	55.4	56.1
0.045	17.1	68.2	12.7	69.8	21.0	67.3	35.5	35.5	36.3
0.038	4.1	68.4	2.5	69.0	5.6	68.1	29.0	28.5	28.8
-0.038	24.6	56.6	0.9	64.6	46.1	56.5	1.8	1.7	2.0
Head		64.6		68.8		60.8		47.6	50.7

S24F**Raw Data**

Run S24F	Feed		Product		Reject	
Sieve aperture (mm)	Mass (wt.%)	Assay (wt.% Fe)	Mass (wt.%)	Assay (wt.% Fe)	Mass (wt.%)	Assay (wt.% Fe)
0.250	0.8	49.8	1.7	62.7	0.3	17.2
0.180	4.0	59.4	9.9	67.3	1.3	34.1
0.125	11.5	65.3	26.9	68.5	4.4	57.7
0.090	15.8	67.3	27.1	69.5	10.2	65.3
0.063	23.5	69.1	22.1	69.8	25.7	68.4
0.045	19.8	69.5	9.2	69.6	24.0	68.3
0.038	4.9	69.0	1.9	69.9	6.1	68.4
-0.038	19.7	65.1	1.1	68.0	27.9	64.6
Head		66.2		68.5		64.7

Standard Deviations

Run S24F	Feed		Product		Reject	
Sieve aperture (mm)	Mass (wt.%)	Assay (wt.% Fe)	Mass (wt.%)	Assay (wt.% Fe)	Mass (wt.%)	Assay (wt.% Fe)
0.250	0.1	0.05	0.1	0.05	0.1	0.05
0.180	0.1	0.05	0.1	0.05	0.1	0.05
0.125	0.1	0.05	0.1	0.05	0.1	0.05
0.090	0.1	0.05	0.1	0.05	0.1	0.05
0.063	0.1	0.05	0.1	0.01	0.1	0.05
0.045	0.1	0.05	0.1	0.01	0.1	0.05
0.038	0.1	0.05	0.1	0.01	0.1	0.05
-0.038	0.1	0.05	0.1	0.05	0.1	0.05
Head		0.05		0.05		0.05
Solids rate		0.1		0.1		0.1

Balanced Data

Run S24F	Feed		Product		Reject		Mass Partition (%)	Solids Yield (wt.%)	Fe Recovery (%)
Sieve aperture (mm)	Mass (wt.%)	Assay (wt.% Fe)	Mass (wt.%)	Assay (wt.% Fe)	Mass (wt.%)	Assay (wt.% Fe)			
0.250	0.8	49.9	1.8	62.3	0.3	17.0	72.6	72.6	90.7
0.180	4.0	59.7	9.9	66.9	1.3	34.2	77.8	77.9	87.3
0.125	11.5	65.4	26.9	68.1	4.4	57.7	73.8	73.6	76.7
0.090	15.6	67.4	27.2	69.4	10.2	64.9	54.9	54.9	56.6
0.063	24.1	68.7	22.0	69.8	25.1	68.2	28.8	29.1	29.5
0.045	19.6	68.7	9.2	69.6	24.4	68.5	14.7	15.5	15.7
0.038	4.9	68.8	1.9	69.9	6.2	68.6	12.4	12.4	12.6
-0.038	19.6	64.6	1.1	68.3	28.1	64.6	1.8	1.6	1.6
Head		66.8		68.8		65.9		31.5	32.4

S24F2**Raw Data**

Run S24F2	Feed		Product		Reject	
Sieve aperture (mm)	Mass (wt.%)	Assay (wt.% Fe)	Mass (wt.%)	Assay (wt.% Fe)	Mass (wt.%)	Assay (wt.% Fe)
0.250	0.8	49.4	1.2	61.2	0.3	12.1
0.180	4.1	60.2	7.5	66.9	1.1	23.1
0.125	11.8	65.6	22.5	68.6	2.8	48.7
0.090	15.9	67.4	26.3	69.3	6.5	61.8
0.063	23.8	68.4	26.7	69.6	21.5	67.2
0.045	19.5	68.4	12.0	69.3	25.7	68.1
0.038	4.8	68.5	2.4	69.4	7.0	67.5
-0.038	19.5	65.9	1.5	68.2	35.1	65.5
Head		67.1		69.1		64.5

Standard Deviations

Run S24F2	Feed		Product		Reject	
Sieve aperture (mm)	Mass (wt.%)	Assay (wt.% Fe)	Mass (wt.%)	Assay (wt.% Fe)	Mass (wt.%)	Assay (wt.% Fe)
0.250	0.1	0.1	0.1	0.1	0.1	0.1
0.180	0.1	0.1	0.1	0.1	0.1	0.1
0.125	0.1	0.1	0.1	0.1	0.1	0.1
0.090	0.1	0.1	0.1	0.05	0.1	0.1
0.063	0.1	0.1	0.1	0.05	0.1	0.1
0.045	0.1	0.1	0.1	0.05	0.1	0.1
0.038	0.1	0.1	0.1	0.05	0.1	0.1
-0.038	0.1	0.1	0.1	0.05	0.1	0.1
Head		0.1		0.05		0.1
Solids rate		0.1		0.1		0.1

Balanced Data

Run S24F2	Feed		Product		Reject		Mass Partition (%)	Solids Yield (wt.%)	Fe Recovery (%)
Sieve aperture (mm)	Mass (wt.%)	Assay (wt.% Fe)	Mass (wt.%)	Assay (wt.% Fe)	Mass (wt.%)	Assay (wt.% Fe)			
0.250	0.7	49.6	1.2	61.1	0.3	11.5	77.5	77.0	94.7
0.180	4.1	60.6	7.6	67.1	1.1	2.3	85.3	90.0	99.6
0.125	11.8	65.9	22.5	68.5	2.8	48.6	87.1	87.1	90.5
0.090	15.6	67.6	26.4	69.3	6.5	61.8	77.5	77.3	79.3
0.063	23.9	68.3	26.5	69.3	21.7	67.2	50.6	51.0	51.8
0.045	19.4	68.2	11.9	69.4	25.7	67.7	28.1	28.1	28.6
0.038	4.9	68.1	2.4	69.7	6.9	67.7	22.6	19.8	20.3
-0.038	19.6	65.5	1.5	68.4	34.9	65.4	3.5	3.5	3.7
Head		66.9		68.9		65.2		45.8	47.1

S24F3**Raw Data**

Run S24F3	Feed		Product		Reject	
Sieve aperture (mm)	Mass (wt.%)	Assay (wt.% Fe)	Mass (wt.%)	Assay (wt.% Fe)	Mass (wt.%)	Assay (wt.% Fe)
0.250	0.7	46.9	0.9	60.7	0.4	8.9
0.180	3.6	58.1	6.3	66.3	1.1	10.6
0.125	10.9	64.8	20.7	67.8	1.4	18.3
0.090	15.7	67.0	27.4	68.9	2.0	42.1
0.063	23.6	69.2	29.9	69.4	16.4	66.1
0.045	20.3	68.3	11.5	69.7	29.7	67.9
0.038	5.3	68.4	2.0	69.3	7.8	68.3
-0.038	20.0	64.9	1.2	68.5	41.1	65.7
Head		66.6		68.5		64.4

Standard Deviations

Run S24F3	Feed		Product		Reject	
Sieve aperture (mm)	Mass (wt.%)	Assay (wt.% Fe)	Mass (wt.%)	Assay (wt.% Fe)	Mass (wt.%)	Assay (wt.% Fe)
0.250	0.1	0.1	0.1	0.1	0.1	0.1
0.180	0.1	0.1	0.1	0.1	0.1	0.1
0.125	0.1	0.1	0.1	0.1	0.1	0.1
0.090	0.1	0.1	0.1	0.05	0.1	0.1
0.063	0.1	0.1	0.1	0.05	0.1	0.1
0.045	0.1	0.1	0.1	0.01	0.1	0.1
0.038	0.1	0.1	0.1	0.05	0.1	0.1
-0.038	0.1	0.1	0.1	0.1	0.1	0.1
Head		0.1		0.1		0.1
Solids rate		0.1		0.1		0.1

Balanced Data

Run S24F3	Feed		Product		Reject		Mass Partition (%)	Solids Yield (wt.%)	Fe Recovery (%)
Sieve aperture (mm)	Mass (wt.%)	Assay (wt.% Fe)	Mass (wt.%)	Assay (wt.% Fe)	Mass (wt.%)	Assay (wt.% Fe)			
0.250	0.7	46.4	0.9	60.8	0.4	9.1	72.2	72.2	94.5
0.180	3.9	58.3	6.3	65.5	1.1	10.3	86.9	86.9	97.7
0.125	11.6	64.8	20.4	67.5	1.4	18.2	94.4	94.4	98.4
0.090	15.7	67.3	27.6	68.9	2.0	41.9	94.1	94.1	96.4
0.063	23.7	68.3	30.0	69.2	16.4	66.4	67.7	68.0	68.9
0.045	19.8	68.7	11.5	69.7	29.4	68.2	31.0	31.7	32.2
0.038	5.0	68.4	2.1	68.9	8.3	68.2	22.4	22.4	22.5
-0.038	19.7	65.1	1.2	68.8	41.0	65.0	3.3	3.3	3.5
Head		66.6		68.5		64.5		53.5	55.0

S24F4**Raw Data**

Run S24F4	Feed		Product		Reject	
Sieve aperture (mm)	Mass (wt.%)	Assay (wt.% Fe)	Mass (wt.%)	Assay (wt.% Fe)	Mass (wt.%)	Assay (wt.% Fe)
0.250	0.7	47.4	1.0	58.1	0.3	7.4
0.180	3.7	58.2	6.2	65.7	0.9	7.8
0.125	11.0	65.2	19.0	68.4	1.2	13.2
0.090	15.8	67.4	25.0	69.4	1.5	31.3
0.063	24.1	68.8	30.6	69.1	10.4	62.3
0.045	19.9	69.1	14.5	69.0	28.4	67.6
0.038	4.8	68.5	2.5	69.9	8.3	67.9
-0.038	20.1	65.9	1.2	67.4	49.0	65.7
Head		66.9		68.4		63.6

Standard Deviations

Run S24F4	Feed		Product		Reject	
Sieve aperture (mm)	Mass (wt.%)	Assay (wt.% Fe)	Mass (wt.%)	Assay (wt.% Fe)	Mass (wt.%)	Assay (wt.% Fe)
0.250	0.1	0.1	0.1	0.1	0.1	0.1
0.180	0.1	0.1	0.1	0.1	0.1	0.1
0.125	0.1	0.1	0.1	0.1	0.1	0.1
0.090	0.1	0.1	0.1	0.05	0.1	0.1
0.063	0.1	0.1	0.1	0.05	0.1	0.1
0.045	0.1	0.1	0.1	0.05	0.1	0.1
0.038	0.1	0.1	0.1	0.01	0.1	0.1
-0.038	0.1	0.1	0.1	0.1	0.1	0.1
Head		0.1		0.1		0.1
Solids rate		0.1		0.1		0.1

Balanced Data

Run S24F4	Feed		Product		Reject		Mass Partition (%)	Solids Yield (wt.%)	Fe Recovery (%)
Sieve aperture (mm)	Mass (wt.%)	Assay (wt.% Fe)	Mass (wt.%)	Assay (wt.% Fe)	Mass (wt.%)	Assay (wt.% Fe)			
0.250	0.7	48.2	1.0	57.4	0.3	7.4	81.7	81.7	97.2
0.180	3.9	59.1	6.1	64.7	0.9	7.8	90.2	90.2	98.7
0.125	11.4	65.7	19.0	68.1	1.2	13.2	95.5	95.5	99.1
0.090	15.0	67.7	25.0	69.3	1.5	31.2	95.7	95.7	98.0
0.063	22.1	67.8	30.7	69.3	10.7	62.3	79.4	79.4	81.1
0.045	20.5	68.4	14.5	69.0	28.7	68.0	40.3	40.3	40.7
0.038	4.9	68.4	2.5	69.9	8.2	67.7	28.8	28.8	29.4
-0.038	21.4	65.7	1.2	67.5	48.5	65.7	3.2	3.2	3.3
Head		66.8		68.6		64.3		57.3	58.9

S24F5**Raw Data**

Run S24F5	Feed		Product		Reject	
Sieve aperture (mm)	Mass (wt.%)	Assay (wt.% Fe)	Mass (wt.%)	Assay (wt.% Fe)	Mass (wt.%)	Assay (wt.% Fe)
0.250	0.4	43.5	0.9	60.4	0.3	7.0
0.180	2.8	57.1	6.0	66.7	0.9	5.3
0.125	9.7	65.1	19.0	67.9	1.3	5.8
0.090	15.2	67.3	24.1	69.0	1.4	11.4
0.063	24.8	68.0	30.5	69.5	3.1	44.7
0.045	20.6	68.3	16.5	69.2	28.6	66.9
0.038	4.9	67.8	2.2	69.2	11.0	67.8
-0.038	21.7	65.8	0.8	66.8	53.5	66.1
Head		66.5		68.7		63.1

Standard Deviations

Run S24F5	Feed		Product		Reject	
Sieve aperture (mm)	Mass (wt.%)	Assay (wt.% Fe)	Mass (wt.%)	Assay (wt.% Fe)	Mass (wt.%)	Assay (wt.% Fe)
0.250	0.1	0.1	0.1	0.1	0.1	0.1
0.180	0.1	0.1	0.1	0.1	0.1	0.1
0.125	0.1	0.1	0.1	0.1	0.1	0.1
0.090	0.1	0.1	0.1	0.05	0.1	0.1
0.063	0.1	0.1	0.1	0.02	0.1	0.1
0.045	0.1	0.1	0.1	0.01	0.1	0.1
0.038	0.1	0.1	0.1	0.02	0.1	0.1
-0.038	0.1	0.1	0.1	0.1	0.1	0.1
Head		0.1		0.1		0.1
Solids rate		0.1		0.1		0.1

Balanced Data

Run S24F5	Feed		Product		Reject		Mass Partition (%)	Solids Yield (wt.%)	Fe Recovery (%)
Sieve aperture (mm)	Mass (wt.%)	Assay (wt.% Fe)	Mass (wt.%)	Assay (wt.% Fe)	Mass (wt.%)	Assay (wt.% Fe)			
0.250	0.5	48.7	0.6	58.7	0.3	7.3	80.5	80.5	97.1
0.180	3.7	59.2	5.1	63.2	0.8	4.9	93.1	93.2	99.4
0.125	13.6	63.7	19.2	65.4	1.3	5.9	97.1	97.1	99.7
0.090	17.3	67.8	24.5	69.2	1.3	11.1	97.6	97.6	99.6
0.063	22.3	68.1	30.9	69.1	3.1	47.1	95.6	95.6	97.0
0.045	19.7	66.4	16.6	69.3	26.7	62.3	57.9	57.9	60.5
0.038	5.2	69.0	2.3	68.9	11.5	69.1	31.2	45.6	45.6
-0.038	17.6	69.7	0.8	69.2	55.0	69.7	3.2	3.2	3.2
Head		67.0		68.1		64.7		69.0	70.1

S24F6**Raw Data**

Run S24F6	Feed		Product		Reject	
Sieve aperture (mm)	Mass (wt.%)	Assay (wt.% Fe)	Mass (wt.%)	Assay (wt.% Fe)	Mass (wt.%)	Assay (wt.% Fe)
0.250	0.7	45.1	1.0	53.4	0.3	6.6
0.180	4.0	58.5	6.9	65.4	1.5	5.1
0.125	12.5	65.5	20.1	68.5	1.9	8.7
0.090	17.0	67.5	23.9	69.1	1.5	14.6
0.063	23.1	68.0	28.1	69.3	3.1	44.1
0.045	19.2	67.9	15.8	69.3	22.4	66.4
0.038	5.0	67.5	2.9	69.0	11.3	67.8
-0.038	18.6	65.3	1.2	67.8	58.0	66.1
Head		66.8		68.8		61.8

Standard Deviations

Run S24F6	Feed		Product		Reject	
Sieve aperture (mm)	Mass (wt.%)	Assay (wt.% Fe)	Mass (wt.%)	Assay (wt.% Fe)	Mass (wt.%)	Assay (wt.% Fe)
0.250	0.1	0.1	0.1	0.1	0.1	0.1
0.180	0.1	0.1	0.1	0.1	0.1	0.1
0.125	0.1	0.1	0.1	0.1	0.1	0.1
0.090	0.1	0.1	0.1	0.02	0.1	0.1
0.063	0.1	0.1	0.1	0.02	0.1	0.1
0.045	0.1	0.1	0.1	0.02	0.1	0.1
0.038	0.1	0.1	0.1	0.02	0.1	0.1
-0.038	0.1	0.1	0.1	0.1	0.1	0.1
Head		0.1		0.1		0.1
Solids rate		0.1		0.1		0.1

Balanced Data

Run S24F6	Feed		Product		Reject		Mass Partition (%)	Solids Yield (wt.%)	Fe Recovery (%)
Sieve aperture (mm)	Mass (wt.%)	Assay (wt.% Fe)	Mass (wt.%)	Assay (wt.% Fe)	Mass (wt.%)	Assay (wt.% Fe)			
0.250	0.7	46.1	0.9	52.4	0.3	6.2	86.3	86.3	98.2
0.180	5.0	58.7	6.8	64.2	1.4	5.0	90.7	90.7	99.2
0.125	14.2	65.1	20.0	67.7	1.9	8.6	95.7	95.7	99.4
0.090	16.6	67.6	23.9	69.2	1.5	14.6	97.1	97.1	99.4
0.063	20.3	68.1	28.5	69.4	3.1	43.8	95.1	95.1	96.8
0.045	18.3	68.0	15.9	69.4	23.2	65.9	59.0	59.0	60.2
0.038	5.4	68.5	2.7	69.2	10.8	68.5	34.7	34.7	35.1
-0.038	19.5	65.2	1.2	67.3	57.8	65.1	4.1	3.9	4.0
Head		66.4		68.5		62.1		67.6	69.7

CF184**Raw Data**

Run CF184	Feed		Product		Reject	
Sieve aperture (μm)	Mass (wt.%)	Assay (wt.% Fe)	Mass (wt.%)	Assay (wt.% Fe)	Mass (wt.%)	Assay (wt.% Fe)
500	2.4	56.9	2.6	56.2		
250	4.6	60.7	5.1	60.7		
125	4.5	62.4	5.4	62.5		
63	5.9	61.2	7.8	60.6		
38	6.3	55.0	11.9	56.5		
20	14.8	54.6	24.9	55.2	1.4	34.7
- 20	61.5	42.1	42.2	51.5	98.6	36.2
Head		47.5		54.1		35.8

Standard Deviations

Run CF184	Feed		Product		Reject	
Sieve aperture (μm)	Mass (wt.%)	Assay (wt.% Fe)	Mass (wt.%)	Assay (wt.% Fe)	Mass (wt.%)	Assay (wt.% Fe)
500	0.1	0.1	0.1	0.1	0.1	0.1
250	0.1	0.1	0.1	0.1	0.1	0.1
125	0.1	0.1	0.1	0.1	0.1	0.1
63	0.1	0.1	0.1	0.1	0.1	0.1
38	0.1	0.1	0.1	0.1	0.1	0.1
20	0.1	0.1	0.1	0.1	0.1	0.1
- 20	0.1	0.1	0.1	0.1	0.1	0.1
Head		0.02		0.02		0.02
Solids rate		0.3		0.3		0.3

Balanced Data

Run CF184	Feed		Product		Reject		Solids Yield (wt.%)	Fe Recovery (%)
Sieve aperture (μm)	Mass (wt.%)	Assay (wt.% Fe)	Mass (wt.%)	Assay (wt.% Fe)	Mass (wt.%)	Assay (wt.% Fe)		
500	2.0	56.7	3.0	56.7				
250	3.9	60.9	5.7	60.9				
125	4.1	62.2	5.9	62.2				
63	5.6	60.8	8.2	60.8				
38	7.3	55.8	10.6	55.8				
20	16.0	54.4	22.6	55.0	1.4	34.7	97.2	69.4
- 20	61.1	42.3	44.0	49.0	98.6	35.6	49.5	79.6
Head		48.1		53.7		35.6	68.7	76.8

CF185**Raw Data**

Run CF185	Feed		Product		Reject	
Sieve aperture (μm)	Mass (wt.%)	Assay (wt.% Fe)	Mass (wt.%)	Assay (wt.% Fe)	Mass (wt.%)	Assay (wt.% Fe)
500	0.6	53.2	1.5	53.8		
250	1.8	57.9	3.2	57.0		
125	3.1	60.7	4.5	59.4		
63	5.4	60.3	7.9	59.4		
38	7.0	56.7	11.9	56.2		
20	15.4	55.5	25.6	55.0	1.5	36.3
- 20	66.7	41.7	45.3	51.3	98.5	35.9
Head		47.1		55.1		36.0

Standard Deviations

Run CF185	Feed		Product		Reject	
Sieve aperture (μm)	Mass (wt.%)	Assay (wt.% Fe)	Mass (wt.%)	Assay (wt.% Fe)	Mass (wt.%)	Assay (wt.% Fe)
500	0.1	0.1	0.1	0.1	0.1	0.1
250	0.1	0.1	0.1	0.1	0.1	0.1
125	0.1	0.1	0.1	0.1	0.1	0.1
63	0.1	0.1	0.1	0.1	0.1	0.1
38	0.1	0.1	0.1	0.1	0.1	0.1
20	0.1	0.1	0.1	0.1	0.1	0.1
- 20	0.1	0.1	0.1	0.1	0.1	0.1
Head		0.02		0.02		0.02
Solids rate		0.3		0.3		0.3

Balanced Data

Run CF185	Feed		Product		Reject		Solids Yield (wt.%)	Fe Recovery (%)
Sieve aperture (μm)	Mass (wt.%)	Assay (wt.% Fe)	Mass (wt.%)	Assay (wt.% Fe)	Mass (wt.%)	Assay (wt.% Fe)		
500	0.7	53.4	1.2	53.4				
250	1.8	57.6	3.2	57.6				
125	2.8	60.1	4.8	60.1				
63	4.9	60.2	8.5	60.2				
38	6.9	56.6	11.9	56.6				
20	15.5	55.4	25.6	56.2	1.5	36.3	96.0	58.9
- 20	67.3	42.3	44.8	52.2	98.5	36.0	38.7	71.7
Head		47.0		55.0		36.0	58.1	67.9

CF186**Raw Data**

Run CF186	Feed		Product		Reject	
Sieve aperture (μm)	Mass (wt.%)	Assay (wt.% Fe)	Mass (wt.%)	Assay (wt.% Fe)	Mass (wt.%)	Assay (wt.% Fe)
500	0.8	55.6	1.0	52.2		
250	2.1	58.7	2.5	56.3		
125	3.4	61.0	4.0	59.4		
63	5.3	61.0	7.6	59.1		
38	8.1	56.7	12.7	57.2		
20	14.7	54.9	26.2	55.7	1.8	36.5
- 20	65.6	42.3	45.9	52.6	98.2	36.3
Head		46.9		54.8		36.1

Standard Deviations

Run CF186	Feed		Product		Reject	
Sieve aperture (μm)	Mass (wt.%)	Assay (wt.% Fe)	Mass (wt.%)	Assay (wt.% Fe)	Mass (wt.%)	Assay (wt.% Fe)
500	0.1	0.1	0.1	0.1	0.1	0.1
250	0.1	0.1	0.1	0.1	0.1	0.1
125	0.1	0.1	0.1	0.1	0.1	0.1
63	0.1	0.1	0.1	0.1	0.1	0.1
38	0.1	0.1	0.1	0.1	0.1	0.1
20	0.1	0.1	0.1	0.1	0.1	0.1
- 20	0.1	0.1	0.1	0.1	0.1	0.1
Head		0.02		0.02		0.02
Solids rate		0.3		0.3		0.3

Balanced Data

Run CF186	Feed		Product		Reject		Solids Yield (wt.%)	Fe Recovery (%)
Sieve aperture (μm)	Mass (wt.%)	Assay (wt.% Fe)	Mass (wt.%)	Assay (wt.% Fe)	Mass (wt.%)	Assay (wt.% Fe)		
500	0.7	54.8	1.0	54.8				
250	1.8	58.2	2.8	58.2				
125	3.1	60.9	4.9	60.9				
63	5.3	61.3	8.4	61.3				
38	7.0	57.6	11.0	57.6				
20	17.6	55.3	26.4	56.0	1.8	36.6	96.3	64.9
- 20	64.5	43.2	45.5	52.1	98.2	35.8	45.2	77.3
Head		48.2		55.1		35.8	64.0	73.3

CF188**Raw Data**

Run CF188	Feed		Product		Reject	
Sieve aperture (μm)	Mass (wt.%)	Assay (wt.% Fe)	Mass (wt.%)	Assay (wt.% Fe)	Mass (wt.%)	Assay (wt.% Fe)
500	1.0	54.5	1.1	54.1		
250	2.8	58.3	2.9	57.3		
125	5.1	61.3	4.8	60.1		
63	8.7	61.6	8.8	60.5		
38	10.0	57.9	13.5	58.0		
20	28.2	56.7	30.8	54.4	5.1	41.6
- 20	44.2	51.4	38.2	57.2	94.9	40.2
Head		55.2		58.2		39.4

Standard Deviations

Run CF188	Feed		Product		Reject	
Sieve aperture (μm)	Mass (wt.%)	Assay (wt.% Fe)	Mass (wt.%)	Assay (wt.% Fe)	Mass (wt.%)	Assay (wt.% Fe)
500	0.1	0.1	0.1	0.1	0.1	0.1
250	0.1	0.1	0.1	0.1	0.1	0.1
125	0.1	0.1	0.1	0.1	0.1	0.1
63	0.1	0.1	0.1	0.1	0.1	0.1
38	0.1	0.1	0.1	0.1	0.1	0.1
20	0.1	0.1	0.1	0.1	0.1	0.1
- 20	0.1	0.1	0.1	0.1	0.1	0.1
Head		0.02		0.02		0.02
Solids rate		0.3		0.3		0.3

Balanced Data

Run CF188	Feed		Product		Reject		Solids Yield (wt.%)	Fe Recovery (%)
Sieve aperture (μm)	Mass (wt.%)	Assay (wt.% Fe)	Mass (wt.%)	Assay (wt.% Fe)	Mass (wt.%)	Assay (wt.% Fe)		
500	1.0	54.8	1.2	54.8				
250	2.8	58.2	3.2	58.2				
125	4.9	60.9	5.5	60.9				
63	8.4	61.3	9.4	61.3				
38	11.0	57.6	12.4	57.6				
20	26.4	56.0	29.2	56.3	5.1	41.0	97.9	89.0
- 20	45.5	52.1	39.1	56.1	94.9	39.3	75.9	95.3
Head		55.1		57.2		39.4	88.5	91.8

CF222**Raw Data**

Run CF222	Feed		Product		Reject	
Sieve aperture (μm)	Mass (wt.%)	Assay (wt.% Fe)	Mass (wt.%)	Assay (wt.% Fe)	Mass (wt.%)	Assay (wt.% Fe)
38	27.8	62.4	46.0	62.0	0.1	
20	16.2	66.2	29.6	66.3	0.2	
- 20	55.9	51.8	24.4	60.9	99.7	47.7
Head		56.1		62.4		47.3

Standard Deviations

Run CF222	Feed		Product		Reject	
Sieve aperture (μm)	Mass (wt.%)	Assay (wt.% Fe)	Mass (wt.%)	Assay (wt.% Fe)	Mass (wt.%)	Assay (wt.% Fe)
38	0.1	0.1	0.1	0.1	0.1	0.1
20	0.1	0.1	0.1	0.1	0.1	0.1
- 20	0.1	0.1	0.1	0.1	0.1	0.1
Head		0.02		0.02		0.02
Solids rate		0.3		0.3		0.3

Balanced Data

Run CF222	Feed		Product		Reject		Solids Yield (wt.%)	Fe Recovery (%)
Sieve aperture (μm)	Mass (wt.%)	Assay (wt.% Fe)	Mass (wt.%)	Assay (wt.% Fe)	Mass (wt.%)	Assay (wt.% Fe)		
38	27.4	63.7	50.2	63.7				
20	15.2	66.0	27.8	66.0				
- 20	57.3	49.9	21.9	59.9	100.0	47.2	20.9	25.1
Head		56.1		63.5		47.2	54.6	61.8

CF223**Raw Data**

Run CF223	Feed		Product		Reject	
Sieve aperture (μm)	Mass (wt.%)	Assay (wt.% Fe)	Mass (wt.%)	Assay (wt.% Fe)	Mass (wt.%)	Assay (wt.% Fe)
38	48.6	61.5	56.4	63.6	0.3	
20	29.0	66.5	28.9	66.8	0.0	
- 20	22.4	61.5	14.6	65.9	99.7	49.2
Head		63.6		64.2		49.3

Standard Deviations

Run CF223	Feed		Product		Reject	
Sieve aperture (μm)	Mass (wt.%)	Assay (wt.% Fe)	Mass (wt.%)	Assay (wt.% Fe)	Mass (wt.%)	Assay (wt.% Fe)
38	0.1	0.1	0.1	0.1	0.1	0.1
20	0.1	0.1	0.1	0.1	0.1	0.1
- 20	0.1	0.1	0.1	0.1	0.1	0.1
Head		0.02		0.02		0.02
Solids rate		0.3		0.3		0.3

Balanced Data

Run CF223	Feed		Product		Reject		Solids Yield (wt.%)	Fe Recovery (%)
Sieve aperture (μm)	Mass (wt.%)	Assay (wt.% Fe)	Mass (wt.%)	Assay (wt.% Fe)	Mass (wt.%)	Assay (wt.% Fe)		
38	50.2	63.7	55.1	63.7				
20	27.8	66.0	30.5	66.0				
- 20	21.9	59.9	14.4	67.1	100.0	49.2	60.0	67.2
Head		63.5		64.9		49.2	91.2	93.2

CF254**Raw Data**

Run CF254	Feed		Product		Reject	
Sieve aperture (μm)	Mass (wt.%)	Assay (wt.% Fe)	Mass (wt.%)	Assay (wt.% Fe)	Mass (wt.%)	Assay (wt.% Fe)
250	0.8	48.6	0.9	49.9		
180	4.1	60.1	4.7	60.6		
125	10.3	65.5	11.4	66.5		
90	17.5	69.2	19.1	67.7		
63	25.3	67.7	28.0	68.3		
45	17.0	68.4	16.5	68.2		
38	1.0	68.1	1.4	68.4	0.2	
20	11.8	66.8	12.6	67.3	0.5	16.6
-20	12.2	51.2	5.5	63.3	99.3	42.6
Head		64.9		67.5		42.3

Standard Deviations

Run CF254	Feed		Product		Reject	
Sieve aperture (μm)	Mass (wt.%)	Assay (wt.% Fe)	Mass (wt.%)	Assay (wt.% Fe)	Mass (wt.%)	Assay (wt.% Fe)
250	0.1	0.05	0.1	0.05	0.1	0.05
180	0.1	0.05	0.1	0.05	0.1	0.05
125	0.1	0.05	0.1	0.05	0.1	0.05
90	0.1	0.05	0.1	0.05	0.1	0.05
63	0.1	0.05	0.1	0.05	0.1	0.05
45	0.1	0.05	0.1	0.05	0.1	0.05
38	0.1	0.05	0.1	0.05	0.1	0.05
20	0.1	0.05	0.1	0.05	0.1	0.05
-20	0.1	0.05	0.1	0.05	0.1	0.05
Head		0.05		0.05		0.05
Solids rate		0.1		0.1		0.1

Balanced Data

Run CF254	Feed		Product		Reject		Solids Yield (wt.%)	Fe Recovery (%)
Sieve aperture (μm)	Mass (wt.%)	Assay (wt.% Fe)	Mass (wt.%)	Assay (wt.% Fe)	Mass (wt.%)	Assay (wt.% Fe)		
250	0.8	48.9	0.9	48.9				
180	4.2	60.5	4.6	60.5				
125	10.4	65.7	11.4	65.7				
90	17.3	68.7	18.9	68.7				
63	25.4	67.8	27.9	67.8				
45	15.7	68.5	17.2	68.5				
38	1.1	68.0	1.2	68.0				
20	11.5	67.2	12.6	67.5	0.7	15.2	99.5	99.9
-20	13.5	50.3	5.2	63.9	99.3	42.9	35.2	44.7
Head		65.0		67.1		42.7	91.2	94.2

Appendix E: Rheology Data

This appendix contains the raw data obtained from the overflow solids rheology experiments and the associated calculations. The slimes volume fraction for each sample was calculated after the measurements by weighing and drying the sample. The calculation converted the slimes mass fraction to a volume fraction assuming a particle density of 4400 kg/m³ for the original samples of Run S24E2 and a density of 4650 kg/m³ for the samples taken from the deslimed Run S24F2. For the original feed (S24E2), the Slimes Vol. Frac. of 0.114 (first sample in table below) was calculated from the solids concentration (for this sample 36.1 wt.%) by,

$$Vol.Frac = \frac{\frac{SolidsConc.}{SolidsDensity}}{\frac{SolidsConc.}{SolidsDensity} + \frac{100 - SolidsConc}{WaterDensity}}$$

$$Vol. Frac. = (36.1/4.4) / ((36.1/4.4) + ((100 - 36.1)/1)) = 0.114$$

S24E2 Overflow -0.038 mm

Slimes Vol. Frac.	Shear Rate (s ⁻¹)	Apparent Viscosity (Pa s)	Shear Stress (Pa)	Measurement Time (s)	Temperature (°C)
0.114	0.002	62.4700	0.100	60.20	24.8
	0.033	3.8550	0.126	125.20	24.8
	0.584	0.2712	0.158	190.23	24.8
	3.403	0.0584	0.199	255.23	24.8
	9.665	0.0258	0.249	310.22	24.8
	22.03	0.0141	0.311	365.20	24.8
	47.07	0.0082	0.387	430.20	24.9
	91.42	0.0052	0.480	495.20	24.9
	152.50	0.0039	0.596	550.22	24.9
	203.00	0.0037	0.747	605.20	24.9
	237.50	0.0040	0.945	650.27	24.9
0.09	0.9620	0.1036	0.100	30.39	23.0
	3.8330	0.0326	0.125	65.39	23.0
	9.1290	0.0171	0.156	100.39	23.1

Slimes Vol. Frac.	Shear Rate	Apparent Viscosity	Shear Stress	Measurement Time	Temperature
	(s ⁻¹)	(Pa s)	(Pa)	(s)	(°C)
0.09	18.4500	0.0106	0.195	135.42	23.0
	35.0700	0.0069	0.242	170.36	23.1
	62.6600	0.0048	0.300	205.38	23.1
	102.1000	0.0036	0.372	240.39	23.1
	151.0000	0.0031	0.464	275.45	23.1
	183.5000	0.0032	0.588	310.36	23.1
	219.2000	0.0034	0.742	345.38	23.1
	263.8000	0.0036	0.938	380.39	23.1
0.079	0.0752	0.1328	0.010	30.45	25.5
	0.1171	0.1072	0.013	65.48	25.6
	0.2985	0.0528	0.016	100.47	25.6
	0.7141	0.0277	0.020	135.48	25.6
	2.0050	0.0123	0.025	170.52	25.6
	4.4650	0.0068	0.030	205.45	25.7
	8.1800	0.0046	0.038	240.45	25.7
	14.0100	0.0033	0.046	275.48	25.7
	22.4900	0.0025	0.057	310.47	25.7
	34.0600	0.0021	0.071	345.45	25.8
48.9000	0.0018	0.088	380.45	25.8	
0.064	0.6967	0.0141	0.010	30.578	24.9
	1.4240	0.0086	0.012	65.578	24.9
	2.8610	0.0053	0.015	100.58	24.9
	5.1460	0.0036	0.019	135.58	24.9
	8.4770	0.0027	0.023	170.58	24.9
	13.3400	0.0021	0.028	205.59	24.9
	19.7200	0.0018	0.035	240.58	24.9
	28.1000	0.0015	0.043	275.59	25.0
	37.8500	0.0014	0.054	310.58	25.0
	49.1100	0.0014	0.067	345.58	25.0
63.2600	0.0013	0.084	380.63	25.0	
69.3600	0.0012	0.084	415.58	25.0	
0.056	0.5720	0.0084	0.005	30.33	25.4
	1.3880	0.0043	0.006	65.33	25.5
	2.5860	0.0028	0.007	100.30	25.5
	4.4780	0.0020	0.009	135.31	25.6
	7.0760	0.0015	0.011	170.33	25.6
	10.4200	0.0013	0.013	205.33	25.6
	14.6100	0.0011	0.016	240.30	25.7
	19.6900	0.0010	0.020	275.31	25.7
25.8000	0.0010	0.025	310.33	25.8	

Slimes Vol. Frac.	Shear Rate (s ⁻¹)	Apparent Viscosity (Pa s)	Shear Stress (Pa)	Measurement Time (s)	Temperature (°C)
0.056	32.9300	0.0010	0.032	345.34	25.8
	40.9700	0.0010	0.040	380.28	25.8
0.043	3.7870	0.0023	0.009	30.42	23.8
	7.3200	0.0015	0.011	65.42	23.8
	10.6900	0.0012	0.013	100.42	23.8
	14.7200	0.0011	0.016	135.42	23.8
	19.6500	0.0010	0.020	170.48	23.8
	25.3700	0.0010	0.025	205.41	23.8
	32.1900	0.0010	0.032	240.42	23.8
	40.3100	0.0010	0.040	275.45	23.8
	50.2600	0.0010	0.051	310.41	23.8
	61.8300	0.0010	0.064	345.47	23.8
	71.7900	0.0012	0.083	380.41	23.8
74.0800	0.0011	0.083	415.42	23.8	
0.036	1.3150	0.0034	0.0045	30.91	24.5
	2.9280	0.0019	0.0055	65.97	24.5
	4.6590	0.0014	0.0067	100.91	24.5
	6.9080	0.0012	0.0082	135.92	24.5
	9.7180	0.0010	0.0101	170.92	24.5
	13.2400	0.0009	0.0125	205.95	24.5
	17.3800	0.0009	0.0156	240.91	24.5
	22.1100	0.0009	0.0196	275.92	24.5
	27.8200	0.0009	0.0247	310.92	24.5
	34.6700	0.0009	0.0312	345.97	24.5
	42.5100	0.0009	0.0395	380.89	24.5
	47.0200	0.0008	0.0390	415.91	24.6

S24F2 Overflow -0.038 mm

Slimes Vol. Frac.	Shear Rate (s ⁻¹)	Apparent Viscosity (Pa s)	Shear Stress (Pa)	Measurement Time (s)	Temperature (°C)
0.401	0.00647	19.3125	0.1	30.593	25.9
	0.264	0.59575	0.1258	65.515	25.9
	3.201	0.061425	0.1573	100.48	25.8
	17.37	0.014	0.1946	135.5	25.8
	41.51	0.007239	0.2404	170.58	25.8
	77.66	0.006088	0.3782	345.23	25.9

Slimes Vol. Frac.	Shear Rate (s^{-1})	Apparent Viscosity (Pa s)	Shear Stress (Pa)	Measurement Time (s)	Temperature ($^{\circ}C$)
	85.33	0.007058	0.4817	380.23	25.9
0.367	0.000433	14.45	0.005	30.266	25.9
	0.000302	26.0875	0.006295	65.313	25.9
	0.05814	0.169625	0.007888	100.25	25.9
	1.21	0.009891	0.009573	135.27	25.9
	2.996	0.004919	0.01179	170.36	25.9
	4.551	0.004041	0.01471	205.3	25.9
	6.427	0.003559	0.0183	240.28	25.9
	9.616	0.002948	0.02267	275.28	25.8
	14.04	0.002496	0.02803	310.3	25.8
	19.73	0.002205	0.03482	345.31	25.8
	26.95	0.002015	0.04343	380.3	25.8
	35.09	0.001941	0.05448	415.27	25.8
	44.57	0.00192	0.06845	450.3	25.8
	54.85	0.001979	0.08685	485.25	25.8
53.28	0.002066	0.0881	520.25	25.8	
0.311	0.09128	0.068113	0.004974	31.016	25.7
	0.6212	0.012128	0.006027	66.031	25.7
	3.293	0.002659	0.007002	101.08	25.7
	6.449	0.001608	0.008293	136.11	25.7
	9.76	0.001296	0.01012	171.03	25.7
	13.42	0.001165	0.01251	206.05	25.6
	17.48	0.001119	0.01565	241	25.6
	21.98	0.001122	0.01972	276.08	25.6
	27.48	0.001133	0.0249	311.03	25.6
	34.19	0.001151	0.03147	346.02	25.7
	42.1	0.001182	0.03981	381.02	25.6
	52.41	0.001202	0.05038	416.06	25.6
	63.56	0.001261	0.06413	451.02	25.6
	74.26	0.001385	0.08231	486.06	25.6
76.45	0.001349	0.08246	521.03	25.7	
0.267	1.064	0.005344	0.004547	31.047	25.3
	5.22	0.001177	0.004915	66.031	25.3
	7.703	0.000979	0.006034	101.02	25.3
	9.803	0.000969	0.007601	136	25.3
	12.17	0.000988	0.009619	171.05	25.3
	15.03	0.001014	0.01219	206.05	25.3
	18.53	0.001041	0.01543	241.05	25.3
	22.64	0.001079	0.01954	276.05	25.3
	28.3	0.001092	0.02473	311.02	25.3
	34.95	0.001119	0.03127	346.06	25.3
	42.98	0.001151	0.03957	381.09	25.3
	53.57	0.001168	0.05004	416.03	25.3
	65.1	0.001223	0.06371	451.08	25.3

Slimes Vol. Frac.	Shear Rate	Apparent Vscosity	Shear Stress	Measurement Time	Temperature
	(s ⁻¹)	(Pa s)	(Pa)	(s)	(°C)
	76.19	0.001341	0.08178	486.02	25.3
	79.39	0.001288	0.08178	521.02	25.4
0.224	5.949	0.001711	0.008143	30.843	24.6
	11.5	0.001058	0.009733	65.843	24.6
	14.95	0.001022	0.01222	100.84	24.6
	18.57	0.001041	0.01546	135.83	24.6
	22.76	0.001075	0.01958	170.89	24.6
	28.31	0.001095	0.02479	205.86	24.6
	35.02	0.00112	0.03137	240.84	24.6
	42.84	0.001159	0.03971	275.84	24.7
	53.39	0.001177	0.05028	310.91	24.7
	64.52	0.001243	0.06418	345.83	24.7
	74.4	0.001385	0.08245	380.83	24.7

Calculations

Linear interpolation was used on the viscosity data in order to obtain the viscosities at a set shear rate.

For the deslimed experiment (S24F2) only data at a shear rate of 10 s⁻¹ was used.

Slimes Vol. Frac.	Apparent Viscosity (Pa s) at Shear Rate:			
	1 s ⁻¹	10 s ⁻¹	20 s ⁻¹	40 s ⁻¹
S24E2				
0.114	0.2398	0.0313	0.0160	0.0099
0.090	0.1027	0.0206	0.0102	0.0055
0.079	0.0243	0.0056	0.0028	0.0020
0.064	0.0118	0.0031	0.0018	0.0014
0.056	0.0062	0.0020	0.0010	0.0010
0.043	0.0040	0.0019	0.0010	0.0010
0.036	0.0030	0.0014	0.0009	0.0009
S24F2				
0.224		0.0011		
0.267		0.001		
0.311		0.0012		
0.367		0.0029		
0.401		0.0387		

The rheology data from Run S24E2 was collapsed into a single empirical model (Equation 5.1) including the terms of shear rate, viscosity and solids volume fraction. The following table lists this data along with the viscosity predicted by the model and the square of error between the predicted and experimental viscosities. In Excel, Solver was used to minimise the *Sum of the Squared Errors* by altering the model exponents a and b and the factors K_1 and K_2 . The values listed in the following table are the best fit that was found. *Note*: the data from the deslimed run (S24F2) is not included in this model as the rheology was quite different to the original feed, as shown in Chapter 7. A sample calculation for the first entry in the table is shown below,

$$\begin{aligned}\mu_s &= \mu(1 + K_1\gamma^a\phi^b + K_2\gamma\phi) \\ &= 0.00089 \times (1 + 1.01 \times 10^6 \times 1.3^{-0.93} \times 0.036^{3.98} + 0.4 \times 1.3 \times 0.036) = 0.0022 \text{ Pa s}\end{aligned}$$

$$\text{Square Error} = (\text{Apparent Visc.} - \text{Model Visc.})^2 = (0.0034 - 0.0022)^2 = 1.51 \times 10^{-6}$$

Appendix E: Rheology Data

Model:				Sum of Square Errors					
Exponents		Factors							
<i>a</i>	<i>b</i>	<i>K</i> ₁	<i>K</i> ₂						
-0.93	3.98	1.01E+06	0.40	0.11					
Slimes Vol. Frac	Shear Rate	Apparent Viscosity	Model Viscosity	Square Error	Slimes Vol. Frac	Shear Rate	Apparent Viscosity	Model Viscosity	Square Error
	(1/s)	(Pa s)	(Pa s)			(1/s)	(Pa s)	(Pa s)	
0.036	1.3	0.0034	0.0022	1.51E-06	0.064	13.3	0.0021	0.0026	2.20E-07
0.036	2.9	0.0019	0.0016	1.15E-07	0.064	19.7	0.0018	0.0023	2.93E-07
0.036	4.7	0.0014	0.0014	7.79E-09	0.064	28.1	0.0015	0.0022	4.72E-07
0.036	6.9	0.0012	0.0013	5.03E-09	0.064	37.9	0.0014	0.0023	7.30E-07
0.036	9.7	0.0010	0.0012	3.28E-08	0.064	49.1	0.0014	0.0024	1.09E-06
0.036	13.2	0.0009	0.0012	7.34E-08	0.064	63.3	0.0013	0.0026	1.72E-06
0.036	17.4	0.0009	0.0012	1.14E-07	0.064	69.4	0.0012	0.0028	2.40E-06
0.036	22.1	0.0009	0.0013	1.49E-07	0.079	0.1	0.1328	0.4093	7.65E-02
0.036	27.8	0.0009	0.0013	1.93E-07	0.079	0.1	0.1072	0.2714	2.70E-02
0.036	34.7	0.0009	0.0014	2.51E-07	0.079	0.3	0.0528	0.1143	3.77E-03
0.036	42.5	0.0009	0.0015	3.17E-07	0.079	0.7	0.0277	0.0513	5.59E-04
0.036	47.0	0.0008	0.0015	5.16E-07	0.079	2.0	0.0123	0.0202	6.38E-05
0.043	3.8	0.0023	0.0019	2.03E-07	0.079	4.5	0.0068	0.0102	1.13E-05
0.043	7.3	0.0015	0.0015	2.39E-09	0.079	8.2	0.0046	0.0063	3.02E-06
0.043	10.7	0.0012	0.0014	3.26E-08	0.079	14.0	0.0033	0.0045	1.29E-06
0.043	14.7	0.0011	0.0014	7.62E-08	0.079	22.5	0.0025	0.0036	1.03E-06
0.043	19.7	0.0010	0.0014	1.32E-07	0.079	34.1	0.0021	0.0032	1.34E-06
0.043	25.4	0.0010	0.0014	1.91E-07	0.079	48.9	0.0018	0.0033	2.15E-06
0.043	32.2	0.0010	0.0015	2.69E-07	0.090	1.0	0.1036	0.0648	1.50E-03
0.043	40.3	0.0010	0.0016	3.74E-07	0.090	3.8	0.0326	0.0187	1.93E-04
0.043	50.3	0.0010	0.0017	5.34E-07	0.090	9.1	0.0171	0.0091	6.47E-05
0.043	61.8	0.0010	0.0019	7.42E-07	0.090	18.5	0.0106	0.0056	2.47E-05
0.043	71.8	0.0012	0.0020	7.94E-07	0.090	35.1	0.0069	0.0043	6.93E-06
0.043	74.1	0.0011	0.0021	9.26E-07	0.090	62.7	0.0048	0.0042	3.31E-07
0.056	0.6	0.0084	0.0170	7.48E-05	0.090	102.1	0.0036	0.0050	1.83E-06
0.056	1.4	0.0043	0.0080	1.40E-05	0.090	151.0	0.0031	0.0063	1.05E-05
0.056	2.6	0.0028	0.0049	4.48E-06	0.090	183.5	0.0032	0.0072	1.64E-05
0.056	4.5	0.0020	0.0034	1.95E-06	0.090	219.2	0.0034	0.0083	2.43E-05
0.056	7.1	0.0015	0.0026	1.15E-06	0.090	263.8	0.0036	0.0097	3.75E-05
0.056	10.4	0.0013	0.0022	8.53E-07	0.114	0.0	62.4700	62.4710	1.03E-06
0.056	14.6	0.0011	0.0020	7.51E-07	0.114	0.0	3.8550	3.7896	4.27E-03
0.056	19.7	0.0010	0.0019	7.46E-07	0.114	0.6	0.2712	0.2606	1.12E-04
0.056	25.8	0.0010	0.0019	8.09E-07	0.114	3.4	0.0584	0.0515	4.80E-05
0.056	32.9	0.0010	0.0019	9.29E-07	0.114	9.7	0.0258	0.0204	2.88E-05
0.056	41.0	0.0010	0.0020	1.09E-06	0.114	22.0	0.0141	0.0107	1.19E-05
0.064	0.7	0.0141	0.0225	7.15E-05	0.114	47.1	0.0082	0.0072	1.09E-06
0.064	1.4	0.0086	0.0121	1.21E-05	0.114	91.4	0.0052	0.0070	2.94E-06
0.064	2.9	0.0053	0.0068	2.24E-06	0.114	152.5	0.0039	0.0085	2.15E-05

0.064	5.1	0.0036	0.0044	5.80E-07	0.114	203.0	0.0037	0.0102	4.30E-05
0.064	8.5	0.0027	0.0032	2.48E-07	0.114	237.5	0.0040	0.0115	5.64E-05

The *Solids Volume Fraction – Apparent Viscosity* data for the original (S24E2) and the deslimed (S24F2)

runs was scaled to fit the Krieger and Dougherty model with maximum packing fraction value of 0.64 and intrinsic viscosity of 2.5, the values for close packing of rigid spheres. Firstly, the model (Equation 2.26) was rearranged to give the Solids Volume Fraction,

$$\phi = \phi_{\max} \left(1 - \left(\frac{\mu_s}{\mu} \right)^{\frac{1}{[\eta]\phi_{\max}}} \right)$$

The *Model Volume Fraction* at the same viscosity as the experimental data was then calculated. For the viscosity of 0.0014 s⁻¹ (first row in the table),

$$\text{Model Vol Frac.} = 0.64 \times (1 - (0.0014/0.00089)^{-1/(2.5(0.64))}) = 0.152$$

The measured *Slimes Volume Fraction* was then multiplied by a *Scaling Factor* to give the *Scaled Volume Fraction* and the *Square of the Error* between this value and the *Model Volume Fraction* calculated. Solver was used to minimise the *Sum of the Squared Errors* by altering the *Scaling Factor*.

The following table lists the data and final values for the best fit to the model for the original and deslimed work.

S24E2 (Original)						
Apparent Viscosity (Pa s)	Slimes Vol. Frac	Scaled Vol. Frac	Model Vol. Frac	Square Error	Sum of Square Error	Scaling Factor
0.0014	0.036	0.200	0.152	0.0024	1.42E-03	5.51
0.0019	0.043	0.236	0.238	0.0000		
0.0020	0.056	0.310	0.254	0.0032		
0.0031	0.064	0.350	0.348	0.0000		
0.0056	0.079	0.435	0.437	0.0000		
0.0206	0.090	0.496	0.550	0.0029		
0.0313	0.114	0.627	0.570	0.0032		
S24F2 (Deslimed)						
Apparent Viscosity (Pa s)	Slimes Vol. Frac	Scaled Vol. Frac	Model Vol. Frac	Square Error	Sum of Square Error	Scaling Factor
0.0011	0.224	0.323	0.079	0.0594	1.23E-32	1.44
0.001	0.267	0.385	0.045	0.1162		
0.0012	0.311	0.449	0.109	0.1159		
0.0029	0.367	0.530	0.334	0.0386		
0.0387	0.401	0.579	0.579	0.0000		

Appendix F: Chapter 5 Calculations

This appendix contains details of calculations used in Chapter 5 not included along the size × assay or rheology data. The first such calculation is for the shear rate estimates within the inclined channel. Sample calculations are provided for Run S24B (first row in table). Firstly, the Overflow solids concentration and total mass flow rate were obtained from the sampling data (Appendix C). Multiplying the *Mass Flow* by $(100 - \text{Solids Conc.})$, and converting units, gives the *Water Rate*.

$$\text{Water rate} = 11836/60 \times (100 - 29.1)/100 = 140 \text{ g/s or } 1.4 \times 10^{-4} \text{ m}^3/\text{s}$$

Dividing this by the *Channel Area* and *Number of Channels* gives the *Single Channel Velocity*.

$$\text{Channel Velocity} = 1.4 \times 10^{-4} / 0.0003 / 26 = 0.01793 \text{ m/s}$$

Equation 3.9 was then used to calculate the shear rate at the four different locations of the channel and an average of all rates determined,

$$\gamma = \frac{6U'}{z} \left(1 - \frac{2x}{z} \right)$$

$$\text{Shear (surface)} = 6 \times 0.01793 / 0.003 \times (1 - (2 \times 0)/0.003) = 36 \text{ s}^{-1}$$

$$\text{Shear (1/3)} = 6 \times 0.01793 / 0.003 \times (1 - (2 \times 0.0005)/0.003) = 24 \text{ s}^{-1}$$

$$\text{Shear (2/3)} = 6 \times 0.01793 / 0.003 \times (1 - (2 \times 0.001)/0.003) = 12 \text{ s}^{-1}$$

$$\text{Shear (middle)} = 6 \times 0.01793 / 0.003 \times (1 - (2 \times 0.0015)/0.003) = 0 \text{ s}^{-1}$$

Run	O/F Solids Conc. (wt.%)	Mass Flow (g/min)	Water Rate		Single Channel Velocity (m/s)	Shear rate (1/s) at:				Average of Shear Rates (1/s)
			(g/s)	(m ³ /s)		Inclined Surface	1/3 Distance to Middle	2/3 Distance to Middle	Middle of Channel	
From Raw Sampling data						Channel Width (m)	Channel Area (m)	No. Channels		
						0.003	0.0003	26		
						0.0018	0.00018	38		
S24B	29.1	11836	140	1.40E-04	0.0179	36	24	12	0	16
S24B2	28.4	6289	75	7.50E-05	0.0096	19	13	6	0	
S24B3	23.9	3498	44	4.44E-05	0.0057	11	8	4	0	
S24D	9.2	5811	88	8.79E-05	0.0113	23	15	8	0	
S24D2	8.4	2812	43	4.29E-05	0.0055	11	7	4	0	
S24E	3.9	12274	197	1.97E-04	0.0252	50	34	17	0	
S24E2	3.6	6223	100	1.00E-04	0.0128	26	17	9	0	
S24F	26.3	10683	131	1.31E-04	0.0168	34	22	11	0	
S24F2	22.2	5401	70	7.00E-05	0.0090	18	12	6	0	
S24F3	8.4	11668	178	1.78E-04	0.0228	46	30	15	0	
S24F4	7.4	5965	92	9.21E-05	0.0118	24	16	8	0	
S24F5	3.2	12754	206	2.06E-04	0.0264	53	35	18	0	
S24F6	2.8	6397	104	1.04E-04	0.0133	27	18	9	0	
S24G	10.6	5881	88	8.76E-05	0.0187	43	28	14	0	
S24G2	19.6	3108	42	4.16E-05	0.0089	20	14	7	0	
S24G3	25.9	6115	76	7.55E-05	0.0161	37	25	12	0	
S24G4	9.9	11234	169	1.69E-04	0.0360	82	55	27	0	

The *Channel Velocity* and *Shear Rate* (at the surface) from the previous calculations were used in the calculations of the hindered settling rates for Figure 5.15. Sample calculations are for Run S24B (first row in table). The *separation size* (d_{50}) was read from the partition to underflow curves and the *Overflow Solids Conc.* obtained from the raw sampling data (Appendix B). The size × assay data gave the *Mass Distribution* above and below 0.038 mm. All conversions from wt.% to vol.% and volume fractions assumed a particle density of 4400 kg/m³, for example in Run S24B the solids concentration of 29.1 wt.% was converted by,

$$Vol.Frac = \frac{\frac{SolidsConc.}{SolidsDensity}}{\frac{SolidsConc.}{SolidsDensity} + \frac{100 - SolidsConc.}{WaterDensity}}$$

$$= (29.1/4.4) / ((29.1/4.4) + ((100 - 29.1)/1)) = 0.085$$

The total overflow solids volume fraction was thus split into the -0.038 mm and +0.038 mm volume fractions. The empirical model created to fit out slimes viscosity data (Equation 5.1) was used to calculate a new effective viscosity for the slimes suspension using the shear rate at the surface and the -0.038 mm volume fraction of solids.

$$\text{Model Visc.} = 0.00089 \times (1 + 1.01 \times 10^6 \times 35.9^{-0.93} \times 0.027^{3.98} + 0.4 \times 35.9 \times 0.027) = 0.0012 \text{ Pa s}$$

Two terminal settling velocities for the d_{50} sized particles were then calculated using Stokes Law (Equation 2.5); a standard velocity using the viscosity of water and one using the calculated effective viscosity.

$$\begin{aligned} u_t(\text{water}) &= d_{50}^2 \times (\text{particle density} - \text{water density}) \times 9.8 / (18 \times \text{water viscosity}) \\ &= (1.24 \times 10^{-4})^2 \times (4400 - 997) \times 9.8 / (18 \times 0.00089) = 0.032 \text{ m/s} \end{aligned}$$

$$\begin{aligned} u_t(\text{slimes}) &= d_{50}^2 \times (\text{particle density} - \text{water density}) \times 9.8 / (18 \times \text{water viscosity}) \\ &= (1.24 \times 10^{-4})^2 \times (4400 - 997) \times 9.8 / (18 \times 0.0012) = 0.023 \text{ m/s} \end{aligned}$$

Two hindered settling factors were calculated in the form of the Richardson and Zaki equation (Equation 2.13) with the exponent $n = 4.6$. The standard factor used the volume fraction of the overflow solids whereas the 'slimes' hindered settling factor used the volume fraction of the +0.038 mm particles. Multiplying the hindered settling factor with the Stokes law settling velocity gives the hindered settling velocity for the standard and slimes cases.

$$\begin{aligned} \text{Hindered settling (standard)} &= (1 - \phi)^{4.6} \times u_t(\text{water}) \\ &= (1 - 0.085)^{4.6} \times 0.032 = 0.0212 \text{ m/s} \end{aligned}$$

$$\begin{aligned} \text{Hindered settling (slimes)} &= (1 - \phi_{+0.038})^{4.6} \times u_t(\text{slimes}) \\ &= (1 - 0.059)^{4.6} \times 0.023 = 0.0173 \text{ m/s} \end{aligned}$$

Appendix G: Chapter 6 Calculations

This appendix contains details of the calculations made for the analysis of the silica feed experiments in Chapter 6. These calculations rely on the partition separation size and Ep values as well as the mass flow data of each stream as given by Appendix B and C. Any conversions from a weight basis to a volume basis, or vice versa, assume a particle density of 2650 kg/m³. Sample calculations in this appendix are for Run CF145 (first row in the table).

The *Underflow Solids Flux* used in Figure 6.9 was calculated by dividing the *Underflow Solids Rate* by the *Underflow Line Area*, and converting the units to m³/(m² s). As the underflow blockage issue occurs on each individual module, this value was divided by 2 to make it the flux for one unit.

$$\begin{aligned} UF \text{ Solids Flux} &= UF \text{ Solids Rate} / UF \text{ Line area} / 1000 / 60 / 2650 / 2 \\ &= 1422 / 1.3 \times 10^{-5} / 1000 / 60 / 2650 / 2 = 0.36 \text{ m}^3/(\text{m}^2 \text{ s}) \end{aligned}$$

The *Channel Velocity* needed for Equation 3.16 was calculated by dividing the *Overflow Flowrate* by the *Total Channel Area*.

$$\begin{aligned} Channel \text{ Vel.} &= Overflow \text{ Flowrate (m}^3/\text{s)} / Total \text{ Channel Area (m}^2) \\ &= 0.0015 / 0.009108 = 0.161 \text{ m/s} \end{aligned}$$

Stokes law was used to calculate the terminal settling velocity for the d_{50} particle (converted from μm to m).

$$\begin{aligned} u_t &= d_{50}^2 \times (\text{particle density} - \text{water density}) \times 9.8 / (18 \times \text{water viscosity}) \\ &= (9.4 \times 10^{-6})^2 \times (2650 - 997) \times 9.8 / (18 \times 0.00089) = 8.97 \times 10^{-5} \text{ m/s} \end{aligned}$$

The Channel velocity was divided by this settling velocity to give the ratio U' / u'_t and the d_{50} size used to calculate the ratio $Gz/3d$,

$$U' / u'_t = 0.161 / 8.97 \times 10^{-5} = 1793$$

$$Gz/3d = 55 \times 0.001 / (3 \times 9.4 \times 10^{-6}) = 1945$$

Rearranging Equation 3.16 for the terminal settling velocity gives,

$$u'_t = \frac{U'3d_{50}}{Gz}$$

Equating this with Stokes Law allows the *Theoretical Separation Size* to be calculated,

$$d_{50} = \frac{54\mu U'}{Ggz\Delta\rho}$$

$$= (54 \times 0.00089 \times 0.161) / (55 \times 9.8 \times 0.001 \times (2650 - 997)) = 8.6 \times 10^{-6} \text{ m}$$

Gravity Separation and Desliming Using Inclined Channels Subject to Different G–Forces

Run no.	Separation size, d_{50} (μm)	Ep (μm)	Feed			Underflow			Overflow				Underflow Line area (m^2)	UF Solids Flux ($\text{m}^3/\text{m}^2\text{s}$)	Channel velocity (m/s)	Terminal settling velocity (m/s)	U'/u'_t $Gz/3d$		Theoretical Separation Size (m)
			Flowrate (L/min)	Solids Conc. ($\text{wt.}\%$)	Solids Rate (g/min)	Flowrate (L/min)	Solids Conc. ($\text{wt.}\%$)	Solids Rate (g/min)	Flowrate (L/min)	Flowrate (m^3/s)	Solids Conc. ($\text{wt.}\%$)	Solids Rate (g/min)							
CF145	9.4	4.6	100	1.9	1910	20	6.9	1422	88	0.0015	0.5	454	1.3E-05	0.36	0.161	8.97E-05	1793	1945	8.6E-06
CF146	14.4	5.7	98	2.0	2028	19	6.5	1307	99	0.0017	0.6	584	1.3E-05	0.33	0.181	2.09E-04	870	1276	9.7E-06
CF147	10.2	5.9	98	2.0	2037	19	7.4	1458	85	0.0014	0.6	473	1.3E-05	0.37	0.155	1.05E-04	1478	1796	8.3E-06
CF148	11.0	5.3	115	4.0	4683	24	12.8	3346	96	0.0016	1.1	1114	1.3E-05	0.85	0.176	1.22E-04	1450	1670	9.4E-06
CF149	10.7	4.1	111	4.0	4529	20	14.3	3212	106	0.0018	0.9	937	1.3E-05	0.82	0.194	1.17E-04	1662	1706	1.0E-05
CF150	10.2	4.1	110	3.9	3662	21	14.0	3275	103	0.0017	1.0	998	1.3E-05	0.84	0.188	1.05E-04	1784	1793	1.0E-05
CF152	12.8	4.5	101	9.9	10618	19	32.5	7712	99	0.0017	2.8	2803	1.3E-05	1.97	0.182	1.65E-04	1099	1432	9.7E-06
CF153	7.8	3.4	49	20.3	11783	20	35.9	8948	49	0.0008	3.1	1544	1.3E-05	2.28	0.090	6.21E-05	1443	2337	4.8E-06
CF154	24.7	14.2	51	29.3	18318	20	47.1	12564	58	0.0010	13.8	8829	1.3E-05	3.20	0.107	6.18E-04	173	741	5.7E-06
CF155	5.4	3.0	37	28.0	11251	18	54.1	12909	33	0.0006	10.2	3615	1.3E-05	3.29	0.061	2.94E-05	2067	3394	3.2E-06
CF156	9.0	4.0	35	28.9	12336	19	41.2	9864	47	0.0008	3.9	1873	1.3E-05	2.52	0.086	8.15E-05	1055	2040	4.6E-06
CF157	20.4	12.0	52	30.1	19267	18	46.6	11833	53	0.0009	12.3	7007	1.3E-05	3.02	0.096	4.20E-04	229	899	5.1E-06
CF158	6.0	4.9	54	30.2	20218	32	40.6	17220	40	0.0007	5.5	2290	2.8E-05	1.95	0.073	3.61E-05	2023	3064	3.9E-06
CF159	31.5	19.2	115	28.3	37815	34	39.8	18089	107	0.0018	16.9	20069	2.8E-05	2.05	0.195	1.00E-03	194	581	1.0E-05
CF160	12.1	5.2	90	28.9	28172	32	47.2	21383	75	0.0012	8.4	6679	2.8E-05	2.42	0.137	1.47E-04	931	1517	7.3E-06
CF162	19.0	10.0	88	29.6	31837	34	44.0	20561	88	0.0015	11.4	10803	2.8E-05	2.33	0.161	3.64E-04	441	965	8.6E-06
CF163	18.6	9.9	82	30.3	30502	31	46.1	20227	76	0.0013	11.8	9682	2.8E-05	2.29	0.140	3.48E-04	402	988	7.4E-06
CF164	13.4	7.3	89	30.8	33775	32	51.2	24143	67	0.0011	10.0	7160	2.8E-05	2.74	0.123	1.83E-04	673	1363	6.5E-06
			Total Channels Area =			0.009108													
			Particle Density =			2650													
			Water Density =			997													
			Water Viscosity =			0.00089													
			G =			55													
			z =			0.001													

Appendix H: Graviton Splashing Raw Data

This appendix contains extra information pertaining to the REFLUX™ Graviton unit. Table H1 contains the data collected to investigate the extent of the internal splashing described in Section 4.1.2. The table shows the volumes of the overflow and underflow samples collected during the tests and the sampling time for each. The volumetric rates were then calculated to generate Figure 4.15. The first, and largest set of data listed in the table is for the system with the underflow blocked off, hence in an ideal system all of the flow would be collected in the overflow. The last sets of data listed are for the various modifications made to help alleviate the splashing issue. The underflow volumes listed are the combine volume of both underflow collection points.

Table H1: Internal splashing test data.

Sample Time (s)	O/F Volume (L)	Sample Time (s)	U/F Volume (L)	O/F Rate (L/s)	U/F Rate (L/s)	Total Flow (L/s)
30	13.4	60	2.9	26.7	2.9	29.6
9	17.3	60	3.9	115.2	3.9	119.1
45	41.4	60	3.1	55.2	3.1	58.3
20	33.0	60	4.0	99.0	4.0	103.0
20	24.2	60	4.2	72.6	4.2	76.8
10	29.4	60	12.8	176.4	12.8	189.2
15	34.7	60	9.0	138.8	9.0	147.8
60	24.8	60	3.0	24.8	3.0	27.8
30	31.1	60	3.2	62.2	3.2	65.4
15	21.9	60	3.7	87.6	3.7	91.3
10	19.3	60	5.7	115.8	5.7	121.5
10	25.4	60	9.1	152.4	9.1	161.5
10	21.3	60	7.4	127.8	7.4	135.2
10	16.1	60	3.4	96.6	3.4	100.0
15	24.0	60	3.4	96.0	3.4	99.4
15	31.7	60	7.4	126.8	7.4	134.2
15	27.8	60	6.8	111.2	6.8	118.0
20	30.5	60	3.3	91.5	3.3	94.8
15	30.7	60	6.7	122.8	6.7	129.5
Upper O/F Blocked						
10	28.7	60	8.6	172.2	8.6	180.8
15	36.6	60	7.0	146.4	7.0	153.4
15	16.9	60	1.0	67.6	1.0	68.6

Gravity Separation and Desliming Using Inclined Channels Subject to Different G-Forces

Sample Time (s)	O/F Volume (L)	Sample Time (s)	U/F Volume (L)	O/F Rate (L/s)	U/F Rate (L/s)	Total Flow (L/s)
Upper O/F Blocked and 1/3 Launder Rail Covered						
10	28.9	60	5.7	173.4	5.7	179.1
Upper O/F Blocked and All of Launder Rail Covered						
10	28.9	60	4.6	173.4	4.6	178.0

Appendix I: Copyright Permissions

This appendix contains the permissions granted by publishers to reproduce their copyrighted material in this thesis. The licences refer to use of the following:

- Figure 3.1. Obtained from Perry & Green (1999)
- Figures 3.3 and 3.5. Obtained from Galvin et al. (2009)
- Figure 3.4 and 3.6. Obtained from Galvin & Liu (2011)
- Figures 3.8, 3.9 and 3.10. Obtained from Das & Sarkar (2018)
- Figure 3.11. Obtained from Singh & Das (2013)
- Figures 3.12 and 3.13. Obtained from Galvin & Dickinson (2013)

Order Number: 1017665

Payment

James Carpenter james.carpenter@uon.edu.au u Payment method: Invoice	Billing Address: Mr. James Carpenter Unit 3 15 Floribunda Close +61 (4)12685828 james.carpenter@uon.edu.au	Customer Location: Mr. James Carpenter Unit 3 15 Floribunda Close
--	---	--

Order Details

1. Perry's chemical engineers' Billing Status:

Order license ID	1017665-1
Order detail status	Completed
ISBN-13	9780070498419
Type of use	Republish in a thesis/dissertation
Publisher	MCGRAW-HILL PROFESSIONAL PUBLISHING

LICENSED CONTENT

Publication Title	Perry's chemical engineers' handbook	Country	United States of America
Author/Editor	GREEN, DONALD W., PERRY, ROBERT H.	Rightsholder	McGraw Hill LLC
Date	01/01/1997		
Language			

REQUEST DETAILS

Image/photo/illustration	Distribution	Worldwide
Number of images / photos / illustrations	Copies for the disabled?	Original language of publication
Format (select all that apply)	Minor editing privileges?	No

Who will republish the content?	Academic institution	Incidental promotional use?	No
Duration of Use	Life of current and all future editions		AUD
Lifetime Unit Quantity	Up to 499		

NEW WORK DETAILS

Title	Gravity Separation and Desliming using Inclined Channels Subject to Different G-Forces	Institution	University of Newcastle
		Expected presentation	2020.02.02
Instructor	James Lachlan Carpenter		

ADDITIONAL DETAILS

The requesting person / organization to appear on the

James L Carpenter

REUSE CONTENT DETAILS

Title, description or numeric reference of the portion(s)	FIG. 19-1 Particle-size range as a guide to the range of applications of various solid-solid operations.	Title of the article/chapter the portion is from	Solid-Solid Operations and Equipment
		Author of portion(s)	GREEN, DONALD W.; PERRY, ROBERT H.
Editor of portion(s)	Kalanadh V. S. Sastry, Harrison Cooper, Richard Hogg, T. L. P. Jespen, Frank Knoll, Bhupendra Parekh, Raj K. Rajamani, Thomas Sorenson, Ionel Wechsler, Chad McCleary, David B. Todd	Publication date of portion	1997-01-01
Volume of serial or monograph	N/A		
Page or page range of portion	19 - 3		

McGraw Hill LLC Terms and Conditions

It is the responsibility of the user to verify that the text, figures, images and other material that they wish to use are owned by McGraw-Hill Education. McGraw-Hill Education can only grant permission for the material

Total Items: 1

Subtotal: 0.00 AUD

Order Total: 0.00 AUD



[My Orders](#)

[My Library](#)

[My Profile](#)

Welcome

[Log out](#) | [Help](#)

[My Orders](#) > [Orders](#) > [All Orders](#)

[Print](#) [Copy](#)

License Number	4766820515393
License date	Feb 12, 2020
Licensed Content	Elsevier
Publisher	Chemical Engineering Science
Licensed Content	No
Publication	Gravity Separation and Desliming using Inclined Channels
Licensed Content	Subject to Different G-Forces University of Newcastle
Publisher	Warabrook, NSW 2304 Australia

[BACK](#)



[My Orders](#)

[My Library](#)

[My Profile](#)

Welcome

[Log out](#) | [Help](#)

[My Orders](#) > [Orders](#) > [All Orders](#)

[Print](#) [Copy](#)

License Number	4766820406747
License date	Feb 12, 2020
Licensed Content	Elsevier
Publisher	Chemical Engineering Science
Licensed Content	Role of inertial lift in elutriating
Publication	No
Licensed Content	Gravity Separation and Desliming using Inclined Channels
Publisher	Subject to Different G-Forces University of Newcastle
	Warabrook, NSW 2304 Australia

[BACK](#)



Mineral Processing and
Extractive Metallurgy
Review

Advanced Gravity Concentration of Fine Particles: A Review

Author: Avimanyu Das, , Biswajit Sarkar

Publication: Mineral Processing and Extractive Metallurgy Review

Rights managed by Taylor & Francis

Thesis/Dissertation Reuse Request

Taylor & Francis is pleased to offer reuses of its content for a thesis or dissertation free of charge contingent on resubmission of permission request if work is published.

[BACK](#)

[CLOSE](#)



[My Orders](#)

[My Library](#)

[My Profile](#)

Welcome

[Log out](#) | [Help](#)

[My Orders](#) > [Orders](#) > [All Orders](#)

[Print](#) [Copy](#)

License Number	4766820150701
License date	Feb 12, 2020
Licensed Content	Fuel Processing Technology
Publisher	Analysis of separation response of Kelsey
Licensed Content	No
Publication	Gravity Separation and Desliming using Inclined Channels
Licensed	Subject to Different G-Forces University of Newcastle
Publisher	Warabrook, NSW 2304 Australia

[BACK](#)



[My Orders](#)

[My Library](#)

[My Profile](#)

Welcome

[Log out](#) | [Help](#)

[My Orders](#) > [Orders](#) > [All Orders](#)

[Print](#) [Copy](#)

License Number	4766800859406
License date	Feb 12, 2020
Licensed Content	Elsevier
Publisher	Chemical Engineering Science
Licensed Content	Particle transport and separation in inclined
Publication	No
Licensed Content	Gravity Separation and Desliming using Inclined Channels
Publisher	Subject to Different G-Forces University of Newcastle
	Warabrook, NSW 2304 Australia

[BACK](#)